Year : 2019

CDK4 as a novel regulator of brown adipose tissue biology

Castillo Armengol Judit

UNIL | Université de Lausanne

Faculté de biologie
et de médecine

Center for Integrative Genomics (CIG)

CDK4 as a novel regulator of brown adipose tissue biology

Thèse de doctorat ès sciences de la vie (PhD)
Cardiovascular and Metabolism program

présentée à la

Faculté de biologie et de médecine
de l'Université de Lausanne

par

Judit CASTILLO ARMENGOL

Biologiste diplômée du Master de
l'Université Pompeu Fabra (Barcelona, Spain)

Jury

Prof. Ian Sanders, Président
Prof. Béatrice Desvergne, Présidente
Prof. Lluis Fajas Coll, Directeur de thèse
Prof. Bernard Thorens, Expert
Prof. Mirko Trajkovski, Expert

Lausanne
2019

UNIL | Université de Lausanne
Faculté de biologie
et de médecine

Ecole Doctorale
Doctorat ès sciences de la vie

Imprimatur

Vu le rapport présenté par le jury d'examen, composé de

Président·e	Madame	Prof.	Beatrice	**Desvergne**
Directeur·trice de thèse	Monsieur	Prof.	Lluis	**Fajas Coll**
Expert·e·s	Monsieur	Prof.	Bernard	**Thorens**
	Monsieur	Prof.	Mirko	**Trajkovski**

le Conseil de Faculté autorise l'impression de la thèse de

Madame Judit Castillo Armengol

Master in biomedical research, Universidad Pompeu Fabra Barcelona, Espagne

intitulée

CDK4 as a novel regulator of brown adipose tissue biology

Lausanne, le 24 juin 2019

pour le Doyen
de la Faculté de biologie et de médecine

Prof. Beatrice Desvergne

Summary

Brown adipose tissue (BAT) is a highly specialized tissue that functions to maintain body temperature during cold challenge through non-shivering thermogenesis. Numerous genes and pathways that regulate brown adipocyte biology have now been identified. However, the role of cell cycle regulators in the development and the function of this oxidative fat depot has not been thoroughly studied yet. Cyclin-dependent kinase 4 (CDK4) is a cell-cycle regulator known to modulate several metabolic processes. This protein is associated to the regulation of oxidative metabolism and now, we aim to determine its role in thermogenesis. Interestingly, *Cdk4* inactivation *in vivo* led to a marked metabolic phenotype in BAT, pointing towards a participation of CDK4 in non-shivering thermogenesis. First, BAT from *Cdk4$^{-/-}$* is smaller and exhibits increased mitochondrial number and decreased lipid droplet size. Moreover, the expression of canonical thermogenic genes is increased in the BAT of these animals, which renders them more resistant to cold exposure. Interestingly, sympathetic innervation of BAT is also increased in these mice maintained at room temperature, a condition of low adrenergic activation. Moreover, neurotrophins' gene expression analysis in *Cdk4$^{-/-}$* mice suggested that CDK4 controls neuronal growth in BAT. On the other hand, specific deletion of *Cdk4* in BAT has no effect in the regulation of thermogenesis. Overall, our findings demonstrate that CDK4 has a major role in BAT biology and in thermoregulation through the central nervous system.

Résumé

Le tissu adipeux brun (BAT) assure la thermogenèse non-frissonnante qui permet le maintien de la température corporelle dans un environnement froid. De nombreux gènes et voies régulant la biologie de l'adipocyte brun ont été découverts jusqu'ici ; cependant, le rôle des régulateurs du cycle cellulaire dans le développement et la fonction de ce tissu adipeux oxydatif n'a jamais été étudié. La protéine cyclin-dependent kinase 4 (CDK4) est un régulateur du cycle cellulaire connu pour également moduler plusieurs processus métaboliques. CDK4 est associée à la régulation du métabolisme oxydatif et au cours de ce travail, nous avions pour objectif de déterminer sa fonction dans la thermogenèse. *In vivo*, l'inactivation de *Cdk4* (souris *Cdk4$^{-/-}$*) induit un phénotype majeur dans le BAT, mettant en évidence le rôle de CDK4 dans la thermogenèse non-frissonnante. Chez ces souris, le BAT est plus petit et contient des gouttelettes lipidiques plus petites et un plus grand nombre de mitochondries. De plus, chez les souris *Cdk4$^{-/-}$*, l'expression des gènes thermogéniques est augmentée et rend ces souris plus résistantes au froid. De plus, l'innervation sympathique du BAT est augmentée chez les souris *Cdk4$^{-/-}$* élevées à température ambiante, une situation où l'activation adrénergique est limitée; enfin, l'analyse de l'expression des gènes de la famille des neurotrophines suggère que CDK4 contrôle la croissance neuronale dans le BAT. D'autre part, la délétion de *Cdk4* spécifiquement dans le BAT n'a pas d'effet sur la régulation de la thermogenèse. En conclusion, nos résultats démontrent que CDK4 joue un rôle majeur dans la biologie du BAT et dans la thermorégulation via le système nerveux central.

Table of contents

Table of contents

_____

Acknowledgements

I would like to express my gratitude to **Professor Lluis Fajas Coll** for giving me the opportunity to do my PhD thesis as part of his lab. Lluis, thank you for helping me during all these years and for having faith on me. I am incredibly grateful to you for all the opportunities that you have given me to develop my abilities and grow as a researcher. Lluis, if among all the things that I have learnt from you, I would have to choose one, it would be to be passionate about science. Your inspiring confidence in science is admirable and this is really something that I am taking with me wherever I am going to continue my science path.

I would also like to thank **Professor Mirko Trajkovski**, **Professor Bernard Thorens**, **Professor Ian Sanders** and **Professor Béatrice Desvergne** for accepting to be part of my committee and for their scientific feedback in the course of this thesis.

This thesis project has been possible thanks to the support and guidance of a team. I would like to thank **Dr. Isabel C. Lopez Mejia**. This work could not have been completed without your advice and excellent scientific feedback. I am very thankful for your guidance and your willingness to talk and advise me on the progress of my project since my first day in the lab.

Many thanks to my friends and colleagues, the "muslonas" **Anita**, **Laia** and **Tiziana** with whom I could share my PhD life, making the time fly a bit faster. The guys, **Valentin** and **Eric**, it has been wonderful spending the end of my PhD with you. My thanks also to **Honglei**. Working with you has been an adventure from which I have learnt a lot. **Lucia**, I am very happy that I could meet you. Always with a smile and giving strong support to me! I am also grateful to **Brigitte** for her technical support, especially with the big amount of genotyping work done.

Thanks to my other colleagues **Yizhe** and **Katharina**. It has been very pleasant meeting you and sharing the lab with you.

Acknowledgements

I want to thank my former colleague **Albert**. I have learnt a lot from the brown adipose tissue world with you. Thank you also for your feedback and willingness to help at all times. **Sylviane** working with you at the beginning of my thesis was wonderful and I missed you a lot when you left the lab. You had faith on me when I was very new in the lab. I am very thankful for your help and ideas. Always with a smile!

I would also like to thank **Frédéric Preitner** for the scientific discussions that help me to advance in the project and **Guy Niederhauser**, **Anabela Rebelo Pimentel** and **Gilles Willemin** for their technical support in the experiments performed with mice.
Additionally, I am grateful to all the people of the Department of Physiology and of the CIG with whom I shared a coffee or a beer enjoying their companionship and encouragement.

A la meva família, els moments que he viscut amb vosaltres durant aquests anys han fet la meva vida més alegre i realment sobren les paraules quan intento descriure el que heu representat per mi en aquests anys de tesi. Com es ben sabut, la família és quelcom que no es tria però tinc la ferma convicció, que no hagués pogut caure en una de millor. **Papa**, **Mama**, tot i la distància, us he tingut molt presents en el meu dia a dia. Us agraeixo el vostre suport incondicional en la meva decisió de venir a fer el doctorat a Lausanne. Les vostres visites a Lausanne han estat fantàstiques i m'han omplert d'alegria en aquests anys. A la meva germana, **Maria**, que podria dir-te si crec que aquests anys separades ens han unit més que mai i això ha estat essencial per mi. I love you, sister! A la meva padrina, **Pimpi**, per sempre present en mi. Fa anys em vas dir: "Qui dia passa, any empeny". Aquesta frase l'he duta al meu cor durant aquests anys a Lausanne i m'ha reconfortat molt quan les coses no han sigut fàcils. Finalment, gràcies **Xavier** pel teu recolzament, suport i amor incondicional. Gràcies també per haver aguantat amb compostura totes les meves "exteeeeenseees" explicacions sobre Cdk4 i companyia... Estic segura que realment podries fer un resum d'aquesta tesi sense massa problemes! ;)

Abbreviations

^{18}FDG-PET/CT	2-[^{18}F]-fluoro-2-deoxy-glucose positron emission tomography
AAV	Adeno-associated virus
ADRB3	Adrenergic receptor beta 3
AMP	Adenosine monphosphate
AMPK	AMP-activated protein kinase
ARC	Arcuate nucleus
AT	Adipose tissue
ATP	Adenosine triphosphate
Atp5a	ATP synthase alpha-subunit
BA	Bile acid
BAT	Brown adipose tissue
Bdnf	Brain derived neurotrophic growth factor
BMI	Body mass index
Bmp8b	Bone morphogenetic protein 8b
CAK	Cdk-activating kinase
cAMP	Cyclic AMP
Ccnd3	Cyclin D3
Cdk	Cyclin-dependent kinase
Cgrp	Calcitonin gene related peptide
Cidea	Cell death activator
CKI	Cdk inhibitor
CKK	Cholecystokinin
CNS	Central nervous system
CoxIV	Cytochrome c oxidase subunit 4
Cpt1b	Carnitine Palmitoyltransferase 1B
Creb	cAMP response element binding
CVD	Cardiovascular diseases

Abstract

_____

DIO	Diet induced obesity
Dio2	2 iodothyronine deiodinase
DIT	Diet induced thermogenesis
DMH	Dorsomedial hypothalamus
DNP	Dinitrophenol
Ebf2	Early b-cell factor 2
EE	Energy expenditure
Ehmt1	Euchromatic histone lysine methyltransferase 1
ETC	Electron transport chain
FGF21	Fibroblast growth factor 21
GLP-1	Glucagon-like peptide 1
HFD	High fat diet
HPT	Hypothalamic-pituitary-thyroid
iBAT	Interscapular BAT
IL	Interleukin
ILC2	Innate lymphoid cell type 2
Irs2	Insulin receptor substrate 2
KO	Knockout
LHA	Lateral hypothalamic area
MAPK	Mitogen-activated protein kinase
MBH	Mediobasal hypothalamus
MEF	Mouse embryonic fibroblasts
Myf5	Myogenic factor 5
NADH	Nicotinamide adenine dinucleotide
Ndufab9	NADH dehydrogenase 1 alpha subcomplex subunit b9
NE	Norepinephrine
Ngf	Nerve growth factor
Npy	Neuropeptide Y
Nrg	Neuroregulin
OPAn	Swiss animal protection ordinance

Pax7	Paired box 7
Pgc1α	Peroxisome proliferator-activated receptor gamma coactivator 1-alpha
PKA	Protein kinase A
PM20D1	Peptidase M20 domain-containing 1
POA	Preoptic area
POMC	Propiomelanocortin
PPARγ	Peroxisome proliferator-activated receptor gamma
Prmd16	PR domain zinc finger protein 16
PSNS	Parasympathetic nervous system
Rb	Retinoblastoma protein
RER	Respiratory exchange ratio
RPA	Raphe pallidus area
scWAT	Subcutaneous WAT
Sdha	Succinate dehydrogenase complex, subunit A
Sema	Semaphorin
SNS	Sympathetic nervous system
T2D	Type-2 diabetes
T3	Triiodothyronine
T4	Thyroxine
TCPTP	T-cell protein tyrosine phosphatase
TG	Triglycerides
TGR5	also known as G protein–coupled bile acid receptor 1, GPBAR1
Th	Tyrosine hydroxylase
Thr	Thyroid hormone receptor
Tomm20	Translocase Of Outer Mitochondrial Membrane 20
TRH	Thyrotropine-releasing hormone
TSH	Thyroid-stimulating hormone
Ubqcr	Ubiquinol cytocrome C reductase
Ucp1	Uncoupling protein 1

VMH   Ventromedial hypothalamus

WAT   White adipose tissue

WT   Wild-type

Chapter 1: Introduction

Chapter 1: Introduction

I.   Therapeutic potential of brown adipose tissue

1) Obesity, metabolic syndrome and energy balance

Nowadays, obesity is a rapid growing epidemic because of the alarming rates of overweight individuals worldwide (1). The prevalence of obesity is increasing constantly and in 2014, 39% of the adult population was overweight. Obesity is defined by using the Body mass index (BMI). A BMI greater or equal to 25 is defined overweight, a BMI greater or equal to 30, obesity and a BMI equal or over 40, extreme obesity.

Obesity is strongly associated to the development of the so-called *metabolic syndrome*, which has been shown to induce the outcome of diabetes and cardiovascular diseases (CVD). The metabolic syndrome appears with the weight gain and in particular with the increase in intra-abdominal fat accumulation represented by larger waist circumference. It includes metabolic disturbances such as high blood pressure, dyslipidemia, insulin resistance and high plasma glucose. All of these pathophysiologies can result in increased risk of type-2 diabetes (T2D) and cardiovascular episodes (2).

Energy balance is described as the equilibrium of energy intake and energy expenditure (EE). When energy balance is positive because energy intake exceeds energy expenditure, it causes weight gain and therefore, obesity. Energy taken in the body includes dietary and food intake in the form of carbohydrates, lipids and proteins. In contrast, energy expenditure is the combination of basal metabolism and physical activity (3-5). Moreover, it is well known that thermogenesis (heat production) contributes to the equation and it is a component of EE (Figure 1-1).
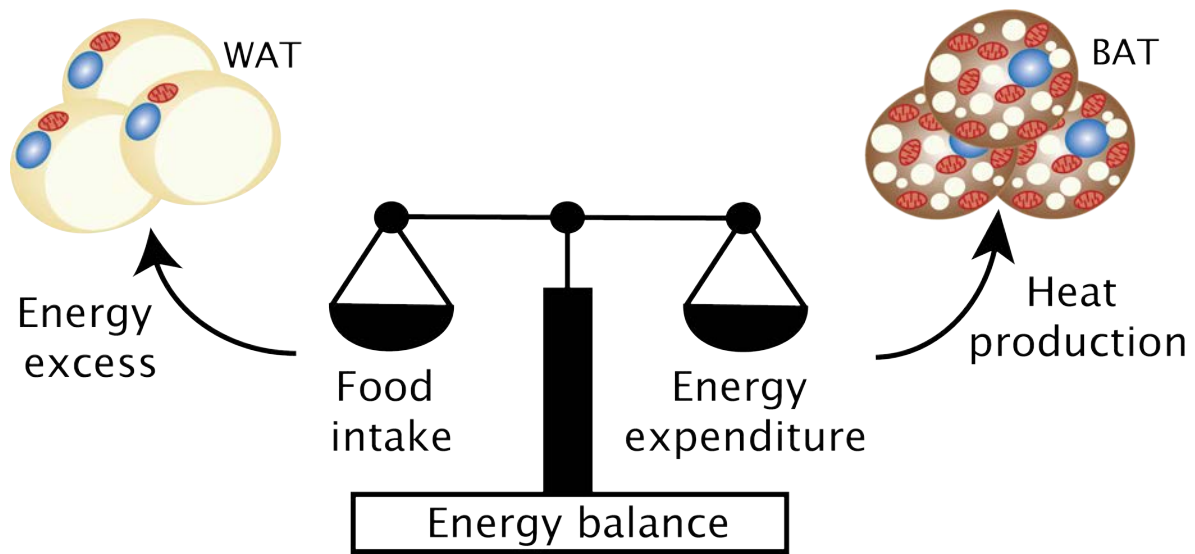
Figure 1-1. Energy balance. Energy balance is the equilibrium between energy taken in by the organism as food and energy dissipated by the body as basal metabolism, physical activity and thermogenesis. Brown adipose tissue (BAT) is dedicated to heat production increasing the whole energy expenditure of the organism. If energy in exceeds energy expenditure, then the extra calories are stored in white adipose tissue (WAT) inducing weight gain. In contrast, if energy expenditure is higher than energy intake, body weight loss is favored.

2) White adipose tissue at the center of obesity

The excess of calories of the positive energy balance is stored in white adipose tissue (WAT) (5, 6). There are several different WAT depots in the organism but there are mainly two different localizations, the visceral and the subcutaneous. The visceral WAT surrounds the organs and includes the omental, mesenteric, perirenal, retroperitoneal and gonadal. On the other hand, the subcutaneous WAT is localized mainly at the abdominal level (Figure 1-2) (7).

Considered a longtime as an inactive tissue, WAT is the main organ of energy storage and it is mainly composed of cells named white adipocytes. They are also called unilocular adipocytes because they have a big lipid droplet that occupies the majority of the cytoplasmic space of the cell. The principal function of white adipocytes is to store energy in the form of triglycerides (TG) to provide fuel to other organs when needed.
WAT is also considered as an endocrine organ because it is capable to secrete several hormones, named adipokines, to communicate with other organs in response of physiological processes (8, 9).

Chronic calorie overconsumption results in hyperplasia and hypertrophy of WAT, which are, respectively, the formation of new adipocytes and the enlargement of the existing ones. However, accumulation of lipids in non-adipose depots, like skeletal muscle or liver, is also possible and results in lipotoxicity, which triggers the failure of the functions of other metabolic organs and a dysregulation of whole-body metabolism (10, 11).

3) Brown adipose tissue (BAT) and energy balance

As an imbalance towards positive energy balance is the cause of obesity, strategies for promoting negative energy balance are of great interest. Reducing food intake through

_____

caloric restriction can decrease energy intake (12). Besides this, increasing EE also promotes negative energy balance. One of the most straightforward methods to increase EE is physical activity that successfully decreases adiposity (13).

As mentioned earlier, thermogenesis, which is the process of generating heat to maintain body temperature, contributes to increase EE. In fact, targeted strategies to chemically stimulate mitochondrial uncoupling have been proved to promote negative energy balance. Adenosine triphosphate (ATP) is considered as the energy exchange factor. Mitochondria are organelles that produce ATP by the enzymatic activity of ATP synthase from the catalysis of carbohydrates, lipids and proteins.

Dinitrophenol (DNP) was broadly used as a weight-loss drug in the early 1930s. The mechanism of action of DNP is to reduce the efficiency of ATP synthase favoring the uncoupling of the energy in the form of heat. Nevertheless, administration of DNP had other side effects because of its non-specific impact in all of the organism's mitochondria and its use was discontinued in the late 1930s (14, 15).

However, increasing uncoupling occurs naturally in BAT. BAT is a highly specialized organ that is capable of maintaining body temperature by regulating heat production. Its more relevant and iconic protein is the Uncoupling protein 1 (UCP1). UCP1 is found in the mitochondria and it is in charge of uncoupling the excess of protons from oxidative phosphorylation in the form of heat. This heat production is called *non-shivering thermogenesis*, to distinguish it from the heat generated from skeletal muscle contraction which is called *shivering thermogenesis* (16).

It has been shown that, when activated, BAT heat production increases EE and diminishes weight gain in diet induced obesity models (17, 18). Moreover, inducing BAT activation in obese mice results in lipid and glucose clearance (17-19). In conclusion, boosting BAT function has beneficial effects to restore the metabolic disorders of obesity

II.   Murine brown and beige adipose tissue

1) BAT in rodents

Small mammals are more susceptible than larger animals to lower ambient temperature because of their higher surface volume ratio that favors the heat loss of body temperature to the environment. Nevertheless, these mammals have developed a new mechanism that replaces body heat lost by new heat production. This is possible because of the existence of BAT, a very highly specialized tissue crucial for these animals to maintain their core body temperature (16).

BAT is considered scientifically a relatively new organ. It was identified for the first time in 1551, but it was not until last century that it was known to be present in all mammals and its function was not described until 1960s (20). BAT biology has been classically studied in rodents. It is found dispersed in several areas of the body. The principal and biggest depot is the interscapular BAT (iBAT) and smaller depots of brown fat can be found in intercostal, axillary, perirenal or periaortic areas (Figure 1-2) (21).

BAT is the major site of non-shivering thermogenesis. It is constituted by brown adipocytes that, like white adipocytes, have the capacity to store lipids. However, brown adipocytes are characterized for having smaller and numerous lipid droplets, which is classifies them as multilocular adipocytes. Moreover, these adipocytes are very rich in mitochondria, which are used to provide the energy for heat dissipation. These mitochondria express UCP1 that is in charge of uncoupling the proton gradient from substrate oxidation to transform energy in the form of heat.

In addition, BAT is a very plastic organ that adapts to external cues. When environmental temperature decreases, body heat loss increases and consequently, BAT

thermogenic capacity is enhanced to compensate it. This process is called *adaptation* or *acclimation* (16).

Furthermore, BAT can also participate in *diet-induced thermogenesis* (DIT) where it is activated in response of high nutrient consumption, for example with high fat diet (HFD) feeding, to compensate for the excess of calories ingested (22). However, in sharp contrast, there are other studies that do not support the concept of DIT (23). Indeed, *Foster and colleagues* remarked that no direct contribution of iBAT, to increased oxygen consumption after high-caloric diet, was assessed to prove its effect on DIT (24). In the same line than this study, it has been reported that oxygen consumption in *Ucp1* wild-type (WT) and knockout (KO) was comparable after switching from chow diet to cafeteria diet (25).

2) Beige adipose tissue in rodents

Apart from the role of BAT in adaptive thermogenesis, other UCP1-expressing adipocytes can emerge from WAT in response to chronic cold exposure. These adipocytes are called "beige" or "brite" (from brown-in-white) adipocytes and the recruitment process of these beige adipiocytes is known as *browning of WAT*. In addition, treatment with β3-adrenergic activators can also mimic browning (26, 27).

Compared to the classical brown adipocytes that are mainly found in the interscapular region, beige adipocytes exist in the subcutaneous WAT of rodents (Figure 1-2). Beige adipocytes share biochemical characteristics with brown adipocytes, such as the multilocularilty and the increased mitochondrial respiratory capacity. As mentioned before, when recruited, they can express UCP1 at similar levels to brown adipocytes. Although the levels of expression of other thermogenic genes can also be shared with brown adipocytes, beige adipocytes have distinctive gene expression signatures (26, 27).
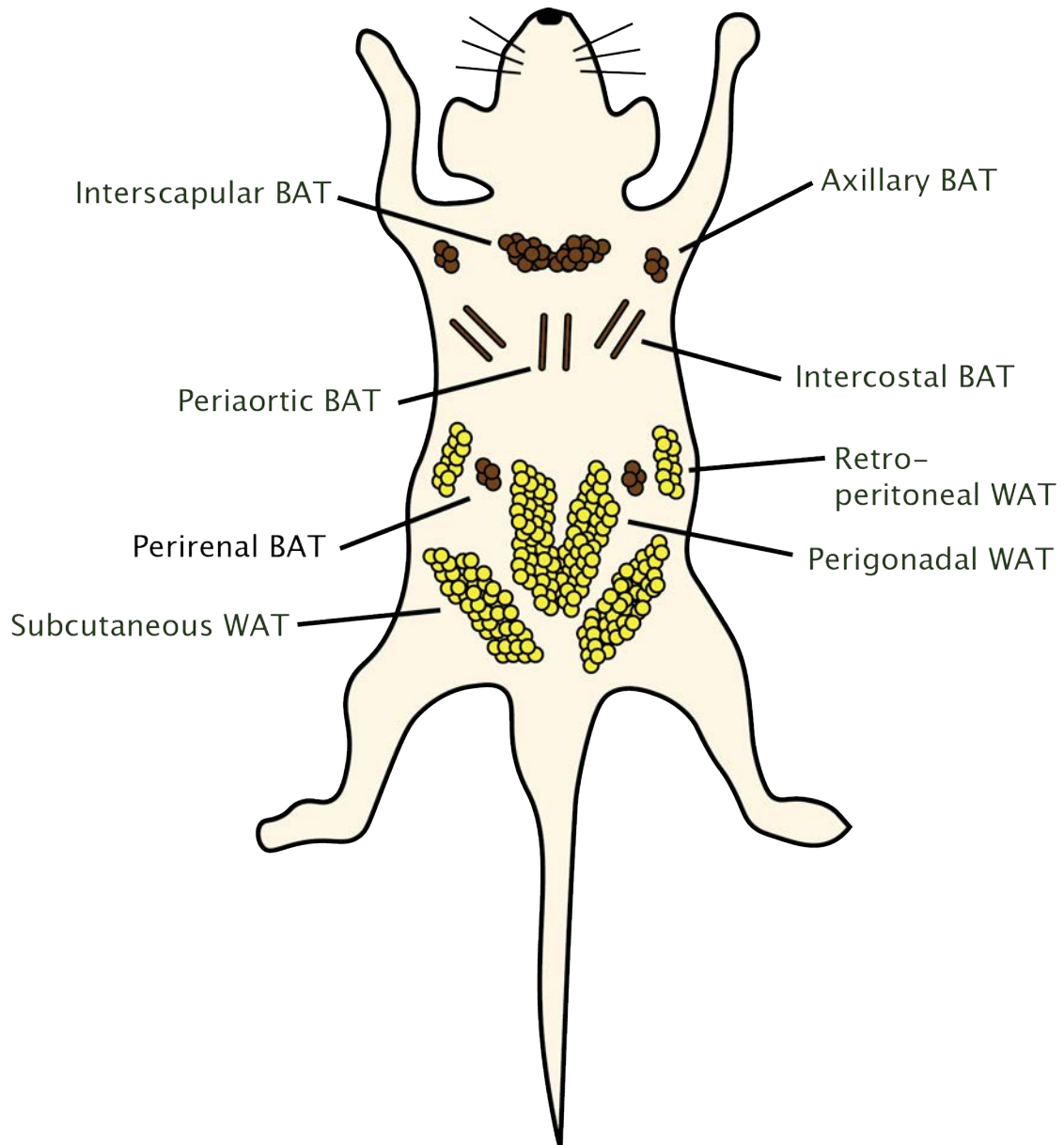
Figure 1-2. Distribution of adipose tissue depots in mouse. BAT is found in different depots in the mouse: interscapular, axillary, periaortic, intercostal and perirenal. WAT depots represented are retro-peritoneal, perigonadal and subcutaneous. Beige adipocytes are preferentially recruited in subcutaneous WAT.

3) Origins and developmental lineages of brown and beige adipocytes

The classical brown adipocytes, that constitute the brown fat depot, arise at late stages of embryonic development. In particular, BAT can be identified in rodents from embryonic day 15.5 (28). In contrast, subcutaneous WAT (scWAT) appears by embryonic day 18 and visceral WAT by post-natal day 6 (29).

Lineage-tracing studies have shown that brown adipocytes arise from precursors that express *Myf5* (myogenic factor 5) and *Pax7* (Paired box 7), two genes known to be expressed in committed skeletal muscle precursors. Both brown adipocytes and myocytes originate from a mesodermal multipotent cell population in the somites (26, 30). There are specific factors that will influence the differentiation of one or the other cell type. For example, PRDM16 (PR domain zinc finger protein 16) is known to promote the differentiation of brown adipocytes and EHMT1 (Euchromatic histone lysine methyltransferase 1), a regulator of PRDM16, is necessary to suppress the expression of factors that are pro-myogenic (31, 32).

The origin of beige adipocytes is not yet fully understood. It is considered that, in contrast to brown adipocytes, beige adipocytes do not derive from the same *Myf5*^{+}-lineage origin. Additionally, *Ebf2* (Early b-cell factor 2) has been identified as marker of a population of cells that can be induced to express UCP1 (33).

On the other, hand, recent evidence suggests that beige adipocytes can be developed directly from the transdifferentiation of white adipocytes under certain external stimuli, such as cold stress or chemical adrenergic stimulation (34). It has been proved that adrenergic stimulation results in browning without affecting adipocyte proliferation or DNA content, suggesting that the new beige adipocytes arise from preexisting white adipocytes (35). Nevertheless, *Wang et al* have labeled mature adipocytes to show that after cold or adrenergic stimulus a large population of beige adipocytes is not emerging from the original white adipocytes (36).

In summary, these studies suggest different mechanisms to explain the origin of beige adipocytes, but further research will be needed to thoroughly determine from where are arising these cells.

4) Networks in rodent brown and beige adipose tissues

Despite the fact that adipocytes are the major cell type of adipose tissue (AT), other cellular compartments are necessary for the tissue to maintain its function, such as the vasculature and the nervous system.

▪ Vasculature of AT

AT is highly vascularized to supply the blood flow essential for developing its own functions. Blood is supplied via arterioles that subdivide into capillaries. BAT is more vascularized than WAT to provide heat and endocrine factors throughout the body and to receive oxygen and oxidative substrates from the blood. Moreover, blood flow is essential not only for adipose tissue function but also for its expansion. The production of new adipocytes is coupled to the generation of new capillaries. Angiogenesis is also associated with the browning of WAT (37).

▪ Innervation of AT

AT is innervated with efferent sensory nerves and afferent sympathetic nerves that communicate with the central nervous system (CNS) (38). The sections that follow describe both types of nerves.

- **Sensory innervation**

Sensory fibers express substance P or calcitonin gene related peptide (CGRP) and their function is not fully understood (38). BAT and WAT sensory nerves report information regarding heat production or lipolysis to key areas of the brain. For example, in WAT the adipokine leptin travels to the brain by sensory nerves to suppress appetite (39).

- **Parasympathetic innervation**

Parasympathetic innervation has been identified by immunohistochemical staining in two depots of BAT, the mediastinal and pericardial BAT depots (40, 41). Nevertheless, no evidence of parasympathetic nervous system (PSNS) has been described for the iBAT depot. Similarly for WAT, neurochemical markers of parasympathetic innervation are absent in this AT (42).

- **Sympathetic innervation**

Neuronal circuits control the functions of brown and beige adipocytes. Sympathetic innervation has been detected in both BAT and WAT. Moreover, several studies have demonstrated that modulations of neuronal activity in the CNS result in regulation of brown/ beige adipocyte thermogenesis (43-45).

Among the parenchymal innervation of BAT, there are thin nerves poorly myelinated that contain the noradrenergic fibers, which express the protein tyrosine hydroxylase (TH) (the rate limiting enzyme for norepinephrine) and co-express the neuropeptide Y (NPY) (38).

In WAT, we can also find sympathetic innervation but to a lower extent (21). The potential of WAT depots to develop browning is proportional to the level of innervation (46).

5) Regulating thermogenic capacity in rodents

There is a complex network between the sympathetic nervous system (SNS), the immune system and autocrine and endocrine factors to regulate the thermogenic capacity of brown and beige adipocytes.

▪ Role of SNS in the control of thermogenesis

The main organ that regulates the response to cold is the CNS. Cold is sensed by the terminals of sensory neurons found in skin, then, these signals are transmitted and integrated in the hypothalamic preoptic area (POA), also known as the thermoregulatory center (47). The transduction of the signal will stimulate other hypothalamic regions, namely the Lateral Hypothalamic Area (LHA), the Ventromedial Hypothalamus (VMH), the Dorsomedial Hypothalamus (DMH) and the Arcuate Nucleus (ARC).

Orexin producing neurons that are located in the LHA, named orexin neurons, participate in the regulation of thermogenesis. The central administration of orexin peptide has been described to stimulate BAT activation and therefore, thermogenesis (48). Moreover, orexin infusion into the VMH can stimulate the sympathetic firing in BAT (49). Both the LHA and the VMH can synergistically interact and activate BAT. Hypothalamic expression of bone morphogenetic protein 8b (BMP8B) in the VMH stimulates orexin secretion in the LHA through a decrease in AMP-activated protein kinase (AMPK) activity, and thus enhances the firing of projections that will stimulate BAT thermogenesis (50). Interestingly, BMP8B can also be produced in BAT and

promote norepinephrine (NE) signaling locally, activating the mitogen-activating protein kinase (MAPK) pathway and lipolysis in brown adipocytes (51).

Several studies have linked the DMH with the response to cold. For instance, a chemical stimulation of this area increases the thermogenic response in rats (52). Similarly, administration of the incretin hormone glucagon-like peptide 1 (GLP-1) in the DMH increases BAT thermogenesis (53). Outflow from these areas is triggered by the premotor neurons found in the brain stem region Raphe Palidus (RPA). It has been broadly discussed that sympathetic nerves are abundant within the parenchyma of adipose tissue. These nerves express tyrosine hydroxylase, the enzyme responsible for the secretion of the catecholamine hormone NE (54). Norephineprine stimulates the β3-adrenergic receptor (ADBR3) and activates the cAMP/PKA pathway, thus triggering lipolysis and increasing the expression of UCP1. Free fatty acids, resulting from the lipolysis, are used both as energy substrates and as activators of UCP1 to uncouple ATP production from mitochondrial respiration into heat (Figure 1-3) (16, 55).

Cold exposure induces sympathetic nerve fiber branching in BAT and scWAT. The main regulators of this process are neurotrophins, molecules that coordinate the growth potential of neurons.

Nerve growth factor (NGF) is a neurotrophin required for sympathetic neuron survival that can be produced by BAT (56). Even though sympathetic innervation is increased in response to cold temperatures, NGF expression is counterintuitively reduced in BAT under these conditions (56, 57).

Brain-derived neurotrophic factor (BDNF) has also been described as a neurotrophin that regulates thermogenesis. Periferal treatment of BDNF, results in increased oxygen consumption, body temperature and UCP1 expression in BAT (58, 59).

On the other hand, semaphorins (SEMA) are a large family of secreted or transmembrane proteins that serves as axonal guidance cues (60). In particular, SEMA3A and SEMA3C act as repulsive signals to cause sympathetic neuron growth cone collapse (61, 62). Another family of secreted or transmembrane proteins involved in

15

axon growth is the neuroregulins (NRG). NRG1, NRG2 and NRG3 promote survival and proliferation of neurons in the development of the brain. NRG4 is expressed in WAT and BAT and it is up-regulated by cold exposure (63, 64). Indeed, the adipokine BMP8B can induce NRG4 secretion to promote sympathetic innervation upon adrenergic stimulation (65).
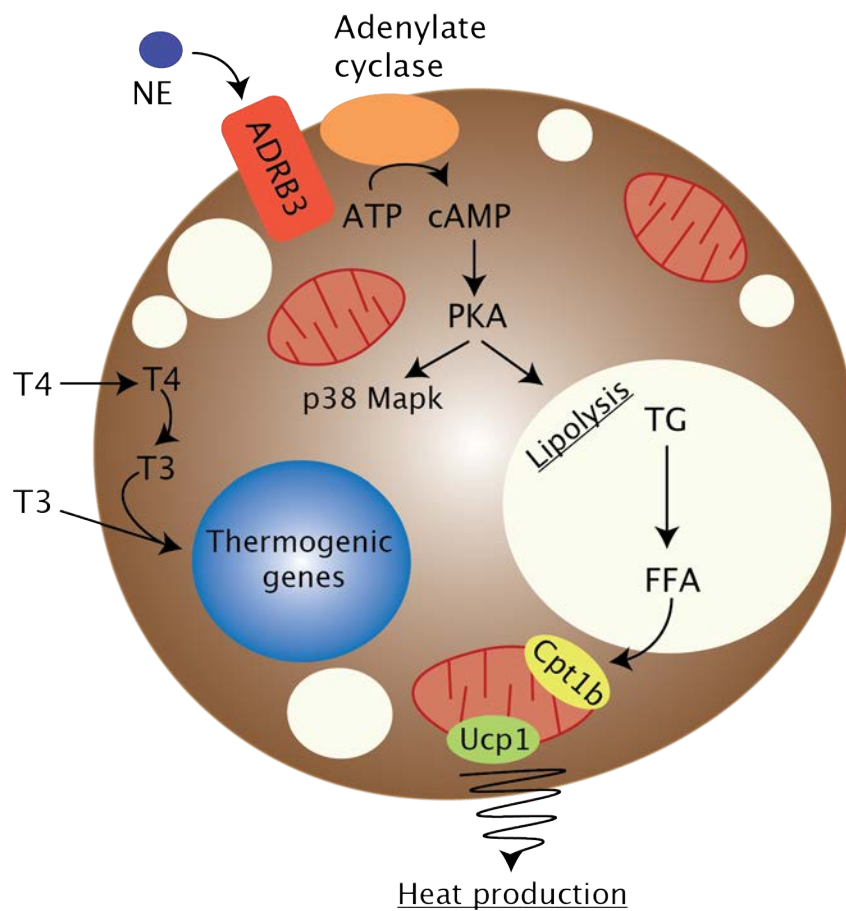
Figure 1-3. PKA pathway in brown adipocyte. The adrenergic stimulation of β3-adrenergic receptor (ADRB3) by norepinephrine (NE) is the main mediator of brown adipocyte functions. This will trigger the enzymatic activity of adenylate cyclase to generate cAMP and stimulate PKA pathway. Therefore, PKA activation will activate the lipolysis of TG to feed the mitochondria with substrates to generate heat by Ucp1-mediated uncoupling. This pathway and the thyroid hormones (T3, T4) will also enhance the expression of thermogenic genes necessary for adipocyte functions.

- **Role of thyroid hormone metabolism in the control of thermogenesis**

Apart from catecholamines, thyroid hormones can also trigger BAT activity (66). The thyroid hormones T3 and T4 are synthetized in the thyroid gland upon hypothalamic stimulation of the pituitary gland, by the thyrotropine-releasing hormone (TRH), and therefore by the production of thyroid-stimulating hormone (TSH) (67). Thyroid hormones access brown adipocytes from the blood stream through specific transporters. In brown adipocytes T4 can be converted to its active form T3 via the type 2 iodothyronine deiodinase (DIO2) thus compensating for the low levels of secreted T3 by the thyroid gland (68). T3 directly activates lipolysis through the PKA pathway. The relevance of thyroid hormone regulation for BAT function is illustrated by the blunted thermogenic response observed in DIO2 knockout mice, despite an increased UCP1 expression (69). Moreover, thyroid hormone status also controls BAT activation. Indeed, hyperthyroid mice have increased BAT activation and upregulation of thermogenic genes (70).

- **Role of the endocrine factors in the control of thermogenesis**

Due to the potential therapeutic effect of increasing overall energy consumption by promoting beige and brown adipose cell metabolism, recent research has focused on the identification of natural hormones or compounds with the capability to promote thermogenic function, such as fibroblast growth factor 21 (FGF21), irisin and bile acids (BAs).

Under cold exposure, FGF21 can be secreted by BAT and WAT and have a paracrine effect to stimulate the expression of thermogenic genes (71). Some groups have reported that FGF21 knockout mice have impaired adaptation to chronic cold exposure and decreased browning of WAT (72). However, others have shown that the lack of FGF21 in long-term cold adaptation does not impair the thermogenic response of mice

(73). Despite the evidence of FGF21 production in WAT, controversial results were published by *Véniant et al* who showed that beneficial effects of weight loss observed after cold were not directly related to FGF21-induced browning (74). However, hepatic FGF21 production can also be induced by cold, and blunted hepatic FGF21 secretion, but not adipocyte-FGF21 secretion, results in impaired cold tolerance and decreased sympathetic nerve activity in BAT (75). Importantly, hepatic FGF21 requires intact expression of the FGF21 receptor β-klotho in adipose tissue for its thermogenic effect, but its expression is increased upon acute cold exposure (6 hours maximum) but decreased after a longer cold exposure (3 days) (75). In conclusion, additional studies are needed to completely elucidate the role of FGF21 in the control of non-shivering thermogenesis.

Besides their role in the digestion of dietary lipids, hepatic BAs can be induced by cold exposure (76). It has been described that BA secretion increases energy expenditure in BAT by enhancing the enzymatic activity of DIO2 and therefore, regulating thyroid hormone metabolism in BAT (77). Moreover, studies using BA receptor TGR5 adipose tissue specific knockout mice proved that BAs also participate in the browning of WAT. These mice show neglectable browning and exhibit reduced cold tolerance due to reduced adipose mitochondrial fusion (78).

Historically, UCP1 has been considered indispensable for thermogenesis in BAT. However, recent research demonstrates that UCP1 is not essential for non-shivering thermogenesis (73, 79, 80). Peptidase M20 domain-containing 1 (PM20D1), a secreted enzyme produced by brown and beige adipocytes, has been recently discovered to contribute to this alternative thermogenesis by participating in the uncoupling of mitochondria in an UCP1-independent manner (79, 80).

▪ **Feeding as an inducer of thermogenesis**

Cold is not the only stimulus that activates non-shivering thermogenesis. It has been demonstrated by several groups that there is a *meal-associated thermogenesis* (81-83). The activation of feeding-responsive thermogenesis has been strongly associated to food intake regulation by inhibiting orexigenic activation in the brain, revealing a Gut-Brain-BAT-Brain axis (84). In particular, feeding activates the secretion of periprandial gut hormones, such as cholecystokinin (CKK), GLP-1 or secretin (85-87). Most of these molecules act through the brain, like GLP-1 and CCK, where they increase sympathetic activation and therefore stimulate the local release of NE in the BAT. Interestingly, secretin can stimulate BAT thermogenesis in a non-sympathetic manner, and contribute to induce satiation. A secretin injection in fasted mice directly activates BAT thermogenesis by increasing lipolysis in this through the cAMP-PKA pathway. Moreover, secretin treatment increases the expression of the anorexigenic proopiomelanocortin (POMC) peptide in the hypothalamus and therefore, reduces food intake (87).

Apart from its role in the regulation of food intake described above, leptin can increase EE by inducing BAT activation. The actions of leptin and insulin in POMC neurons, can also be triggered by a decrease of the hypothalamic levels of T cell-protein tyrosine phosphatase (TCPTP), which is a negative regulator the insulin signaling, to further increase the browning of WAT and EE (44, 88). This mechanism can limit the effects of *diet-induced obesity* (DIO).

▪ **Regulation of thermogenesis by immune cells**

WAT and BAT also include immune cells, like macrophages, eosinophils and innate lymphoid type 2 cells (ILC2s). Interestingly, a role in the control of thermogenesis has been described for macrophages. In fact, cold exposure triggers the polarization of macrophages to M2-like phenotype. M2 macrophages seem to release NE in AT to

contribute to the activation of thermogenesis (89). In the same line, BAT macrophages were also reported to be involved in sympathetic innervation of the tissue (90). Nevertheless, opposite findings were reported by *Fisher et al* claim that deletion of Th (a key gene in the catecholamine synthesis) expression in AT macrophages does not alter energy expenditure in response to cold exposure (91).

III.   Human brown adipose tissue

Although described in the 16th century to be present in small mammals, evidence of an active BAT in adult humans was only found in 2002 by using 2-[^{18}F]-fluoro-2-desoxy-glucose positron emission tomography coupled with computed tomography (^{18}FDG-PET/CT) (92). ^{18}FDG-PET measures the uptake and accumulation of a radioactive analogue of glucose (^{18}FDG). This procedure, normally used to detect tumors, can also identify other tissues that have high rates of glucose uptake and indeed, some scans using this method showed areas of ^{18}FDG uptake around the neck and shoulders with similar characteristics to AT (93).

Moreover, BAT has long been known to be present in newborns (16, 94). BAT is essential for human infants after birth to maintain their core body temperature and defend the ambient colder temperatures. Nevertheless, BAT is known to progressively disappear through adulthood (95).

Evidence suggests that human BAT contains both "brown"-like and "beige"-like adipocytes (96, 97). For example, the BAT of human infants is structurally similar to the one of rodents because it has UCP1-expressing adipocytes separated from the surrounding-white adipocytes (96).

Interestingly, human BAT also responds to external cues and it is thermogenically active under lower ambient temperatures (98). Its potential role in enhancing energy expenditure, glucose clearance and lipid utilization make it a special target for new developing therapeutic strategies.

_____

IV.   Cyclin-dependent kinase 4

1) Cell cycle

Eukaryotic cell cycle is divided into: DNA replication, mitosis and interphase. During DNA replication, all chromosomes are duplicated. Mitosis consists of the separation of daughter chromosomes and ends with cell division (cytokinesis) and during interphase, chromosomes are decondensed and distributed uniformly thorough the nucleus. These cell cycle phases are called M phase, G1 phase and S phase. M phase is mitosis, and it is followed by the G1 phase, which corresponds to the interval between mitosis and initiation of DNA replication in S phase (synthesis). Finally in G2 phase, cell grows and proteins are synthesized in preparation for mitosis (99).

Cell cycle regulators control cell cycle progression to extracellular stimuli. The major components of the cell cycle regulatory machinery are cyclin dependent kinases (CDKs), cyclins, the retinoblastoma family of proteins (RB) and the E2F transcription factors (99).

The activity of these kinases is regulated during the cell cycle and these results in phosphorylations / dephosphorylations of cell cycle regulatory proteins (100).

2) Cyclin-dependent kinases

CDKs are a family of cell-cycle regulators that control the successions of cell cycle. There are over thirteen different genes that code for CDKs. The activity of these proteins is dependent on their dimerization with Cyclins (101, 102). There are four types of Cyclins:

1) G1/S phase cyclins. They activate specific CDKs at the end of G1 phase and their expression is decreased in S phase.
2) S phase cyclins. They bind specific CDKs to stimulate chromosome duplication.
3) M phase cyclins. They activate specific CDKs that stimulate mitosis.
4) G1 phase cyclins. They control the activity of G1/S CDKs.

Moreover, CDKs are formed by a catalytic subunit and an activating cyclin subunit. When a CDK forms a complex with a Cyclin, it becomes active and it is able to phosphorylate several substrates that will allow the progression of the cell cycle (101, 102). CDKs are serine/threonine kinases that can phosphorylate consensus sequences that are [S/T]-Px-[K/R] (where S is serine, T threonine, P proline, K lysine and R argine) (103).

3) The CDK4-pRB-E2F pathway

CDK4 is a serine/threonine kinase that can be activated by D-type cyclins (cyclin D1, D2 or D3). The complex CDK4/D-type cyclin participates in the transition of the G1/S phase of the cell cycle. In animal cells, the key function of the CDK4/6-D-type cyclin complex is to activate a group of transcription factors: the E2F proteins. These proteins bind to the promoter of specific genes encoding for proteins important for DNA synthesis and chromosome duplication.

Under non-proliferative stimuli, E2F is repressed by the members of the RB family of proteins. On the other hand, under proliferative stimuli CDK4 is activated and phosphorylates the protein pRB, releasing the repression of E2F, thus it activates the transcription of different proliferative genes (104).

The hyperactivity of the CDK4-pRB-E2F pathway is associated with the abnormal proliferation of cancer cells (105). In fact, there is a described mutation of CDK4, which renders the protein hyperactive because it cannot be inhibited by the INK4 family of

_____

inhibitors. The mutation happens when the arginine in position 24 is replaced by a cysteine and it is called R24C. Mice homozygous for this mutation naturally develop endocrine and epithelial tumors and also sarcomas (105).

4) The regulation of the complex CDK4/D-type cyclins

To orchestrate the cell cycle process, CDKs receive multiple regulatory signals. Indeed, extracellular growth factors will activate CDKs. The activation of CDK4 depends on a CDK-activating kinase (CAK) that will phosphorylate CDK4 to fully activate it. On the other hand, antiproliferative signals will induce the activity of CDK inhibitors (CKIs). There are two different families of CDK inhibitors: the INK4 including $p16^{INK4A}$, $p15^{INK4B}$, $p18^{INK4C}$ and $p19^{INK4}$ and the CIP-KIP family formed by $p21^{CIP1}$, $p27^{KIP1}$ and $p57^{KIP2}$ (102). The inhibitors from the INK4 family can interfere to repress the CAK activating phosphorylation and also by avoiding the formation of the complex CDK4/D-type cyclin. In contrast, the CIP-KIP inhibitors can be associated to both CDK and cyclins to avoid their interaction (106).
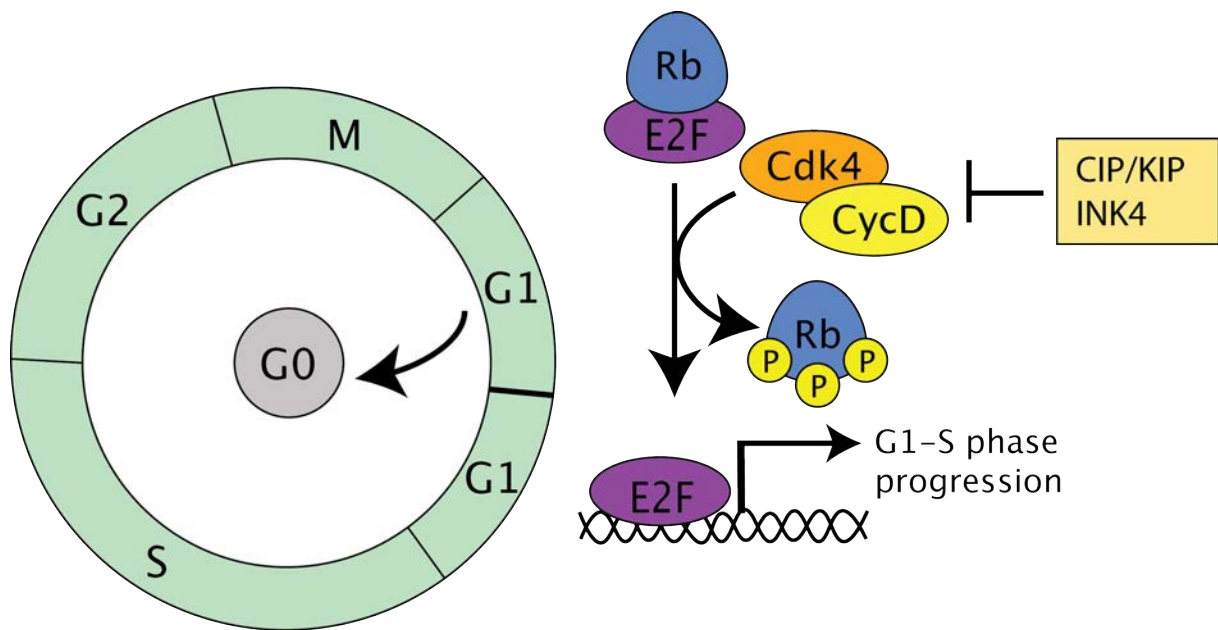
Figure 1-4. CDK4-pRB-E2F pathway in cell cycle. E2F is a transcription factor normally repressed by the members of the retinoblastoma family of proteins (RB). When mitogenic or proliferative stimuli are sensed by the cell, a D-type cyclin is activated to form a complex with the protein cyclin-dependent kinase 4 (CDK4). CDK4 is a kinase that will phosphorylate RB, releasing the repression of E2F, which will therefore; activate the transcription of different proliferative genes needed for the progression of G1-S phase. CDK-inhibitors (CKI) from the CIP/KIP and INK4 families can repress the kinase function of CDK4.

_____

5) CDK4-pRB-E2F pathway in metabolic processes

Metabolic reprogramming is not only a hallmark of normal physiological homeostasis, but also of pathological conditions. Growing evidences exist about the regulatory crosstalk between metabolic pathways, cell cycle progression and cell division. Our laboratory has been focusing for a long time on the function of the CDK4-pRB-E2F pathway in the control of metabolism. We, and others, have clearly demonstrated that these G1 and S-phase cell cycle regulators unequivocally control metabolic processes, to ensure the metabolic reprogramming required for cell cycle, and independently of cell cycle (107-111).

Actually, E2F1 was shown to be a positive regulator of adipogenesis, while E2F4 is a negative regulator of adipocyte differentiation (112). This regulation is orchestrated through the control of the key adipogenic regulator peroxisome proliferator-activated receptor gamma (PPARγ). Similarly, it has been shown that pRB, the pocket protein that represses E2F1 transcriptional activity, plays numerous roles in adipogenesis, as reviewed by *Galderisi et al* (113). Moreover, CDK4 and one of its partners, cyclin D3, can also promote adipocyte differentiation via the direct activation of PPARγ (114, 115).
Cyclin D1 (CCND1) and cyclin D3 (CCND3), two possible partners of CDK4, have independently been revealed to play opposite roles in adipogenesis, since CCND3 has been shown to promote adipogenesis (115), whereas CCND1 inhibits both PPARγ activity and adipogenesis (115). These findings are in agreement with the discovery that the association between CDK4 and CCND2 and CCND3 increases during adipocyte differentiation, whereas the association between CDK4 and CCND1 is limited to the proliferative phase and the clonal expansion of 3T3-L1 adipocytes (116).

Studies using mouse models have further underscored the role of the CDK4-pRB-E2F1 pathway in metabolism, since transgenic animal models for these proteins exhibit marked metabolic phenotypes. For instance, *E2f1* $^{-/-}$ mice and *Ccnd3* $^{-/-}$ mice are resistant to high-fat diet-induced obesity and show increased insulin sensitivity (112,

115, 117). *E2f1* $^{-/-}$ mice also exhibit increased oxidative metabolism in brown adipose tissue (118). *pRb* adipose-specific knockout (119) are protected from diet-induced obesity and exhibit browning of the white adipose tissue, and *pRb* haploinsufficient animals express brown adipocyte-related genes in white adipose tissue (120). Furthermore, like *pRb* deficient animals, mice lacking *p107* are lean and displayed a conversion of WAT into BAT (121). Additionally, mice lacking *p130* showed a marked reduction in subcutaneous fat (122).

The above-mentioned studies highlight the dual role of cell cycle regulators in adipogenesis and mature adipocyte function. On the one hand, the positive cell cycle regulators CDK4, CCND3 and the transcription factors E2F1 promote adipocyte differentiation by promoting PPARγ expression or activity (112, 114, 115). This positive effect on PPARγ can partially explain the protection from diet-induced obesity observed in *E2f1* $^{-/-}$ mice and *Ccnd3* $^{-/-}$ mice (115, 117).

On the other hand, the negative cell cycle regulators of the retinoblastoma family play controversial roles in adipogenesis. The lack of *pRb* inhibits adipogenesis in 3T3 and MEF cells (119, 123), whereas the lack of *p107* and *p130* increases the differentiation potential in 3T3 cells (123). However, pRB can directly repress PPARγ thus the lack of *pRb* promotes adipogenesis in the presence of PPARγ agonists (124). Despite the dual role of retinoblastoma proteins in adipogenesis, *pRb-*, *p107-* and *p130-* deficient mice are also leaner than their control counter parts (119-122). However, the use of the adipose-specific model by *Dali-Youcef et al* allows focusing on the function of pRB in mature adipocytes (119).

The similarities between *pRb-*, *p107-* and *p130*-deficient mice, which are expected to have increased E2F1 activity, and *E2f1* $^{-/-}$ mice underscore the importance of E2F1 both as a transcriptional repressor, when complexed with a pocket protein, and as a transcriptional activator. Moreover, they suggest that there are other factors implicated in the regulation of gene expression by the pocket protein/E2F1 complexes.

In addition, *Cdk4* full knockout (*Cdk4⁻/⁻*) mice are smaller in size compared to the control mice and insulin-deficient diabetic because of a striking decrease in the amount of β-cells (125). The phenotyping of *Cdk4⁻/⁻* mice revealed that CDK4 is involved in the insulin secretion describing a new role of CDK4 in the pancreatic function.

Other roles of CDK4 related to the control of glucose homeostasis have been described. *Lee et al* found that CDK4 shuts down hepatic gluconeogenesis by inhibiting the activity of the transcription factor peroxisome proliferator-activated receptor gamma coactivator 1-alpha (PGC1α) (126).

Finally, *Cdk4 ⁿᶜ/ⁿᶜ* mice, expressing *Cdk4* only in pancreatic beta cells, have decreased fat mass, and exhibit insulin resistance; whereas *Cdk4 R24C/R24C* mice, carrying a point mutation that prevents the interaction between CDK4 and the INK4 family members, have increased fat mass and improved insulin sensitivity in an E2F1-independent manner, via increased phosphorylation of the insulin receptor substrate 2 (IRS2) protein (127). Recombinant adeno-associated virus (AAV) were used to trigger an acute deletion of *Cdk4*, and conclusively prove that the effects of CDK4 in the insulin signaling pathway are due to the modulation of terminally differentiated adipocytes, and not to its role in adipogenesis (127).

Interestingly, CDK4 has also been placed in the center of the control of muscle metabolism to regulate fatty acid oxidation through the modulation of AMPK activity (128).

Cell cycle regulators have been shown to modulate the activity of several metabolic tissues via the regulation of master metabolic regulators like PPARγ, PGC1α and IRS2. The studies described before suggest that there might be other cell cycle independent functions in metabolic tissues remaining to be discovered. These findings place the CDK4-pRB-E2F1 axis as a key sensor of metabolism at the cellular and at the organismal level.

Chapter 2: Aim of the thesis

_____

Chapter 2: Aim of the thesis

As already mentioned in the introduction, BAT research has gained strong relevance on the field of metabolic studies. Indeed, the importance of this fat depot relies on its potential to increase energy expenditure and glucose clearance through its activation. The above-mentioned functions of BAT are seen as novel strategies against obesity and diabetes.

Several novel proteins have been newly identified as participants of the BAT activity regulation. Among them, numerous cell cycle regulators have been attributed to regulate brown fat activity (118, 119, 129, 130). However, no role for CDK4 has been yet described.

The aim of this thesis rests on the following observations from rodent models:

1. CDK4 has a role independent from cell cycle
2. CDK4 is a protein that is highly expressed in BAT
3. CDK4 has been described to regulate metabolic pathways in mature white adipocytes

Overall, the aim of this thesis was to further investigate the role of CDK4 in other metabolic tissues and in particular, in BAT and thermoregulation.

The first objective was to determine whether or not CDK4 plays a role in the regulation of BAT non-shivering thermogenesis. The second objective was to investigate how CDK4 regulates thermoregulation, if it is direct effect in the BAT or not. As this part of the study revealed that the effect was not cell autonomous, the third objective of the thesis was to further study the mechanism by which CDK4 regulates BAT activity.

Chapter 3: Results

_____

Chapter 3: Results

I. CDK4 regulates non-shivering thermogenesis through modulation of thyroid hormone metabolism and sympathetic innervation

The first part of the results is the manuscript of the unpublished article that we have entitled *"CDK4 regulates non-shivering thermogenesis through modulation of thyroid hormone metabolism and sympathetic innervation"* which includes the studies of BAT in *Cdk4* knockout (*Cdk4*$^{-/-}$) and *Cdk4* BAT-specific knockout (*Cdk4* bKO) mice.

_____

CDK4 regulates non-shivering thermogenesis through modulation of thyroid hormone metabolism and sympathetic innervation

Judit Castillo-Armengol[1], Honglei Ji[1], Ilenia Severi[2], Valentin Barquissau[1], Anita Nasrallah[1], Laia Martinez-Carreres[1], Eric Aria Fenandez[1], Catherine Moret[1], Guy Neiderhauser[1], Brigitte Delacuisine[1], Sylviane Lagarrigue[3], Frédéric Preitner[1], Antonio Giordano[2], Isabel C. Lopez-Mejia[1], Lluis Fajas[1*]

[1] Center for Integrative Genomics, University of Lausanne, Lausanne CH-1015, Switzerland

[2] Department of Experimental and Clinical Medicine, Marche Polytechnic University, Via Tronto 10/A, 60020 Ancona, Italy

[3] Department of Physiology, University of Lausanne, Lausanne CH-1005, Switzerland

*Corresponding author:

Prof. Lluis Fajas, Center for Integrative Genomics, University of Lausanne

CH-1015 Lausanne

Phone: +41 21 692 41 11

Email: lluis.fajas@unil.ch

_____

Abstract

Brown adipose tissue (BAT) is a highly specialized tissue that functions to maintain body temperature during cold challenge through non-shivering thermogenesis. Cyclin-dependent kinase 4 (CDK4) has been described as a regulator of oxidative metabolism. However, the role of cell cycle regulators in the development and the function of this oxidative depot has not been thoroughly studied yet. We now aim to determine the role of CDK4 in the function of BAT. Interestingly, *Cdk4* inactivation in vivo led to a marked metabolic phenotype in BAT, pointing towards a participation of CDK4 in non-shivering thermogenesis. BAT from *Cdk4$^{-/-}$* mice are smaller, and exhibit a decreased number of lipid droplets. Moreover, mitochondrial number and the expression of canonical thermogenic genes are increased in the BAT of these mice, which renders them more resistant to cold exposure. Nevertheless, these effects are not cell-auntonomous because BAT-specific deletion of *Cdk4* does not alter the regulation of thermogenesis. Importantly, deiodinase 2 (*Dio2*) and Thyroid hormone receptor beta (*Thrβ*) expression is increased in the BAT of *Cdk4$^{-/-}$* mice, suggesting that there might be an increased intracellular thyroid hormone signaling. Interestingly, BAT sympathetic innervation is also increased in these mice indicating that a higher level of BAT activation by the sympathetic nervous system. Overall, our findings suggest that CDK4 has a major role in brown adipose tissue biology and in temperature regulation through thyroid hormone metabolism and sympathetic innervation.

_____

Introduction

Energy balance is controlled by food intake and energy expenditure. A dysregulation in this equation might produce excess in white adipose tissue (WAT) mass and therefore, obesity (1). Cardiovascular diseases and diabetes are pathologies, which are highly associated with obesity, a worldwide growing problem (2).

WAT is an organ dedicated to lipid storage in the form of triglycerides (TG) to provide fuel to other organs when needed (3, 4). In the last years, special attention has been placed into brown adipose tissue (BAT) because of its ability to increase energy expenditure and glucose clearance (5-7). Although described in the 16th century to be present in small mammals, evidence of an active BAT in humans came in 2002 (8). BAT is a highly specialized organ dedicated to thermogenesis aiming to maintain body temperature in cold stress (9). It is formed by brown adipocytes that contain numerous lipid droplets and a high number of mitochondria, in which is present the uncoupling protein 1 (UCP1). UCP1 uncouples ATP production from mitochondrial respiration into heat (9, 10).

Cold exposure is sensed by motor neurons found in the skin that send sensory information to the central nervous system (CNS) (11). In the hypothalamus there are several nuclei known to be involved in the thermogenic response (11-15). In particular, the sympathetic nervous system directly innervates BAT to control heat production (16-18). Thyroxine hydroxylase-expressing nervous fibers (TH-fibers) in BAT will locally secrete norepinephrine, the principal inductor of BAT activity (18). Norepinephrine stimulates β-adrenergic receptors in brown adipocytes to increase intracellular cAMP levels by adenylyl cyclase and activate the PKA pathway to increase lipid mobilization and thermogenesis (19). Moreover, sympathetic innervation also affects mitochondrial number and activity (20-22).

Other neuro-endocrine pathways had been described to regulate BAT thermogenesis. The Hypothalamic-Pituitary-Thyroid (HPT) axis is one of them, which controls the

_____

production of thyroid hormones by the thyroid gland (23, 24). Thyroid hormones (T3, T4) are known to stimulate energy expenditure and heat production (25). Type II iodothyronine deiodinase 2 (*Dio2*) is the key enzyme to generate T3, the active form of the thyroid hormones, from T4. Numerous studies have studied the role of TH in BAT (26-28). Indeed, there is evidence that T3 signaling induces *Ucp1* and thermogenic gene expression by binding to nuclear thyroid hormone receptor (THR) (29).

CDK4 is a cell-cycle regulator that participates in the G1/S transition phase of the cell cycle. Growth factors or mitotic stimuli activate this kinase by promoting its interaction to its regulatory proteins, D-type cyclins. Once active, CDK4 is able to phosphorylate the retinoblastoma protein (pRB) to release the repression of the E2F protein. E2F will thus bind to the promoter of specific genes encoding for proteins important for DNA synthesis and chromosome duplication (30).

Apart from that, growing evidences exist about the role of CDK4 in adaptive metabolic responses (31-33). Indeed, our lab reported that CDK4 is a mediator of insulin signaling in mature adipocytes (31) and the treatment with a chemical inhibitor of CDK4/6 proteins, protects against diet induced obesity and decreases fat mass through increasing lipid utilization (34). Because of the role of CDK4 in the regulation of oxidative metabolism (33), we want to explore the function of CDK4 in the BAT biology.

In the present study, we focused on the study of CDK4 in BAT function by investigating the thermogenic phenotype of the already described *Cdk4* knockout mice (*Cdk4*[nc/nc], mentioned in this manuscript as *Cdk4*^{-/-}) (31) and of a new model of *Cdk4* BAT-specific knockout mice (*Cdk4*-bKO). BAT thermogenesis was increased in the *Cdk4*^{-/-}, and this was accompanied by a global increase in energy expenditure. Nevertheless, *Cdk4*-bKO mice did not show any metabolic phenotype related to BAT, suggesting that CDK4 has no cell-autonomous effect of in mature brown adipocytes. Furthermore, we demonstrated that sympathetic innervation and thyroid hormone metabolism were highly increased in BAT of *Cdk4*^{-/-}, which could explain its higher activation. Collectively, our results indicate

_____

that CDK4 reduces BAT thermogenesis through the regulation of TH metabolism and sympathetic innervation.

Results

Cdk4 knockout mice are smaller and have increased energy expenditure

Cdk4 knockout mice (_Cdk4-/-_) were used to explore the role of CDK4 in brown adipose tissue metabolism. As described before by our lab, _Cdk4-/-_ mice are smaller in size (Supplemental figure 1 A-B) and present decreased fat mass (data not shown) (31). Despite their smaller size and leaner phenotype, these mice have a 20% increase in food intake, when corrected by body weight (Supplemental figure 1 C-D). Moreover, _Cdk4-/-_ mice showed and important increased oxygen consumption and energy expenditure (calculated as EE=((RERx1.232)+3.815)xVO2)/1000) in the dark and light phases, when compared to wild-type mice (Supplemental figure 1 E-F).

Increased adaptation to cold in _Cdk4_ knockout mice

The contribution of BAT in increasing whole-body energy expenditure has been broadly studied. We therefore hypothesized that the increased energy expenditure observed in the _Cdk4-/-_ could be explained by increased BAT activation. BAT is functional mainly under cold exposure where it plays a role in maintaining body temperature. To explore the activation of this tissue, we exposed _Cdk4-/-_ mice to 6°C to and measured oxygen consumption and respiratory exchange ratio (RER) by indirect calorimetry. Cold exposure increases oxygen consumption and decreases RER in the control animals (Figure 1, A-B). Interestingly, the differences between control and knockout mice were even bigger at 6°C, where _Cdk4-/-_ have higher levels of oxygen consumption and a bigger switch towards lipid utilization shown by the measurements of RER. These data strongly suggested that _Cdk4-/-_ mice could have developed a system to adapt to cold exposure. To test this hypothesis, we exposed the animals to cold and followed their body temperature for 6 hours. Even if their basal body temperature was just slightly

_____

increased compared to their control littermates (Figure 1C), *Cdk4*$^{-/-}$ mice maintained a higher body temperature during the 6 hours of cold exposure (Figure 1D). These results suggest that deletion of CDK4 promotes thermogenic capacity.

The interscapular brown fat depot of *Cdk4* knockout mice was smaller and darker, suggesting an increased activation of the tissue (Figure 2A-B). By analyzing the morphology of this tissue by hematoxylin eosin staining, we observed a decreased lipid droplet size in the knockout mice (Figure 2C), suggesting an increased activation of the tissue. The most iconic BAT protein is the uncoupling protein 1 (UCP1), which is involved in the uncoupling of protons to generate heat. *Cdk4*$^{-/-}$ mice presented an increased amount of this protein at room temperature conditions, demonstrated by immunohistochemical analysis (Figure 2C) and western blot (Figure 2D). Moreover, gene expression analysis of BAT revealed a high up-regulation of thermogenic and brown markers in the *Cdk4*$^{-/-}$ mice; where especially *Ucp1* and *Bmp8b* were highly increased (Figure 2E). These results suggest that there is a marked pro-thermogenic phenotype in the *Cdk4* deficient mice.

Specific deletion of *Cdk4* in BAT does not affect thermogenic capacity

To determine the tissue-specificity of the phenotype found in the *Cdk4*$^{-/-}$ mice and to further explore the cell-autonomous role of Cdk4 in BAT, we generated BAT specific knockout mice by crossing *Cdk4*$^{flox/flox}$ mice with Ucp1-Cre transgenic mice, which express Cre recombinase specifically in brown adipocytes, generating *Cdk4*$^{flox/flox}$ Ucp1-Cre mice (*Cdk4*-bKO). As shown in Supplemental Figure 2 A, *Cdk4*-bKO had decreased expression of CDK4 in BAT but not in subcutaneous white adipose tissue (scWAT) or perigonadal WAT (pgWAT). No differences in size, body weight or fat mass were observed in these mice compared to their control littermates (Supplemental figure 2B, C, D).

For assessment of thermogenesis, *Cdk4*-bKO and control mice were exposed to cold for 6 hours. No differences in basal body temperature (Figure 3A) or response to cold

_____

exposure were observed (Figure 3B). Interscapular BAT mass from *Cdk4*-bKO mice was similar to the one of the controls (Figure 3C, D) and hematoxylin eosin analysis revealed no apparent difference in the lipid content or the morphology of the tissue between the two genotypes (Figure 3E). Likewise, western blot analysis of UCP1 (Figure 3F) or thermogenic and brown gene expression levels (Figure 3G) was indistinguisable between both models.

Altogether, these results demonstrate that there is not autonomous effect of CDK4 in the thermogenic function of brown adipocytes. Therefore, we focused on exploring what is the organ crosstalk and upstream regulation of the BAT in the Cdk4$^{-/-}$ mice.

Cdk4 knockout mice have enhanced intracellular thyroid hormone signaling

BAT activity can be regulated by different mechanisms, among them, the endocrine system and the sympathetic innervation. Thyroid hormones regulate BAT metabolism and thermogenesis. First, we analyzed the morphology of the thyroid gland. Histological analysis of this tissue by hematoxylin eosin staining did not show any apparent difference between both genotypes (Supplemental Figure 3A). Similarly, analysis of the most abundant thyroid hormone, T4, levels in serum did not show differences between both genotypes (Supplemental Figure 3B).

As T4 is more aboundantly synthetized than its active form T3, there is a special enzyme in charge of its conversion to T3. This enzyme is the deiodinase 2 (DIO2). The higher expression of *Dio2* found in the BAT of the *Cdk4*$^{-/-}$ mice (Supplemental Figure 3C), led us to suspect that thyroid hormones might play a role in the regulation of increased thermogenesis in the *Cdk4* knockout mice. We therefore determined the expression levels of the thyroid hormone receptors in BAT and found that *Thrβ* expression was increased in the *Cdk4*$^{-/-}$ mice suggesting that there might be an increased intracellular thyroid hormone metabolism in the BAT of *Cdk4*$^{-/-}$ mice.

_____

Increased sympathetic innervation in BAT and browning of scWAT in *Cdk4* knockout mice

It is well established that, BAT-dependent thermogenesis is controlled by sympathetic innervation. TH-positive fibers are found within BAT and are responsible of the local production of norepinephrine to stimulate the tissue. Therefore, we hypothesized that an increase in sympathetic innervation could explain the phenotype of *Cdk4*$^{-/-}$ mice. For this reason, we explored innervation of BAT in *Cdk4*$^{-/-}$ mice by immunohistochemical analysis of TH-fibers in tissue sections. Mice deficient in Cdk4 presented higher levels of TH-expressing fibers than the wild-type mice (Figure 4A-B). In addition to its role in regulating BAT activity, sympathetic innervation can also stimulate the browning of WAT. As we saw an increased activation of BAT in *Cdk4*$^{-/-}$ mice, we suspected that morphological differences towards thermogenesis would also be found in the WAT of these mice. Accordingly, *Cdk4*$^{-/-}$ mice also presented browning of scWAT at room temperature conditions as showed by hematoxylin eosin staining and thermogenic or brown gene expression (Supplemental Figure 4A-B).

As thermogenic activation of brown adipocytes mainly involve beta 3 adrenergic receptor (ADRB3), we treated the mice with a specific ADRB3 antagonist (SR59230A) and we analyzed their response to cold after the treatment. *Cdk4*$^{+/+}$ mice treated with the antagonist (SR) were more sensitive to cold test than the vehicle-treated group (NaCl). Nevertheless, to our surprise, knockout mice treated with SR, did not decrease their body temperature and exhibited the same cold resistance than the *Cdk4*$^{-/-}$ with NaCl (Figure 4C-D). To understand this paradox, we analyzed the expression of p-CREB Ser133 as a measurement of the activation of the PKA pathway by western blot. This experiment showed that under SR treatment where β3-adrenergic signaling is blocked, *Cdk4*$^{-/-}$ mice have increased activation of the PKA pathway in BAT, suggesting that there is a higher thermogenic activity of this tissue despite the inhibition of the ADRB3 by the antagonist (Figure 4E).

_____

***Cdk4* deletion favors mitochondrial biogenesis and activity**

Since mitochondria are crucial organelles for heat production, we decided to determine the role of Cdk4 in brown adipose tissue mitochondrial number and function. We first assessed mitochondrial number by transmission electron microscopy (TEM). This analysis showed that there was 40% more of mitochondrial volume in the BAT of *Cdk4$^{-/-}$* mice (Figure 5A-B). Next, we determined the oxidative capacity of this tissue by respirometry analysis using the Oroboros system. Coupled respiration through complex I (CI) or complex 1 + 2 (CI+CII) and maximal electron transport system capacity was strongly increased in the BAT homogenates from the knockout mice (Figure 5C). Nevertheless, isolated mitochondria showed equal amounts of proteins from the complexes of the electron transport chain in both wild-type and knockout models (Figure 2D). Taken together these results suggest that *Cdk4$^{-/-}$* mice have a bigger thermogenic response due to an increased mitochondrial number, which therefore increased the efficiency of the tissue to uncouple and generate heat.

Discussion

The study of BAT thermogenesis has gained great attention in the past years. BAT activation increases energy expenditure and helps to maintain glucose homeostasis (5, 7, 35, 36). These traits make this organ a tissue of interest to be studied in detail to design targeted therapies against obesity and diabetes (37-39).

The cell-cycle regulator CDK4 is known to be involved in adipose tissue metabolism, in processes such as adipogenesis and insulin signaling in mature white adipocytes (31, 32). Moreover, CDK4 activity has also been associated to the regulation of oxidative metabolism (33). Here, we provide evidences that CDK4 impairs non-shivering thermogenesis by modulating intra-adipocyte thyroid hormone metabolism and sympathetic innervation.

_____

First we showed that *Cdk4* knockout mice have increased energy expenditure and oxygen consumption, especially under cold exposure where there is also an increased metabolic switch towards lipids utilization. These data suggested a role of CDK4 in thermoadaptation.

Moreover, *Cdk4*$^{-/-}$ mice showed an increased cold tolerance accompanied by an enhanced expression of *Ucp1* and other thermogenic genes in BAT. Nevertheless, experiments with *Cdk4*-bKO mice proved that CDK4 does not have cell autonomous effects in BAT. Therefore, we hypothesized that the increased thermogenic capacity of the *Cdk4* knockout mice was due to the regulation by other organs. While investigating this we found that thyroid hormone metabolism in BAT was highly relevant in these mice, represented by the enhanced expression of *Dio2* and *Thrβ*. These results suggested an enhanced intracellular thyroid hormone metabolism that could explain a greater activation of the PKA-pathway and in turn, of heat production.

This study has also illustrated that Cdk4 deficiency leads to increased mitochondrial number in BAT. Several studies have associated that thyroid hormones play a role in the regulation of mitochondrial biogenesis (39-42). As shown by our results, *Cdk4* knockout mice might have increased thyroid hormones signaling in BAT and this could explain the higher amount of mitochondria found in the BAT of these mice by electron microscopy analysis.

On the other hand, the increased presence of TH-positive fibers in the BAT of *Cdk4*$^{-/-}$ mice, a measurement of sympathetic innervation, suggested that CDK4 acts at the level of sympathetic nervous system to repress sympathetic innervation in adipose tissue.

The modulation of adrenergic stimulation of brown adipocytes is mediated by β3-adrenergic receptor. However, blocking this receptor by a selective β3-antagonist did not prevent the enhanced cold-tolerance of *Cdk4*$^{-/-}$ mice. The mechanisms of thermogenesis from *Cdk4*$^{-/-}$ could include compensating pathways, such as other adrenergic receptors, such as β1-adrenergic receptor that has been described to

_____

compensate the lack of β3-adrenergic receptor *in vivo* (43). Moreover, PKA-activation can be triggered by other molecules, such as thyroid hormones (44). Therefore, lack of β3-adrenergic mediating effects in *Cdk4$^{-/-}$* could be compensated by increased intracellular thyroid hormone signaling. Further investigation would be required to determine the mechanisms driving the heat production of *Cdk4$^{-/-}$* mice under these conditions.

Other cell-cycle regulators had been associated to the regulation of obesity and the metabolic adaptation (45, 46). *Cdk6* deficient mice present recruitment of beige adipocytes in WAT demonstrating that CDK6 impairs the transition of white to beige adipocytes (46). Besides this, CDK4 has recently gained attention as a possible target against obesity. In addition to its previously reported effects in modulating fat mass (34), here we are describing that *Cdk4$^{-/-}$* mice present multilocular adipocytes in the subcutaneous WAT, highlighting the relevance of CDK4 as a regulator of adrenergic activation and therefore, of WAT remodeling.

It is worth noting that we also found that Cdk4 regulates the expression of *Bmp8b*, a key protein involved not only in browning of WAT but also in BAT differentiation and function (47, 48). Increased *Bmp8b* levels in adipose tissue are associated to increased thermogenesis and increased innervation (48). This could explain the enhanced parenchymal innervation of BAT in the *Cdk4$^{-/-}$* mice.

Although this study does not describe the specific region where CDK4 is controlling sympathetic innervation, it would be interesting to define the central impact of CDK4 in *Cdk4$^{-/-}$* mice. To accomplish this goal, Nkx2.1-Cre transgenic mice could be use to delete Cdk4 in multiple hypothalamic cellular subtypes (49, 50).

In summary, we have shown that *Cdk4* deletion contributes to BAT activation and function. CDK4 is an upstream regulator of neuro-remodeling for thermogenic demands.

_____

Thus, targeting CDK4 represents an alternative mechanism to control the coordination of adipocyte thermogenic activity and its neuroregulation.

Materials and Methods

Animals. The generation of $Cdk4^{-/-}$ ($Cdk4^{nc/nc}$) mice has been previously described (28). $Cdk4^{flox/flox}$ and Ucp1-Cre mice on a C57BL6/J background were intercrossed to generate the experimental cohorts (Cdk4-bKO). Animals were maintained in a temperature-controlled animal facility with a 12-hour light/12-hour dark cycle and had access to food and water according to Swiss Animal Protection Ordinance (OPAn). Only male animals were used in this study. Body composition (fat and lean mass) was measured using EchoMRI. Oxygen consumption and Respiratory Exchange ratio (RER) were measured with Oxymax apparatus (Columbus Instruments) and normalized by body weight. Energy expenditure was calculated as the following formula: EE=((RERx1.232)+3.815)xVO2)/1000 as previously described in (51). Acute cold test was carried out on animals individually housed at 4°C for 6h and rectal temperature was measured every hour using a thermal probe (Bioseb Lab Instruments). Animals were sacrificed by cervical dislocation and tissues were collected, a piece was taken for histological analysis and the rest, directly snap-frozen in liquid nitrogen. All animal care and treatment procedures were performed in accordance with Swiss guidelines and were approved by the Canton of Vaud SCAV (authorization VD 3121.h).

β3-Antagonist experiment

For the β3-antagonist experiment, SR-59230A (S8688, Sigma) was injected i.p. at 3mg/kg/day during 7 days. Acute cold test was performed on the day 5. The day before sacrifice, mice were injected with β3-agonist CL-316243 (1mg/kg, ab144605, Abcam) or vehicle (NaCl).

_____

Measurement of respirometry.

BAT was freshly homogenized after dissection to assess respirometry using high-resolution respirometry (Oroboros Oxygraph-2k, Oroboros Instruments, Innsbruck, Australia). Homogenization was performed by mechanical permeabilization in MiR05 medium (0.5mM EGTA, 3mM $MgCl_2$, 60mM Lactobionic acid, 20mM Taurine, 10mM KH_2PO_4, 20mM HEPES, 110mM D-Sucrose, 1g/l BSA, pH 7.1) and the equivalent of 2mg of tissue was added to the experimental chamber. Malate (2mM), Pyruvate (10mM) and Glutamate (20mM) were added to the chamber in the absence of ADP to measure oxygen flux (also called "Leak" in the figure). Complex-I-dependent respiration ("CI", in the figure) was measured after adding ADP (5mM). After, succinate (10mM) was added to analyze electron flow through both complex I and II ("CI+CII", in the figure). This was followed by addition of carbonylcyanide-4-(trifluoromethoxy)-phenyl-hydrazone (FCCP) to obtain maximum flux through the electron transfer system ("ETS," in the figure). Finally, oxidative phosphorylation was fully inhibited by addition of rotenone (0.1μM) and antimycin A (2.5μM), respectively ("ETS (CII)", in the figure). The remaining O_2 flux resulting from the inhibition with Antimycin A (ETS independent flux) was substracted from the values of each of the previous measurements. O_2 flux values are expressed as relative to leak respiration.

Histology. Hematoxylin-eosin staining was performed in 4μM formalin-fixed paraffin-embedded tissue sections. Immunohisotchemical analyses of UCP1 and TH expression were performed using the antibodies anti-UCP1 (ab10983, Abcam) and anti-TH (AB1542, Merck Millipore). TH expression was analysed by counting TH-positive fibers per a total of 100 adipocytes.

Mitochondria and lipid droplet quantification. Mitochondria and lipid droplet surfaces were quantified using electromicrographs from BAT of $Cdk4^{-/-}$ and $Cdk4^{+/+}$ mice. In brief, samples were fixed, embedded and cut in ultra-thin sections. Four micrographs were taken and assembled to form a final image that was analyzed using

the program IMOD. Mitochondrial volume was obtained using the point-counting technique with a superimposed grid of 500 × 500 nm.

RNA extraction, RT-PCR. Adipose tissues were powdered manually and thyroid gland and hypothalamus were homogenized using the Precelly's system with tubes with beads. RNA was isolated with Tri-Reagent (T9424, Sigma-Aldrich). For BAT, 500μL of Tri-Reagent were used to lyse the tissue powder. After centrifugation to remove debris, 100μL of Chrloroform were used for phase separation. Aqueous fase was recovered and precipitated with Isopropanol and after centrifugation; RNA pellets were washed with 500μL of 75% ethanol. Pellets were resuspended in 200μL of MiliQ water. A second step of 1:1 Chloroform was used to obtain better-purified RNA. Aqueous fase was recovered and incubated O/N at -20°C with 70μL of ammonium acetate (NH_4AC) and 600μL of absolute ethanol. Then, precipitation of RNA pellets was done by centrifugation. Pellets were washed with 75% ethanol followed by centrifugation and resuspended in MiliQ water. For thyroid gland, RNA was extracted according to the manufacturer's protocol. RNA concentrations were determined using Nanodrop and reversed transcribed using 1000ng of RNA and Superscript II enzyme (18064014, Invitrogen). qPCR analysis were performed using SYBR green detection (04913914001, Roche) on a 7900HT Fast Real-Time PCR System (Applied Biosystems). Relative mRNA expression was calculated from the comparative threshold cycle (Ct) values of the gene of interest relative to RS9 mRNA. Specific primer sequences are listed in Table S1.

Protein extraction and western blot analysis. Proteins were lysed using mammalian protein extraction reagent (MPER, Pierce) and analysed by gel electrophoresis and using the antibodies anti-UCP1 (ab10983, Abcam), anti-CDK4 (C-22, sc-260, SantaCruz), anti-p-CREB Ser133 (87G3, 9198S, Cell Signaling Technology) and anti-CREB total (48H2, 9197S, Cell Signaling Technology).

Mitochondria isolation and mitoproteins analysis. Mitochondria were isolated from BAT from $Cdk4^{-/-}$ and $Cdk4^{+/+}$ mice were homogenized in 2ml cold isolation buffer

_____

(10mM Tris, 200mM sucrose, 1mM EGTA/Tris). Tissue homogenization was obtained at 1500rpm after 20 strikes. The homogenized extract was centrifuged at 600g for 10 min at 4°C in order to remove cellular debris. This step was performed two times. The mitochondrial fraction was pelleted at 10 000g for 10min at 4°C and subsequently washed using the isolation buffer. The mitochondrial pellet was resuspended in isolation buffer to assess protein quantification. Expression of mitochondrial proteins was analyzed by western blot and using the antibodies anti-NDUFAB9 for Complex I (20C11B11B11, ab14713, Abcam), anti-SDHA for Complex II (2^E3GC12FB2AE2, ab14715), anti-UQCRC1 for Complex III (16D10AD9AH5, ab110252), anti-COXIV for Complex IV (20E8C12, ab14744), anti-ATP5A for Complex IV (15H4C4, ab14748), anti-UCP1 (ab10983, Abcam) and anti-TOMM20 used as loading control (EPR15581-54, ab186735, Abcam).

Statistical analysis. Data are presented as mean ±s.e.m. Statistical analyses were carried out with unpaired Student's t-tests. Differences were considered statistically significant at *p-value<0.05, **p-value<0.01, ***p-value<0.001.

_____

References

1.   Hill JO, Wyatt HR, Peters JC. Energy balance and obesity. Circulation. 2012 Jul 3;126(1):126-32. PubMed PMID: 22753534. Pubmed Central PMCID: 3401553.

2.   Bell CG, Walley AJ, Froguel P. The genetics of human obesity. Nature reviews Genetics. 2005 Mar;6(3):221-34. PubMed PMID: 15703762.

3.   Sethi JK, Vidal-Puig AJ. Thematic review series: adipocyte biology. Adipose tissue function and plasticity orcheastrate nutritional adaptation. Journal of lipid research. 2007 Jun;48(6):1253-62. PubMed PMID:17374880. PubMed Central PMCID: 4303760.

4.   Scherer PE. Adipose tissue: from lipid storage compartment to endocrine organ. Diabetes. 2006 Jun;55(6):1537-45. PubMed PMID: 16731815.

5.   Lowell BB, V SS, Hamann A, Lawitts JA, Himms-Hagen J, Boyer BB, et al. Development of obesity in transgenic mice after genetic ablation of brown adipose tissue. Nature. 1993 Dec 23-30;366(6457):740-2. PubMed PMID: 8264795.

6.   Harper JA, Dickinson K, Brand MD. Mitochondrial uncoupling as a target for drug development for the treatment of obesity. Obesity reviews: an official journal of the International Association for the Study of Obesity. 2001 Nov;2(4):255-65. PubMed PMID: 12119996.

7.   Cannon B, Nedergaard J. Thermogenesis challenges the adipostat hypothesis for body-weight control. The Proceedings of the Nutrition Society. 2009 Nov;68(4):401-7. PubMed PMID: 19775494.

8.   Nedergaard J, Bengtsson T, Cannon B. Unexpected evidence for active brown adipose tissue in adult humans. American journal of physiology Endocrinology and metabolism. 2007 Aug;293(2):E444-52. PubMed PMID: 17473055.

9.   Cannon B, Nedergaard J. Brown adipose tissue: function and physiological significance. Physiological reviews. 2004 Jan;84(1):277-359. PubMed PMID: 14715917.

10.   Fedorenko A, Lishko PV, Kirichok Y. Mechanism of fatty-acid-dependent UCP1 uncoupling in brown fat mitochondria. Cell. 2012 Oct 12;151(2):400-13. PubMed PMID: 23063128. Pubmed Central PMCID: 3782081.

_____

11.   Morrison SF, Madden CJ, Tupone D. Central control of brown adipose tissue thermogenesis. Frontiers in endocrinology. 2012 Jan 24;3(5). PubMed PMID: 22389645. Pubmed Central PMCID: 3292175.

12.   Oldfield BJ, Giles ME, Watson A, Anderson C, Colvill LM, McKinley MJ. The neurochemical characterisation of hypothalamic pathways projecting polysynaptically to brown adipose tissue in the rat. Neuroscience. 2002;110(3):515-26. PubMed PMID: 11906790.

13.   Lee SJ, Sanchez-Watts G, Krieger JP, Pignalosa A, Norell PN, Cortella A, et al. Loss of dorsomedial hypothalamic GLP-1 signaling reduces BAT thermogenesis and increases adiposity. Molecular metabolism. 2018 May;11:33-46. PubMed PMID: 29650350. Pubmed Central PMCID: 6001878.

14.   Monda M, Viggiano AN, Viggiano A, Viggiano E, Lanza A, De Luca V. Hyperthermic reactions induced by orexin A: role of the ventromedial hypothalamus. The European journal of neuroscience. 2005 Sep;22(5):1169-75. PubMed PMID: 16176359.

15.   Martins L, Seoane-Collazo P, Contreras C, Gonzalez-Garcia I, Martinez-Sanchez N, Gonzalez F, et al. A Functional Link between AMPK and Orexin Mediates the Effect of BMP8B on Energy Balance. Cell reports. 2016 Aug 23;16(8):2231-42. PubMed PMID: 27524625. Pubmed Central PMCID: 4999418.

16.   De Matteis R, Ricquier D, Cinti S. TH-, NPY-, SP-, and CGRP-immunoreactive nerves in interscapular brown adipose tissue of adult rats acclimated at different temperatures: an immunohistochemical study. Journal of neurocytology. 1998 Dec;27(12):877-86. PubMed PMID: 10659680.

17.   Murano I, Barbatelli G, Giordano A, Cinti S. Noradrenergic parenchymal nerve fiber branching after cold acclimatisation correlates with brown adipocyte density in mouse adipose organ. Journal of anatomy. 2009 Jan;214(1):171-8. PubMed PMID: 19018882. Pubmed Central PMCID: 2667925.

18.   Bartness TJ, Vaughan CH, Song CK. Sympathetic and sensory innervation of brown adipose tissue. International journal of obesity. 2010 Oct;34 Suppl 1:S36-42. PubMed PMID: 20935665. Pubmed Central PMCID: 3999344.

19.   Collins S, Surwit RS. The beta-adrenergic receptors and the control of adipose tissue metabolism and thermogenesis. Recent progress in hormone research. 2001;56:309-28. PubMed PMID: 11237219.

20.   Klingenspor M, Ivemeyer M, Wiesinger H, Haas K, Heldmaier G, Wiesner RJ. Biogenesis of thermogenic mitochondria in brown adipose tissue of Djungarian hamsters during cold adaptation. The Biochemical journal. 1996 Jun 1;316 (Pt 2):607-13. PubMed PMID: 8687407. Pubmed Central PMCID: 1217391.

21.   Puigserver P, Wu Z, Park CW, Graves R, Wright M, Spiegelman BM. A cold-inducible coactivator of nuclear receptors linked to adaptive thermogenesis. Cell. 1998 Mar 20;92(6):829-39. PubMed PMID: 9529258.

22.   Sanchez-Alavez M, Conti B, Wood MR, Bortell N, Bustamante E, Saez E, et al. ROS and Sympathetically Mediated Mitochondria Activation in Brown Adipose Tissue Contribute to Methamphetamine-Induced Hyperthermia. Frontiers in endocrinology. 2013;4:44. PubMed PMID: 23630518. Pubmed Central PMCID: 3632801.

23.   Bianco AC, Silva JE. Intracellular conversion of thyroxine to triiodothyronine is required for the optimal thermogenic function of brown adipose tissue. The Journal of clinical investigation. 1987 Jan;79(1):295-300. PubMed PMID: 3793928. Pubmed Central PMCID: 424048.

24.   Bianco AC, Silva JE. Optimal response of key enzymes and uncoupling protein to cold in BAT depends on local T3 generation. The American journal of physiology. 1987 Sep;253(3 Pt 1):E255-63. PubMed PMID: 3631256.

25.   Vaitkus JA, Farrar JS, Celi FS. Thyroid Hormone Mediated Modulation of Energy Expenditure. International journal of molecular sciences. 2015 Jul 16;16(7):16158-75. PubMed PMID: 26193258. Pubmed Central PMCID: 4519944.

26.   Broeders EP, Vijgen GH, Havekes B, Bouvy ND, Mottaghy FM, Kars M, et al. Thyroid Hormone Activates Brown Adipose Tissue and Increases Non-Shivering Thermogenesis--A Cohort Study in a Group of Thyroid Carcinoma Patients. PloS one. 2016;11(1):e0145049. PubMed PMID: 26784028. Pubmed Central PMCID: 4718641.

27.   de Jesus LA, Carvalho SD, Ribeiro MO, Schneider M, Kim SW, Harney JW, et al. The type 2 iodothyronine deiodinase is essential for adaptive thermogenesis in brown

_____

adipose tissue. The Journal of clinical investigation. 2001 Nov;108(9):1379-85. PubMed PMID: 11696583. Pubmed Central PMCID: 209445.

28.   Endo T, Kobayashi T. Thyroid-stimulating hormone receptor in brown adipose tissue is involved in the regulation of thermogenesis. American journal of physiology Endocrinology and metabolism. 2008 Aug;295(2):E514-8. PubMed PMID: 18559984.

29.   Martinez de Mena R, Scanlan TS, Obregon MJ. The T3 receptor beta1 isoform regulates UCP1 and D2 deiodinase in rat brown adipocytes. Endocrinology. 2010 Oct;151(10):5074-83. PubMed PMID: 20719854.

30.   Malumbres M. Cyclin-dependent kinases. Genome biology. 2014;15(6):122. PubMed PMID: 25180339. Pubmed Central PMCID: 4097832.

31.   Lagarrigue S, Lopez-Mejia IC, Denechaud PD, Escote X, Castillo-Armengol J, Jimenez V, et al. CDK4 is an essential insulin effector in adipocytes. The Journal of clinical investigation. 2016 Jan;126(1):335-48. PubMed PMID: 26657864. Pubmed Central PMCID: 4701556.

32.   Abella A, Dubus P, Malumbres M, Rane SG, Kiyokawa H, Sicard A, et al. Cdk4 promotes adipogenesis through PPARgamma activation. Cell metabolism. 2005 Oct;2(4):239-49. PubMed PMID: 16213226.

33.   Lopez-Mejia IC, Lagarrigue S, Giralt A, Martinez-Carreres L, Zanou N, Denechaud PD, et al. CDK4 Phosphorylates AMPKalpha2 to Inhibit Its Activity and Repress Fatty Acid Oxidation. Molecular cell. 2017 Oct 19;68(2):336-49 e6. PubMed PMID: 29053957.

34.   Iqbal NJ, Lu Z, Liu SM, Schwartz GJ, Chua S, Jr., Zhu L. Cyclin-dependent kinase 4 is a preclinical target for diet-induced obesity. JCI insight. 2018 Sep 6;3(17). PubMed PMID: 30185666. Pubmed Central PMCID: 6171799.

35.   Stanford KI, Middelbeek RJ, Townsend KL, An D, Nygaard EB, Hitchcox KM, et al. Brown adipose tissue regulates glucose homeostasis and insulin sensitivity. The Journal of clinical investigation. 2013 Jan;123(1):215-23. PubMed PMID: 23221344. Pubmed Central PMCID: 3533266.

36.   Chondronikola M, Volpi E, Borsheim E, Porter C, Annamalai P, Enerback S, et al. Brown adipose tissue improves whole-body glucose homeostasis and insulin sensitivity

_____

in humans. Diabetes. 2014 Dec;63(12):4089-99. PubMed PMID: 25056438. Pubmed Central PMCID: 4238005.

37.   Cypess AM, Kahn CR. Brown fat as a therapy for obesity and diabetes. Current opinion in endocrinology, diabetes, and obesity. 2010 Apr;17(2):143-9. PubMed PMID: 20160646. Pubmed Central PMCID: 3593105.

38.   Soler-Vazquez MC, Mera P, Zagmutt S, Serra D, Herrero L. New approaches targeting brown adipose tissue transplantation as a therapy in obesity. Biochemical pharmacology. 2018 Sep;155:346-55. PubMed PMID: 30030977.

39.   Trayhurn P. Recruiting Brown Adipose Tissue in Human Obesity. Diabetes. 2016 May;65(5):1158-60. PubMed PMID: 27208185.

40.   Carmona MC, Iglesias R, Obregon MJ, Darlington GJ, Villarroya F, Giralt M. Mitochondrial biogenesis and thyroid status maturation in brown fat require CCAAT/enhancer-binding protein alpha. The Journal of biological chemistry. 2002 Jun 14;277(24):21489-98. PubMed PMID: 11940593.

41.   Wulf A, Harneit A, Kroger M, Kebenko M, Wetzel MG, Weitzel JM. T3-mediated expression of PGC-1alpha via a far upstream located thyroid hormone response element. Molecular and cellular endocrinology. 2008 Jun 11;287(1-2):90-5. PubMed PMID: 18336995.

42.   Weitzel JM, Iwen KA, Seitz HJ. Regulation of mitochondrial biogenesis by thyroid hormone. Experimental physiology. 2003 Jan;88(1):121-8. PubMed PMID: 12552316.

43.   Susulic VS, Frederich RC, Lawitts J, Tozzo E, Kahn BB, Harper ME, et al. Targeted disruption of the beta 3-adrenergic receptor gene. The Journal of biological chemistry. 1995 Dec 8;270(49):29483-92. PubMed PMID: 7493988.

44   Obregon MJ. Adipose tissues and thyroid hormones. Frontiers in physiology. 2014;5:479. PubMed PMID: 25566082. Pubmed Central PMCID: 4263094.

45.   Petrov PD, Ribot J, Palou A, Bonet ML. Improved metabolic regulation is associated with retinoblastoma protein gene haploinsufficiency in mice. American journal of physiology Endocrinology and metabolism. 2015 Jan 15;308(2):E172-83. PubMed PMID: 25406261.

_____

46.   Hou X, Zhang Y, Li W, Hu AJ, Luo C, Zhou W, et al. CDK6 inhibits white to beige fat transition by suppressing RUNX1. Nature communications. 2018 Mar 9;9(1):1023. PubMed PMID: 29523786. Pubmed Central PMCID: 5845007.

47.   Whittle AJ, Carobbio S, Martins L, Slawik M, Hondares E, Vazquez MJ, et al. BMP8B increases brown adipose tissue thermogenesis through both central and peripheral actions. Cell. 2012 May 11;149(4):871-85. PubMed PMID: 22579288. Pubmed Central PMCID: 3383997.

48.   Pellegrinelli V, Peirce VJ, Howard L, Virtue S, Turei D, Senzacqua M, et al. Adipocyte-secreted BMP8b mediates adrenergic-induced remodeling of the neuro-vascular network in adipose tissue. Nature communications. 2018 Nov 26;9(1):4974. PubMed PMID: 30478315. Pubmed Central PMCID: 6255810.

49.   Xu Q, Tam M, Anderson SA. Fate mapping Nkx2.1-lineage cells in the mouse telencephalon. The Journal of comparative neurology. 2008 Jan 1;506(1):16-29. PubMed PMID: 17990269.

50.   Ring LE, Zeltser LM. Disruption of hypothalamic leptin signaling in mice leads to early-onset obesity, but physiological adaptations in mature animals stabilize adiposity levels. The Journal of clinical investigation. 2010 Aug;120(8):2931-41. PubMed PMID: 20592471. Pubmed Central PMCID: 2912188.

51.   Nie Y, Gavin TP, Kuang S. Measurement of Resting Energy Metabolism in Mice Using Oxymax Open Circuit Indirect Calorimeter. Bio-protocol. 2015;5(18). PubMed PMID: 26878029. Pubmed Central PMCID: 4751037

_____

Supplemental Table 1. List of oligonucleotide sequences used for RT-PCR analysis

Gene	Forward primer	Reverse primer
Adrb3	CACCGCTCAACAGGTTTGATG	TCTTGGGGCAACCAGTCAAG
Bmp8b	TCCACCAACCACGCCACTAT	CAGTAGGCACACAGCACACCT
Cdk4	GCCTGTGTCTATGGTCTG	AAGCAGGGGATCTTACGC
Cidea	TGCTCTTCTGTATCGCCCAGT	GCCGTGTTAAGGAATCTGCTG
Cpt1b	CCGGAAAGGTATGGCCACTT	GAAGAAAATGCCTGTCGCCC
Dio2	CAAACAGGTTAAACTGGGTGAAGA	GTCAAGAAGGTGGCATTCGG
Pgc1α	CCGATCACCATATTCCAGGTC	GTGTGCGGTGTCTGTAGTGG
Prdm16	CAGCACGGTGAAGCCATTC	GCGTGCATCCGCTTGTG
RS9	CGGCCCGGGAGCTGTTGACG	CTGCTTGCGGACCCTAATGTGACG
Thrα	ATGACACGGAAGTGGCTCTG	ACTCTGCACTTCTCTCTCCTTC
Thrβ	AACCAGTGCCAGGAATGTCG	CTCTTCTCACGGTTCTCCTC
Ucp1	CACCTTCCCGCTGGACACTGC	TTGCCAGGGTGGTGATGGTCC

_____

Figure legends

Figure 1. Increased whole body oxygen consumption, lipid utilization and resistance to cold exposure. Indirect calorimetry was performed using the monitoring system Columbus Instruments in 10w-old *Cdk4*$^{+/+}$ (n=6) and *Cdk4*$^{-/-}$ (n=5) mice. **A.** Whole-body oxygen consumption rate (VO$_2$) and **B.** respiratory exchange ratio (RER) were measured at 24°C and at 6°C. **C.** Basal rectal temperature was measured at 24°C and **D.** Rectal temperature was monitored during acute cold exposure at 4°C during 6h in 10w-old *Cdk4*$^{+/+}$ (n=10) and *Cdk4*$^{-/-}$ (n=8) mice. All data are shown as mean +/- SEM. *P<0.05; **<0.01, ***<0.001.

Figure 2. *Cdk4* deficiency promotes BAT-thermogenic response. 14w-old *Cdk4*$^{+/+}$ (n=6) and *Cdk4*$^{-/-}$ (n=6) mice were fed with Chow diet and sacrificed after O/N fasting at RT. **A.** General morphology of BAT **B.** Interscapular BAT weight compared to body weight **C.** Hematoxylin and eosin staining and UCP1 immunohistochemical staining of BAT sections. **D.** Brown gene expression in BAT. **E.** UCP1 and CDK4 protein expression were analyzed by western blot in *Cdk4*$^{+/+}$ (n=4) and *Cdk4*$^{-/-}$ (n=4) mice. Ponceau was used as loading control. All data are shown as mean +/- SEM. *P<0.05; **<0.01; ***<0.001.

Figure 3. Specific *Cdk4* deletion in BAT does not affect thermogenic characteristics. **A.** Rectal temperature was measured at 24°C and **B.** Rectal temperature was monitored during acute cold exposure at 4°C during 6h in 10w-old *Cdk4*$^{flox/flox}$ (*Cdk4-WT*) (n=9) and *Cdk4*$^{flox/flox}$ *Ucp1-Cre* (*Cdk4 –bKO*) mice (n=9). 14w-old Cdk4$^{flox/flox}$ (*Cdk4-WT*) (n=6) and *Cdk4*$^{flox/flox}$ *Ucp1-Cre* (*Cdk4 –bKO*) (n=6) mice were fed with Chow diet and sacrificed after O/N fasting at RT. **C.** General morphology of BAT **D.** Interscapular BAT weight compared to body weight E. Hematoxylin and eosin staining and UCP1 immunohistochemical staining of BAT sections. **F.** Brown gene expression in BAT. **G.** UCP1 and CDK4 protein expression were analyzed by western blot in *Cdk4*$^{flox/flox}$ (*Cdk4-*

_____

WT) (n=4) and *Cdk4^flox/flox^ Ucp1-Cre* (*Cdk4 –bKO*) (n=4) mice. Ponceau was used as loading control. All data are shown as mean +/- SEM. *P<0.05; **<0.005.All data are shown as mean +/- SEM. *P<0.05; **<0.005.

Figure 4. Innervation is increased in BAT of *Cdk4* knockout mice. 14w-old *Cdk4^+/+^* (n=6) and *Cdk4^-/-^* (n=6) mice were fed with Chow diet and sacrificed after O/N fasting at RT. **A.** TH immunohistochemical staining in BAT sections and **B.** quantification. **C.** Acute cold test after 5 days of β3-adrenergic antagonist (SR) (12w-old, *Cdk4^+/+^* (n=8) and *Cdk4^-/-^* (n=8)) or vehicle (NaCl) (*Cdk4^+/+^* (n=5) and *Cdk4^-/-^* (n=5)) treatment and **D.** quantification of area under the curve (AUC) **E.** p-CREB S133 and CREB protein expression in BAT of *Cdk4^+/+^* (n=3) and *Cdk4^-/-^* (n=3) mice treated with β3-adrenergic antagonist (SR). All data are shown as mean +/- SEM. *P<0.05; **<0.01.

Figure 5. *Cdk4* deficiency promotes mitochondrial biogenesis and activity in BAT. 14w-old *Cdk4^+/+^* and *Cdk4^-/-^* mice were fed with Chow diet and sacrificed after O/N fasting at RT. **A.** Transmission electron microscopy (TEM) of BAT **B.** and quantification of lipid droplets (LD) and mitochondria (Mito) (*Cdk4^+/+^* (n=4) and *Cdk4^-/-^* (n=4)) **C.** Protein levels of proteins from mitochondrial electron transport chain complexes in isolated mitochondria (*Cdk4^+/+^* (n=2) and *Cdk4^-/-^* (n=2)). **D.** Respirometry analysis of BAT measured by Oroboros (*Cdk4^+/+^* (n=6) and *Cdk4^-/-^* (n=6)). All data are shown as mean +/- SEM. *P<0.05; **<0.01; ***<0.001.

_____

Supplemental Figure legends

Supplemental Figure 1. *Cdk4* knockout mice are smaller, have increased food intake and energy expenditure at RT. **A.** Whole body image and **B.** Body weight of *Cdk4$^{+/+}$* (n=5) and *Cdk4$^{-/-}$* (n=6) mice. Food intake was measured using the Phenomaster system. **C, D.** Daily cummulative food intake of 14w-old *Cdk4$^{+/+}$* (n=7) and *Cdk4$^{-/-}$* (n=8) mice. Indirect calorimetry was performed using the monitoring system Columbus Instruments in 10w-old *Cdk4$^{+/+}$* (n=6) and *Cdk4$^{-/-}$* (n=6) mice. **E.** Whole-body oxygen consumption rate (VO$_2$) and **F.** Energy expenditure were measured at 24°C. All data are shown as mean +/- SEM. *P<0.05; **<0.01, ***<0.001

Supplemental Figure 2. *Cdk4* BAT specific knockout mice have normal body composition. **A.** Western blot for CDK4 and Tubulin in BAT, scWAT and pgWAT of *Cdk4$^{flox/flox}$* (*Cdk4-WT*) (n=3) and *Cdk4$^{flox/flox}$ Ucp1-Cre* (*Cdk4 –bKO*) (n=3) mice. **B.** Whole body image, **C.** Body weight and **D.** Body composition (fat and lean mass) of 14w-old *Cdk4$^{flox/flox}$* (*Cdk4-WT*) (n=8) and *Cdk4$^{flox/flox}$ Ucp1-Cre* (*Cdk4 –bKO*) (n=8) mice. All data are shown as mean +/- SEM. *P<0.05; **<0.01, ***<0.001

Supplemental figure 3. *Cdk4* knockout mice have enhanced intracellular thyroid hormone signaling. *Cdk4$^{+/+}$* and *Cdk4$^{-/-}$* mice were fed with Chow diet and sacrificed at RT. **A.** H&E staining of thyroid gland **B.** T4 levels in serum (14w-old, *Cdk4$^{+/+}$* (n=14) and *Cdk4$^{-/-}$* (n=10)) **C.** Gene expression of *Dio2* in BAT (14w-old, *Cdk4$^{+/+}$* (n=6) and *Cdk4$^{-/-}$* (n=6)). **D.** Gene expression of thyroid receptors in BAT (14w-old, *Cdk4$^{+/+}$* (n=6) and *Cdk4$^{-/-}$* (n=6)). All data are shown as mean +/- SEM. *P<0.05.

Supplemental figure 4. *Cdk4* deficiency promotes browning of subcutaneous WAT. 27w-old *Cdk4$^{+/+}$* (n=5) and *Cdk4$^{-/-}$* (n=6) mice were fed with Chow diet and sacrificed after O/N fasting at RT. **A.** Hematoxylin and eosin staining in scWAT. **B.** Brown gene expression in scWAT. All data are shown as mean +/- SEM. *P<0.05; **<0.01; ***<0.001.

Figure 1

Castillo-Armengol, J. et al

_____
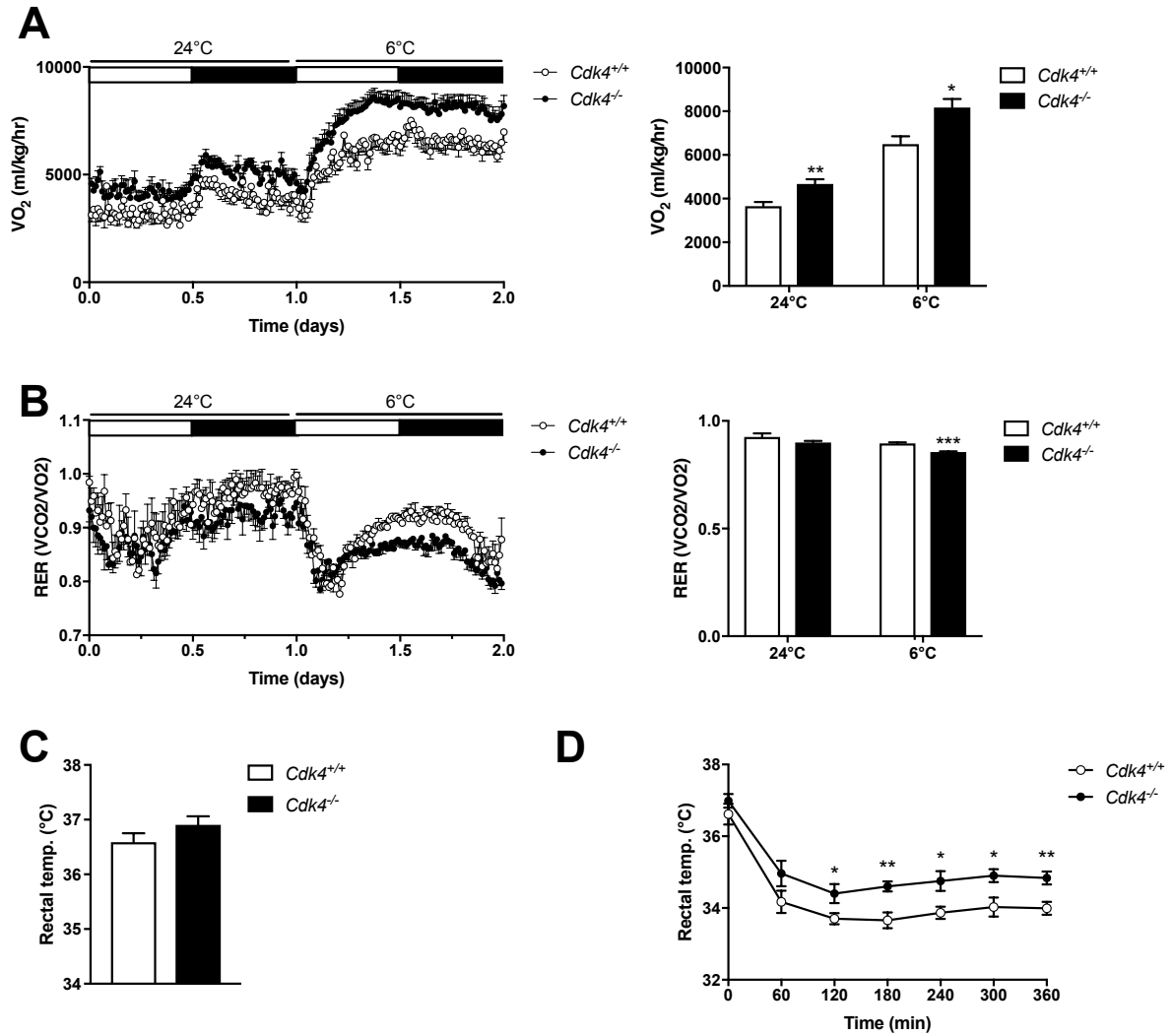
Figure 2

Castillo-Armengol, J. et al

_____
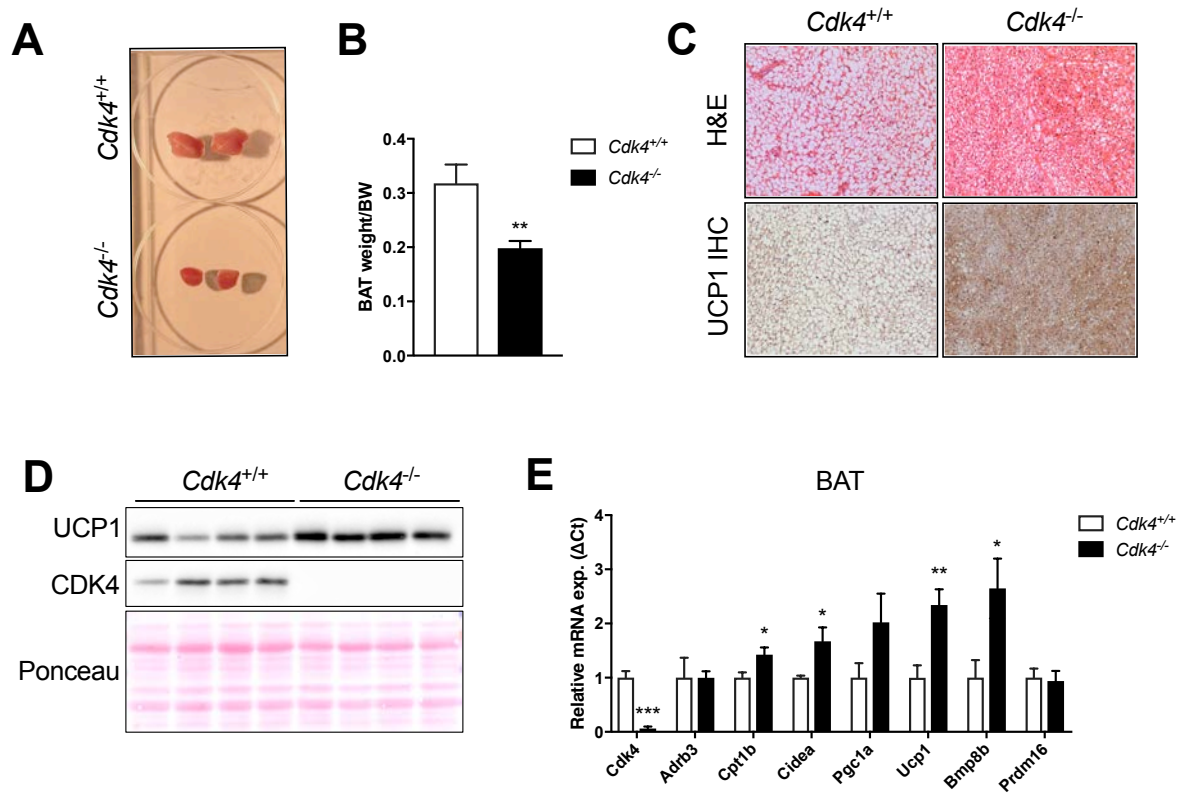
Figure 3

Castillo-Armengol, J. et al
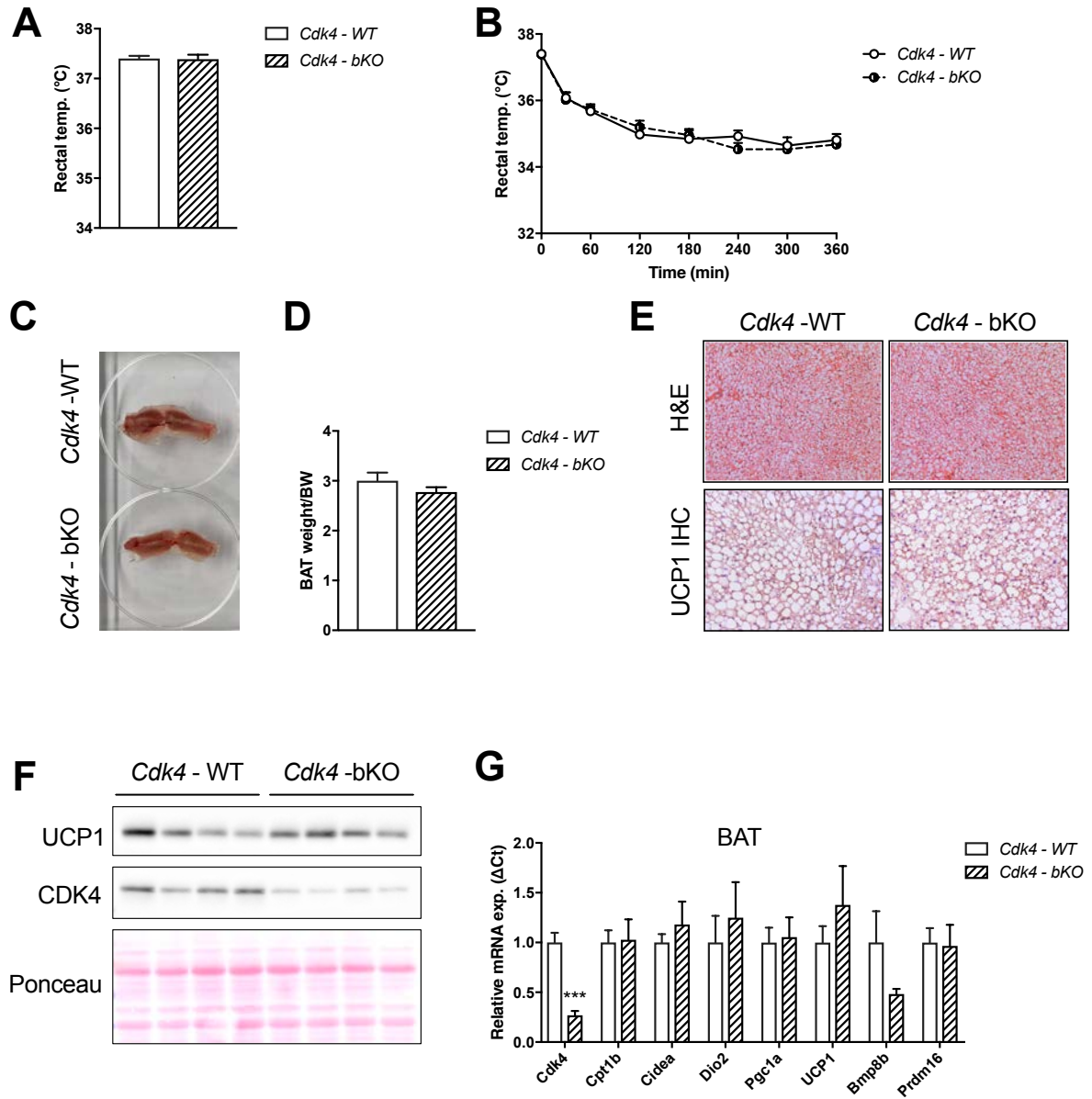
Figure 4

Castillo-Armengol, J. et al

_____
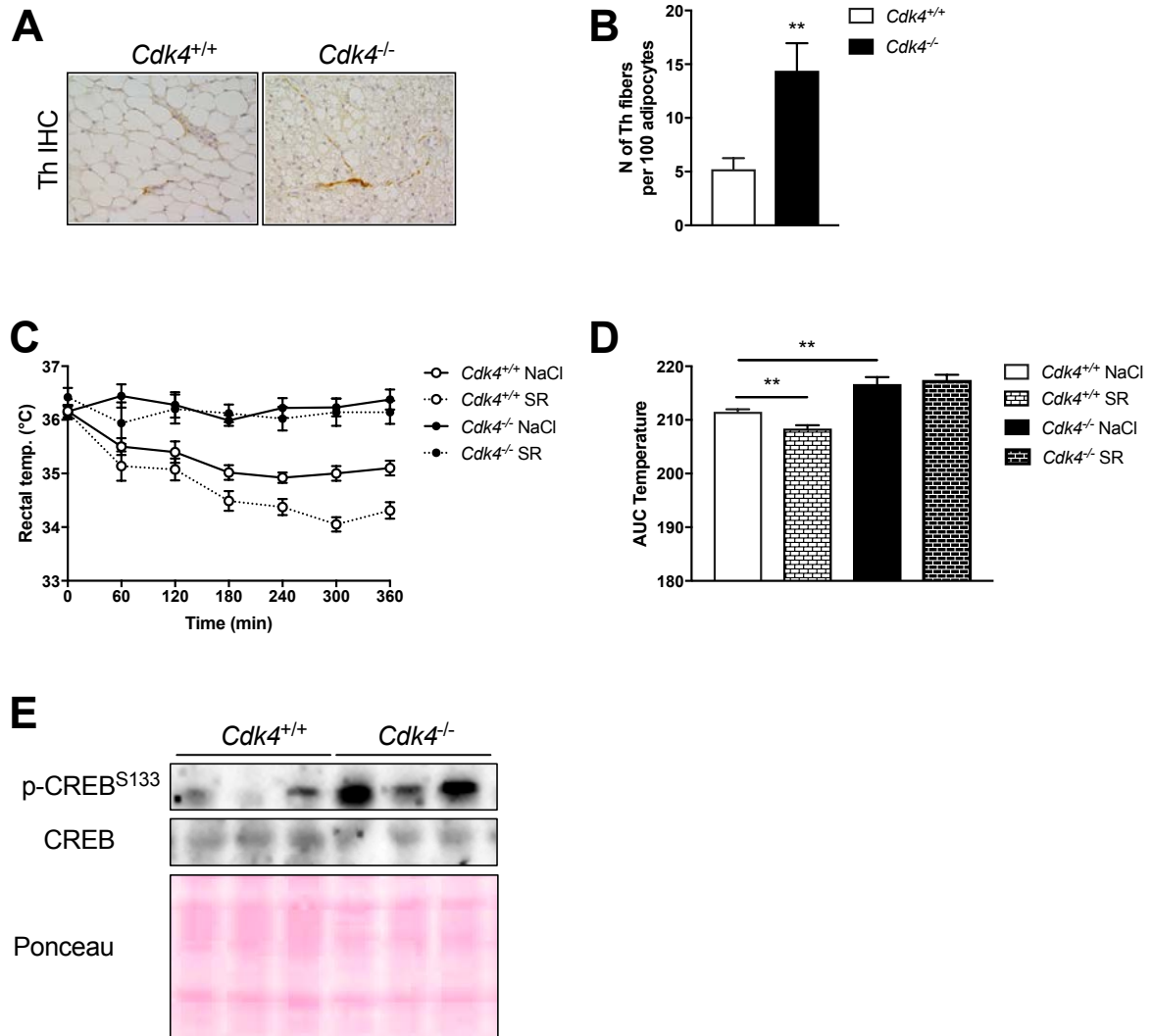
Figure 5

Castillo-Armengol, J. et al

A

B

C

D

_____
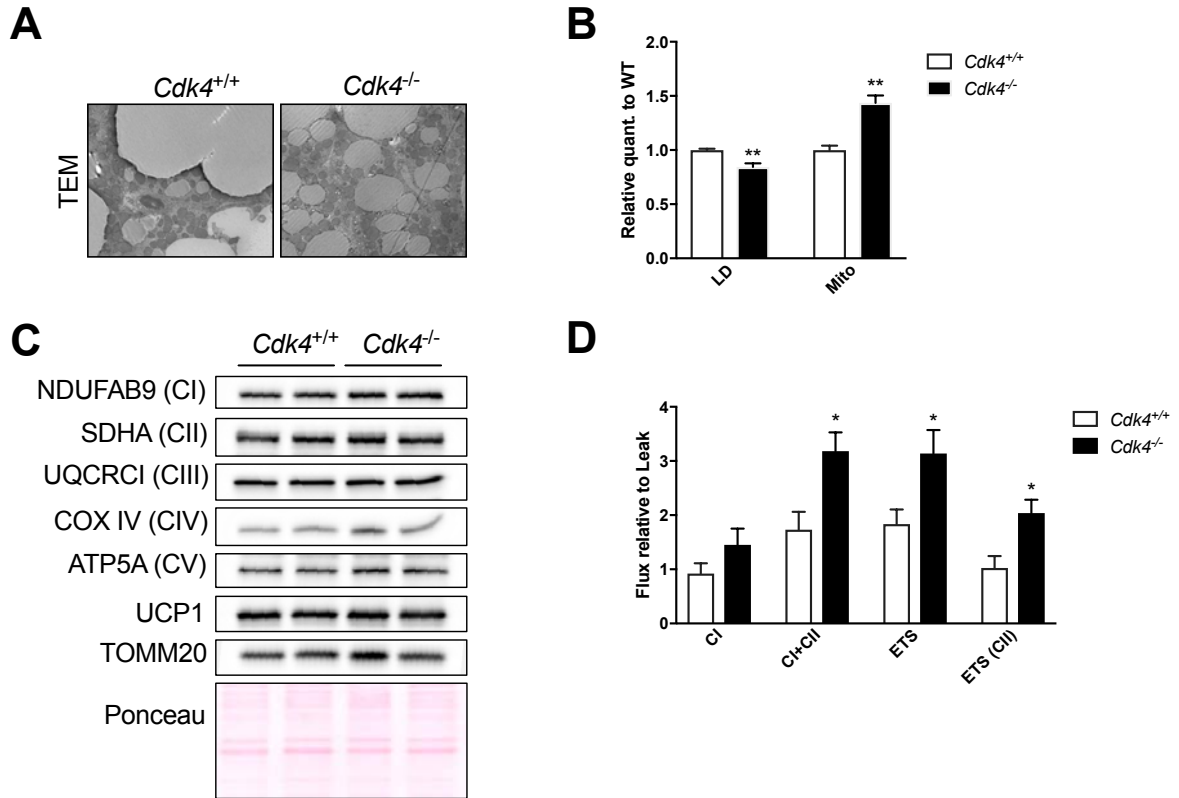
Supplemental Figure 1

Castillo-Armengol, J. et al

A $Cdk4^{+/+}$ $Cdk4^{-/-}$

B

C

D

E

F

_____
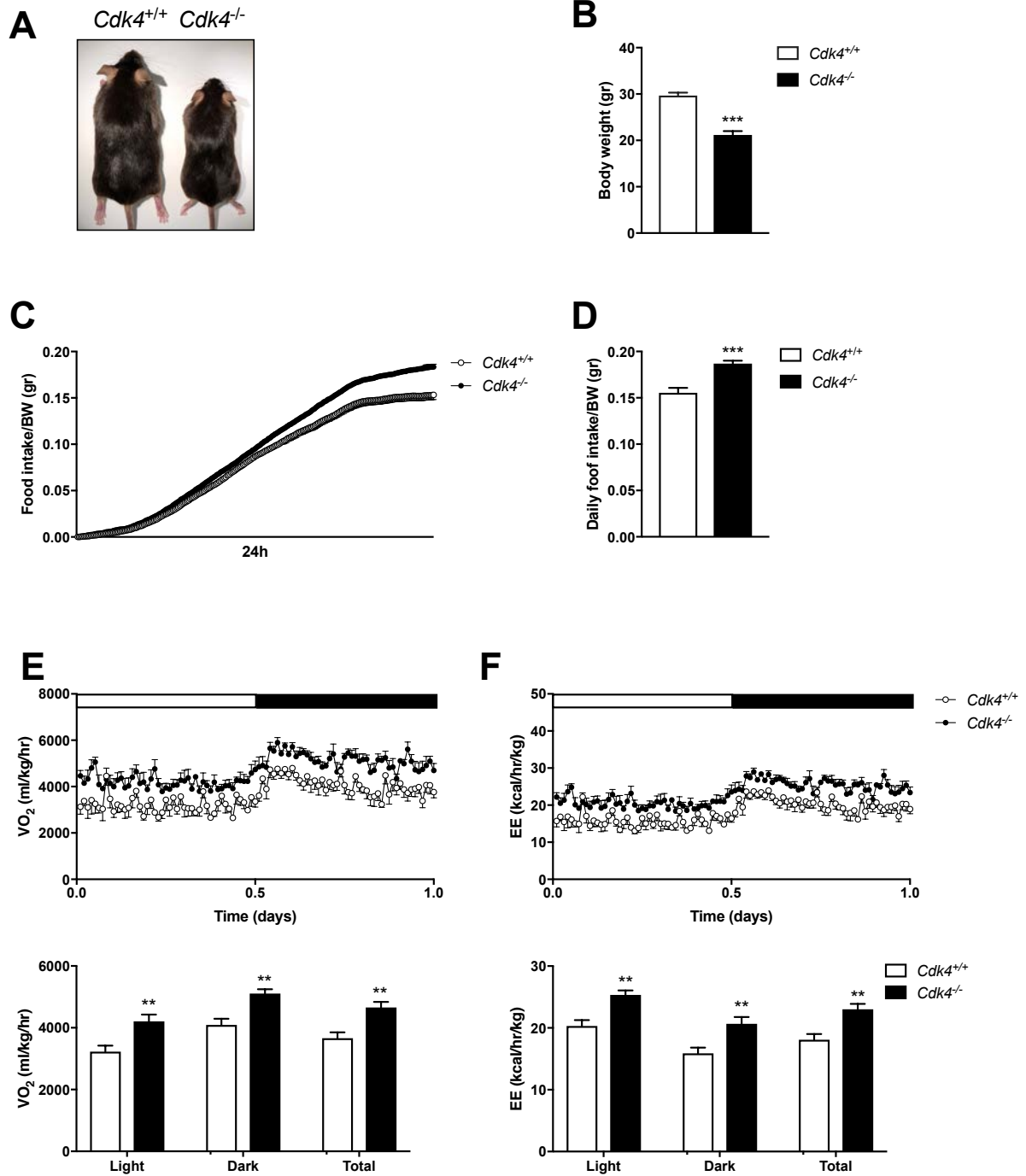
Supplemental Figure 2

Castillo-Armengol, J. et al

A

B

C

D
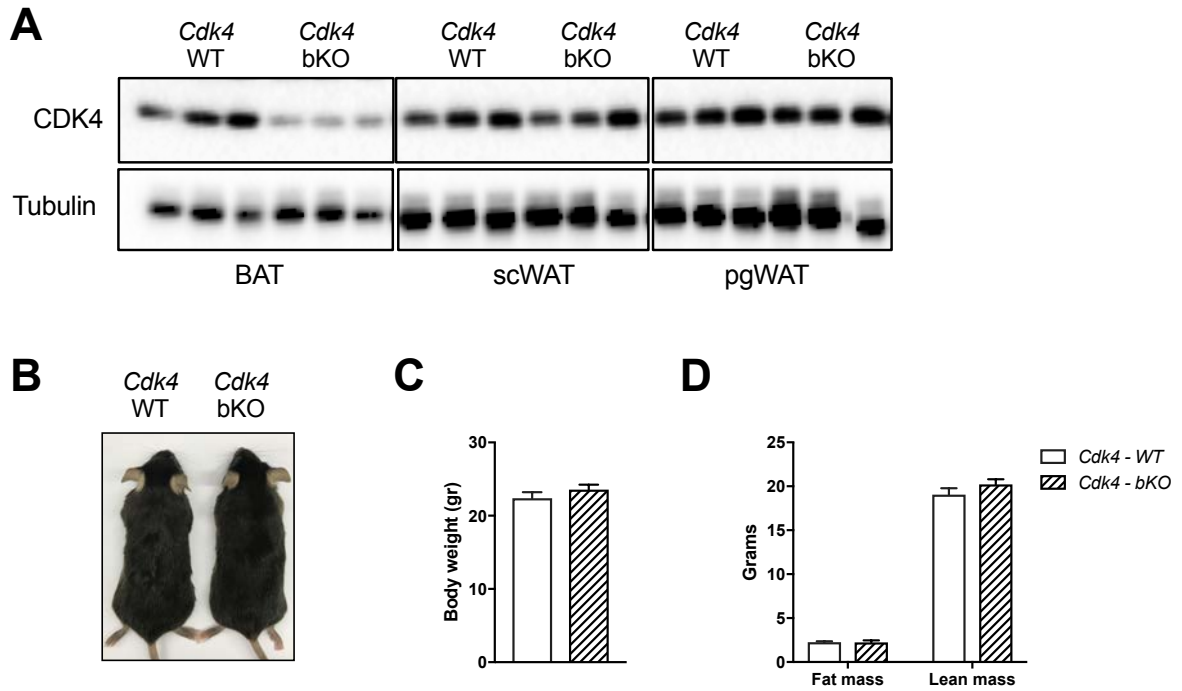
Supplemental Figure 3

Castillo-Armengol, J. et al

A

$Cdk4^{+/+}$ $Cdk4^{-/-}$

B

C BAT

D BAT

Supplemental Figure 4

A

$Cdk4^{+/+}$ $Cdk4^{-/-}$

H&E

B

scWAT

_____
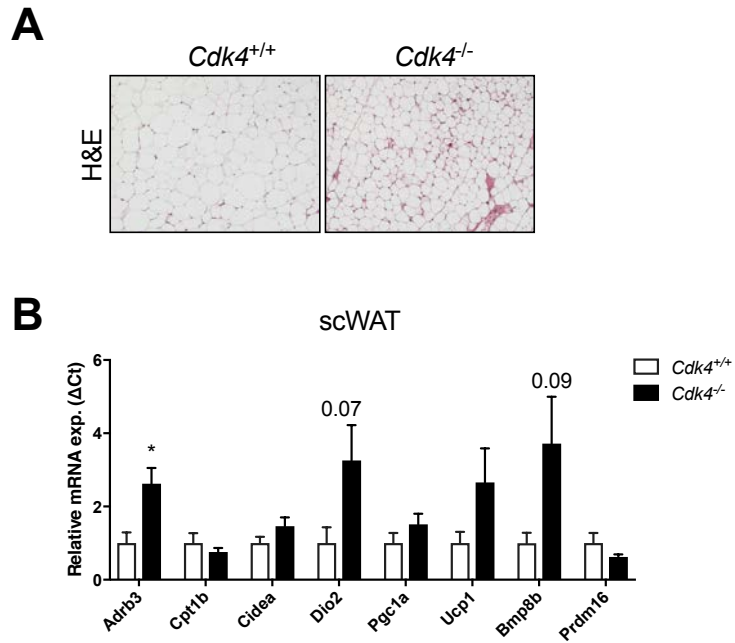
II.   Study of BAT thermogenesis in *Cdk4*^{R24C/R24C} mice

As described in the first part of the results, *Cdk4* knockout mice (*Cdk4*^{-/-}) clearly showed a marked phenotype of increased thermogenesis and BAT activation. To further analyze the effects of CDK4 in BAT biology, we decided to analyze the effects of a genetic hyperactivation of CDK4 in vivo.

Cdk4^{R24C/R24C} mice are homozygous for the non-synonymous point mutation R24C. This mutation is the substitution of the arginine (R) located at the position 24 for a cysteine (C). This modification at the sequence of the protein results in a conformational change that prevents the inhibition of CDK4 by the INK4A family of inhibitors, therefore resulting in a highly active CDK4 protein (125).

1) Hyperactivation of CDK4 does not impair BAT thermogenesis, but increases lipid content in BAT

To elucidate the effects of CDK4 hyperactivation in BAT, we examined the response of *Cdk4*^{R24C/R24C} mice to an acute cold stress. Surprisingly, we were not able to see the expected opposite results to *Cdk4*^{-/-} mice. Both *Cdk4*^{+/+} and *Cdk4*^{R24C/R24C} mice had very similar responses to the cold exposure by decreasing to the same extent their body temperature (Figure 3-1A).

Nevertheless, hematoxylin eosin staining of BAT revealed that *Cdk4*^{R24C/R24C} present bigger lipid droplets in the brown fat depot (Figure 3-1B). On the other hand, gene expression analysis identified *Dio2* and *Bmp8b* differentially expressed between genotypes with a higher expression in the knock-in mice, although UCP1 and other thermogenic or brown genes were not changed between the two genotypes (Figure 3-1C). Moreover, both *Cdk4*^{+/+} and *Cdk4*^{R24C/R24C} responded equally to adrenergic stimulation with β3-agonist treatment (Figure 3-1D). In conclusion, *Cdk4*^{R24C/R24C} mice

74

do not have impaired BAT thermogenesis in response to cold or chemically induced adrernergic stimulation.

_____
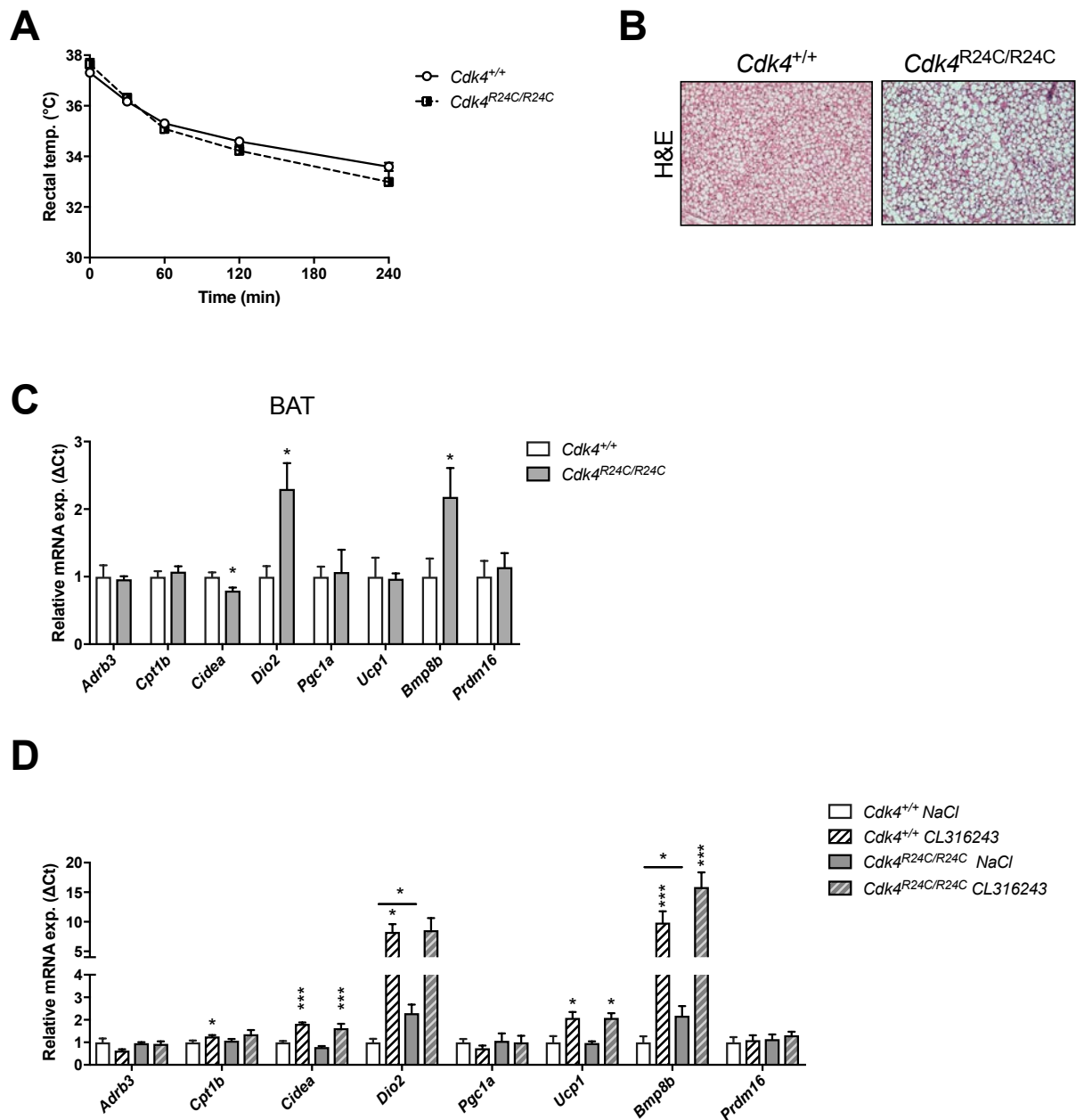
Figure 3-1. Hyperactivation of CDK4 results in increased lipid content in BAT and normal response to cold. A. Rectal temperature was monitored during acute cold exposure at 4°C during 4h in 16w-old *Cdk4+/+* (n=12) and *Cdk4R24C/R24C* (n=10) mice. **B.** Hematoxylin and eosin staining of BAT sections. **C.** Brown gene expression in BAT in basal and after chronic (10 days) β3-agonist treatment 18w-old *Cdk4+/+* (n=6) and *Cdk4R24C/R24C* (n=6) mice. **D.** All data are shown as mean +/- SEM. *P<0.05; **<0.01, ***<0.001.

_____

III.   Study of BAT thermogenesis in *Cdk4*-adKO mice

To elucidate if the effects seen in the *Cdk4* knockout (*Cdk4$^{-/-}$*) mice are tissue autonomous or due to a secondary effect of the deletion of *Cdk4* in other tissues and before generating the BAT-specific knockout mice, we explored the result of the deletion of *Cdk4* in brown and white adipose tissue with the *Cdk4*-adKO mice. These mice were generated by breeding *Cdk4*$^{flox/flox}$ mice with transgenic mice that express the *Cre* recombinase from the adipose-specific fatty acid binding protein (*aP2*) promoter/enhancer.

1) Ablation of *Cdk4* in adipose tissue does not impair body weight or body composition

The efficiency and specificity of the *Cdk4* deletion were analyzed by Western blot. CDK4 expression was preserved in liver, brain, gastrocnemius heart, kidney, pancreas and spleen, but decreased in BAT, subcutaneous WAT and perigonadal WAT (Figure 3-2A, data not shown). Body weight of wild-type and *Cdk4* ad-KO mice was not different. Moreover, by using EchoMRI, we could determine that body composition was not affected by the deletion of *Cdk4* in adipose tissues (Figure 3-2B, C).

2) Adipose tissue-specific deletion of *Cdk4* triggers BAT gene expression

The evidences of BAT activation in *Cdk4$^{-/-}$* mice prompted us to study the response to cold from *Cdk4* ad-KO mice. No differences were observed between wild-type and *Cdk4* ad-KO mice on the response to the lower ambient temperatures and both genotypes were equally resistant to the cold stress (Figure 3-2D).

_____

Histological analysis with hematoxylin eosin staining of these mice indicated that BAT of wild-type and *Cdk4* ad-KO mice was morphologically similar. However, the expression levels of certain brown genes (*Adrb3*, *Cpt1b*, *Pgc1α*, *Bmp8b*, *Prdm16*) were increased in BAT, as revealed by RT-PCR analysis (Figure 3-2F).

In conclusion, *Cdk4*-adKO mice have increased thermogenic and brown gene expression but no difference in the response to the cold exposure when compared to wild-type mice.
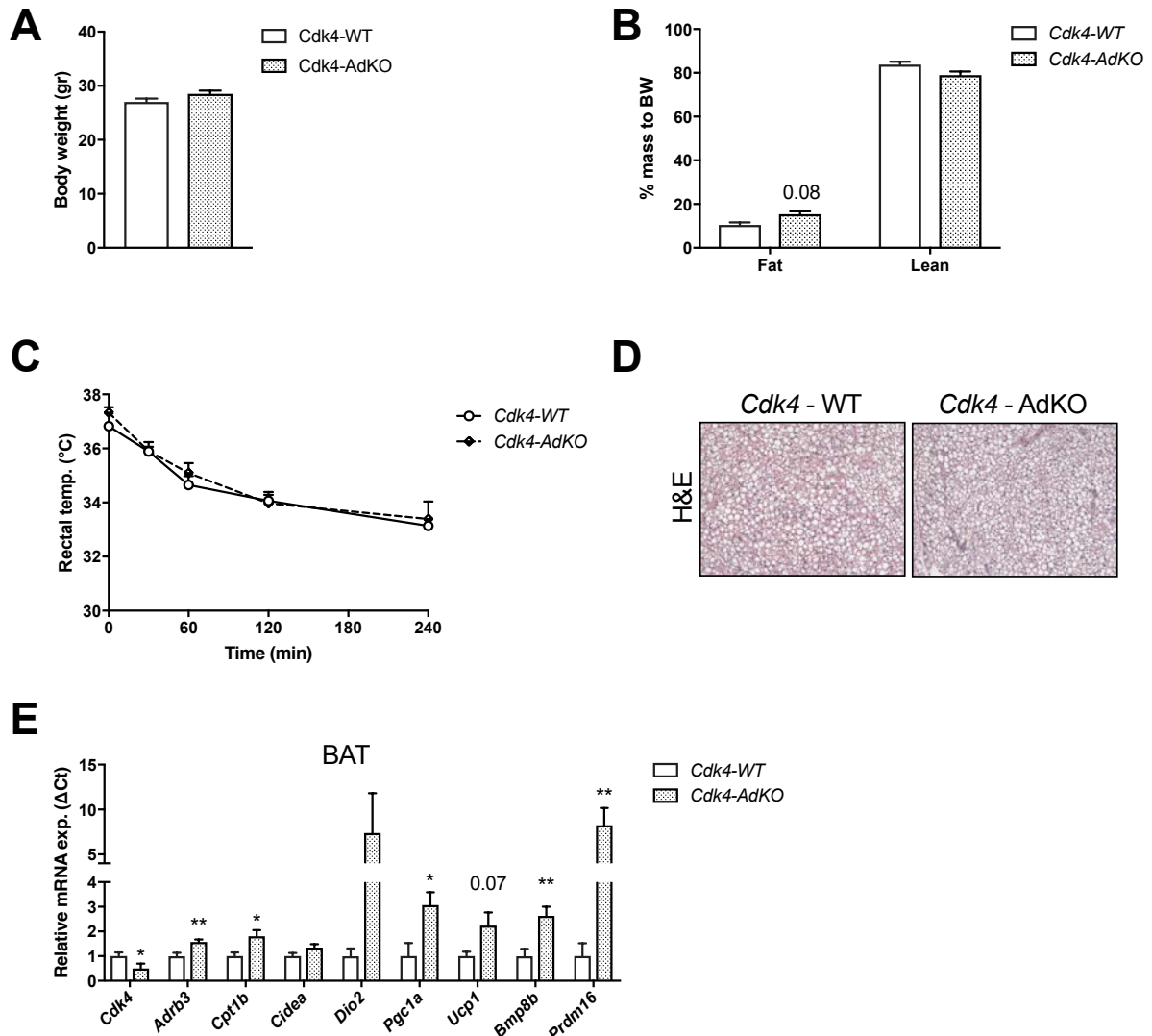
Figure 3-2. AT deletion of *Cdk4* in vivo increases thermogenic gene expression but not cold tolerance. A. Body weight and **B.** Body composition (fat and lean mass) of 18w-old *Cdk4*-WT (n=9) and *Cdk4*-AdKO (n=7) mice. **C.** Rectal temperature was monitored during acute cold exposure at 4°C during 4h in 16w-old *Cdk4*-WT (n=8) and *Cdk4*-AdKO (n=9) mice. **D.** Hematoxylin and eosin staining of BAT sections. **E.** Brown gene expression in BAT of *Cdk4*-WT (n=5) and *Cdk4*-AdKO (n=6) mice. All data are shown as mean +/- SEM. *P<0.05; **<0.01, ***<0.001.

_____

IV.   Study of BAT thermogenesis in *Cdk4*-Sf1Cre mice

The studies that we have done on the *Cdk4*-AdKOCre and *Cdk4*-bKO helped us to discriminate that the effects observed in the *Cdk4*$^{-/-}$ mice are not tissue autonomous, but originated from other organs that regulate thermogenesis. In fact, as previously described in the introduction, the CNS plays a very important role at the level of thermoregulation. Indeed, several hypothalamic regions have been described to control brown fat thermogenesis (47-50, 52, 53), among them, the VMH region.

As *Cdk4* is a highly expressed in hypothalamus, we decided to explore the effects of the deletion of *Cdk4* in Sf1 neurons with the *Cdk4*-Sf1Cre mice. These mice were generated by breeding *Cdk4*$^{flox/flox}$ mice with transgenic mice, kindly provided by Prof. Bernard Thorens, that express the *Cre* recombinase from the steroidogenic factor-1 (*Sf1*) promoter/enhancer. *Sf1*-positive neurons are present in the VMH, as well as pituitary, gonad and adrenal tissue.

1) Ablation of *Cdk4* in *Sf1*-positive neurons results in a mild decrease in body weight and fat mass

Under chow diet feeding, body weight of *Cdk4* Sf1-Cre mice was slightly reduced at 14 weeks old (Figure 3-3A). Moreover, body composition analysis using EchoMRI, showed that these mice also have a mild decrease in the percentage of fat mass (Figure 3-3B).

2) *Cdk4* deletion in Sf1 neurons promotes cold tolerance but not thermogenic gene expression in BAT

We evaluated whether *Cdk4*-Sf1Cre mice were more cold tolerant by performing an acute cold exposure to these animals. *Cdk4*-Sf1Cre animals fed with chow diet showed

_____

an improved response to the cold stress as compared to the wild-type littermates (*Cdk4*$^{\text{flox/flox}}$) (Figure 3-3C). However, no changes in brown fat depot morphology were seen in *Cdk4*-Sf1Cre mice when compared to wild-type mice (Figure 3-3D). Next, we aimed to identify the effects of *Cdk4* deletion in Sf1 neurons on the thermogenic gene expression in BAT. These analyses showed that thermogenic gene expression was unaffected (Figure 3-3E).

All together, these data demonstrate that *Cdk4*-specific deletion in Sf1-positive neurons results in increased cold-induced thermogenesis with no effect in brown fat gene expression.
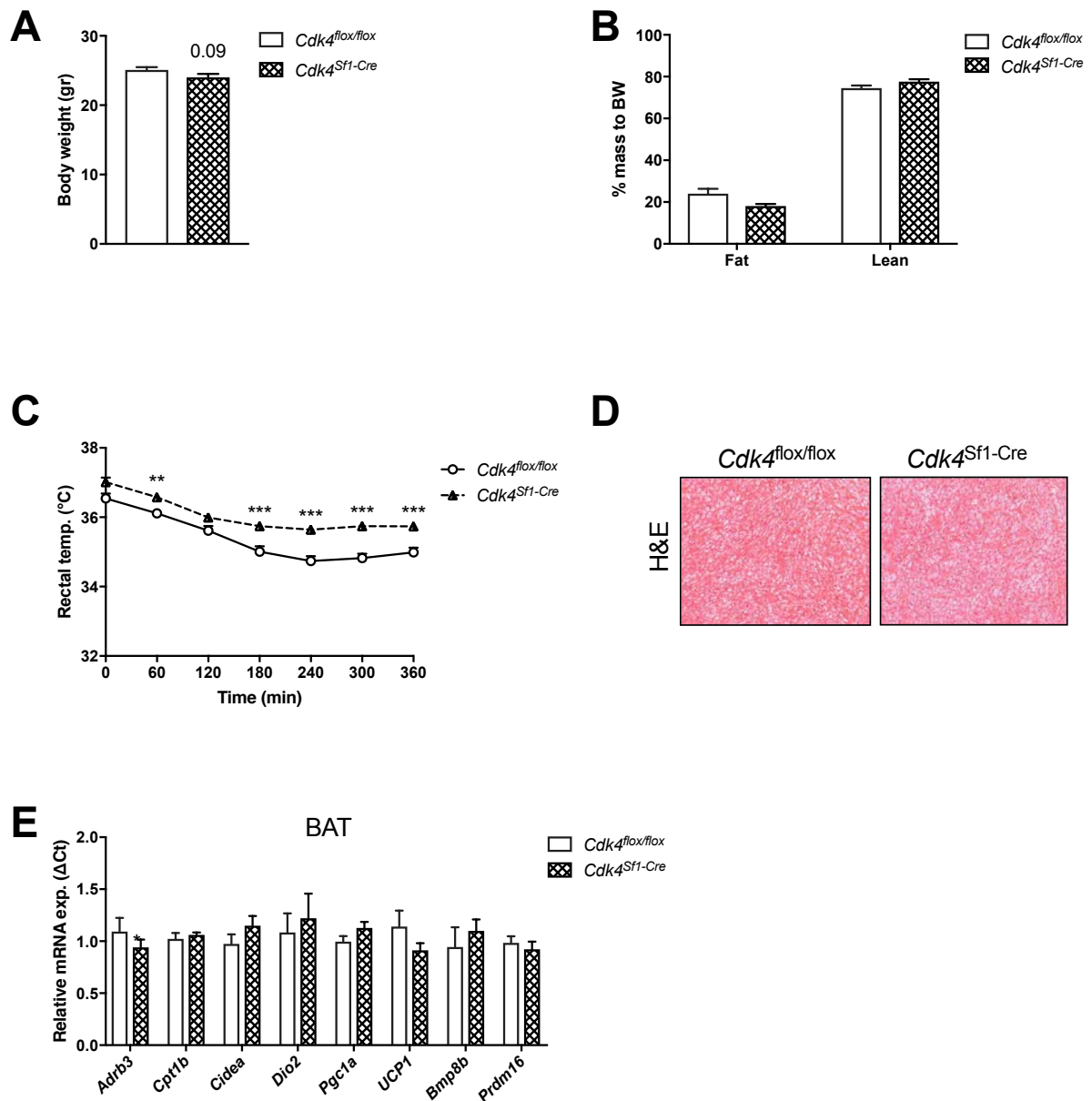
Figure 3-3. Increased cold tolerance without changes in BAT in *Cdk4*^flox/flox Sf1-Cre mice. A. Body weight and **B.** Body composition (fat and lean mass) of 18w-old *Cdk4^flox/flox* (n=17) and *Cdk4^flox/flox Sf1-Cre* (n=11) mice. **C.** Rectal temperature was monitored during acute cold exposure at 4°C during 4h in 16w-old *Cdk4^flox/flox* (n=27) and *Cdk4^flox/flox Sf1-Cre* (n=20) mice. **D.** Hematoxylin and eosin staining of BAT sections. **E.** Brown gene expression in BAT of *Cdk4^flox/flox* (n=15) and *Cdk4^flox/flox Sf1-Cre* (n=12) mice. All data are shown as mean +/- SEM. *P<0.05; **<0.01, ***<0.001.

_____

V.   Effects of *Cdk4* deletion in thyroid gland

The main objective of this thesis was to determine the participation of CDK4 in the regulation of brown fat thermogenesis. Since the results described in the previous sections revealed that *Cdk4* deletion in adipose tissue or Sf1 neurons has no impact in BAT thermoregulation, we explored the participation of this protein in thyroid hormone thyroid hormone metabolism. A part of this investigation in thyroid hormone metabolism is already addressed in the manuscript found in section I.

1) *Trh* expression is enhanced in hypothalamus of *Cdk4*$^{-/-}$ mice

As previously mentioned in the introduction, thyroid hormones are known to be involved in the control of BAT heat production. The thyroid gland is the organ in charge of the secretion of, T4 and T3, hormones that stimulate brown adipocytes activation (66, 68, 69). The first level of stimulation of thyroid hormone secretion is the hypothalamus where there is the secretion of TRH to activate the pituitary-dependent secretion of TSH, main activator of thyroid hormone production (67). To elucidate the role of CDK4 in the hypothalamic regulation of thyroid hormone metabolism, we analyzed the gene expression of *Trh* in whole hypothalamus of *Cdk4*$^{-/-}$ mice. *Cdk4*$^{-/-}$ mice presented higher levels of this gene compared to wild-type mice (Figure 3-4 A). This result prompted us to study in detail the thyroid gland of these mice.

2) Increased expression of deiodinases in *Cdk4*$^{-/-}$ thyroid gland

As already shown in the manuscript of the Results Section I, no apparent morphological differences were found in this organ between both genotypes. Nevertheless, gene expression analysis of the thyroid gland revealed that *Dio2* and *Dio3* levels were increased in the knockout mice (Figure 3-4B). These results were clearly controversial

_____

because of the natural roles of these deiodinases. DIO2 is the key enzyme in charge of the conversion of T4 to its metabolic active form, T3. On the other hand, DIO3 has an opposite action because it mediates the degradation of T3 to maintain normal levels of this hormone (131). Other thyroid-specific genes such as the precursor of thyroid hormones thyroglobulin (Tg), the thyroid hormone-synthesis enzyme thyroperoxidase (Tpo) or the thyroid-stimulating hormone receptor (Tshr) were not affected (Figure 3-4 B).
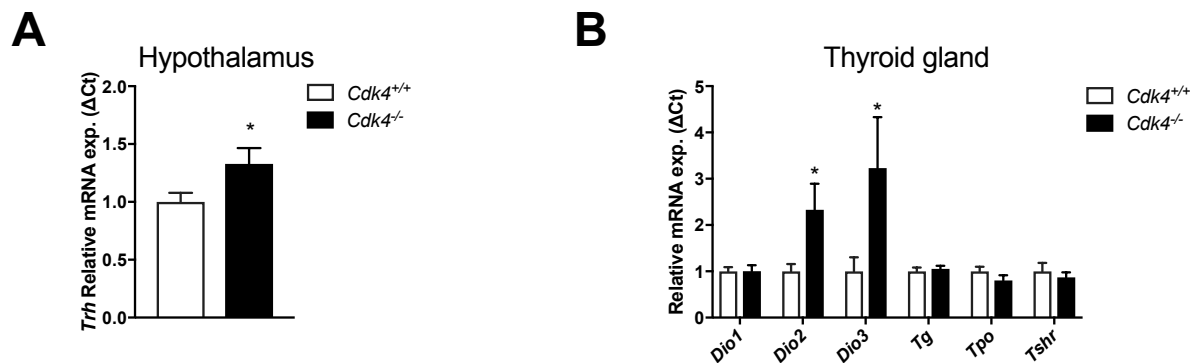
Figure 3-4. Thyroid hormone metabolism in *Cdk4*^{-/-} mice A. *Trh* gene expression in whole hypothalamus of *Cdk4*^{+/+} (n=14) and *Cdk4*^{-/-} (n=9) mice. **B.** Thyroid hormone metabolism gene expression in BAT of *Cdk4*^{+/+} (n=12) and *Cdk4*^{-/-} (n=10) mice. All data are shown as mean +/- SEM. *P<0.05; **<0.01, ***<0.001.

_____

VI.   Effects of *Cdk4* deletion in adrenal gland

The adrenal gland is a small endocrine organ located above the kidney and responsible of the catecholamine's synthesis. It is the main site of epinephrine (EPI) and norepinephrine (NE) synthesis for the general circulation (132). The secretion of these catecholamines is controlled by the sympathetic innervation of the adrenal glands (133).

1) Gene expression of cathecolamine-synthesizing enzymes is increased in *Cdk4$^{-/-}$* adrenal gland

The conclusion that we extracted from the first part of the results (mentioned in the manuscript found in Section I) is that CDK4 inhibits sympathetic innervation in BAT, confirmed by the increased levels of TH-positive fibers in the brown fat depot of *Cdk4$^{-/-}$* mice. As a consequence, we thought that general sympathetic innervation is enhanced in *Cdk4$^{-/-}$*. In order to elucidate this hypothesis, we checked the gene expression levels of the catecholamine synthesis genes (*Dbh*, *Pnmt*, *Th*) in adrenal gland as readout of its sympathetic activation. We found a 2.5 to 4-fold increase in the expression of these genes in the adrenal gland of *Cdk4*-deficient mice, suggesting an overall increase in the levels of sympathetic stimulation of these mice (Figure 3-5).

_____
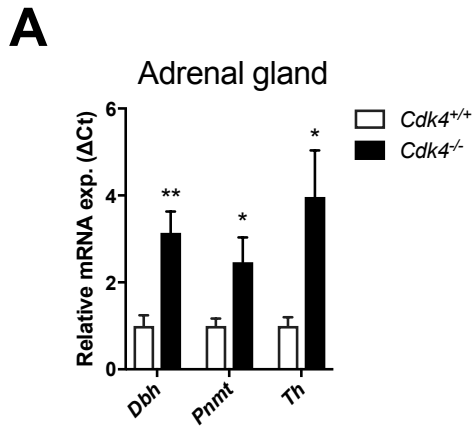
Figure 3-5. Catecholamine synthesis gene expression is enhanced in _Cdk4_-deficient mice A. Catecholamine synthesis gene expression in BAT of _Cdk4+/+_ (n=8) and _Cdk4-/-_ (n=8) mice. All data are shown as mean +/- SEM. *P<0.05; **<0.01, ***<0.001.

VII.   Aging and thermogenesis in *Cdk4*-deficient mice

BAT non-shivering thermogenesis is a crucial process for the survival of rodents (16). However, aging has been associated with a loss-of-function of this fat depot. Brown adipocytes get enlarged and accumulate more lipids in elderly animals. Moreover, thermogenic gene expression is reduced in BAT of older mice and in consequence, cold tolerance is also diminished (134-136).

1) Differences in cold tolerance between *Cdk4*$^{-/-}$ and *Cdk4*$^{+/+}$ mice are greater in older animals

To determine how aging altered the phenotype of *Cdk4*$^{-/-}$ mice, we exposed 30 weeks old mice to cold ambient temperature during 6h. Surprisingly, *Cdk4*$^{-/-}$ mice maintained their body temperature during the cold test whereas *Cdk4*$^{+/+}$ mice had a strong decrease in their core body temperature of almost 2°C (Figure Annex 3-6A). Next, we conducted histological analysis to explore the morphology of the BAT. The differences found on the hematoxylin eosin staining were striking. BAT of *Cdk4*$^{-/-}$ mice was clearly delipidated and only small lipid droplets were present. In contrast, BAT of *Cdk4*$^{+/+}$ mice showed increased lipid droplet size and number (Figure 3-6B). In addition, brown and thermogenic gene expression (*Adrb3*, *Cpt1b*, *Cidea*, *Dio2*, *Ucp1*, ...) was higher in the BAT of *Cdk4*-deficient mice (Figure 3-6C). In conclusion, differences in thermogenic response between *Cdk4*$^{-/-}$ and *Cdk4*$^{+/+}$ mice are magnified by aging.
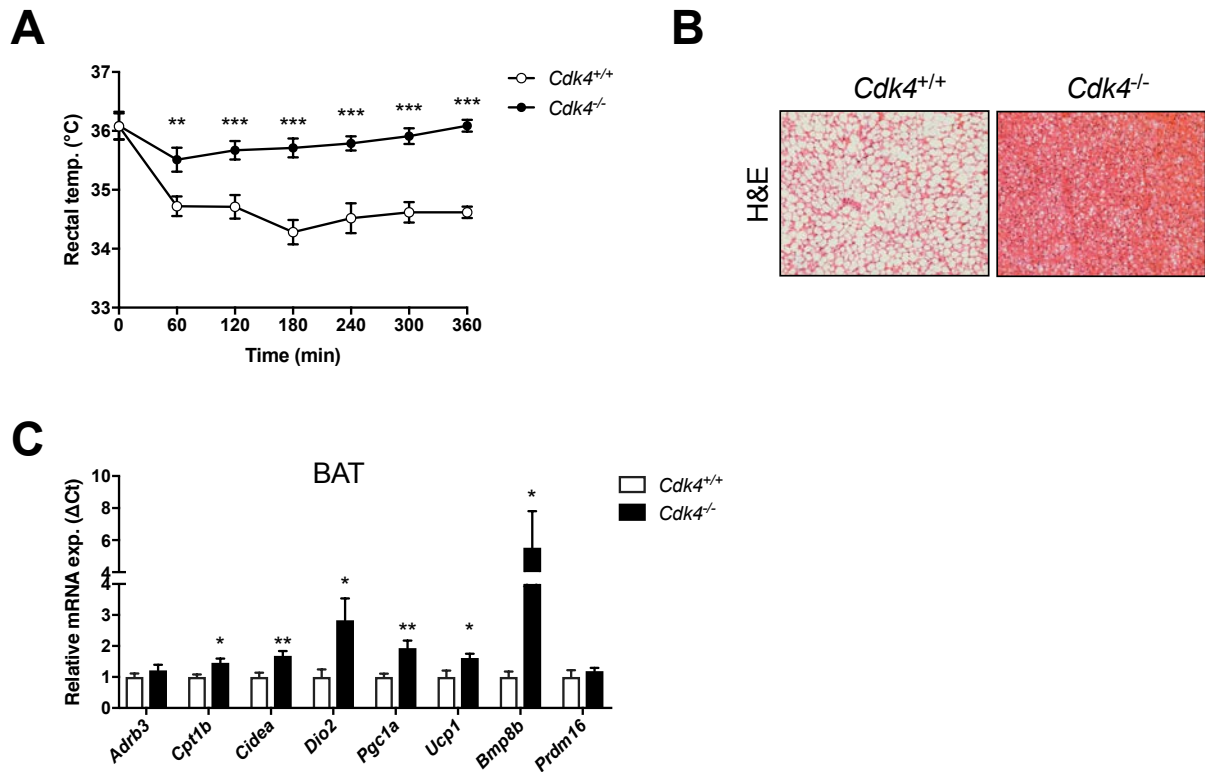
Figure 3-6. Old *Cdk4⁻ᐟ⁻* mice are hyperthermic under cold exposure and have a very marked thermogenic phenotype in BAT A. Rectal temperature was monitored during acute cold exposure at 4°C during 4h in 30w-old *Cdk4⁺ᐟ⁺* (n=10) and *Cdk4⁻ᐟ⁻* (n=10) mice. **B.** Hematoxylin and eosin staining of BAT sections. **C.** Brown gene expression in BAT in 30w-old *Cdk4⁺ᐟ⁺* (n=6) and *Cdk4⁻ᐟ⁻* (n=6) mice. All data are shown as mean +/- SEM. *P<0.05; **<0.01, ***<0.001.

_____

2) *Cdk4*$^{-/-}$ increased thermogenesis is not present at younger stages of development

Sympathetic innervation occurs early in the mouse development and it is controlled by transcriptional regulators but also, secreted factors like BMP8B. To better characterize if the phenotype observed in the *Cdk4*$^{-/-}$ mice was a result of the adaptation to the innervation, we studied the BAT of juvenile individuals in 3 weeks old mice. The BAT of these young *Cdk4*$^{-/-}$ animals was not smaller when normalized by body weight but was darker than the tissue of the controls (Figure 3-7 A-B). Hematoxylin-eosin staining revealed that, similarly to what we found in older animals, *Cdk4*$^{-/-}$ mice had a substantial decrease in the amount of lipid droplets compared with wild-type controls (Figure 3-7 C).

We also defined the characteristics of the BAT of these mice by gene expression analysis. In contrast to the 14 weeks old *Cdk4*$^{-/-}$ (described in Section I), we noted that most of the genes that were found increased in those^{-} mice were not changed in the BAT of the 3 weeks old knockout mice and only Bmp8b was highly increased in those samples (Figure 3-7 D). These results indicate that the phenotype gets stronger with aging.

Additionally, we tested the gene expression of certain factors that are involved in mediating axon guidance and innervation. *Sema3c* expression, a gene that encodes for a protein that stops axon growth, was reduced whereas *Nrg4*, which encodes for axon growth, was increased in the BAT of *Cdk4* deficient mice suggesting that there might be a role of *Cdk4* in mediating axon growth and innervation (Figure 3-7E).

In conclusion, *Cdk4*$^{-/-}$ mice at post-weaning age, present a milder BAT phenotype compared with animals from the same genotype at older stages, such as 14 or 30 weeks old.

_____
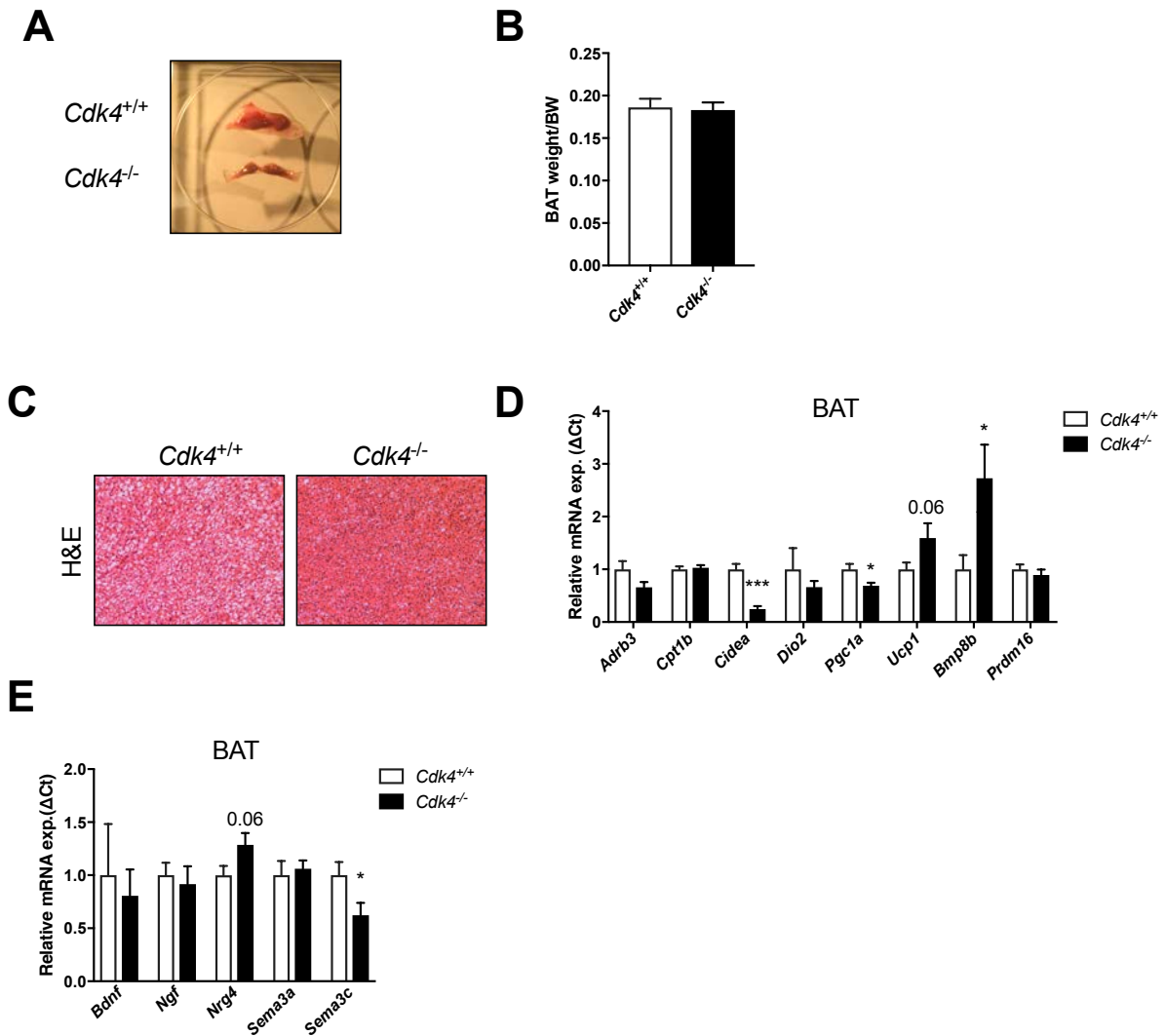
Figure 3-7. Young *Cdk4*⁻/⁻ mice have a very mild thermogenic phenotype in BAT and **enhanced neuronal growth gene expression in BAT A.** General morphology of BAT **B.** Interscapular BAT weight compared to body weight **C.** Hematoxylin and eosin staining of BAT sections. **D.** Brown gene expression and **E.** Neurotrophins gene expression in BAT in 3w-old *Cdk4*⁺/⁺ (n=8) and *Cdk4*⁻/⁻ (n=7) mice. All data are shown as mean +/- SEM. *P<0.05; **<0.01, ***<0.001.

Chapter 4: General discussion

_____

Chapter 4: General discussion

The number of publications that attribute metabolic processes to cell cycle proteins has been growing in the past 10 years (107-109, 111). Indeed, the CDK4-RB-E2F pathway has been described as a mediator of physiological adaptation by regulating not only cell cycle but also metabolic pathways (112-115, 119-122, 125, 127, 128). This thesis has been focused on the study of the protein CDK4.

CDK4 is a protein kinase that is only active when complexed with D-type cyclins. Its kinase activity is induced by extracellular signals, like growth factors, and triggers cell cycle progression (104). On the other hand, several studies have proved that it is a metabolic regulator. For example, it is known that CDK4 participates in adipocyte differentiation via direct regulation of PPARγ (114). Moreover, it also regulates insulin secretion, fatty acid oxidation and insulin signaling in mature adipocytes (127, 128, 137).

Even though it has been reported that cold induces enhanced levels of phosphorylated pRB, a well-known CDK4 target, in BAT (118), no specific role of CDK4 in this tissue has been reported before.

Nowadays, obesity has been the focus of attention in research due to the increased prevalence of metabolic diseases derived from it. BAT activation by chronic cold-exposure or pharmacological approaches increases energy expenditure, glucose clearance and lipolysis (18, 19). All of these processes result in a decrease in weight gain and fat mass. Therefore, identifying new factors that regulate BAT thermogenesis can help to design new-targeted strategies to stimulate brown fat as a new therapeutic approach against obesity (138-140).

_____

Interestingly, BAT activation and browning of scWAT are processes that are closely related to the remodeling of nervous and vascular networks (38, 46, 141). For this reason, the remodeling of nervous networks could be targeted by novel therapeutic approaches to optimize the efficiency of directed strategies to increase weight-loss.

As we found that *Cdk4* deletion augments EE and lipid oxidative metabolism in mice especially in cold ambient temperatures, we decided to analyze the characteristics of the brown fat depot of mice that are depleted from *Cdk4*. *Cdk4*$^{-/-}$ mice showed a very marked thermogenic phenotype. Even though basal temperature was not affected, *Cdk4*$^{-/-}$ mice were more resistance to short periods of cold-exposure. The upregulated thermogenic gene expression and the decreased lipid content in BAT also indicated a more active brown fat depot in these animals. These observations led us to hypothesize that CDK4 was affecting BAT biology and thermogenic capacity.

This hypothesis was first explored using the AT-specific knockout (*Cdk4*-AdKO) in which *Cdk4* was depleted in AT by *Cre* expression under the *aP2*-driven promoter. Gene expression analysis of BAT from *Cdk4*-AdKO showed increased thermogenic gene expression. It was expected that due to the differences in gene expression, *Cdk4*-AdKO mice would have increased cold tolerance or morphological differences in BAT, but neither of these two hypotheses were confirmed and no alterations were found in these parameters. As the construction of the *Cdk4*-AdKO mice was not only targeting brown and white AT, but also macrophages and some hypothalamic areas (142, 143), we decided to design a new animal model with the *Ucp1*-driven Cre expression to specifically target brown adipocytes.

Revealing the effect of CDK4 in *Cdk4* BAT-specific knockout mice was surprisingly challenging. In spite of the high levels of expression of this protein in this AT depot (127), we could not demonstrate the results that we expected when we deleted *Cdk4* from BAT in vivo. We hypothesized that *Cdk4*-bKO mice would show increased thermogenesis, leading to reduced body weight and increased EE compared to WT.

_____

Nevertheless, this was not the case in these animals housed at 21°C fed a chow diet or housed at 6°C during 6 weeks (data not shown). So, the enhanced thermogenesis of $Cdk4^{-/-}$ mice was not due to cell autonomous effects in BAT, but from its activation by other tissues.

Subsequent experiments with the $Cdk4$ knockout model ($Cdk4^{-/-}$) were needed to investigate the different hypotheses of the thermogenic regulation in these mice by other organs. BAT activity is regulated by the SNS (46, 47). Sympathetic innervation was assessed directly in BAT by immunohistochemistry against TH, one of the key enzymes of catecholamine synthesis expressed in nervous fibers innervating BAT (38, 46). These measurements showed that lack of Cdk4 increased innervation of TH-positive fibers in BAT, inducing an enhanced adrenergic activation of the tissue.

The adrenergic dependence of the thermogenic response in $Cdk4^{-/-}$ mice was tested by inhibiting the activation of the β3-adrenergic receptor in vivo using a selective β3-antagonist. Surprisingly, the higher cold-resistance of $Cdk4^{-/-}$ mice was not affected by this treatment. We believe that other mechanisms could compensate the blockade of this receptor, such as the activation of other NE-responding receptors (144). Indeed, it has been reported that ADRB3 disruption in vivo does not affect thermogenic capacity, due to the compensative overexpression of other β–receptors (145-147). On the other hand, as PKA-pathway can also be activated by other mechanisms such as thyroid hormone stimulation (66); enhanced thyroid hormone intracellular metabolism could induce PKA activation in $Cdk4^{-/-}$ mice in the context of ADRB3 inhibition. Nevertheless, other experiments would be necessary to clarify this point.

The UCP1-mediated heat production takes place in the mitochondria of brown adipocytes. Therefore, alterations in mitochondria number or activity have an influence on thermogenic capacity (148, 149). By comparing the electromicrographs of BAT from $Cdk4^{+/+}$ and $Cdk4^{-/-}$ mice, we could also notice a remarkable increase in mitochondria content in the $Cdk4^{-/-}$ animals. Respirometry analysis of BAT homogenates from these

_____

mice revealed that *Cdk4*^{-/-} have highly efficient ETC machinery that could explain why these animals can generate more heat compared to their WT littermates. This increased mitochondrial biogenesis might be explained by the overall enhanced innervation and therefore activation of BAT (150, 151). However, several authors have also demonstrated that thyroid hormones can influence mitochondrial number by upregulating mitochondrial biogenesis' gene expression (152-154).

During the course of our studies, we attempted to determine the effects of CDK4 in thyroid hormone metabolism by first analyzing the gene expression levels of *Trh*. The expression levels of this gene were increased in the hypothalamus of *Cdk4*^{-/-} mice. This suggested that there was an upregulated activation of the HPT axis (155). Experiments in the thyroid gland of *Cdk4*^{-/-} mice showed that the expression of deiodinases was affected. However, controversial results were found because the enzyme *Dio2*, which is relevant for the intracellular levels of T3, was augmented but also the counteractive *Dio3* enzyme that inactivates T3 was enhanced (131).

On the other hand, no differences were found in fed levels of T3 or T4 in serum. Nevertheless, we are aware that other parameters could be tested to further investigate the thyroid metabolism of *Cdk4*^{-/-} mice. For example, slight differences in TSH circulating levels could explain a hyperthyroid phenotype (156). In conclusion, further work is required to demonstrate whether CDK4 affects thyroid hormone secretion or not.

However, *Dio2* and *Thrβ* expression is enhanced in BAT of *Cdk4*^{-/-} suggesting that there is an increased intracellular thyroid hormone metabolism. Hence, the enhanced expression of these genes could explain an increased activation of BAT function by thyroid hormones (157).

Furthermore, we have shown that CDK4 also affects the remodeling of other AT depots. Older (30- weeks old) *Cdk4*^{-/-} mice present cells containing smaller and multiple lipid droplets, which are characteristic of brown adipocytes within WAT (30). Consistent with this, thermogenic genes are also induced in the scWAT of *Cdk4*^{-/-} mice. Besides this,

_____

another important piece of evidence comes from our analysis of the adrenal gland of these mice. We observed increased gene expression of catecholamine-synthesizing enzymes in the adrenal glands of $Cdk4^{-/-}$ mice. Both findings could be associated to an overall increased sympathetic tone in $Cdk4^{-/-}$ mice, as it has been described that the SNS controls AT remodeling and catecholamine synthesis in adrenal glands (46, 133, 141).

Another point that I would like to strengthen in this discussion is the impact of CDK4 on $Bmp8b$ expression. BMP8B is an adipokine known to be upregulated in BAT and scWAT by cold-exposure (51). It also contributes to the expansion of nervous networks in BAT to enhance the adrenergic response of the tissue (65). It is likely that $Cdk4^{-/-}$ mice have an enhanced thermogenic response to cold and have increased adrenergic innervation via BMP8B signaling. However, the contribution of CDK4 into the regulation of BMP8B secretion would require further investigation.

First, it was confirmed that $Cdk4^{-/-}$ mice have an increased thermogenic phenotype at 14- weeks old. Further analysis of BAT thermogenesis in this model revealed that in older mice (30- weeks old) the differences between $Cdk4^{+/+}$ and $Cdk4^{-/-}$ are bigger. As previously described in numerous publications, BAT atrophy is associated with aging (48, 135, 136, 158-160). Thus, $Cdk4^{+/+}$ mice presented whitening of BAT and reduced cold-tolerance at 30- weeks of age while $Cdk4^{-/-}$ mice maintained their thermogenic phenotype both at the level of gene expression and also in their response to cold exposure.

The temperature under which we house our animals (21°C) is a great thermogenic challenge for them (161). This is especially important regarding younger animals. Younger animals are more susceptible to low temperature due to greater heat loss to the environment compared to older mice because of their larger surface area to volume ratio. It is in these younger mice in which BAT is more active (161). Therefore, young (3- week old) $Cdk4^{-/-}$ mice were analyzed for a thermogenic phenotype. To our surprise, thermogenic gene expression in these mice was almost restored to WT values.

Nevertheless, preliminary data showed that the semaphorin *Sema3c*, which is a repressor of axon growth (62), was reduced in the BAT of young *Cdk4*^{-/-} mice whereas *Nrg4*, a neuroregulin induced by cold that promotes neuronal outgrowth (65), was enriched in the same depot. These two observations prompted us to consider that young *Cdk4*^{-/-} mice have enhanced remodeling of AT depots through the formation and growth of nervous networks.

As mentioned earlier, smaller animals are more cold-sensitive because of a greater energy dissipation due to their unfavorable surface to volume ratio (161). Therefore, the reduced size of *Cdk4*^{-/-} mice could explain an enhanced heat dissipation that needs to be compensated by an increase in thermogenesis.

So far, we do not know at which level CDK4 is acting in the formation of nervous networks but we hypothesize that it is at the level of SNS development, probably due to the challenge posed by housing at room temperature. To test this hypothesis, *Cdk4*^{-/-} mice could be bred and housed at 30°C, a temperature at which cold-induced sympathetic tone to AT is reduced due to the almost absence of thermogenic challenge (thermoneutral conditions for mice are defined at 30°C). In principle, under these conditions, *Cdk4*^{-/-} should not have the need to develop adrenergical networks to stimulate heat production. Moreover, the total dependence of the *Cdk4*^{-/-} phenotype on sympathetic tone to BAT could be verified by measuring thermogenic gene expression in BAT from denervated *Cdk4*^{-/-} mice. However, these experiments were not possible during the course of my PhD studies.

Nevertheless, it would be interesting to quantify the central impact of the lack of *Cdk4* in the thermogenesis of *Cdk4*^{-/-} mice. *Cdk4* mRNA is expressed in multiple hypothalamic areas, but it is unknown which specific neuronal populations express *Cdk4*. The importance of *Cdk4* expression in the hypothalamic areas that regulate thermogenesis could be investigated using a brain-specific *Cdk4*^{-/-} model via a generic hypothalamic Cre recombinase driver such as *Nkx2.1* (162, 163).

_____

Although *Cdk4* expression in specific neuronal populations is unknown, it has been reported that this protein is active in the mediobasal hypothalamus (MBH), a region that includes the Arc and the VMH. Increased phosphorylation of the CDK4-target RB was found in this area in mice after HFD-feeding (164).

Therefore, we explored the role of CDK4 in the VMH by generating a new mouse model of *Cdk4* deletion in the neurons of this area using the *Sf1*-Cre recombinase driver. The resulting animal did not present any phenotype at the level of BAT gene expression but an increase in cold tolerance when animals were exposed to cold ambient temperature for a short period of time. Further experiments would be necessary to clarify the relevance of the deletion of *Cdk4* in this area, such as long-term cold exposure or β3-agonist stimulation in these mice.

As a complement to the studies on *Cdk4* deletion in vivo, we also analyzed the phenotype of *Cdk4*$^{R24C/R24C}$ mice in BAT. These animals are characterized by the expression of a point mutation that renders CDK4 hyperactive because of the conformational change that avoids the repression by p16, one CKI. Conversely, the expected inversed phenotype was not observed in the *Cdk4*$^{R24C/R24C}$ mice. These mice did not show impaired thermogenesis or reduced expression of *Ucp1* in BAT. These results are in disagreement with the work done on *p16*-deficient mice, which report increased *Ucp1* expression in BAT under chow diet conditions (165). It is worth noting that the R24C mutation causes the inability of p16 to bind and inhibit CDK4. Nevertheless, other inhibitors can still access the protein to repress it. Thus, it is possible that in the context where CDK4 has a role in thermogenesis, p16 is not its major repressor and therefore, *Cdk4*$^{R24C/R24C}$ mice have a normal regulation of the protein and not a hyperactivation.

To sum up, we suspect that *Cdk4*$^{-/-}$ mice had upregulated BAT thermogenic gene expression as a response to BAT adrenergic hyperactivation due to the enhanced level of

catecholaminergic fibers that are populating this AT depot. Overall CDK4 seems to act as a repressor of thermogenesis through its inhibitory effect on innervation.

Chapter 5: Conclusions

_____

Chapter 5: Conclusions

The figure 5-1 summarizes the findings described in this PhD thesis. Cold or pharmacological stimulation of BAT results in heat production by brown adipocytes. Under these stimuli, expansion of BAT and recruitment of beige adipocytes in scWAT are also induced and followed by the remodeling of vascular and nervous networks in AT. The adaptive process of sympathetic nervous outgrowth and branching will induce an increased catecholaminergic stimulation of the tissue and in turn, NE-stimulation will result in the adaptation of the tissue to increase lipolysis and heat production.

During this PhD studies, we have demonstrated that Cdk4 deficient mice ($Cdk4^{-/-}$) have a marked thermogenic phenotype in BAT with enhanced heat production. Moreover, the analysis of $Cdk4$ BAT-specific knockout ($Cdk4$-bKO) mice revealed that the effects from CDK4 observed in BAT are not cell autonomous but derived from another upstream organ. In fact, the characterization of the $Cdk4$ knockout mice ($Cdk4^{-/-}$) showed an increased sympathetic innervation of BAT that could explain the thermogenic activation seen in these animals. In conclusion, here we propose CDK4 as a novel regulator of non-shivering thermogenesis through nervous network remodeling of AT.

Our results demonstrate a new role for CDK4 on the control of thermogenesis and its function in the biology of BAT. We suspect that CDK4 plays a role in development at the level of CNS to repress sympathetic innervation outgrowth. That is why, $Cdk4^{-/-}$ mice have enhanced sympathetic innervation of BAT which triggers the adaptation over time of the tissue to adrenergic stimulation, with evidences of enhanced thermogenic gene expression at 14- weeks old and not at 3- weeks old mice. Moreover, we have also observed that this BAT activation induces mitochondrial biogenesis in $Cdk4^{-/-}$ mice.

On the other hand, we have also noticed that, in older mice (30- weeks old), lack of $Cdk4$ promotes beige cell recruitment in scWAT and the induction of thermogenic machinery

in this tissue. This is likely due to the impact of CDK4 in general sympathetic tone. Similarly, the elevated expression of the genes responsible of catecholamine synthesis in adrenal glands of $Cdk4^{-/-}$ mice could be also derived from it.

Overall the findings in this thesis suggest that CDK4 acts as a repressor of sympathetic innervation during development affecting the thermogenic response of BAT and the remodeling of WAT.

_____

_____
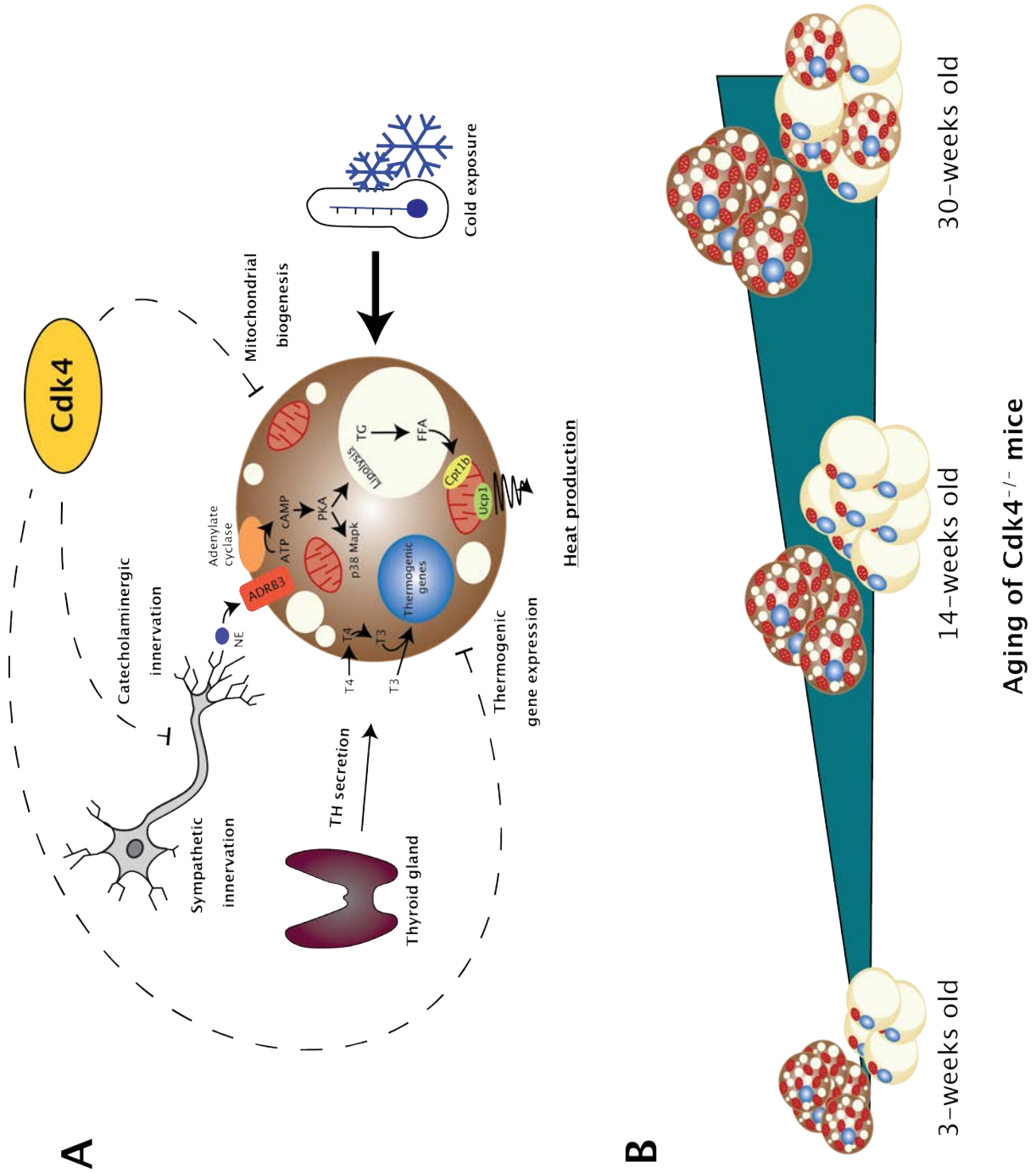
Figure 5-1. Summary of the proposed roles of CDK4 in brown and beige adipocytes. Brown adipocytes respond to cold exposure by generating heat. Apart from that, the stimulus of cold induces the expansion of sympathetic nervous networks in BAT. The findings of this thesis prompted us to assume that CDK4 is an inhibitor of the outgrowth and branching of sympathetic nerves. In parallel the impairment of BAT innervation by CDK4 also affects thermogenic gene expression, mitochondrial biogenesis and therefore, heat production (A). Cold also induces the recruitment of thermogenic beige adipocytes in scWAT. CDK4 would also act as a repressor of sympathetically-mediated beige cell recruitment. In this way, $Cdk4^{-/-}$ mice have overall enhanced sympathetic innervation and they adapt over time to this nervous networks remodeling their AT depots. That is why, young (3- weeks old) $Cdk4^{-/-}$ mice have a very mild phenotype in BAT, but when they are 14- weeks old the phenotype is more evident and differences are stronger between $Cdk4^{+/+}$ and $Cdk4^{-/-}$ mice at older stages (30- weeks old). It is also at this point; in which we can see spontaneous recruitment of beige adipocytes in scWAT (B).

References

References

1.   Ogden CL, Flegal KM, Carroll MD, Johnson CL. Prevalence and trends in overweight among US children and adolescents, 1999-2000. Jama. 2002 Oct 9;288(14):1728-32. PubMed PMID: 12365956.

2.   Han TS, Lean ME. A clinical perspective of obesity, metabolic syndrome and cardiovascular disease. JRSM cardiovascular disease. 2016 Jan-Dec;5:2048004016633371. PubMed PMID: 26998259. Pubmed Central PMCID: 4780070.

3.   Romieu I, Dossus L, Barquera S, Blottiere HM, Franks PW, Gunter M, et al. Energy balance and obesity: what are the main drivers? Cancer causes & control : CCC. 2017 Mar;28(3):247-58. PubMed PMID: 28210884. Pubmed Central PMCID: 5325830.

4.   Hill JO, Wyatt HR, Peters JC. Energy balance and obesity. Circulation. 2012 Jul 3;126(1):126-32. PubMed PMID: 22753534. Pubmed Central PMCID: 3401553.

5.   Hill JO, Wyatt HR, Peters JC. The Importance of Energy Balance. European endocrinology. 2013 Aug;9(2):111-5. PubMed PMID: 29922364. Pubmed Central PMCID: 6003580.

6.   Sethi JK, Vidal-Puig AJ. Thematic review series: adipocyte biology. Adipose tissue function and plasticity orchestrate nutritional adaptation. Journal of lipid research. 2007 Jun;48(6):1253-62. PubMed PMID: 17374880. Pubmed Central PMCID: 4303760.

7.   Kwok KH, Lam KS, Xu A. Heterogeneity of white adipose tissue: molecular basis and clinical implications. Experimental & molecular medicine. 2016 Mar 11;48:e215. PubMed PMID: 26964831. Pubmed Central PMCID: 4892883.

8.   Kershaw EE, Flier JS. Adipose tissue as an endocrine organ. The Journal of clinical endocrinology and metabolism. 2004 Jun;89(6):2548-56. PubMed PMID: 15181022.

9.   Scherer PE. Adipose tissue: from lipid storage compartment to endocrine organ. Diabetes. 2006 Jun;55(6):1537-45. PubMed PMID: 16731815.

10.   Lelliott C, Vidal-Puig AJ. Lipotoxicity, an imbalance between lipogenesis de novo and fatty acid oxidation. International journal of obesity and related metabolic disorders : journal of the International Association for the Study of Obesity. 2004 Dec;28 Suppl 4:S22-8. PubMed PMID: 15592482.

11.   Virtue S, Vidal-Puig A. Adipose tissue expandability, lipotoxicity and the Metabolic Syndrome--an allostatic perspective. Biochimica et biophysica acta. 2010 Mar;1801(3):338-49. PubMed PMID: 20056169.

12.   Sjostrom L, Lindroos AK, Peltonen M, Torgerson J, Bouchard C, Carlsson B, et al. Lifestyle, diabetes, and cardiovascular risk factors 10 years after bariatric surgery. The New England journal of medicine. 2004 Dec 23;351(26):2683-93. PubMed PMID: 15616203.

13.   van Baak MA. Physical activity and energy balance. Public health nutrition. 1999 Sep;2(3A):335-9. PubMed PMID: 10610070.

14.   Colman E. Dinitrophenol and obesity: an early twentieth-century regulatory dilemma. Regulatory toxicology and pharmacology : RTP. 2007 Jul;48(2):115-7. PubMed PMID: 17475379.

References

_____

15.   Cannon B, Nedergaard J. Thermogenesis challenges the adipostat hypothesis for body-weight control. The Proceedings of the Nutrition Society. 2009 Nov;68(4):401-7. PubMed PMID: 19775494.

16.   Cannon B, Nedergaard J. Brown adipose tissue: function and physiological significance. Physiological reviews. 2004 Jan;84(1):277-359. PubMed PMID: 14715917.

17.   Vallerand AL, Lupien J, Bukowiecki LJ. Cold exposure reverses the diabetogenic effects of high-fat feeding. Diabetes. 1986 Mar;35(3):329-34. PubMed PMID: 3005094.

18.   Himms-Hagen J, Cui J, Danforth E, Jr., Taatjes DJ, Lang SS, Waters BL, et al. Effect of CL-316,243, a thermogenic beta 3-agonist, on energy balance and brown and white adipose tissues in rats. The American journal of physiology. 1994 Apr;266(4 Pt 2):R1371-82. PubMed PMID: 7910436.

19.   Arbeeny CM, Meyers DS, Hillyer DE, Bergquist KE. Metabolic alterations associated with the antidiabetic effect of beta 3-adrenergic receptor agonists in obese mice. The American journal of physiology. 1995 Apr;268(4 Pt 1):E678-84. PubMed PMID: 7733267.

20.   Smith RE, Horwitz BA. Brown fat and thermogenesis. Physiological reviews. 1969 Apr;49(2):330-425. PubMed PMID: 4888392.

21.   Cinti S. The adipose organ. Prostaglandins, leukotrienes, and essential fatty acids. 2005 Jul;73(1):9-15. PubMed PMID: 15936182.

22.   Stock MJ. The role of brown adipose tissue in diet-induced thermogenesis. The Proceedings of the Nutrition Society. 1989 Jul;48(2):189-96. PubMed PMID: 2678114.

23.   Kozak LP. Brown fat and the myth of diet-induced thermogenesis. Cell metabolism. 2010 Apr 7;11(4):263-7. PubMed PMID: 20374958. Pubmed Central PMCID: 2867325.

24.   Ma SW, Foster DO, Nadeau BE, Triandafillou J. Absence of increased oxygen consumption in brown adipose tissue of rats exhibiting "cafeteria" diet-induced thermogenesis. Canadian journal of physiology and pharmacology. 1988 Nov;66(11):1347-54. PubMed PMID: 3242772.

25.   Anunciado-Koza R, Ukropec J, Koza RA, Kozak LP. Inactivation of UCP1 and the glycerol phosphate cycle synergistically increases energy expenditure to resist diet-induced obesity. The Journal of biological chemistry. 2008 Oct 10;283(41):27688-97. PubMed PMID: 18678870. Pubmed Central PMCID: 2562063.

26.   Harms M, Seale P. Brown and beige fat: development, function and therapeutic potential. Nature medicine. 2013 Oct;19(10):1252-63. PubMed PMID: 24100998.

27.   Kajimura S, Spiegelman BM, Seale P. Brown and Beige Fat: Physiological Roles beyond Heat Generation. Cell metabolism. 2015 Oct 6;22(4):546-59. PubMed PMID: 26445512. Pubmed Central PMCID: 4613812.

28.   Schulz TJ, Tseng YH. Brown adipose tissue: development, metabolism and beyond. The Biochemical journal. 2013 Jul 15;453(2):167-78. PubMed PMID: 23805974. Pubmed Central PMCID: 3887508.

29.   Hudak CS, Gulyaeva O, Wang Y, Park SM, Lee L, Kang C, et al. Pref-1 marks very early mesenchymal precursors required for adipose tissue development and expansion. Cell reports. 2014 Aug 7;8(3):678-87. PubMed PMID: 25088414. Pubmed Central PMCID: 4138044.

30.   Wang W, Seale P. Control of brown and beige fat development. Nature reviews Molecular cell biology. 2016 Nov;17(11):691-702. PubMed PMID: 27552974. Pubmed Central PMCID: 5627770.

31.   Seale P, Bjork B, Yang W, Kajimura S, Chin S, Kuang S, et al. PRDM16 controls a brown fat/skeletal muscle switch. Nature. 2008 Aug 21;454(7207):961-7. PubMed PMID: 18719582. Pubmed Central PMCID: 2583329.

32.   Ohno H, Shinoda K, Ohyama K, Sharp LZ, Kajimura S. EHMT1 controls brown adipose cell fate and thermogenesis through the PRDM16 complex. Nature. 2013 Dec 5;504(7478):163-7. PubMed PMID: 24196706. Pubmed Central PMCID: 3855638.

33.   Wang W, Kissig M, Rajakumari S, Huang L, Lim HW, Won KJ, et al. Ebf2 is a selective marker of brown and beige adipogenic precursor cells. Proceedings of the National Academy of Sciences of the United States of America. 2014 Oct 7;111(40):14466-71. PubMed PMID: 25197048. Pubmed Central PMCID: 4209986.

34.   Rosenwald M, Perdikari A, Rulicke T, Wolfrum C. Bi-directional interconversion of brite and white adipocytes. Nature cell biology. 2013 Jun;15(6):659-67. PubMed PMID: 23624403.

35.   Ghorbani M, Himms-Hagen J. Appearance of brown adipocytes in white adipose tissue during CL 316,243-induced reversal of obesity and diabetes in Zucker fa/fa rats. International journal of obesity and related metabolic disorders : journal of the International Association for the Study of Obesity. 1997 Jun;21(6):465-75. PubMed PMID: 9192230.

36.   Wang QA, Tao C, Gupta RK, Scherer PE. Tracking adipogenesis during white adipose tissue development, expansion and regeneration. Nature medicine. 2013 Oct;19(10):1338-44. PubMed PMID: 23995282. Pubmed Central PMCID: 4075943.

37.   Xue Y, Petrovic N, Cao R, Larsson O, Lim S, Chen S, et al. Hypoxia-independent angiogenesis in adipose tissues during cold acclimation. Cell metabolism. 2009 Jan 7;9(1):99-109. PubMed PMID: 19117550.

38.   De Matteis R, Ricquier D, Cinti S. TH-, NPY-, SP-, and CGRP-immunoreactive nerves in interscapular brown adipose tissue of adult rats acclimated at different temperatures: an immunohistochemical study. Journal of neurocytology. 1998 Dec;27(12):877-86. PubMed PMID: 10659680.

39.   Murphy KT, Schwartz GJ, Nguyen NL, Mendez JM, Ryu V, Bartness TJ. Leptin-sensitive sensory nerves innervate white fat. American journal of physiology Endocrinology and metabolism. 2013 Jun 15;304(12):E1338-47. PubMed PMID: 23612999. Pubmed Central PMCID: 3680695.

40.   Giordano A, Frontini A, Castellucci M, Cinti S. Presence and distribution of cholinergic nerves in rat mediastinal brown adipose tissue. The journal of histochemistry and cytochemistry : official journal of the Histochemistry Society. 2004 Jul;52(7):923-30. PubMed PMID: 15208359.

41.   Schafer MK, Eiden LE, Weihe E. Cholinergic neurons and terminal fields revealed by immunohistochemistry for the vesicular acetylcholine transporter. II. The peripheral nervous system. Neuroscience. 1998 May;84(2):361-76. PubMed PMID: 9539210.

42.   Bartness TJ, Liu Y, Shrestha YB, Ryu V. Neural innervation of white adipose tissue and the control of lipolysis. Frontiers in neuroendocrinology. 2014 Oct;35(4):473-93. PubMed PMID: 24736043. Pubmed Central PMCID: 4175185.

_____

43.   Liu C, Bookout AL, Lee S, Sun K, Jia L, Lee C, et al. PPARgamma in vagal neurons regulates high-fat diet induced thermogenesis. Cell metabolism. 2014 Apr 1;19(4):722-30. PubMed PMID: 24703703. Pubmed Central PMCID: 4046333.

44.   Dodd GT, Decherf S, Loh K, Simonds SE, Wiede F, Balland E, et al. Leptin and insulin act on POMC neurons to promote the browning of white fat. Cell. 2015 Jan 15;160(1-2):88-104. PubMed PMID: 25594176. Pubmed Central PMCID: 4453004.

45.   Ruan HB, Dietrich MO, Liu ZW, Zimmer MR, Li MD, Singh JP, et al. O-GlcNAc transferase enables AgRP neurons to suppress browning of white fat. Cell. 2014 Oct 9;159(2):306-17. PubMed PMID: 25303527. Pubmed Central PMCID: 4509746.

46.   Murano I, Barbatelli G, Giordano A, Cinti S. Noradrenergic parenchymal nerve fiber branching after cold acclimatisation correlates with brown adipocyte density in mouse adipose organ. Journal of anatomy. 2009 Jan;214(1):171-8. PubMed PMID: 19018882. Pubmed Central PMCID: 2667925.

47.   Zhang W, Bi S. Hypothalamic Regulation of Brown Adipose Tissue Thermogenesis and Energy Homeostasis. Frontiers in endocrinology. 2015;6:136. PubMed PMID: 26379628. Pubmed Central PMCID: 4553396.

48.   Sellayah D, Bharaj P, Sikder D. Orexin is required for brown adipose tissue development, differentiation, and function. Cell metabolism. 2011 Oct 5;14(4):478-90. PubMed PMID: 21982708.

49.   Monda M, Viggiano AN, Viggiano A, Viggiano E, Lanza A, De Luca V. Hyperthermic reactions induced by orexin A: role of the ventromedial hypothalamus. The European journal of neuroscience. 2005 Sep;22(5):1169-75. PubMed PMID: 16176359.

50.   Martins L, Seoane-Collazo P, Contreras C, Gonzalez-Garcia I, Martinez-Sanchez N, Gonzalez F, et al. A Functional Link between AMPK and Orexin Mediates the Effect of BMP8B on Energy Balance. Cell reports. 2016 Aug 23;16(8):2231-42. PubMed PMID: 27524625. Pubmed Central PMCID: 4999418.

51.   Whittle AJ, Carobbio S, Martins L, Slawik M, Hondares E, Vazquez MJ, et al. BMP8B increases brown adipose tissue thermogenesis through both central and peripheral actions. Cell. 2012 May 11;149(4):871-85. PubMed PMID: 22579288. Pubmed Central PMCID: 3383997.

52.   Zaretskaia MV, Zaretsky DV, Shekhar A, DiMicco JA. Chemical stimulation of the dorsomedial hypothalamus evokes non-shivering thermogenesis in anesthetized rats. Brain research. 2002 Feb 22;928(1-2):113-25. PubMed PMID: 11844478.

53.   Lee SJ, Sanchez-Watts G, Krieger JP, Pignalosa A, Norell PN, Cortella A, et al. Loss of dorsomedial hypothalamic GLP-1 signaling reduces BAT thermogenesis and increases adiposity. Molecular metabolism. 2018 May;11:33-46. PubMed PMID: 29650350. Pubmed Central PMCID: 6001878.

54.   Bartness TJ, Vaughan CH, Song CK. Sympathetic and sensory innervation of brown adipose tissue. International journal of obesity. 2010 Oct;34 Suppl 1:S36-42. PubMed PMID: 20935665. Pubmed Central PMCID: 3999344.

55.   Fedorenko A, Lishko PV, Kirichok Y. Mechanism of fatty-acid-dependent UCP1 uncoupling in brown fat mitochondria. Cell. 2012 Oct 12;151(2):400-13. PubMed PMID: 23063128. Pubmed Central PMCID: 3782081.

56.   Nisoli E, Tonello C, Benarese M, Liberini P, Carruba MO. Expression of nerve growth factor in brown adipose tissue: implications for thermogenesis and obesity. Endocrinology. 1996 Feb;137(2):495-503. PubMed PMID: 8593794.

57.   Sornelli F, Fiore M, Chaldakov GN, Aloe L. Adipose tissue-derived nerve growth factor and brain-derived neurotrophic factor: results from experimental stress and diabetes. General physiology and biophysics. 2009;28 Spec No:179-83. PubMed PMID: 19893098.

58.   Nakagawa T, Tsuchida A, Itakura Y, Nonomura T, Ono M, Hirota F, et al. Brain-derived neurotrophic factor regulates glucose metabolism by modulating energy balance in diabetic mice. Diabetes. 2000 Mar;49(3):436-44. PubMed PMID: 10868966.

59.   Tsuchida A, Nonomura T, Ono-Kishino M, Nakagawa T, Taiji M, Noguchi H. Acute effects of brain-derived neurotrophic factor on energy expenditure in obese diabetic mice. International journal of obesity and related metabolic disorders : journal of the International Association for the Study of Obesity. 2001 Sep;25(9):1286-93. PubMed PMID: 11571589.

60.   Fiore R, Puschel AW. The function of semaphorins during nervous system development. Frontiers in bioscience : a journal and virtual library. 2003 May 1;8:s484-99. PubMed PMID: 12700098.

61.   Giordano A, Coppari R, Castellucci M, Cinti S. Sema3a is produced by brown adipocytes and its secretion is reduced following cold acclimation. Journal of neurocytology. 2001 Jan;30(1):5-10. PubMed PMID: 11577241.

62.   Mejhert N, Wilfling F, Esteve D, Galitzky J, Pellegrinelli V, Kolditz CI, et al. Semaphorin 3C is a novel adipokine linked to extracellular matrix composition. Diabetologia. 2013 Aug;56(8):1792-801. PubMed PMID: 23666167.

63.   Wang GX, Zhao XY, Meng ZX, Kern M, Dietrich A, Chen Z, et al. The brown fat-enriched secreted factor Nrg4 preserves metabolic homeostasis through attenuation of hepatic lipogenesis. Nature medicine. 2014 Dec;20(12):1436-43. PubMed PMID: 25401691. Pubmed Central PMCID: 4257907.

64.   Rosell M, Kaforou M, Frontini A, Okolo A, Chan YW, Nikolopoulou E, et al. Brown and white adipose tissues: intrinsic differences in gene expression and response to cold exposure in mice. American journal of physiology Endocrinology and metabolism. 2014 Apr 15;306(8):E945-64. PubMed PMID: 24549398. Pubmed Central PMCID: 3989735.

65.   Pellegrinelli V, Peirce VJ, Howard L, Virtue S, Turei D, Senzacqua M, et al. Adipocyte-secreted BMP8b mediates adrenergic-induced remodeling of the neuro-vascular network in adipose tissue. Nature communications. 2018 Nov 26;9(1):4974. PubMed PMID: 30478315. Pubmed Central PMCID: 6255810.

66.   Obregon MJ. Adipose tissues and thyroid hormones. Frontiers in physiology. 2014;5:479. PubMed PMID: 25566082. Pubmed Central PMCID: 4263094.

67.   Brent GA. Mechanisms of thyroid hormone action. The Journal of clinical investigation. 2012 Sep;122(9):3035-43. PubMed PMID: 22945636. Pubmed Central PMCID: 3433956.

68.   Bianco AC, McAninch EA. The role of thyroid hormone and brown adipose tissue in energy homoeostasis. The lancet Diabetes & endocrinology. 2013 Nov;1(3):250-8. PubMed PMID: 24622373. Pubmed Central PMCID: 4976626.

References

_____

69.   Christoffolete MA, Linardi CC, de Jesus L, Ebina KN, Carvalho SD, Ribeiro MO, et al. Mice with targeted disruption of the Dio2 gene have cold-induced overexpression of the uncoupling protein 1 gene but fail to increase brown adipose tissue lipogenesis and adaptive thermogenesis. Diabetes. 2004 Mar;53(3):577-84. PubMed PMID: 14988240.

70.   Weiner J, Kranz M, Kloting N, Kunath A, Steinhoff K, Rijntjes E, et al. Thyroid hormone status defines brown adipose tissue activity and browning of white adipose tissues in mice. Scientific reports. 2016 Dec 12;6:38124. PubMed PMID: 27941950. Pubmed Central PMCID: 5150531.

71.   Hondares E, Iglesias R, Giralt A, Gonzalez FJ, Giralt M, Mampel T, et al. Thermogenic activation induces FGF21 expression and release in brown adipose tissue. The Journal of biological chemistry. 2011 Apr 15;286(15):12983-90. PubMed PMID: 21317437. Pubmed Central PMCID: 3075644.

72.   Fisher FM, Kleiner S, Douris N, Fox EC, Mepani RJ, Verdeguer F, et al. FGF21 regulates PGC-1alpha and browning of white adipose tissues in adaptive thermogenesis. Genes & development. 2012 Feb 1;26(3):271-81. PubMed PMID: 22302939. Pubmed Central PMCID: 3278894.

73.   Keipert S, Kutschke M, Ost M, Schwarzmayr T, van Schothorst EM, Lamp D, et al. Long-Term Cold Adaptation Does Not Require FGF21 or UCP1. Cell metabolism. 2017 Aug 1;26(2):437-46 e5. PubMed PMID: 28768181.

74.   Veniant MM, Sivits G, Helmering J, Komorowski R, Lee J, Fan W, et al. Pharmacologic Effects of FGF21 Are Independent of the "Browning" of White Adipose Tissue. Cell metabolism. 2015 May 5;21(5):731-8. PubMed PMID: 25955208.

75.   Ameka M, Markan KR, Morgan DA, BonDurant LD, Idiga SO, Naber MC, et al. Liver Derived FGF21 Maintains Core Body Temperature During Acute Cold Exposure. Scientific reports. 2019 Jan 24;9(1):630. PubMed PMID: 30679672. Pubmed Central PMCID: 6345819.

76.   Worthmann A, John C, Ruhlemann MC, Baguhl M, Heinsen FA, Schaltenberg N, et al. Cold-induced conversion of cholesterol to bile acids in mice shapes the gut microbiome and promotes adaptive thermogenesis. Nature medicine. 2017 Jul;23(7):839-49. PubMed PMID: 28604703.

77.   Watanabe M, Houten SM, Mataki C, Christoffolete MA, Kim BW, Sato H, et al. Bile acids induce energy expenditure by promoting intracellular thyroid hormone activation. Nature. 2006 Jan 26;439(7075):484-9. PubMed PMID: 16400329.

78.   Velazquez-Villegas LA, Perino A, Lemos V, Zietak M, Nomura M, Pols TWH, et al. TGR5 signalling promotes mitochondrial fission and beige remodelling of white adipose tissue. Nature communications. 2018 Jan 16;9(1):245. PubMed PMID: 29339725. Pubmed Central PMCID: 5770450.

79.   Long JZ, Roche AM, Berdan CA, Louie SM, Roberts AJ, Svensson KJ, et al. Ablation of PM20D1 reveals N-acyl amino acid control of metabolism and nociception. Proceedings of the National Academy of Sciences of the United States of America. 2018 Jul 17;115(29):E6937-E45. PubMed PMID: 29967167. Pubmed Central PMCID: 6055169.

80.   Long JZ, Svensson KJ, Bateman LA, Lin H, Kamenecka T, Lokurkar IA, et al. The Secreted Enzyme PM20D1 Regulates Lipidated Amino Acid Uncouplers of Mitochondria.

Cell. 2016 Jul 14;166(2):424-35. PubMed PMID: 27374330. Pubmed Central PMCID: 4947008.

81.   Glick Z. Inverse relationship between brown fat thermogenesis and meal size: the thermostatic control of food intake revisited. Physiology & behavior. 1982 Dec;29(6):1137-40. PubMed PMID: 7163393.

82.   Saito M. Brown adipose tissue as a regulator of energy expenditure and body fat in humans. Diabetes & metabolism journal. 2013 Feb;37(1):22-9. PubMed PMID: 23441053. Pubmed Central PMCID: 3579148.

83.   M UD, Saari T, Raiko J, Kudomi N, Maurer SF, Lahesmaa M, et al. Postprandial Oxidative Metabolism of Human Brown Fat Indicates Thermogenesis. Cell metabolism. 2018 Aug 7;28(2):207-16 e3. PubMed PMID: 29909972.

84.   Kelsey R. BAT is involved in control of satiation. Nature reviews Endocrinology. 2018 Dec;15(1):1. PubMed PMID: 30487533.

85.   Beiroa D, Imbernon M, Gallego R, Senra A, Herranz D, Villarroya F, et al. GLP-1 agonism stimulates brown adipose tissue thermogenesis and browning through hypothalamic AMPK. Diabetes. 2014 Oct;63(10):3346-58. PubMed PMID: 24917578.

86.   Blouet C, Schwartz GJ. Duodenal lipid sensing activates vagal afferents to regulate non-shivering brown fat thermogenesis in rats. PloS one. 2012;7(12):e51898. PubMed PMID: 23251649. Pubmed Central PMCID: 3522613.

87.   Li Y, Schnabl K, Gabler SM, Willershauser M, Reber J, Karlas A, et al. Secretin-Activated Brown Fat Mediates Prandial Thermogenesis to Induce Satiation. Cell. 2018 Nov 29;175(6):1561-74 e12. PubMed PMID: 30449620.

88.   Dodd GT, Andrews ZB, Simonds SE, Michael NJ, DeVeer M, Bruning JC, et al. A Hypothalamic Phosphatase Switch Coordinates Energy Expenditure with Feeding. Cell metabolism. 2017 Aug 1;26(2):375-93 e7. PubMed PMID: 28768176.

89.   Nguyen KD, Qiu Y, Cui X, Goh YP, Mwangi J, David T, et al. Alternatively activated macrophages produce catecholamines to sustain adaptive thermogenesis. Nature. 2011 Nov 20;480(7375):104-8. PubMed PMID: 22101429. Pubmed Central PMCID: 3371761.

90.   Wolf Y, Boura-Halfon S, Cortese N, Haimon Z, Sar Shalom H, Kuperman Y, et al. Brown-adipose-tissue macrophages control tissue innervation and homeostatic energy expenditure. Nature immunology. 2017 Jun;18(6):665-74. PubMed PMID: 28459435. Pubmed Central PMCID: 5438596.

91.   Fischer K, Ruiz HH, Jhun K, Finan B, Oberlin DJ, van der Heide V, et al. Alternatively activated macrophages do not synthesize catecholamines or contribute to adipose tissue adaptive thermogenesis. Nature medicine. 2017 May;23(5):623-30. PubMed PMID: 28414329. Pubmed Central PMCID: 5420449.

92.   Nedergaard J, Bengtsson T, Cannon B. Unexpected evidence for active brown adipose tissue in adult humans. American journal of physiology Endocrinology and metabolism. 2007 Aug;293(2):E444-52. PubMed PMID: 17473055.

93.   Hany TF, Gharehpapagh E, Kamel EM, Buck A, Himms-Hagen J, von Schulthess GK. Brown adipose tissue: a factor to consider in symmetrical tracer uptake in the neck and upper chest region. European journal of nuclear medicine and molecular imaging. 2002 Oct;29(10):1393-8. PubMed PMID: 12271425.

_____

94.   Hu HH, Tovar JP, Pavlova Z, Smith ML, Gilsanz V. Unequivocal identification of brown adipose tissue in a human infant. Journal of magnetic resonance imaging : JMRI. 2012 Apr;35(4):938-42. PubMed PMID: 22180228. Pubmed Central PMCID: 3310283.

95.   Carpentier AC, Blondin DP, Virtanen KA, Richard D, Haman F, Turcotte EE. Brown Adipose Tissue Energy Metabolism in Humans. Frontiers in endocrinology. 2018;9:447. PubMed PMID: 30131768. Pubmed Central PMCID: 6090055.

96.   Lidell ME, Betz MJ, Dahlqvist Leinhard O, Heglind M, Elander L, Slawik M, et al. Evidence for two types of brown adipose tissue in humans. Nature medicine. 2013 May;19(5):631-4. PubMed PMID: 23603813.

97.   Cypess AM, White AP, Vernochet C, Schulz TJ, Xue R, Sass CA, et al. Anatomical localization, gene expression profiling and functional characterization of adult human neck brown fat. Nature medicine. 2013 May;19(5):635-9. PubMed PMID: 23603815. Pubmed Central PMCID: 3650129.

98.   Au-Yong IT, Thorn N, Ganatra R, Perkins AC, Symonds ME. Brown adipose tissue and seasonal variation in humans. Diabetes. 2009 Nov;58(11):2583-7. PubMed PMID: 19696186. Pubmed Central PMCID: 2768171.

99.   Barnum KJ, O'Connell MJ. Cell cycle regulation by checkpoints. Methods in molecular biology. 2014;1170:29-40. PubMed PMID: 24906307. Pubmed Central PMCID: 4990352.

100.   Pavletich NP. Mechanisms of cyclin-dependent kinase regulation: structures of Cdks, their cyclin activators, and Cip and INK4 inhibitors. Journal of molecular biology. 1999 Apr 16;287(5):821-8. PubMed PMID: 10222191.

101.   Malumbres M, Harlow E, Hunt T, Hunter T, Lahti JM, Manning G, et al. Cyclin-dependent kinases: a family portrait. Nature cell biology. 2009 Nov;11(11):1275-6. PubMed PMID: 19884882. Pubmed Central PMCID: 2914104.

102.   Satyanarayana A, Kaldis P. Mammalian cell-cycle regulation: several Cdks, numerous cyclins and diverse compensatory mechanisms. Oncogene. 2009 Aug 20;28(33):2925-39. PubMed PMID: 19561645.

103.   Malumbres M. Cyclin-dependent kinases. Genome biology. 2014;15(6):122. PubMed PMID: 25180339. Pubmed Central PMCID: 4097832.

104.   Malumbres M, Barbacid M. Mammalian cyclin-dependent kinases. Trends in biochemical sciences. 2005 Nov;30(11):630-41. PubMed PMID: 16236519.

105.   Malumbres M, Barbacid M. Cell cycle, CDKs and cancer: a changing paradigm. Nature reviews Cancer. 2009 Mar;9(3):153-66. PubMed PMID: 19238148.

106.   Besson A, Dowdy SF, Roberts JM. CDK inhibitors: cell cycle regulators and beyond. Developmental cell. 2008 Feb;14(2):159-69. PubMed PMID: 18267085.

107.   Blanchet E, Annicotte JS, Fajas L. Cell cycle regulators in the control of metabolism. Cell cycle. 2009 Dec 15;8(24):4029-31. PubMed PMID: 19946202. Pubmed Central PMCID: 3323501.

108.   Aguilar V, Fajas L. Cycling through metabolism. EMBO molecular medicine. 2010 Sep;2(9):338-48. PubMed PMID: 20721988. Pubmed Central PMCID: 3118222.

109.   Fajas L. Re-thinking cell cycle regulators: the cross-talk with metabolism. Frontiers in oncology. 2013;3:4. PubMed PMID: 23355973. Pubmed Central PMCID: 3555080.

References

_____

110.   Lopez-Mejia IC, Fajas L. Cell cycle regulation of mitochondrial function. Current opinion in cell biology. 2015 Apr;33:19-25. PubMed PMID: 25463842.

111.   Lopez-Mejia IC, Castillo-Armengol J, Lagarrigue S, Fajas L. Role of cell cycle regulators in adipose tissue and whole body energy homeostasis. Cellular and molecular life sciences : CMLS. 2018 Mar;75(6):975-87. PubMed PMID: 28988292.

112.   Fajas L, Landsberg RL, Huss-Garcia Y, Sardet C, Lees JA, Auwerx J. E2Fs regulate adipocyte differentiation. Developmental cell. 2002 Jul;3(1):39-49. PubMed PMID: 12110166.

113.   Galderisi U, Cipollaro M, Giordano A. The retinoblastoma gene is involved in multiple aspects of stem cell biology. Oncogene. 2006 Aug 28;25(38):5250-6. PubMed PMID: 16936744.

114.   Abella A, Dubus P, Malumbres M, Rane SG, Kiyokawa H, Sicard A, et al. Cdk4 promotes adipogenesis through PPARgamma activation. Cell metabolism. 2005 Oct;2(4):239-49. PubMed PMID: 16213226.

115.   Sarruf DA, Iankova I, Abella A, Assou S, Miard S, Fajas L. Cyclin D3 promotes adipogenesis through activation of peroxisome proliferator-activated receptor gamma. Molecular and cellular biology. 2005 Nov;25(22):9985-95. PubMed PMID: 16260612. Pubmed Central PMCID: 1280250.

116.   Phelps DE, Xiong Y. Regulation of cyclin-dependent kinase 4 during adipogenesis involves switching of cyclin D subunits and concurrent binding of p18INK4c and p27Kip1. Cell growth & differentiation : the molecular biology journal of the American Association for Cancer Research. 1998 Aug;9(8):595-610. PubMed PMID: 9716177.

117.   Fajas L, Annicotte JS, Miard S, Sarruf D, Watanabe M, Auwerx J. Impaired pancreatic growth, beta cell mass, and beta cell function in E2F1 (-/-)mice. The Journal of clinical investigation. 2004 May;113(9):1288-95. PubMed PMID: 15124020. Pubmed Central PMCID: 398423.

118.   Blanchet E, Annicotte JS, Lagarrigue S, Aguilar V, Clape C, Chavey C, et al. E2F transcription factor-1 regulates oxidative metabolism. Nature cell biology. 2011 Aug 14;13(9):1146-52. PubMed PMID: 21841792. Pubmed Central PMCID: 3849758.

119.   Dali-Youcef N, Mataki C, Coste A, Messaddeq N, Giroud S, Blanc S, et al. Adipose tissue-specific inactivation of the retinoblastoma protein protects against diabesity because of increased energy expenditure. Proceedings of the National Academy of Sciences of the United States of America. 2007 Jun 19;104(25):10703-8. PubMed PMID: 17556545. Pubmed Central PMCID: 1965576.

120.   Petrov PD, Ribot J, Palou A, Bonet ML. Improved metabolic regulation is associated with retinoblastoma protein gene haploinsufficiency in mice. American journal of physiology Endocrinology and metabolism. 2015 Jan 15;308(2):E172-83. PubMed PMID: 25406261.

121.   Scime A, Grenier G, Huh MS, Gillespie MA, Bevilacqua L, Harper ME, et al. Rb and p107 regulate preadipocyte differentiation into white versus brown fat through repression of PGC-1alpha. Cell metabolism. 2005 Nov;2(5):283-95. PubMed PMID: 16271529.

122.   Vormer TL, Wojciechowicz K, Dekker M, de Vries S, van der Wal A, Delzenne-Goette E, et al. RB family tumor suppressor activity may not relate to active silencing of

E2F target genes. Cancer research. 2014 Sep 15;74(18):5266-76. PubMed PMID: 25056122.

123. Classon M, Kennedy BK, Mulloy R, Harlow E. Opposing roles of pRB and p107 in adipocyte differentiation. Proceedings of the National Academy of Sciences of the United States of America. 2000 Sep 26;97(20):10826-31. PubMed PMID: 10995476. Pubmed Central PMCID: 27108.

124. Fajas L, Egler V, Reiter R, Hansen J, Kristiansen K, Debril MB, et al. The retinoblastoma-histone deacetylase 3 complex inhibits PPARgamma and adipocyte differentiation. Developmental cell. 2002 Dec;3(6):903-10. PubMed PMID: 12479814.

125. Rane SG, Dubus P, Mettus RV, Galbreath EJ, Boden G, Reddy EP, et al. Loss of Cdk4 expression causes insulin-deficient diabetes and Cdk4 activation results in beta-islet cell hyperplasia. Nature genetics. 1999 May;22(1):44-52. PubMed PMID: 10319860.

126. Lee Y, Dominy JE, Choi YJ, Jurczak M, Tolliday N, Camporez JP, et al. Cyclin D1-Cdk4 controls glucose metabolism independently of cell cycle progression. Nature. 2014 Jun 26;510(7506):547-51. PubMed PMID: 24870244. Pubmed Central PMCID: 4076706.

127. Lagarrigue S, Lopez-Mejia IC, Denechaud PD, Escote X, Castillo-Armengol J, Jimenez V, et al. CDK4 is an essential insulin effector in adipocytes. The Journal of clinical investigation. 2016 Jan;126(1):335-48. PubMed PMID: 26657864. Pubmed Central PMCID: 4701556.

128. Lopez-Mejia IC, Lagarrigue S, Giralt A, Martinez-Carreres L, Zanou N, Denechaud PD, et al. CDK4 Phosphorylates AMPKalpha2 to Inhibit Its Activity and Repress Fatty Acid Oxidation. Molecular cell. 2017 Oct 19;68(2):336-49 e6. PubMed PMID: 29053957.

129. Molchadsky A, Shats I, Goldfinger N, Pevsner-Fischer M, Olson M, Rinon A, et al. p53 plays a role in mesenchymal differentiation programs, in a cell fate dependent manner. PloS one. 2008;3(11):e3707. PubMed PMID: 19002260. Pubmed Central PMCID: 2577894.

130. Van De Pette M, Tunster SJ, McNamara GI, Shelkovnikova T, Millership S, Benson L, et al. Cdkn1c Boosts the Development of Brown Adipose Tissue in a Murine Model of Silver Russell Syndrome. PLoS genetics. 2016 Mar;12(3):e1005916. PubMed PMID: 26963625. Pubmed Central PMCID: 4786089.

131. Gereben B, Zavacki AM, Ribich S, Kim BW, Huang SA, Simonides WS, et al. Cellular and molecular basis of deiodinase-regulated thyroid hormone signaling. Endocrine reviews. 2008 Dec;29(7):898-938. PubMed PMID: 18815314. Pubmed Central PMCID: 2647704.

132. Perlman RL, Chalfie M. Catecholamine release from the adrenal medulla. Clinics in endocrinology and metabolism. 1977 Nov;6(3):551-76. PubMed PMID: 338214.

133. Wong DL. Epinephrine biosynthesis: hormonal and neural control during stress. Cellular and molecular neurobiology. 2006 Jul-Aug;26(4-6):891-900. PubMed PMID: 16645894.

134. Sellayah D, Sikder D. Orexin restores aging-related brown adipose tissue dysfunction in male mice. Endocrinology. 2014 Feb;155(2):485-501. PubMed PMID: 24248466.

135. Hansen JB, Kristiansen K. Regulatory circuits controlling white versus brown adipocyte differentiation. The Biochemical journal. 2006 Sep 1;398(2):153-68. PubMed PMID: 16898874. Pubmed Central PMCID: 1550312.

_____

136. McDonald RB, Horwitz BA, Hamilton JS, Stern JS. Cold- and norepinephrine-induced thermogenesis in younger and older Fischer 344 rats. The American journal of physiology. 1988 Mar;254(3 Pt 2):R457-62. PubMed PMID: 3348440.

137. Annicotte JS, Blanchet E, Chavey C, Iankova I, Costes S, Assou S, et al. The CDK4-pRB-E2F1 pathway controls insulin secretion. Nature cell biology. 2009 Aug;11(8):1017-23. PubMed PMID: 19597485. Pubmed Central PMCID: 2824657.

138. Stanford KI, Goodyear LJ. The therapeutic potential of brown adipose tissue. Hepatobiliary surgery and nutrition. 2013 Oct;2(5):286-7. PubMed PMID: 24570961. Pubmed Central PMCID: 3924699.

139. Bhatt PS, Dhillo WS, Salem V. Human brown adipose tissue-function and therapeutic potential in metabolic disease. Current opinion in pharmacology. 2017 Dec;37:1-9. PubMed PMID: 28800407.

140. Trayhurn P. Brown Adipose Tissue-A Therapeutic Target in Obesity? Frontiers in physiology. 2018;9:1672. PubMed PMID: 30532712. Pubmed Central PMCID: 6265308.

141. Vitali A, Murano I, Zingaretti MC, Frontini A, Ricquier D, Cinti S. The adipose organ of obesity-prone C57BL/6J mice is composed of mixed white and brown adipocytes. Journal of lipid research. 2012 Apr;53(4):619-29. PubMed PMID: 22271685. Pubmed Central PMCID: 3307639.

142. Makowski L, Boord JB, Maeda K, Babaev VR, Uysal KT, Morgan MA, et al. Lack of macrophage fatty-acid-binding protein aP2 protects mice deficient in apolipoprotein E against atherosclerosis. Nature medicine. 2001 Jun;7(6):699-705. PubMed PMID: 11385507. Pubmed Central PMCID: 4027052.

143. Antonson P, Matic M, Portwood N, Kuiper RV, Bryzgalova G, Gao H, et al. aP2-Cre-mediated inactivation of estrogen receptor alpha causes hydrometra. PloS one. 2014;9(1):e85581. PubMed PMID: 24416430. Pubmed Central PMCID: 3885723.

144. Collins S, Surwit RS. The beta-adrenergic receptors and the control of adipose tissue metabolism and thermogenesis. Recent progress in hormone research. 2001;56:309-28. PubMed PMID: 11237219.

145. Atgie C, D'Allaire F, Bukowiecki LJ. Role of beta1- and beta3-adrenoceptors in the regulation of lipolysis and thermogenesis in rat brown adipocytes. The American journal of physiology. 1997 Oct;273(4 Pt 1):C1136-42. PubMed PMID: 9357756.

146. Rohrer DK. Physiological consequences of beta-adrenergic receptor disruption. Journal of molecular medicine. 1998 Oct;76(11):764-72. PubMed PMID: 9826121.

147. Susulic VS, Frederich RC, Lawitts J, Tozzo E, Kahn BB, Harper ME, et al. Targeted disruption of the beta 3-adrenergic receptor gene. The Journal of biological chemistry. 1995 Dec 8;270(49):29483-92. PubMed PMID: 7493988.

148. Paulo E, Wu D, Wang Y, Zhang Y, Wu Y, Swaney DL, et al. Sympathetic inputs regulate adaptive thermogenesis in brown adipose tissue through cAMP-Salt inducible kinase axis. Scientific reports. 2018 Jul 20;8(1):11001. PubMed PMID: 30030465. Pubmed Central PMCID: 6054673.

149. Wu Z, Puigserver P, Andersson U, Zhang C, Adelmant G, Mootha V, et al. Mechanisms controlling mitochondrial biogenesis and respiration through the thermogenic coactivator PGC-1. Cell. 1999 Jul 9;98(1):115-24. PubMed PMID: 10412986.

150. Klingenspor M, Ivemeyer M, Wiesinger H, Haas K, Heldmaier G, Wiesner RJ. Biogenesis of thermogenic mitochondria in brown adipose tissue of Djungarian

_____

hamsters during cold adaptation. The Biochemical journal. 1996 Jun 1;316 (Pt 2):607-13. PubMed PMID: 8687407. Pubmed Central PMCID: 1217391.

151.   Puigserver P, Wu Z, Park CW, Graves R, Wright M, Spiegelman BM. A cold-inducible coactivator of nuclear receptors linked to adaptive thermogenesis. Cell. 1998 Mar 20;92(6):829-39. PubMed PMID: 9529258.

152.   Weitzel JM, Iwen KA. Coordination of mitochondrial biogenesis by thyroid hormone. Molecular and cellular endocrinology. 2011 Aug 6;342(1-2):1-7. PubMed PMID: 21664416.

153.   Weitzel JM, Iwen KA, Seitz HJ. Regulation of mitochondrial biogenesis by thyroid hormone. Experimental physiology. 2003 Jan;88(1):121-8. PubMed PMID: 12552316.

154.   Yau WW, Singh BK, Lesmana R, Zhou J, Sinha RA, Wong KA, et al. Thyroid hormone (T3) stimulates brown adipose tissue activation via mitochondrial biogenesis and MTOR-mediated mitophagy. Autophagy. 2019 Jan;15(1):131-50. PubMed PMID: 30209975. Pubmed Central PMCID: 6287687.

155.   Chiamolera MI, Wondisford FE. Minireview: Thyrotropin-releasing hormone and the thyroid hormone feedback mechanism. Endocrinology. 2009 Mar;150(3):1091-6. PubMed PMID: 19179434.

156.   Sheehan MT. Biochemical Testing of the Thyroid: TSH is the Best and, Oftentimes, Only Test Needed - A Review for Primary Care. Clinical medicine & research. 2016 Jun;14(2):83-92. PubMed PMID: 27231117. Pubmed Central PMCID: 5321289.

157.   de Jesus LA, Carvalho SD, Ribeiro MO, Schneider M, Kim SW, Harney JW, et al. The type 2 iodothyronine deiodinase is essential for adaptive thermogenesis in brown adipose tissue. The Journal of clinical investigation. 2001 Nov;108(9):1379-85. PubMed PMID: 11696583. Pubmed Central PMCID: 209445.

158.   Scarpace PJ, Matheny M, Borst SE. Thermogenesis and mitochondrial GDP binding with age in response to the novel agonist CGP-12177A. The American journal of physiology. 1992 Feb;262(2 Pt 1):E185-90. PubMed PMID: 1539643.

159.   Lecoultre V, Ravussin E. Brown adipose tissue and aging. Current opinion in clinical nutrition and metabolic care. 2011 Jan;14(1):1-6. PubMed PMID: 21088572.

160.   Goncalves LF, Machado TQ, Castro-Pinheiro C, de Souza NG, Oliveira KJ, Fernandes-Santos C. Ageing is associated with brown adipose tissue remodelling and loss of white fat browning in female C57BL/6 mice. International journal of experimental pathology. 2017 Apr;98(2):100-8. PubMed PMID: 28543963. Pubmed Central PMCID: 5485357.

161.   Cannon B, Nedergaard J. Nonshivering thermogenesis and its adequate measurement in metabolic studies. The Journal of experimental biology. 2011 Jan 15;214(Pt 2):242-53. PubMed PMID: 21177944.

162.   Xu Q, Tam M, Anderson SA. Fate mapping Nkx2.1-lineage cells in the mouse telencephalon. The Journal of comparative neurology. 2008 Jan 1;506(1):16-29. PubMed PMID: 17990269.

163.   Ring LE, Zeltser LM. Disruption of hypothalamic leptin signaling in mice leads to early-onset obesity, but physiological adaptations in mature animals stabilize adiposity levels. The Journal of clinical investigation. 2010 Aug;120(8):2931-41. PubMed PMID: 20592471. Pubmed Central PMCID: 2912188.

164.   Iqbal NJ, Lu Z, Liu SM, Schwartz GJ, Chua S, Jr., Zhu L. Cyclin-dependent kinase 4 is a preclinical target for diet-induced obesity. JCI insight. 2018 Sep 6;3(17). PubMed PMID: 30185666. Pubmed Central PMCID: 6171799.

165.   Rabhi N, Hannou SA, Gromada X, Salas E, Yao X, Oger F, et al. Cdkn2a deficiency promotes adipose tissue browning. Molecular metabolism. 2018 Feb;8:65-76. PubMed PMID: 29237539. Pubmed Central PMCID: 5985036.

Appendix: Contributions and articles

Appendix: Contributions and articles
_____

125

Appendix: Contributions and articles

Throughout these years of research in the lab of Prof. Lluis Fajas, I had the chance to contribute to several research projects, which resulted in publications from which I am co-author of the manuscript. Most of them are already published but others are under revisions or submitted. All the manuscripts of these articles can be found in this appendix.

_____

CDK4 is an essential insulin effector in adipocytes

Lagarrigue S, Lopez-Mejia IC, Denechaud PD, Escoté X, **Castillo-Armengol J**, Jimenez V, Chavey C, Giralt A, Lai Q, Zhang L, Martinez-Carreres L, Delacuisine B, Annicotte JS, Blanchet E, Huré S, Abella A, Tinahones FJ, Vendrell J, Dubus P, Bosch F, Kahn CR, Fajas L.

This study describes a novel role of CDK4 in mature white adipocytes. CDK4 modulates create a positive feedback loop to maintain insulin signaling active. My contributions to this project included: analyzing the expression of phosphorylated IRS2 at the specific site of CDK4 (Ser188) by western blot in WAT samples from mice and performing experiments of colocalization of CDK4 and IRS2 in adipocytes (data not shown in the article).

CDK4 is an essential insulin effector in adipocytes

Sylviane Lagarrigue, … , C. Ronald Kahn, Lluis Fajas

Research Article   **Metabolism**

Insulin resistance is a fundamental pathogenic factor that characterizes various metabolic disorders, including obesity and type 2 diabetes. Adipose tissue contributes to the development of obesity-related insulin resistance through increased release of fatty acids, altered adipokine secretion, and/or macrophage infiltration and cytokine release. Here, we aimed to analyze the participation of the cyclin-dependent kinase 4 (CDK4) in adipose tissue biology. We determined that white adipose tissue (WAT) from CDK4-deficient mice exhibits impaired lipogenesis and increased lipolysis. Conversely, lipolysis was decreased and lipogenesis was increased in mice expressing a mutant hyperactive form of CDK4 (CDK4^{R24C}). A global kinome analysis of CDK4-deficient mice following insulin stimulation revealed that insulin signaling is impaired in these animals. We determined that insulin activates the CCND3-CDK4 complex, which in turn phosphorylates insulin receptor substrate 2 (IRS2) at serine 388, thereby creating a positive feedback loop that maintains adipocyte insulin signaling. Furthermore, we found that CCND3 expression and IRS2 serine 388 phosphorylation are increased in human obese subjects. Together, our results demonstrate that CDK4 is a major regulator of insulin signaling in WAT.

Find the latest version:

CDK4 is an essential insulin effector in adipocytes

Sylviane Lagarrigue,[1,2] Isabel C. Lopez-Mejia,[1] Pierre-Damien Denechaud,[1] Xavier Escoté,[1] Judit Castillo-Armengol,[1] Veronica Jimenez,[3] Carine Chavey,[2] Albert Giralt,[1] Qiuwen Lai,[1] Lianjun Zhang,[4] Laia Martinez-Carreres,[1] Brigitte Delacuisine,[1] Jean-Sébastien Annicotte,[2,5] Emilie Blanchet,[2] Sébastien Huré,[1,2] Anna Abella,[6] Francisco J. Tinahones,[7,8] Joan Vendrell,[9] Pierre Dubus,[10] Fatima Bosch,[3] C. Ronald Kahn,[11] and Lluis Fajas[1,2]

[1]Department of Physiology, Université de Lausanne, Lausanne, Switzerland. [2]Institut de Génétique Moléculaire de Montpellier (IGMM), Université de Montpellier, Montpellier, France. [3]Center of Animal Biotechnology and Gene Therapy and Department of Biochemistry and Molecular Biology, School of Veterinary Medicine, Universitat Autònoma de Barcelona, Bellaterra, and Centro de Investigación Biomédica en Red de Diabetes y Enfermedades Metabólicas Asociadas, Barcelona, Spain. [4]Translational Tumor Immunology, Ludwig Center for Cancer Research, Université de Lausanne, Epalinges, Switzerland. [5]European Genomic Institute for Diabetes, Université Lille Nord de France, UMR 8199 CNRS, Lille, France. [6]INSERM U834, Montpellier, France. [7]Unidad de Gestión Clínica de Endocrinología y Nutrición, Hospital Universitario Virgen de la Victoria, Málaga, Spain. [8]Centro de Investigación Biomédica en Red-Fisiopatología de la Obesidad y la Nutrición (CIBERobn CB06/003), Instituto de Salud Carlos III, Madrid, Spain. [9]CIBERDEM, Institut d'Investigació Pere Virgili, Universitat Rovira i Virgili, Hospital Universitari Joan XXIII, Tarragona, Spain. [10]EA2406, Histologie et pathologie moléculaire des tumeurs, Université de Bordeaux, Bordeaux, France. [11]Section on Integrative Physiology and Metabolism, Joslin Diabetes Center, Harvard Medical School, Boston, Massachusetts, USA.

Insulin resistance is a fundamental pathogenic factor that characterizes various metabolic disorders, including obesity and type 2 diabetes. Adipose tissue contributes to the development of obesity-related insulin resistance through increased release of fatty acids, altered adipokine secretion, and/or macrophage infiltration and cytokine release. Here, we aimed to analyze the participation of the cyclin-dependent kinase 4 (CDK4) in adipose tissue biology. We determined that white adipose tissue (WAT) from CDK4-deficient mice exhibits impaired lipogenesis and increased lipolysis. Conversely, lipolysis was decreased and lipogenesis was increased in mice expressing a mutant hyperactive form of CDK4 (CDK4^{R24C}). A global kinome analysis of CDK4-deficient mice following insulin stimulation revealed that insulin signaling is impaired in these animals. We determined that insulin activates the CCND3-CDK4 complex, which in turn phosphorylates insulin receptor substrate 2 (IRS2) at serine 388, thereby creating a positive feedback loop that maintains adipocyte insulin signaling. Furthermore, we found that CCND3 expression and IRS2 serine 388 phosphorylation are increased in human obese subjects. Together, our results demonstrate that CDK4 is a major regulator of insulin signaling in WAT.

Introduction

Insulin signaling is a versatile system that coordinates growth, proliferation, and development of multiple tissues and organs by controlling metabolic processes that accommodate the energy needs of cellular function (1). Defects in insulin signaling contribute to insulin resistance, a common complication of obesity that occurs early in the pathogenesis of type 2 diabetes and cardiovascular disease (2, 3). Insulin response depends on tissue and cellular functions. In white adipose tissue (WAT), insulin signaling regulates lipid synthesis (1) and glucose transport (4–6) and represses lipolysis (7). However, the exact mechanism by which insulin signaling coordinates regulated cellular functions is not fully understood. Cyclin-dependent kinase 4 (CDK4) plays an important role in the G$_1$/S transition of the cell cycle. Its kinase activity is regulated through interaction with the D-type cyclins (CCND1, CCND2, and CCND3) (8). The resulting cyclin D–CDK4 complexes catalyze the phosphorylation of the members of the retinoblastoma (RB) protein family (RB1, RBL1, and RBL2). Phosphorylation of RB1 by cyclin D–CDK4 releases the E2F

transcription factors, thereby ensuring the expression of genes required for cell-cycle progression (9). Conversely, members of the family of CDK inhibitors (INK and CIP/KIP) block CDK activity in response to quiescence stimuli. Many studies have assessed the roles of CDK4 in cell growth, proliferation, and cancer (10), but the role of CDK4 in adipose tissue function has never been explored. The most marked phenotypes of mice lacking CDK4 (*Cdk4$^{neo/neo}$*) are reduced body size and insulin-deficient diabetes due to a severe decrease in pancreatic β cell growth (11). β Cell–specific reexpression of the *Cdk4^{R24C}* allele renders CDK4 resistant to the inhibitory effects of INK4 proteins (12) and restores β cell proliferation and normoglycemic conditions (13). Interestingly, CDK4 reexpression in pancreatic β cells does not rescue body size reduction, suggesting that this phenotype is not due to endocrine defects secondary to decreased insulin levels. We previously demonstrated that CDK4 regulates adipogenesis, suggesting a role of CDK4 in WAT function (14).

Results

CDK4 activity is positively correlated with WAT mass. The first suggestion of a role of CDK4 in adipose tissue biology came from the finding that CDK4 and 2 D-type cyclins (CCND2 and CCND3) are highly expressed in epididymal WAT (eWAT) compared with the other tissues analyzed (Figure 1A). The high levels of expres-
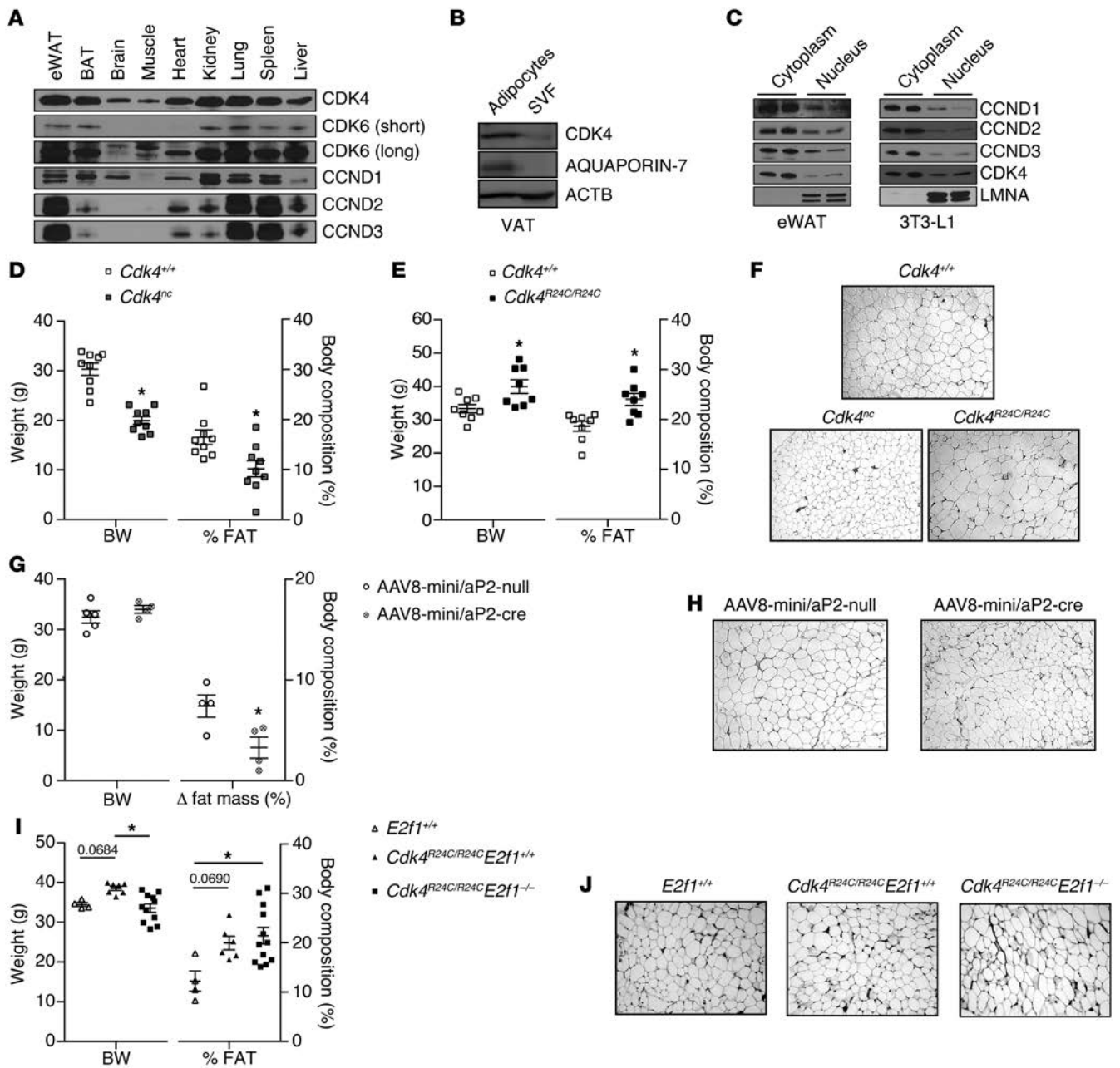
Figure 1. Positive correlation between CDK4 activity and WAT mass. (**A**) Expression levels of CCND1, CCND2, CCND3, CDK4, and CDK6 proteins in mouse eWAT, BAT, brain, muscle, heart, kidney, lung, spleen, and liver. Representative blot of several animals analyzed is shown. (**B**) CDK4 protein level in the SVF and mature adipocytes isolated from VAT. (**C**) Subcellular localization of CCND1, CCND2, CCND3, and CDK4 proteins in cytoplasm and nuclear fractions of eWAT and mature 3T3-L1 adipocytes. LMNA was used as a control for the nuclear fraction. (**B** and **C**) Representative blots out of 3 independent experiments are shown. (**D** and **E**) Body weight and percentage of fat mass of 20-week-old $Cdk4^{+/+}$ and $Cdk4^{nc}$ mice (n = 9) (**D**) and 30-week-old $Cdk4^{+/+}$ and $Cdk4^{R24C/R24C}$ mice (n = 8) (**E**) as obtained using EchoMRI technology. (**F**) H&E staining of eWAT sections from $Cdk4^{+/+}$, $Cdk4^{nc}$, and $Cdk4^{R24C/R24C}$ mice. (**G**) Body weight, Δ fat mass of 20-week-old $Cdk4^{flox/flox}$ mice infected with AAV8-mini/aP2-null (n = 5) or AAV8-mini/aP2-cre (n = 4) analyzed by EchoMRI technology (we show the difference between the percentage of fat before and the percentage of fat 3 weeks after infection). (**H**) H&E staining of eWAT sections from $Cdk4^{flox/flox}$ mice infected with AAV8-mini/aP2-null or AAV8-mini/aP2-cre. (**I**) Body weight and percentage of fat mass of 30-week-old $E2f1^{+/+}$ (n = 4), $Cdk4^{R24C/R24C} E2f1^{+/+}$ (n = 6), and $Cdk4^{R24C/R24C} E2f1^{-/-}$ mice (n = 12). (**J**) H&E staining of eWAT sections from $E2f1^{+/+}$, $Cdk4^{R24C/R24C} E2f1^{+/+}$, and $Cdk4^{R24C/R24C} E2f1^{-/-}$ mice. Statistically significant differences were determined with unpaired 2-tailed Student's t tests (**D**, **E**, and **G**) or 1-way ANOVA followed by Tukey's multiple comparisons test (**I**). *$P < 0.05$. Original magnification, ×100.

sion of CCND3 in eWAT (Figure 1A and Supplemental Figure 1, A and B; supplemental material available online with this article; doi:10.1172/JCI81480DS1) are consistent with previous findings showing increased CCND3 expression during adipogenesis (15).

Protein expression analysis in visceral adipose tissue (VAT) cellular fractions showed that CDK4 was better expressed in mature adipocytes compared with the stromal vascular fraction (SVF) (Figure 1B and Supplemental Figure 1C). Furthermore, CDK4 expression
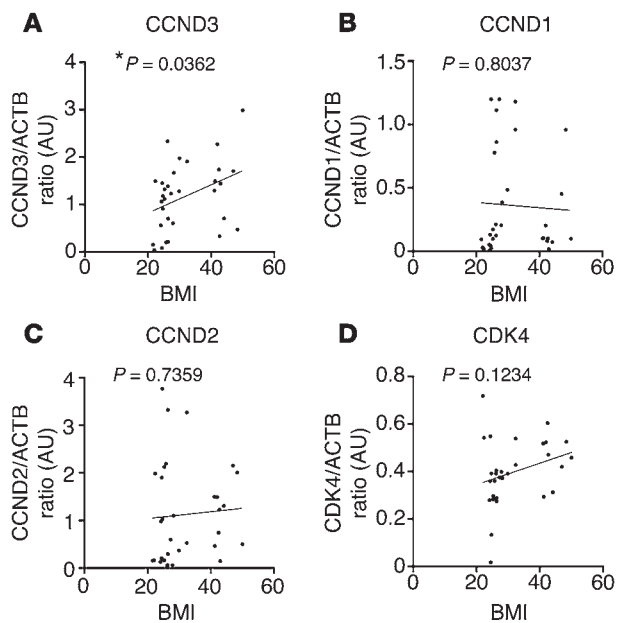
Figure 2. Positive correlation between CCND3 expression and human VAT mass. (**A**–**D**) Correlation between the CCND3/ACTB ratio ($n = 32$, Pearson's $r = 0.3717$, $P < 0.05$) (**A**), the CCND1/ACTB ratio ($n = 32$, Pearson's $r = -0.04574$, $P < 0.05$) (**B**), the CCND2/ACTB ratio ($n = 32$, Pearson's $r = 0.06203$, $P < 0.05$) (**C**), and the CDK4/ACTB ratio ($n = 30$, Pearson's $r = 0.2875$, $P < 0.05$) (**D**) and BMI in VAT of human subjects. Data are normalized to ACTB. *$P < 0.05$.

engineering of white and brown adipocytes in adult mice and has very poor tropism for macrophages (17). We infected $Cdk4^{flox/flox}$ mice (Supplemental Figure 1I) with AAV8 vectors expressing the Cre recombinase under the control of the mini/aP2 adipose tissue–specific promoter (AAV8-mini/aP2-cre) or with the control vector (AAV8-mini/aP2-null). First of all, we determined the tissues that were infected by assessing the presence of viral genome (vg) using Cre PCR. The vg was only present in brown adipose tissue (BAT), eWAT, s.c. WAT, and liver, whereas we could not detect it in pancreas and muscle (Supplemental Figure 1J). Quantitative reverse-transcription–PCR (RT-qPCR) analysis showed a significant decrease of $Cdk4$ mRNA in eWAT and s.c. WAT, whereas no changes were observed in liver and BAT (Supplemental Figure 1K). After 3 weeks, the systemic administration of AAV8-mini/aP2-cre triggered a decrease in fat mass gain; indeed, AAV8-mini/aP2-cre–infected mice gained significantly less fat mass (Figure 1G) and experienced a reduction in adipocyte size (Figure 1H). However, no differences were found in body weight and lean mass in $Cdk4^{flox/flox}$ mice infected with AAV8-mini/aP2-cre vector (Figure 1G and Supplemental Figure 1L). The use of this adipose tissue–specific $Cdk4$ depletion model supports a cell-autonomous contribution for CDK4 in adipose tissue. Overall, these 3 models ($Cdk4^{nc}$, $Cdk4^{R24C/R24C}$, and $Cdk4^{flox/flox}$ mice infected with AAV8 mini/aP2-cre) clearly demonstrate a positive correlation between CDK4 activity and WAT mass/size.

E2F1, a known proproliferative downstream effector of CDK4, was previously shown to promote adipogenesis (16). Therefore, in order to determine whether adipocyte proliferation was not affected with the modulation of CDK4 activity, we generated $Cdk4^{R24C/R24C}$ $E2f1^{-/-}$ mice. No significant changes were observed in adiposity, adipocyte size, lean mass, or adipocyte proliferation as measured by Ki67 expression in $Cdk4^{R24C/R24C}$ $E2f1^{-/-}$ compared with $Cdk4^{R24C/R24C}$ $E2f1^{+/+}$ mice (Figure 1, I and J, and Supplemental Figure 1, M and N). These results demonstrate that when CDK4 is hyperactive, the deletion of E2f1 does not affect fat mass, mature adipocyte size, and proliferation. Because $Cdk4^{R24C/R24C}$ mice develop a wide spectrum of tumors (18, 19), we investigated to determine whether the WAT phenotype observed in these mice could be secondary to tumor development. We could not find any correlation between fat mass and tumor development. Indeed, all mice used in this study were tumor free (Supplemental Figure 1O). Moreover, tumor development was negatively correlated with fat mass in 60-week-old $Cdk4^{R24C/R24C}$ mice, proving that the increased WAT mass in these mice was not secondary to tumor formation (Supplemental Figure 1P).

CCND3 is positively correlated with WAT mass in human subjects. Our data suggesting the involvement of CCND3-CDK4 in adipose tissue was further supported by the positive correlation between CCND3 protein expression in visceral WAT samples from human subjects and their BMI (Figure 2A and Supplemental Figure 1, Q

was also higher in differentiated 3T3-L1 adipocytes compared with nondifferentiated 3T3-L1 preadipocytes (Supplemental Figure 1C). Interestingly, the subcellular localization of CDK4 and CCND3 as well as of the other D-type cyclins revealed that these proteins are not only found in the nucleus; rather, they are mainly localized in the cytoplasm of adipocytes (Figure 1C and Supplemental Figure 1D), suggesting a role for CDK4 that is independent of the RB/E2F pathway in these cells. Moreover, since the duplication rate in mature adipocytes is low (16), these results suggested a novel cell-cycle independent role for CDK4. In order to analyze the participation of CDK4 in adipose tissue biology, we set to determine the phenotype of CDK4 mutant mice. The previously generated $Cdk4^{neo/neo}$ mice are diabetic and have impaired pancreatic β cell development and decreased insulin levels (11). Analysis of adipose tissue function in these mice would be confusing, since any observed effect could be secondary to insulin deficiency. We therefore used $Cdk4^{neo/neo}$ Rip-Cre ($Cdk4^{neo/neo;cre/cre}$; herein referred to as $Cdk4^{nc}$) mice that reexpress $Cdk4$ in β cells and thus have normal insulin levels (13). We also used a mouse model of CDK4 hyperactivation, the R24C model. $Cdk4^{R24C/R24C}$ mice express a mutant CDK4 protein that is not sensitive to INK4a inhibitors (11) and is consequently more active. A first analysis showed that $Cdk4^{nc}$ mice had decreased body weight, whereas $Cdk4^{R24C/R24C}$ mice exhibited increased body weight compared with $Cdk4^{+/+}$ mice (Figure 1, D and E). Significant changes in WAT mass accounted for body weight variation. $Cdk4^{nc}$ and $Cdk4^{R24C/R24C}$ mice had decreased and increased WAT mass, respectively, as measured by EchoMRI (Figure 1, D and E, and Supplemental Figure 1, E and F). Changes in fat mass were consistent with variation in adipocyte size (Figure 1F and Supplemental Figure 1G). Overall, severe atrophy could be observed in fat pads from $Cdk4^{nc}$ mice, whereas $Cdk4^{R24C/R24C}$ mice developed adipose tissue hypertrophy (Supplemental Figure 1H).

To demonstrate that the effects of Cdk4 deletion in adipose tissue were cell autonomous, we used an approach involving systemic administration of adeno-associated viral vectors of serotype 8 (AAV8), which has been previously reported as leading to genetic

Figure 3. CDK4 promotes insulin sensitivity in vivo. (**A–C**) Fasting glycemia in *Cdk4+/+* and *Cdk4nc* (*n* = 8) mice (**A**), *Cdk4flox/flox* infected with AAV8-mini/aP2-null or AAV8-mini/aP2-cre vectors (*n* = 5–4) (**B**), and *Cdk4+/+* and *Cdk4R24C/R24C* (*n* = 12) mice (**C**). (**D–F**) Fed serum insulin in *Cdk4+/+* and *Cdk4nc* (*n* = 7) (**D**), *Cdk4flox/flox* infected with AAV8-mini/aP2-null or AAV8-mini/aP2-cre vectors (*n* = 5–4) (**E**), and *Cdk4+/+* and *Cdk4R24C/R24C* mice (*n* = 8) (**F**). (**G–I**) GTT in *Cdk4+/+* and *Cdk4nc* (*n* = 7) (**G**), *Cdk4flox/flox* infected with AAV8-mini/aP2-null or AAV8-mini/aP2-cre (*n* = 5–4) (**H**), and *Cdk4+/+* and *Cdk4R24C/R24C* (*n* = 6) mice (**I**). (**J–L**) ITT in *Cdk4+/+* and *Cdk4nc* (*n* = 5) (**J**), *Cdk4flox/flox* infected with AAV8-mini/aP2-null or AAV8-mini/aP2-cre vectors (*n* = 5–4) (**K**), and *Cdk4+/+* and *Cdk4R24C/R24C* (*n* = 12) mice (**L**). AUC for GTT and ITT was analyzed and is shown below the curves. Data were expressed as mean ± SEM. Statistically significant differences were determined with unpaired 2-tailed Student's *t* tests. *P < 0.05.

and R). No association was found for CCND1, CCND2, or CDK4 (Figure 2, B–D). These results confirmed a positive correlation between WAT mass and CCND3-CDK4 expression and activity and suggested that these proteins participate in WAT function.

CDK4 promotes insulin sensitivity in vivo. No differences in fasting and feeding glycemia were observed in *Cdk4nc* or *Cdk4flox/flox* infected with AAV8-mini/aP2-cre vector and *Cdk4R24C/R24C* mice

compared with their respective control mice (Figure 3, A–C). Insulin quantification in plasma showed, however, a significant decrease in *Cdk4R24C/R24C* mice, whereas no differences were observed in *Cdk4nc* or *Cdk4flox/flox* mice infected with AAV8-mini/aP2-cre vector in fed conditions (Figure 3, D–F). Decreased insulin levels are indicative of either better insulin sensitivity or of a defect in insulin secretion by pancreatic β cells. *Cdk4nc* mice were glucose intolerant (Figure 3G)

Figure 4. CDK4 represses lipolysis and is a positive modulator of lipogenesis. (**A**) Quantification of TG content of eWAT from $Cdk4^{+/+}$ and $Cdk4^{nc}$ mice ($n = 3$). (**B**) Quantification of TG content of eWAT of $Cdk4^{+/+}$ and $Cdk4^{R24C/R24C}$ mice ($n = 3$). (**C**) Rate of NEFA release in eWAT explants from fasting $Cdk4^{+/+}$ and $Cdk4^{nc}$ mice ($n = 3$). (**D**) Rate of NEFA release in eWAT explants from f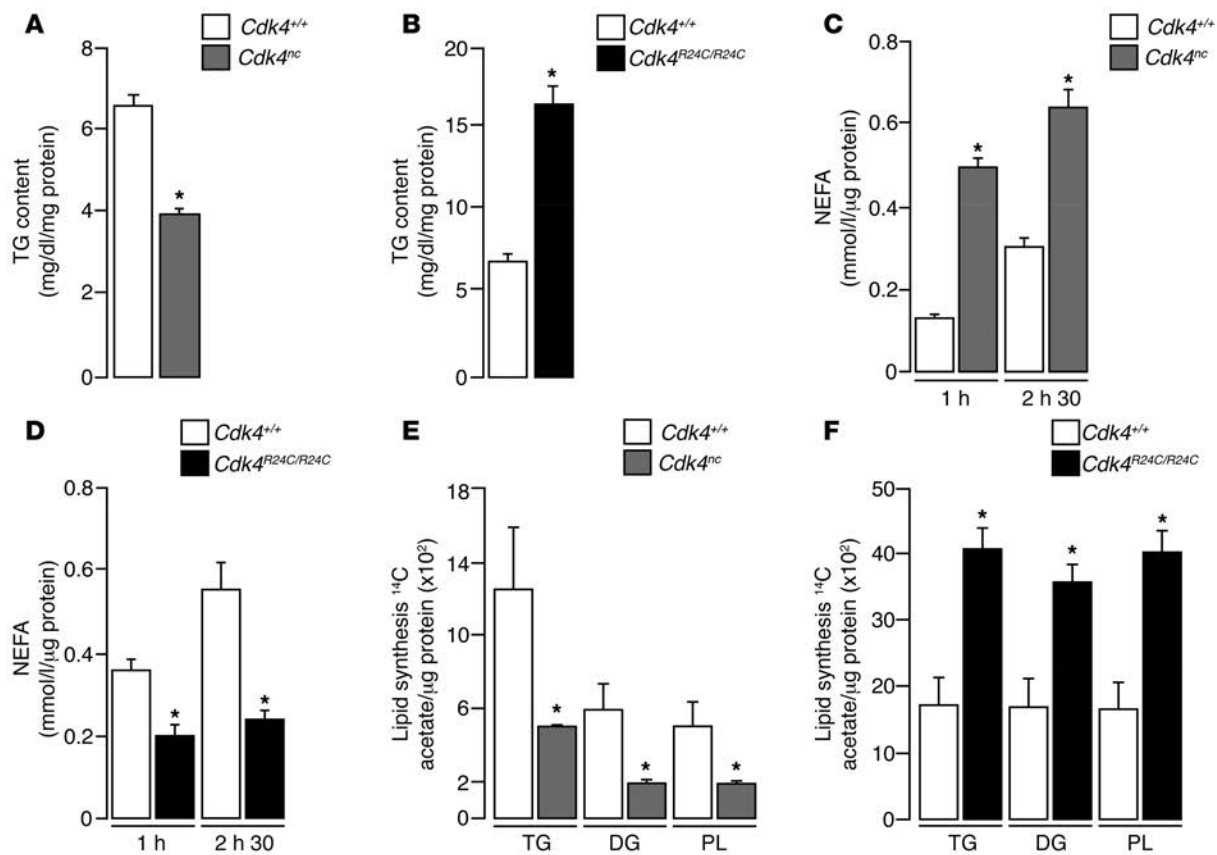asting $Cdk4^{+/+}$ and $Cdk4^{R24C/R24C}$ mice ($n = 6$). (**E**) Ex vivo lipogenesis experiments in eWAT explants using labeled ^{14}C-acetate incorporation to detect TG, DG, and PL synthesis in $Cdk4^{+/+}$ and $Cdk4^{nc}$ mice ($n = 3$). (**F**) Ex vivo lipogenesis experiments in eWAT explants from $Cdk4^{+/+}$ and $Cdk4^{R24C/R24C}$ mice. ^{14}C-acetate incorporation was used to detect TG, DG, and PL synthesis by TLC ($n = 3$). Data are expressed as mean ± SEM. Statistically significant differences were determined with unpaired 2-tailed Student's t tests. $*P < 0.05$.

and cleared glucose at a slower rate than $Cdk4^{+/+}$ mice, a characteristic of insulin resistance (Figure 3J). We did not observe any significant differences in glucose tolerance tests (GTTs) in $Cdk4^{flox/flox}$ mice infected with AAV8-mini/aP2-cre vector; however, these mice had a trend toward insulin resistance compared with $Cdk4^{flox/flox}$ mice infected with AAV8-mini/aP2-null vector ($P = 0.0829$) (Figure 3, H and K). In contrast, $Cdk4^{R24C/R24C}$ mice were more glucose tolerant and insulin sensitive than $Cdk4^{+/+}$ mice (Figure 3, I and L). Together, these results show that CDK4 activity is positively correlated with insulin sensitivity.

CDK4 represses lipolysis and stimulates lipogenesis. We previously showed the participation of CDK4 and CCND3 in adipogenesis. We proved that these proteins control the activity of the master regulator of adipocyte differentiation, PPARγ (14). In this study, we analyze the participation of CDK4 in the function of mature adipocytes. Lipids are mobilized from WAT through lipolysis, a breakdown of triglycerides (TG) into glycerol and free fatty acids (FFA) (20). As expected, changes in WAT mass were positively correlated with alterations in TG content in our mouse models: $Cdk4^{nc}$ and $Cdk4^{R24C/R24C}$ mice had less and more TG in eWAT, respectively (Figure 4, A and B). Decreased TG content in $Cdk4^{nc}$ eWAT was likely the result of an imbalanced lipogenesis/lipolysis ratio. Indeed, treatment of fully differentiated 3T3-L1

adipocytes with a chemical CDK4 inhibitor (PD0332991) (21) resulted in the delipidation of these adipocytes and in a 40% decrease in their TG content (Supplemental Figure 2, A and B). Lipolysis experiments in eWAT explants from mice revealed a 4-fold increase of nonesterified fatty acid (NEFA) release in $Cdk4^{nc}$ eWAT compared with $Cdk4^{+/+}$ eWAT (Figure 4C). Similarly, glycerol release was also increased in these mice (Supplemental Figure 2C). Conversely, $Cdk4^{R24C/R24C}$ eWAT showed significantly decreased NEFA (Figure 4D) and glycerol release (Supplemental Figure 2D), which suggested impaired lipolysis. Interestingly, eWAT explants from $Cdk4^{nc}$ mice, in addition to increased lipolysis, had reduced lipogenesis, as measured by acetate incorporation into the distinct TG, diacyclycerols (DG), and phospholipid (PL) lipid fractions (Figure 4E). On the other hand, eWAT explants from mice expressing the hyperactive $Cdk4^{R24C}$ allele showed increased lipogenesis (Figure 4F). However, we could not detect any differences in liver TG content in $Cdk4^{+/+}$, $Cdk4^{nc}$, and $Cdk4^{R24C/R24C}$ mice (Supplemental Figure 2, E and F). This validated a positive correlation between CDK4 activity and lipogenesis and a negative correlation between CDK4 activity and lipolysis. Strikingly, these are exactly the effects of insulin in adipocytes, suggesting that CDK4 could mediate the effects of insulin in adipose tissue.
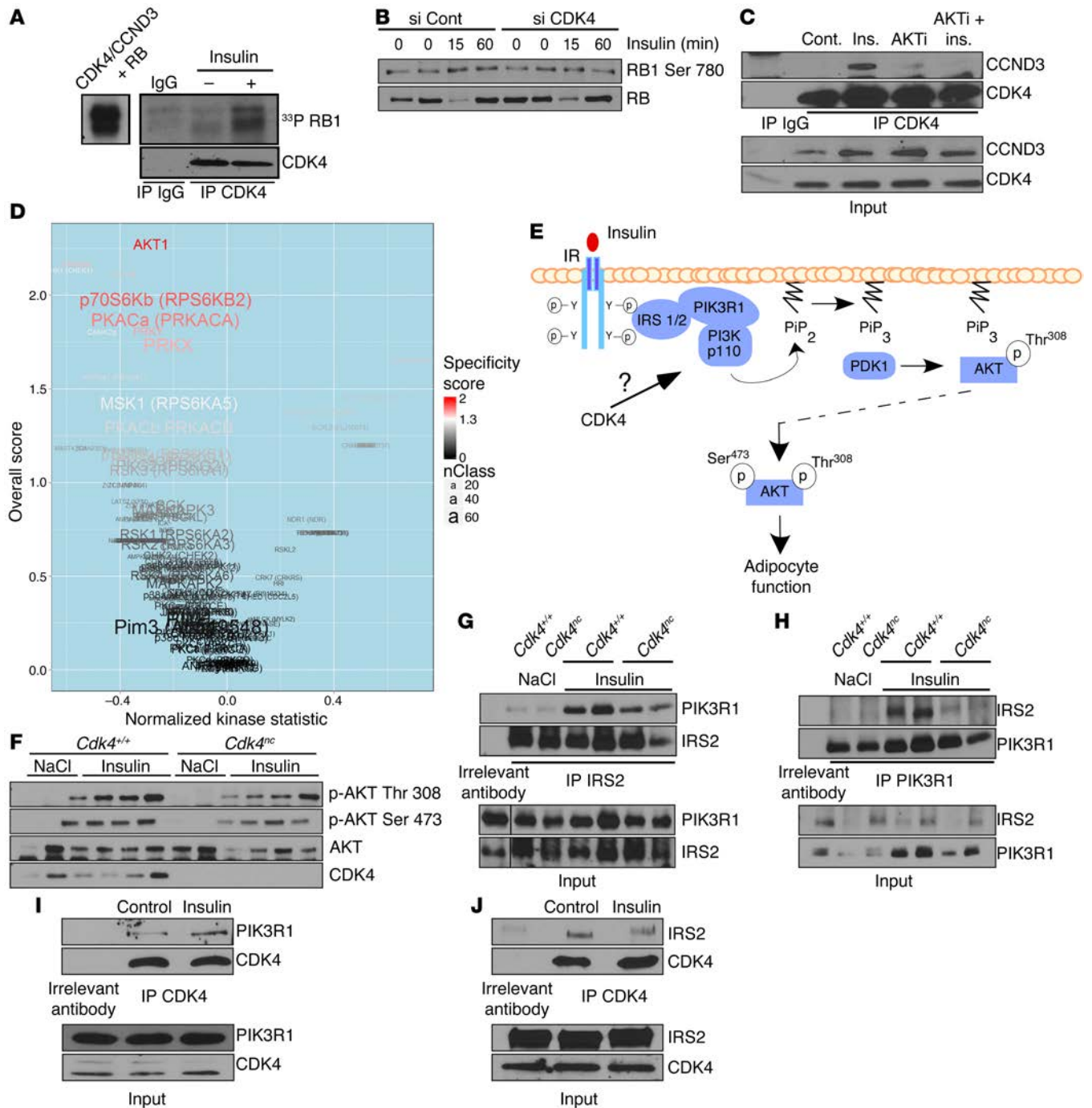
Figure 5. CDK4 is activated by insulin and translates insulin signaling in adipocytes. (**A**) CDK4 activity in vivo. SDS-PAGE autoradiography showing RB1 phosphorylation by CDK4 immunoprecipitated from 3T3-L1 mature adipocytes after insulin stimulation. The left panel shows RB1 phosphorylation by recombinant CDK4 used as a positive control. (**B**) Western blot analysis showing the inhibition of insulin-induced RB1 phosphorylation on Ser780 by CDK4 knockdown in mature 3T3-L1 adipocytes. (**C**) CCND3 and CDK4 association is increased upon insulin stimulation, but decreased upon cotreatment with insulin and AKT inhibitor in mature 3T3-L1 adipocytes. (**D**) Volcano plot showing differences in putative kinase activities between control and $Cdk4^{nc}$ mice injected (portal vein) with insulin for 3 minutes ($n = 4$). Kinases with a positive kinase statistic show higher activity in $Cdk4^{nc}$ samples compared with control samples, whereas kinases with negative kinase statistic show lower activity in $Cdk4^{nc}$ samples compared with control samples. (**E**) Based on the upstream kinase activity (**D**) results and on the GeneGO analysis of the PamGene experiment, the putative role of CDK4 upstream of AKT in the insulin signaling pathway is represented. (**F**) Immunoblot showing AKT phosphorylation on Thr308 and Ser473 in response to insulin injection (3 minutes) in fasted control and $Cdk4^{nc}$ mice ($n = 2$ for NaCl and $n = 4$ for insulin treatment). (**G** and **H**) Coimmunoprecipitation experiments showing the interaction between endogenous IRS2 and PIK3R1. IRS2 (**G**) and PIK3R1 (**H**) were immunoprecipitated and the presence of PIK3R1 (**G**) and IRS2 (**H**) was detected by Western blot analysis in $Cdk4^{+/+}$ and $Cdk4^{nc}$ mice treated with insulin for 3 minutes ($n = 2$ for NaCl and $n = 3$ for insulin treatment). (**I** and **J**) Coimmunoprecipitation experiments showing the interaction between endogenous PIK3R1 or IRS2 and CDK4. CDK4 was immunoprecipitated and the presence of PIK3R1 ($n = 3$) (**I**) and IRS2 ($n = 1$) (**J**) was detected by Western blot analysis in 3T3-L1 mature adipocytes treated with insulin. A representative Western blot is shown. Unless specified otherwise, all experiments are representative of 3 independent experiments.

Table 1. CDK consensus sites in mouse IRS1, IRS2, PDKP1, and PIK3R1

Protein	Site position	Sequence	CDK4 Interaction
PIK3R1	Thr86	TPKP	+
PDPK1	Thr357	TPPP	−
	Thr521	TPNP	
IRS1	Ser1209	SPRR	+
IRS2	Ser388	SPGP	+
	Thr576	TPAR	
	Ser980	SPKP	
	Ser1004	SPYP	
	Ser1226	SPMR	

CDK4 is activated by insulin and mediates insulin signaling in adipocytes. We wanted next to uncover the mechanisms of CDK4 activation following insulin stimulation in adipocytes. CDK4 activity was stimulated by insulin in differentiated 3T3-L1 cells, as suggested by increased phosphorylation of PIK3R1 by immunoprecipitated CDK4 (Figure 5A). Similar results were observed when eWAT from insulin-treated mice was used (Supplemental Figure 3A). Interestingly, CDK4 knockdown (Figure 5B) or treatment of 3T3-L1 adipocytes with PD0332991 (Supplemental Figure 3B) abrogated the effects of insulin on PIK3R1 phosphorylation. Furthermore, association of CDK4 with its regulatory subunit CCND3 was dependent on the insulin signaling pathway, since AKT inhibition abolished this association (Figure 5C).

Next, we addressed how CDK4 could participate in the insulin-signaling pathway in adipocytes. Since the insulin signaling cascade is dependent on the rapid activation of a series of tyrosine and serine/threonine protein kinases (STKs), we used a new technology developed by PamGene to determine differential global kinase activity in $Cdk4^{nc}$ and control mice in response to insulin. We used arrays that consisted of 140 immobilized serine/threonine-containing peptides that are targets of most known kinases (STK PamChips) (22). These chips were incubated with lysates prepared from eWAT from $Cdk4^{nc}$ or control mice injected with insulin. The same experiment was performed using lysates from cells treated with PD0332991 and stimulated with insulin. Peptides whose phosphorylation varied significantly between the control and $Cdk4^{nc}$-treated mice or between the control and PD0332991-treated samples (Supplemental Figure 3, C and D) were indicative of differential specific kinase activities. Putative upstream kinase analysis underscored significant differences in the AKT pathway (Figure 5D and Supplemental Figure 3, E and F). This suggested that CDK4 activity played a role upstream of AKT, as indicated in Figure 5E. Western blot analyses further proved that AKT activity, as measured by phosphorylation in Ser473 and Thr308, was decreased in $Cdk4^{nc}$ mice in response to insulin (Figure 5F). Similarly, chemical inhibition of CDK4 also attenuated AKT signaling in 3T3-L1 adipocytes (Supplemental Figure 3G). This further supports the hypothesis that CDK4 regulates insulin signaling upstream of AKT. Upon insulin stimulation, the intrinsic tyrosine kinase domain of the insulin receptor leads to receptor

autophosphorylation at tyrosine residues. The subsequent recruitment and phosphorylation of insulin receptor substrate 1 (IRS1) and IRS2 are the pivotal events that, in turn, activate the downstream PI3K-PDK1-AKT axis to regulate lipogenesis and lipolysis in adipocytes (23). We therefore investigated whether CDK4 regulated the insulin-signaling pathway by facilitating the recruitment of IRS into PIK3R1, the PI3K subunit p85a. We found that *Cdk4* deletion greatly impaired the ability of IRS2 to bind with PIK3R1 in response to insulin stimulation (Figure 5, G and H). Furthermore, CDK4 was recruited to PIK3R1 (Figure 5I) and IRS2 (Figure 5J) complexes in adipocytes. However, we only detected an increase of interaction in response to insulin between PIK3R1 and CDK4.

IRS2 is a substrate of CDK4. Interestingly, in silico analysis highlighted the presence of CDK4 consensus phosphorylation sites in the p85A subunit of PI3K (PIK3R1), phosphoinositide-dependent kinase 1 (PDK1), IRS1, and IRS2 (Table 1). However, in vitro kinase assays showed no phosphorylation of PIK3R1, or PDPK1 by CDK4 (data not shown). In vitro kinase assays showed, however, that CDK4 could phosphorylate recombinant glutathione S–transferase–purified (GST-purified) IRS2 protein (Figure 6A). IRS2 contains 5 CDK4 consensus sites distributed along the protein (Ser388, Thr576, Ser980, Ser1004, and Ser1226) (Table 1 and Supplemental Figure 4A). Site-directed mutagenesis (serine to alanine) and protein truncation approaches helped us to map the CDK4 phosphorylation sites of IRS2 at Ser388 and Ser1226 (Figure 6, B and C). Interestingly, these 2 potential phosphorylation sites are highly conserved through evolution (Supplemental Figure 4B).

We next evaluated the functional relevance of IRS2[S388A] and IRS2[S1226A] mutants that cannot be phosphorylated by CDK4. Rescue of IRS2 activity in *Irs2^{-/-}* preadipocytes with ectopic expression of WT IRS2 resulted in the restoration of insulin signaling as assessed by immunofluorescence staining of AKT phosphorylation (Figure 6, D and E). In contrast, IRS2[S388A] mutants, which cannot be phosphorylated by CDK4, could not restore insulin signaling in these cells (Figure 6, D and E). No significant phenotype was observed for IRS2[S1226A] mutants (data not shown). Moreover, IRS2[S388A] mutants were not recruited to PIK3R1 protein complexes upon insulin stimulation when ectopically expressed in 293T cells (Figure 6, F and G). This demonstrated that the phosphorylation of IRS2 on Ser388 by CDK4 is essential for its activity.

CDK4 regulates insulin signaling in vivo via IRS2[Ser388] phosphorylation. To determine the potential roles of CDK4 on IRS2 phosphorylation, we generated a phosphospecific antibody to Ser388 of IRS2 that we validated by in vitro CDK4 kinase assay (Supplemental Figure 5A). IRS2 Ser388 was highly phosphorylated in the adipose tissue of *Cdk4^{+/+}* mice after 50 minutes of insulin stimulation (Figure 7, A and B). This phosphorylation was almost abrogated in the adipose tissue of insulin-treated *Cdk4[nc]* mice. Moreover, decreased IRS2 Ser388 phosphorylation resulted in impaired insulin signaling pathways, as demonstrated by reduced AKT phosphorylation (Figure 7, A and B). In sharp contrast, CDK4 hyperactivity, as observed in *Cdk4[R24C/R24C]* mice, resulted in a robust increase in IRS2 Ser388 phosphorylation (Figure 7, C and D). Consequently, AKT phosphorylation was also increased (Figure 7, C and D). Chemical inhibition of CDK4 also resulted in the abrogation of both IRS2 Ser388 and AKT phosphorylations (Figure 7, E and F). From these results, we can conclude that this

Figure 6. CDK4 phosphorylates IRS2. (**A**) CCND3-CDK4 complex directly phosphorylates full-length GST-IRS2 in vitro (*n* = 3). (**B**) In vitro phosphorylation of GST-IRS2 fragments (1–494aa, 495–744aa, 745–993aa, 994–1099aa, 1100–1321aa) by CCND3/CDK4. Left panel, SDS-PAGE stained with Coomassie blue for the loading control. Middle panels, autoradiography of the SDS-PAGE gels containing the different GST-IRS2 fragments, incubated with CCND3/CDK4. Right panel, RB1 recombinant protein was used as a positive control (*n* = 3). (**C**) Defective IRS2[S388A] and IRS2[S1226A] phosphorylation by CCND3-CDK4. Upper panel, autoradiography; lower panel, SDS-PAGE gel stained with Coomassie blue for the loading control. (*n* = 2). (**D**) Decrease in pAKT Ser473 phosphorylation in Flag-IRS2[S388A] electroporated *Irs2*^{−/−} cells upon insulin stimulation, compared with the WT Flag-IRS2–transfected cells (*n* = 3). Original magnification, ×400. (**E**) Quantification of pAKT Ser473 fluorescence intensity for untransfected, Flag-IRS2–transfected, and Flag-IRS IRS2[S388A] electroporated *Irs2*^{−/−} preadipocytes was performed with ImageJ software (http://imagej.nih.gov/ij/). At least 100 cells were quantified per condition. (**F**) Representative Western blot analysis showing impaired interaction between PIK3R1 and Flag-IRS2[S388A] mutant after insulin stimulation compared with cells transfected with Flag-IRS2 in 293T cells. (**G**) Quantification of the blot shown in **F**. A representative Western blot is shown. Data are expressed as mean ± SEM. Statistically significant differences were determined with 2-way ANOVA followed by Tukey's multiple comparisons test (**E–G**). *$P < 0.05$.
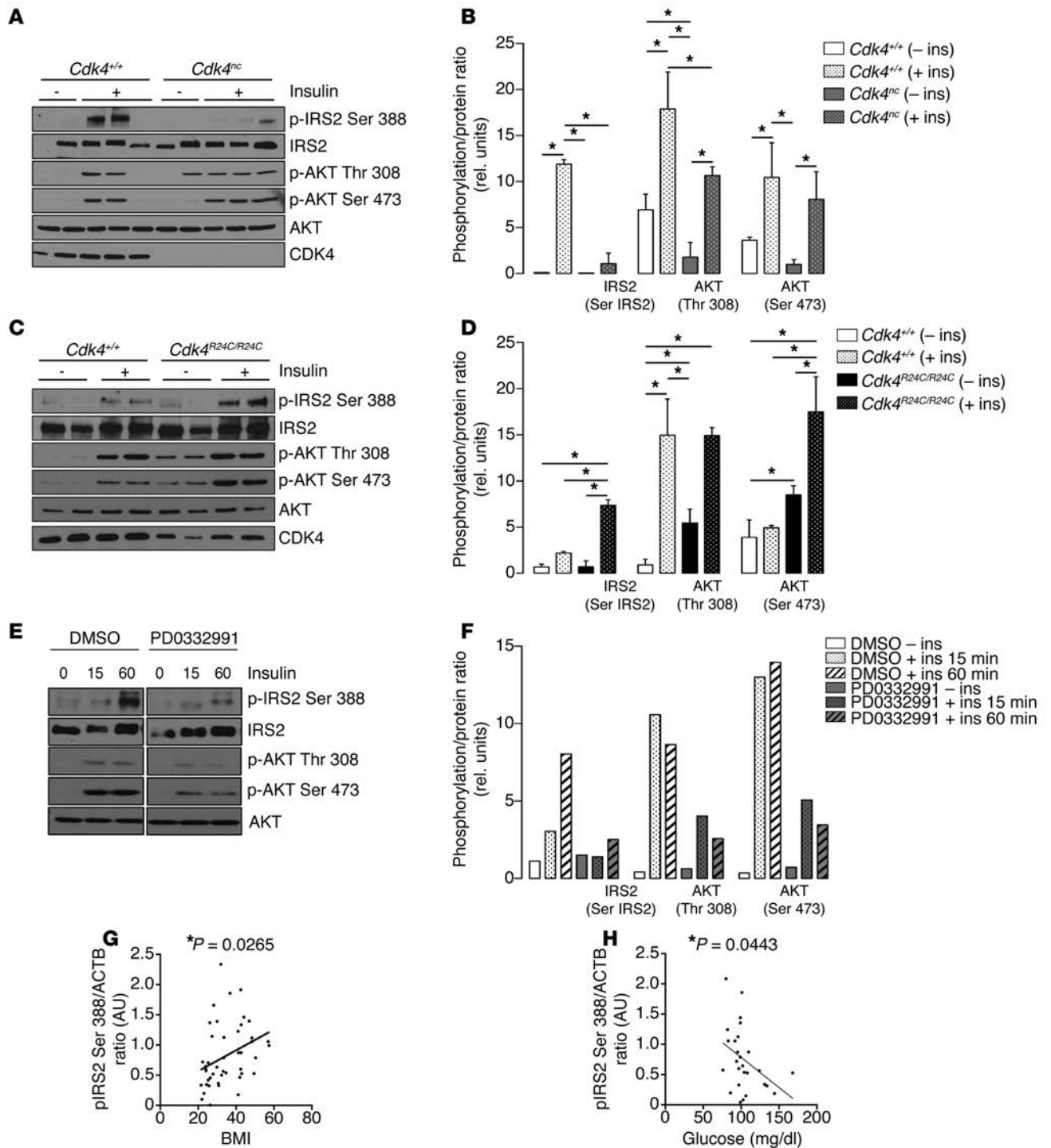
Figure 7. CDK4 phosphorylates in vivo the IRS2 protein at the Ser388. (**A**–**D**) Immunoblot analysis of IRS2 phosphorylation on Ser388 and AKT phosphorylation on Thr308 and Ser473 in control and *Cdk4^nc^* (*n* = 2 starved/5 insulin for *Cdk4^+/+^* and *n* = 2 starved/5 insulin for *Cdk4^nc^*) mice (**A**). (**B**) Quantification of the blot shown in **A** using ImageJ software. *Cdk4^R24C/R24C^* (*n* = 2 starved/3 insulin for both *Cdk4^+/+^* and *Cdk^R24C/R24C^*). (**C**) Mice were treated for 50 minutes with insulin. (**D**) Quantification of the blot shown in **C** using ImageJ software. (**E**) Immunoblot analysis of IRS2 phosphorylation on Ser388 and AKT phosphorylation on Thr308 and Ser473 in 3T3-L1 mature adipocytes during a time course insulin stimulation with or without PD0332991 (*n* = 1). (**F**) Quantification of the blot shown in **E** using ImageJ software. (**G**) Correlation between the pIRS2 Ser388/ACTB ratio in VAT and the BMI of the subjects (*n* = 45, Pearson's *r* = 0.3307, *P* < 0.05). (**H**) Correlation between the pIRS2 Ser388/ACTB ratio in VAT and the glycemia of the subjects (*n* = 27, Pearson's *r* = –0.3900, *P* < 0.05). Data are expressed as mean ± SEM. Statistically significant differences were determined with 2-way ANOVA followed by Tukey's multiple comparisons test (**B**–**D**). *P* < 0.05.

newly identified site in IRS2, which is phosphorylated by CDK4, maintains the activation of the insulin signaling pathway. To further investigate the status of IRS2 Ser388 in type 2 diabetic mouse models, such as *db/db* mice, that are known to be hyperinsulinemic, we analyzed this phosphorylation in the basal state and upon insulin stimulation in adipose tissue. The *db/db* mice have a tendency toward an increased IRS2 Ser388 phosphorylation under basal conditions, compared with *db/+* mice ($P = 0.0511$) (Supplemental Figure 5B). However, insulin-resistant *db/db* mice did not show increased IRS2 Ser388 phosphorylation upon insulin stimulation (Supplemental Figure 5B). Most important was the finding that IRS2 Ser388 phosphorylation in human visceral WAT samples was positively correlated with the BMI of the subjects (Figure 7G and Supplemental Figure 5, C and D). Interestingly, we found a negative correlation between IRS2 Ser388 phosphorylation and fasting glucose in human subjects. This further advocates for a role of CDK4 in both adipose tissue biology and glucose homeostasis (Figure 7H and Supplemental Figure 5E).

Discussion

We showed throughout this study that the cell-cycle regulatory kinase CDK4 is a key regulator of adipocyte function. The participation of this kinase in the control of proliferation through the control of the activity of E2F transcription factors has been extensively studied (24). The results of our study provide 3 lines of evidence that CDK4 acts independently of E2F to regulate adipocyte function. First, we discovered a role of the cell-cycle kinase CDK4 in the control of the insulin-signaling pathway. CDK4, through phosphorylation of IRS2, maintains insulin action in adipocytes. This is consistent with the phenotypes of genetic CDK4 mouse models. Indeed, adipose tissue from *Cdk4^nc^* mice has decreased lipogenesis as well as increased lipolysis. In contrast, mice that express hyperactive CDK4^R24C exhibit decreased lipolysis and increased lipogenesis in WAT. These findings place CDK4 at the initiation of the insulin-triggered adipocyte-signaling pathway.

We show in this study a function of CDK4, that of a mediator of insulin signaling. Indeed, we show that the effects of CDK4 in adipocytes are independent of E2F activity and, therefore, most likely independent of the control of the cell cycle. E2F1 is the most studied member of the E2F family. E2F1 has numerous metabolic functions, such as the participation in adipose tissue metabolism through the transcriptional regulation of the master adipogenic factor PPARγ during early stages of adipogenesis (16). Here, we demonstrate, by generation of *Cdk4^R24C/R24 E2f1^+/+* and *Cdk4^R24C/R24C E2f1^-/-* mice, that CDK4 has E2F1-independent functions in mature adipose tissue. Indeed, the genetic deletion of E2F1 in the R24C background does not affect adiposity or adipocyte proliferation (Figure 1, I and J, and Supplemental Figure 1N).

Based on our results, we propose that CDK4 is integrated in the insulin-signaling pathway as follows. In response to insulin, the canonical cascade of events is elicited. This includes the sequential activation of IR, IRS1-2, PI3K, PDPK1, and AKT. AKT then activates CDK4 (because inhibition of AKT blocks CDK4 activation), which then phosphorylates IRS2, creating a positive feedback loop. The activation of CDK4 by AKT is likely an indirect event. Several studies previously reported that AKT phosphorylates and inhibits p21 and p27, which are both CDK4 inhibitors (25, 26).

Interestingly, IRS proteins are also involved in the activation of several growth factor receptor pathways other than the insulin receptor pathway, such as the IGF 1 receptor (IGF1R) pathway (27). The prooncogenic activities of IGF1R (26) are mediated by its downstream effectors, IRS1 and IRS2. IRS proteins transduce mitogenic, antiapoptotic, and antidifferentiation signals to the cell, mainly through the PI3K–AKT module (28). Although antioncogenic synergistic effects have been observed using either CDK4 and IGF1R inhibitors or CDK4 and PI3K inhibitors, no crosstalk between both pathways has been described (29–32). The CDK4/CDK6 inhibitor (PD0332991, palbociclib) has been approved for the treatment of breast cancer (33). Two other CDK4/CDK6 inhibitors, LY-2835219 (also known as abemaciclib) and LEE011 (also known as ribociclib), are also currently in advanced stages of clinical trials (34). Interestingly, it has previously been reported that a major enzyme of de novo lipogenesis, the fatty acid synthase (FASN), is increased in numerous cancers, including breast cancer (35). The activity of FASN is known to be stimulated by insulin through the PI3K/AKT pathway, and here, we demonstrate that CDK4 is a key effector of insulin, thus promoting de novo lipid synthesis. Based on our findings, we can speculate that CDK4, through phosphorylation and regulation of IRS activity, could simultaneously sustain de novo lipid synthesis and the oncogenic activity of the aforementioned pathways in transformed cells.

The second major finding of our study is the discovery of a residue in IRS2 that is phosphorylated by CDK4 in response to insulin. A large number of publications previously focused on the effects of IRS1 and IRS2 phosphorylation on the insulin-signaling pathway. Both positive and negative phosphorylation sites finely regulate IRS1 and IRS2 activity and are a paradigm of the flexibility of insulin and IGF signaling (36). The final serine/threonine phosphorylation state of IRS proteins is a consequence of the combined action of several kinases that are activated by different pathways in a spaciotemporal manner. Multiple site phosphorylation of these proteins by distinct kinases, such as JNK (37), GSK3 (38), ERK1, or mTOR (39), provides a large number of combinations of phosphorylating events that generate a very complex network (40). We show that CDK4 phosphorylates IRS2 at the new Ser388 site. Moreover, we show that this phosphorylation renders IRS2 more active. Our results add more complexity to the understanding of the physiology of the phosphorylation of the IRS proteins. Phosphorylation by CDK4 may also have an impact on the phosphorylation of IRS2 by other kinases; however, the relative contribution of CDK4 to the final activation or inhibition of IRS compared with other kinases and the identification of which serine/threonine residues are the most critical in regulating IRS function in response to insulin remain to be elucidated. Similarly, we still do not understand why CDK4 activates IRS2 whereas AKT inhibits it through a negative feedback loop. The same stimulus, insulin, triggers concomitantly inhibitory and stimulatory phosphorylations in IRS. The fine regulation of these positive versus negative phosphorylation events requires further investigation. Interestingly, we were able to observe the stimulation of IRS2 Ser388 phosphorylation with insulin not only in adipocytes, but also in other cell types, such as C2C12 myotubes and primary hepatocytes. IRS2 Ser388 phosphorylation could also be detected in Min6 cells, but was not so insulin responsive. As shown in Supplemental Figure 6, A–C, upon insulin stimulation, IRS2 Ser388 phosphoryla-

tion was stronger after 1 hour of treatment, which is in agreement with our findings in mature adipocytes. These results open interesting perspectives into the contribution of CDK4 to IRS2 Ser388 phosphorylation in other insulin-sensitive tissues; CDK4 could, for instance, participate in the control of de novo lipid synthesis in liver upon insulin stimulation.

RNAi-mediated depletion of CDK6, the CDK4 ortholog, suggests that this kinase is also able to phosphorylate IRS2 at Ser388 in mature adipocytes upon insulin stimulation, but to a lesser extent (Supplemental Figure 6D). The effects of CDK6 on IRS2 in other tissues remain to be studied.

Defects in insulin action and insulin secretion are both features of type 2 diabetes. In line with previous publications reporting that CDK4 regulates β cell growth (11) and insulin secretion in β cells (41), it would be interesting to explore the relative contribution of this IRS2 Ser388 phosphorylation in β cell function. The involvement of IRS2 in the pathogenesis of type 2 diabetes is highlighted by the phenotype of *Irs2*^{-/-} mice. Indeed, these animals develop type 2 diabetes with impaired peripheral insulin signaling and pancreatic β cell function without compensation by IRS1 (42).

Third, the importance of our findings goes beyond the control of adipocyte biology in normal physiology. Here, we also report a significant ($P = 0.0362$) correlation between CCND3 expression and BMI in human subjects. Our model is further supported by the observed increase in the phosphorylation of the Ser388 of IRS2 in human obese subjects (BMI > 27). Insulin resistance is a major feature in various metabolic disorders, such as obesity and type 2 diabetes. We show here an inverse correlation of IRS2 Ser388 levels in VAT with the blood glucose levels from the subjects (Figure 7H). This strongly supports the notion that this phosphorylation participates in glucose homeostasis in humans.

In conclusion, our results demonstrate that CDK4 is a regulator of adipocyte insulin signaling. By combining experimental data from cellular and mouse models and data obtained using human samples, our study provides insights into the complex pathogenesis of obesity and insulin resistance.

Methods

Materials. All experiments with the CDK4 inhibitor (PD0332991, Azasynth Co.) were done using 1 μM of PD0332991 in mature 3T3-L1 adipocytes. All chemicals, unless stated otherwise, were purchased from Sigma-Aldrich. Actrapid human recombinant insulin was purchased from Novo Nordisk Pharma SA. AKT inhibitor (catalog 124017) was purchased from Calbiochem and used at 10 μM for 30 minutes. ^{14}C-acetate, and γ-^{33}P-ATP were purchased from PerkinElmer.

Animals. The generation of *Cdk4[nc]* and *Cdk4[R24C/R24C]* mice has been previously described (11, 13). The 8- to 12-week-old male db/+ and db/db as well as C57BL/6J (B6) mice were obtained from Janvier. *E2f1^{+/+}* and *E2f1^{-/-}* mice (B6;129S4-E2f1tm1 Meg/J) were purchased from The Jackson Laboratory. *Cdk4[flox/flox]* mice were generated for this study in collaboration with Cyagen Biosciences. The targeting vector included a Neo resistance cassette flanked by FRT sites as well as CRE-dependent lox P sites in introns 1 and 8 (Supplemental Figure 1I).

C57BL/6 embryonic stem cells were used for gene targeting, and the positive cells were bred into albino B6 female mice. This strategy allowed us to have a pure B6 background. *Cdk4[flox/+]* mice were then crossed with mice expressing Flp recombinase (B6.Cg-Tg[Pgk1-

FLPo]10Sykr/J) in order to remove the Neo resistance cassette. With one subsequent cross with B6 animals, the Flp transgene was removed and the obtained *Cdk4[flox/+]* mice were then intercrossed in order to generate the *Cdk4[flox/flox]* mice used in this study.

Animals were maintained in a temperature-controlled animal facility with a 12-hour light/12-hour dark cycle and had access to food and water according to the Swiss Animal Protection Ordinance (OPAn). Only male animals were used in this study. For the GTT, mice were starved for 16 hours and then injected i.p. with glucose (2 g/kg). Tail vein blood glucose was measured at the indicated times. For the insulin tolerance test (ITT), 6-hour–fasted mice were injected i.p. with 0.75 U/kg insulin and tail vein blood glucose was then measured at the indicated times. For the in vivo insulin-stimulation assay, mice were fasted overnight and injected in the portal vein or i.p. with 0.75 U/kg insulin or an equal volume of saline. After 3 or 50 minutes, the mice were sacrificed via cervical dislocation. For insulin level measurements, tail vein blood was collected under fed conditions 2 hours after the beginning of the 12-hour dark cycle.

Plasmid constructs and mutagenesis. pDONR-IRS2 was subcloned from pBS mouse IRS-2 (Addgene plasmid catalog 11372) (43) and generated using the pDONR221 vector of Gateway Cloning Technology (Invitrogen). Flag-IRS2 and GST-IRS2 were obtained using the pDEST pCMV14-3XFlag and pGEX-2T vectors of Gateway Cloning Technology starting from the above-described pDONR-IRS2 constructs. A similar strategy was used to obtain the truncated versions of GST-IRS2. The Flag-PIK3R1 and Flag-PDPK1 plasmids were obtained from the Montpellier Genomic Collection (MGC). pDONR-hRB 379–928aa was subcloned from pCMV human RB1 and generated using the pDONR221 vector of Gateway Cloning Technology. pGEX-2T hRB 379–928aa was obtained using the pDEST pGEX-2T from Gateway Cloning Technology. The different serine-to-alanine mutants of GST-IRS2 were generated using a QuikChange Site-Directed Mutagenesis Kit (Stratagene).

Cell culture. 3T3-L1 and 293T were obtained from ATCC. *Irs2^{-/-}* cells were cultured in DMEM with 10% FBS (PAA Laboratories) in 5% CO_2 in an incubator set at 37°C. Two days after reaching confluence, 3T3-L1 cells were differentiated with DMEM, 10% FBS, 0.5 mM 3-isobutyl-1methylxanthine (IBMX), 1.7 μM insulin, 1 μM dexamethasone, and 1 μM rosiglitazone for 2 days. From day 3 onward, the cells were incubated with DMEM, 10% FBS, and 10 μg/ml insulin, and the medium was changed every 2 days until day 8 of differentiation. 3T3-L1 mature adipocytes were maintained in medium containing FBS only. For insulin (100 nM) or isoproterenol (100 nM) treatments, fully differentiated 3T3-L1 adipocytes were incubated in serum-free DMEM containing 0.2% fatty acid–free BSA. Primary hepatocytes were obtained from B6 mice. Mouse hepatocytes were harvested and cultured as previously described (44). Min6 cells were provided by Christian Widmann (Department of Physiology, Université de Lausanne, Lausanne). They were maintained as previously described (45) and incubated in DMEM supplemented with 15% FBS and 5 mM glucose overnight. The day after, cells were incubated in serum-free DMEM containing 0.1% fatty acid–free BSA for 6 hours. C2C12 myoblasts were obtained from ATCC and were cultured in low-glucose DMEM with 10% FBS in 5% CO_2 in an incubator set at 37°C. For myotube differentiation, C2C12 myoblasts were seeded in 6-cm plates. When the cells reached 95% confluency, the culture medium was switched to DMEM containing 2% horse serum. The medium was changed every 2 days until day 5 of

differentiation. C2C12 myotubes were incubated in α-MEM overnight to induce starvation. Primary hepatocytes, Min6 cells, and C2C12 myotubes were stimulated with insulin (100 nM).

Proteins extraction, coimmunoprecipitation assays, and immunoblot analyses. For endogenous immunoprecipitation experiments between CDK4 and IRS2, mature 3T3-L1 adipocytes were lysed in a buffer containing 0.3% CHAPS, 40 mM Hepes, pH 7.5, 120 mM NaCl, 1 mM EDTA, 10 mM pyrophosphate, 10 mM glycerophosphate, and protease inhibitor cocktail. Lysates were precleared with protein A/G–agarose beads (Life Technologies) and 4 μg of control antibody (HA antibody) for 1 hour. After this step, anti-CDK4 antibodies or HA antibodies were added to the precleared lysates overnight to immunoprecipitate CDK4 or for the control immunoprecipitation, respectively. For endogenous immunoprecipitation experiments, mature 3T3-L1 adipocytes or eWAT from mice was lysed in a buffer containing 20 mM Tris, pH 7.5, 150 mM NaCl, 1 mM EDTA, 1% Triton X-100, 1 mM Na_3VO_4, 1 mM β-glycerophosphate, 50 mM NaF, and protease inhibitor cocktail. Whole protein extracts were precleared with protein A/G–agarose beads (Life Technologies) for 1 hour, and anti-CDK4 antibody (Santa Cruz Biotechnology Inc., sc-260AC) and negative control (Rabbit IgG) (Santa Cruz Biotechnology Inc., sc-2345) were added to immunoprecipitate CDK4 overnight at 4°C. For IRS2 and PIK3R1 immunoprecipitation experiments from mature adipocytes and mice, whole protein extracts were precleared with protein A/G–agarose beads (Life Technologies) and 4 μg of control antibody (HA antibody) for 1 hour. Then anti-IRS2 anti-PIK3R1 antibody and negative control (HA antibody) were added to the precleared lysates for immunoprecipitation overnight at 4°C. Immunoprecipitation experiments in 293T cells were performed using the same buffer as above. Anti-CDK4 antibody (Santa Cruz Biotechnology Inc., sc-601) and negative control (rabbit IgG) (Santa Cruz Biotechnology Inc., sc-2027) were used for the immunoprecipitation. Flag-PIK3R1, Flag-PDKP1, and Flag-IRS2 were transfected with Lipofectamine 2000 (Invitrogen) and immunoprecipitated with Flag beads (Sigma-Aldrich A2220). Proteins were extracted with the same lysis buffer described above and subjected to SDS-PAGE electrophoresis. Protein extractions from the different tissues (eWAT, BAT, brain, muscle, heart, kidney, lung, spleen, and liver) were prepared using M-PER mammalian extraction buffer (Thermo Scientific) containing 1:100 Halt phosphatase inhibitor cocktail (Thermo Scientific) and 1:100 Halt protease inhibitor cocktail, EDTA-free (Thermo Scientific). All the tissues were snap-frozen and then ground with Liquid N2 before lysis. The following antibodies were used for Western blot analysis: anti-CCND1 (NeoMarkers Rb-010-P0), anti-CCND3 (clone sc-6283), anti-CDK4 (clone sc-260), anti-HSL (clone sc-25843), anti-HA (clone sc-805), anti-IRS2 (clone sc-8299) (Santa Cruz Biotechnology Inc.); anti-CCND2 (clone ab3085), anti-CDK4 (clone DSC-35), anti-Ki67 (clone ab15580) (Abcam); anti–LMNA (clone 2032), anti-pHSL Ser573 (clone 4139), anti–RB1 Ser780 (clone 9307), anti–pAKT Thr308 (clone 4056), anti–pAKT Ser473 (clone 4060), anti-AKT (clone 9272), anti-CDK6 (clone DCS83) (Cell Signaling Technology); anti-Flag (clone F3165), anti-actin (clone A2066), anti-tubulin (clone T6199) (Sigma-Aldrich); anti-PI3K3R1 (clone 06-195) (Upstate); and anti-IRS2 (Millipore MABS15). The phosphospecific antibody against IRS2 Ser388 was synthesized and purchased from GenScript.

Kinase assays. 3T3-L1 mature adipocytes were incubated overnight in serum-free DMEM containing 0.2% fatty acid–free BSA and either stimulated with insulin (100 nM) or left untreated with lysates

of these cells used to immunoprecipitate CDK4, as described above. Additionally, CDK4 was immunoprecipitated from eWAT collected from mice that had fasted for 16 hours and were injected i.p. with insulin (0.75 U/kg) for 30 minutes. Kinase assays were performed using immunoprecipitated CDK4 and 500 ng of recombinant RB1 protein (Santa Cruz Biotechnology Inc.) as a substrate in kinase buffer (25 mM Tris/HCl, pH 7.5, 150 mM NaCl, 10 mM $MgCl_2$, 1 mM DTT, 5 mM $Na_4P_2O_7$, 50 mM NaF, 1 mM vanadate, and protease inhibitor cocktail) with 40 μM ATP and 8 μCi γ-^{33P}ATP for 30 minutes at 30°C. Recombinant CDK4/CCND3 (ProQinase) was used as positive control. Boiling the samples for 5 minutes in the presence of denaturing sample buffer stopped the reaction. Samples were subsequently subjected to SDS-PAGE, and the gels were then dried in a gel dryer for 1 hour and exposed to an x-ray film at −80°C.

When using GST-purified proteins as substrates, kinase assays were performed using 500 ng of recombinant RB1 protein (Santa Cruz Biotechnology Inc.) as a positive control and recombinant CDK4/CCND3 kinase (ProQinase) and incubated in kinase buffer (described above) supplemented with 40 μM ATP and 8 μCi γ-^{33P}ATP for 30 minutes at 30°C.

PamChip peptide microarrays for kinome analysis following insulin stimulation. For kinome analysis, STK microarrays were purchased from PamGene International BV. Each array contained 140 phosphorylatable peptides as well as 4 control peptides. Sample incubation, detection, and analysis were performed in a PamStation 12 according to the manufacturer's instructions. Briefly, extracts from *Cdk4+/+* and *Cdk4nc* mice or mature 3T3-L1 adipocytes were made using M-PER mammalian extraction buffer (Thermo Scientific) containing 1:50 Halt phosphatase inhibitor cocktail (Thermo Scientific) and 1:50 Halt protease inhibitor cocktail, EDTA-free (Thermo Scientific), for 20 minutes on ice. The lysates were then centrifuged at 15,871 *g* for 20 minutes to remove all debris. The supernatant was aliquoted, snap-frozen in liquid nitrogen, and stored at −80°C until further processing. Prior to incubation with the kinase reaction mix, the arrays were blocked with 2% BSA in water for 30 cycles and washed 3 times with PK assay buffer. Kinase reactions were performed for 1 hour with 5 μg of total extract for the mouse experiment or 2.5 μg of total extract for the mature adipocyte and 400 μM ATP at 30°C. Phosphorylated peptides were detected with an anti-rabbit–FITC antibody that recognizes a pool of anti–phospho serine/threonine antibodies. The instrument contains a 12-bit CCD camera suitable for imaging of FITC-labeled arrays. The images obtained from the phosphorylated arrays were quantified using the BioNavigator software (PamGene International BV), and the list of peptides whose phosphorylation was significantly different between control (3 minutes of insulin treated in *Cdk4+/+* mice or 5 minutes of insulin stimulation in cells starved in the presence of DMSO) and test (3 minutes of insulin treated in *Cdk4nc* mice or 5 minutes of insulin stimulation in cells starved in the presence of PD0332991) conditions was uploaded to GeneGo for pathway analysis. The list of the significantly different peptides is shown in Supplemental Figure 3, C and D. The BioNavigator software was used to perform the upstream STK analysis that is shown in Figure 4D.

Statistics. All statistics are described in the figure legends. The results were expressed as mean ± SEM. Pearson's correlation coefficient was calculated to test for correlation between 2 parameters. Comparisons between 2 groups were performed with an unpaired

2-tailed Student's *t* test, and multiple group comparisons were performed by 1-way ANOVA followed by Tukey's test and 2-way ANOVA followed by Tukey's test. *P* < 0.05 was considered significant.

Study approval. All animal care and treatment procedures were performed in accordance with Swiss guidelines and were approved by the Canton of Vaud SCAV (authorization VD 2627.b). For human samples, the protocol concerning the use of biopsy from patients was approved in agreement with Spanish regulations, either by the Ethics and Research Committee of Virgen de la Victoria Clinical University Hospital or by the Institutional Ethics Committee of the Joan XXIII University Hospital. All patients provided written informed consent.

Supplemental data. Additional methods information is available in Supplemental Experimental Procedures. The sequences of the primers used for RT-qPCR are available in Supplemental Table 1.

Author contributions

LF designed the project. SL, ICLM, PDD, XE, JCA, CC, AG, QL, LMC, BD, JSA, EB, SH, AA, and PD designed and carried out the experiments. The design and execution of the PamGene experiment was done by ICLM. VJ and FB provided the AAV8 vectors.

LZ performed the tail-vein injections. CRK provided pBS mouse IRS-2 and *Irs2*^{−/−} cells. JV and FJT provided human VAT samples. SL, ICLM, and LF wrote the manuscript.

Address correspondence to: Lluis Fajas, Department of Physiologie, Université de Lausanne, CH-1005 Lausanne, Switzerland. Phone: 41.21.692.55.10; E-mail: lluis.fajas@unil.ch.

1. Saltiel AR, Kahn CR. Insulin signalling and the regulation of glucose and lipid metabolism. *Nature*. 2001;414(6865):799–806.
2. White MF. Insulin signaling in health and disease. *Science*. 2003;302(5651):1710–1711.
3. Rask-Madsen C, Kahn CR. Tissue-specific insulin signaling, metabolic syndrome, and cardiovascular disease. *Arterioscler Thromb Vasc Biol*. 2012;32(9):2052–2059.
4. Vazquez-Vela ME, Torres N, Tovar AR. White adipose tissue as endocrine organ and its role in obesity. *Arch Med Res*. 2008;39(8):715–728.
5. Koch L, et al. Central insulin action regulates peripheral glucose and fat metabolism in mice. *J Clin Invest*. 2008;118(6):2132–2147.
6. Abel ED, et al. Adipose-selective targeting of the GLUT4 gene impairs insulin action in muscle and liver. *Nature*. 2001;409(6821):729–733.
7. Choi YH, et al. Alterations in regulation of energy homeostasis in cyclic nucleotide phosphodiesterase 3B-null mice. *J Clin Invest*. 2006;116(12):3240–3251.
8. Matsushime H, et al. Identification and properties of an atypical catalytic subunit (p34PSK-J3/cdk4) for mammalian D type G1 cyclins. *Cell*. 1992;71(2):323–334.
9. Connell-Crowley L, Harper JW, Goodrich DW. Cyclin D1/Cdk4 regulates retinoblastoma protein-mediated cell cycle arrest by site-specific phosphorylation. *Mol Biol Cell*. 1997;8(2):287–301.
10. Malumbres M, Barbacid M. Cell cycle, CDKs and cancer: a changing paradigm. *Nat Rev Cancer*. 2009;9(3):153–166.
11. Rane SG, et al. Loss of Cdk4 expression causes insulin-deficient diabetes and Cdk4 activation results in beta-islet cell hyperplasia. *Nat Genet*. 1999;22(1):44–52.
12. Serrano M, Hannon GJ, Beach D. A new regulatory motif in cell-cycle control causing specific inhibition of cyclin D/CDK4. *Nature*. 1993;366(6456):704–707.

13. Martin J, et al. Genetic rescue of Cdk4 null mice restores pancreatic beta-cell proliferation but not homeostatic cell number. *Oncogene*. 2003;22(34):5261–5269.
14. Abella A, et al. Cdk4 promotes adipogenesis through PPARgamma activation. *Cell Metab*. 2005;2(4):239–249.
15. Sarruf DA, Iankova I, Abella A, Assou S, Miard S, Fajas L. Cyclin D3 promotes adipogenesis through activation of peroxisome proliferator-activated receptor gamma. *Mol Cell Biol*. 2005;25(22):9985–9995.
16. Fajas L, Landsberg RL, Huss-Garcia Y, Sardet C, Lees JA, Auwerx J. E2Fs regulate adipocyte differentiation. *Dev Cell*. 2002;3(1):39–49.
17. Jimenez V, et al. In vivo adeno-associated viral vector-mediated genetic engineering of white and brown adipose tissue in adult mice. *Diabetes*. 2013;62(12):4012–4022.
18. Sotillo R, et al. Wide spectrum of tumors in knock-in mice carrying a Cdk4 protein insensitive to INK4 inhibitors. *EMBO J*. 2001;20(23):6637–6647.
19. Rodriguez-Diez E, et al. Cdk4 and Cdk6 cooperate in counteracting the INK4 family of inhibitors during murine leukemogenesis. *Blood*. 2014;124(15):2380–2390.
20. Zechner R, et al. FAT SIGNALS — lipases and lipolysis in lipid metabolism and signaling. *Cell Metab*. 2012;15(3):279–291.
21. Fry DW, et al. Specific inhibition of cyclin-dependent kinase 4/6 by PD 0332991 and associated antitumor activity in human tumor xenografts. *Mol Cancer Ther*. 2004;3(11):1427–1438.
22. Hilhorst R, Houkes L, Mommersteeg M, Musch J, van den Berg A, Ruijtenbeek R. Peptide microarrays for profiling of serine/threonine kinase activity of recombinant kinases and lysates of cells and tissue samples. *Methods Mol Biol*. 2013;977:259–271.
23. Thirone AC, Huang C, Klip A. Tissue-specific

roles of IRS proteins in insulin signaling and glucose transport. *Trends Endocrinol Metab*. 2006;17(2):72–78.
24. Malumbres M, Barbacid M. Mammalian cyclin-dependent kinases. *Trends Biochem Sci*. 2005;30(11):630–641.
25. Viglietto G, et al. Cytoplasmic relocalization and inhibition of the cyclin-dependent kinase inhibitor p27(Kip1) by PKB/Akt-mediated phosphorylation in breast cancer. *Nat Med*. 2002;8(10):1136–1144.
26. Zhou BP, Liao Y, Xia W, Spohn B, Lee MH, Hung MC. Cytoplasmic localization of p21Cip1/WAF1 by Akt-induced phosphorylation in HER-2/neu-overexpressing cells. *Nat Cell Biol*. 2001;3(3):245–252.
27. Reuveni H, et al. Therapeutic destruction of insulin receptor substrates for cancer treatment. *Cancer Res*. 2013;73(14):4383–4394.
28. Baserga R. The insulin receptor substrate-1: a biomarker for cancer? *Exp Cell Res*. 2009;315(5):727–732.
29. Heilmann AM, et al. CDK4/6 and IGF1 receptor inhibitors synergize to suppress the growth of p16INK4A-deficient pancreatic cancers. *Cancer Res*. 2014;74(14):3947–3958.
30. Vora SR, et al. CDK 4/6 inhibitors sensitize PIK3CA mutant breast cancer to PI3K inhibitors. *Cancer Cell*. 2014;26(1):136–149.
31. Muranen T, Meric-Bernstam F, Mills GB. Promising rationally derived combination therapy with PI3K and CDK4/6 inhibitors. *Cancer Cell*. 2014;26(1):7–9.
32. Miller ML, et al. Drug synergy screen and network modeling in dedifferentiated liposarcoma identifies CDK4 and IGF1R as synergistic drug targets. *Sci Signal*. 2013;6(294):ra85.
33. Turner NC, et al. Palbociclib in hormone-receptor-positive advanced breast cancer. *N Engl J Med*. 2015;373(3):209–219.
34. Asghar U, Witkiewicz AK, Turner NC, Knudsen

ES. The history and future of targeting cyclin-dependent kinases in cancer therapy. *Nat Rev Drug Discov*. 2015;14(2):130–146.

35. Menendez JA, Lupu R. Fatty acid synthase and the lipogenic phenotype in cancer pathogenesis. *Nat Rev Cancer*. 2007;7(10):763–777.

36. Copps KD, White MF. Regulation of insulin sensitivity by serine/threonine phosphorylation of insulin receptor substrate proteins IRS1 and IRS2. *Diabetologia*. 2012;55(10):2565–2582.

37. Solinas G, Naugler W, Galimi F, Lee MS, Karin M. Saturated fatty acids inhibit induction of insulin gene transcription by JNK-mediated phosphorylation of insulin-receptor substrates. *Proc Natl Acad Sci U S A*. 2006;103(44):16454–16459.

38. Sharfi H, Eldar-Finkelman H. Sequential phosphorylation of insulin receptor substrate-2 by glycogen synthase kinase-3 and c-Jun NH2-terminal kinase plays a role in hepatic insulin signaling. *Am J Physiol Endocrinol Metab*. 2008;294(2):E307–E315.

39. Fritsche L, et al. Insulin-induced serine phosphorylation of IRS-2 via ERK1/2 and mTOR: studies on the function of Ser675 and Ser907. *Am J Physiol Endocrinol Metab*. 2011;300(5):E824–E836.

40. Boura-Halfon S, Zick Y. Phosphorylation of IRS proteins, insulin action, and insulin resistance. *Am J Physiol Endocrinol Metab*. 2009;296(4):E581–E591.

41. Blanchet E, et al. E2F transcription factor-1 regulates oxidative metabolism. *Nat Cell Biol*. 2011;13(9):1146–1152.

42. Withers DJ, et al. Disruption of IRS-2 causes type 2 diabetes in mice. *Nature*. 1998;391(6670):900–904.

43. Tsuruzoe K, Emkey R, Kriauciunas KM, Ueki K, Kahn CR. Insulin receptor substrate 3 (IRS-3) and IRS-4 impair IRS-1- and IRS-2-mediated signaling. *Mol Cell Biol*. 2001;21(1):26–38.

44. Benhamed F, et al. The lipogenic transcription factor ChREBP dissociates hepatic steatosis from insulin resistance in mice and humans. *J Clin Invest*. 2012;122(6):2176–2194.

45. Annicotte JS, et al. The CDK4-pRB-E2F1 pathway controls insulin secretion. *Nat Cell Biol*. 2009;11(8):1017–1023.

CDK4 Phosphorylates AMPKα2 to Inhibit Its Activity and Repress Fatty Acid Oxidation

Lopez-Mejia IC, Lagarrigue S, Giralt A, Martinez-Carreres L, Zanou N, Denechaud PD, **Castillo-Armengol J**, Chavey C, Orpinell M, Delacuisine B, Nasrallah A, Collodet C, Zhang L, Viollet B, Hardie DG, Fajas L.

In this article, it is demonstrated that CDK4 regulates oxidative metabolism by modulating AMPK activity. In fact, here we show that AMPK is a new target of CDK4 to repress its activation and therefore, inhibit fatty acid oxidation. My work in this project included tissue dissection and analysis of AMPK activation checking downstream effectors by western blot.

Article

CDK4 Phosphorylates AMPKα2 to Inhibit Its Activity and Repress Fatty Acid Oxidation

Graphical Abstract
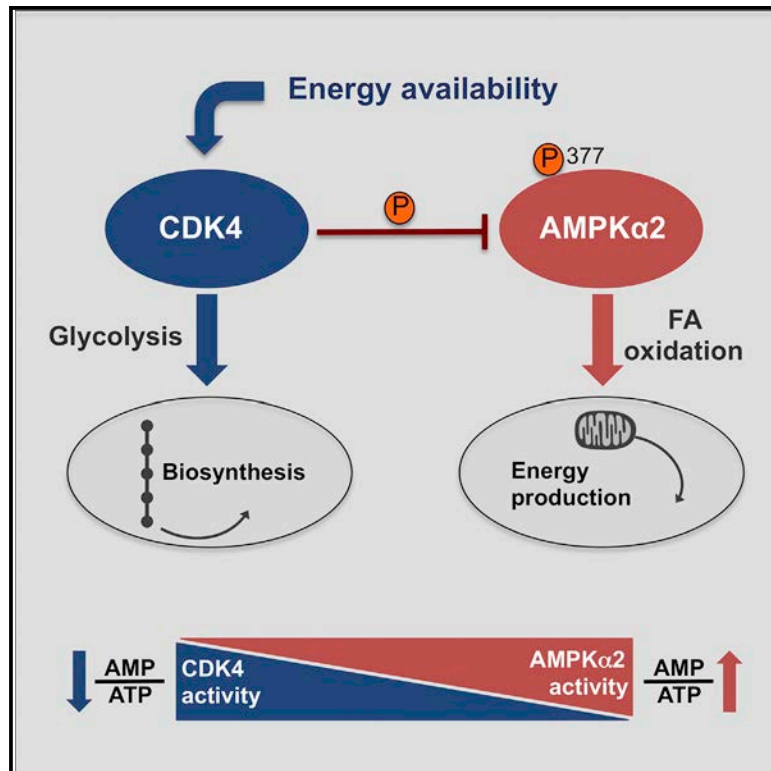
Authors

Isabel C. Lopez-Mejia,
Sylviane Lagarrigue, Albert Giralt, ...,
Benoît Viollet, D. Grahame Hardie,
Lluis Fajas

Correspondence

lluis.fajas@unil.ch

In Brief

Lopez-Mejia et al. show in this study that CDK4, a protein that is usually involved in the control of cell division, is an important regulator of the energy balance of the cell through the direct inhibition of the activity of AMPK, which is a major regulator of energy consuming processes.

Highlights

- CDK4 promotes glycolysis and inhibits fatty acid oxidation

- CDK4 inhibits AMPK activity through direct phosphorylation of the AMPK-α2 subunit

- Mice treated with CDK4 inhibitor have AMPK-dependent increased oxidative metabolism

CellPress

CDK4 Phosphorylates AMPKα2 to Inhibit Its Activity and Repress Fatty Acid Oxidation

Isabel C. Lopez-Mejia,[1,2] Sylviane Lagarrigue,[2] Albert Giralt,[1] Laia Martinez-Carreres,[1] Nadège Zanou,[2,3]
Pierre-Damien Denechaud,[1,2] Judit Castillo-Armengol,[1] Carine Chavey,[4] Meritxell Orpinell,[2] Brigitte Delacuisine,[1,2]
Anita Nasrallah,[1] Caterina Collodet,[5,6] Lianjun Zhang,[7] Benoît Viollet,[8,9,10] D. Grahame Hardie,[11] and Lluis Fajas[1,2,12,*]
[1]Center for Integrative Genomics, University of Lausanne, 1015 Lausanne, Switzerland
[2]Department of Physiology, University of Lausanne, 1005 Lausanne, Switzerland
[3]Institute of Sport Sciences, University of Lausanne, 1015 Lausanne, Switzerland
[4]IGMM, Université de Montpellier, UMR 5535 CNRS, 34293 Montpellier, France
[5]Nestlé Institute of Health Sciences SA, EPFL Innovation Park, 1015 Lausanne, Switzerland
[6]École Polytechnique Fédérale de Lausanne, School of Life Sciences, 1015 Lausanne, Switzerland
[7]Ludwig Center for Cancer Research, University of Lausanne, 1066 Epalinges, Switzerland
[8]Institut Cochin, INSERM U1016, Paris, France
[9]CNRS, UMR 8104, Paris, France
[10]Université Paris Descartes, Sorbonne Paris Cité, Paris, France
[11]School of Life Sciences, University of Dundee, Dundee, Scotland, UK
[12]Lead Contact
*Correspondence: lluis.fajas@unil.ch
https://doi.org/10.1016/j.molcel.2017.09.034

SUMMARY

The roles of CDK4 in the cell cycle have been extensively studied, but less is known about the mechanisms underlying the metabolic regulation by CDK4. Here, we report that CDK4 promotes anaerobic glycolysis and represses fatty acid oxidation in mouse embryonic fibroblasts (MEFs) by targeting the AMP-activated protein kinase (AMPK). We also show that fatty acid oxidation (FAO) is specifically induced by AMPK complexes containing the α2 subunit. Moreover, we report that CDK4 represses FAO through direct phosphorylation and inhibition of AMPKα2. The expression of non-phosphorylatable AMPKα2 mutants, or the use of a CDK4 inhibitor, increased FAO rates in MEFs and myotubes. In addition, $Cdk4^{-/-}$ mice have increased oxidative metabolism and exercise capacity. Inhibition of CDK4 mimicked these alterations in normal mice, but not when skeletal muscle was AMPK deficient. This novel mechanism explains how CDK4 promotes anabolism by blocking catabolic processes (FAO) that are activated by AMPK.

INTRODUCTION

Promitotic signals such as growth factors increase the levels of D-type cyclins (cyclins D1, D2, and D3), which bind and activate CDK4/6 to trigger the phosphorylation of the retinoblastoma-associated protein pRB and other pocket proteins (i.e., p107 and p130) (Malumbres and Barbacid, 2005). Rb phosphorylation enables release of the E2F transcription factors that promote the

transcription of genes necessary for the replication of the genome (Malumbres and Barbacid, 2005). The role of CDK4 in the regulation of cell-cycle progression has been extensively studied in eumetazoan organisms, and alterations in CDK4 activity have been associated with cancer development and progression (Malumbres and Barbacid, 2001, 2009; O'Leary et al., 2016). For example, the R24C mutation, which is used in this study, renders CDK4 resistant to inhibition by INK4 inhibitors and has been reported to confer a genetic predisposition to melanoma (Rane et al., 1999, 2002; Wölfel et al., 1995).

Cell division requires substantial amounts of ATP, and numerous metabolic intermediates to support biosynthesis of essential molecules, such as lipids and nucleic acids. Proliferating cells preferentially use anaerobic glycolysis to generate large amounts of ATP and provide metabolic intermediates to support cell growth (Jones and Thompson, 2009). Growing evidence demonstrates that regulatory crosstalk exists between metabolic pathways and regulators of cell-cycle progression. Mitochondrial respiration and metabolism are coordinated with cell-cycle progression by cell-cycle regulators (Lopez-Mejia and Fajas, 2015; Salazar-Roa and Malumbres, 2016). Our laboratory and others have demonstrated that CDK4 is one such "metabolic" cell-cycle regulator (Blanchet et al., 2011; Icreverzi et al., 2012; Lagarrigue et al., 2016; Lee et al., 2014). Indeed, we have previously shown that CDK4 regulates oxidative metabolism via the E2F1 transcription factor in muscle and brown adipose tissue (Blanchet et al., 2011) and promotes the insulin-signaling pathway in mature adipocytes (Lagarrigue et al., 2016). Overall, the participation of cell-cycle regulators in the control of energy homeostasis occurs mainly through the activation of anabolic processes (Aguilar and Fajas, 2010). The AMP-activated protein kinase (AMPK) is a central inhibitor of such anabolic processes and might therefore be repressed by cell-cycle regulators. Under conditions of low cellular energy, AMP and ADP are increased relative to ATP, and this is sensed by AMPK.

AMPK exists as heterotrimeric complexes composed of a catalytic subunit (α) and two regulatory subunits (β and γ); the α and β subunits exist as two isoforms ($\alpha1/\alpha2$ and $\beta1/\beta2$, encoded by the *PRKAA1/2* and *PRKAB1/2* genes), and the γ subunit exists as three isoforms ($\gamma1/\gamma2/\gamma3$, encoded by *PRKAG1/2/3*), thus generating up to 12 combinations of heterotrimeric complex (Carling, 2004; Grahame Hardie, 2016; Hardie et al., 2012; Ross et al., 2016b). AMPK is regulated both by phosphorylation/dephosphorylation and by the relative cellular concentrations of adenine nucleotides, with the two mechanisms being intimately linked. First, the upstream kinases LKB1 (liver kinase B1) (Hawley et al., 2003; Shaw et al., 2004; Woods et al., 2003) or CaMKK2 (calmodulin-dependent kinase kinase-2/-β) (Hawley et al., 2005; Hurley et al., 2005; Woods et al., 2005) activate AMPK through the phosphorylation of Thr^{172} of the α subunit (Hawley et al., 1996). Second, AMPK is regulated through the competitive binding of ATP or AMP and ADP at up to three sites on the γ subunit. When cellular energy levels are low, binding of AMP or ADP enhances Thr^{172} phosphorylation by LKB1 and inhibits Thr^{172} dephosphorylation by protein phosphatases, while binding of AMP (but not ADP) causes further allosteric activation (Ross et al., 2016a). Metabolic stresses that reduce intracellular ATP concentrations are therefore the best-characterized activators of AMPK, although it has recently been shown that glucose deprivation can activate AMPK by an adenine nucleotide-independent mechanism (Zhang et al., 2017). Once activated, AMPK promotes catabolic pathways that generate ATP (e.g., fatty acid oxidation [FAO]) while switching off anabolic pathways and other ATP-requiring processes to restore cellular ATP levels (Carling, 2004; Grahame Hardie, 2016; Hardie et al., 2012; Ross et al., 2016b).

Other kinase activities that are induced by growth stimuli are known to inhibit AMPK. This includes AKT a key effector of the insulin/insulin growth factor 1 (IGF1)-signaling pathway that antagonizes the AMPK pathway through phosphorylation of AMPKα1 on Ser^{487} (Horman et al., 2006), or extracellular signal-regulated kinase (ERK), which was shown to phosphorylate the same residue (López-Cotarelo et al., 2015). The cyclic-AMP-dependent protein kinase (PKA) also phosphorylates and negatively regulates AMPK (Djouder et al., 2010; Hurley et al., 2006), and Thr^{481} and Ser^{477} on AMPKα1 are phosphorylated by glycogen synthase kinase 3 (GSK3) (Suzuki et al., 2013), following a "priming" phosphorylation of Ser^{487} by AKT.

Muscle function requires a finely tuned balance between anabolism and catabolism in order to respond to physiological challenges within the available energy supply. AMPK is a major coordinator of energy intake and utilization in exercising muscle (Hoffman et al., 2015), functioning to enhance energy availability. Among other effects, AMPK promotes FAO to maintain ATP cellular stores, although the exact role of AMPK in regulation of muscle FAO has been controversial (Mounier et al., 2015).

In this study, we sought to determine whether CDK4 participates in energy homeostasis by inhibiting catabolic processes. The mechanisms by which the activity of AMPK is inhibited under anabolic conditions, such as during cell-cycle progression or in resting muscle, have not been thoroughly studied. We report here that CDK4 enhances anaerobic glycolysis and represses fatty acid oxidation. Surprisingly, the AMPKα1 and α2 subunits play distinct roles. We provide here a molecular mechanism whereby CDK4-CycD3 complexes directly repress α2-containing complexes to inhibit FAO. We show that chemical and genetic inhibition of CDK4 also promotes oxidative metabolism *in vivo*, as evidenced by decreased respiratory exchange ratio (RER) and increased exercise performance in mice lacking CDK4 activity.

RESULTS

CDK4 Modulates FAO in an E2F1-Independent Manner

We previously demonstrated that CDK4 is a major mediator of insulin signaling and therefore contributes to the positive regulation of biosynthetic processes, such as fatty acid synthesis, and the inhibition of catabolic pathways, such as lipolysis (Lagarrigue et al., 2016). To further investigate the contribution of CDK4 to metabolic regulation, Seahorse analyses were performed. *Cdk4$^{R24C/R24C}$* mouse embryonic fibroblasts (MEFs), which express a hyperactive CDK4 mutant, exhibited a significant increase in anaerobic glycolysis, as measured by the extracellular acidification rate (ECAR), whereas *Cdk4$^{-/-}$* MEFs had impaired anaerobic glycolysis (Figures 1A and 1B). In contrast, CDK4 activity was inversely correlated with FAO. *Cdk4$^{R24C/R24C}$* MEFs metabolized palmitate at a low rate, whereas *Cdk4$^{-/-}$* MEFs showed increased palmitate oxidation (Figures 1C and 1D). Interestingly, the effects of CDK4 on substrate use were independent of E2F1 activity, since deletion of E2F1 in *Cdk4$^{R24C/R24C}$* MEFs failed to reverse the effects of *Cdk4^{R24C}* on anaerobic glycolysis or palmitate oxidation (Figures 1E–1H). These results suggest that CDK4 controls substrate utilization in MEFs independently of E2F1.

CDK4 Regulation of FAO Is AMPK Dependent

The decrease in FAO observed in response to constitutive activation of CDK4 is the opposite of the effect seen with AMPK activation (Fullerton et al., 2013; Hardie, 2015; Hardie and Pan, 2002; O'Neill et al., 2014). Therefore, we analyzed the involvement of AMPK in the CDK4-mediated regulation of FAO in MEFs. Basal levels of phosphorylated ACC (pACC), which is a known target and marker of AMPK activity, were decreased in *Cdk4$^{R24C/R24C}$* MEFs but increased 3-fold in the *Cdk4$^{-/-}$* cells (Figures 2A, 2B, S1A, and S1B), suggesting that CDK4 antagonizes AMPK function. Moreover, the activation of AMPK by the specific activator A769662 (Göransson et al., 2007; Moreno et al., 2008) was reduced in *Cdk4$^{R24C/R24C}$* MEFs (Figures 2A and 2B), suggesting that CDK4 can prevent AMPK activation. In addition, increased AMP/ATP and ADP/ATP ratios were observed in MEFs expressing the hyperactive CDK4 mutant, which suggested a lower catabolic rate (Figures 2C and 2D). Interestingly, in *Cdk4$^{-/-}$* MEFs, comparable pACC levels were measured both in the basal state and upon AMPK stimulation (Figures 2A and 2B). This finding implies that in the absence of CDK4, AMPK reaches its activated state without need for any further stimulation. Likewise in *Cdk4$^{-/-}$* cells and wild-type (WT) MEFs treated with A769662, we observed a significant decrease of AMP/ATP and ADP/ATP ratios (Figures 2C–2F).
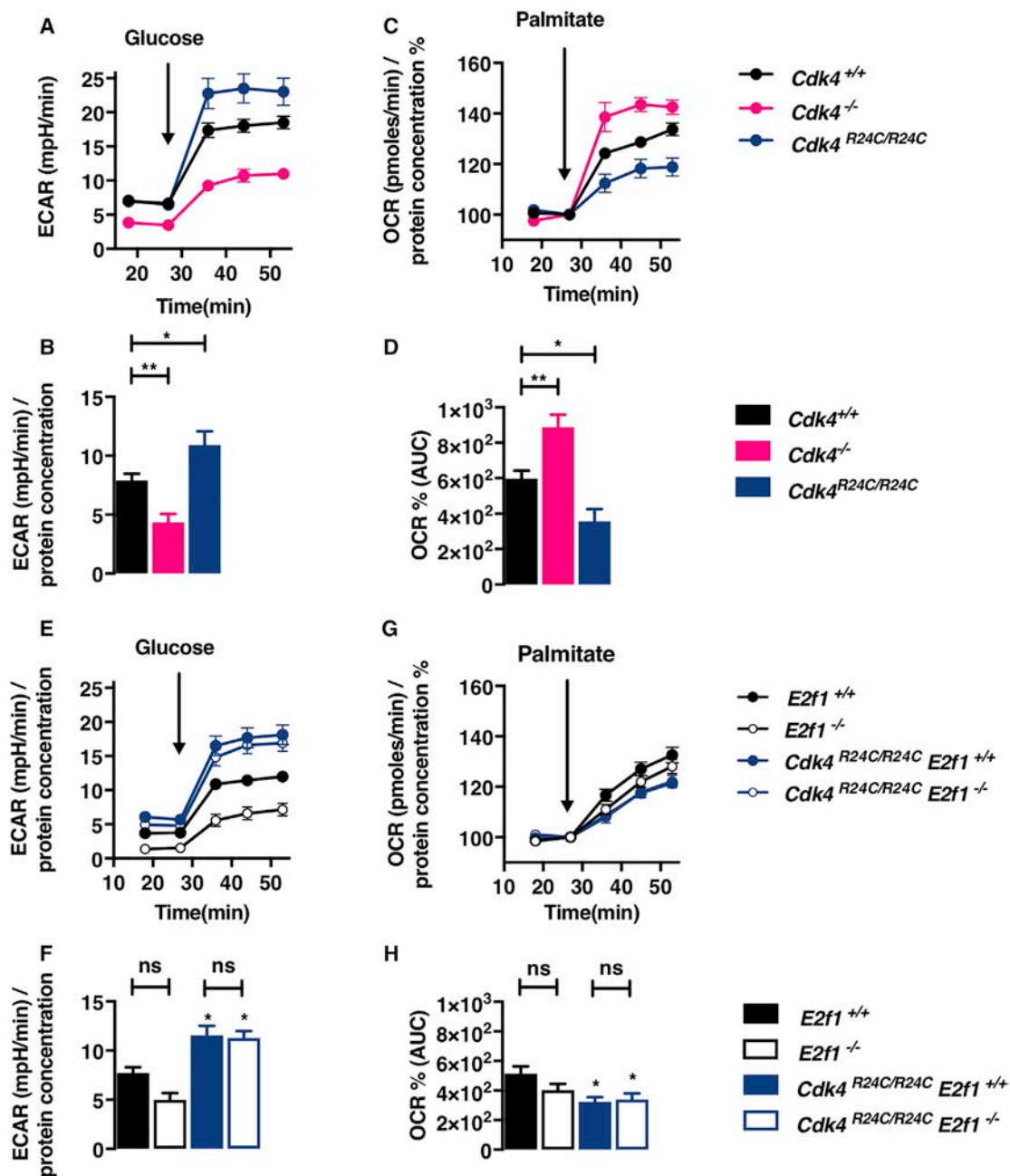
Figure 1. CDK4 Modulates FAO in an E2F1-Independent Manner

(A–D) *Cdk4*$^{+/+}$, *Cdk4*$^{-/-}$, and *Cdk4*$^{R24C/R24C}$ MEFs were submitted to a glycolysis assay, during which ECAR was measured at the basal level and upon glucose injection (A), or to a FAO assay, in which the palmitate induced OCR was measured (in % OCR compared to the basal OCR) (C). The glycolytic rate was calculated (B). The area under curve of the palmitate induced OCR was quantified (D).

(E–H) *E2f1*$^{+/+}$, *E2f1*$^{-/-}$, *Cdk4*$^{R24C/R24C}$ *E2f1*$^{+/+}$, and *Cdk4*$^{R24C/R24C}$ *E2f1*$^{-/-}$ MEFs were submitted to a glycolysis assay, during which ECAR was measured at the basal level and upon glucose injection (E), or to a FAO assay, in which the palmitate induced OCR was measured (in % OCR compared to the basal OCR) (G). The glycolytic rate was calculated in (F). The area under curve of the palmitate induced OCR was quantified in (H).

Data are expressed as mean ± SEM.

Next, we studied the physiological relevance of the increase in AMPK activity in *Cdk4*$^{-/-}$ cells using FAO assays in MEFs treated with A769662 and with the non-selective AMPK inhibitor compound C. As expected, the levels of palmitate oxidation in WT MEFs were at least 25% higher in A769662-treated cells (Figures 2G, S1C, and S1D). However, *Cdk4*$^{-/-}$ cells did not respond in the same assay to A769662 treatment. By contrast, AMPK activation by A769662 in *Cdk4*$^{R24C/R24C}$ MEFs was only able to
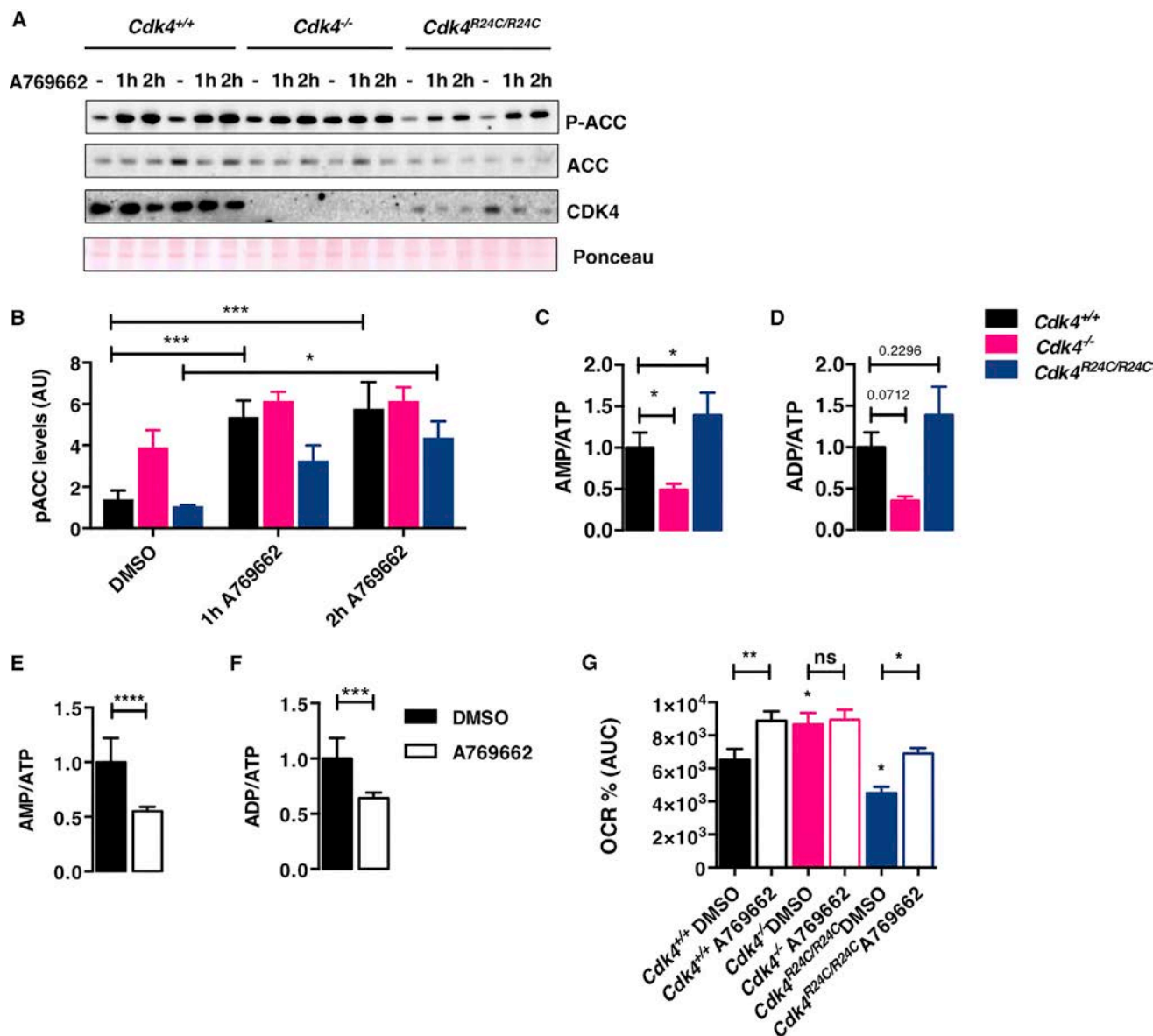
Figure 2. CDK4 Regulation of FAO Is AMPK Dependent

(A) $Cdk4^{+/+}$, $Cdk4^{-/-}$, and $Cdk4^{R24C/R24C}$ MEFs were starved for 3 hr and then stimulated with 50 μM A769662; western blot analysis shows the A769662-induced ACC phosphorylation in $Cdk4^{+/+}$, $Cdk4^{-/-}$, and $Cdk4^{R24C/R24C}$ cells.

(B) Quantification of pACC levels.

(C and D) SV40 immortalized cells were placed in KHB medium containing 1.5 mM carnitine and 300 μM oleate for AMP, ADP, and ATP quantification by HPLC, and AMP/ATP (C) and ADP/ATP (D) ratios are shown.

(E and F) AMP/ATP (E) and ADP/ATP (F) ratios of WT SV40 immortalized cells treated with 50 μM A769662 for 8 hr.

(G) $Cdk4^{+/+}$, $Cdk4^{-/-}$, and $Cdk4^{R24C/R24C}$ MEFs were treated with DMSO or 50 μM A769662 for 2 hr in KHB medium and submitted to a FAO assay in which the palmitate induced OCR was measured (in % OCR compared to the basal OCR). The area under curve of the palmitate-induced OCR was quantified.

Data are expressed as mean ± SEM. See also Figure S1.

restore WT levels of FAO (Figures 2G, S1C, and S1D). AMPK inhibition in $Cdk4^{-/-}$ cells (albeit by the non-selective inhibitor compound C) produced consistent results. The levels of pACC in CDK4-null MEFs, as well as the increased FAO levels, were restored back to basal levels (Figures S1E–S1G). Taken together, these results suggest that CDK4 inhibits the AMPK pathway.

The AMPKα2 Subunit Is Required for Efficient FAO in MEFs

Our results suggested that CDK4 has a negative effect on FAO via the regulation of AMPK activity, raising the question of which AMPK subunits contribute to this effect. Interestingly, the deletion of either AMPKα subunit in MEFs resulted in increased
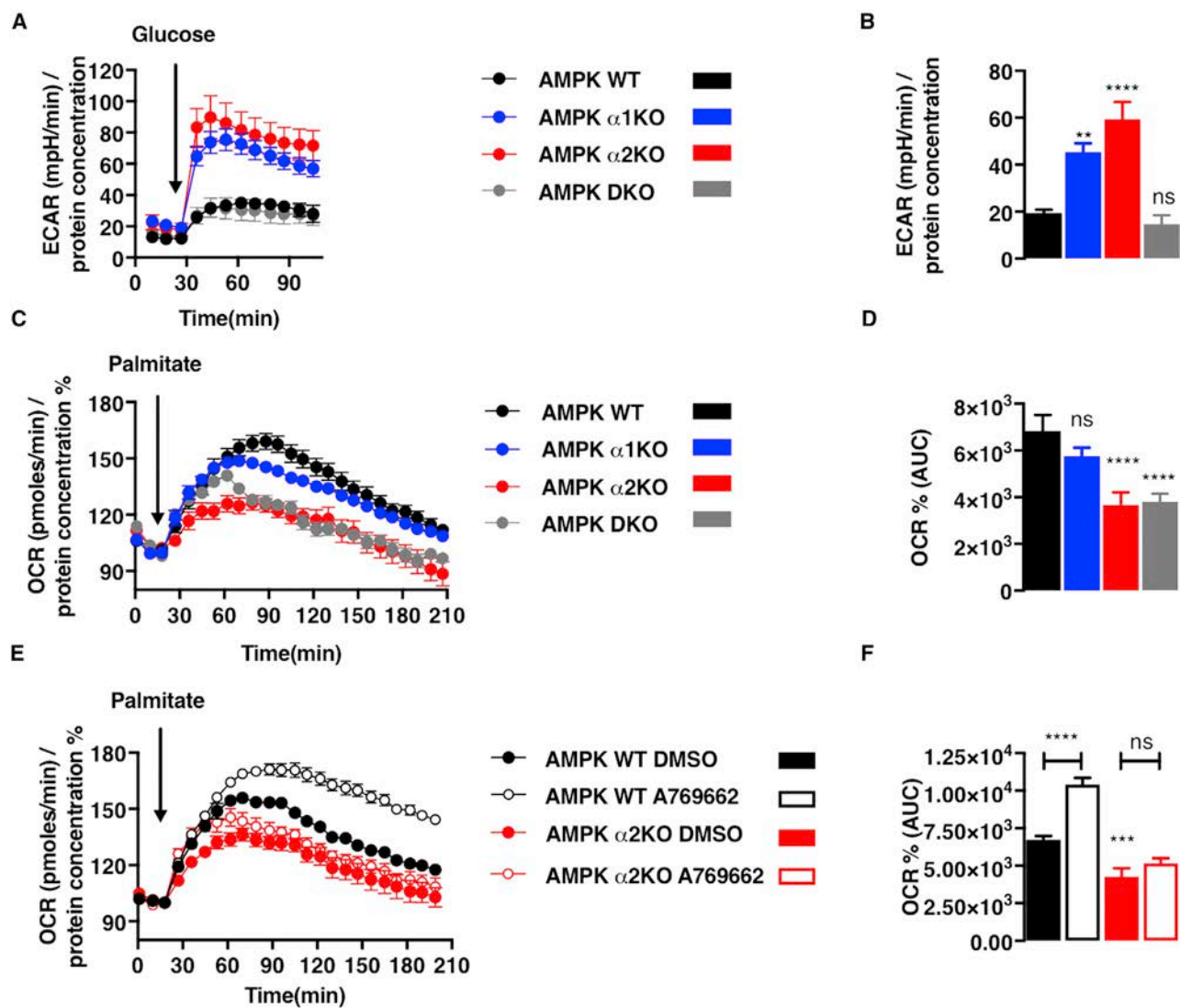
Figure 3. The AMPKα2 Subunit Is Required for Efficient Fatty Acid Oxidation in MEFs

(A–D) AMPK WT, AMPK α1 KO, AMPK α2 KO, and AMPK DKO SV40-immortalized MEFs were submitted to a glycolysis assay, during which ECAR was measured at the basal level and upon glucose injection (A), or to a FAO assay, in which the palmitate induced OCR was measured (in % OCR compared to the basal OCR) (C). The glycolytic rate was calculated (B). The area under curve of the palmitate induced OCR was quantified (D).

(E and F) AMPK WT and AMPK α2 KO SV40-immortalized MEFs were treated for 2 hr with DMSO or 50 μM A769662 for 2 hr in KHB medium and submitted to a FAO assay in which the palmitate induced OCR was measured (in % OCR compared to the basal OCR) (E). The area under curve of the palmitate induced OCR was quantified (F).

Data are expressed as mean ± SEM. See also Figure S2.

ECAR, indicating increased glycolysis, whereas the complete abrogation of AMPK activity had no effect, perhaps due to disruption of glucose transport into the cells (Figures 3A and 3B). However, although AMPKα1 knockout (KO) MEFs metabolized palmitate as efficiently as control cells, both AMPKα2KO and AMPK α1/α2 double-knockout (DKO) cells exhibited significantly reduced levels of FAO (Figures 3C and 3D). Consistently, A769662 failed to trigger FAO in cells lacking the α2 subunit (both α2KO and DKO). Thus, despite being more abundant in MEFs (Morizane et al., 2011), the AMPKα1 subunit cannot substitute for the α2 subunit in the control of FAO, even when allosterically

activated by A769662 (Figures 3E, 3F, S1H, and S1I). In addition, ACC phosphorylation could be detected upon stimulation with A769662 in both AMPK α1KO and AMPK α2KO MEFs (Figure S1J), suggesting that both AMPK subunits can phosphorylate ACC1 and therefore inhibit lipid synthesis, but only AMPKα2 can promote FAO. Taken together, these results suggest that AMPK complexes containing α2 specifically control FAO.

CDK4 Phosphorylates the AMPK α2 Subunit

The inhibition of AMPKα2-dependent FAO could be the result of a direct phosphorylation by CDK4. *In vitro* kinase assays showed
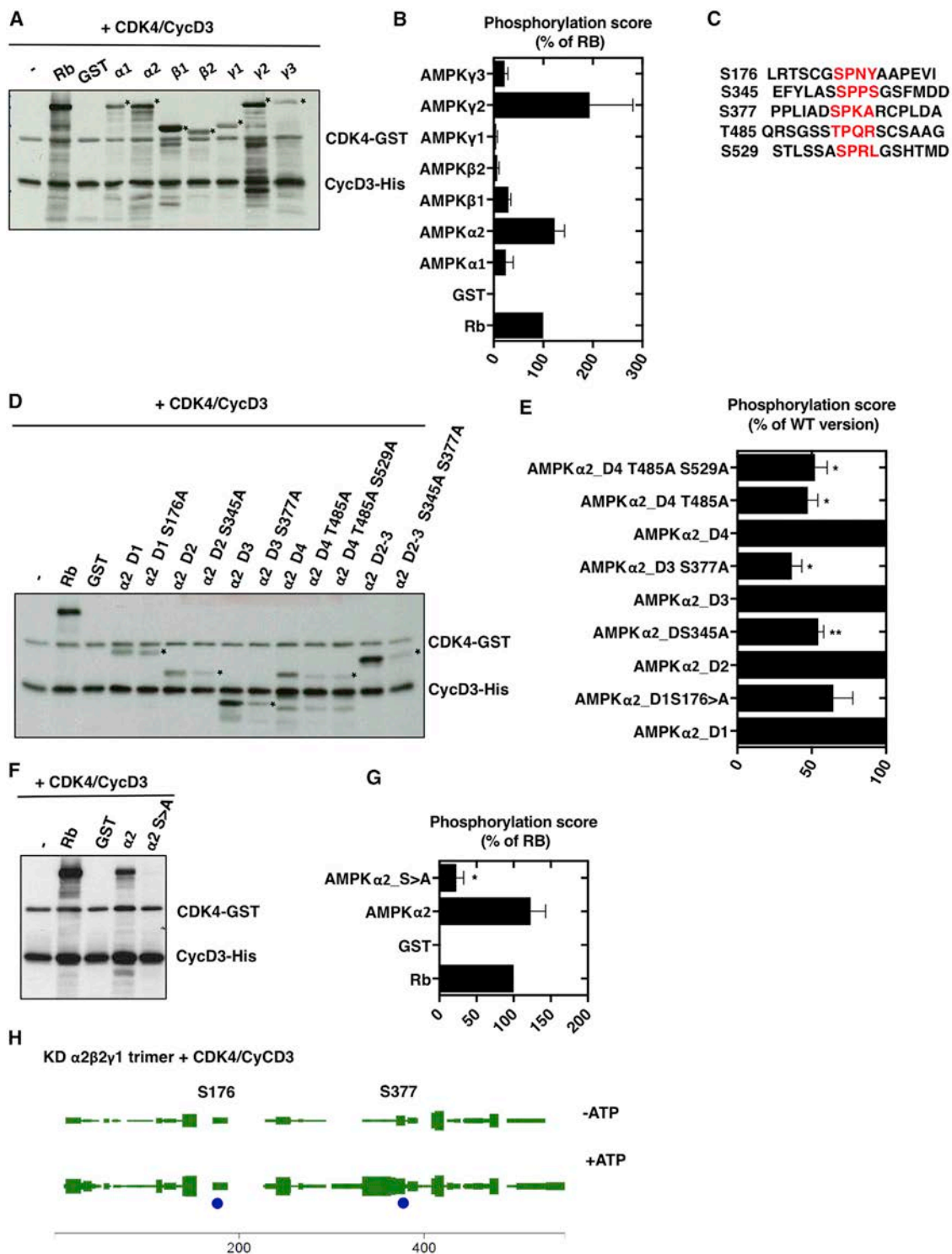
Figure 4. CDK4 Phosphorylates the AMPKα2 Subunit

(A) Cyclin D3-CDK4 directly phosphorylates full-length GST-AMPK subunits *in vitro* (n = 3). Asterisks mark the proteins of interest.

(B) Phosphorylation score (in percentage of RB phosphorylation).

(C) CDK consensus sites in human AMPKα2 (*PRKAA2*).

(D) *In vitro* phosphorylation of WT and mutated (Ser or Thr to Ala) GST-AMPK α2 fragments (D1, 1–245 aa; D2, 246–356 aa; D3, 357–422 aa; D4, 432–522; and D2–D3, 246–422 aa) by cyclin D3/CDK4 (n = 3).

(legend continued on next page)

that recombinant CDK4/CycD3 phosphorylated all glutathione S-transferase (GST) fusions of AMPK subunits tested at different levels (Figure 4A; loading control in Figure S2A). Interestingly, AMPKα2 and AMPKγ2 were phosphorylated by CDK4 to a greater extent than pRB, which is the canonical CDK4 substrate (Figure 4B). Since the specificity of CDKs is partially determined by substrate docking on the cyclin subunit, kinase assays were also performed using recombinant CDK4/CycD1 instead of CDK4/CycD3. The phosphorylation of the AMPK subunits was very low under these conditions (Figure S2B), suggesting that AMPK phosphorylation by CDK4 requires recognition by cyclin D3.

AMPKα2 was predicted to contain 6 CDK4 phosphorylation sites (Thr^{85}, Ser^{176}, Ser^{345}, Ser^{377}, Thr^{485}, and Ser^{529}). Out of these six potential sites, five were listed in the phosphoNET database (Figure 4C). Site-directed mutagenesis (S > A or T > A) combined with protein truncation studies (Figure S3C) identified Ser^{345}, Ser^{377}, Thr^{485}, and Ser^{529} as CDK4 phosphorylation sites (Figures 4D and 4E; loading control in Figure S3D). Phosphorylation by CDK4 was completely abrogated in a full-length recombinant protein carrying Ser to Ala or Thr to Ala mutations at the four CDK4 phosphosites (α2 S > A mutant), suggesting that the four newly identified residues account for all sites phosphorylated on GST-AMPKα2 by CDK4 in cell-free assays (Figure 4F and 4G; loading control in Figure S2E). The phosphorylation of Ser^{377} and Thr^{485} has been previously described in proteomic studies (Figure S2F) (Dinkel et al., 2011; Gnad et al., 2011; Hornbeck et al., 2015), including cell-cycle-related phosphoproteomes (Daub et al., 2008; Kettenbach et al., 2011), and in liver upon insulin stimulation (Humphrey et al., 2015), suggesting that the regulation of AMPK by CDK4 is important for cell-cycle progression and for the insulin signaling pathway. Moreover, we found the four newly identified CDK4 phosphosites to be conserved among the AMPKα2 subunits of several mammalian species (Figure S3A), but not between the AMPKα1 and AMPKα2 isoforms (Figure S3B).

In intact cells, AMPK is found as a heterotrimeric complex; therefore recombinant kinase-inactive α2β2γ1 complexes were also used as substrate for recombinant CDK4-CycD3 complexes. After mass spectrometry analysis, we obtained 83% coverage of the AMPKα2 subunit and observed the phosphorylation in Ser^{176} and Ser^{377} (Figure 4H). A targeted analysis to increase coverage showed phosphorylation of Thr^{485} and Ser^{529} with low detectability. The phosphorylation of Ser^{345} and Ser^{377} was also detected in myotubes and muscle tissue, which express high levels of the α2 subunit (Figures S4A and S4B; Table S1). Interestingly, our results suggest that these phosphorylations are present when AMPK is inactive, since the activating Thr^{172} phosphorylation was not found in 5 out of 6 experiments

(Figures S4A and S4B). Taken together, these data indicate that the α2 subunit of AMPK is a substrate for CDK4-CycD3 complexes in cell-free assays and that some of these phosphorylations occur *in vivo*, in conditions in which CDK4 is active (Blanchet et al., 2011; Lagarrigue et al., 2016) but AMPK is inactive.

AMPKα2 Phosphorylation Is Necessary and Sufficient for FAO Repression by CDK4

To elucidate the functional relevance of the phosphorylation of AMPKα2 by CDK4, we compared the regulatory activities of AMPKα2 S > A, AMPKα2, and AMPKα1 in the context of FAO. Transfection of AMPK DKO MEFs with the AMPKα2 S > A mutant conferred ACC phosphorylation levels that where higher than those observed in AMPKα1- or α2-transfected cells in the basal state and upon stimulation by A769662 (Figure 5A). Similarly, ectopic expression of the AMPKα2 S > A mutant in the FAO-defective AMPK DKO MEFs rescued palmitate oxidation to a greater extent than that observed upon transfection with WT AMPKα2 (Figures 5B and S5A). Taken together, these results indicate that defective targeting of AMPKα2 by CDK4 at Ser^{345}, Ser^{377}, Thr^{485}, and Ser^{529} results in increased AMPKα2 FAO-promoting activity.

In order to demonstrate that CDK4 represses FAO by inhibiting AMPK activity, WT and AMPK mutant cells were treated with CDK4 inhibitors. Inhibition of CDK4 activity by LY2835219 significantly increased FAO after 24 hr (Figures 5C and S5B) or 2 hr (Figure S5C) of treatment. Strikingly, the CDK4 inhibitor failed to increase FAO in both AMPK α2KO and AMPK DKO cells, but not in AMPK α1KO cells, demonstrating that CDK4 targets AMPKα2 to alter cellular metabolism (Figures 5C, S5B, and S5E–S5G). The overall positive effect of CDK4 inhibition on AMPK activity was confirmed by analyzing ACC phosphorylation. Indeed, LY2835219 treatment induced a dose-dependent increase in the phosphorylation of ACC (Figures S5H and S5I). This effect correlated with decreased CDK4 activity given that phosphorylation of RB Ser^{780} was also reduced (Figure S5I). Of note, increased ACC phosphorylation and increased FAO could be detected after 2 hr of CDK4 inhibition, whereas inhibition of RB phosphorylation required longer treatments. Moreover, LY2835219 had an effect comparable to that of A769662, significantly decreasing AMP/ATP and ADP/ATP ratios in WT MEFs (Figures 2E, 2F, 5D, and 5E). The use of LY2835219 suggests that CDK4 inhibition promotes catabolic processes in an AMPKα2-subunit-dependent manner.

We next decided to validate our findings in a more physiological cellular model. LY2835219 treatment induced an increase in FAO in C2C12 myotubes, which are known to express high levels of AMPKα2 (Figures S6A and S6B). In this model, CDK4 inhibition correlated with a dose-dependent increase of the

(E) Phosphorylation score (in percentage of the WT fragment).
(F) *In vitro* phosphorylation of full-length WT GST-AMPKα2 and full-length S > A GST-AMPKα2 by cyclin D3/CDK4 (n = 3).
(G) Phosphorylation score (in percentage of RB phosphorylation).
(H) Kinase-dead AMPK α2β2γ1 trimers were used as a substrate for cyclin D3-CDK4 complex and analyzed by mass spectrometry. A graphical overview of the sequence coverage of AMPKα2 human protein in samples displayed by MsViz is depicted. The thickness of the green bars is a function of the number of spectra matching the sequence region, while modification sites are labeled and shown as circles with size proportional to the number of spectra matching a given position. A truncated form of RB (hRB; 379–928 aa) was used as a positive control. A representative autoradiography for each kinase assay is shown.
See also Figure S3.
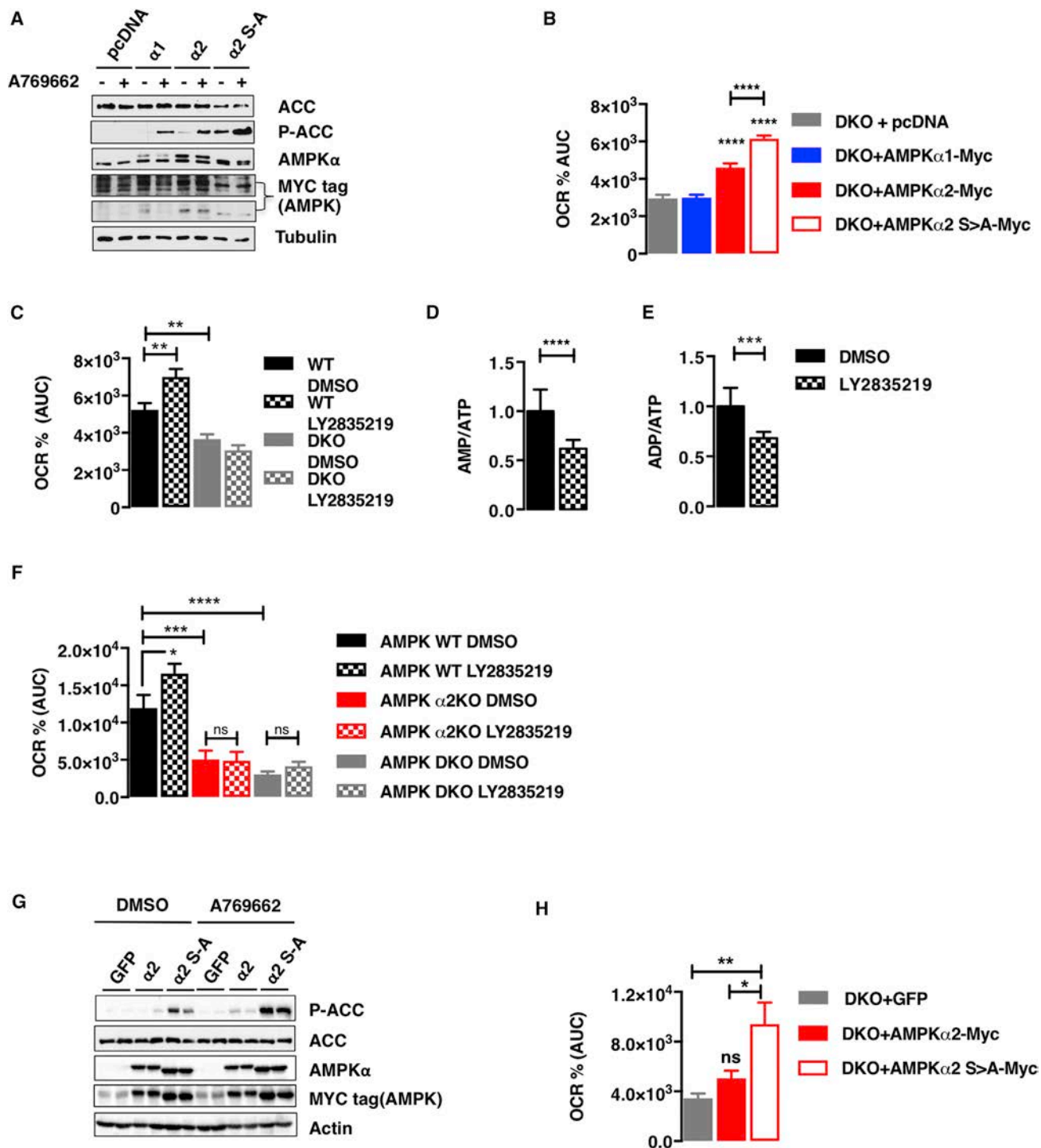
Figure 5. AMPKα2 Phosphorylation Is Necessary and Sufficient for FAO Repression by CDK4

(A) AMPK DKO SV40-immortalized MEFs were electroporated with plasmids encoding Myc-tagged AMPK α1, Myc-tagged AMPK α2 and Myc-tagged AMPK α2 S > A. 48 hr later, MEFs were starved for 3 hr and treated for 2 hr with DMSO or 50 μM A769662 before protein extraction. Western blot analysis shows the A769662-induced ACC phosphorylation in transfected cells.

(B) Electroporated MEFs were submitted to a FAO assay 48 hr after transfection, in which the palmitate induced OCR was measured (in % OCR compared to the basal OCR). The area under curve of the palmitate induced OCR was quantified.

(C) AMPK WT and AMPK DKO SV40-immortalized MEFs were treated with DMSO or LY2835219 (1.5 μM) for 24 hr and submitted to a FAO assay, in which the palmitate-induced OCR was measured (in % OCR compared to the basal OCR). The area under curve of the palmitate induced OCR was quantified.

(legend continued on next page)

phosphorylation of ACC, without significant increase of AMPK Thr^{172} phosphorylation (Figures S6C–S6E). The direct involvement of AMPKα2 was confirmed by analyzing myotubes lacking AMPKα2 or both the α1 and α2 subunits (Lantier et al., 2010). Like in MEFs, FAO was impaired in the α2KO and DKO myotubes. Similarly, the CDK4 inhibitor failed to increase FAO in α2KO and DKO myotubes (Figures 5F and S6F). Rescue of AMPK DKO myotubes with the AMPKα2 S > A mutant triggered ACC phosphorylation levels that where higher than those observed in AMPK α2-transfected cells both in the basal state or upon stimulation with A769662 (Figure 5G). Similarly, ectopic expression of the AMPKα2 S > A mutant in the FAO-defective AMPK DKO myotubes rescued palmitate oxidation to levels similar to those of WT myotubes (Figures 5H and S6G). Taken together, these results in muscle cells confirm that CDK4 modulates FAO through the specific inhibition of AMPKα2 activity and that a non-phosphorylatable AMPKα2 mutant has a FAO-promoting activity.

CDK4 Modulates Oxidative Metabolism and Exercise Capacity *In Vivo*

We next investigated the contribution of CDK4 to oxidative metabolism and muscle function *in vivo*. Isolated mitochondria from $Cdk4^{-/-}$ muscles showed increased oxygen consumption, suggesting increased fatty acid oxidation capacity (Figures 6A and 6B). Increased FAO was further demonstrated by using intact muscle fibers from flexor digitorum brevis (FDB) muscle (Figure 6C). Fibers from $Cdk4^{-/-}$ FDB muscle metabolized palmitate at a higher rate (Figures 6C and 6D) and were capable to reach a higher maximal respiration (Figures 6C and 6E). The increased capacity of the muscles of $Cdk4^{-/-}$ mice to oxidize fatty acids suggested an overall metabolic phenotype in these mice.

$Cdk4^{-/-}$ mice have decreased body weight (Figure 6F). Consistent with increased AMPK activity, $Cdk4^{-/-}$ mice exhibit increased exercise capacity and decreased RER, indicating a preference toward fat oxidation (Figures 6G–6I). An 8-day treatment with LY2835219 did not trigger significant alterations in body weight and food intake (Figures 6J and S7D), although it induced a consistent albeit non-significant decrease in fat mass (Figure S7C) and a modest but significant increase in exercise performance (Figure 6K). A decrease in RER was observed after 4–5 days of treatment (Figures 6L and 6M). *In vivo*, the inhibition of CDK4 triggered an increase in the phosphorylation of ACC in quadriceps muscle (Figures S7E and S7G), suggesting increased AMPK activity. This was accompanied by an increase of the slow-twitch fiber marker MyHC I (Figure S7I). MyHC I mRNA levels were also increased in gastrocnemius and tibialis muscles from LY2835219-treated animals (Figures S7H–S7J).

Overall, these data suggest that CDK4 is a negative regulator of exercise capacity and whole-body oxidative metabolism in mice.

CDK4 Regulation of Oxidative Metabolism and Exercise Capacity *In Vivo* Requires Muscle AMPK

To determine if the effects of CDK4 inhibition in exercise performance and whole-body oxidative metabolism require muscle AMPK, we treated muscle-specific AMPK α1/α2 KO mice (MDKO) (Lantier et al., 2014) with the CDK4 inhibitor. Consistently, treatment with LY2835219 did not trigger significant alterations in body weight or food intake (Figures 7A and S7M) in control or in AMPK MDKO animals. In control animals, LY2835219 was sufficient to trigger a decrease (albeit not significant [p = 0.1243]) in fat mass, a modest increase in exercise performance, and a decrease in RER (Figures 7B–7D and S7L). In agreement with previous reports (Lantier et al., 2014; O'Neill et al., 2011), AMPK MDKO animals showed decreased RER and decreased exercise capacity (Figures 7B–7D). However, they were not affected by the treatment with LY2835219 under our experimental conditions (Figures 7A–7D and S7K–S7M). Taken together, these results show that the negative effects of CDK4 in oxidative metabolism and exercise performance *in vivo* involve muscle AMPK activity.

DISCUSSION

The contribution of CDK4 to the control of cell-cycle progression, via pocket proteins and E2F transcription factors, has been extensively studied (Malumbres, 2014) for more than two decades. However, the CDK4/6-pRB/E2F1 pathway was only recently implicated in metabolic regulation (Aguilar and Fajas, 2010; Blanchet et al., 2011; Denechaud et al., 2016; Lagarrigue et al., 2016; Lee et al., 2014; Lopez-Mejia and Fajas, 2015; Petrov et al., 2016; Salazar-Roa and Malumbres, 2016). Our study provides evidence that the cell-cycle kinase CDK4 is a key player in the control of cellular energy homeostasis and can also act independently of E2F1 to regulate metabolic pathways.

Three major findings are described here. First, we found that CDK4 negatively regulates the AMPK pathway and thus inhibits FAO through phosphorylation of the AMPKα2 subunit. Indeed, $Cdk4^{-/-}$ MEFs behaved like cells treated with an AMPK activator and exhibited high FAO levels and low levels of anaerobic glycolysis. Consistently, $Cdk4^{R24C/R24C}$ cells exhibited increased anaerobic glycolysis and very low FAO levels. A similar phenotype was observed in AMPK α2KO MEFs. Therefore, CDK4 activity is inversely correlated with AMPKα2-dependent activity. These findings indicate that CDK4 plays a central role in

(D and E) AMPK WT SV40 immortalized cells were treated for 8 hr with DMSO or LY2835219 (1.5 μM). AMP, ADP, and ATP were quantified by HPLC. The AMP/ATP (D) and ADP/ATP (E) ratios are shown.

(F–H) AMPK WT, AMPK α2 KO and AMPK DKO myotubes were treated with DMSO or 1.5μM LY2835219 for 24, and submitted to a FAO assay, in which the palmitate induced OCR was measured (in % OCR compared to the basal OCR). The area under curve of the palmitate induced OCR was quantified in (F). AMPK DKO myotubes were transfected with plasmids encoding Myc-tagged AMPK α2 and Myc-tagged AMPK α2 S > A. B. 48 hr later, myotubes were treated for 2 hr with DMSO or 50 μM A769662 before protein extraction; western blot analysis shows the A769662-induced ACC phosphorylation in transfected cells (G). Transfected myotubes were submitted to a FAO assay in which the palmitate-induced OCR was measured (in % OCR compared to the basal OCR). The area under curve of the palmitate-induced OCR was quantified in (H).

Data are expressed as mean ± SEM. See also Figure S4 and S5.
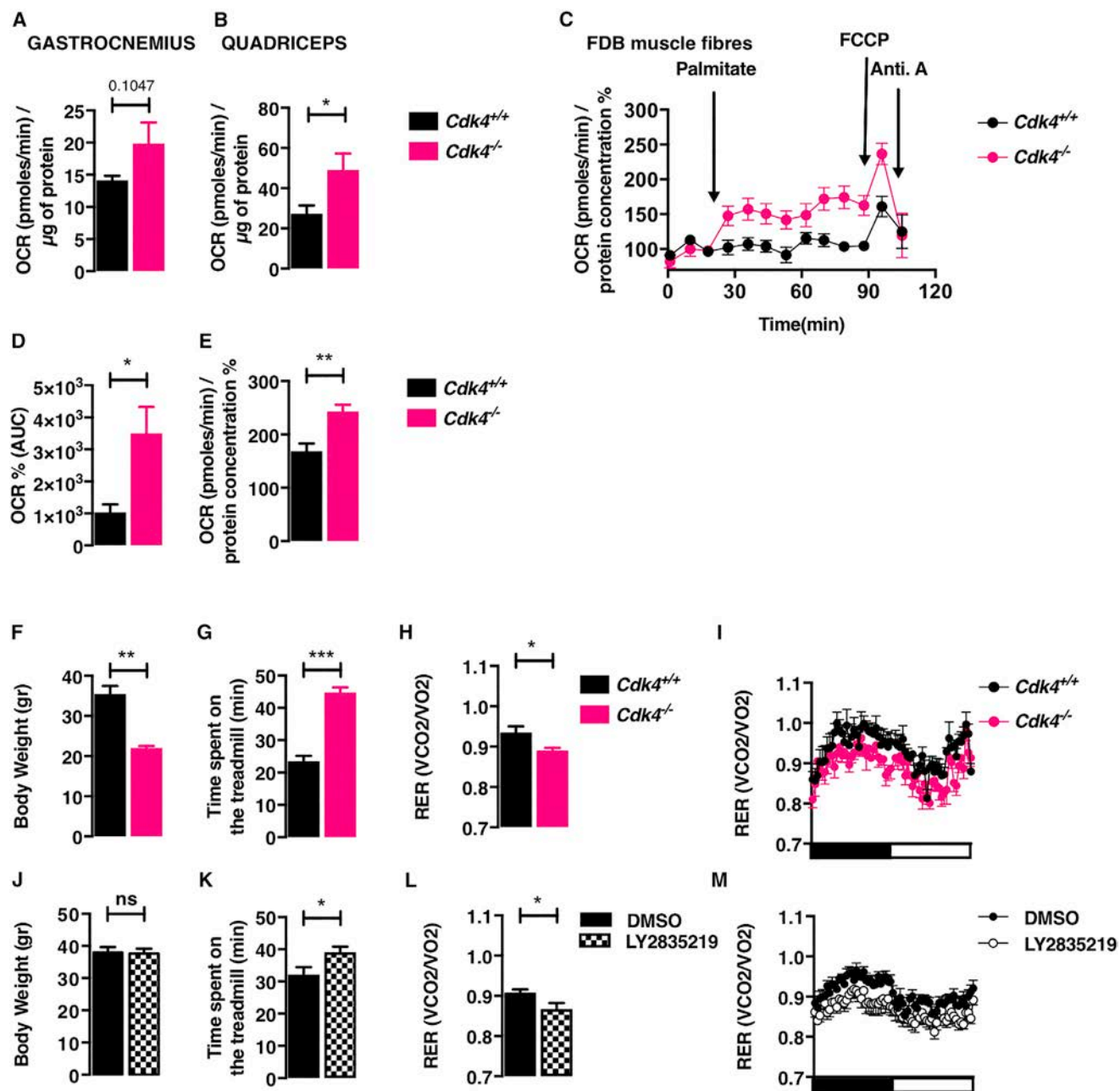
Figure 6. CDK4 Modulates Oxidative Metabolism and Exercise Capacity *In Vivo*

(A–E) Mitochondria isolated from gastrocnemius (A) and quadriceps (B) muscle from $Cdk4^{+/+}$ and $Cdk4^{-/-}$ mice were submitted to a respiration assay using fatty acids as a substrate. Isolated FDB muscle fibers from $Cdk4^{+/+}$ and $Cdk4^{-/-}$ mice were submitted to a FAO assay in which the palmitate-induced OCR was measured (in % OCR compared to the basal OCR) (C). The area under curve of the palmitate-induced OCR is shown (D). The maximal respiration was induced by FCCP (E).

(F) Body weight of 25- to 30-week-old male $Cdk4^{+/+}$ and $Cdk4^{-/-}$ mice was measured.

(G) $Cdk4^{+/+}$ and $Cdk4^{-/-}$ were submitted to an exercise capacity testing on treadmill, and the time before exhaustion was recorded.

(H and I) RER of the aforementioned mice is depicted.

(J and K) 30-week-old WT mice were gavaged with 37 mg/kg LY2835219 or vehicle for 8 days. Body weight (K) and exercise capacity (K) were measured the day after the last treatment.

(L and M) RER of the aforementioned mice after 5 days of treatment is depicted.

Data are expressed as mean ± SEM. See also Figure S6.
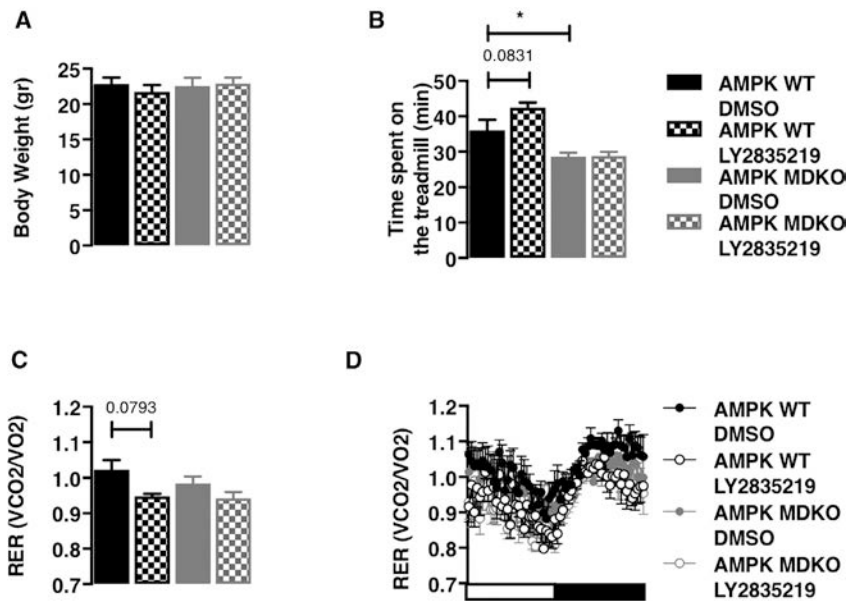
Figure 7. CDK4 Regulation of Oxidative Metabolism and Exercise Capacity *In Vivo* Requires Muscle AMPK

(A) Body weight of 12- to 16-week-old AMPK WT and AMPK MDKO females gavaged with 37 mg/kg LY2835219 or vehicle for 8 days was measured.

(B–D) Body weight of 12–16 weeks old AMPK WT and AMPK MDKO females gavaged with 37mg/kg of LY2835219 or vehicle for 8 days was measured in (A). To measure exercise capacity on treadmill, the time before exhaustion was recorded in (B). RER of the aforementioned mice is depicted in (C) and (D).

Data are expressed as mean ± SEM. See also Figure S7.

mitochondrial FAO that involves AMPKα2 inhibition and is independent of other downstream effectors, such as E2F1.

Cell division requires high cellular energy levels. Despite the recent evidence that underscores the existence of a crosstalk between cell-cycle regulators and energy metabolism (Lopez-Mejia and Fajas, 2015; Salazar-Roa and Malumbres, 2016), the molecular mechanisms coupling energy production and cell-cycle progression remain to be elucidated. Based on our results, we propose that to exert its role in both cell-cycle progression and the insulin-signaling pathway, CDK4 represses catabolism by directly targeting at least one of the catalytic subunits of AMPK, namely the α2 subunit. Interestingly, AKT, another key player of the insulin-signaling pathway, phosphorylates the α1 subunit of AMPK, thus reducing α1 Thr172 phosphorylation and the subsequent activation of the AMPK heterotrimer (Hawley et al., 2014; Horman et al., 2006). Remarkably, previous evidence from our laboratory demonstrates that CDK4 is a key effector of the AKT pathway (Lagarrigue et al., 2016). Surprisingly, GSK3 has been reported to inhibit AMPK activity after phosphorylation of the α subunit by AKT (Suzuki et al., 2013). This finding is somehow unexpected, since GSK3 activity is negatively regulated via phosphorylation by AKT upon insulin stimulation. Moreover, GSK3 is known to inhibit rather than promote anabolic pathways, like the synthesis of glycogen (Cohen and Frame, 2001).

The second major finding in our study is the observation that the function of AMPK heterotrimers can differ depending on their α subunit isoform. Few studies have focused on the specific function of each AMPK subunit (but see a recent review by Ross et al., 2016b), and models completely lacking AMPK activity are often used to study the function of AMPK. Liver-specific deletion or overexpression of the AMPKα2 subunit suggested that this isoform is involved in regulating the balance between lipid synthesis and FAO (Andreelli et al., 2006; Foretz et al., 2005), but these studies did not assess the differences in spec-

ificity between α1 and α2. Interestingly, leptin was shown to directly trigger FAO in muscle (Minokoshi et al., 2002) and trigger an anorexigenic response in hypothalamus (Minokoshi et al., 2004) in an AMPKα2-dependent manner. The effect on food intake may be triggered through AKT signaling via phosphorylation of AMPKα2 by p70S6K (Dagon et al., 2012). Other positive energy balance signals can also reduce food intake via AMPKα2 activity in the brain (Claret et al., 2007; Kim et al., 2004). The isoform-specific roles of the different AMPK subunits in whole-body energy homeostasis were further highlighted by the fact that the AMPKα2 subunit is essential for nicotine-triggered lipolysis in adipocytes (Wu et al., 2015). However, the specific regulation of energy homeostasis by AMPKα2, and the molecular mechanisms regulating α2-isoform specific AMPK activity have remained largely unknown.

The third major finding in our study is that the modulation of CDK4 activity *in vivo* can result in modifications in whole-body energy homeostasis and exercise performance. These modifications require the expression of AMPK in skeletal muscle. Our results are in agreement with previous studies demonstrating that the use of 5-aminoimidazole-4-carboxamide ribonucleotide (AICAR) can increase exercise performance in sedentary mice while increasing the proportion of slow-twitch fibers (Narkar et al., 2008). However, the exact mechanisms that mediate this phenotype remain to be studied. Global approaches to determine muscle reprograming at the proteomics and gene expression level will allow further study of the involvement of CDK4 in muscle biology, particularly during exercise. Given that muscle expresses the AMPKα2 subunit highly and responds to exercise by downregulating CDK activity (Hoffman et al., 2015), we believe that the study of the CDK4-AMPKα2 interaction in skeletal muscle will be very relevant to the discovery of pharmacological interventions to promote or enhance the beneficial effects of exercise on general health.

By identifying 4 new specific CDK4 phosphosites in the α2 subunit of AMPK, we have discovered a specific role for this subunit in the control of fatty acid metabolism that we could not demonstrate for the α1 subunit. Interestingly, we detected the phosphorylation of two of these residues, Ser[377] and Ser[345], in

muscle samples from resting mice and myotubes stimulated with insulin or IGF1.

FAO repression by CDK4 emerges as an additional level of metabolic regulation by this kinase, which also mediates other effects of the insulin-signaling pathway (Lagarrigue et al., 2016), including lipid synthesis, glycolysis (Denechaud et al., 2016), and proliferation (Malumbres and Barbacid, 2005).

In conclusion, our results demonstrate that CDK4 is a major regulator of cellular energy homeostasis. By combining experimental data from cellular metabolism analyses, biochemistry and molecular biology studies, and *in vivo* experiments, our work provides insights into the complex regulation of anabolic and catabolic pathways. These novel findings can have broad implications not only in the regulation of cell metabolism during proliferation but also in the control of energy utilization at the level of the whole organism. Moreover, they highlight the need to delve deeper into the specific functions of the different AMPK heterotrimers, as well as in the regulation of AMPK inactivation.

STAR★METHODS

Detailed methods are provided in the online version of this paper and include the following:

- ● KEY RESOURCES TABLE
- ● CONTACT FOR REAGENT AND RESOURCE SHARING
- ● EXPERIMENTAL MODEL AND SUBJECT DETAILS
  - ○ Cell culture
  - ○ Animal studies
- ● METHOD DETAILS
  - ○ Materials
  - ○ Immunoblot
  - ○ Plasmid constructs and mutagenesis
  - ○ GST production
  - ○ CDK4 Kinase assay
  - ○ Mitochondrial isolation
  - ○ Isolation of adult skeletal muscle fibers
  - ○ Seahorse analyses
  - ○ Immunoprecipitation
  - ○ Mass spectrometry
  - ○ HPLC
  - ○ mRNA analysis
- ● QUANTIFICATION AND STATISTICAL ANALYSES

SUPPLEMENTAL INFORMATION

Supplemental Information includes seven figures and three tables and can be found with this article online at https://doi.org/10.1016/j.molcel.2017.09.034.

AUTHOR CONTRIBUTIONS

I.C.L.-M. and L.F. designed this study. I.C.L.-M. guided and performed most experiments, with assistance from S.L., A.G., L.M.-C., P.-D.D., N.Z., C. Chavey, B.D., J.C.-A., A.N., L.Z., and C. Collodet. M.O. performed HPLC analysis for AMP-ADP-ATP quantification. B.V. generated the *Prkaa1*$^{-/-}$, *Prkaa2*$^{-/-}$ individual KOs and *Prkaa1*$^{-/-}$; *Prkaa2*$^{-/-}$ double-KO MEF cells and myoblasts, as well as the muscle-specific *Prkaa1*$^{-/-}$; *Prkaa2*$^{-/-}$ double-KO mice. D.G.H. helped to design the experiments and provided AMPK constructs. I.C.L.-M. and L.F. wrote the manuscript.

REFERENCES

Aguilar, V., and Fajas, L. (2010). Cycling through metabolism. EMBO Mol. Med. *2*, 338–348.

Andreelli, F., Foretz, M., Knauf, C., Cani, P.D., Perrin, C., Iglesias, M.A., Pillot, B., Bado, A., Tronche, F., Mithieux, G., et al. (2006). Liver adenosine monophosphate-activated kinase-alpha2 catalytic subunit is a key target for the control of hepatic glucose production by adiponectin and leptin but not insulin. Endocrinology *147*, 2432–2441.

Blanchet, E., Annicotte, J.S., Lagarrigue, S., Aguilar, V., Clapé, C., Chavey, C., Fritz, V., Casas, F., Apparailly, F., Auwerx, J., and Fajas, L. (2011). E2F transcription factor-1 regulates oxidative metabolism. Nat. Cell Biol. *13*, 1146–1152.

Carling, D. (2004). Ampk. Curr. Biol. *14*, R220.

Claret, M., Smith, M.A., Batterham, R.L., Selman, C., Choudhury, A.I., Fryer, L.G., Clements, M., Al-Qassab, H., Heffron, H., Xu, A.W., et al. (2007). AMPK is essential for energy homeostasis regulation and glucose sensing by POMC and AgRP neurons. J. Clin. Invest. *117*, 2325–2336.

Cohen, P., and Frame, S. (2001). The renaissance of GSK3. Nat. Rev. Mol. Cell Biol. *2*, 769–776.

Dagon, Y., Hur, E., Zheng, B., Wellenstein, K., Cantley, L.C., and Kahn, B.B. (2012). p70S6 kinase phosphorylates AMPK on serine 491 to mediate leptin's effect on food intake. Cell Metab. *16*, 104–112.

Daub, H., Olsen, J.V., Bairlein, M., Gnad, F., Oppermann, F.S., Körner, R., Greff, Z., Kéri, G., Stemmann, O., and Mann, M. (2008). Kinase-selective enrichment enables quantitative phosphoproteomics of the kinome across the cell cycle. Mol. Cell *31*, 438–448.

Denechaud, P.D., Lopez-Mejia, I.C., Giralt, A., Lai, Q., Blanchet, E., Delacuisine, B., Nicolay, B.N., Dyson, N.J., Bonner, C., Pattou, F., et al. (2016). E2F1 mediates sustained lipogenesis and contributes to hepatic steatosis. J. Clin. Invest. *126*, 137–150.

Dinkel, H., Chica, C., Via, A., Gould, C.M., Jensen, L.J., Gibson, T.J., and Diella, F. (2011). Phospho.ELM: a database of phosphorylation sites–update 2011. Nucleic Acids Res. *39*, D261–D267.

Djouder, N., Tuerk, R.D., Suter, M., Salvioni, P., Thali, R.F., Scholz, R., Vaahtomeri, K., Auchli, Y., Rechsteiner, H., Brunisholz, R.A., et al. (2010). PKA phosphorylates and inactivates AMPKalpha to promote efficient lipolysis. EMBO J. *29*, 469–481.

Foretz, M., Ancellin, N., Andreelli, F., Saintillan, Y., Grondin, P., Kahn, A., Thorens, B., Vaulont, S., and Viollet, B. (2005). Short-term overexpression of a constitutively active form of AMP-activated protein kinase in the liver leads to mild hypoglycemia and fatty liver. Diabetes *54*, 1331–1339.

Fullerton, M.D., Galic, S., Marcinko, K., Sikkema, S., Pulinilkunnil, T., Chen, Z.P., O'Neill, H.M., Ford, R.J., Palanivel, R., O'Brien, M., et al. (2013). Single phosphorylation sites in Acc1 and Acc2 regulate lipid homeostasis and the insulin-sensitizing effects of metformin. Nat. Med. *19*, 1649–1654.

Gnad, F., Gunawardena, J., and Mann, M. (2011). PHOSIDA 2011: the post-translational modification database. Nucleic Acids Res. *39*, D253–D260.

Göransson, O., McBride, A., Hawley, S.A., Ross, F.A., Shpiro, N., Foretz, M., Viollet, B., Hardie, D.G., and Sakamoto, K. (2007). Mechanism of action of A-769662, a valuable tool for activation of AMP-activated protein kinase. J. Biol. Chem. *282*, 32549–32560.

Grahame Hardie, D. (2016). Regulation of AMP-activated protein kinase by natural and synthetic activators. Acta Pharm. Sin. B *6*, 1–19.

Hardie, D.G. (2015). AMPK: positive and negative regulation, and its role in whole-body energy homeostasis. Curr. Opin. Cell Biol. *33*, 1–7.

Hardie, D.G., and Pan, D.A. (2002). Regulation of fatty acid synthesis and oxidation by the AMP-activated protein kinase. Biochem. Soc. Trans. *30*, 1064–1070.

Hardie, D.G., Ross, F.A., and Hawley, S.A. (2012). AMPK: a nutrient and energy sensor that maintains energy homeostasis. Nat. Rev. Mol. Cell Biol. *13*, 251–262.

Hawley, S.A., Davison, M., Woods, A., Davies, S.P., Beri, R.K., Carling, D., and Hardie, D.G. (1996). Characterization of the AMP-activated protein kinase kinase from rat liver and identification of threonine 172 as the major site at which it phosphorylates AMP-activated protein kinase. J. Biol. Chem. *271*, 27879–27887.

Hawley, S.A., Boudeau, J., Reid, J.L., Mustard, K.J., Udd, L., Mäkelä, T.P., Alessi, D.R., and Hardie, D.G. (2003). Complexes between the LKB1 tumor suppressor, STRAD alpha/beta and MO25 alpha/beta are upstream kinases in the AMP-activated protein kinase cascade. J. Biol. *2*, 28.

Hawley, S.A., Pan, D.A., Mustard, K.J., Ross, L., Bain, J., Edelman, A.M., Frenguelli, B.G., and Hardie, D.G. (2005). Calmodulin-dependent protein kinase kinase-beta is an alternative upstream kinase for AMP-activated protein kinase. Cell Metab. *2*, 9–19.

Hawley, S.A., Ross, F.A., Gowans, G.J., Tibarewal, P., Leslie, N.R., and Hardie, D.G. (2014). Phosphorylation by Akt within the ST loop of AMPK-α1 down-regulates its activation in tumour cells. Biochem. J. *459*, 275–287.

Hoffman, N.J., Parker, B.L., Chaudhuri, R., Fisher-Wellman, K.H., Kleinert, M., Humphrey, S.J., Yang, P., Holliday, M., Trefely, S., Fazakerley, D.J., et al. (2015). Global phosphoproteomic analysis of human skeletal muscle reveals a network of exercise-regulated kinases and AMPK substrates. Cell Metab. *22*, 922–935.

Horman, S., Vertommen, D., Heath, R., Neumann, D., Mouton, V., Woods, A., Schlattner, U., Wallimann, T., Carling, D., Hue, L., and Rider, M.H. (2006). Insulin antagonizes ischemia-induced Thr172 phosphorylation of AMP-activated protein kinase alpha-subunits in heart via hierarchical phosphorylation of Ser485/491. J. Biol. Chem. *281*, 5335–5340.

Hornbeck, P.V., Zhang, B., Murray, B., Kornhauser, J.M., Latham, V., and Skrzypek, E. (2015). PhosphoSitePlus, 2014: mutations, PTMs and recalibrations. Nucleic Acids Res. *43*, D512–D520.

Humphrey, S.J., Azimifar, S.B., and Mann, M. (2015). High-throughput phosphoproteomics reveals in vivo insulin signaling dynamics. Nat. Biotechnol. *33*, 990–995.

Hurley, R.L., Anderson, K.A., Franzone, J.M., Kemp, B.E., Means, A.R., and Witters, L.A. (2005). The Ca2+/calmodulin-dependent protein kinase kinases are AMP-activated protein kinase kinases. J. Biol. Chem. *280*, 29060–29066.

Hurley, R.L., Barré, L.K., Wood, S.D., Anderson, K.A., Kemp, B.E., Means, A.R., and Witters, L.A. (2006). Regulation of AMP-activated protein kinase by multisite phosphorylation in response to agents that elevate cellular cAMP. J. Biol. Chem. *281*, 36662–36672.

Icreverzi, A., de la Cruz, A.F., Van Voorhies, W.A., and Edgar, B.A. (2012). Drosophila cyclin D/Cdk4 regulates mitochondrial biogenesis and aging and sensitizes animals to hypoxic stress. Cell Cycle *11*, 554–568.

Jones, R.G., and Thompson, C.B. (2009). Tumor suppressors and cell metabolism: a recipe for cancer growth. Genes Dev. *23*, 537–548.

Kettenbach, A.N., Schweppe, D.K., Faherty, B.K., Pechenick, D., Pletnev, A.A., and Gerber, S.A. (2011). Quantitative phosphoproteomics identifies substrates and functional modules of Aurora and Polo-like kinase activities in mitotic cells. Sci. Signal. *4*, rs5.

Kim, M.S., Park, J.Y., Namkoong, C., Jang, P.G., Ryu, J.W., Song, H.S., Yun, J.Y., Namgoong, I.S., Ha, J., Park, I.S., et al. (2004). Anti-obesity effects of alpha-lipoic acid mediated by suppression of hypothalamic AMP-activated protein kinase. Nat. Med. *10*, 727–733.

Laderoute, K.R., Amin, K., Calaoagan, J.M., Knapp, M., Le, T., Orduna, J., Foretz, M., and Viollet, B. (2006). 5′-AMP-activated protein kinase (AMPK) is induced by low-oxygen and glucose deprivation conditions found in solid-tumor microenvironments. Mol. Cell. Biol. *26*, 5336–5347.

Lagarrigue, S., Lopez-Mejia, I.C., Denechaud, P.D., Escoté, X., Castillo-Armengol, J., Jimenez, V., Chavey, C., Giralt, A., Lai, Q., Zhang, L., et al. (2016). CDK4 is an essential insulin effector in adipocytes. J. Clin. Invest. *126*, 335–348.

Lantier, L., Mounier, R., Leclerc, J., Pende, M., Foretz, M., and Viollet, B. (2010). Coordinated maintenance of muscle cell size control by AMP-activated protein kinase. FASEB J. *24*, 3555–3561.

Lantier, L., Fentz, J., Mounier, R., Leclerc, J., Treebak, J.T., Pehmøller, C., Sanz, N., Sakakibara, I., Saint-Amand, E., Rimbaud, S., et al. (2014). AMPK controls exercise endurance, mitochondrial oxidative capacity, and skeletal muscle integrity. FASEB J. *28*, 3211–3224.

Lee, Y., Dominy, J.E., Choi, Y.J., Jurczak, M., Tolliday, N., Camporez, J.P., Chim, H., Lim, J.H., Ruan, H.B., Yang, X., et al. (2014). Cyclin D1-Cdk4 controls glucose metabolism independently of cell cycle progression. Nature *510*, 547–551.

López-Cotarelo, P., Escribano-Díaz, C., González-Bethencourt, I.L., Gómez-Moreira, C., Deguiz, M.L., Torres-Bacete, J., Gómez-Cabañas, L., Fernández-Barrera, J., Delgado-Martín, C., Mellado, M., et al. (2015). A novel MEK-ERK-AMPK signaling axis controls chemokine receptor CCR7-dependent survival in human mature dendritic cells. J. Biol. Chem. *290*, 827–840.

Lopez-Mejia, I.C., and Fajas, L. (2015). Cell cycle regulation of mitochondrial function. Curr. Opin. Cell Biol. *33*, 19–25.

Malumbres, M. (2014). Cyclin-dependent kinases. Genome Biol. *15*, 122.

Malumbres, M., and Barbacid, M. (2001). To cycle or not to cycle: a critical decision in cancer. Nat. Rev. Cancer *1*, 222–231.

Malumbres, M., and Barbacid, M. (2005). Mammalian cyclin-dependent kinases. Trends Biochem. Sci. *30*, 630–641.

Malumbres, M., and Barbacid, M. (2009). Cell cycle, CDKs and cancer: a changing paradigm. Nat. Rev. Cancer *9*, 153–166.

Manfredi, G., Yang, L., Gajewski, C.D., and Mattiazzi, M. (2002). Measurements of ATP in mammalian cells. Methods *26*, 317–326.

Martín-Campos, T., Mylonas, R., Masselot, A., Waridel, P., Petricevic, T., Xenarios, I., and Quadroni, M. (2017). MsViz, a graphical software tool for in-depth manual validation and quantitation of post-translational modifications. J. Proteome Res. *16*, 3092–3101.

Minokoshi, Y., Kim, Y.B., Peroni, O.D., Fryer, L.G., Müller, C., Carling, D., and Kahn, B.B. (2002). Leptin stimulates fatty-acid oxidation by activating AMP-activated protein kinase. Nature *415*, 339–343.

Minokoshi, Y., Alquier, T., Furukawa, N., Kim, Y.B., Lee, A., Xue, B., Mu, J., Foufelle, F., Ferré, P., Birnbaum, M.J., et al. (2004). AMP-kinase regulates food intake by responding to hormonal and nutrient signals in the hypothalamus. Nature *428*, 569–574.

Moreno, D., Knecht, E., Viollet, B., and Sanz, P. (2008). A769662, a novel activator of AMP-activated protein kinase, inhibits non-proteolytic components of the 26S proteasome by an AMPK-independent mechanism. FEBS Lett. *582*, 2650–2654.

Morizane, Y., Thanos, A., Takeuchi, K., Murakami, Y., Kayama, M., Trichonas, G., Miller, J., Foretz, M., Viollet, B., and Vavvas, D.G. (2011). AMP-activated protein kinase suppresses matrix metalloproteinase-9 expression in mouse embryonic fibroblasts. J. Biol. Chem. *286*, 16030–16038.

Mounier, R., Théret, M., Lantier, L., Foretz, M., and Viollet, B. (2015). Expanding roles for AMPK in skeletal muscle plasticity. Trends Endocrinol. Metab. *26*, 275–286.

Narkar, V.A., Downes, M., Yu, R.T., Embler, E., Wang, Y.X., Banayo, E., Mihaylova, M.M., Nelson, M.C., Zou, Y., Juguilon, H., et al. (2008). AMPK and PPARdelta agonists are exercise mimetics. Cell *134*, 405–415.

Nesvizhskii, A.I., Keller, A., Kolker, E., and Aebersold, R. (2003). A statistical model for identifying proteins by tandem mass spectrometry. Analytical Chemistry *75*, 4646–4658.

O'Leary, B., Finn, R.S., and Turner, N.C. (2016). Treating cancer with selective CDK4/6 inhibitors. Nat. Rev. Clin. Oncol. *13*, 417–430.

O'Neill, H.M., Maarbjerg, S.J., Crane, J.D., Jeppesen, J., Jørgensen, S.B., Schertzer, J.D., Shyroka, O., Kiens, B., van Denderen, B.J., Tarnopolsky, M.A., et al. (2011). AMP-activated protein kinase (AMPK) beta1beta2 muscle null mice reveal an essential role for AMPK in maintaining mitochondrial content and glucose uptake during exercise. Proc. Natl. Acad. Sci. USA *108*, 16092–16097.

O'Neill, H.M., Lally, J.S., Galic, S., Thomas, M., Azizi, P.D., Fullerton, M.D., Smith, B.K., Pulinilkunnil, T., Chen, Z., Samaan, M.C., et al. (2014). AMPK phosphorylation of ACC2 is required for skeletal muscle fatty acid oxidation and insulin sensitivity in mice. Diabetologia *57*, 1693–1702.

Petrov, P.D., Ribot, J., López-Mejía, I.C., Fajas, L., Palou, A., and Bonet, M.L. (2016). Retinoblastoma protein knockdown favors oxidative metabolism and glucose and fatty acid disposal in muscle cells. J. Cell. Physiol. *231*, 708–718.

Rane, S.G., Dubus, P., Mettus, R.V., Galbreath, E.J., Boden, G., Reddy, E.P., and Barbacid, M. (1999). Loss of Cdk4 expression causes insulin-deficient diabetes and Cdk4 activation results in beta-islet cell hyperplasia. Nat. Genet. *22*, 44–52.

Rane, S.G., Cosenza, S.C., Mettus, R.V., and Reddy, E.P. (2002). Germ line transmission of the Cdk4(R24C) mutation facilitates tumorigenesis and escape from cellular senescence. Mol. Cell. Biol. *22*, 644–656.

Ross, F.A., Jensen, T.E., and Hardie, D.G. (2016a). Differential regulation by AMP and ADP of AMPK complexes containing different γ subunit isoforms. Biochem. J. *473*, 189–199.

Ross, F.A., MacKintosh, C., and Hardie, D.G. (2016b). AMP-activated protein kinase: a cellular energy sensor that comes in 12 flavours. FEBS J. *283*, 2987–3001.

Salazar-Roa, M., and Malumbres, M. (2016). Fueling the cell division cycle. Trends Cell Biol. *27*, 69–81.

Schindelin, J., Arganda-Carreras, I., Frise, E., Kaynig, V., Longair, M., Pietzsch, T., Preibisch, S., Rueden, C., Saalfeld, S., Schmid, B., et al. (2012). Fiji: an open-source platform for biological-image analysis. Nat. Methods *9*, 676–682.

Shaw, R.J., Kosmatka, M., Bardeesy, N., Hurley, R.L., Witters, L.A., DePinho, R.A., and Cantley, L.C. (2004). The tumor suppressor LKB1 kinase directly activates AMP-activated kinase and regulates apoptosis in response to energy stress. Proc. Natl. Acad. Sci. USA *101*, 3329–3335.

Suzuki, T., Bridges, D., Nakada, D., Skiniotis, G., Morrison, S.J., Lin, J.D., Saltiel, A.R., and Inoki, K. (2013). Inhibition of AMPK catabolic action by GSK3. Mol. Cell *50*, 407–419.

Wölfel, T., Hauer, M., Schneider, J., Serrano, M., Wölfel, C., Klehmann-Hieb, E., De Plaen, E., Hankeln, T., Meyer zum Büschenfelde, K.H., and Beach, D. (1995). A p16INK4a-insensitive CDK4 mutant targeted by cytolytic T lymphocytes in a human melanoma. Science *269*, 1281–1284.

Woods, A., Johnstone, S.R., Dickerson, K., Leiper, F.C., Fryer, L.G., Neumann, D., Schlattner, U., Wallimann, T., Carlson, M., and Carling, D. (2003). LKB1 is the upstream kinase in the AMP-activated protein kinase cascade. Curr. Biol. *13*, 2004–2008.

Woods, A., Dickerson, K., Heath, R., Hong, S.P., Momcilovic, M., Johnstone, S.R., Carlson, M., and Carling, D. (2005). Ca2+/calmodulin-dependent protein kinase kinase-beta acts upstream of AMP-activated protein kinase in mammalian cells. Cell Metab. *2*, 21–33.

Wu, Y., Song, P., Zhang, W., Liu, J., Dai, X., Liu, Z., Lu, Q., Ouyang, C., Xie, Z., Zhao, Z., et al. (2015). Activation of AMPKα2 in adipocytes is essential for nicotine-induced insulin resistance in vivo. Nat. Med. *21*, 373–382.

Zhang, C.S., Hawley, S.A., Zong, Y., Li, M.Q., Wang, Z.C., Gray, A., Ma, T., Cui, J.W., Feng, J.W., Zhu, M.J., et al. (2017). Fructose-1,6-bisphosphate and aldolase mediate glucose sensing by AMPK. Nature *548*, 112–116.

STAR★METHODS

KEY RESOURCES TABLE

REAGENT or RESOURCE	SOURCE	IDENTIFIER
Antibodies		
Rabbit polyclonal anti-ACC	Cell Signaling Technology	Cat#3662
Rabbit polyclonal anti-Phospho-ACC	Cell Signaling Technology	Cat#3661
Rabbit polyclonal anti-AMPKa	Cell Signaling Technology	Cat#2532
Rabbit monoclonal anti-Phospho-AMPKa(Thr172)(40H9)	Cell Signaling Technology	Cat#2535
Mouse monoclonal anti-Myc-Tag (9B11)	Cell Signaling Technology	Cat#2276
Rabbit monoclonal anti-Phospho Rb (ser780)(D59B7)	Cell Signaling Technology	Cat#8180
Rabbit polyclonal anti-Cdk4 (C-22)	Santa Cruz biotechnology	Sc-260
Mouse monoclonal anti-Rb (C-2)	Santa Cruz biotechnology	Sc-74562
Goat polyclonal anti-AMPK a2 (C-20)	Santa Cruz biotechnology	Sc-19131
Goat polyclonal anti-Actin (C11)	Santa Cruz biotechnology	Sc-1615
Rabbit polyclonal anti-Myc-Tag	Abcam	Ab9106
Mouse monoclonal anti-a-Tubulin	Sigma-Aldrich	T6199
Chemicals, Peptides, and Recombinant Proteins		
LY2835219	MedChemExpress	HY-16297
PD0332991	MedChemExpress	HY-50767
LEE011	MedChemExpress	HY-15777
A769662	MedChemExpress	HY-50662
Compound C	MedChemExpress	HY-13418
FCCP	Sigma Aldrich	C2920
Antimycine A	Sigma Aldrich	A8674
CDK4/CycD3	ProQinase	0142-0373-1
CDK4/CycD1	ProQinase	0142-0143-1
Recombinant kinase dead AMPK trimers ($\alpha2\beta2\gamma1$)	DG. Hardie lab.	
Experimental Models: Cell Lines		
C2C12	ATCC	CRL-1772
Primary and SV40 immortalized $Cdk4^{-/-}$ MEFs	This paper	N/A
Primary and SV40 immortalized $Cdk4^{+/+}$ MEFs,	This paper	N/A
Primary and SV40 immortalized $Cdk4^{R24C/R24C}$ MEFs	This paper	N/A
Primary $E2f1^{+/+}$ MEFs	This paper	N/A
Primary $E2f1^{-/-}$ MEFs	This paper	N/A
Primary $Cdk4^{R24C/R24C}$ $E2f1^{+/+}$ MEFs	This paper	N/A
Primary $Cdk4^{R24C/R24C}$ $E2f1^{-/-}$ MEFs	This paper	N/A
$Prkaa1^{-/-}$ SV40 immortalized MEFs	(Laderoute et al., 2006)	N/A
$Prkaa2^{-/-}$ SV40 immortalized MEFs	(Laderoute et al., 2006)	N/A
$Prkaa1^{-/-}$; $Prkaa2^{-/-}$ double KO SV40 immortalized MEFs	(Laderoute et al., 2006)	N/A
AMPK alpha2 KO Myoblasts	(Lantier et al., 2010)	N/A
AMPK alpha1, alpha2 double KO Myoblasts	(Lantier et al., 2010)	N/A
AMPK WT Myoblasts	(Lantier et al., 2010)	N/A
Experimental Models: Organisms/Strains		
Skeletal muscle AMPK-deficient mice [AMPK_1fl/fl _2fl/fl human skeletal actin (HSA)-Cre_ mice on a C57Bl6- 129Sv mixed background]	(Lantier et al., 2014)	N/A
The generation of $Cdk4^{-/-}$, that lack CDK4 in all tissues except pancreatic beta cells and were referred as $Cdk4^{nc/nc}$ in our previous study.	(Lagarrigue et al., 2016)	N/A
C57BL/6JRj mice.		Janvier Labs

(*Continued on next page*)

Continued

REAGENT or RESOURCE	SOURCE	IDENTIFIER
Oligonucleotides		
See Table S2		N/A
See Table S3		N/A
Recombinant DNA		
pDONR223-hPRKAA1	Addgene	(ref:23871)
pDONR223-hPRKAA2	Addgene	(ref:23671)
pDONR223-hPRKAB1	Addgene	(ref:23360)
pDONR223-hPRKAB2	Addgene	(ref:23647)
pDONR223-hPRKAG1,	Addgene	(ref:23718)
pDONR223-hPRKAG2	Addgene	(ref:23689)
pDONR223-hPRKAG3	Addgene	(ref:23549)
pDEST pGEX-2T-hPRKAA1	This paper	N/A
pDEST pGEX-2T -hPRKAA2	This paper	N/A
pDEST pGEX-2T -hPRKAB1	This paper	N/A
pDEST pGEX-2T -hPRKAB2	This paper	N/A
pDEST pGEX-2T -hPRKAG1,	This paper	N/A
pDEST pGEX-2T -hPRKAG2	This paper	N/A
pDEST pGEX-2T -hPRKAG3	This paper	N/A
pDEST pGEX-2T -hPRKAA2 D1	This paper	N/A
pDEST pGEX-2T -hPRKAA2 D1 S176A	This paper	N/A
pDEST pGEX-2T -hPRKAA2 D2	This paper	N/A
pDEST pGEX-2T -hPRKAA2 D2 S345A	This paper	N/A
pDEST pGEX-2T -hPRKAA2 D3	This paper	N/A
pDEST pGEX-2T -hPRKAA2 D3 S377A	This paper	N/A
pDEST pGEX-2T -hPRKAA2 D4	This paper	N/A
pDEST pGEX-2T -hPRKAA2 D4 T485A	This paper	N/A
pGEX-2T -hPRKAA2 D4 T485A S529A	This paper	N/A
pDEST pGEX-2T -hPRKAA2 D2-D3	This paper	N/A
pDEST pGEX-2T -hPRKAA2 D2-D3 S345A S377A	This paper	N/A
pDEST pGEX-2T -hPRKAA2 S377A S345A T485A S529A	This paper	N/A
pCDNA3 MYC hPRKAA1	This paper	N/A
pCDNA3 MYC hPRKAA2	This paper	N/A
pCDNA3 MYC hPRKAA2 S377A S345A T485A S529A	This paper	N/A
Software and Algorithms		
Protein Prophet algorithm	(Nesvizhskii et al., 2003)	N/A
MsViz software	(Martín-Campos et al., 2017)	N/A
Fiji image processing package	(Schindelin et al., 2012).	N/A

CONTACT FOR REAGENT AND RESOURCE SHARING

Further information and requests for resources and reagents should be directed to and will fulfilled by Lluis Fajas (lluis.fajas@unil.ch).

EXPERIMENTAL MODEL AND SUBJECT DETAILS

Cell culture

MEFs were derived from embryos that were dissected 13.5 days after vaginal plugs. The $Cdk4^{-/-}$ ($Cdk4^{nc}$), $Cdk4^{R24C/R24C}$ and $E2f1^{-/-}$ mice have been previously described (Denechaud et al., 2016; Lagarrigue et al., 2016).

Prkaa1$^{-/-}$, *Prkaa2*$^{-/-}$ individual KOs; and *Prkaa1*$^{-/-}$; *Prkaa2*$^{-/-}$ double KO SV40 immortalized MEF cells were prepared as described (Laderoute et al., 2006). They are referred in the manuscript as AMPK α1KO, AMPK α2KO and AMPK DKO.

MEFs were cultured in DMEM/F12 supplemented with 10% fetal bovine serum (FBS, PAA Laboratories), glutamax (1mM), sodium pyruvate (1mM), non-essential amino-acids, 2-Mercapto-ethanol (50μM) and antibiotics in 5% CO_2 37°C incubator.

C2C12 myoblasts were obtained from ATCC and were cultured in low-glucose DMEM with 10% FBS in 5% CO_2 37°C incubator. For myotube differentiation, when the cells reached 80%–90% confluency, the culture medium was switched to DMEM containing 2% horse serum. The medium was changed every 2 days until day 5 to 7 of differentiation.

Primary myoblasts were grown in collagen coated plates cultured DMEM/F12 supplemented with 20% fetal bovine serum, 2mM Glutamine and FGF (5ng/ml) in 5% CO_2 37°C incubator. For myotube differentiation, cells were plated on matrigel-coated plates when the cells reached 80%–90% confluency, the culture medium was switched to DMEM/F12 supplemented with 2% horse serum and 2mM Glutamine. The medium was changed every 2 days until day 4-5 of differentiation. For rescue experiments, myotubes were transfected using lipofectamine 3000 (Thermo Fisher Scientific), at day 1 and day 3 of differentiation. The cells were assayed 48 hr after the 2nd round of transfection.

Primary *Cdk4*$^{+/+}$, *Cdk4*$^{-/-}$ and *Cdk4*$^{R24C/R24C}$ MEFs, as well as primary *E2f1*$^{+/+}$, *E2f1*$^{-/-}$, *Cdk4*$^{R24C/R24C}$ *E2f1*$^{+/+}$ and *Cdk4*$^{R24C/R24C}$ *E2f1*$^{-/-}$ MEFs, between P2 and P5, were used for Figures 1 and 2. SV40 immortalized MEFs were used for all other figures.

Animal studies

The generation of *Cdk4*$^{-/-}$, that lack CDK4 in all tissues except pancreatic beta cells and were referred as *Cdk4*$^{nc/nc}$ in our previous study, was described in (Lagarrigue et al., 2016). Male mice were used.

For gavage experiments, C57BL/6J male mice were obtained from Janvier Labs. Animals were gavaged daily with 37mg/kg of LY2835219 or vehicle for 8 days. Mice were acclimated and submitted to indirect calorimetry between day 4 and day 6. Exercise capacity testing was performed the day after the last gavage. Body weight was controlled daily. Food intake was measured in the metabolic cages.

To obtain skeletal muscle AMPK-deficient mice [AMPK_1fl/fl _2fl/fl human skeletal actin (HSA)-Cre_ mice on a C57Bl6- 129Sv mixed background], AMPK_1$^{fl/fl}$-2$^{fl/fl}$ mice were interbred with transgenic mice expressing Cre recombinase under the control of the HSA promoter. Female mice were used.

The mice were housed in a facility on a 12-h light-dark cycle with free access to standard rodent chow and water.

Mice were familiarized to the motorized rodent treadmill (Columbus Instruments, Columbus OH) on the J-2 and J-1 before the evaluation of exercise capacity. Familiarization consisted of an initial 10 min period where the treadmill speed and incline were set to zero with a slight electric shock grid at the back of the carpet set to 20 V, 0.34 mA, and 2 Hz. The treadmill speed was then increased steadily to 10 m/min (J-2) and 12 m/min (J-1) for an additional 10 min.

The day immediately following familiarization to the treadmill, mice were subjected to an exercise capacity test. For this, the mice were acclimated to the treadmill for 10 min, with the speed and incline set initially to zero. The treadmill speed was then increase to 8.5 m/min with an angle of inclination set to 0° for 9 min. Next, the treadmill speed and incline was increased to 10 m/min and 5°, respectively, for 3 min. The speed was then increased by 2.5 m/min every 3 min to a maximum speed of 40 m/min, while inclination was increased by 5° every 9 min until a maximum incline of 15°.

Strict a priori criteria for exercise-induced exhaustion consisted in: (1) 10 consecutive seconds on the electric grid; (2) spending more than 50% of time on the grid; and/or (3) lack of motivation to manual prodding. Mice were immediately removed from their respective lane once one or more of these criteria were reached.

Following the protocol, mice were killed by cervical dislocation and skeletal muscles were isolated for analysis.

All animal care and treatment procedures were performed in accordance with Swiss guidelines and were approved by the Canton of Vaud, Service de la Consommation et des Affaires Vétérinaires (SCAV) (authorization VD 3121.a).

METHOD DETAILS

Materials

All cell culture reagents were purchased from GIBCO (Thermo Fisher Scientific). All chemicals, except if stated otherwise, were purchased from Sigma-Aldrich. The CDK4 *inhibitor (LY2835219) and* Compound C. were purchased from MedChem Express. Experiments were done using 1μM of LY2835219, unless stated otherwise. The AMPK allosteric activator was purchased from Abcam or MedChem Express. Unless stated otherwise, A769662 was used at a concentration of 50μM. γ-^{33}P-ATP was purchased from Perkin Elmer.

Immunoblot

For western blot analysis, the cells were seeded in 6-well plates 48 hr before the experiment, serum starved for 3 hr, and treated with either LY2835219 or A769662 for 2 hr.

Total proteins extracts were subjected to SDS-PAGE analysis and transferred to nitrocellulose membranes for immunoblotting. The following antibodies were obtained from Cell Signaling Technology: ACC (no. 3662), phosphorylated ACC (ser79) (no. 3661), AMPK (no.2532), phosphorylated AMPK (Thr172) (no 2535), Myc-tag (no. 2276), phosphorylated RB (Ser780) (no. 8180). The

following antibodies were obtained from Santa Cruz Technology: Cdk4 (C-22; sc-260), Rb (C-2; sc-74562), AMPK α2 (sc-19131). A second Myc-tag antibody was used to analyze myotube samples (Abcam ab9106)

The α Tubulin (no. T6199) antibody was obtained from Sigma Aldrich, the actin (sc-1615) was obtained from Santa Cruz Technology.

The levels of total proteins and the levels of phosphorylation of proteins were analyzed on separate gels. The band intensities on developed films, fusion FX images or chemidoc images or were quantified using Fiji image processing package (Schindelin et al., 2012).

Plasmid constructs and mutagenesis

pDONR223-hPRKAA1 (ref:23871), pDONR223-hPRKAA2 (ref:23671), pDONR223-hPRKAB1 (ref:23360), pDONR223-hPRKAB2 (ref:23647), pDONR223-hPRKAG1 (ref:23718), pDONR223-hPRKAG2 (ref:23689), pDONR223-hPRKAG3 (ref:23549) were provided from Addgene. The different GST subunits of human AMPK were obtained using the pDEST pGEX-2T vector of Gateway Cloning Technology (Invitrogen) starting from previously described pDONR223AMPK constructs. The different serine-to-alanine mutants of GST-hPRKAA2 were generated using a Quick-Change Site-Directed Mutagenesis kit (Stratagene) with the following primers (Table S2). A similar strategy was used to obtain the truncated versions of GST-hPRKAA2 and the different serine-to-alanine mutants using the following primers (Table S2).

The Myc-hPRKAA1, the Myc-hPRKAA2 and the Myc-hPRKAA2-S345A-S377A-T485A-S529A were obtained using the pDEST pCDNA3 MYC vector previously and the above described pDONR223-human AMPK constructs. pDONR-hRB 379-928aa was subcloned from pCMV human RB and generated using the pDONR221 vector of Gateway Cloning Technology. The pGEX-2T hRB 379-928aa was obtained using the pDEST pGEX-2T from Gateway Cloning Technology.

GST production

Independent AMPK subunits were cloned in the pDEST pGEX-2T and expressed in BL21 bacteria. GST-purified proteins were re-suspended in 50mM Tris.HCl [pH 8], 100 mM NaCl, 5 mM DTT and 20% glycerol buffer.

CDK4 Kinase assay

Kinase assays were performed using independent AMPK subunits proteins and 500ng of recombinant RB protein (Santa Cruz) as a substrate in kinase buffer (25 mM Tris.HCl [pH 7.5], 150 mM NaCl, 10 mM MgCl$_2$, 1 mM DTT, 5 mM Na$_4$P$_2$O$_7$, 50 mM NaF, 1 mM vanadate and protease inhibitor cocktail) with 40 μM ATP and 8 μCi γ-^{33P}ATP (Perkin Elmer) for 30 min at 30°C. Recombinant CDK4/cyclin D3 kinase and CDK4/Cyclin D1 (ProQinase) were used. RB was used as a positive control.

Boiling the samples for 5 min in the presence of denaturing sample buffer stopped the reaction. Samples were subsequently subjected to SDS–PAGE, and transferred to a nitrocellulose membrane before being exposed to an X-ray film at −80°C during 4 hr or over night. Recombinant protein loading was confirmed by SYPRO Ruby protein Blot Staining (Life Technologies).

For mass spectrometry, recombinant kinase dead AMPK trimers (α2β2γ1) were used as a substrate for CDK4/CyCD3. Recombinant kinase dead AMPK trimers (α2β2γ1) were produced by the DG. Hardie lab.

Mitochondrial isolation

Quadriceps muscle from *Cdk4$^{+/+}$* or *Cdk4$^{-/-}$* mice were homogenized in 2ml cold buffer I. Tissue homogenization was obtained at 1500rpm after 30 strokes. The homogenized extract was then centrifuged at 600 g for 10 min at 4°C in order to remove cellular debris. This step was performed three times. The mitochondrial fraction was pelleted at 10000 g for 10 min at 4°C and subsequently washed using buffer II. The mitochondrial pellet was suspended in 80ul cold buffer II. Mitochondria were immediately used for seahorse analysis. Buffers I composition is as follows: 210 mM mannitol, 70 mM sucrose, 5 mM HEPES, 1 mM EGTA, 0.5% BSA pH to 7.4. Buffer II composition is as follows: 210 mM mannitol, 70 mM sucrose, 10 mM MgCl2, 5 mMK2HPO4, 10 mM MOPS, 1 mM EGTA pH to 7.4.

Isolation of adult skeletal muscle fibers

Flexor digitorum brevis (FDB) muscles were incubated for 45 min at 37°C in an oxygenated 'Krebs-HEPES' solution containing 0.2% collagenase type IV (GIBCO). Muscles were then washed twice in DMEM/F12 supplemented with 2% fetal bovine serum and mechanically dissociated by repeated passages through fire-polished Pasteur pipettes of progressively decreasing diameter. Dissociated fibers were plated directed onto Seahorse XF24 tissue culture dishes coated with Matrigel and allowed to adhere to the bottom of the dish for 2h. After checking the adhesion of the fibers, a seahorse Fatty acid oxidation was performed as described

The Krebs-HEPES solution contains NaCl 135.5mM, MgCl$_2$ 1.2mM, KCl 5.9mM, glucose 11.5mM, HEPES 11.5mM and CaCl$_2$ mM.

Seahorse analyses

For seahorse analysis, the cells were seeded 16 hr before the experiment.

Mitochondrial function was determined with an XF-24 extracellular flux analyzer (Seahorse Bioscience). Oxygen consumption Rate (OCR) and Extracellular acidification rate (ECAR) was measured in adherent MEFs. Control and mutant fibroblast cells were seeded in an XF 24-well cell culture microplate at a density of 7×10^5 cells per cell in 200 μL DMEM/F12 media. Cells were incubated for 16 hr at 37°C in 5% CO$_2$ before the assay. OCR was expressed as pmol of O$_2$ per minute and was normalized by protein content a Pierce BCA

Protein Assay protocol (Thermo Fisher Scientific). ECAR was expressed as mpH per minute and was normalized by protein content a Pierce BCA Protein Assay protocol (Thermo Fisher Scientific).

For glycolysis experiments, just before the experiment the cells were washed, and the growth medium was replaced with DMEM medium containing only 2mM Glutamine. Cells were then pre-incubated for 1 hr at 37°C without CO_2 to allow cells to pre-equilibrate with the assay media before starting the glycolysis test procedure. After measuring baseline ECAR, ECAR was measured after an acute injection of 25mM Glucose. The glycolytic rate was calculated as glucose dependent ECAR. It was calculated as follows: Glucose induced ECAR-basal ECAR.

For fatty acid oxidation experiments, just before the experiment the cells are washed, and the growth medium was replaced with KHB containing 2.5mM Glucose and 1.5mM of carnitine. Cells were then pre-incubated for 1 hr at 37°C without CO_2 to allow cells to pre-equilibrate with the assay media before starting the fatty acid oxidation procedure. After measuring baseline OCR as an indication of basal respiration, OCR was measured after an acute injection of 400μM or 150μM of palmitate coupled to BSA (for MEFs and myotubes respectively).

For FDB muscle fibers 125μM of palmitate coupled to BSA, 400nM of FCCP and 1μM of Antimycine A were injected directly onto the fibers using the seahorse analyzer. Fatty acid oxidation was induced by the palmitate injection. The uncoupling agent FCCP induced the maximal respiration.

OCR was expressed as pmol of O_2 per minute and was normalized by total DNA content.

For mitochondrial respiration, 50 μL of mitochondrial suspension (containing 10μg of freshly isolated mitochondria) were used per well. The XF24 cell culture microplate was centrifuged at 2000 g for 20 min at 4°C. The assay medium contained 250 mM sucrose, 15 mM KCl, 1 mM EGTA, 5 mMMgCl2, 30 mM K2HPO4, 2mM HEPES and 0.2% FFA-Free BSA. 0.5mM Malate, 80μM PalmitoylCoA, 240μM Carnitine and 4mM ADP diluted in assay medium were added after the centrifugation of the mitochondria to obtain a final volume of 525μl per well. After 10 min of incubation at 37°C without CO2 the mitochondrial respiration was measured using the seahorse analyzer.

Immunoprecipitation

Myotubes or liquid N2 grinded muscle samples were lysed in M-PER buffer (Thermo Fisher Scientific) and incubated in agitation for one hour at 4°C. 2-5 mg of protein was immunoprecipitated overnight with an AMPKα2 antibody (Santa Cruz, sc-19131) and Protein G coupled with magnetic beads (Sigma, 1004D) in the following buffer (IP buffer): 25 mM TRIS pH 7.9, 5 mM $MgCl_2$, 10% Glycerol, 100 mM KCl, 0.1% NP40, 0.3 mM DTT. Next day, beads were washed for times with the IP buffer and frozen. Samples were used for mass spectrometry.

Mass spectrometry

In the *in vitro* assays, protein samples were loaded on a 12% mini polyacrylamide gel and migrated about 3 cm, while in the immunoprecipitation experiments proteins were loaded on an 8% gel and fully migrated. After Coomassie staining, visible band between 50 and 75 kDa corresponding to AAPK2 was excised and digested with sequencing-grade trypsin (Promega). Extracted tryptic peptides were dried and resuspended in 0.05% trifluoroacetic acid, 2% (v/v) acetonitrile for mass spectrometry analyses.

Tryptic peptide mixtures were injected on an Ultimate RSLC 3000 nanoHPLC system (Dionex, Sunnyvale, CA, USA) interfaced via a nanospray source to a high resolution mass spectrometer based on Orbitrap technology: Fusion Tribrid or QExactive Plus (Thermo Fisher, Bremen, Germany), depending on the experiments considered. Peptides were loaded onto a trapping microcolumn Acclaim PepMap100 C18 (20 mm x 100 μm ID, 5 μm, Dionex) before separation on a C18 reversed-phase analytical nanocolumn at a flowrate of 0.25 μl/min, using a gradient from 4 to 76% acetonitrile in 0.1% formic acid (total time: 65min).

The *in vitro* experiments were analyzed with a Fusion mass spectrometer interfaced to a custom packed 40-cm C18 column (75 μm ID, 100Å, Reprosil Pur 1.9 um particles). Full MS survey scans were performed at 120'000 resolution. Data-dependent acquisition was controlled by Xcalibur 3.0 software (Thermo Fisher) and applied a top speed precursor selection strategy to maximize acquisition of peptide tandem MS spectra with a maximum cycle time of 3 s. Multiple-charge precursor ions were isolated in the quadrupole with a window of 1.6 m/z width and then dynamically excluded from further selection during 60 s. HCD fragmentation was performed in the ion routing multipole with 32% normalized collision energy and fragment ions were measured in the ion trap.

The immunoprecipitation experiments were analyzed with a Q-Exactive Plus instrument interfaced to an Easy Spray C18 PepMap column (50cm x 75μm ID, 2μm, 100Å, Dionex). Full MS survey scans were performed at 70'000 resolution. In data-dependent acquisition controlled by Xcalibur 3.1 software (Thermo Fisher), the 10 most intense multiple-charge precursor ions detected in the full MS survey scan were selected for higher energy collision-induced dissociation (HCD, normalized collision energy NCE = 27%) and analysis in the orbitrap at 17'500 resolution. The window for precursor isolation was of 1.5 m/z units around the precursor and selected fragments were excluded for 60 s from further analysis.

MS data were analyzed using Mascot 2.6 (Matrix Science, London, UK) set up to search the UniProt database (www.uniprot.org) restricted to *Homo sapiens* (*in vitro* experiments) or *Mus musculus* (immunoprecipitation experiments) taxonomy (SwissProt, November 2016 version: 20'130 and 16'846 sequences, respectively). Trypsin (cleavage at K,R) was used as the enzyme definition, allowing 3 missed cleavages. Mascot was searched with a parent ion tolerance of 10 ppm and a fragment ion mass tolerance of 0.5

(Fusion MS data) or 0.02 Da (QExactive MS data). Iodoacetamide derivative of cysteine was specified in Mascot as a fixed modification. N-terminal acetylation of protein, oxidation of methionine, and phosphorylation of serine, threonine or tyrosine were specified as variable modifications.

Scaffold software (version 4.7.5, Proteome Software Inc., Portland, OR) was used to validate MS/MS based peptide and protein identifications, and to perform dataset alignment. Peptide identifications were accepted if they could be established at greater than 90.0% probability by the Scaffold Local FDR algorithm. Protein identifications were accepted if they could be established at greater than 95.0% probability and contained at least 2 identified peptides. Protein probabilities were assigned by the Protein Prophet algorithm. Proteins that contained similar peptides and could not be differentiated based on MS/MS analysis alone were grouped to satisfy the principles of parsimony. Proteins sharing significant peptide evidence were grouped into clusters.

MsViz software (Martín-Campos et al., 2017) was used to compare sequence coverage and phosphorylation of the AMPK alpha 2 protein in the *in vitro* experiments.

HPLC

Cells were grown in 10 cm dishes and treated as indicated in the figure legends. Culture medium was removed by aspiration, rinsed with ultra pure water, flash frozen with liquid nitrogen, thawed on ice, and followed by immediate addition of ice-cold 0.4M perchloric acid (500 μl). Cells were scrapped off thoroughly, and transferred to 1.5 mL microfuge eppendorf tubes. Samples were incubated at 4°C for 45 min, and centrifuged at 14,000 rpm at 4C for 10 min. The supernatant (500 μl) was collected, mixed with 500μl K_2CO_3 4M, and incubated at least 1h at −80°C. The samples were again centrifugated at 4C for 10 min, the supernatant collected and tested on HPLC.

External standards stocks were prepared in ultra pure water, at 10 mg/ml, and treated in exactly the same way as the samples.

For normalization, protein measurements were performed using a Pierce BCA Protein Assay protocol (Thermo Fisher Scientific). In parallel DNA was extracted from the pellets and quantified.

The gradient elution was performed as described (Manfredi et al., 2002) on a 4.6-mmi.d, 150-mm, Kinetex 5u EVO C18 100A HPLC column (Phenomenex) with two buffers at a rate of 0.5 ml/min. Buffer A contained 25mM NaH2PO4, 100 mg/liter tetrabutylammonium hydrogen sulfate, pH 5. Organic buffer B was composed of 10% (v/v) acetonitrile in 200mM NaH2PO4, 100 mg/liter tetrabutylammonium hydrogen sulfate, pH 4.0. Buffers were filtered and degassed. The gradient was 100% buffer A from 0–5 min, 100% buffer A to 100% buffer B from 5–20 min, and 100% buffer A from 20 to 31 min for column reequilibration, which was sufficient to achieve stable baseline conditions. 25 μl of prepared sample was autoinjected and UV monitored at 260nm from 0 to 31 min for phosphorylated nucleotides. Peaks were identified by their retention times and by using co-chromatography with standards.

Each standard of interest was first subjected to chromatography individually to obtain its retention time (Manfredi et al., 2002) and to be able to later identify each compound in a standard mixture. A standard curve for each compound was constructed by plotting peakheight s (IV) versus concentration. Linear curves were obtained with R^2 values > 0.95. The quantification of nucleotides in the sample was performed using the external standard calibration, integrating sample peak heights against corresponding standard curves.

mRNA analysis

Muscle tissues were grinded to powder in liquid nitrogen. mRNAs from muscle was isolated using TRIREAGENT according to the manufacturer's protocol. One microgram of the RNA was subsequently reverse-transcribed (Superscript II, Life Technologies) and quantified via real-time quantitative PCR using an ABI 7900HT instrument. qPCR analysis was performed using a 7900HT Fast Real-Time PCR System (Applied Biosystems) and SYBR Green detection of the amplified products. The relative quantification for a given gene was corrected to RS9 mRNA values (oligonucleotide sequences are provided in Table S3).

QUANTIFICATION AND STATISTICAL ANALYSES

The results were expressed as means ± standard error of the means (s.e.m). Comparisons between 2 groups were performed with an unpaired 2-tailed Student's t test and multiple group comparisons were performed by unpaired 1-way ANOVA followed by Tukey's test and 2-way ANOVA, followed by Tukey's test. All *p-value*s below 0.05 were considered significant. Statistical significance values were represented by asterisks corresponding to $*p < 0.05$, $**p < 0.01$, $***p < 0.001$ and $****p < 0.0001$.

_____

Role of cell cycle regulators in adipose tissue and whole body energy homeostasis

Lopez-Mejia IC, **Castillo-Armengol J**, Lagarrigue S, Fajas L.

During this PhD studies, I also had the chance to write a review on a topic very related to my thesis. In this article, we have tried to summarize the principal findings that associate cell cycle regulatory proteins to adipose tissue metabolism.

Cellular and Molecular Life Sciences

CrossMark

Role of cell cycle regulators in adipose tissue and whole body energy homeostasis

I. C. Lopez-Mejia[1,2] · J. Castillo-Armengol[1,2] · S. Lagarrigue[2] · L. Fajas[1,2]

Abstract In the course of the last decades, metabolism research has demonstrated that adipose tissue is not an inactive tissue. Rather, adipocytes are key actors of whole body energy homeostasis. Numerous novel regulators of adipose tissue differentiation and function have been identified. With the constant increase of obesity and associated disorders, the interest in adipose tissue function alterations in the XXIst century has become of paramount importance. Recent data suggest that adipocyte differentiation, adipose tissue browning and mitochondrial function, lipogenesis and lipolysis are strongly modulated by the cell division machinery. This review will focus on the function of cell cycle regulators in adipocyte differentiation, adipose tissue function and whole body energy homeostasis; with particular attention in mouse studies.

Keywords Cell cycle · CDKs · Cyclins · Adipose tissue · Metabolism · Obesity · Insulin resistance

Introduction

Metabolic adaptation to dietary consumption and composition involves changes in the pattern of gene expression that allow the organism to optimally utilize, and respond to, available nutrients. However, excess intake of certain nutrients will interfere with body homeostasis and physiology,

leading to maladaptation and disease, i.e., obesity and associated disorders.

Adipose tissue, which is composed mostly of adipocytes, is a major endocrine organ and plays a key role in energy homeostasis. Hence, adipose tissue is an important player in the development of obesity-induced insulin resistance, and therefore in the onset of the metabolic syndrome [19].

Three types of adipose tissue: white adipose tissue (WAT), brown adipose tissue (BAT), and brite adipose tissue (or beige adipose tissue) have been identified [70]. The main functions of WAT are to store excess energy in the form of triglycerides (TGs), and to produce numerous hormones (adipokines) [52]. In contrast, brown and brite adipose tissues oxidize substrates and dissipate energy in the form of heat [23]. Excessive WAT promotes obesity and related diseases, whereas the activity of brown and brite adipose tissues has a positive effect in metabolic health. Therefore, gaining insight about the regulation of the function of the different adipose tissue depots can pave the way for new therapies to counteract obesity and obesity-associated metabolic diseases.

Cell cycle regulators respond to extracellular stimuli, control the progression through the cell cycle, and ensure the different quality control checkpoints for cell duplication. Cell cycle dependent kinases (CDKs), cyclins, and CDK inhibitors of the CIP/KIP (CDK inhibitors (CKIs)) and INK4 families, as well as the pocket proteins of the retinoblastoma family and the E2F transcription factors, are major components of the cell cycle regulatory machinery. The activity of the CDKs is positively regulated by their interaction with their regulatory subunits, the cyclins. They can also be negatively regulated by their interaction with CKIs and INK4 family members. Upon mitogen activation, CDK4/6 and CDK2, with the D-type and E-type cyclins respectively, phosphorylate the retinoblastoma proteins (pRB, p107

✉ L. Fajas
lluis.fajas@unil.ch

1 Center for Integrative Genomics, University of Lausanne, Lausanne, Switzerland

2 Department of Physiology, University of Lausanne, Lausanne, Switzerland

and p130), thereby releasing the E2F transcription factors and allowing the transcription of genes necessary for the G1/S transition and for DNA synthesis [47]. CDK2 and CDK1, with the A-type and B-type cyclins, respectively, ensure the progression of the G2 and M phases (Table 1 and Fig. 1). To prevent unhealthy cells from proliferating, several quality control checkpoints trigger cell cycle arrest to permit either the repair of identified defects, or to prevent

the multiplication of the severely injured cells [51]. These checkpoints are controlled, amongst other, by the ATM/ATR and CHK1/CHK2 kinases [2, 83]; as well as by the transcriptional regulator p53 [33] (Fig. 2).

Growing evidence about the regulatory crosstalk between metabolic pathways, cell cycle progression and cell division is found. Our laboratory and others have shown that cell metabolism is reprogrammed through the regulation of

Table 1 Cell cycle regulators

Cell cycle stage	Cyclins	CDKs	Function
G1	CCND1, CCND2, CCND3	CDK4, CDK6	Respond to external stimuli and mitogens. CDK4/6 activation initiates the phosphorylation of key substrates including Rb. Rb phosphorylation by CDK4/6 releases E2F1 to regulate the transcription of cell cycle related genes
G1/S	CCNE1, CCNE2	CDK2	CDK2/CCNE complexes contribute to the hyperphosphorylation of Rb and to the initiation of DNA replication. Induction of histone synthesis
S	CCNA1, CCNA2	CDK1, CDK2	Duplication of the genome. Targets helicases and polymerases
G2/M	CCNB1, CCNB2, CCNB3	CDK1	CDK1/B-type cyclin complexes are the major regulator of G2/M transition. CDK1/B-type cyclin complexes also act by priming certain substrates (including INCENP and BubR1) for phosphorylation by another mitotic kinase, polo kinase (Plk1)
M	CCNB1, CCNB2, CCNB3	CDK1	The activation of CDK1/B-type cyclin complexes promotes mitosis progression in the absence of DNA damage and following appropriate preparation for chromosomal segregation
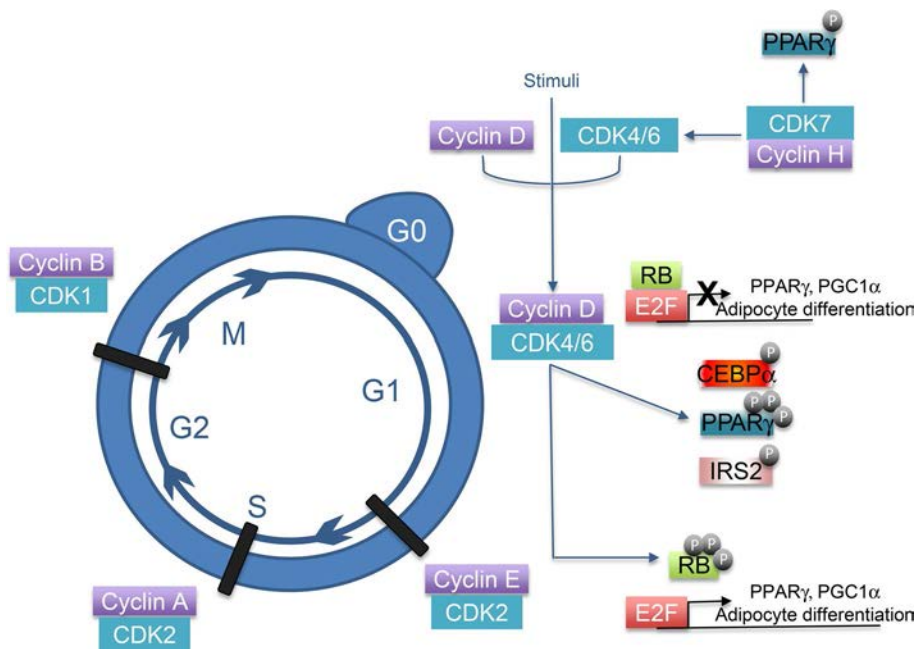
Fig. 1 Cell cycle regulators participate in adipose tissue function. Stimuli and CAK (CDK-activating kinase CDK7/CyclinH/MAT1) induced activation of the cyclin D-CDK4/6 complex early in G1 phase leads to the partial inactivation of the pocket proteins, pRB, p107 and p130. Inactivated pocket proteins will release E2Fs transcription factor activity and thus, allow the expression of genes necessary for the G1 > S transition. Next, CDK2 is active, as a complex with cyclin E or A-type cyclins, during S phase and G phase.

Finally, CDK1 with B-type cyclins, will drive cells through mitosis. Cell cycle checkpoints are depicted in black. Upon activation, CDK4 also participates in white adipocyte differentiation and function by directly phosphorylating PPARγ, CEBPα and IRS2. The activation of CDK4, via the E2F transcription factors also triggers the transcription of adipogenic genes, PPARγ, and PGC1α. Moreover, CDK7 also phosphorylates PPARγ
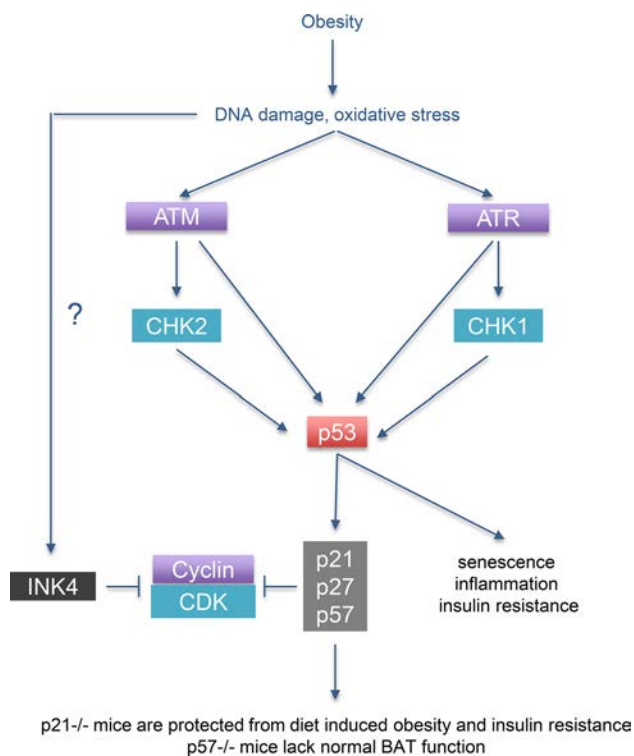
Fig. 2 Negative cell cycle regulators participate in adipose tissue function. Obesity induces the accumulation of damaged DNA and oxidative stress. It has also been linked to shortened telomeres and to increased senescence. This processes trigger the induction of the cell cycle checkpoint control and lead to the activation of p53. p53 will then participate in the onset of insulin resistance. Therefore the adipose-specific p53 KO protects from diet-induced insulin resistance. p21 is a transcriptional target of p53, and $p21^{-/-}$ mice are also protected against diet-induced obesity and insulin resistance. On the other hand, $p57^{-/-}$ mice lack proper brown function, suggesting that the CKIs members play independent roles in adipose tissue function. The role of the kinases upstream p53 (ATM, ATR, CHK1 and CHK2) remains to be studied

metabolic processes, like lipogenesis, lipolysis and mitochondrial function [43, 49, 72] by various cell cycle regulators. In this review, we describe the recent advances in the study of the regulation of white, brown, and brite adipocytes by cell cycle regulators in cellular models of adipose tissue and mouse models, and discuss what is currently known in humans.

The role of the CDK4-pRB-E2F1 pathway in adipose tissue function

Our laboratory has been focusing for a long time in the function of the CDK4-pRB-E2F1 pathway in the control of metabolism. We, and others, have clearly demonstrated that these G1 and S-phase cell cycle regulators unequivocally control metabolic processes, to ensure the metabolic

reprogramming required for cell cycle, and independently of cell cycle [4, 49, 72].

Indeed, E2F1 was demonstrated to be a positive regulator of adipogenesis, whereas E2F4 is a negative regulator of adipocyte differentiation [28]. This regulation takes place through the control of the key adipogenic regulator PPARγ. In agreement with this finding, it has been shown that pRB, the pocket protein that represses E2F1 transcriptional activity, plays numerous roles in adipogenesis, as reviewed by [31]. Moreover, CDK4 and one of its partners, cyclin D3, can also promote adipocyte differentiation via the direct activation of PPARγ [1, 73].

Cyclin D1 and cyclin D3, two possible partners of CDK4, have independently been revealed to play opposite roles in adipogenesis, since cyclin D3 has been shown to promote adipogenesis [73], whereas cyclin D1 inhibits both PPARγ activity and adipogenesis [30]. These findings are in agreement with the discovery that the association between CDK4 and cyclins D2 and D3 increases during adipocyte differentiation, whereas the association between CDK4 and cyclin D1 is limited to the proliferative phase and the clonal expansion of 3T3-L1 adipocytes [66].

Studies using mouse models have further underscored the role of the CDK4-pRB-E2F1 pathway in metabolism, since transgenic animal models for these proteins exhibit marked metabolic phenotypes. For instance, $E2f1^{-/-}$ mice and $Ccnd3^{-/-}$ mice are resistant to high-fat diet-induced obesity and show increased insulin sensitivity [26, 28, 73]. $E2f1^{-/-}$ mice also exhibit increased oxidative metabolism in brown adipose tissue [11]. pRB adipose-specific knockout [24] are protected from diet-induced obesity and exhibit browning of the white adipose tissue, and pRB haploinsufficient animals express brown adipocyte-related genes in white adipose tissue [65]. Furthermore, like pRB deficient animals, mice lacking p107 are lean and displayed a conversion of WAT into BAT [74]. Additionally, mice lacking p130 showed a marked reduction in subcutaneous fat [79].

The above-mentioned studies highlight the dual role of cell cycle regulators in adipogenesis and mature adipocyte function. On the one hand, the positive cell cycle regulators CDK4, Cyclin D3 and the transcription factors E2F1 promote adipocyte differentiation by promoting PPARγ expression or activity [1, 28, 73]. This positive effect on PPARγ can partially explain the protection from diet-induced obesity observed in $E2f1^{-/-}$ mice and $Ccnd3^{-/-}$ mice [26, 73].

On the other hand, the negative cell cycle regulators of the retinoblastoma family play controversial roles in adipogenesis. The lack of pRB inhibits adipogenesis in 3T3 and MEF cells [22, 24], whereas the lack of p107 and p130 increases the differentiation potential in 3T3 cells [22]. However, pRB can directly repress PPARγ thus the lack of pRB promotes adipogenesis in the presence of PPARγ agonists [27]. Despite the dual role of retinoblastoma proteins

in adipogenesis, pRB-, p107- and p130- deficient mice are also leaner than their control counter parts [24, 65, 74, 79]. However, the use of the adipose-specific model in the Dali-Youcef et al. allows focusing on the function of pRB in mature adipocytes.

The similarities between pRB-, p107- and p130-deficient mice, which are expected to have increased E2F1 activity, and *E2f1*$^{-/-}$ mice underscore the importance of E2F1 both as a transcriptional repressor, when complexed with a pocket protein, and as a transcriptional activator. Moreover, they suggest that there are other factors implicated in the regulation of gene expression by the pocket protein/E2F1 complexes.

Finally, *Cdk4*$^{nc/nc}$ mice, expressing CDK4 only in pancreatic beta cells, have decreased fat mass, and exhibit insulin resistance; whereas *Cdk4*$^{R24C/R24C}$ mice, carrying a point mutation that prevents the interaction between CDK4 and the INK4 family members, have increased fat mass and improved insulin sensitivity in an E2F1-independent manner, via increased phosphorylation of the IRS2 protein [43]. Recombinant adeno-associated virus (AAV) were used to trigger an acute deletion of CDK4, and formally prove that the effects of CDK4 in the insulin signaling pathway are due to the modulation of terminally differentiated adipocytes, and not to its role in adipogenesis [43]. This finding suggests that CDK4 and D-type cyclins may have other cell cycle independent functions in metabolic tissues that remain to be discovered.

Cell cycle regulators have been shown to modulate adipose tissue via the regulation of master metabolic regulators like PPARγ, PGC1α and IRS2 [1, 11, 43]. These findings place the CDK4-pRB-E2F1 axis as a key sensor of metabolism at the cellular and at the organismal level.

The role of CKIs in adipose tissue function

The CKIs (CDK inhibitors), namely p21^{Cip1}, p27^{Kip1}, and p57^{Kip2}, inhibit CDKs in a stoichiometric manner [15]. However, they have also been proposed to stabilize the complexes formed between CDK4 and the D-type cyclins [10, 17, 42]. p21 has been shown to increase during adipocyte differentiation. Its inhibition prevents adipogenesis [41]. In agreement with these findings, p21 knockout male mice are resistant to diet-induced insulin resistance and obesity [41]. Surprisingly, it has also been reported that p21 knockout, p27 knockout and p21/p27 double knockout female mice have increased adiposity, suggesting a repressive synergistic role of p21 and p27 in adipose tissue hyperplasia [59]. However, the molecular mechanisms by which p21 and p27 modulate the onset of obesity have not yet been established.

Interestingly, the overexpression of p57 leads to an increase of BAT and BAT-like depots within white adipose tissue in mice. This increasing brown and brown-like functions trigger a lean phenotype. Conversely, the mice that are deficient for p57 lack functional BAT. This is due to the effect of p57 in the stabilization of PRDM16, a key factor for brown fat development [77].

Despite our finding that CDK4 activity is positively correlated with adiposity and with insulin signaling using the R24C model [43], the exact role of the INK4 inhibitors in adipose differentiation and function remains to be studied.

The role of atypical cell cycle regulators in adipose tissue function

Cell cycle CDKs (CDK1, CDK2, CDK4 and CDK6) play important roles in the control of cell division. Out of these CDKs, only CDK4 has been demonstrated to play a role in adipose tissue metabolism. A second subset of CDKs plays roles outside cell cycle, like CDK5, or rather regulate transcription in response to several extra- and intracellular cues [50]. CDK5, CDK7 and CDK9 are of particular interest for this review.

CDK5 is considered an atypical CDK because it is activated by the non-cyclin proteins Cdk5R1 (p35) or Cdk5R2 (p39), and because it does not require the phosphorylation in the T-loop to be active [18]. Even if CDK5 is ubiquitously expressed, the expression of p35 and p39 is restricted to specific cell types [18]. Obesity has been demonstrated to increase the expression/activity of CDK5 in adipose tissue, thus triggering direct phosphorylation of PPARγ S273. The activation of CDK5 in obesity is mediated by the cleavage of p35, into the more active p25 [20, 21]. Surprisingly, the adipose-specific knockout of CDK5 leads to increased PPARγ S273 phosphorylation, because of a lack of repression of CDK5 on kinase MEK2 [9], underscoring the complexity of the regulation of insulin sensitivity in adipose tissue.

CDK7, and its partners MAT1 and cyclin H, have essential roles in both the cell cycle, as a CDK-activating kinase (CAK) that functions upstream cell cycle CDKs, and in transcriptional initiation as the kinase submodule of the general transcription factor TFIIH [25]. The CDK7-cyclin H-MAT1 complex was shown to repress adipocyte differentiation by directly phosphorylating PPARγ. Accordingly, the levels of MAT1 and CDK7 decrease during adipocyte differentiation, and *Mat1*$^{-/-}$ MEFs exhibit increased adipocyte differentiation [37].

CDK9, as the catalytic subunit of p-TEFb, controls the elongation phase [63]. The inhibition of the activity of CDK9 results in decreased adipogenesis, since CDK9 interacts with, phosphorylates and activates PPARγ. Importantly, the expression of CDK9 is increased in the adipose tissue in two models of obesity in mice: the high-fat diet model, and the db/db model [40].

Overall, these results suggest that CDK5 and the transcriptional CDKs, CDK7 and CDK9, play precise roles in metabolic tissues and therefore in whole body energy homeostasis.

Other atypical cell cycle regulators include the highly conserved, membrane bound, cyclin Y, which activates the poorly characterized CDK16, CDK17 and CDK18 [53]; and the G1 and G2 cyclins that actually oppose cell cycle progression. The expression of cyclin G2 is higher in differentiated cells and cell cycle arrested cells. It is believed to actually promote the quiescent state of terminally differentiated cells and has no associated kinase activity [82]. The expression of cyclin G2 is increased during adipocyte differentiation, and it promotes PPARγ-dependent transcription [3]. Cyclin G2 is also expressed in mature adipocytes, most likely to maintain the quiescent state in those differentiated cells [82].

Cyclin Y deficiency leads to impaired adipogenesis, and cyclin Y-deficient animals have decreased fat mass, are resistant to high-fat diet-induced obesity, and show increased BAT function and overall metabolic rates [5].

The role of the cell cycle checkpoint regulators in adipose tissue function

Proper cell cycle progression requires a tight quality control. This quality control relies on three major checkpoints: the G1/S checkpoint, the S-phase checkpoint and the G2/M checkpoint (Fig. 2). ATM/ATR, CHK1/CHK2 and p53 are master regulators of these checkpoints.

Interestingly, p53 is a dominant regulator of the CDK inhibitor p21 [7, 75]. It exerts a negative effect in white adipocyte differentiation, but a positive effect in brown adipocyte differentiation [56, 57]. p53 expression levels remain stable during adipocyte differentiation; however, the phosphorylation levels of S15 and S20 are increased during the terminal steps of adipocyte differentiation [41].

Importantly, the expression of p53 in WAT is tightly entangled in the development of insulin resistance. Indeed, the excessive energy intake that characterizes the western diet leads to the accumulation of oxidative damage in WAT. This leads to the increased expression of the tumor suppressor p53 [54], perhaps due to an increase in the levels of DNA damage, and to a decrease in telomere length [78].

Despite the fact that the full KO of p53 have increased sensitivity to high-fat diet-induced obesity [56], adipose-specific inhibition of the activity of p53 corrected the diet-induced inflammation and insulin resistance, but not the diet-induced increase in fat mass; whereas the overexpression of p53 triggered increased inflammation in adipose tissue, and therefore, insulin resistance [54]. The observations made in p53 adipose-specific knockout animals suggest that p53 plays a dual role in adipose tissue function by repressing adipocyte differentiation and by triggering stress-induced inflammation in mature adipocytes.

The importance of oxidative stress and p53 in the onset of insulin resistance was further demonstrated by the fact that mice carrying a germline mutation replacing the p53 S15, which is phosphorylated by ATM upon stress, with an alanine have severe defects in glucose homeostasis and develop insulin resistance [6]. It is worth noting that an increase of p53 levels was also observed in omental adipose tissue in a cohort of human obese patients [60].

Moreover, *trp53*$^{-/-}$ mice are protected against ghrelin-induced gains in body weight and fat mass. However, it is

Table 2 Mouse models

Cell cycle regulator	Phenotype	References
Cdk4 KO	Lean, decreased fat mass, insulin resistant	[43, 69]
Cdk4 R24C	Overweight, increased fat mass, increased insulin sensitivity	[43, 69]
Cyclin D3 KO	Resistant to high-fat diet, smaller adipocytes	[73]
E2F1 KO	Increased oxidative activity in brown adipose tissue	[11]
Rb, adipose tissue-specific KO	Decreased body weight and fat content, increased mitochondrial activity in WAT and BAT	[24]
Rb$^{+/-}$	Reduced in body fat content, improved blood lipids, enhanced insulin and leptin sensitivity	[65]
p21 KO	Resistant to high-fat diet	[41]
p21, p27 DBKO	Increased body weight and adipocyte hyperplasia	[41]
p107 KO	Less differentiated WAT depots and browning of WAT	[74]
Cdk5, adipose tissue-specific KO	Insulin resistant, increased of fasting insulin, no change in body weight and glucose tolerance	[9]
CCNY KO	Decreased total body fat mass and smaller adipocytes	[5]
p53, adipose tissue-specific transgenic	Accumulation of oxidative stress, increased senescence and inflammation, increased insulin resistance	[54]
p53, adipose tissue-specific KO	Reduction of oxidative stress, reduction of senescence and inflammation, reduced insulin resistance	[54]

Table 3 Literature review

Cell cycle regulator	Mechanism of action	Target genes/proteins	Model	Species	References
CCND1, CCND2, CCND3, CDK4	D-type cyclin expression levels are regulated during adipogenesis. Levels of CCND2 and CCND3 and their associations with Cdk4 increased during adipogenesis. CCND3 is the predominant cyclin partner of Cdk4 in mature adipocyte		3T3-L1	Mouse	[66]
CCND1	CCND1 increases histone deacetylase (HDAC1) activity and inhibit both PPARγ activity and adipogenesis	HDAC1, PPARγ	NIH 3T3 cells, MEFs	Mouse	[30]
CCND2, CCND3, Cdk4	miR-125b-5p inhibits cell proliferation and induces cell cycle arrest in 3T3L1 to promote adipogenesis by decreasing the expression of CCND2, CCND3 and CDK4	C/EBPα, PPARγ, CCND2, CCND3, CDK4	3T3-L1	Mouse	[61]
CCND3	CCND3 promotes adipocyte differentiation via a coactivation of PPARγ	PPARγ	3T3-L1, white adipose tissue	Mouse	[73]
CCND3, CDK4	CDK4-CCND3 phosphorylates C/EBPα to induce growth arrest and further differentiation	C/EBPα (S193)	3T3-L1, Liver	Mouse	[80]
CDK2/CDK4	CDK2/CDK4 interaction is involved in in vitro adipocyte differentiation	C/EBPα	NIH 3T3 cells	Mouse	[67]
CDK4	db/db- CDK4 R24C mice have decreased peripheral lipolysis		Plasma	Mouse	[55]
CDK4	Inhibition of CDK4 reduces the adipogenic fate in human Adipocyte Derived Mesenchymal Stem Cells (hAD-MSCs)	Adiponectin, Lipoprotein lipase and PPARγ2	hAD-MSCs	Human	[46]
CDK4	Overexpression of CDK4/CycD leads to an increase of mitochondrial activity in the adipose tissue of Drosophila	Delg, drosophila homolog of NRF2/GABP	Drosophila larvae fat body	Drosophila	[8]
CDK4	Cdk4 participates in adipocyte differentiation through PPARγ activation	PPARγ	3T3-L1, MEFs	Mouse	[1]
CDK4	Cdk4 mediates the effects of insulin by repressing lipolysis and stimulating lipogenesis in white adipose tissue	IRS2 (S388)	3T3-L1, white adipose tissue, mice, human visceral adipose tissue	Mouse Human	[43]
CDK4	ZnO treatment increases CDK4-PPARγ colocalization and lipid accumulation	PPARγ, FABP4, CEBPα, SREBP1	3T3-L1	Mouse	[62]
CDK4, p21, p27 and Cdc2	CDKs are regulated by antioxidants to modulate the cell cycle progression of hAD-MSCs and enhance their differentiation potential	CDK4, p21, p27 and Cdc2	hAD-MSCs	Human	[76]
E2F1	E2F1 represses oxidative metabolism in murine brown adipose tissue	UCP1, CPT1, PGC1α	Brown adipose tissue, mice	Mouse	[11]

Table 3 (continued)

Cell cycle regulator	Mechanism of action	Target genes/proteins	Model	Species	References
E2F1	Oxidative damage decreases E2F1 expression and inhibits adipogenesis in 3T3L1 cells	aP2, p21, p27, pRB	3T3-L1, primary adipocytes from subcutaneous adipose tissue	Mouse	[29]
E2F1	E2F1 expression is increased in visceral fat of obese humans to, probably, mediate autophagy	ATG5, MAP1LC3B/LC3B	human visceral adipose tissue, MEFs	Human	[35]
E2F1, E2F3, E2F4	E2F1 and E2F3 promote adipogenesis in murine MEFs. E2F4 has a negative effect on adipogenesis	PPARγ	3T3L1, NIH-3T3, MEFs, ES cells	Mouse	[28]
E2F4	Loss of E2F4 increases the differentiation potential of MEFs into adipocytes		MEFs	Mouse	[45]
pRb	Impaired Rb activity leads to the conversion of white adipose tissue into brown adipose tissue	UCP, aP2, LPL	aP2-SV-40 transgenic mice	Mouse	[71]
pRb	Adipose tissue-specific Rb knockout are protected from HFD and browning of WAT with an increased of energy expenditure	UCP1, CCND2, PGC1α	MEFs	Mouse	[24]
pRb	Rb/HDAC3 complex blocks adipocyte differentiation by a negative regulation of PPARγ	PPARγ, HDAC3	3T3L1, MEFs	Mouse	[27]
pRb	Rb negatively regulates the adipogenic commitment at the initial stage of adipogenesis	PPARγ, aP2, LPL, adiponectin	Porcine mature adipocytes	Pig	[38]
pRb	Rb loss favors the adipogenic fate in in vitro osteoblasts and increases the levels of brown fat	Runx2, PPARγ	osteoblast cell lines, primary osteoblast	Mouse	[13]
pRb	Rb is essential for the differentiation of fibroblasts into adipocytes	C/EBPβ	MEFs	Mouse	[16]
pRb	Inactivation of Rb converts WAT into BAT	UCP1	3T3L1, MEFs	Mouse	[36]
pRb	Lack of Rb increases the expression of thermogenesis-related genes but not of brite fat-specific markers	PPARγ, PPARγ1a, PPARγ1b, Prdm16, Cpt1b	Primary preadipocytes	Mouse	[64]
pRb	Aged Rb$^{+/-}$ mice were leaner and more insulin sensitive than their WT littermates. They also exhibit increased expression of fatty acid oxidation genes in WAT	UCP1, PPARα, CPT1b	White adipose tissue	Mouse	[65]

Table 3 (continued)

Cell cycle regulator	Mechanism of action	Target genes/proteins	Model	Species	References
pRb	Lack of Rb increases the percentage of uncommitted bone marrow stem cells (BMSC) towards adipocytes	C/EBPα, C/EBPβ	Bone marrow stromal cells	Human	[14]
pRb, p107	Overexpression of Rb promotes adipocyte differentiation in wild-type cells and p107 does the opposite	C/EBPα	NIH-3T3	Mouse	[22]
p107	Lack of p107 results in a decrease of adipocyte differentiation and increases browning in WAT	PGC1α	Primary preadipocytes, white adipose tissue	Mouse	[74]
p130	Absence of p130 reduces the subcutaneous fat deposition		Subcutaneous adipose depots	Mouse	[79]
p21	p21 has a positive effect in the latter stages of adipocyte differentiation by inducing C/EBPβ expression. p21$^{-/-}$ male mice are protected against diet-induced obesity	C/EBPβ	3T3-L1, white adipose tissue, mice,	Mouse	[41]
p21, p27	Decreased expression of p21 and p27 in the subcutaneous white adipose tissue of high-fat diet rats		Subcutaneous white adipose tissue, rats	Rat	[12]
p27	p27 loss increases the levels of PPARγ and induces apoptosis in inguinal fat		White adipose tissue, mice,	Mouse	[48]
p27, p21	Lack of p27 or p21 causes adipocyte hyperplasia and obesity in female mice		White adipose tissue, mice,	Mouse	[59]
CDKN1C	CDKN1C promotes the formation of BAT and the browning of WAT by increasing Prdm16 expression	Prdm16	MEFs, white and brown adipose tissue, mice	Mouse	[77]
CCNG2/CDK4	CDK4 and CCNG2 expression are inversely associated with glucose and insulin resistance	Correlates with Cdk4 expression	Human visceral adipose tissue	Human	[32]
CCNG2	CCNG2 stimulates the transcriptional activity and interacts with PPARγ to promote adipocyte differentiation	PPARγ	3T3-F442A	Mouse	[3]
CCNG2	CCNG2 expression is increased during adipogenic differentiation in porcine subcutaneous adipose tissue probably to inhibit cell cycle and maintain the quiescent state of mature adipocytes	PPARγ	3T3-L1, isolated preadipocytes	Pig	[82]
CCNY	CCNY promotes adipocyte differentiation. CCNY also promotes insulin signaling in liver cells		3T3-L1, white adipose tissue, mice	Mouse	[5]

Table 3 (continued)

Cell cycle regulator	Mechanism of action	Target genes/proteins	Model	Species	References
CDK5	CDK5 activation is stimulated by insulin and regulates glucose transport in adipocytes. In the absence of CDK5, GLUT4-mediated glucose transport is decreased		3T3L1	Mouse	[44]
CDK5	CDK5-mediated phosphorylation of PPARγ is linked to obesity induced in mice by high-fat feeding. The phosphorylation of PPARγ by CDK5 is blocked by anti-diabetic PPARγ ligands	PPARγ S273	3T3-L1, MEFs, white adipose tissue, mice	Mouse	[20]
CDK5	A novel class of anti-diabetic drugs, that are not PPARγ agonists, act by blocking Cdk5-mediated PPARγ phosphorylation	PPARγ S273	3T3-L1, white adipose tissue, mice	Mouse	[21]
CDK5	Adipose-specific CDK5 knockout mice have an increase in PPARγ S273 phosphorylation and worsened insulin resistance	PPARγ S273	White adipose tissue, mice	Mouse	[9]
CDK7	The CDK7/MAT1 complex is an inhibitor of adipogenesis through the phosphorylation of PPARγ S112	PPARγ S112	3T3L1, MEFs	Mouse	[37]
CDK9	CDK9 participates in adipogenesis by promoting the clonal expansion and the terminal differentiation and by interacting with PPARγ	PPARγ	NIH 3T3, 3T3-L1	Mouse	[40]
p53	p53 KO MEFs exhibit increased adipogenic differentiation		MEFs	Mouse	[57]
p53	p53 exerts a suppressive effect on white adipocyte differentiation, while promoting brown adipocyte differentiation. P53 null mice are protection against diet-induced obesity, but have and atrophied BAT		C3H10T1/2 and 3T3L1cell line	Mouse human	[56]
p53	p53 is induced in ob/ob fed mice to negatively regulate the effects of insulin	p21, MDM2, Bax, Insulin-like growth factor binding protein-3 (IGFBP-3)	White adipose tissue	Mouse	[81]
p53	p53 expression is involved in the development of insulin resistance in adipose tissue		Human preadipocytes, human visceral adipose tissue	Mouse human	[54]
p53	Inflammation and insulin resistance exert dual effects on adipose tissue tumor protein 53 expression		Omental and subcutaneous adipose tissue, explants of SC adipose tissue, isolated pre-adipocytes	human	[60]

Table 3 (continued)

Cell cycle regulator	Mechanism of action	Target genes/proteins	Model	Species	References
p53	p53 suppresses adipogenesis by regulating adipocyte gene expression and the AKT signaling pathway	PPARγ, C/EBPα	3T3L1, MEFs	Mouse	[39]
p53	The p53 pathway and DNA damage mediate alterations in metabolic and secretory functions of adipocytes		3T3L1, human visceral preadipocytes	Mouse human	[78]
ATM/p53	Mice with a targeted mutation in the ATM phosphorylation site on p53 (S18) exhibit insulin resistance	p53 (S18)	MEFs	Mouse	[6]
p53/Ghrelin	The lack of p53 abolishes the stimulation of lipid storage induced by chronically administered ghrelin in WAT	p53	White adipose tissue, mice	Mouse	[68]

not clear if this is due to the effects of p53 in central nervous system, or directly in adipose tissue [68].

These recent findings concerning the role of p53 in adipose tissue biology suggest that there could be a more general, and largely unexplored, role for cell cycle checkpoint regulators in metabolism and adipose tissue biology, via peripheral and central mechanisms.

Human studies

Despite the increasing number of studies describing the function of cell cycle regulators in mouse and cellular models, relatively few studies have confirmed this in humans.

In cultured human mesenchymal stem cells, the inhibition of CDK4, a pro-adipogenic factor, reduces adipogenic potential [46]. In a similar way, antioxidants promote the proliferation and adipogenic potential of human adipose-derived stem cells, partially via the upregulation of CDK4 and CDK2 and the downregulation of p21 and p27 expression [76]. E2F4, an anti-adipogenic factor, is decreased under rosiglitazone therapy in human adipose tissue samples [34].

The levels of cyclin D3 and E2F1, as well as the activity of CDK4, have been shown to be increased in adipose tissue of obese patients [35, 43]. Interestingly, the expression of CDK4 is decreased in morbid obese patients with high insulin resistance, compared to low insulin resistant morbid obese patients [32].

The role of p53 in obesity was also confirmed in humans, since adipose tissue from diabetic subjects [54] or obese subjects [60] exhibit higher p53 expression. Moreover, aging, DNA damage and inflammation also correlate with increased p53 activation and decreased insulin signaling [54, 78].

Overall, these studies in human confirm the proadipogenic function of the CDK4-pRB-E2F1 pathway, the role of CDK4-Cyclin D3 in insulin signaling and the anti-adipogenic function of E2F4; as well as the importance of the p53 pathway in obesity and insulin resistance. Thus, the CDK4-pRB-E2F1 and p53 pathways may be pharmacologically target to prevent obesity and/or the onset of the metabolic syndrome.

Concluding remarks

Proper adipose tissue function is required for whole body energy homeostasis and is an essential part of the metabolic flexibility at the level of the whole organism. Cell cycle progression requires great metabolic adaptation, and cell cycle regulators are emerging as a large class of sensors and effectors of this metabolic adaptation. In this review, we discussed how typical and atypical cyclins and CDKs,

cell cycle inhibitors, E2F transcription factors and the tumor suppressors pRb and p53 regulate diverse key functions of white adipose tissue, as well as its differentiation. Importantly, for most of these factors, roles in the proliferation and differentiation of progenitor cells and in mature adipocytes have been identified. The frequent use of whole body, or constitutive knockout models; rather than tissue-specific knockouts and AAV-mediated approaches has not allowed to fully separate the function of these cell cycle regulators in adipogenesis from their function in mature cells.

Yet, the role of cell cycle regulators in brite and brown adipose tissue biology stands mostly unstudied. Likewise, the role of the cell cycle checkpoint kinases ATM/ATR, CHK1/CHK2, and of the INK4 family of CDK inhibitors in white and brown adipose tissue biology remains to be explored.

While some treatments for the obesity and associated pathologies are available, no therapeutic strategies, other than bariatric surgery have proven effective [53]. The study of the function of cell cycle regulators could lead to the identification of novel pathways [9] and therefore of promising therapeutic avenues in the long term, even if this may prove difficult due to the dose-limiting toxicities of drugs targeting cell cycle regulators [58].

Note

For the sake of clarity, key information concerning the role of cell cycle regulators in adipose tissue function, and the adipose tissue phenotypes of different mouse models that are of interest for this review are recapitulated in Tables 2 and 3.

References

1. Abella A, Dubus P, Malumbres M, Rane SG, Kiyokawa H, Sicard A, Vignon F, Langin D, Barbacid M, Fajas L (2005) Cdk4 promotes adipogenesis through PPARgamma activation. Cell Metab 2:239–249

2. Abraham RT (2001) Cell cycle checkpoint signaling through the ATM and ATR kinases. Genes Dev 15:2177–2196

3. Aguilar V, Annicotte JS, Escote X, Vendrell J, Langin D, Fajas L (2010) Cyclin G2 regulates adipogenesis through PPAR gamma coactivation. Endocrinology 151:5247–5254

4. Aguilar V, Fajas L (2010) Cycling through metabolism. EMBO Mol Med 2:338–348

5. An W, Zhang Z, Zeng L, Yang Y, Zhu X, Wu J (2015) Cyclin Y is involved in the regulation of adipogenesis and lipid production. PLoS One 10:e0132721

6. Armata HL, Golebiowski D, Jung DY, Ko HJ, Kim JK, Sluss HK (2010) Requirement of the ATM/p53 tumor suppressor pathway for glucose homeostasis. Mol Cell Biol 30:5787–5794

7. Ashcroft M, Kubbutat MH, Vousden KH (1999) Regulation of p53 function and stability by phosphorylation. Mol Cell Biol 19:1751–1758

8. Baltzer C, Tiefenbock SK, Marti M, Frei C (2009) Nutrition controls mitochondrial biogenesis in the Drosophila adipose tissue through Delg and cyclin D/Cdk4. PLoS One 4:e6935

9. Banks AS, McAllister FE, Camporez JP, Zushin PJ, Jurczak MJ, Laznik-Bogoslavski D, Shulman GI, Gygi SP, Spiegelman BM (2015) An ERK/Cdk5 axis controls the diabetogenic actions of PPARgamma. Nature 517:391–395

10. Blain SW, Montalvo E, Massague J (1997) Differential interaction of the cyclin-dependent kinase (Cdk) inhibitor p27Kip1 with cyclin A-Cdk2 and cyclin D2-Cdk4. J Biol Chem 272:25863–25872

11. Blanchet E, Annicotte JS, Lagarrigue S, Aguilar V, Clape C, Chavey C, Fritz V, Casas F, Apparailly F, Auwerx J et al (2011) E2F transcription factor-1 regulates oxidative metabolism. Nat Cell Biol 13:1146–1152

12. Boque N, Campion J, Milagro FI, Moreno-Aliaga MJ, Martinez JA (2009) Some cyclin-dependent kinase inhibitors-related genes are regulated by vitamin C in a model of diet-induced obesity. Biol Pharm Bull 32:1462–1468

13. Calo E, Quintero-Estades JA, Danielian PS, Nedelcu S, Berman SD, Lees JA (2010) Rb regulates fate choice and lineage commitment in vivo. Nature 466:1110–1114

14. Capasso S, Alessio N, Di Bernardo G, Cipollaro M, Melone MA, Peluso G, Giordano A, Galderisi U (2014) Silencing of RB1 and RB2/P130 during adipogenesis of bone marrow stromal cells results in dysregulated differentiation. Cell Cycle 13:482–490

15. Cerqueira A, Martin A, Symonds CE, Odajima J, Dubus P, Barbacid M, Santamaria D (2014) Genetic characterization of the role of the Cip/Kip family of proteins as cyclin-dependent kinase inhibitors and assembly factors. Mol Cell Biol 34:1452–1459

16. Chen PL, Riley DJ, Chen Y, Lee WH (1996) Retinoblastoma protein positively regulates terminal adipocyte differentiation through direct interaction with C/EBPs. Genes Dev 10:2794–2804

17. Cheng M, Olivier P, Diehl JA, Fero M, Roussel MF, Roberts JM, Sherr CJ (1999) The p21(Cip1) and p27(Kip1) CDK 'inhibitors' are essential activators of cyclin D-dependent kinases in murine fibroblasts. EMBO J 18:1571–1583

18. Cheung ZH, Ip NY (2012) Cdk5: a multifaceted kinase in neurodegenerative diseases. Trends Cell Biol 22:169–175

19. Choe SS, Huh JY, Hwang IJ, Kim JI, Kim JB (2016) Adipose tissue remodeling: its role in energy metabolism and metabolic disorders. Front Endocrinol 7:30

20. Choi JH, Banks AS, Estall JL, Kajimura S, Bostrom P, Laznik D, Ruas JL, Chalmers MJ, Kamenecka TM, Bluher M et al (2010) Anti-diabetic drugs inhibit obesity-linked phosphorylation of PPARgamma by Cdk5. Nature 466:451–456

21. Choi JH, Banks AS, Kamenecka TM, Busby SA, Chalmers MJ, Kumar N, Kuruvilla DS, Shin Y, He Y, Bruning JB et al (2011) Antidiabetic actions of a non-agonist PPARgamma ligand blocking Cdk5-mediated phosphorylation. Nature 477:477–481

22. Classon M, Kennedy BK, Mulloy R, Harlow E (2000) Opposing roles of pRB and p107 in adipocyte differentiation. Proc Natl Acad Sci USA 97:10826–10831

23. Cohen P, Spiegelman BM (2015) Brown and beige fat: molecular parts of a thermogenic machine. Diabetes 64:2346–2351

24. Dali-Youcef N, Mataki C, Coste A, Messaddeq N, Giroud S, Blanc S, Koehl C, Champy MF, Chambon P, Fajas L et al (2007) Adipose tissue-specific inactivation of the retinoblastoma protein protects against diabesity because of increased energy expenditure. Proc Natl Acad Sci USA 104:10703–10708

25. Egly JM, Coin F (2011) A history of TFIIH: two decades of molecular biology on a pivotal transcription/repair factor. DNA Repair 10:714–721

26. Fajas L, Annicotte JS, Miard S, Sarruf D, Watanabe M, Auwerx J (2004) Impaired pancreatic growth, beta cell mass, and beta cell function in E2F1(−/−) mice. J Clin Invest 113:1288–1295

27. Fajas L, Egler V, Reiter R, Hansen J, Kristiansen K, Debril MB, Miard S, Auwerx J (2002) The retinoblastoma-histone deacetylase 3 complex inhibits PPARgamma and adipocyte differentiation. Dev Cell 3:903–910

28. Fajas L, Landsberg RL, Huss-Garcia Y, Sardet C, Lees JA, Auwerx J (2002) E2Fs regulate adipocyte differentiation. Dev Cell 3:39–49

29. Findeisen HM, Pearson KJ, Gizard F, Zhao Y, Qing H, Jones KL, Cohn D, Heywood EB, de Cabo R, Bruemmer D (2011) Oxidative stress accumulates in adipose tissue during aging and inhibits adipogenesis. PLoS One 6:e18532

30. Fu M, Rao M, Bouras T, Wang C, Wu K, Zhang X, Li Z, Yao TP, Pestell RG (2005) Cyclin D1 inhibits peroxisome proliferator-activated receptor gamma-mediated adipogenesis through histone deacetylase recruitment. J Biol Chem 280:16934–16941

31. Galderisi U, Cipollaro M, Giordano A (2006) The retinoblastoma gene is involved in multiple aspects of stem cell biology. Oncogene 25:5250–5256

32. Garrido-Sanchez L, Roca-Rodriguez Mdel M, Fernandez-Veledo S, Vendrell J, Yubero-Serrano EM, Ocana-Wilhelmi L, Garcia-Fuentes E, Tinahones FJ (2014) CCNG2 and CDK4 is associated with insulin resistance in adipose tissue. Surg Obes Relat Dis 10:691–696

33. Giono LE, Manfredi JJ (2007) Mdm2 plays a positive role as an effector of p53-dependent responses. Cell Cycle 6:2143–2147

34. Goldfine AB, Crunkhorn S, Costello M, Gami H, Landaker EJ, Niinobe M, Yoshikawa K, Lo D, Warren A, Jimenez-Chillaron J et al (2006) Necdin and E2F4 are modulated by rosiglitazone therapy in diabetic human adipose and muscle tissue. Diabetes 55:640–650

35. Haim Y, Bluher M, Slutsky N, Goldstein N, Kloting N, Harman-Boehm I, Kirshtein B, Ginsberg D, Gericke M, Guiu Jurado E et al (2015) Elevated autophagy gene expression in adipose tissue of obese humans: a potential non-cell-cycle-dependent function of E2F1. Autophagy 11:2074–2088

36. Hansen JB, Jorgensen C, Petersen RK, Hallenborg P, De Matteis R, Boye HA, Petrovic N, Enerback S, Nedergaard J, Cinti S et al (2004) Retinoblastoma protein functions as a molecular switch determining white versus brown adipocyte differentiation. Proc Natl Acad Sci USA 101:4112–4117

37. Helenius K, Yang Y, Alasaari J, Makela TP (2009) Mat1 inhibits peroxisome proliferator-activated receptor gamma-mediated adipocyte differentiation. Mol Cell Biol 29:315–323

38. Hu X, Luo P, Peng X, Song T, Zhou Y, Wei H, Peng J, Jiang S (2015) Molecular cloning, expression pattern analysis of porcine Rb1 gene and its regulatory roles during primary dedifferentiated fat cells adipogenic differentiation. Gen Comp Endocrinol 214:77–86

39. Huang Q, Liu M, Du X, Zhang R, Xue Y, Zhang Y, Zhu W, Li D, Zhao A, Liu Y (2014) Role of p53 in preadipocyte differentiation. Cell Biol Int 38:1384–1393

40. Iankova I, Petersen RK, Annicotte JS, Chavey C, Hansen JB, Kratchmarova I, Sarruf D, Benkirane M, Kristiansen K, Fajas L (2006) Peroxisome proliferator-activated receptor gamma recruits the positive transcription elongation factor b complex to activate transcription and promote adipogenesis. Mol Endocrinol 20:1494–1505

41. Inoue N, Yahagi N, Yamamoto T, Ishikawa M, Watanabe K, Matsuzaka T, Nakagawa Y, Takeuchi Y, Kobayashi K, Takahashi A et al (2008) Cyclin-dependent kinase inhibitor, p21WAF1/CIP1, is involved in adipocyte differentiation and hypertrophy, linking to obesity, and insulin resistance. J Biol Chem 283:21220–21229

42. LaBaer J, Garrett MD, Stevenson LF, Slingerland JM, Sandhu C, Chou HS, Fattaey A, Harlow E (1997) New functional activities for the p21 family of CDK inhibitors. Genes Dev 11:847–862

43. Lagarrigue S, Lopez-Mejia IC, Denechaud PD, Escote X, Castillo-Armengol J, Jimenez V, Chavey C, Giralt A, Lai Q, Zhang L et al (2016) CDK4 is an essential insulin effector in adipocytes. J Clin Investig 126:335–348

44. Lalioti V, Muruais G, Dinarina A, van Damme J, Vandekerckhove J, Sandoval IV (2009) The atypical kinase Cdk5 is activated by insulin, regulates the association between GLUT4 and E-Syt1, and modulates glucose transport in 3T3-L1 adipocytes. Proc Natl Acad Sci USA 106:4249–4253

45. Landsberg RL, Sero JE, Danielian PS, Yuan TL, Lee EY, Lees JA (2003) The role of E2F4 in adipogenesis is independent of its cell cycle regulatory activity. Proc Natl Acad Sci USA 100:2456–2461

46. Lee J, Baek JH, Choi KS, Kim HS, Park HY, Ha GH, Park H, Lee KW, Lee CG, Yang DY et al (2013) Cyclin-dependent kinase 4 signaling acts as a molecular switch between syngenic differentiation and neural transdifferentiation in human mesenchymal stem cells. Cell Cycle 12:442–451

47. Lim S, Kaldis P (2013) Cdks, cyclins and CKIs: roles beyond cell cycle regulation. Development 140:3079–3093

48. Lin J, Della-Fera MA, Li C, Page K, Choi YH, Hartzell DL, Baile CA (2003) P27 knockout mice: reduced myostatin in muscle and altered adipogenesis. Biochem Biophys Res Commun 300:938–942

49. Lopez-Mejia IC, Fajas L (2015) Cell cycle regulation of mitochondrial function. Curr Opin Cell Biol 33:19–25

50. Malumbres M (2014) Cyclin-dependent kinases. Genome Biol 15:122

51. Malumbres M, Barbacid M (2009) Cell cycle, CDKs and cancer: a changing paradigm. Nat Rev Cancer 9:153–166

52. Maury E, Brichard SM (2010) Adipokine dysregulation, adipose tissue inflammation and metabolic syndrome. Mol Cell Endocrinol 314:1–16

53. Mikolcevic P, Rainer J, Geley S (2012) Orphan kinases turn eccentric: a new class of cyclin Y-activated, membrane-targeted CDKs. Cell cycle 11(20):3758–3768

54. Minamino T, Orimo M, Shimizu I, Kunieda T, Yokoyama M, Ito T, Nojima A, Nabetani A, Oike Y, Matsubara H et al (2009) A crucial role for adipose tissue p53 in the regulation of insulin resistance. Nat Med 15:1082–1087

55. Miyawaki K, Inoue H, Keshavarz P, Mizuta K, Sato A, Sakamoto Y, Moritani M, Kunika K, Tanahashi T, Itakura M (2008) Transgenic expression of a mutated cyclin-dependent kinase 4 (CDK4/R24C) in pancreatic beta-cells prevents progression of diabetes in db/db mice. Diabetes Res Clin Pract 82:33–41

56. Molchadsky A, Ezra O, Amendola PG, Krantz D, Kogan-Sakin I, Buganim Y, Rivlin N, Goldfinger N, Folgiero V, Falcioni R et al (2013) p53 is required for brown adipogenic differentiation and has a protective role against diet-induced obesity. Cell Death Differ 20:774–783

57. Molchadsky A, Shats I, Goldfinger N, Pevsner-Fischer M, Olson M, Rinon A, Tzahor E, Lozano G, Zipori D, Sarig R et al (2008) p53 plays a role in mesenchymal differentiation programs, in a cell fate dependent manner. PLoS One 3:e3707

58. Murphy CG, Dickler MN (2015) The role of CDK4/6 inhibition in breast cancer. Oncologist 20:483–490

59. Naaz A, Holsberger DR, Iwamoto GA, Nelson A, Kiyokawa H, Cooke PS (2004) Loss of cyclin-dependent kinase inhibitors produces adipocyte hyperplasia and obesity. FASEB J 18:1925–1927

60. Ortega FJ, Moreno-Navarrete JM, Mayas D, Serino M, Rodriguez-Hermosa JI, Ricart W, Luche E, Burcelin R, Tinahones FJ, Fruhbeck G et al (2014) Inflammation and insulin resistance exert dual

effects on adipose tissue tumor protein 53 expression. Int J Obes 38:737–745

61. Ouyang D, Ye Y, Guo D, Yu X, Chen J, Qi J, Tan X, Zhang Y, Ma Y, Li Y (2015) MicroRNA-125b-5p inhibits proliferation and promotes adipogenic differentiation in 3T3-L1 preadipocytes. Acta Biochim Biophys Sin 47:355–361

62. Pandurangan M, Jin BY, Kim DH (2016) ZnO nanoparticles upregulates adipocyte differentiation in 3T3-L1 Cells. Biol Trace Elem Res 170:201–207

63. Peterlin BM, Price DH (2006) Controlling the elongation phase of transcription with P-TEFb. Mol Cell 23:297–305

64. Petrov PD, Palou A, Bonet ML, Ribot J (2016) Cell-autonomous brown-like adipogenesis of preadipocytes from retinoblastoma haploinsufficient mice. J Cell Physiol 231:1941–1952

65. Petrov PD, Ribot J, Palou A, Bonet ML (2015) Improved metabolic regulation is associated with retinoblastoma protein gene haploinsufficiency in mice. Am J Physiol Endocrinol Metab 308:E172–E183

66. Phelps DE, Xiong Y (1998) Regulation of cyclin-dependent kinase 4 during adipogenesis involves switching of cyclin D subunits and concurrent binding of p18INK4c and p27Kip1. Cell Growth Differ Mol Biol J Am Assoc Cancer Res 9:595–610

67. Porse BT, Pedersen TA, Hasemann MS, Schuster MB, Kirstetter P, Luedde T, Damgaard I, Kurz E, Schjerling CK, Nerlov C (2006) The proline-histidine-rich CDK2/CDK4 interaction region of C/EBPalpha is dispensable for C/EBPalpha-mediated growth regulation in vivo. Mol Cell Biol 26:1028–1037

68. Porteiro B, Diaz-Ruiz A, Martinez G, Senra A, Vidal A, Serrano M, Gualillo O, Lopez M, Malagon MM, Dieguez C et al (2013) Ghrelin requires p53 to stimulate lipid storage in fat and liver. Endocrinology 154:3671–3679

69. Rane SG, Dubus P, Mettus RV, Galbreath EJ, Boden G, Reddy EP, Barbacid M (1999) Loss of Cdk4 expression causes insulin-deficient diabetes and Cdk4 activation results in beta-islet cell hyperplasia. Nat Genet 22:44–52

70. Rosen ED, Spiegelman BM (2014) What we talk about when we talk about fat. Cell 156:20–44

71. Ross SR, Choy L, Graves RA, Fox N, Solevjeva V, Klaus S, Ricquier D, Spiegelman BM (1992) Hibernoma formation in transgenic mice and isolation of a brown adipocyte cell line expressing the uncoupling protein gene. Proc Natl Acad Sci USA 89:7561–7565

72. Salazar-Roa M, Malumbres M (2017) Fueling the cell division cycle. Trends Cell Biol 27(1):69–81

73. Sarruf DA, Iankova I, Abella A, Assou S, Miard S, Fajas L (2005) Cyclin D3 promotes adipogenesis through activation of peroxisome proliferator-activated receptor gamma. Mol Cell Biol 25:9985–9995

74. Scime A, Grenier G, Huh MS, Gillespie MA, Bevilacqua L, Harper ME, Rudnicki MA (2005) Rb and p107 regulate preadipocyte differentiation into white versus brown fat through repression of PGC-1alpha. Cell Metab 2:283–295

75. Shieh SY, Ahn J, Tamai K, Taya Y, Prives C (2000) The human homologs of checkpoint kinases Chk1 and Cds1 (Chk2) phosphorylate p53 at multiple DNA damage-inducible sites. Genes Dev 14:289–300

76. Sun LY, Pang CY, Li DK, Liao CH, Huang WC, Wu CC, Chou YY, Li WW, Chen SY, Liu HW et al (2013) Antioxidants cause rapid expansion of human adipose-derived mesenchymal stem cells via CDK and CDK inhibitor regulation. J Biomed Sci 20:53

77. Van De Pette M, Tunster SJ, McNamara GI, Shelkovnikova T, Millership S, Benson L, Peirson S, Christian M, Vidal-Puig A, John RM (2016) Cdkn1c boosts the development of brown adipose tissue in a murine model of Silver Russell syndrome. PLoS Genet 12:e1005916

78. Vergoni B, Cornejo PJ, Gilleron J, Djedaini M, Ceppo F, Jacquel A, Bouget G, Ginet C, Gonzalez T, Maillet J et al (2016) DNA damage and the activation of the p53 pathway mediate alterations in metabolic and secretory functions of adipocytes. Diabetes 65:3062–3074

79. Vormer TL, Wojciechowicz K, Dekker M, de Vries S, van der Wal A, Delzenne-Goette E, Naik SH, Song JY, Dannenberg JH, Hansen JB et al (2014) RB family tumor suppressor activity may not relate to active silencing of E2F target genes. Can Res 74:5266–5276

80. Wang GL, Shi X, Salisbury E, Sun Y, Albrecht JH, Smith RG, Timchenko NA (2006) Cyclin D3 maintains growth-inhibitory activity of C/EBPalpha by stabilizing C/EBPalpha-cdk2 and C/EBPalpha-Brm complexes. Mol Cell Biol 26:2570–2582

81. Yahagi N, Shimano H, Matsuzaka T, Najima Y, Sekiya M, Nakagawa Y, Ide T, Tomita S, Okazaki H, Tamura Y et al (2003) p53 activation in adipocytes of obese mice. J Biol Chem 278:25395–25400

82. Zhang J, Suh Y, Choi YM, Ahn J, Davis ME, Lee K (2014) Differential expression of cyclin G2, cyclin-dependent kinase inhibitor 2C and peripheral myelin protein 22 genes during adipogenesis. Anim Int J Anim Biosci 8:800–809

83. Zhou BB, Bartek J (2004) Targeting the checkpoint kinases: chemosensitization versus chemoprotection. Nat Rev Cancer 4:216–225

CDK4 regulates lysosomal function and mTORC1 activation to promote cancer cells survival

Martínez-Carreres L, Puyal J, Orpinell M, **Castillo-Armengol J**, Giralt A, Moret C, Barquissau V, Nasrallah A, Pabois A, Zhang L, Romero P, Lopez-Mejia IC and Fajas L.

This study emphasizes the regulation of lysosomal biology in a crosstalk between CDK4 and mTORC1 in cancer cells. CDK4 phosphorylates foliculin (FLCN) affecting the recruitment of mTORC1 to the lysosomal surface. Moreover, a direct role of CDK4 in lysosomes is also described in this study conferring to CDK4 a new role in lysosomal degradation and autophagy. My contribution to this project was to analyze the expression of lysosomal and senescence markers by RT-PCR in cells and tumors from mice.

CDK4 regulates lysosomal function and mTORC1 activation to promote cancer cells survival

Laia Martínez-Carreres[1], Julien Puyal[2], Meritxell Orpinell[3], Judit Castillo-Armengol[1], Albert Giralt[1], Catherine Moret[1], Valentin Barquissau[1], Anita Nasrallah[1], Angélique Pabois[4,5], Lianjun Zhang[4,6,7], Pedro Romero[4], Isabel C. Lopez-Mejia[1] and Lluis Fajas[1*]

[1]Center for Integrative Genomics, University of Lausanne, 1015 Lausanne, Switzerland.

[2]Department of Fundamental Neurosciences, University of Lausanne, 1005 Lausanne, Switzerland.

[3]Department of Physiology, University of Lausanne, 1005 Lausanne, Switzerland

[4]Department of Fundamental Oncology, University of Lausanne, 1066 Epalinges, Switzerland.

[5]Ludwig Institute for Cancer Research, University of Lausanne, 1066 Epalinges, Switzerland.

[6]Present address: Center for Systems Medicine, Institute of Basic Medical Sciences, Chinese Academy of Medical Sciences and Peking Union Medical College, 100005 Beijing, China.

[7]Present address: Suzhou Institute of Systems Medicine, Suzhou, Jiangsu 215123, China.

Corresponding author: Lluis Fajas, University of Lausanne, Center for Integrative Genomics, Quartier UNIL-Sorge, Bat. Genopode, CH-1015 Lausanne, Switzerland. Phone: +41.21.692.4111; E-mail: Lluis.Fajas@unil.ch.

Summary

CDK4 has been at the centerstage of cancer research for years. However, its role on cancer metabolism, especially in the mTOR signaling pathway, is as yet undefined. For the first time, in this study we connect CDK4 with lysosomes, the emerging metabolic organelles, crucial for mTORC1 activation. On one hand, we show that CDK4 phosphorylates the tumor suppressor FLCN, which regulates mTORC1 recruitment to the lysosomal surface in response to amino acids. On the other hand, we unravel that CDK4 has a direct role in lysosomal function and is essential for lysosomal degradation, ultimately regulating mTORC1 activity. We show here that chemical inhibition or genetic inactivation of CDK4, other than retaining FLCN at the lysosomal surface, lead to the accumulation of undigested material inside lysosomes, impairing the autophagic flux and inducing cancer cell senescence in vitro and xenograft models. Importantly, the use of CDK4 inhibitors in therapy results in cancer cell senescence but not in cell death. To overcome this resistance, and based on our findings, we increased the autophagic flux in cancer cells by using an AMPK activator in combination with a CDK4 inhibitor. We prove that the cotreatment induces autophagy (AMPK), and impairs lysosomal function (CDK4), finally resulting in cell death and tumor regression. Altogether we uncovered a previously unknown role for CDK4 in lysosomal biology and propose a novel therapeutic strategy to kill cancer cells.

Introduction

Cyclin-dependent kinase 4 (CDK4) has a well-established major role in cell cycle control (Malumbres and Barbacid, 2009) and CDK4-cyclin complexes are commonly deregulated in tumorigenesis (Deshpande et al., 2005). These complexes are of great interest as therapeutic targets, especially since the FDA has approved the specific CDK4/6 kinase inhibitors PD0332991 (palbociclib), LEE011 (ribociclib) and LY2835219 (abemaciclib) for treating advanced or metastatic hormone receptor (HR)-positive and HER2-negative breast cancer. Clinical studies using CDK4/6 inhibitors to treat other malignancies are being conducted (O'Leary et al., 2016).

Research from our group and others has shown that the role of CDK4 is not limited to the control of the cell cycle. Indeed CDK4 is also a major regulator of energy homeostasis (Aguilar and Fajas, 2010; Lee et al., 2014; Salazar-Roa and Malumbres, 2017) through E2F1-RB complex (Blanchet et al., 2011), AMP-activated protein kinase (AMPK) (Lopez-Mejia et al.,

2017) and insulin receptor substrate 2 (IRS2) (Lagarrigue et al., 2016). Importantly, the CDK4 pathway has been shown to cross-talk with the mechanistic target of Rapamycin (mTOR) pathway, which is a major regulator of cell growth and metabolism (Albert and Hall, 2015; Saxton and Sabatini, 2017). CDK4/6 inhibition attenuates mTOR Complex 1 (mTORC1) activity in some cancer models (Goel et al., 2016; Olmez et al., 2017), yet the effects of CDK4/6 inhibitors on mTORC1 seem to be cell-type specific, since opposite results were found in pancreatic ductal adenocarcinoma (Franco et al., 2016). Given that mTOR activity is amplified in numerous cancer types and participates in the translational regulation of several oncogenic proteins, mTOR inactivation is an attractive strategy for cancer treatment (Wang and Sun, 2009). The exact mechanism underlying the CDK4-mTOR cross-talk in mammals is unknown, although in Drosophila it occurs via the phosphorylation of TSC2 (Romero-Pozuelo et al., 2017).

Lysosomes, considered for years as only the digestive system of the cell, have since become key effectors in metabolism, due to their role as platforms in the activation of mTOR pathway (Bar-Peled and Sabatini, 2014; Dibble and Cantley, 2015; Puertollano, 2014). mTORC1 is recruited to the surface of lysosomes in a complex procedure sensitive to amino-acids (Bar-Peled and Sabatini, 2014). Among the multiple regulators of this process, we focused on FLCN, a tumor suppressor which functions as a complex with its partner FNIP. FLCN-FNIP complex interacts with the Rag GTPases in the absence of amino acids repressing their activity, and when amino acids are sensed, FLCN-FNIP complex dissociate from Rag GTPases eliciting their activation. Rag GTPases activation is crucial for mTORC1 recruitment to lysosomes (Petit et al., 2013). Importantly, mTORC1 activation is also triggered by the accumulation of amino acids in the lysosomal lumen (Zoncu et al., 2011). Therefore, alterations in lysosomal function directly impact mTORC1 activity (Jia et al., 2018; Li et al., 2013). For this reason, and because these organelles also play a role in cell survival and cell proliferation, lysosomes have become emerging targets for cancer therapy (Fehrenbacher and Jaattela, 2005; Martinez-Carreres et al., 2017; Piao and Amaravadi, 2016).

In this study we reveal that CDK4 is capable of modulating mTORC1 activity in a direct manner, through the phosphorylation of FLCN, and in an indirect manner, by promoting lysosomal function. Indeed, CDK4 chemical inhibition or genetic inactivation prevent mTORC1 recruitment to lysosomal surface, not only due to the lack of FLCN phosphorylation, but also because of the accumulation of undigested material inside the lysosomes. This lack of

lysosomal function, in turn, induces senescence in triple-negative breast cancer (TNBC) cells, as well as in a mouse xenograft model. CDK4 inhibition as single treatment reduces notably tumor size since cells enter to senescent programs. Moreover, a combination between AMPK activation and CDK4 inhibition was used in an attempt to trigger autophagy in conditions when lysosomes are dysfunctional, and results in cell death and tumor regression. This finding is of a high relevance in TNBC, a highly invasive and aggressive cancer type that does not have a clear therapeutic strategy yet (Elsamany and Abdullah, 2014).

Results

CDK4 activity is required for mTORC1 localization at lysosomes

It was previously demonstrated that CDK4/6 inhibition results in the deregulation of mTORC1 in certain models of human cancer, suggesting a cross-talk between the two pathways (Franco et al., 2016; Goel et al., 2016; Olmez et al., 2017). To determine the cell-type specificity of this cross-talk, eight human cancer cell lines were stimulated with IGF-1 to induce mTORC1 activation in the presence or absence of the CDK4/6 inhibitor LY2835219 (abemaciclib). The efficiency of CDK4/6 inhibition was measured by RB-Ser^{780} phosphorylation. Treatment with LY2835219 caused a decrease in p70S6K and 4E-BP1 phosphorylation (two well-known targets of mTORC1 used as a readout of its activity), both in the unstimulated and in the IGF-1 stimulated conditions (Sup. Figure 1A). mTORC1 activity showed the highest sensitivity to CDK4/6 inhibition in CCRF-CEM, MDA-MB-231 and HT29 cells, whereas IB115, MCF7 and PC3 were the least responsive. It is worth noting that, despite showing considerable mTORC1 inhibition, some cell lines showed only a mild decrease in AKT phosphorylation in the presence of LY2835219 (HCT116, IB115, MDA-MB-231, SKOV3, PC3), suggesting that the effects observed in mTORC1 activity were at least partially independent of decreased AKT signaling.

We decided to focus our experiments on the triple negative breast cancer (TNBC) cell line MDA-MB-231 because it was one of the most responsive to CDK4/6 inhibition and due to the lack of a clearly defined treatment strategy for this cancer type. We first investigated whether CDK4 inhibition or depletion affects the translocation of mTORC1 to the lysosomal surface, a key step for mTORC1 activation. We found that MDA-MB-231 wild-type (WT) cells treated with the CDK4/6 inhibitor LY2835219 or CDK4 knock-out (KO) MDA-MB-231 cells showed impaired translocation of mTORC1 to lysosomes in response to amino acids (Figure

1A–B) and decreased mTORC1 activity, as measured by the phosphorylation of 4E-BP1 and p70S6K (Figure 1C-D). Inhibition of glutaminolysis has been shown to prevent lysosomal recruitment and subsequent activation of mTORC1 (Duran et al., 2012). To check whether mTORC1 translocation was affected due to an impairment in glutamine metabolism, we treated MDA-MB-231 cells with a cell-permeable α-ketoglutarate analog. We found that α-ketoglutarate stimulation could not rescue the defective translocation of mTORC1 to the lysosomal surface upon CDK4 inhibition or depletion (Sup. Fig 2 A-B), indicating that CDK4 inhibition or depletion does not affect mTORC1 translocation to the lysosomal surface by impairing glutamine metabolism.

Interestingly, MDA-MB-231 cells lacking E2F1 showed normal mTORC1 translocation to the lysosomal surface and increased mTORC1 activation (Sup. Fig 2 C-D-E–F) but were still sensitive to CDK4 inhibition. This suggests that the effects of CDK4 on mTORC1 activity are independent of E2F1 transcriptional activity, pointing to other cell cycle-independent targets of CDK4.

CDK4 regulates mTORC1 activity through phosphorylating FLCN

Given the kinase properties of CDK4, we hypothesize that CDK4 potentially regulates mTORC1 pathway through phosphorylation of one of its regulators. To test our hypothesis, first, we performed a bioinformatics search of the proteins of mTORC1 pathway containing the putative phosphorylation site for CDK4: [ST]Px[KRP]. Due to the tight relationship of FLCN with lysosomes and nutrient sensing, we decided to focus on this protein. We performed *in vitro* kinase assays with CDK4/CycD3 recombinant protein and gluthatione S-transferase (GST) fusion of full length FLCN. The Mass Spectrometry analysis of post-translational modifications revealed that FLCN could be phosphorylated by recombinant CDK4/CycD3 at different sites, being S62, S73, T227 and S571 the ones with higher score (Figure 2A). Importantly, S62, S73 and S571 phosphorylation sites were found when we overexpressed and immunoprecipitated FLCN in MDA-MB-231 cells upon amino acid and IGF-1 stimulation (Figure 2B).

We, then, monitored the localization of overexpressed FLCN by immunofluorescence under amino acid depletion or stimulation in wild type MDA-MB-231 cells untreated or treated with LY2835219, and in CDK4 KO MDA-MB-231 cells. In the absence of amino acids, FLCN is localized at the surface of lysosomes, preventing mTORC1 recruitment to lysosomal surface. When amino acids are sensed, FLCN translocates to the cytoplasm, allowing the

RagGTPases to recruit mTORC1. Importantly, we found that FLCN is retained at the lysosomes in the presence of amino acids upon CDK4 inhibition or depletion (Figure 2C). Therefore, our results suggests that CDK4 phosphorylations on FLCN are necessary for mTORC1 activation.

CDK4 inhibition or depletion increases lysosomal mass

Lysosomal biogenesis is a biological process coordinated by transcription factor EB (TFEB), which is repressed by mTORC1. Under nutrient-rich conditions, TFEB is phosphorylated by mTORC1, causing its retention in the cytoplasm. By contrast, when mTORC1 is inactivated, unphosphorylated TFEB translocates to the nucleus and promotes the transcription of genes encoding numerous lysosomal and autophagic proteins (Puertollano, 2014). To test whether CDK4 inhibition or depletion affected TFEB transcription and the resulting upregulation of lysosomal biogenesis genes, we treated WT and CDK4 KO MDA-MB-231 cells with complete or serum-starvation media, with or without the CDK4/6 inhibitor LY2835219, and studied the expression of TFEB target genes. As expected, under starvation conditions, WT MDA-MB-231 cells showed an increase in the expression of genes regulated by TFEB (Figure 3A; cathepsins B and D and SQSTM1). Moreover, we found that CDK4/6 inhibition synergized with starvation to further increase the expression of those genes. CDK4 KO cells also presented increased expression of those genes under basal conditions, but no further increase was found upon CDK4/6 inhibition (Figure 3A).

We next used LysoTracker staining and flow cytometry to look at the percentage of lysosome-positive cells upon CDK4 inhibition or depletion. The percentage of LysoTracker positive cells and the size of the LysoTracker positive particles were consistently and markedly increased in the absence of CDK4 activity (Figure 3B-C-D). Similarly, when we quantified the size of lysosomal-associated membrane protein 1 (LAMP1)-positive particles, we found a significant increase in lysosomal density in CDK4 KO cells compared to WT MDA-MB-231 cells (Figure 3E-F). These results suggested a new function of CDK4 in the control of lysosomal biology.

CDK4 is required for lysosomal function

It is well known that the inhibition of mTORC1 results in the induction of autophagy, a conserved catabolic process that triggers the degradation of intracellular constituents and organelles in the lysosome (Kaur and Debnath, 2015). To investigate the effects of CDK4

inhibition on autophagy, we treated MDA-MB-231 cells for 24h with LY2835219. Also we used the mTOR inhibitor rapamycin and serum-starvation (-FBS) media as autophagy inducers. Then, we measured the amounts of the autophagosome marker LC3-II and the degradation marker SQSTM1. As expected, serum-starvation conditions, as well as mTOR inhibition by rapamycin, increased the amounts of the autophagosome marker LC3-II (Figure 4A-B, long exposure). CDK4/6 inhibition also increased LC3-II levels to the same extent (Figure 4A-B). Moreover, CDK4 KO cells showed increased levels of LC3-II in basal conditions and were more sensitive to starvation-mediated autophagic stimuli (Figure 4A-B). The observed increase of LC3-II levels suggested that there is either an increase of autophagosome biogenesis or an impairment of the autophagic flux. Indeed, these effects could be secondary to mTOR inactivation, since the decreased mTORC1 activity caused by CDK4 inhibition or depletion shown in Figure 1 could ultimately induce lysosomal biogenesis.

To further study the autophagic flux, we treated cells as described above (Figure 4A-B), including the addition of bafilomycin A1 (BafA1), a potent V-ATPase inhibitor that blocks autophagosome-lysosome fusion. In WT cells, under starvation conditions and in the presence of rapamycin treatment, BafA1 further increased LC3-II levels, indicating that rapamycin induces autophagosome biogenesis. In contrast, in CDK4 KO cells or cells treated with CDK4 inhibitor, BafA1 failed to cause any additional increase in LC3-II levels (Figure 4A-C). These results suggested that CDK4 does not directly participate in autophagosome biogenesis. On the other hand, no abnormal SQSTM1 accumulation was observed after CDK4 inhibition or depletion, despite observing a consistent SQSTM1 increase with BafA1 (Figure 4A). SQSTM1 protein levels are often negatively correlated with autophagic degradation. However, it has been already observed that the expression of SQSTM1 does not always inversely correlate with autophagic activity, given that they can be restored during prolonged starvation (Sahani et al., 2014).

Given that CDK4 inhibition or depletion result in an increase in lysosomal and autophagosomal markers, we next used transmission electron microscopy (TEM) to analyze the ultrastructure of these organelles in WT and CDK4 KO MDA-MB-231 cells incubated with serum-starvation media to trigger autophagy. As expected, serum-starvation medium induced autophagosome and lysosome formation in MDA-MB-231 WT cells. Interestingly, CDK4 KO MDA-MB-231 cells displayed higher densities of autophagosomes and lysosomes than WT cells, in agreement with our previous results. Moreover, TEM analysis revealed that the

lysosomes in CDK4 KO cells were full of electron-dense material, indicating that they accumulated undigested material inside the lysosomes under both complete and serum-free conditions (Figure 5A-B-C-D, Sup. Figure 3A). LY2835219 treated WT cells yielded the same results as CDK4 KO cells (Figure 5E-F-G-H, Sup. Figure 3B). To further investigate these observations, we measured intracellular lysosomal activity and cathepsin B activity and found that both were decreased in CDK4 KO cells (Figure 5I-J).

Overall, these results suggest that CDK4 is fundamental for the activity of lysosomes and that its absence impairs autophagic flux at the lysosomal degradation step.

Dysfunctional lysosomes, but not mTORC1 inhibition, induce senescence

The above results suggest that CDK4 has a direct impact on lysosomal function and that CDK4 depletion or inhibition leads to the accumulation of enlarged and non-functional lysosomes that impair autophagic flux. Lysosomal processes are associated with aging and longevity (Carmona-Gutierrez et al., 2016), and the increase of lysosomal content is characteristic of senescence progression (Cho and Hwang, 2012). This led us to investigate the fate of cells lacking CDK4 activity. We therefore measured levels of proliferation, apoptosis and senescence in cells after treatment with CDK4/6 inhibitor. Analysis of Ki-67 levels showed that CDK4/6 inhibition significantly decreased the proliferation rate of cells in complete medium (Figure 6A). Yet, when the cells were serum-starved, no differences were observed in response to CDK4/6 inhibition (Figure 6A). Apoptosis, measured by Annexin V staining, was not significantly induced when cells were treated with the CDK4/6 inhibitor in complete medium (Figure 6B). A slight increase of apoptosis was seen when CDK4/6 inhibition was combined with serum starvation, but the overall percentage of apoptotic cells was relatively low (Figure 6B). Interestingly, when WT and CDK4 KO cells were incubated for eight days with LY2835219 in complete medium, we observed increased senescence, as measured by senescence-associated beta-galactosidase (SA-βGal) staining. Moreover, CDK4 KO cells in complete medium showed abundant SA-βGal staining under basal conditions, an indication of increased senescence (Figure 6C-D). When the same experiment was conducted in serum starvation conditions, senescence was induced in WT cells but was not further increased in CDK4 KO cells. To test whether these effects were dependent on mTORC1, we also treated cells with rapamycin. Levels of SA-βGal staining in the rapamycin treated cells were similar to

those of untreated cells, indicating that the induction of senescence in the absence of CDK4 was not due to mTORC1 inhibition (Figure 6C-E).

To further characterize the senescent phenotype in cells lacking CDK4 activity, we additionally measured the expression of senescence markers in MDA-MB-231 WT cells cultured in complete medium after an eight-days treatment with DMSO, LY2835219 or rapamycin (Figure 6F). Consistently with the SA-βGal data, LY2835219 treatment induced the expression of most of the senescence-related genes evaluated (Figure 6F). Some of the genes that did not respond to CDK4/6 inhibition are p53-regulated genes, reinforcing the idea of a cell cycle-independent induction of senescence. It is worth noting that MDA-MB-231 cells lack CDKN2A, a p53 target gene that is known to promote cellular senescence. Additionally, similar to SA-βGal data in Figure 6C-E, mTOR inhibition by rapamycin failed to induce the expression of genes related to senescence. Only RKHD3 and IGFBP5 were induced by rapamycin, but always to a minor extent than with LY2835219 treatment (Figure 6F).

Our results suggest that the lysosomal dysfunction induced by CDK4 inhibition or depletion is the cause of the senescent phenotype in these cells, and that mTORC1 inhibition is a secondary effect of the impairment of lysosomal function. In fact, SA-βGal derives from a lysosomal enzyme, and the increase of this parameter in senescent cells is likely due to an expansion of the lysosomal compartment (reviewed in Kuilman et al 2010).

The CDK4 inhibitor LY2835219 alters lysosomal function, attenuates mTORC1 activity, and decreases tumor growth in a breast cancer xenograft mouse model

To investigate the effects of CDK4/6 inhibition on lysosomal function *in vivo*, we used a breast cancer xenograft model created by injecting MDA-MB-231 cells into the mammary glands of NSG mice. Intratumoral inhibition of RB phosphorylation in mice treated eight days with LY2835219 compared with vehicle confirmed that CDK4/6 was effectively inhibited in the tumor (Figure 7A-B). Consistent with the previously observed anticancer activity of CDK4 inhibition (Hamilton and Infante, 2016), we observed that the tumors from LY2835219-treated group halted their growth (Figure 7C) and reduced cell proliferation (Figure 7D-E) whereas the untreated ones continued growing and highly proliferating. Of note, the observed effects of CDK4/6 inhibition in tumor size are independent of the immune system in our model because NSG mice are immunodeficient. This was confirmed by the lack of immune cell infiltration in the H-E staining of the tumors in any of the groups (Sup. Figure 4A).

Consistent with our *in vitro* data, xenograft tumors treated with LY2835219 had increased expression levels of the lysosomal marker LAMP1 (Figure 7F-G) and increased expression levels of TFEB target genes (Sup. Figure 4B). In addition, LY2835219 treatment also decreased the activity of mTORC1, assessed by the phosphorylation of p70S6K Thr^{389} (Figure 7H-I). Ultrastructural analysis by TEM confirmed that tumors from LY2835219 treated mice had higher densities of autophagosomes and lysosomes, and that those lysosomes accumulated non-digested material (Figure 7J-K-L-M, Sup. Figure 4C). Furthermore, we show that the tumors of mice treated with LY2835219, which harbored non-functional lysosomes, had increased SA-βGal staining (Figure 7N) and increased expression of senescence markers (Sup. Figure 4D), revealing that the tumor cells had become senescent, in agreement with our *in vitro* data. Together, these results further demonstrate that CDK4 plays an essential role in the regulation of lysosomal function in vivo, and that this alteration in lysosomal function leads to tumor cell senescence in a mouse model of breast cancer.

The CDK4 inhibitor LY2835219 in combination with the AMPK activator A769662 induces cell death in breast cancer cells and tumors.

Given that lysosomes are essential for autophagy, we set to determine the consequences of the activation of autophagy in conditions when lysosomes were dysfunctional. Thus, we tested the combination of LY2835219, to impair lysosomal function, with the AMPK activator A769662, to induce autophagy. Breast cancer xenografts of NSG mice co-treated for eight days with A769662 and LY2835219 showed smaller tumor size than the ones treated only with LY2835219, whereas tumors from mice treated only with A769662 were similar in size than the untreated ones (DMSO group) (Figure 8A-B). Strikingly, the combination treatment resulted in tumor regression; almost 50% of the tumors decreased their size upon the co-treatment using both A769662 and LY2835219. In contrast, no reduction in tumor size was observed when individual drugs were used (Figure 8C-D). Cell proliferation in tumors, assessed by Ki67 staining, significantly decreased with LY2835219 treatment. However, comparing this group with de co-treated group, there was only a light tendency for the percentage of Ki67 positive cells to further decrease in the co-treated group (Figure 8E-F). Moreover, cleaved-Caspase-3 staining revealed a significant induction of intratumoral cell death when mice were co-treated with A769662 and LY2835219, which was at least six-fold higher than the apoptosis rate in mice treated with LY2835219 as a single

agent (Figure 8E-G). This result suggested that increased apoptosis was underlying the decrease in tumor size in the co-treatment group.

In vitro studies with MDA-MB-231 cell line in culture were consistent with the *in vivo* data; CDK4 inhibition and AMPK activation as single treatments failed to induce cell death after one week treatment as shown by the low levels of Annexin V-positive cells (Sup. Figure 5A). Only the combination of LY2835219 with A769662 increased notably the percentage of Annexin V-positive cells (Sup. Figure 5A).

As previously reported, CDK4 inhibition resulted in the intratumoral decrease of RB phosphorylation, but no differences were observed between LY2835219 and the co-treated tumors (Figure 8H-I). As for mTORC1 activity, LY2835219 treatment as well as AMPK activation decreased p70S6K phosphorylation (Figure 8H-J). However, mTORC1 inactivation by A769662 treatment was not sufficient to decrease tumor size in our model. Importantly, and consistent with other studies (Lopez-Mejia et al., 2017), CDK4 inhibition was able to trigger AMPK activation, as observed with the increased phosphorylation of Acetyl-CoA Carboxylase (ACC), a known target of AMPK (Figure 8H-K).

TEM analysis of the tumors revealed that the percentage of the autophagosome and lysosome area per cell was increased in the single treatments, as well as in the A769662 and LY2835219 co-treated group (Sup. Figure 5B-C-D). When we quantified the percentage of autolysosomes with digested material, we found that the mice co-treated with both A769662 and LY2835219 still display a significant decrease in this parameter, despite LY2835219 as a single treatment showed a greater decrease (Sup. Figure 5B-E). The underlying mechanism of this apparent paradox could be that A769662 induced cell death only in cells in which LY2835219 treatment impaired lysosomal function. Indeed, some of the co-treated cells displayed mixed morphological features of apoptotic cell death (highly condensed chromatin, shrinkage of the cytoplasm) and autophagic cell death (numerous autophagosomes and autolysosomes, focal swelling of the perinuclear membrane (Sup. Figure 5B (indicated by *)).

Taken together, these results showed that the combination treatment using A769662 and LY2835219 provided a better outcome than LY2835219 alone, inducing cell death and tumor regression in the MDA-MB-231 breast cancer xenograft model.

Discussion

We show here for the first time that CDK4 regulates lysosomal function and mTORC1 activity in cancer cells. We demonstrate that CDK4, through phosphorylation of FLCN in specific residues, facilitates the migration of mTOR to the lysosomes in order to be activated. The abrogation of mTOR activation by depletion or chemical inhibition of CDK4 consequently resulted in a substantial increase in the numbers of lysosomes and autophagosomes. This proves that CDK4 is necessary for the dissociation of FLCN from the lysosomes, and for the subsequent recruitment and activation of mTORC1.

However, this increase was not correlated with greater lysosomal activity, which suggested that CDK4 has an mTOR-independent role in this process. Importantly, we prove that CDK4 inhibition or depletion leads to the accumulation of intra-lysosomal undigested material, which, through recycling of amino acids, might serve as a signal to mTORC1. mTORC1 activation is initiated at the lysosome and requires the presence of amino acids, products of macromolecule degradation, in the cytosol, but also in the lysosomal lumen (Zoncu et al., 2011). We show now that an additional mechanism by which CDK4 favors mTORC1 activation by promoting the digestion of proteins in the lysosome, in turn providing metabolic intermediates that sustain cell growth and survival via downstream effectors. This pathway would be particularly crucial during prolonged starvation conditions, such as the typical environment of some tumors.

Cells initially respond to nutrient deprivation by inactivating their energy-consuming processes, such as protein or lipid biosynthesis, and by activating catabolism. At the same time, other mechanisms are activated to recycle molecules to provide the cell with enough substrates and metabolic intermediates to survive – an important function of autophagy. In the long term, autophagy reactivates the mTORC1 pathway by replenishing the lysosomes with digested proteins and amino acids (Tan et al., 2017). CDK4 inhibition or depletion could therefore mimic a starvation signal. This hypothesis is in agreement with previous studies showing that CDK4/6 inhibitors induce autophagy (Bourdeau and Ferbeyre, 2016; Iriyama et al., 2018). We also observed an increase in the number of autophagosomes upon CDK4 inhibition in this study. However, when analyzing the ultimate fate of the autophagosomes, we found that they accumulate due to the impairment of lysosomal degradation upon CDK4 inhibition or depletion. Indeed, others have demonstrated that the inhibition of lysosomal activity causes decreased fusion with autophagosomes and vice-versa (Renna et al., 2011; Seranova et al., 2017; Settembre and Ballabio, 2014). In this study, we showed that inhibiting

or depleting CDK4, in addition to inducing autophagy, likely through mTORC1 inactivation, impairs the autophagic flux at the lysosomal degradation step. This observation may explain the increased susceptibility of CDK4 KO cells to autophagic stimuli.

We also found that CDK4 inhibition or depletion increased the expression of many lysosomal genes. It is well known that mTORC1 negatively regulates lysosomal biogenesis (Zhou et al., 2013). This could be secondary to mTORC1 inhibition, or due to a compensatory mechanism to create new lysosomes as the existing ones are dysfunctional and ensure their function.

CDK4/6 inhibitors have been shown to accumulate into lysosomes, a phenomenon called lysosomal trapping (Llanos et al., 2019). However, the use of CDK4 KO cells in our work demonstrates that CDK4 rather stimulates lysosomal function, and that the lysosomal trapping of the drug is secondary to the lysosomal impairment induced by CDK4 inhibition. In addition, CDK4/6 inhibition has been found to result in proteasomal activation (Miettinen et al., 2018). Moreover, a negative-feedback exist between proteasomal activity and autophagic flux (Lee et al., 2019). Thus, the impairment of autophagic flux at the lysosomal degradation step can result in proteasomal activation and viceversa.

Despite the known requirement for lysosomes in cell cycle progression (Hubbi et al., 2014; Jin and Weisman, 2015), little is known about the relationship between lysosomes and senescence. Importantly, in eukaryotes, autophagy impairment via lysosomal dysfunction has been described to be an important characteristic of oxidative stress-induced senescence (Tai et al., 2017). Our findings suggest that the ultimate fate of cells that lack CDK4 is the activation of senescence due to lysosomal dysfunction. The absence of senescence when cells are treated with rapamycin further demonstrates that mTORC1 inactivation is a consequence of lysosomal impairment due to CDK4 inhibition or depletion. However, the CDK4 inhibitor induced lysosomal dysfunction, was not sufficient to induce cell death in the tumors of the treated mice. Instead, cancer cells were arrested, but were still alive, which explained that the tumor burden was not decreased, but only stabilized (Figure 7). We reasoned that further forcing the autophagic flux would create an additional stress that could kill these tumor cells. With this aim, we used the AMPK activator A769662, which is known to increase autophagy, in combination with the CDK4 inhibitor. Indeed, co-treatment of the cells resulted in increased cancer cell death and therefore tumor regression (Figure 8). This is a major finding that represents a paradigm switch regarding the use of CDK4 inhibitors for the treatment of cancer.

Strikingly, and consistent with our findings, CDK4 inhibitors are not efficient as a single drug in the clinical practice and are often used in combination with other drugs (Klein et al., 2018b; Ku et al., 2016; Michaloglou et al., 2018).

We show here that the effects of CDK4 in MDA-MB-231 cells are independent of E2F1, the transcription factor modulated by CDK4 during the cell cycle. It has been reported, however, that E2F1 regulates lysosomal positioning and activates mTORC1 by promoting its recruitment to the lysosomal surface (Meo-Evoli et al., 2015; Real et al., 2011). This suggests a dual and complementary role for CDK4 in the regulation of the mTORC1 pathway: first, through regulation of the lysosomal function; and second, through FLCN phosphorylation .

It was previously described that CDK4/6 inhibitors display anti-tumor activity only in RB-positive cells (Polk et al., 2016). In addition, it was unclear whether CDK4/6 inhibition had an effect on TNBCs. Our findings are consistent with other studies showing that CDK4/6 inhibitors still have some effects on RB-negative cells (Rivadeneira et al., 2010), and that CDK4/6 inhibitors do have anti-tumor effects in TNBCs. Indeed, depending on the cell type, CDK4/6 inhibition triggers either a quiescence or senescence response, not necessarily via the canonical RB-E2F pathway (reviewed in (Klein et al., 2018a); (Brown et al., 2012)).

Overall, the present study demonstrates a new role for CDK4 in the regulation of lysosomal function, which ultimately leads to senescence in cancer cells and mTORC1 inactivation. , In addition, we highlight the importance of lysosomes in cancer and we propose that CDK4/6 inhibitors could be used in combination with other drugs to target lysosomal function as a novel anticancer strategy.

Materials and Methods

Materials

LY2835219 (abemaciclib), a specific CDK4/6 inhibitor, was purchased from MedChem Express and used at a concentration of 0.5 µM for cancer cell lines. R[3] human IGF-1 (I11146, Sigma) was used at a concentration of 30 ng/ml. Minimal Essential Media (MEM) Amino Acids Solution (50X, ThermoFisher) was used at the indicated concentrations. Rapamycin was kindly provided by Professor Pedro Romero (Université de Lausanne, Switzerland) and was used at the indicated concentrations. Bafilomycin A1 (BafA1) was purchased from Enzo Life Sciences (ALX-380-030-M001) and used at a concentration of 0.3 µM.

Cell culture and transfection

The cancer cell lines MDA-MB-231, CCRF-CEM, HTC116, IB115, HT29, SKOV, MCF7 and PC3 were cultured in RPMI 1640 (1×) + GlutaMAX media (Life Technologies, USA) containing 10% fetal bovine serum (FBS) (PAA Laboratories), 1% HEPES (Life Technologies) and 1% sodium pyruvate (Sigma).

MDA-MB-231 CDK4 knockout (KO) and E2F1 KO stable cell lines were generated with CRISPR/cas9 technology. The lentiCRISPR v2 plasmid was a gift from Feng Zhang (Cambridge University, Cambridge, England; Addgene plasmid # 52961); a description of this plasmid can be found in Shalem et al. 2014 (Shalem et al., 2014). The pMD2.G and psPAX2 plasmids were gifts from Didier Trono (Université de Lausanne; Addgene plasmids # 12259 and # 12260, respectively). The target sequences for the guide RNA were as follows:

CDK4	5'-CACCGCTTGCCAGCCGAAACGATCA-3'
	5'-AAACTGATCGTTTCGGCTGGCAAGC-3'
E2F1	5'-CACCGTCTGACCACCAAGCGCTTCC-3'
	5'-AACGGAAGCGCTTGGTGGTCAGAC-3'

The oligonucleotides were synthesized and cloned into the digested LentiCrispR vector as described by Shalem et al., 2014. Lentiviral production was based on the standard protocol established by Salmon and Trono, 2006 (Salmon and Trono, 2006). The resulting lentivirus (2ml) was then used to infect MDA-MB-231 cells for 72 hours. Infected cells were treated with 5 μg/ml puromycin for five consecutive days. Western blotting was performed to ensure that the protein of interest was not expressed.

For pRK5-FLAG-FLCN (Addgene #72290) transfection, cells were grown in 10cm diameter dishes. 10μg of plasmid were transfected with X-treme gene HP in a ratio 1:2 (μg DNA: μl reagent) in Optimem media. The following day the media was changed to the normal growing media, and cells were grown for 48h.

Cell treatments

For insulin pathway stimulation, the different tumor cell lines were first treated with a CDK4/6 inhibitor (or the same volume of DMSO as a control) diluted in FBS-free media for 15 h. The cells were subsequently treated with IGF-1 for 20 min before lysis or fixation.

For amino acid stimulation, after a 15 h treatment with FBS-free media with or without the CDK4/6 inhibitor, the cells were incubated for two hours in KRBB media containing 111 mM NaCl, 25 mM NaHCO$_3$, 5 mM KCl, 2.5 mM CaCl$_2$, 1 mM MgCl$_2$, 25 mM HEPES, 25 mM glucose and dialyzed FBS with or without the CDK4/6 inhibitor. For the last 20 min, 2× MEM amino acids solution and 2 mM glutamine were added to the cells.

Western blotting

Cell lysates were obtained with M-PER mammalian extraction buffer (Thermo Scientific) containing 1:100 Halt phosphatase inhibitor cocktail (Thermo Scientific) and 1:100 Halt EDTA-free protease inhibitor cocktail (Thermo Scientific). Lysate proteins were separated by SDS-PAGE and transferred onto nitrocellulose membranes. The membranes were incubated overnight at 4°C with the corresponding primary antibodies and then incubated with the corresponding secondary antibodies and developed with ECL. The band intensities on the developed films, fusion FX images and ChemiDoc images were quantified using the Fiji image-processing package (Schindelin et al., 2012). The following antibodies were used for Western blot analysis: anti-CDK4 (clone H22), anti-CDK6 (clone C21) and anti-RB (C15) from Santa Cruz Biotechnology; anti-phospho Rb-S780 (clone D59B7), anti-phospho P70S6K-T389 (clone 108D2), anti-4E-BP1 (clone 53H11), anti-phospho AKT-T308 (clone 244F9), anti-phospho AKT- S472/3 (clone D9E), anti-p70S6 kinase (49D7), anti-LC3B (polyclonal), anti-SQSTM1 (polyclonal), anti AcetylCoA Carboxylase (p-ACC) (polyclonal) and anti phospho AcetylCoA Carboxylase (p-ACC) from Cell Signaling Technology; and anti-alpha-tubulin (clone DM1A) from Sigma-Aldrich. The bands were quantified with FIJI software (Schindelin et al., 2012).

Immunofluorescence

For in vitro immunofluorescence, cells were grown on glass coverslips. After the different treatments or stimulation, the slides were rinsed with PBS once and fixed for 15 min with 4% paraformaldehyde in PBS at room temperature (RT). The slides were rinsed twice with PBS, permeabilized with 0.01% saponin for 10 min and blocked with PBS containing 2% BSA

and 0.05% Tween 20 for 30-60 min, then, incubated with the primary antibodies for 2-3 h at RT. After 3 washes with PBS, they were incubated with 1:1000 anti-mouse Alexa 488 and anti-rabbit Alexa 561 secondary antibodies for 45 min. Finally, they were washed twice with PBS for 10 minutes, and the nuclei were stained with Hoechst (1:10000 in PBS). The coverslips were mounted with Fluoromont mounting media on the glass slides. Images were obtained with a Zeiss LSM710 inverted confocal microscope with a 63× objective. The following antibodies were used for immunofluorescence experiments: anti-mTOR (7C10), anti-FLCN (clone D14G9) and anti-Lamp1 (clone D401S) from Cell Signaling Technology (USA) and anti-CDK4 (clone EPR4513) from Abcam. Images were processed with Fiji software (Schindelin et al., 2012). Colocalization was analyzed with JACoP (Just Another Colocalization Plugin) for ImageJ, and the volume of LAMP1 positive particles was analyzed with Imaris 9.0.0.

For fluorescence immunohistochemistry in tissue sections, mouse xenograft tumors were dissected, fixed in 4% paraformaldehyde and embedded in paraffin. Next, 4-μm sections were deparaffined with xylene and rehydrated in a graded ethanol series. Antigen retrieval was performed by heating the sections in the microwave at 750 W for 10 minutes in citrate buffer (0.01 M, pH 6). After cooling, the sections were washed with PBS, and blocked for 1 hour with NGS 2.5%. Primary anti-LAMP1, Ki67 and Cleaved-Caspase-3 antibodies were incubated overnight at 4°C. The following day, the sections were incubated with the corresponding Alexa 488 or 568 secondary antibody and counterstained with DAPI. The sections were mounted and observed with a 20X objective and a fluorescence microscope. Images were processed and analyzed with Fiji software (Schindelin et al., 2012).

Immunoprecipitation

48 h after pRK5-FLAG-FLCN transfection, cells were lysated as described above with M-PER buffer. With 1 mg of total protein, FLAG was over night immunoprecipitated using FLAG-M2 affinity gel. After some washes with buffer, the samples were analyzed by western blotting.

GST production

pDON-FLCN and pDON-RB were cloned in pDEST pGEX-2T and expressed in BL21 bacteria. The GST-purified proteins were resuspended in 50mM Tris.HCl (pH 8), 100 mM NaCl, 5 mM DTT and 20% glycerol buffer.

In vitro kinase assay

Kinase assays were performed using GST-FLCN and recombinant RB protein (Santa Cruz) as a substrate in kinase buffer (25 mM Tris.HCl (pH 7.5), 150 mM NaCl, 10 mM MgCl$_2$, 1 mM DTT, 5 mM Na$_4$P$_2$O$_7$, 50 mM NaF, 1 mM vanadate and protease inhibitor cocktail) with 40 μM ATP (PAMGENE ATP- Perkin Elmer) for 30 min at 30°C. RecombinantCDK4/cyclin D3 kinase (ProQinase) were used. RB was used as positive control. Boiling the samples for 5 min in the presence of denaturing sample buffer stopped the reaction. As an experimental control, westernblot with RB samples was done with phospho-RB antibody. FLCN samples were analyzed by mass spectrometry.

Mass spectrometry

Protein samples were loaded on a 10% mini polyacrylamide gel, and after Coomassie staining visible band between 75 and 100 kDa corresponding to FLCN-GST or FLCN-FLAG construct was excised and digested with sequencing-grade trypsin (Promega) as described (Shevchenko et al., 2006). Extracted tryptic peptides were dried and resuspended in 0.05% trifluoroacetic acid, 2% (v/v) acetonitrile, for mass spectrometry analyses. Tryptic peptide mixtures were injected on an Ultimate RSLC 3000 nanoHPLC system (Dionex, Sunnyvale, CA, USA) interfaced to an Orbitrap Fusion Tribrid or to a QExactive Plus high resolution mass spectrometer (Thermo Scientific, Bremen, Germany). Peptides were loaded onto a trapping microcolumn Acclaim PepMap100 C18 (20 mm x 100 μm ID, 5 μm, 100Å, Thermo Scientific) before separation on a reversed-phase analytical nanocolumn at a flowrate of 0.25 μl/min, using a gradient from 4 to 76% acetonitrile in 0.1% formic acid (total time: 140min). A custom packed nanocolumn was used with Fusion MS instrument (75 μm ID × 40 cm, 1.8 μm particles, Reprosil Pur, Dr. Maisch), and an Easy-Spray PepMap C18 column was used with QExactive MS (50 cm x 75 μm ID, 2 μm, 100Å, Thermo Scientific). In Fusion instrument, full survey scans were performed at a 120'000 resolution, and a top speed precursor selection strategy was applied to maximize acquisition of peptide tandem MS spectra with a maximum cycle time of 3s. HCD fragmentation mode was used at a normalized collision energy of 32%, with a precursor isolation window of 1.6 m/z, and MS/MS spectra were acquired at a 15'000 resolution. Peptides selected for MS/MS were excluded from further fragmentation during 60s. In QExactive instrument, full MS survey scans were

performed at 70'000 resolution, and the 10 most intense multiple-charge precursor ions detected in the full MS survey scan were selected for higher energy collision-induced dissociation (HCD, normalized collision energy NCE=27 %) and analysis in the orbitrap at 17'500 resolution. The window for precursor isolation was of 1.5 m/z units around the precursor and selected fragments were excluded for 60s from further analysis.

MS data were analyzed using Mascot 2.6 (Matrix Science, London, UK) set up to search the SwissProt database (www.uniprot.org) restricted to *Homo sapiens* taxonomy (December 2017 version, 20'245 sequences) and including common contaminants (keratins, digestion enzymes, etc.). Trypsin (cleavage at K,R) was used as the enzyme definition, allowing 3 missed cleavages. Mascot was searched with a parent ion tolerance of 10 ppm and a fragment ion mass tolerance of 0.02 Da. Iodoacetamide derivative of cysteine was specified in Mascot as a fixed modification. N-terminal acetylation of protein, oxidation of methionine, and phosphorylation of serine, threonine or tyrosine were specified as variable modifications.

Scaffold software (version 4.8.4, Proteome Software Inc., Portland, OR) was used to validate MS/MS based peptide and protein identifications, and to perform dataset alignment. Peptide identifications were accepted if they could be established at greater than 90.0% probability by the Scaffold Local FDR algorithm. Protein identifications were accepted if they could be established at greater than 95.0% probability and contained at least 5 identified peptides. Protein probabilities were assigned by the Protein Prophet algorithm (Nesvizhskii et al., 2003). Proteins that contained similar peptides and could not be differentiated based on MS/MS analysis alone were grouped to satisfy the principles of parsimony. Proteins sharing significant peptide evidence were grouped into clusters. MsViz software (Martin-Campos et al., 2017) was used for comparison of sequence coverage and phosphorylation of FLCN protein in the different treatments.

Flow cytometry

To study cell death and proliferation following treatment with CDK4 inhibitors, the amounts of Annexin V-PE and Ki67 expression were measured by flow cytometry. Cultured cells were trypsinized and stained with Annexin V-PE (BioLegend, 640907) according to the manufacturer's protocol, and the cells were analyzed on either a Gallios™ (Beckman Coulter) or LSR II flow cytometer (BD Biosciences). For intracellular Ki67 staining, cells were fixed and permeabilized (Biolegend) according to the manufacturer's protocol. Cells were then

incubated with a permeabilization buffer that detects anti-Ki67-FITC (Biolegend) for 30 min on ice. After washing twice with permeabilization buffer, the cells were resuspended in PBS prior to analysis. For each sample, at least 10000 events were acquired. Flow cytometry analysis was performed with FlowJo software (Version 7.6.5, Treestar).

For the LysoTracker experiments, fluorescence was analyzed with an ImageStreem III Flow Cytometer. After treating the cells with the CDK4 inhibitor and/or IGF1, 100 nM Lysotracker Green DND-26 (Life Technologies) was added to live cells 1 h before fixation. The cells were then trypsinized and fixed in suspension with 4% PFA for 15 min at RT and washed twice with PBS. Nuclear staining was performed with DAPI, and the cells were resuspended in PBS with 2% FBS. For each sample, 10000 events were acquired at a magnification power equivalent to 60X.

Flow cytometry was also used to analyze the intracellular lysosomal activity with a lysosomal intracellular activity assay kit (Cell-Based) (Biovision) according to the manufacturer's instructions. Briefly, a self-quenched substrate was added to the cultured cells with freshly prepared media containing 0.5% FBS, incubated for one hour at 37°C with 5% CO_2 and trypsinized; 1000 events were acquired with an ACCURI C6 flow cytometer. All flow cytometry analyses were performed with FlowJo software (Version 7.6.5, Treestar).

Quantitative Real-Time PCR Analysis.

Total RNA was prepared using Trizol reagent (Sigma) and then reverse transcribed using Super Script II (Invitrogen). qPCR analysis was performed using SYBR green (Roche Diagnostics) and a 7900HT Fast Real-Time PCR System (Applied Biosystems). Relative mRNA expression levels were calculated from the comparative threshold cycle (Ct) values of the gene of interest relative to RS9 and TBP mRNA. Specific primer sequences are listed in Table S1, S2 and S3.

Table S1. Primers used for qPCR Analysis of Transcription Factor EB (TFEB) regulated genes (human)

Gene	Forward	Reverse
ATP6V0E1	CATTGTGATGAGCGTGTTCTGG	AACTCCCCGGTTAGGACCCTTA
ATP6V1H	GGAAGTGTCAGATGATCCCCA	CCGTTTGCCTCGTGGATAAT

CTSA	CAGGCTTTGGTCTTCTCTCCA	TCACGCATTCCAGGTCTTTG
CTSB	AGTGGAGAATGGCACACCCTA	AAGAAGCCATTGTCACCCCA
CTSD	GCTGATTCAGGGCGAGTACATGAT	TGCGACACCTTGAGCGTGTA
CTSF	ACAGAGGAGGAGTTCCGCACTA	GCTTGCTTCATCTTGTTGCCA
CTSL1	CACCGGCTTTGTGGACATC	ATGACCTGCATCAATAGCAACA
CTSO	TAGATGCAGTGAGCTGGCAA	AACGGAATCTGCAATACCACA
LAMP1	ACGTTACAGCGTCCAGCTCAT	TCTTTGGAGCTCGCATTGG
SQSTM1	CACCTGTCTGAGGGCTTCTC	CACACTCTCCCCAACGTTCT
TFEB	CCAGAAGCGAGAGCTCACAGAT	TGTGATTGTCTTTCTTCTGCCG

Table S2. Primers used for qPCR Analysis of Senescence genes (human)

Gene	Forward	Reverse
CDKN1A	GACACCACTGGAGGGTGACT	CAGGTCCACATGGTCTTCCT
CDKN2A	CCAACGCACCGAATAGTTACG	GCGCTGCCCATCATCATG
COL1A1	GGAGGAATTTCCGTGCCTGG	CAATCCTCGAGCACCCTGAG
CXCL14	GGACCCAAGATCCGCTACAG	CTTCGTAGACCCTGCGCTTC
MFAP2	AGCAGTGAACGGAGTCACAAA	GCCGAGGAGTCACCTCTTGA
MMP2	TGATGTCCAGCGAGTGGATG	AAGAAGTAGCTGTGACCGCC
P311	GGGGCTTTTGTCTGTTGGTC	GAAGCCTTCCCTCCATGTCC
RKHD3	GGGCGGCAAGGTTGTAAAAT	TGTTCTTATTCCGGGGAGGCG
IGFBP5	GAAAGCAGTGCAAACCTTCCC	AGGTGTGGCACTGAAAGTCC
RBL2	CGGGATCTCTGTGCCAAACT	ACTTCTATACACCTGGCTCCG

Table S3. Primers used for qPCR Analysis of housekeeping genes (human)

Gene	Forward	Reverse
RS9	CACACTCTCCCCAACGTTCT	ACCACCTGCTTGCGGACCCTGATA
TBP	TGCACAGGAGCCAAGAGTGAA	CACATCACAGCTCCCCACCA

Cathepsin B activity assay kit (fluorometric)

Cathepsin B activity was assessed with a fluorometric kit (ab65300, Abcam). Cell lysates that contain cathepsin B cleave the synthetic substrate RR-AFC to release free AFC, which

emits fluorescence that can be measured. Cells were lysed with chilled cell lysis buffer provided in the kit; the lysates were then incubated on ice for 10-30 minutes and centrifuged for 5 minutes at 4°C. The supernatants were saved, and the protein concentrations were measured. In a 96-well plate, 200 μg of protein was loaded per well, and 50 μl of cathepsin B reaction buffer and 2 μl of 10 mM cathepsin B substrate Ac-RR-AFC (200 μM final concentration) were added. The plates were incubated at 37°C for 1 hour in the dark, and the fluorescence was measured with a Tecan plate reader (Ex/Em = 400/505 nm).

Colorimetric detection of senescence-associated β galactosidase

Senescence-associated β-galactosidase (SA-β-Gal) analysis was performed in cultured cells and mouse xenograft tumors.

Cells in culture were fixed with 2% PFA and 0.2% glutaraldehyde for five minutes at RT, washed with PBS and stained with a solution containing 40 mM citric acid/Na phosphate buffer, 5 mM $K_4[Fe(CN)_6]$ $3H_2O$, 5 mM $K_3[Fe(CN)_6]$, 150 mM sodium chloride, 2 mM magnesium chloride and 1 mg ml^{-1} X-gal in distilled water for 15h at 37°C. After staining, the cells were washed twice with PBS and once with methanol, and the plates were allowed to air dry. Bright field images were obtained with an upright light microscope (CarlZeiss) with a 20X objective. Positive cells and the total number of cells per field were counted manually.

For SA-β-Gal analysis of mouse tumors, tissues were OCT embedded and stored at -80°C. On the day of the experiment, the tissues were cut into 8-μm-thick sections and mounted onto glass slides. After air-drying for 30 minutes, the sections were fixed with 2% PFA and 0.2% glutaraldehyde and stained as previously for cultured cells. The sections were washed and counterstained with 0.1% Fast Red (Sigma). Images were taken at different magnifications with a bright field microscope.

Electron microscopy

Cells were plated on poly-L-lysine (0.01%, Sigma, catalog n°P4832)-coated glass slides (LabTek Chamber Slides, catalog n°177399) cultured for two days and treated with CDK4/6 inhibitor or DMSO as control. The cells were then fixed for two hours in 2.5% glutaraldehyde (Electron Microscopy Sciences, catalog n°16220) dissolved in 0.1 M phosphate buffer (PB), pH 7.4. After three washes with PB, the cells were post-fixed for one hour in 1% osmium tetroxide

(Electron Microscopy Sciences, catalog n°19150) in PB and then stained with 70% ethanol containing 1% uranyl acetate (Sigma, catalog n°73943) for 20 minutes. The cells were dehydrated in a graded alcohol series and embedded in Epon (Electron Microscopy Sciences, catalog n°13940). Mouse tumors were cut into small pieces (approximately 1 mm^3) and then analysed in the same way as cells, outlined below.

For EM analysis, mouse tumors and cultured cells were fixed in a 2.5% glutaraldehyde solution (EMS, Hatfield, PA, US) in PB for one hour at RT. Then, they were rinsed three times for five minutes with PB buffer and post-fixed with a fresh mixture of 1% osmium tetroxide (EMS, Hatfield, PA, US) and 1.5% potassium ferrocyanide (Sigma, St Louis, MO, US) in PB buffer for one hour at RT. The samples were then washed three times with distilled water and dehydrated in acetone solutions (Sigma, St Louis, MO, US) of graded concentrations (30%-40 min; 50%-40 min; 70%-40 min; 100%-3x1 h). This was followed by incubation with Epon (Sigma, St Louis, MO, US) at graded concentrations (Epon 1/3 acetone-2 h; Epon 3/1 acetone-2 h, Epon 1/1-4 h; Epon 1/1-12 h) and finally polymerization for 48 h at 60°C in an oven.

Ultrathin sections of 50 nm were cut on a Leica Ultracut (Leica Mikrosysteme GmbH, Vienna, Austria) and picked up on a 2x1 mm copper slot grid (EMS, Hatfield, PA, US) coated with a polystyrene film (Sigma, St Louis, MO, US). Sections were post-stained with 4% uranyl acetate (Sigma, St Louis, MO, US) in H$_2$O for 10 minutes, rinsed several times with H$_2$O followed by Reynolds lead citrate in H$_2$O (Sigma, St Louis, MO, US) for 10 minutes and then again with H$_2$O several times. Micrographs were taken with a Philips CM100 transmission electron microscope (Thermo Fisher Scientific, Waltham, MA USA) at an acceleration voltage of 80 kV with a TVIPS TemCam-F416 digital camera (TVIPS GmbH, Gauting, Germany). Large montage alignment was performed using the Blendmont command-line program from IMOD software (Kremer et al., 1996) (for the in vivo analyses) or Adobe Photoshop CC 2015 (for in vitro analyses).

The areas of autolysosomes, autophagosomes and cell cytoplasm were measured using ImageJ software. The densities of the autolysosomes and autophagosomes were expressed as a percentage of the cell area using the formula: area of the autolysosomes (or autophagosomes) / area of the cell cytoplasm x 100. The mean autolysosome area per cell and the percentage of autolysosomes containing degraded material per cell were also analyzed.

Animal studies

MDA-MB-231 cells were injected into the fourth mammary gland of eight-week-old female NSG mice (NOD.*Cg-Prkdc^{scid}Il2rg^{tm1Wjl}*/Sz strain, The Jackson Laboratory). Tumor growth and body weight were measured twice per week until the tumor size of each mouse reached 50 mm^3. Optical imaging measurements using an IVIS Xenogen system were conducted on mice under anesthesia once per week for the duration of the study to follow the progression of the primary tumor.

For the first experiment, mice were divided randomly into two groups, one (n=15) for treatment with vehicle (DMSO) and the other (n=15) for treatment with a CDK4/6 inhibitor (LY2835219, 75 mg/kg, formulated in 1% HEC in distilled water). The treatments were administered orally (gavage), with approximately 300 µl of solution (depending on the body weight) gavaged every day for a total of 8 days. During this time, body weight and tumor growth were also monitored. After eight days, the animals were anesthetized with isoflurane (3%) in an induction chamber for 3 minutes and were sacrificed by cervical dislocation. Tumors from n=10 mice from each treatment group were dissected and cut into two pieces; one piece was fixed in PFA for histological staining, and the other piece was snap frozen for protein and RNA analysis. Tumors from n=5 mice from each treatment group were processed for transmission electron microscopy analysis and SA-β-Gal staining.

The injections and monitoring for second experiment was exactly the same. However, mice were divided into four groups of n=9-10 as follows:

1. DMSO gavage + intraperitoneal injection (IP) NaCl 0.9%

2. DMSO gavage + IP A-769662 (20mg/kg)

3. LY2835219 gavage (75 mg/Kg) + IP NaCl 0.9%

4. LY2835219 gavage (75 mg/Kg) + IP A-769662 (20mg/kg)

As before, the CDK4/6 inhibitor LY2835219 was administrated orally (gavage) in approximately 350µl of volume (depending on the body weight). A-769662 was administrated by intraperitoneal injection (IP) of 100µl in saline solution (NaCl 0.9%).

Quantification and Statistical Analyses

The results are expressed as the means ± standard error of the means (S.E.M.). Comparisons between 2 groups were performed with an unpaired two-tailed Student's t test, and multiple group comparisons were performed by unpaired one-way ANOVA and two-way ANOVA, both followed by Tukey's test or otherwise indicated. All *p-value*s below 0.05 were considered significant. Statistically significant values are represented by asterisks corresponding to *p < 0.05, **p < 0.01, ***p < 0.001 and ****p < 0.0001.

Author contributions

L.M-C. and L.F. designed this study. L.M-C. conducted most of the experiments, with assistance from I.C.L-M., M.O., J.C-A., A.G., L.Z, V.B and A.Nasrallah. J.P performed electron microscopy experiments, acquisition and analysis. C.M. performed histological stainings. A.P. assisted in the *in vivo* work. P.R. contributed to the conception and experimental design of FACS analysis. L.M-C, I.C.L-M and L.F wrote the manuscript.

Declaration of interests

The authors declare no competing interests.

References

Aguilar, V., and Fajas, L. (2010). Cycling through metabolism. EMBO molecular medicine *2*, 338-348.

Albert, V., and Hall, M.N. (2015). mTOR signaling in cellular and organismal energetics. Current opinion in cell biology *33*, 55-66.

Argiles, J.M., Orpi, M., Busquets, S., and Lopez-Soriano, F.J. (2012). Myostatin: more than just a regulator of muscle mass. Drug Discov Today *17*, 702-709.

Bar-Peled, L., and Sabatini, D.M. (2014). Regulation of mTORC1 by amino acids. Trends Cell Biol *24*, 400-406.

Blanchet, E., Annicotte, J.S., Lagarrigue, S., Aguilar, V., Clape, C., Chavey, C., Fritz, V., Casas, F., Apparailly, F., Auwerx, J*., et al.* (2011). E2F transcription factor-1 regulates oxidative metabolism. Nature cell biology *13*, 1146-1152.

Bourdeau, V., and Ferbeyre, G. (2016). CDK4-CDK6 inhibitors induce autophagy-mediated degradation of DNMT1 and facilitate the senescence antitumor response. Autophagy *12*, 1965-1966.

Brown, N.E., Jeselsohn, R., Bihani, T., Hu, M.G., Foltopoulou, P., Kuperwasser, C., and Hinds, P.W. (2012). Cyclin D1 activity regulates autophagy and senescence in the mammary epithelium. Cancer Res *72*, 6477-6489.

Carmona-Gutierrez, D., Hughes, A.L., Madeo, F., and Ruckenstuhl, C. (2016). The crucial impact of lysosomes in aging and longevity. Ageing research reviews *32*, 2-12.

Cho, S., and Hwang, E.S. (2012). Status of mTOR activity may phenotypically differentiate senescence and quiescence. Molecules and cells *33*, 597-604.

Deshpande, A., Sicinski, P., and Hinds, P.W. (2005). Cyclins and cdks in development and cancer: a perspective. Oncogene *24*, 2909-2915.

Dibble, C.C., and Cantley, L.C. (2015). Regulation of mTORC1 by PI3K signaling. Trends in cell biology *25*, 545-555.

Duran, R.V., Oppliger, W., Robitaille, A.M., Heiserich, L., Skendaj, R., Gottlieb, E., and Hall, M.N. (2012). Glutaminolysis activates Rag-mTORC1 signaling. Mol Cell *47*, 349-358.

Elsamany, S., and Abdullah, S. (2014). Triple-negative breast cancer: future prospects in diagnosis and management. Medical oncology *31*, 834.

Fehrenbacher, N., and Jaattela, M. (2005). Lysosomes as targets for cancer therapy. Cancer research *65*, 2993-2995.

Franco, J., Balaji, U., Freinkman, E., Witkiewicz, A.K., and Knudsen, E.S. (2016). Metabolic Reprogramming of Pancreatic Cancer Mediated by CDK4/6 Inhibition Elicits Unique Vulnerabilities. Cell Rep *14*, 979-990.

Goel, S., Wang, Q., Watt, A.C., Tolaney, S.M., Dillon, D.A., Li, W., Ramm, S., Palmer, A.C., Yuzugullu, H., Varadan, V*., et al.* (2016). Overcoming Therapeutic Resistance in HER2-Positive Breast Cancers with CDK4/6 Inhibitors. Cancer cell *29*, 255-269.

Hamilton, E., and Infante, J.R. (2016). Targeting CDK4/6 in patients with cancer. Cancer Treat Rev *45*, 129-138.

Hubbi, M.E., Gilkes, D.M., Hu, H., Kshitiz, Ahmed, I., and Semenza, G.L. (2014). Cyclin-dependent kinases regulate lysosomal degradation of hypoxia-inducible factor 1alpha to promote cell-cycle progression. Proceedings of the National Academy of Sciences of the United States of America *111*, E3325-3334.

Iriyama, N., Hino, H., Moriya, S., Hiramoto, M., Hatta, Y., Takei, M., and Miyazawa, K. (2018). The cyclin-dependent kinase 4/6 inhibitor, abemaciclib, exerts dose-dependent cytostatic and cytocidal effects and induces autophagy in multiple myeloma cells. Leuk Lymphoma *59*, 1439-1450.

Jia, J., Abudu, Y.P., Claude-Taupin, A., Gu, Y., Kumar, S., Choi, S.W., Peters, R., Mudd, M.H., Allers, L., Salemi, M.*, et al.* (2018). Galectins Control MTOR and AMPK in Response to Lysosomal Damage to Induce Autophagy. Autophagy.

Jin, Y., and Weisman, L.S. (2015). The vacuole/lysosome is required for cell-cycle progression. eLife *4*.

Kaur, J., and Debnath, J. (2015). Autophagy at the crossroads of catabolism and anabolism. Nat Rev Mol Cell Biol *16*, 461-472.

Klein, M.E., Kovatcheva, M., Davis, L.E., Tap, W.D., and Koff, A. (2018a). CDK4/6 Inhibitors: The Mechanism of Action May Not Be as Simple as Once Thought. Cancer cell.

Klein, M.E., Kovatcheva, M., Davis, L.E., Tap, W.D., and Koff, A. (2018b). CDK4/6 Inhibitors: The Mechanism of Action May Not Be as Simple as Once Thought. Cancer cell *34*, 9-20.

Kremer, J.R., Mastronarde, D.N., and McIntosh, J.R. (1996). Computer visualization of three-dimensional image data using IMOD. J Struct Biol *116*, 71-76.

Ku, B.M., Yi, S.Y., Koh, J., Bae, Y.H., Sun, J.M., Lee, S.H., Ahn, J.S., Park, K., and Ahn, M.J. (2016). The CDK4/6 inhibitor LY2835219 has potent activity in combination with mTOR inhibitor in head and neck squamous cell carcinoma. Oncotarget *7*, 14803-14813.

Lagarrigue, S., Lopez-Mejia, I.C., Denechaud, P.D., Escote, X., Castillo-Armengol, J., Jimenez, V., Chavey, C., Giralt, A., Lai, Q., Zhang, L.*, et al.* (2016). CDK4 is an essential insulin effector in adipocytes. J Clin Invest *126*, 335-348.

Lee, J.H., Park, S., Kim, E., and Lee, M.J. (2019). Negative-feedback coordination between proteasomal activity and autophagic flux. Autophagy, 1-3.

Lee, Y., Dominy, J.E., Choi, Y.J., Jurczak, M., Tolliday, N., Camporez, J.P., Chim, H., Lim, J.H., Ruan, H.B., Yang, X.*, et al.* (2014). Cyclin D1-Cdk4 controls glucose metabolism independently of cell cycle progression. Nature *510*, 547-551.

Li, M., Khambu, B., Zhang, H., Kang, J.H., Chen, X., Chen, D., Vollmer, L., Liu, P.Q., Vogt, A., and Yin, X.M. (2013). Suppression of lysosome function induces autophagy via a feedback down-regulation of MTOR complex 1 (MTORC1) activity. J Biol Chem *288*, 35769-35780.

Llanos, S., Megias, D., Blanco-Aparicio, C., Hernandez-Encinas, E., Rovira, M., Pietrocola, F., and Serrano, M. (2019). Lysosomal trapping of palbociclib and its functional implications. Oncogene.

Lopez-Mejia, I.C., Lagarrigue, S., Giralt, A., Martinez-Carreres, L., Zanou, N., Denechaud, P.D., Castillo-Armengol, J., Chavey, C., Orpinell, M., Delacuisine, B.*, et al.* (2017). CDK4 Phosphorylates AMPKalpha2 to Inhibit Its Activity and Repress Fatty Acid Oxidation. Mol Cell *68*, 336-349 e336.

Martin-Campos, T., Mylonas, R., Masselot, A., Waridel, P., Petricevic, T., Xenarios, I., and Quadroni, M. (2017). MsViz: A Graphical Software Tool for In-Depth Manual Validation and Quantitation of Post-translational Modifications. Journal of proteome research *16*, 3092-3101.

Martinez-Carreres, L., Nasrallah, A., and Fajas, L. (2017). Cancer: Linking Powerhouses to Suicidal Bags. Frontiers in oncology *7*, 204.

Meo-Evoli, N., Almacellas, E., Massucci, F.A., Gentilella, A., Ambrosio, S., Kozma, S.C., Thomas, G., and Tauler, A. (2015). V-ATPase: a master effector of E2F1-mediated lysosomal trafficking, mTORC1 activation and autophagy. Oncotarget *6*, 28057-28070.

Michaloglou, C., Crafter, C., Siersbaek, R., Delpuech, O., Curwen, J.O., Carnevalli, L.S., Staniszewska, A.D., Polanska, U.M., Cheraghchi-Bashi, A., Lawson, M.*, et al.* (2018). Combined Inhibition of mTOR and CDK4/6 Is Required for Optimal Blockade of E2F Function and Long-term Growth Inhibition in Estrogen Receptor-positive Breast Cancer. Molecular cancer therapeutics *17*, 908-920.

Miettinen, T.P., Peltier, J., Hartlova, A., Gierlinski, M., Jansen, V.M., Trost, M., and Bjorklund, M. (2018). Thermal proteome profiling of breast cancer cells reveals proteasomal activation by CDK4/6 inhibitor palbociclib. The EMBO journal *37*.

Nesvizhskii, A.I., Keller, A., Kolker, E., and Aebersold, R. (2003). A statistical model for identifying proteins by tandem mass spectrometry. Analytical chemistry *75*, 4646-4658.

O'Leary, B., Finn, R.S., and Turner, N.C. (2016). Treating cancer with selective CDK4/6 inhibitors. Nature reviews Clinical oncology *13*, 417-430.

Olmez, I., Brenneman, B., Xiao, A., Serbulea, V., Benamar, M., Zhang, Y., Manigat, L., Abbas, T., Lee, J., Nakano, I., *et al.* (2017). Combined CDK4/6 and mTOR Inhibition Is Synergistic against Glioblastoma via Multiple Mechanisms. Clin Cancer Res *23*, 6958-6968.

Petit, C.S., Roczniak-Ferguson, A., and Ferguson, S.M. (2013). Recruitment of folliculin to lysosomes supports the amino acid-dependent activation of Rag GTPases. The Journal of cell biology *202*, 1107-1122.

Piao, S., and Amaravadi, R.K. (2016). Targeting the lysosome in cancer. Ann N Y Acad Sci *1371*, 45-54.

Polk, A., Kolmos, I.L., Kumler, I., and Nielsen, D.L. (2016). Specific CDK4/6 inhibition in breast cancer: a systematic review of current clinical evidence. ESMO open *1*, e000093.

Puertollano, R. (2014). mTOR and lysosome regulation. F1000Prime Rep *6*, 52.

Real, S., Meo-Evoli, N., Espada, L., and Tauler, A. (2011). E2F1 regulates cellular growth by mTORC1 signaling. PLoS One *6*, e16163.

Renna, M., Schaffner, C., Winslow, A.R., Menzies, F.M., Peden, A.A., Floto, R.A., and Rubinsztein, D.C. (2011). Autophagic substrate clearance requires activity of the syntaxin-5 SNARE complex. J Cell Sci *124*, 469-482.

Rivadeneira, D.B., Mayhew, C.N., Thangavel, C., Sotillo, E., Reed, C.A., Grana, X., and Knudsen, E.S. (2010). Proliferative suppression by CDK4/6 inhibition: complex function of the retinoblastoma pathway in liver tissue and hepatoma cells. Gastroenterology *138*, 1920-1930.

Romero-Pozuelo, J., Demetriades, C., Schroeder, P., and Teleman, A.A. (2017). CycD/Cdk4 and Discontinuities in Dpp Signaling Activate TORC1 in the Drosophila Wing Disc. Dev Cell *42*, 376-387 e375.

Sahani, M.H., Itakura, E., and Mizushima, N. (2014). Expression of the autophagy substrate SQSTM1/p62 is restored during prolonged starvation depending on transcriptional upregulation and autophagy-derived amino acids. Autophagy *10*, 431-441.

Salazar-Roa, M., and Malumbres, M. (2017). Fueling the Cell Division Cycle. Trends in cell biology *27*, 69-81.

Salmon, P., and Trono, D. (2006). Production and titration of lentiviral vectors. Current protocols in neuroscience *Chapter 4*, Unit 4 21.

Saxton, R.A., and Sabatini, D.M. (2017). mTOR Signaling in Growth, Metabolism, and Disease. Cell *169*, 361-371.

Schindelin, J., Arganda-Carreras, I., Frise, E., Kaynig, V., Longair, M., Pietzsch, T., Preibisch, S., Rueden, C., Saalfeld, S., Schmid, B., *et al.* (2012). Fiji: an open-source platform for biological-image analysis. Nat Methods *9*, 676-682.

Seranova, E., Connolly, K.J., Zatyka, M., Rosenstock, T.R., Barrett, T., Tuxworth, R.I., and Sarkar, S. (2017). Dysregulation of autophagy as a common mechanism in lysosomal storage diseases. Essays Biochem *61*, 733-749.

Settembre, C., and Ballabio, A. (2014). Lysosomal adaptation: how the lysosome responds to external cues. Cold Spring Harb Perspect Biol *6*.

Shalem, O., Sanjana, N.E., Hartenian, E., Shi, X., Scott, D.A., Mikkelson, T., Heckl, D., Ebert, B.L., Root, D.E., Doench, J.G., *et al.* (2014). Genome-scale CRISPR-Cas9 knockout screening in human cells. Science *343*, 84-87.

Shevchenko, A., Tomas, H., Havlis, J., Olsen, J.V., and Mann, M. (2006). In-gel digestion for mass spectrometric characterization of proteins and proteomes. Nature protocols *1*, 2856-2860.

Tai, H., Wang, Z., Gong, H., Han, X., Zhou, J., Wang, X., Wei, X., Ding, Y., Huang, N., Qin, J., *et al.* (2017). Autophagy impairment with lysosomal and mitochondrial dysfunction is an important characteristic of oxidative stress-induced senescence. Autophagy *13*, 99-113.

Tan, H.W.S., Sim, A.Y.L., and Long, Y.C. (2017). Glutamine metabolism regulates autophagy-dependent mTORC1 reactivation during amino acid starvation. Nature communications *8*, 338.

Wang, X., and Sun, S.Y. (2009). Enhancing mTOR-targeted cancer therapy. Expert opinion on therapeutic targets *13*, 1193-1203.

Zhou, J., Tan, S.H., Nicolas, V., Bauvy, C., Yang, N.D., Zhang, J., Xue, Y., Codogno, P., and Shen, H.M. (2013). Activation of lysosomal function in the course of autophagy via mTORC1 suppression and autophagosome-lysosome fusion. Cell research *23*, 508-523.

Zoncu, R., Bar-Peled, L., Efeyan, A., Wang, S., Sancak, Y., and Sabatini, D.M. (2011). mTORC1 senses lysosomal amino acids through an inside-out mechanism that requires the vacuolar H(+)-ATPase. Science *334*, 678-683.
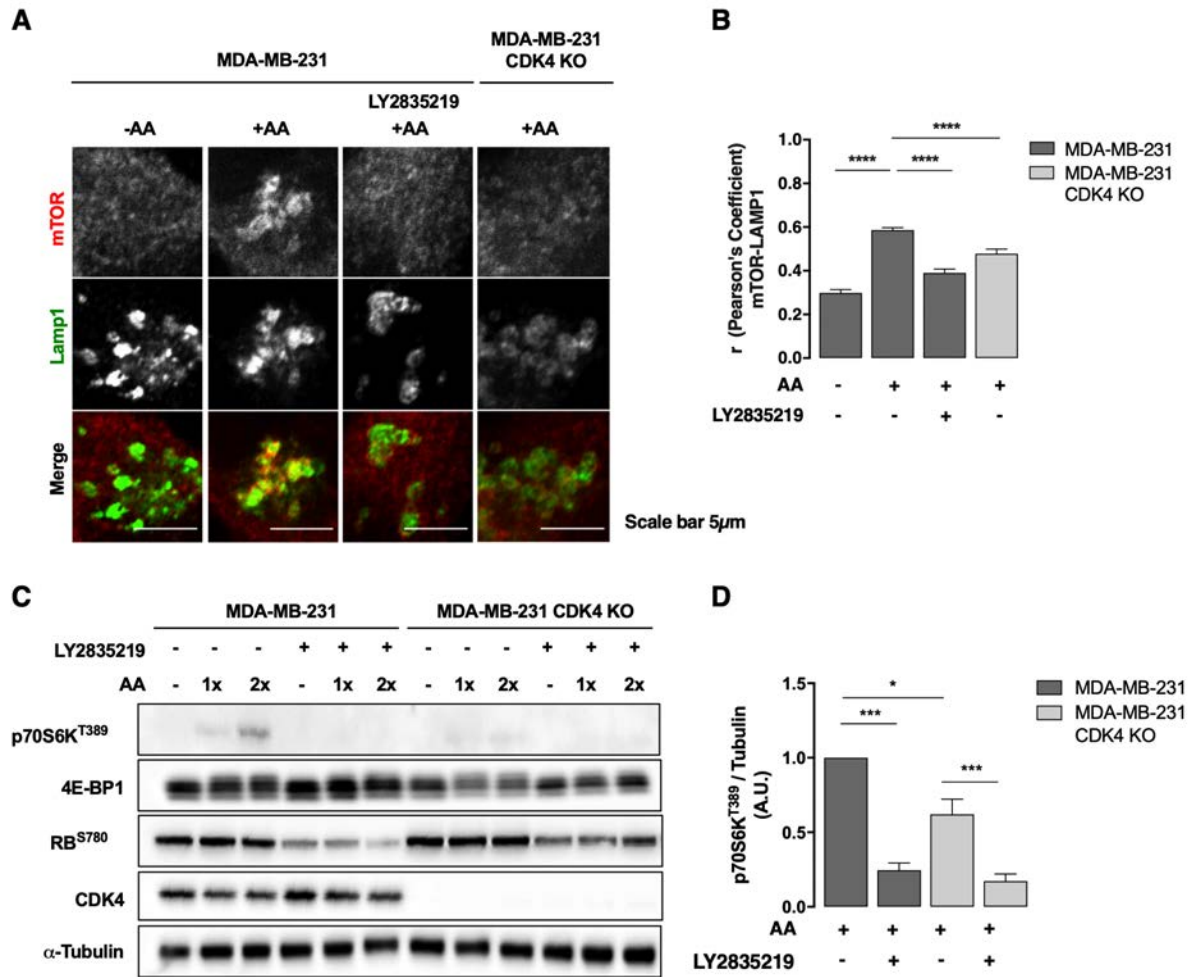
Figure 1.- CDK4 inhibition or depletion prevents the recruitment of mTOR to the lysosomal surface in response to amino acid stimulation. A, Confocal immunofluorescence analysis showing the colocalization of mTOR with lysosomes (visualized by LAMP1 and mTOR staining) in WT and CDK4 KO MDA-MB-231 cells, with or without amino acid stimulation and in the presence of 0.5 µM of the CDK4/6 inhibitor LY2835219 or vehicle control (DMSO). B, Quantification of mTOR-LAMP1 colocalization from A using Pearson's coefficient. At least 40 fields per treatment condition from 3 independent experiments were analyzed. C, Western blot showing levels of phospho-RB (S780), CDK4, mTORC1 target genes (phospho-p70S6K (T389) and 4E-BP1). α-tubulin was used as a loading control in WT and CDK4 KO MDA-MB-231 cells with or without amino acid stimulation and in presence or absence of 0.5 µM LY2835219. D, Quantification of phospho-p70S6K (T389) levels from three independent experiments like C normalized to α-tubulin.
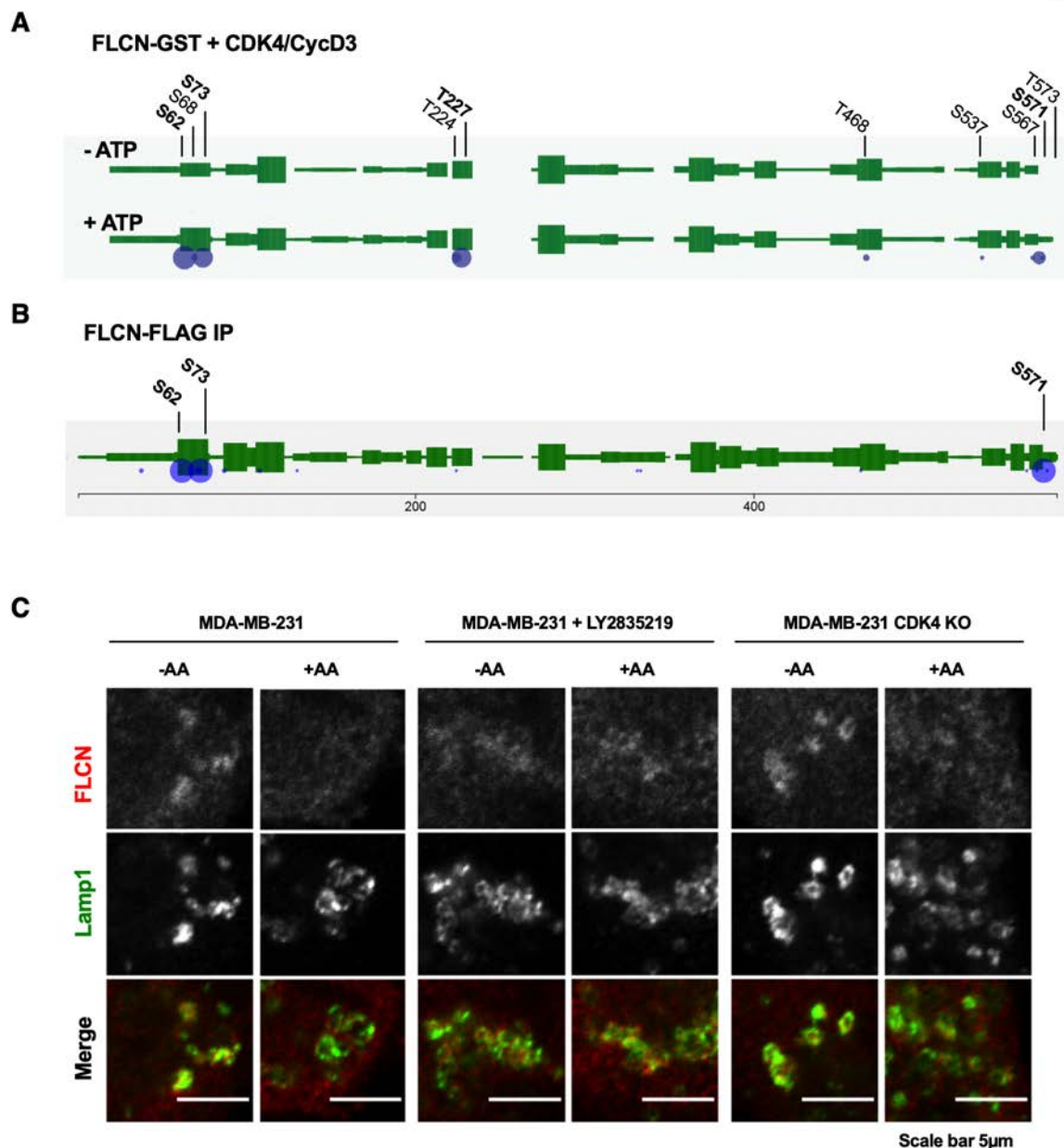
Figure 2.- CDK4 regulates mTORC1 activity through phosphorylating FLCN. A, Representation of the phosphorylation sites detected by mass spectrometry analysis in the *In vitro* kinase assay with FLCN-GST and CDK4/CyclinD3. In green is represented the protein sequence. Blue dots represent the phosphorylation sites, and their size correlates with their abundance. Conditions without ATP (-ATP) were used as negative control. B, Representation of the phosphorylation sites detected by mass spectrometry analysis in the overexpressed and immunoprecipitated FLCN-FLAG. As in A, green represents the protein sequence. Blue dots represent the phosphorylation sites, the size of which correlates with their abundance. C, Confocal immunofluorescence analysis showing the colocalization of overexpressed FLCN

32

with lysosomes (visualized by LAMP1 and FLCN staining) in WT and CDK4 KO MDA-MB-231 cells, with or without amino acid stimulation and in the presence of 0.5 µM of the CDK4/6 inhibitor LY2835219 or vehicle control (DMSO).
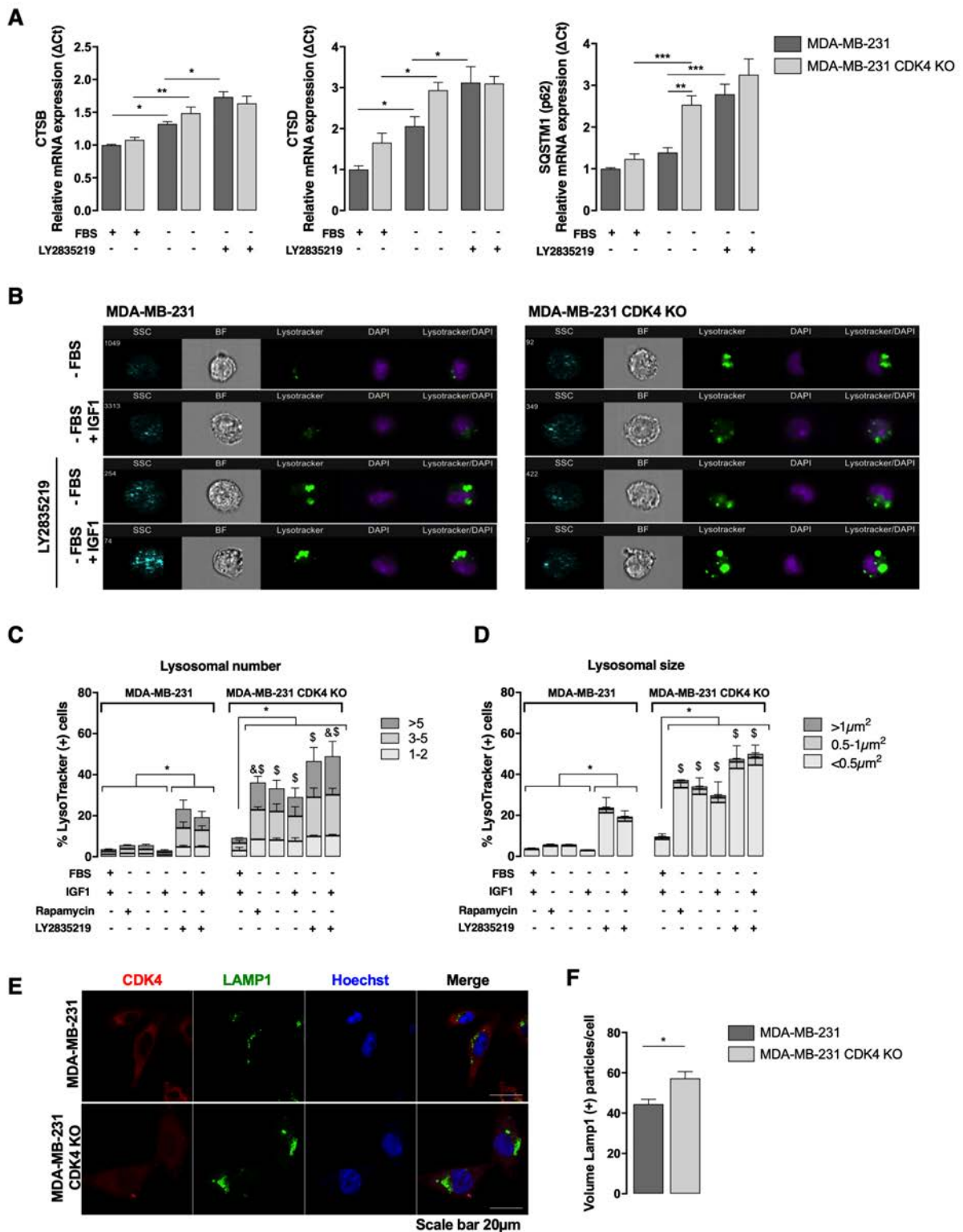
Figure 3.- CDK4 inhibition or depletion increases lysosomal mass. A, Quantitative PCR analysis showing the expression of transcription factor EB (TFEB) regulated genes that are involved in lysosomal or autophagic processes (cathepsins B and D and SQSTM1) in WT or

CDK4 KO MDA-MB-231 cells in complete (+FBS) or serum-starvation media (-FBS), treated with or without 0.5μM LY2835219. Each condition was assessed in duplicates for three independent experiments. B, Representative flow cytometry images of WT or CDK4 KO MDA-MB-231 cells treated with or without LY2835219 and stained with LysoTracker Green DND-26 under the indicated conditions. C, Proportions of cells containing lysosomes, estimated by quantification of fluorescence from LysoTracker Green DND-26 stained cells from two independent experiments. At least 10.000 events were acquired. Data are subdivided into categories of the number of lysosomes per cell. Significant differences between WT and KO MDA-MB-231 cells are indicated by: * total lysosomal particles (P<0.05); $ lysosomal particles per cell (3-5 particles) (P<0.05); & lysosomal particles per cell (>5 particles) (P<0.05); Two-way ANOVA followed by Tukey's multiple comparisons test. D, As for panel C, but subdivided into categories of the sizes of lysosomes per cell. Significant differences between WT and KO MDA-MB-231 cells are indicated by: * lysosomal particles <0.5μm^2 (P<0.05); $ lysosomal particles per cell (<0.5 μm^2) (P<0.05). E, Immunofluorescence analysis showing LAMP1 and CDK4 expression in WT and CDK4 KO MDA-MB-231 cells in complete media. F, Quantification of the total volume of LAMP1-positive particles in z-stack images. At least 30 cells in total from three independent experiments were analyzed.
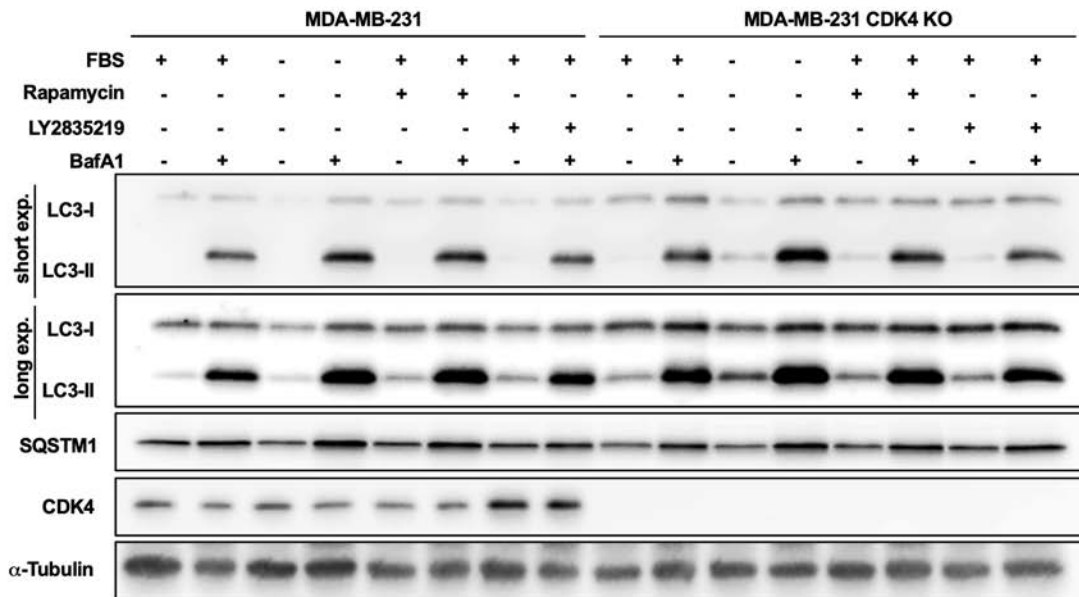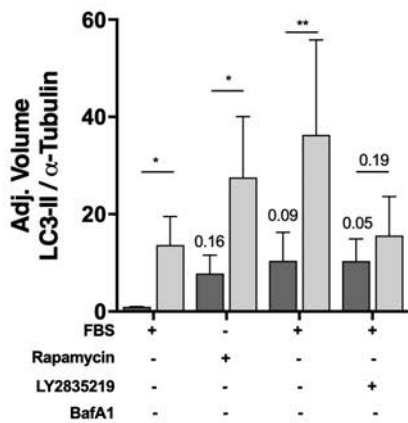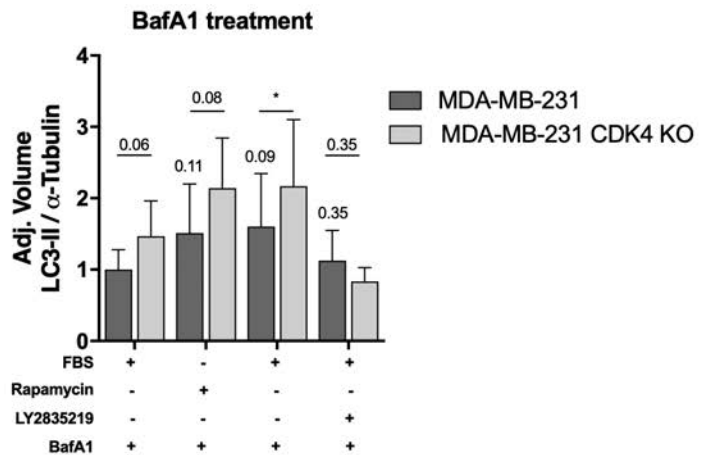
Figure 4.- Autophagic flux is impaired when CDK4 is inhibited or depleted. A, Western blot analysis of autophagosomal markers LC3-I, LC3-II, SQSTM1 in WT and CDK4 KO MDA-MB-231 cells treated 24h with complete media (+FBS) or serum-starvation media (-FBS), presence/absence of the mTOR inhibitor 0.5 μM rapamycin and of the CDK4 inhibitor 0.5 μM LY2835219 and presence/absence of 0.3 μM bafilomycin A1, 6 h before the treatment. B, Quantification of protein expression of LC3-II normalized to α-tubulin from three independent experiments like A, only the conditions without bafilomycin A1. C, Quantification of protein expression of LC3-II normalized to α-tubulin from three independent experiments like A, only

the conditions with bafilomycin A1. Statistical analysis was performed using a paired sample

T-test.

Figure 5.- Absence of CDK4 alters lysosomal function.
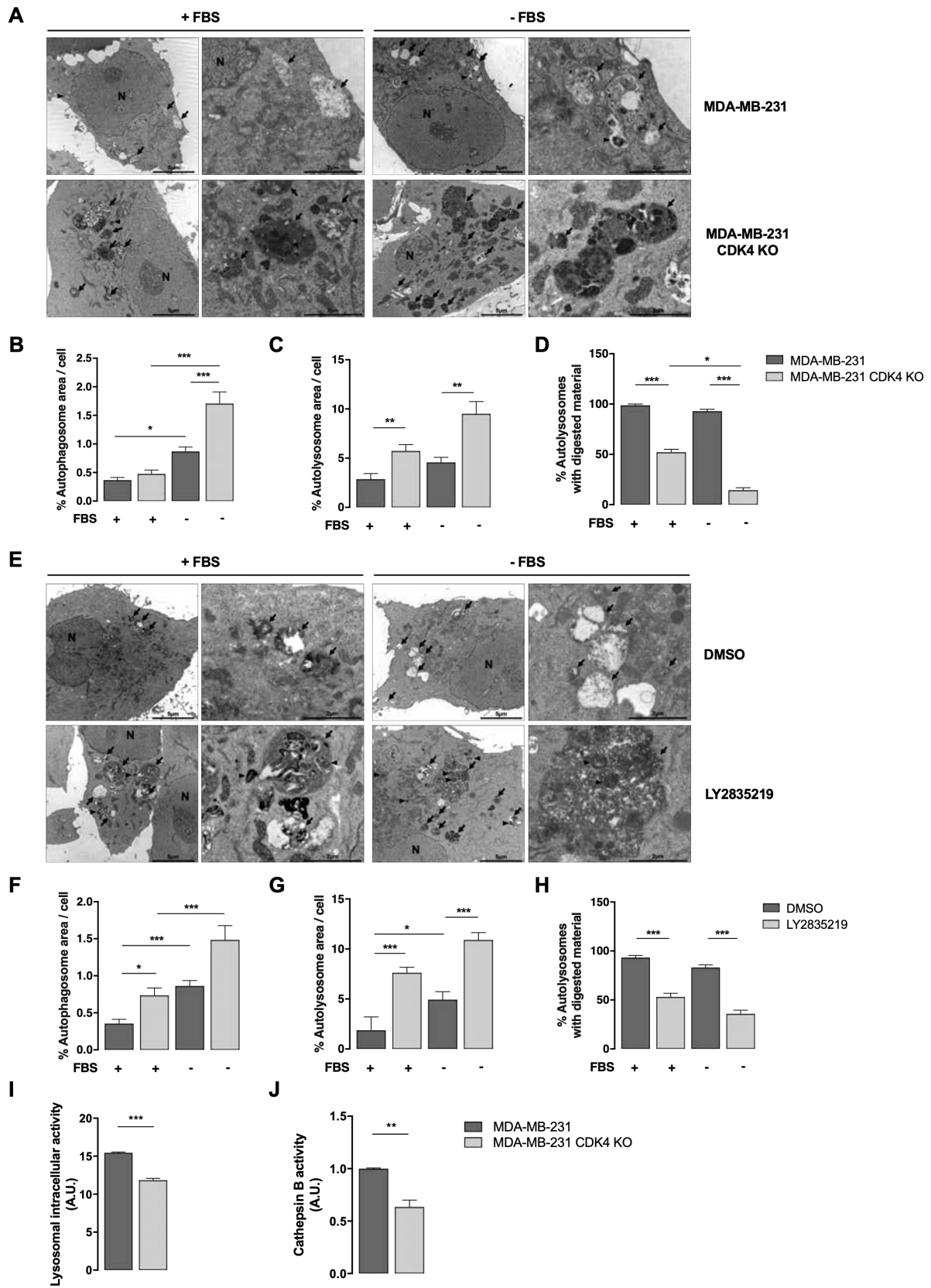
A, Representative electron micrographs of WT and CDK4 KO MDA-MB-321 cells showing that cells lacking CDK4 have increased autolysosome (arrows) density and size. In CDK4 KO cells, autolysosomes accumulated non-degraded material, such as undegraded autophagosomes (arrowheads), in both complete (+FBS) and serum-starvation media (-FBS). In cell cultures without FBS, an increase in autophagosomes (arrowheads) was also observed in CDK4 KO cells as compared to wild-type cells. N: nucleus. B–D, Quantification of the autophagosome (B) and autolysosome (C) area per cell, and the percentage of autolysosomes containing degraded material (D), quantified for the conditions shown in Figure 4A. n = 20 cells per condition. E, Representative electron micrographs of MDA-MB-321 cells showing increased density of autolysosomes (arrows), accumulation of non-degraded materials (including undegraded autophagosomes; arrowheads) and autophagosomes (arrowheads) in DMSO or LY2835219-treated WT MDA-MB-321 cells in complete and serum-starvation media. N: nucleus. F–H, Quantification of autophagosome area per cell (F), autolysosome area per cell (G) and percentage of autolysosomes containing degraded material per cell (H) quantified for conditions shown in Figure 4E. n = 20 cells per condition. I, Quantification of intracellular lysosomal activity of WT and CDK4 KO MDA-MB-231 cells in complete media. J, Quantification of cathepsin B activity in WT and CDK4 KO MDA-MB-231 cells in complete media.
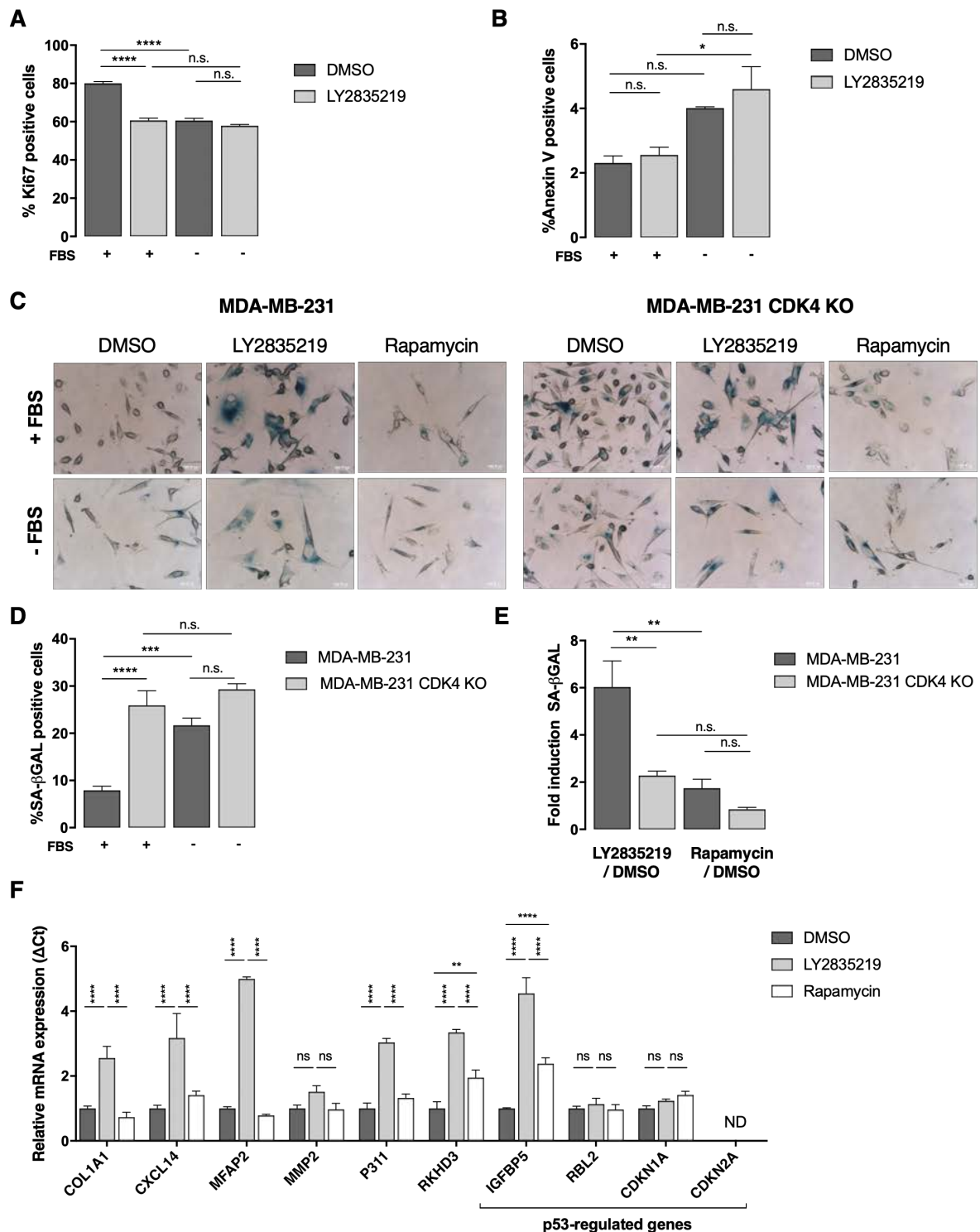
Figure 6.- Dysfunctional lysosomes, but not mTORC1 inhibition, induce senescence.

A, Proliferation of WT MDA-MB-231 cells cultured in either complete (+FBS) or serum-starvation (-FBS) media, with or without LY2835219, as shown by the percentage of Ki67-positive cells. B, Apoptosis under the same conditions, as shown by the percentage of Annexin

V-positive cells. C, mTOR-independent induction of senescence by LY2835219, visualized by colorimetric senescence-associated β-Galactosidase (SA-β-Gal) staining of WT and CDK4 KO MDA-MB-231 cells cultured in -/+ FBS media for the last 16 h of 8 days' treatment with DMSO, 0.5 μM LY2835219, or 0.5μM rapamycin. D, Quantification of the percentage of SA-β-Gal-positive WT and CDK4 KO MDA-MB-231 cells from triplicates, at least five fields per replicate. E, Quantification of the fold induction of SA-β-Gal induced by LY2835219 or rapamycin treatment from triplicates, at least five fields per replicate. F, Quantitative PCR analysis showing expression of genes usually upregulated in senescence (including p53-regulated genes), in WT MDA-MB-231 cells treated for 8 days with DMSO, LY2835219, or rapamycin in complete media. Each condition was assessed in triplicates.
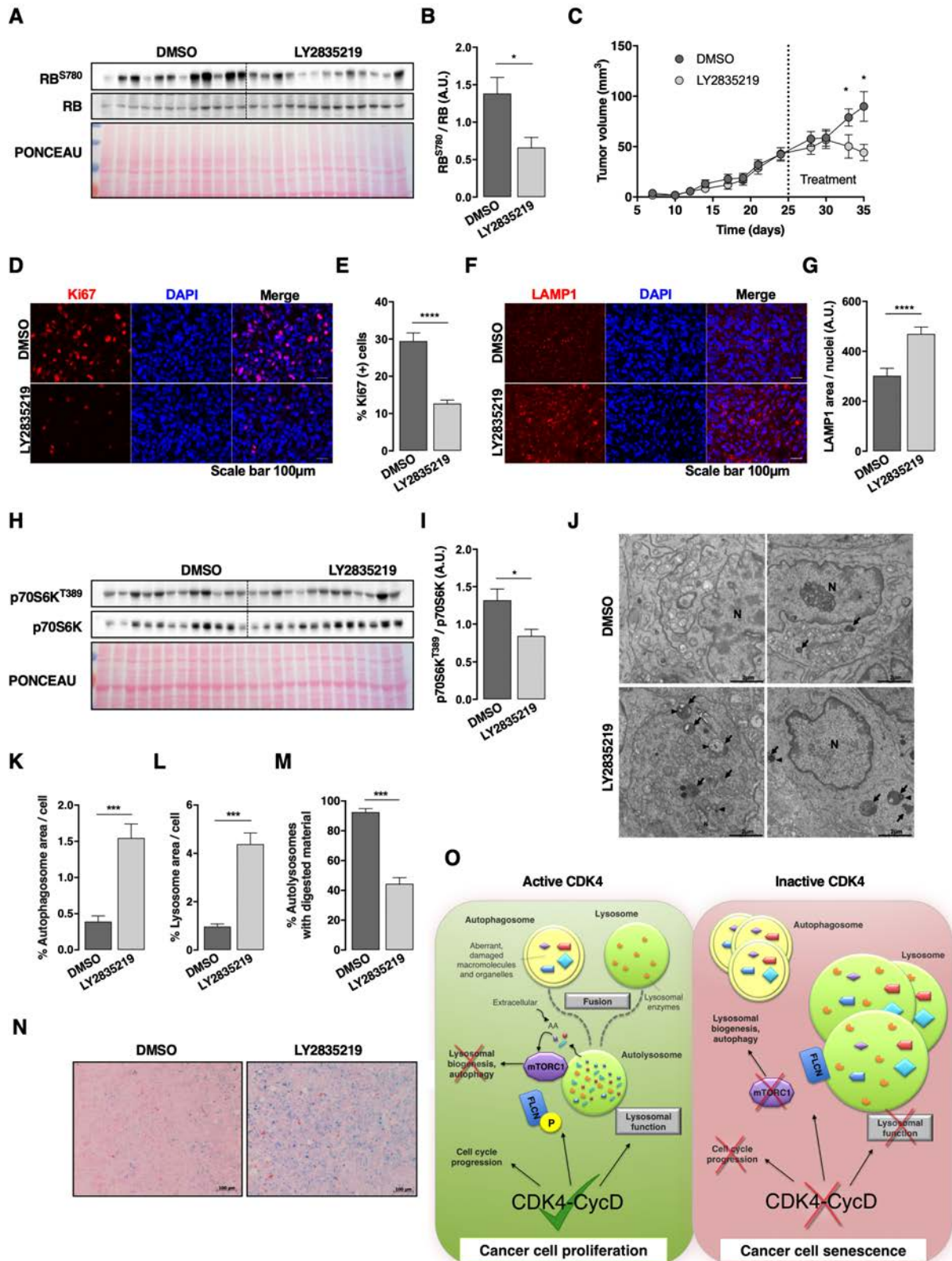
Figure 7- The CDK4/6 inhibitor LY2835219 alters lysosome morphology in a breast cancer xenograft mouse model. A, Western blot for RB and phospho-RB (S780) in tumor protein extracts of mice from both groups as a control for CDK4/6 inhibition. B, Quantification of A, as

arbitrary levels of phospho-RB (S780) normalized to total RB. C, Volume of MDA-MB-231 tumors from mice throughout the entire experiment from 8 or 9 mice per condition. When the tumors reached a volume of 50 mm^3 (day 25), gavage with either DMSO or LY2835219 started and lasted for 8 days. D, Immunohistochemistry with Ki67 antibody and DAPI for tumor sections from DMSO- or LY2835219-gavaged mice. E, Percentage of Ki67-positive cells from D. Three images per section were analyzed for 8 or 9 mice. F, Immunohistochemistry with LAMP1 antibody and DAPI of tumor sections from mouse xenograft models treated with either LY2835219 or DMSO. G, Quantification in arbitrary units of the area of LAMP1 staining normalized to the number of nuclei per field. Three images per section were analyzed for 8 or 9 mice. H, Western blot for the mTOR target protein p70S6K and its phosphorylated variant (phospho-p70S6K (T389)) from mouse tumor xenograft lysate, following gavage with either DMSO or LY2835219. I, Quantification of H, showing arbitrary levels of phospho-p70S6K (T389) normalized to total p70S6K. J, Representative electron micrographs of mouse tumor xenograft cells, showing that LY2835219 treatment increases notably the density of autolysosomes (arrows) and that these autolysosomes accumulate non-degraded materials, such as undegraded autophagosomes (arrowheads). N: nucleus. K-M, Quantification for conditions shown in J, as percentage of autophagosome area per cell (K), percentage of autolysosome area per cell (L) and the percentage of autolysosomes containing degraded material per cell (M) from EM images of mouse xenograft tumors treated with LY2835219 or control. n = 30 cells per condition. N, Colorimetric SA-β-Gal staining of tumor cell senescence in tumor xenograft sections taken from mice gavaged with LY2835219 or DMSO. O, Schematic representation of the proposed model. In cancer cells, activated CDK4 (left) promotes cancer cell proliferation through regulating cell cycle, but also through FLCN phosphorylation to ensure mTORC1 recruitment to lysosomes in the presence of amino acids (AA). In addition, CDK4 can also promote lysosomal degradation to generate amino acids, which also serve to activate mTORC1. When CDK4 is inhibited or depleted (right), cancer cell senescence is induced through impairment of cell cycle progression, and by suppressing lysosomal function, which results in mTORC1 inactivation, lysosomal biogenesis and impairment of autophagic flux. mTORC1 is dually inhibited, since unphosphorylated FLCN is retained at the surface of lysosomes also abrogating mTORC1 recruitment.
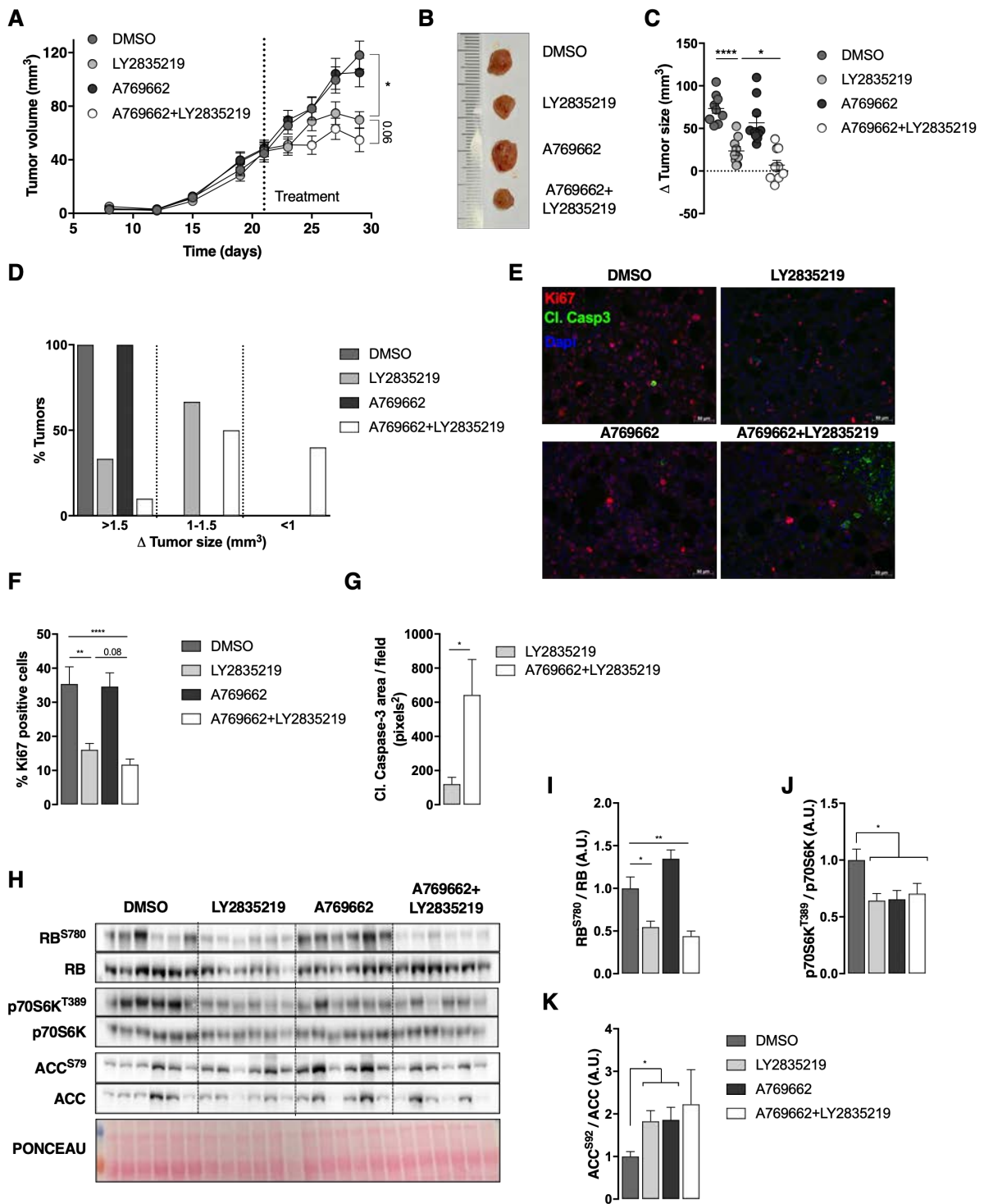
Figure 8- The CDK4 inhibitor LY2835219 in combination with the AMPK activator A769661 induces cell death in breast cancer cells and tumors.

A, Tumor volume of breast cancer xenograft in NSG mice was monitored throughout the whole experiment. Treatment started on day 21 and lasted for 8 days (n=9-10). B, Representative images from tumors at the day of sacrifice, after the corresponding treatment. C, Increment of tumor

volume per mouse: Vol day29/Vol day21. D, Representation of percentage of tumors, which increases more than 1.5 fold, from 1 to 1.5 folds or less than 1 fold. E, Ki67 and Cleaved Caspase-3 immunostaining in tumor sections after the corresponding treatment. F, Quantification from E of % Ki67 positive cells. G, Quantification from E of Cleaved-Caspase-3 area per field, comparing LY2835219 and A769662+LY2935219. H, Westernblot analysis of activation of RB, p70S6K and ACC proteins in tumor samples. I, Quantification from H of phospho-RB normalized with total RB. J, Quantification from H of phospho-p70S6K normalized with total p70S6K. K, Quantification from H of phospho-ACC, normalized with total ACC.
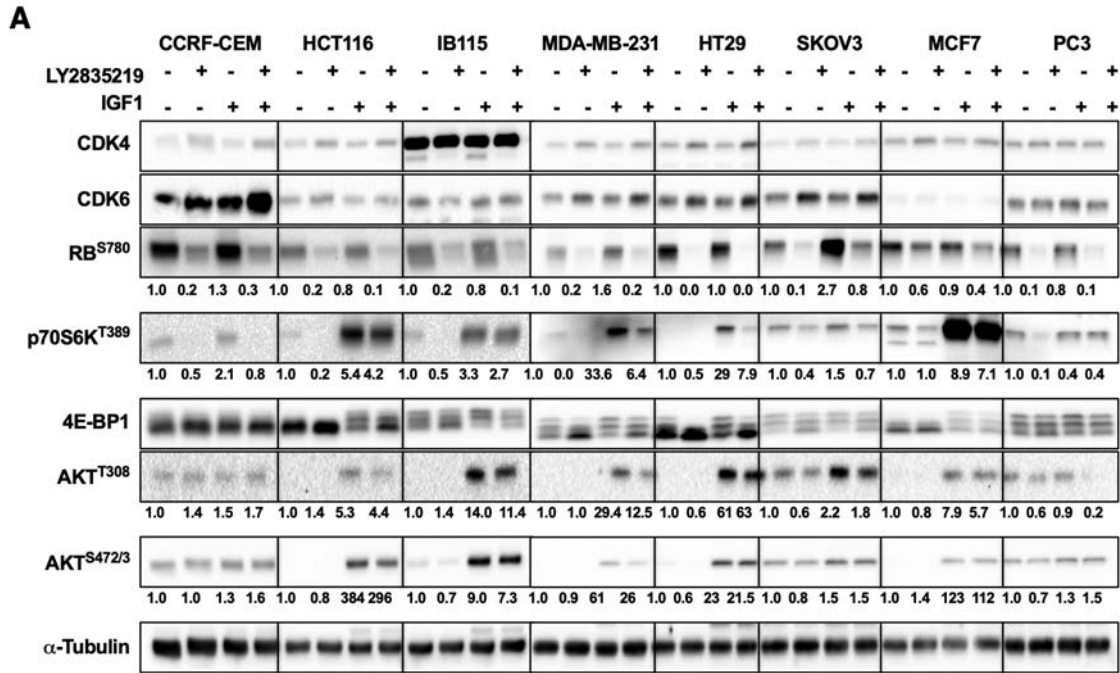
Sup. Figure 1.- CDK4 inhibition or depletion decreases mTORC1 activity in several cancer cell lines. A, Western blot showing the impact of the lack of CDK4 on downstream PI3K pathway proteins in different cancer cell lines, with or without the PI3K pathway stimulating ligand IGF-1. The relative phosphorylation level normalized to α-tubulin is indicated below the corresponding panels normalized to 1 in every cell line.
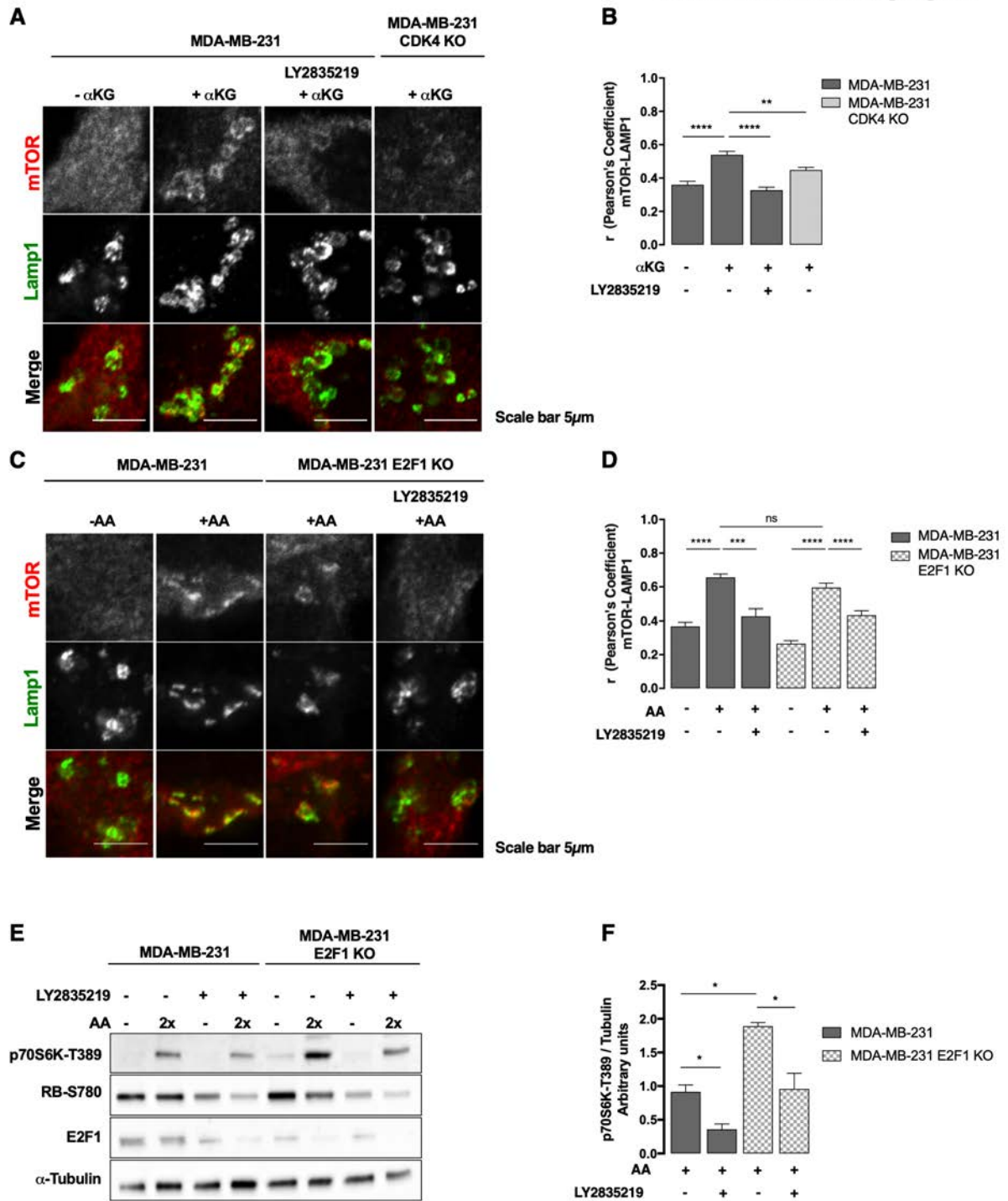
Sup. Figure 2.- CDK4 effects on mTORC1 are α-ketoglutarate and E2F1-independent. To check whether the effects of LY2835219 on MDA-MB-231 cells were due to an impairment in glutamine metabolism, we treated the cells with a cell-permeable α-ketoglutarate analog. A, Confocal immunofluorescence analysis showing mTOR colocalization with lysosomes (Lamp1) in WT and CDK4 KO MDA-MB-231, with or without 5 mM α-KG and/or 0.5 μM LY2835219. B, Quantification of colocalization from A using Pearson's coefficient. At least 20 fields per

condition were analyzed. C, Effect of CDK4 inhibition on the colocalization of mTORC1, examined using confocal immunofluorescence analysis of mTOR colocalization with lysosomes (Lamp1) in MDA-MB-231 cells lacking E2F1, and the sensitivity of these cells to LY2835219 in presence or absence of amino acid stimulation. D, Quantification of the colocalization in C using Pearson's coefficient. At least 20 fields per condition were analyzed. E, Western blot analysis of phospho-p70S6K (T389), 4E-BP1, phospho-RB (S780), E2F1 and α-tubulin in WT and E2F1 KO MDA-MB-231 cells, in the presence of glutamine and different concentrations of amino acids (AA) (0×, 1× or 2× Minimal Essential Media AA) and in the presence of DMSO or 0.5 μM LY2835219. F, Quantification of Western blot analysis in E showing phosphorylation levels of mTORC1 target molecule phospho-p70S6K (T389) normalized to α-tubulin from three independent experiments like E.

A

B
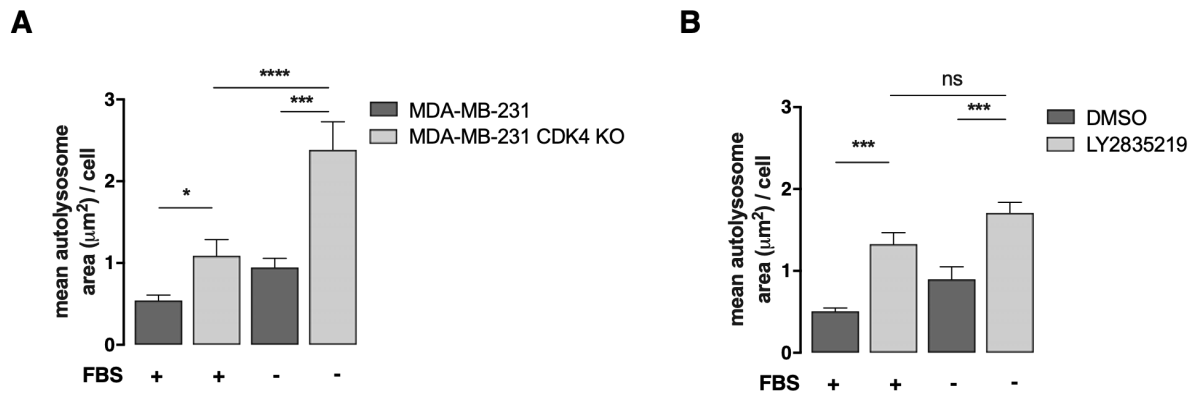
Sup. Figure 3.- CDK4 inhibition or depletion increases lysosomal mass. A, Quantifications of the mean autolysosome area per cell from electron microscope images in MDA-MB-321 WT and CDK4 KO cells, either in complete medium (+FBS) or in serum starvation conditions (-FBS). B, Quantifications of the mean autolysosome area per cell from electron microscope images in MDA-MB-321 WT cells under DMSO or LY2835219 treatment, either in complete medium or in starvation conditions (medium - FBS). n = 20 cells per condition.
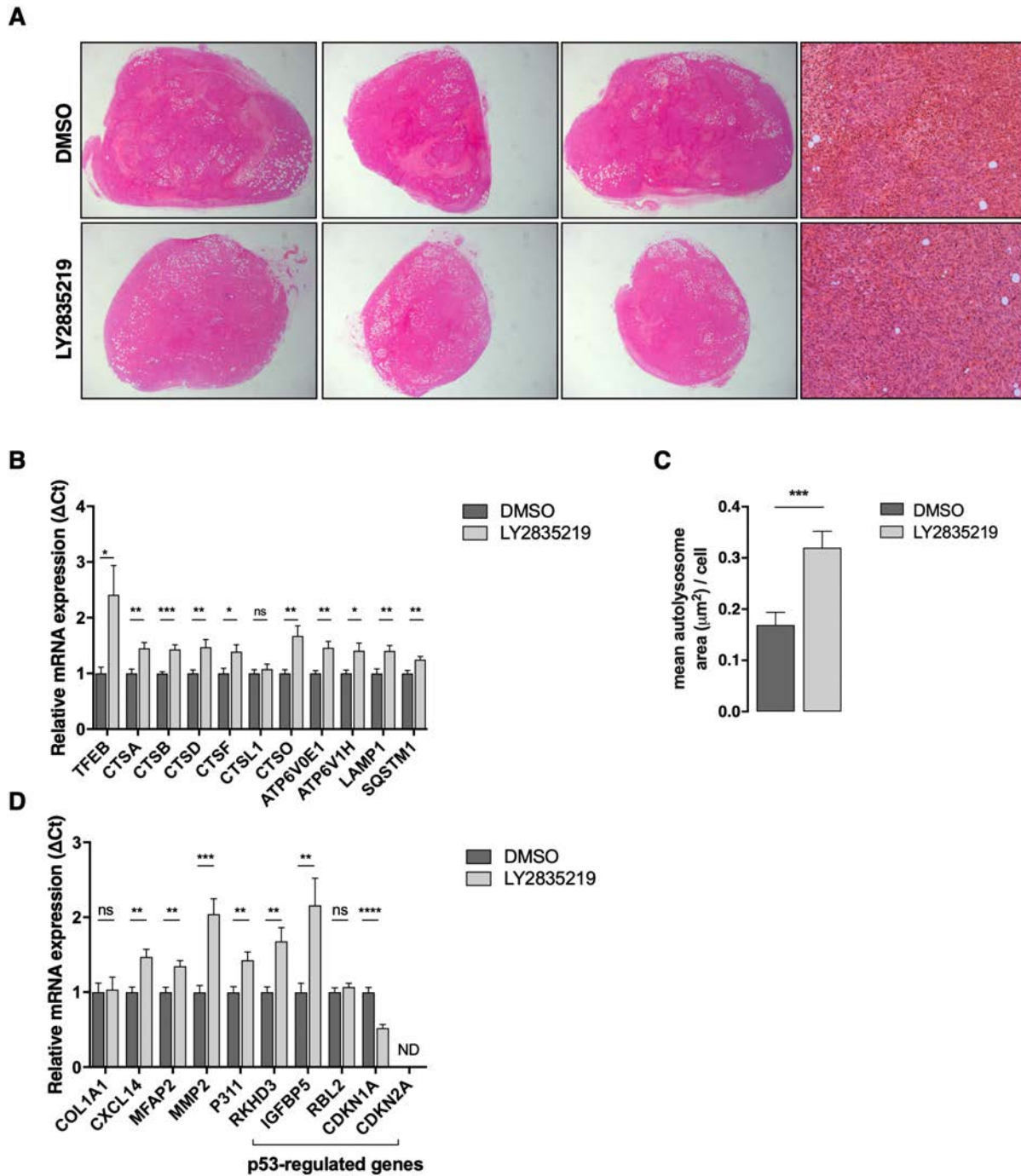
Sup. Figure 4.- Hematoxylin and eosin staining and gene expression analysis of tumors from mice treated with or without LY2835219.

A, Hematoxylin and eosin staining of tumor sections from DMSO- or LY2835219-treated mice, to confirm the lack of immune cell infiltration (whole tumor and with 20X objective). B, Gene expression of all lysosomal and autophagic genes examined by qPCR from DMSO- or LY2835219-treated mice. 8 or 9 mice per condition were analyzed C, Quantifications of the

mean autolysosome area per cell from electron microscope images of tumor sections from DMSO- or LY2835219-treated mice. n=30 cells per condition. D, Gene expression of genes usually upregulated in senescence (including p53-regulated genes) examined by qPCR from DMSO- or LY2835219-treated mice. 8 or 9 mice per condition were analyzed.
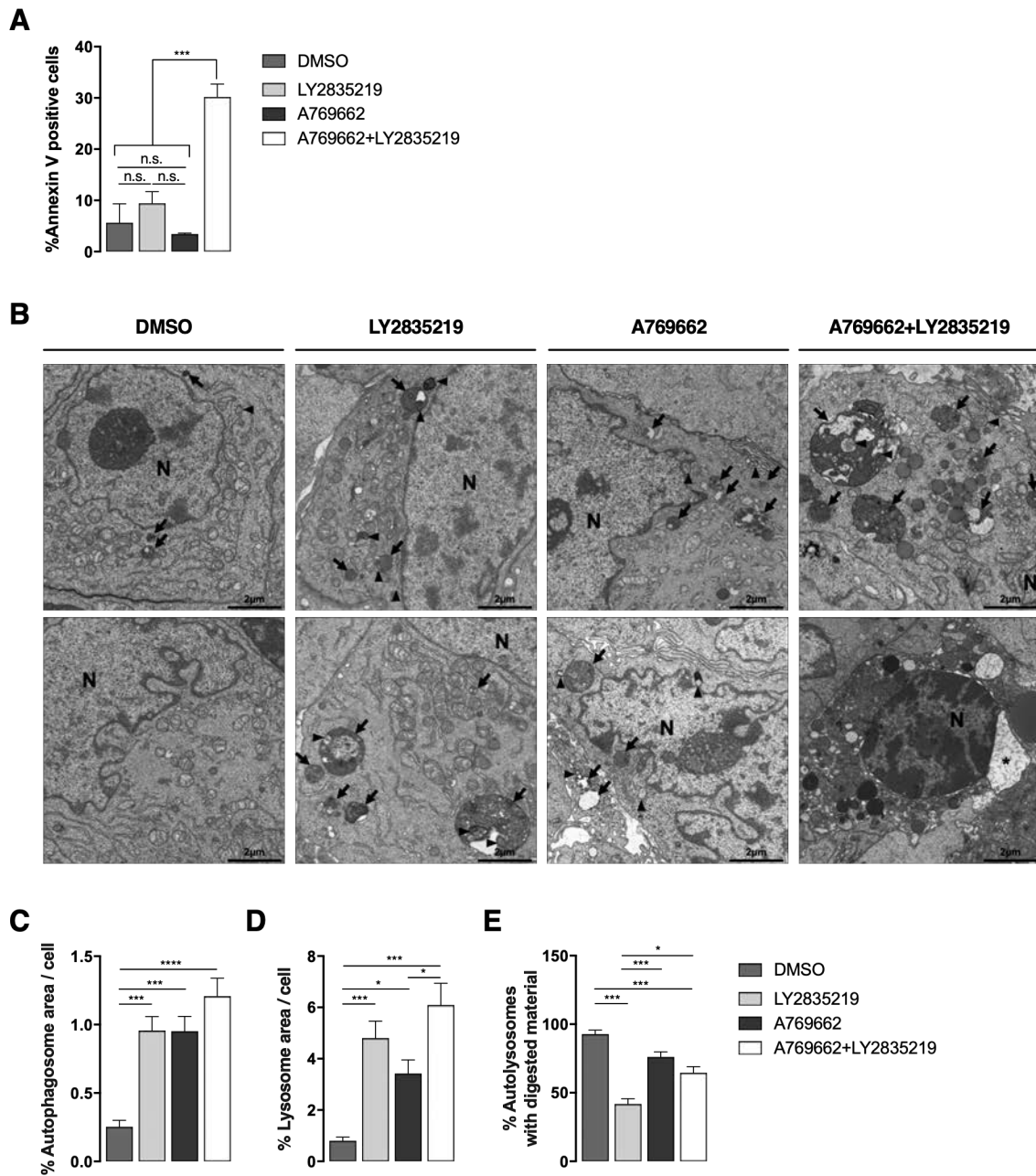
Sup. Figure 5. *In vitro* **cell death analysis and** *in vivo* **electron microscopy analysis of tumors treated with DMSO, LY2835219, A769662 and the combination of A769662 with LY2835219.** A, Percentage of Annexin V positive cells assessed by flow cytometry of MDA-MB-231 cells cultured for 8 days with the corresponding treatment. B, Representative electron micrographs of tumors from mice treated with DMSO, LY2835219, A769662 and the combination of A769662 with LY2835219. The arrowheads represent the autophagosomes and the arrows, the autolysosomes with undigested material inside. * Indicates the focal swelling of the perinulear membrane, and N represents nucleus. C, Quantification from B, of the percentage of autophagosome area per

cell. D, Quantification from B, of the percentage of lysosome area per cell. E, Quantification from B, of the percentage of autolysosomes with digested material inside. n = 30 cells per condition. Values are mean ± SEM, *$P < 0.05$;***$P < 0.001$

_____

241

Inter-organ communication: a gatekeeper for metabolic health

Castillo-Armengol J, Fajas L and Lopez-Mejia IC.

More recently, I had the chance to write an invited review from EMBO Reports on a very interesting subject, which is the inter-organ communication in metabolism. This very challenging article summarizes some of the interactions between organs related to physiological conditions.

Inter-organ communication: a gatekeeper for metabolic health

Judit Castillo-Armengol[1,] Lluis Fajas[1]* and Isabel C. Lopez-Mejia[1]*

[1]Center for Integrative Genomics, University of Lausanne, 1015 Lausanne, Switzerland.

*Corresponding authors: Isabel C. Lopez-Mejia and Lluis Fajas, University of Lausanne, Center for Integrative Genomics, Quartier UNIL-Sorge, Bâtiment Génopode, CH-1015 Lausanne, Switzerland

E-mail : lluis.fajas@unil.ch, isabel.lopezmejia@unil.ch

Abstract

Multidirectional interactions between metabolic organs in the periphery and the central nervous system have evolved concomitantly with multicellular organisms to maintain whole-body energy homeostasis and ensure the organism's adaptation to external cues. These interactions are altered in pathological conditions such as obesity and type 2 diabetes. Bioactive peptides and proteins, such as hormones and cytokines, produced both by peripheral organs and the central nervous system, are the key messengers in this inter-organ communication. Despite the early discovery of the first hormones more than one hundred years ago, recent studies taking advantage of novel technologies have shed light on the multiple ways the cells in the body communicate to maintain energy balance. This review focuses on how the crosstalk between gut, brain, and other peripheral metabolic organs maintains energy homeostasis and how the improved knowledge about these interorgan networks is helping us redefine therapeutic strategies to fight metabolic disease and promote healthy living.

<u>Introduction</u>

In order to maintain homeostasis and adapt to external conditions the different tissues of multicellular organisms communicate with each other via different sorts of signals. Peripheral organs produce a plethora of bioactive molecules, including hormones (from the Greek *horme* that means impulsion), that ensure intercellular signaling in an autocrine, paracrine or endocrine manner. Peripheral organs and immune cells can also produce smaller bioactive proteins, namely cytokines (Dinarello, 2007), that also participate in inter-organ communication. On the other hand, the nervous system coordinates whole body metabolism not only by the production of neurohormones that act locally, but also by direct innervation of the target tissues. Indeed, sympathetic and parasympathetic fibers innervating peripheral tissues express enzymes crucial for the biosynthesis and transport of specific molecules (neurotransmitters and neuropeptides) necessary for the response to tissue-specific adaptation to external cues.

Work from the nineteenth century, notably from Claude Bernard, first suggested that a system involving chemical messengers ensured the communication between the different organs of the body (Bernard, 1853). The term "hormone" was first used in 1905 by the british physiologist Ernest Stalling, that had described the gut hormone Secretin, just three years prior (Bayliss & Starling, 1902, Tata, 2005). Carl Ferdinand Cori and Gerty Cori then described the cycle in which lactate produced by anaerobic glycolysis in muscles can be recycled by liver and converted to glucose, to then returns to the muscle and be metabolized back to lactate (Cori & Cori, 1946). The Cori cycle was one of the first described examples of an efficient communication system between organs which functions to facilitate the metabolic adaptation to the energy demands.

Key metabolic hormones, like pancreatic insulin and glucagon, were successfully identified, synthesized and used for therapy in the course of the XXth century; however the identification of signaling molecules produced by metabolic organs has increased exponentially in recent years, giving rise to the terms hepatokines (Meex & Watt, 2017), myokines (Giudice & Taylor, 2017), adipokines (Fasshauer & Bluher, 2015) and batokines (Villarroya, Cereijo et al., 2017), for the hormones produced by liver, muscle, white adipose tissue (WAT) and brown adipose tissue (BAT) respectively. The secretion of these signaling molecules varies according to the metabolic status of the body. They respond for instance to fasting and feeding cycles, to the circadian rhythm (Gnocchi & Bruscalupi, 2017), to cold exposure and to exercise, thus participating in the organism adaptive response and ensuring metabolic flexibility. Inter-organ communication is altered in different pathologic conditions, for example in conditions related to adipose tissue dysfunction, like obesity. As such, alterations in hormones and cytokines are currently known to notably contribute to the spectrum of obesity-associated pathologies. Therefore, pharmacological interventions to modify the production of hormones/cytokines, or directly delivering recombinant hormones/cytokines, are currently being explored as promising pharmacological approaches to treat a wide variety of obesity-related endocrine diseases. In this review we will focus in how recent research has highlighted the importance of the crosstalk between gut, brain and other peripheral metabolic organs, like WAT, BAT, pancreas, liver and muscle, in the maintenance of metabolic fitness.

<u>Inter-organ communication in the control of fasting/feeding cycles</u>

Gut-WAT-Brain axis

The physiological response to a meal ingestion initiates in the gut and is triggered by the presence of nutrients. Entero-endocrine cells sense nutrients in the intestinal lumen and produce peptides such as cholecystokinin (CCK), secretin and the incretins glucose-dependent insulinotropic peptide (GIP) and glucagon-like peptide 1 (GLP-1) (Batterham, Cowley et al., 2002, Turton, O'Shea et al., 1996). Gut hormones play their role by directly acting on target tissues via the circulation or by activating intestinal neurons in a paracrine manner. A major target for gut-derived hormones is the vagal afferent neurons (VANs) (Ronveaux, Tome et al., 2015). Endogenous GLP-1 acts on VANs to inhibit food intake. The actions of GLP-1 are further modulated by the fact that GLP-1 receptors (GLP-1R) are internalized upon fasting conditions, but translocate to the plasma membrane after a meal, when ghrelin levels are low. Indeed GLP-1 and GIP work synergistically to potentiate glucose-stimulated insulin secretion by pancreatic β-cells (Ronveaux et al., 2015). Moreover, GLP-1 inhibits glucagon production by pancreatic α-cells. Secretin stimulates exocrine pancreas activity to ensure a proper environment for digestion and absorption of nutrients. Moreover, secretin can also inhibit food intake via the activation of secretin receptor (SctR) in vagal sensory nerves and melanocortin signaling in the brain (Cheng, Chu et al., 2011, Chu, Cheng et al., 2013).

After the postprandial regulation initiated in the gut, the changes in circulating levels of nutrients, mainly glucose and triglycerides (TG), will also engage the response of several peripheral organs and the nervous system. An increase in circulating glucose levels will be sensed by pancreatic β-cells through the glucose transporter GLUT2. Glucose sensing will lead to a β-cell response that ultimately leads to insulin secretion (Tokarz, MacDonald et al., 2018). In parallel, glucose

inhibits the release of glucagon from the pancreatic α-cells (Kersten, 2001, Vieira, Salehi et al., 2007). Insulin will target insulin-sensitive organs, like brain, WAT, muscle and liver to induce glucose utilization and storage to prevent hyperglycemia. In the brain, insulin regulates feeding behavior, and modifies energy metabolism in liver and adipose tissue, as well as several more cognitive functions (Bruning, Gautam et al., 2000, Gray, Meijer et al., 2014, Lee, Zabolotny et al., 2016). In liver, insulin promotes metabolization of glucose by hexokinases, while decreasing hepatic glucose production. Intact hepatic insulin signaling is however dispensable for the postprandial repression of hepatic glucose production in the absence of hepatic FoxO1 (I, Zhang et al., 2015, Titchenell, Chu et al., 2015), highlighting the importance of hypothalamic insulin signaling in the control of liver glucose metabolism (Obici, Zhang et al., 2002). On the other hand, insulin triggers glucose uptake by promoting the externalization of the glucose transporter GLUT4 in WAT and muscle, glycogen synthesis in muscle, and *de novo* lipogenesis by promoting the expression and activity of fatty acid synthesis enzymes specifically in WAT. In WAT, glucose- derived glycerol serves as building blocks for TGs, in turn TGs serve as a fuel stock for energy scarcity conditions. In order to avoid excessive food intake, excessive adiposity and needless energy storage, which have deleterious effects for the organism, WAT also has the capability to act as a hormone producing organ. Leptin is secreted by white adipocytes proportionally to TG stores (Frederich, Hamann et al., 1995, Ingalls, Dickie et al., 1950, Zhang, Proenca et al., 1994). Leptin is widely known to target the central nervous system, that highly expresses the long from of leptin receptor (LepRb). By binding LepRb and signaling via Janus Kinase 2 (JAK2) and signal transducer and activators of transcription 3 (STAT3) in the brain, leptin signals to maintain energy stores constant. Indeed, leptin

suppresses food intake and the production of adrenal corticosteroids while promoting energy expenditure and decreasing insulin secretion (Pan & Myers, 2018, Stern, Rutkowski et al., 2016). Leptin can also activate glucose uptake in BAT, as well as glucose uptake and fatty acid oxidation in muscle in an AMP-activated protein kinase (AMPK) dependent manner (Minokoshi, Kim et al., 2002), but whether this is direct or indirect remains to be fully elucidated (D'Souza A, Neumann et al., 2017).

More recently, the liver-expressed antimicrobial peptide 2 (LEAP2), a peptide first described as an antimicrobial liver produced peptide, was described to be produced also by the gut. LEAP2 is produced by the liver and the small intestine in the fed state and its secretion is suppressed by fasting. Importantly, LEAP2 was reported to be an endogenous antagonist of the growth hormone secretagogue receptor (GHSR), the ghrelin receptor. Indeed, LEAP2 can fully blunt GHSR activation by ghrelin, thus reducing food intake and Growth Hormone (GH) release (Ge, Yang et al., 2018). This recent study adds LEAP2 to the growing list of hormones that connect gut, brain and other peripheral organs in the metabolic control.

As such, we have described in this section how several organs from the body, mainly gut, brain, pancreas and WAT, communicate in the fed state. Upon ingestion of a meal the aforementioned organs orchestrate a coordinated response in order to ensure proper digestion and storage of energy substrates, while initiating a negative feedback loop involving satiety and increased energy expenditure to maintain energy homeostasis by preventing an excessive "positive energy balance" **(Figure1)**.

Gut-brain and brain-periphery axes

When the organism's energy levels are low, the lack of food in the stomach, as well as the decrease in blood glucose, are sensed in order to replenish energy stores and to produce alternative substrates to keep all organs functioning. Ghrelin is mainly secreted by the gastric epithelium when the stomach is empty. Plasma concentrations of ghrelin are high during fasting and robustly decrease in a postprandial state (Cummings, Purnell et al., 2001). Ghrelin was first described as a potent inducer of GH secretion (Kojima, Hosoda et al., 1999), but is now known to stimulate food intake, adiposity, and to maintains glucose levels by binding to its receptor GHSR. Ghrelin exerts its orexigenic effects centrally in the arcuate nucleus (ARC) of the hypothalamus by triggering the expression of agouti-related protein (AgRP) and Neuropeptide Y (NPY) in order to increase appetite. However, the exact mechanism by which ghrelin plays its central role remains unclear. So far 3 hypotheses have been put forward: 1) ghrelin acts by activating VANs, 2) ghrelin is synthesized locally in response to feeding and 3) ghrelin will cross the blood–brain barrier and activate its receptor in the hypothalamus (Al Massadi, Lopez et al., 2017). Ghrelin attenuates insulin production and increases blood glucose concentration by promoting the intracellular localization of the pancreatic β-cell GLP-1R under fasting conditions, thus counteracting GLP-1 signaling (Ronveaux et al., 2015). Ghrelin also stimulates glucagon secretion in pancreatic α-cells (Chuang, Sakata et al., 2011). Moreover, ghrelin can directly promote adiposity, independently of food intake or GH secretion, by increasing carbohydrate use, stimulating lipid synthesis and reducing fatty acid oxidation (Al Massadi et al., 2017, Tschop, Smiley et al., 2000). The effects of ghrelin on adiposity have been shown to require intact sympathetic nervous system signaling (Theander-Carrillo, Wiedmer et al., 2006).

Adipokine secretion is also modified in low energy conditions. Leptin circulating levels rapidly decrease upon fasting. This reduction in leptin promotes a switch between the "fasted state" and the "fed state" by promoting food intake and reducing energy expenditure (Jackson & Ahima, 2006). In contrast to leptin, adiponectin levels increase in low glucose and low insulin conditions, at least in the cerebrospinal fluid (CSF) (Kubota, Yano et al., 2007, Steinberg & Kemp, 2007). Adiponectin levels are overall inversely proportional to adiposity and correlate with improved metabolic fitness. Numerous studies have reported that adiponectin targets numerous tissues (Adiponectin receptors AdipoR1/2 are essentially ubiquitous). In the brain, adiponectin activates AMPK signaling in hypothalamic ARC, resulting in an increase in food intake and a reduction in energy expenditure, suggesting that in the hypothalamus adiponectin promotes feeding and inhibits the anorexigenic effects of leptin (Kubota et al., 2007, Steinberg & Kemp, 2007). In the peripheral tissues, adiponectin promotes liver insulin sensitivity via several independent mechanisms: an AMPK-dependent mechanism involving increased ACC phosphorylation, an AMPK-independent mechanism that involves a reduction in liver ceramide levels (Holland, Miller et al., 2011) and an IL6-dependent mechanism that involves the upregulation of Insulin receptor substrate 2 (IRS-2) through the activation of STAT3 (Awazawa, Ueki et al., 2011). Adiponectin reduces hepatic de novo lipid synthesis and increases hepatic fatty acid oxidation (Stern et al., 2016). The effects of adiponectin in hepatic glucose production remain debated (Stern et al., 2016). Asprosin, a novel fasting-induced adipokine that promotes hepatic glucose production was recently described (Romere, Duerrschmid et al., 2016). Asprosin is the C-terminal cleavage product of profibrillin (FBN1 gene). It is encoded by the last 2 exons of FBN1 and is mainly produced by adipose tissue in

mice. Asprosin directly targets liver and promotes glucose release, without increasing plasma levels of glucagon, catecholamines and glucocorticoids, and independently from the glucagon receptor signaling and from the β-adrenergic receptor (Romere et al., 2016). Importantly, insulin can counteract the effects of Asprosin on hepatic protein kinase A (PKA) signaling and glucose release (Romere et al., 2016).

Fibroblast growth factor 21 (FGF21) was first identified as an hepatokine (Kharitonenkov, Shiyanova et al., 2005). It was shown to be necessary for the adaptation to fasting in 2007 (Badman, Pissios et al., 2007, Inagaki, Dutchak et al., 2007). Indeed, liver expression and plasma levels of FGF21 levels are markedly increased upon fasting. FGF21 then increases adipose tissue lipolysis, as well as hepatic fatty acid oxidation and ketogenesis, thus ensuring the availability of substrates for the brain. It is worth noting that FGF21 knockout mice are viable and "only" show lower glycemia in the fasted state, and lower plasma levels of ketone bodies in both the fasted and the fed state (BonDurant & Potthoff, 2018, Potthoff, Inagaki et al., 2009).

Fasting induced hypoglycemia also results in the stimulated secretion of glucagon. Hypoglycemia is directly sensed by GLUT2 positive hypothalamic neurons that promote glucagon secretion via an increase in parasympathetic input (Lamy, Sanno et al., 2014). Glucagon signals to the liver through the PKA signaling pathway to stimulate 1) the mobilization of hepatic glycogen (glycogenolysis) and, if the fasting is prolonged, 2) hepatic de novo glucose synthesis (gluconeogenesis) and 3) to repress glycolysis and glycogenesis. To ensure the availability of alternative substrates for the peripheral organs, and to allow glucose production for the brain, glucagon also triggers lipolysis in WAT. TGs are metabolized into free

fatty acids and glycerol. Glycerol is transported to the liver to be oxidized or used as a substrate for gluconeogenesis. Albumin-bound fatty acids are transported in the bloodstream to serve as oxidation substrates for the liver, muscle and other tissues. WAT lipolysis can also directly be promoted by direct sympathetic nervous system (SNS) innervation. Indeed, SNS fibers can release norepinephrine (NE) locally and exert the "same" effects as glucagon. This increased SNS tone in WAT could be directly triggered by hypoglycemia sensing in the brain (Garretson, Szymanski et al., 2016, Geerling, Boon et al., 2014). Notably, direct innervation of WAT is sparse (Zeng, Pirzgalska et al., 2015), therefore cell-to-cell communication via connexin 43 (CX43) containing gap junctions is essential to disseminate adrenergic activation signals (Zhu, Gao et al., 2016).

Overall, in this section we described how inter-organ communication in situations of food deprivation **(Figure 2)**. This counter regulatory response aims to promote food intake, maintain blood glucose levels high enough to prevent alterations in brain function and ensure that other substrates are available to all organs. This is accompanied by an overall reduction of energy expenditure in order to preserve energy.

Inter-organ communication in non-shivering thermogenesis

In order to adapt to cold exposure and maintain body temperature, different strategies have been developed by homeotherms. Mammals have BAT, a highly specialized tissue that functions to produce heat(Cannon & Nedergaard, 2004). BAT is especially abundant in hibernating mammals (Gesta, Tseng et al., 2007), but can also be found in adult humans (Cypess & Kahn, 2010).

Brain – BAT axis

The main organ that regulates the response to cold is the central nervous system (CNS). Cold is sensed by the terminals of sensory neurons found in skin, then, these signals are transmitted and integrated in the hypothalamic preoptic area (POA), also known as the thermoregulatory center (Zhang & Bi, 2015). The transduction of the signal will stimulate other hypothalamic regions, namely the Lateral Hypothalamic Area (LHA), the Ventromedial Hypothalamus (VMH), the Dorsomedial Hypothalamus (DMH) and the Arcuate Nucleus (ARC).

Orexin producing neurons that are located in the LHA, named orexin neurons, participate in the regulation of thermogenesis. The central administration of orexin peptide has been described to stimulate BAT activation and therefore, thermogenesis (Sellayah, Bharaj et al., 2011). Moreover, orexin infusion into the VMH can stimulate the sympathetic firing in BAT (Monda, Viggiano et al., 2005). Both the LHA and the VMH can synergistically interact and activate BAT. Hypothalamic expression of Bone morphogenetic protein 8b (BMP8b) in the VMH stimulates orexin secretion in the LHA through a decrease in AMPK activity, and thus enhances the firing of projections that will stimulate BAT thermogenesis (Martins, Seoane-Collazo et al., 2016). Interestingly, BMP8b can also be produced

in BAT and promote NE signaling locally, activating the mitogen-activating protein kinase (MAPK) pathway and lipolysis in brown adipocytes (Whittle, Carobbio et al., 2012).

Several studies have linked the DMH with the response to cold. For instance, a chemical stimulation of this area increases the thermogenic response in rats (Zaretskaia, Zaretsky et al., 2002). Similarly, administration of the incretin hormone GLP-1 in the DMH increases BAT thermogenesis (Lee, Sanchez-Watts et al., 2018).

Outflow from these areas is triggered by the premotor neurons found in the brain stem region Raphe Palidus (RPA). It has been broadly discussed that sympathetic nerves are abundant within the parenchyma of adipose tissue. These nerves express tyrosine hydroxylase, the enzyme responsible for the secretion of the catecholamine hormone NE (Bartness, Vaughan et al., 2010). BAT is the major catecholamine-responsive tissue. It is mainly constituted by brown adipocytes that contain numerous lipid droplets and a high number of mitochondria. Norephineprine stimulates the β3-adrenergic receptor (ADBR3) and activates the cAMP/PKA pathway, thus triggering lipolysis and increasing the expression of uncoupling protein 1 (UCP1). Free fatty acids, resulting from the lipolysis, are used both as energy substrates and as activators of UCP1 to uncouple ATP production from mitochondrial respiration into heat (Cannon & Nedergaard, 2004, Fedorenko, Lishko et al., 2012).

Apart from catecholamines, thyroid hormones can also trigger BAT activity (Obregon, 2014). The thyroid hormones T3 and T4 are synthetized in the thyroid gland upon hypothalamic stimulation of the pituitary gland and Thyroid-stimulating hormone (TSH) production (Brent, 2012). Thyroid hormones access brown adipocytes from the blood stream through specific transporters. In brown adipocytes

T4 can be converted to its active form T3 via the type 2 iodothyronine deiodinase (DIO2) thus compensating for the low levels of secreted T3 by the thyroid gland (Bianco & McAninch, 2013). T3 directly activates lipolysis through the PKA pathway. The relevance of thyroid hormone regulation for BAT function is illustrated by the blunted thermogenic response observed in DIO2 knockout mice, despite an increased UCP1 expression (Christoffolete, Linardi et al., 2004).

Liver-BAT-WAT axis

If cold stress is sustained overtime, a process that is called browning is triggered. This process is characterized by the appearance of brite (from **br**own-in-wh**ite**) adipocytes, also called beige adipocytes, mainly in subcutaneous WAT. Brite adipocytes can express UCP1 and as such, can participate in the maintenance of body temperature (Wu, Cohen et al., 2013). Brown and brite adipocytes play a key role in energy homeostasis. Their potential contribution to global energy expenditure has opened the door to new human therapeutic strategies against obesity and diabetes. UCP1-expressing adipocytes (brown and brite) are capable of participating in the regulation of glucose homeostasis due to their high capability to uptake glucose. They can also contribute enormously to the clearance of circulating lipids, and can therefore increase insulin sensitivity. Due to the potential therapeutic effect of increasing overall energy consumption by promoting brite and brown adipose cell metabolism, recent research has focused on the identification of natural hormones or compounds with the capability to promote thermogenic function, such as FGF21, irisin and Bile acids (BAs).

Under cold exposure, FGF21 can be secreted by BAT and WAT, have a paracrine effect and stimulate the expression of thermogenic genes (Hondares,

Iglesias et al., 2011). Some teams have reported that FGF21 knockout mice have impaired adaptation to chronic cold exposure and decreased browning of WAT (Fisher, Kleiner et al., 2012). However, others have shown that the lack of FGF21 in long-term cold adaptation does not impair the thermogenic response of mice (Keipert, Kutschke et al., 2017). Despite the evidence of FGF21 production in WAT, controversial results were published by Véniant *et al* who showed that beneficial effects of weight loss observed after cold were not directly related to FGF21-induced browning (Veniant, Sivits et al., 2015). However, hepatic FGF21 production can also be induced by cold, and blunted hepatic FGF21 secretion, but not adipocytic FGF21 secretion, results in impaired cold tolerance and decreased sympathetic nerve activity in BAT (Ameka, Markan et al., 2019). Importantly, hepatic FGF21 requires intact expression of the FGF21 receptor β-klotho in adipose tissue for its thermogenic effect, but its expression is increased upon acute cold exposure (6 hours maximum) but decreased after a longer cold exposure (3 days) (Ameka et al., 2019). In conclusion, additional studies are needed to completely elucidate the role of FGF21 in the control of non-shivering thermogenesis.

Besides their role in the digestion of dietary lipids, hepatic BAs can be induced by cold exposure (Worthmann, John et al., 2017). It has been described that BA secretion increases energy expenditure in BAT by enhancing the enzymatic activity of DIO2 and therefore, regulating thyroid hormone metabolism in BAT(Watanabe, Houten et al., 2006). Moreover, studies using BA receptor TGR5 adipose tissue specific knockout mice proved that BAs also participate in the browning of WAT. These mice show neglectable browning and exhibit reduced cold tolerance due to reduced adipose mitochondrial fusion (Velazquez-Villegas, Perino et al., 2018).

Historically, UCP1 has been considered indispensable for thermogenesis in BAT. However, recent research demonstrates that UCP1 is not essential for non-shivering thermogenesis (Keipert et al., 2017, Long, Roche et al., 2018, Long, Svensson et al., 2016). Peptidase M20 domain-containing 1 (PM20D1), a secreted enzyme produced by brown and brite adipocytes, has been recently discovered to contribute to this alternative thermogenesis by participating in the uncoupling of mitochondria in an UCP1-independent manner (Long et al., 2018, Long et al., 2016).

Gut - Brain - BAT axis

Cold is not the only stimulus that activates non-shivering thermogenesis. It has been demonstrated by several groups that there is a meal-associated thermogenesis (Glick, 1982, M, Saari et al., 2018, Saito, 2013). The activation of feeding-responsive thermogenesis has been strongly associated to food intake regulation by inhibiting orexigenic activation in the brain, revealing a Gut-Brain-BAT-Brain axis (Kelsey, 2018). In particular, feeding activates the secretion of periprandial gut hormones, such as CKK, GLP-1 or secretin (Beiroa, Imbernon et al., 2014, Blouet & Schwartz, 2012, Li, Schnabl et al., 2018). Most of these

molecules act through the brain, like GLP-1 and CCK, where they increase sympathetic activation and therefore stimulate the local release of NE in the BAT. Interestingly, secretin can stimulate BAT thermogenesis in a non-sympathetic manner, and contribute to induce satiation. A secretin injection in fasted mice directly activates BAT thermogenesis by increasing lipolysis in this through the cAMP-PKA pathway. Moreover, secretin treatment increases the expression of the anorexigenic proopiomelanocortin (POMC) peptide in the hypothalamus and therefore, reduces food intake (Li et al., 2018).

WAT-Brain-WAT axis

Apart from its role in the regulation of food intake described above, leptin can increase energy expenditure by inducing BAT activation. The actions of leptin and insulin actions in POMC neurons, can also be triggered by a decrease of the hypothalamic levels of T cell-protein tyrosine phosphatase (TCPTP), which is a negative regulator the insulin signaling, to further increase the browning of WAT and energy expenditure (Dodd, Andrews et al., 2017, Dodd, Decherf et al., 2015). This mechanism can limit the effects of diet-induced obesity (DIO).

In this section we described how brown and beige adipose tissue thermogenesis are activated not only to adapt to cold stress **(Figure 3)**, but also to prevent the excessive energy storage that could lead to obesity and thus maintain general energy homeostasis in the organism.

Inter-organ communication during exercise

Physical exercise was first described to have beneficial effects for health in 450 BC by Hippocrates (Febbraio, 2017). Despite early hypothesis suggesting that

muscle releases a hypoglycemic "humoral factor" in response to glucose demand (Goldstein, 1961), part of the molecular mechanisms behind this observation have only been described in the past years. Indeed, physical exercise is not only beneficial because of the immediate increase in energy expenditure, it also remodels whole body energy metabolism. The ensemble of muscle derived peptides and proteins, currently referred to as myokines is, at least in part, responsible for exercise whole body health benefits. Recent analysis of muscle secretome revealed that aerobic exercise or strength training trigger the secretion of numerous myokines (Giudice & Taylor, 2017). Importantly, it is worth noting that the production of "positive" myokines is as much promoted by physical exercise as it is repressed by physical inactivity, further highlighting the importance of lifestyle for health span (Hoffmann & Weigert, 2017).

More precisely, during exercise skeletal muscle tightly interacts with adipose tissue, pancreas and liver to sustain the energy demands of physical activity and mediate positive effects in whole body energy metabolism. The first exercise-induced myokine to be described was Interleukin 6 (IL6) (Petersen & Pedersen, 2005). Exercise-induced IL6 production was initially believed to be linked to muscle damage, but has now been proven to directly depend on contraction and to mediate muscle glucose uptake, increased insulin sensitivity, as well as increased fatty acid oxidation. IL6 also triggers insulin production in pancreas, hepatic glucose production and adipose tissue lipolysis, thus ensuring the availability of energy substrates for exercising muscle (Giudice & Taylor, 2017, Pedersen & Febbraio, 2012). IL6 also has the ability to induce an anti-inflammatory response by reducing tumor necrosis factor α (TNFα) production while increasing the levels of interleukin 10 (IL10), interleukin 1 receptor antagonist (IL1Ra) and interleukin 15 (IL15) (Leal,

Lopes et al., 2018, Pedersen & Febbraio, 2012). Future studies using tissue specific IL6 knockout mice will be required, however, to fully elucidate to which extent muscle IL6 contributes to the positive effects of exercise and to determine if the anti-inflammatory effects of IL6 are muscle-cell autonomous or not (Giudice & Taylor, 2017, Leal et al., 2018).

Irisin (FDNC5), an exercise-dependent myokine, was first described in 2012 by Bostrom and colleagues (Bostrom, Wu et al., 2012). Irisin was shown to trigger WAT remodeling by increasing p38 signaling, UCP1 expression and therefore browning (Bostrom et al., 2012, Zhang, Li et al., 2014). Irisin can also increase muscle oxidative metabolism and substrate (glucose and fatty acid) uptake, reduce hepatic glucose output (Perakakis, Triantafyllou et al., 2017) and increase cognitive function (Lourenco, Frozza et al., 2019). Interestingly, cold-induced muscle shivering can increase circulating irisin levels and promote brown fat thermogenesis (Lee, Linderman et al., 2014) **(Figure 3)**.

Some groups have suggested that irisin can also be produced and secreted by adipose tissue and liver (Roca-Rivada, Castelao et al., 2013). Nonetheless, some inconsistencies have been found between human and mice and in the methodology used (Fiuza-Luces, Santos-Lozano et al., 2018), which adds more complexity to the functions of irisin in energy homeostasis. In addition, FGF21 has also been proposed to be produced by skeletal muscle in response to the PI3K-AKT pathway and to act in autocrine manner to reduce muscle insulin resistance. Moreover, under cold exposure, when shivering thermogenesis is induced, FGF21 can synergize with Irisin to promote BAT non-shivering thermogenesis (Lee et al., 2014).

Finally, a recent study using proteomic approaches, demonstrated that the secreted form of lysosomal enzyme Cathepsin B (CTSB) is also an exercise

responsive myokine, that targets the brain, promotes hippocampal neurogenesis, and therefore enhances cognitive abilities (Moon, Becke et al., 2016).

Overall in this section we described how, in order to satisfy the energy demands generated by exercise, muscle communicates with other organs in order to ensure energy substrate availability. Moreover, physical exercise also promotes the browning of WAT and BAT thermogenesis, probably in order to meet the increased demand for fatty acid and glucose oxidation and prevent the accumulation energy substrates in circulation (Aldiss, Betts et al., 2018, Virtanen, 2014). Importantly, during exercise, muscle signals directly to the brain to promote cognitive function, providing an additional interest for lifestyle modifications including an increase in physical activity (Suzuki, 2016).

Inter-organ communication in pathological conditions: the case of obesity and related disorders.

In pathological situations, WAT can account for more than 50% of human body weight. The increasing prevalence of obesity has triggered considerable interest in understanding the physiological mechanisms promoting calorie storage, and energy expenditure, in order to prevent the deleterious metabolic consequences of obesity such as hyperglycemia, insulin resistance, dyslipidaemia and hepatic steatosis. Insulin resistance is characterized by a decrease in insulin-stimulated glucose uptake in adipocytes and muscle, as well as by a blunted insulin-stimulated repression of hepatic glucose production (Kahn & Flier, 2000). Most humans with obesity as well as diet-induced obesity (DIO) mice, fed highly caloric palatable diets, develop insulin resistance and exhibit high plasma levels of leptin (Frederich et al., 1995). Despite this, they do not show the expected reduction in food intake and

increase in energy expenditure, thus leading to the concept of leptin resistance, probably due to a decrease in JAK2-STAT3 signaling in pathologic conditions (Munzberg, Flier et al., 2004). Increasing the activation of the leptin-LepRb signaling in the brain remains a target for obesity treatment. In obesity conditions, increased NPY expression in the ARC decreases the expression of tyrosine hydroxylase neurons in the Paraventricular nucleus (PVN) of the hypothalamus and consequently, diminishes the thermogenic activation of BAT and overall energy expenditure (Shi, Lau et al., 2013).

On the other hand, mouse models of obesity and unhealthy obese individuals exhibit lower circulating levels of adiponectin. This finding that adiponectin levels are proportional to metabolic fitness has prompted the use of recombinant adiponectin and other adiponectin receptor agonists in several mouse models of obesity. So far, the activation of adiponectin signaling has improved glucose tolerance, insulin sensitivity and longevity in mice (Fasshauer & Bluher, 2015, Okada-Iwabu, Yamauchi et al., 2013). Importantly, adiponectin has been shown to improve the metabolic profile in leptin deficient ob/ob mice by overall increasing energy expenditure, despite not triggering a reduction in food intake (Qi, Takahashi et al., 2004). In pathological conditions of obesity, the reduction in CSF levels of adiponectin that is accompanied by feeding is lost, thus maintaining a "high food intake behavior" even in conditions that are not of energy scarcity (high energy conditions)(Kubota et al., 2007).

Interestingly, some studies suggest that the beneficial effects of FGF21 in glucose homeostasis are at least partially mediated by an increase in adiponectin production by WAT (Holland, Adams et al., 2013). However, other groups show that adiponectin is dispensable for the metabolic effects of FGF21 (BonDurant, Ameka

et al., 2017). Moreover, despite evidence showing improved metabolic fitness in FGF21 treatment or overexpression studies, clinical studies in humans have revealed high FGF21 circulating concentrations in obese and insulin resistant subjects, as well as the onset of a so called "FGF21 resistance"(Fisher, Chui et al., 2010). These findings highlight the fact that the importance of FGF21 in metabolic health still debated.

The levels of the gluconeogenic adipokine asprosin are elevated in obese mice. This observation suggests high plasma asprosin may contribute to the onset of hyperglycemia and insulin resistance in mice and humans. Moreover, the improvement of the metabolic phenotype of obese insulin resistant mice when using an antibody to sequester circulating asprosin places this novel adipokine as a potential therapeutic target against diabetes (Romere et al., 2016).

An example of the use of novel strategies for the discovery of endocrine interactions with physiological relevance for whole body metabolism is the recent discovery of a novel adipokine, mouse lipocalin 5 (LCN5) (LCN6 in humans), that has the ability to promote insulin sensitivity by enhancing muscle mitochondrial function (Seldin, Koplev et al., 2018). Seldin and colleagues developed a bioinformatic framework that takes advantage of publicly available data generated with different OMICS approaches to identify new circuits of inter-organ communication, thus contributing to increase our understanding about the mechanism by which WAT communicates with other organs to maintain homeostasis. Of note, despite showing significant effects in promoting muscle mitochondrial function in cellular models, the effects of the novel adipokine LCN5 in promoting glucose and insulin sensitivity *in vivo* were more pronounced in a High-Fat High-Sucrose (HF-HS) model. However, it is worth noting that LCN5

overexpression had positive effect on the metabolic status whether at the beginning or after several weeks of HF-HS diet (Seldin et al., 2018). These findings highlight the fact that improving muscle oxidative capacity is beneficial both to prevent metabolic disease and to cure metabolic disease, however, if this is relevant in normal physiology remains to be determined.

The effect of gut hormones is also altered in obesity. Indeed, ghrelin displays lowered orexigenic action in diet-induced obesity rodents due to a reduction in activation and plasticity of NPY/AgRP neurons (Briggs, Enriori et al., 2010). Moreover, a reduced incretin effect is seen in subjects with type 2 diabetes and obesity. Interestingly, postprandial GLP- 1 secretion is increased in obese patients following bariatric surgery, and correlates with weight loss maintenance (Madsbad, 2014).

Despite the positive effects of muscle-derived IL6 that are mentioned in the previous section, IL6 can also be released by adipose tissue. Chronically high levels of circulating IL6 in response to HFD contribute to obesity by promoting macrophage recruitment to WAT (Kraakman, Kammoun et al., 2015). In conditions of insulin resistance, WAT secretome is substantially altered and includes a broad range of pro-inflammatory factors, such $TNF\alpha$, IL6, interleukin 8 (IL8), and interleukin 1β (IL1B) and monocyte chemotactic protein 1 (MCP1) (Fasshauer & Bluher, 2015). The secretion of these proinflammatory cytokines and chemokines, as well as the secretion of other adipokines like retinol binding protein 4 (RBP4) (Graham, Yang et al., 2006, Yang, Graham et al., 2005), is now well admitted to contribute to the onset of the physiological alterations accompanying obesity (Fasshauer & Bluher, 2015) .

Physical inactivity, that can be both a cause and a consequence of obesity, is known to be associated with decreased insulin sensitivity, reduced postprandial lipid metabolism, decreased muscle mass and obesity. Alterations in myokine production associated with physical inactivity may also mediate the onset of obesity. This may be the case for myostatin (also known as GDF8), a member of the TGFβ superfamily. Myostatin was first described to be secreted during development to limit muscle growth (McPherron, Lawler et al., 1997), but is also known today to be produced in adults (Argiles, Orpi et al., 2012), and to promote muscle atrophy, in part by inhibiting AKT and mTOR signaling. Importantly, the inhibition of myostatin signaling increases PGC1α and mitochondrial biogenesis (LeBrasseur, Schelhorn et al., 2009), while mice deficient for myostatin show an improved metabolic phenotype and a resistance to HFD (Shan, Liang et al., 2013, Zhao, Wall et al., 2005). However, myostatin deficient mice also develop insulin resistance via

alterations in AMPK activity (Zhang, McFarlane et al., 2011), highlighting the need to determine the exact effects of myostatin signaling, as well as of other myokines correlating with obesity, in whole body energy homeostasis (Hoffmann & Weigert, 2017).

Overall, the finding that inter-organ communication is altered in conditions of obesity has gathered increasing attention in research aiming to manipulate those preestablished axis to counteract metabolic alterations.

Taking advantage of inter-organ communication to treat obesity and associated diseases

Understanding the biological networks that are involved in the induction of energy expenditure and promote satiety is crucial to target metabolic organs to increase weight loss in the context of the current obesity epidemic. Therefore, numerous efforts are currently being done to further understand the role of the signaling molecules described in this review, and to identify novel mechanisms of inter-organ communication that could contribute to the establishment of new therapeutic approaches against obesity and diabetes. Efforts to include recombinant adipokines or adipokine analogs as pharmacotherapy against obesity started more than 20 years ago. However, most of these efforts have not yet reached significant success. Indeed, leptin therapy alone has failed to induce significant weight loss or insulin sensitization (Heymsfield, Greenberg et al., 1999, Hukshorn, Saris et al., 2000). However, the use of leptin analogs in combination with other agents, namely amylin, has given more encouraging results, but was stopped due to adverse secondary effects (Fasshauer & Bluher, 2015). Importantly, despite apparently promoting hepatic glucose output by increasing the availability of gluconeogenic substrates in

the presence of insulin, in conditions in which insulin levels are low, like in type-2 (diabetes) T2D, leptin inhibits lipolysis thus decreasing the circulating levels gluconeogenic substrates such as glycerol, fatty acids and ketone bodies, which may play a role in suppressing gluconeogenesis under leptin therapy (D'Souza A et al., 2017). Adiponectin receptor analogs have successfully been used in preclinical mouse models (Okada-Iwabu et al., 2013), but have not yet been used in human patients. A truncated globular form of adiponectin has also been shown to promote muscle fatty acid oxidation, decrease muscle ceramides and overall improve insulin sensitivity, whether this globular adiponectin mimics the function of the multimeric adiponectin complexes found in circulation (Stern et al., 2016).

Extensive efforts have also been placed in the use of recombinant FGF21or FGF21 variants as potential therapy, due to beneficial metabolic effects observed in mice (Xu, Lloyd et al., 2009, Zhang, Huang et al., 2015), however only a small trend towards glucose lowering was reported in humans (Gaich, Chien et al., 2013). Moreover, there is increased concern about the use of FGF21 in therapy due to potential adverse effects in the skeletal system, more specifically in bones (Kharitonenkov & Adams, 2014, Wei, Dutchak et al., 2012). Finally, despite evidence that irisin treatment can positively affect glucose and lipid metabolism in mice, no real consensus exists as of yet concerning the link between irisin and the metabolic syndrome in humans, and no irisin analog has been used for studies in humans (Perakakis et al., 2017).

Significant preclinical and clinical success however has been encountered by using GLP1 receptor agonists (GLP-1Ras), that trigger a reduction in body weight by promoting satiety and reducing food intake, and profit from a longer half-life than endogenous GLP-1. Moreover GLP1-Ras improve glycemic control and reduce liver

inflammation and fibrosis (Andersen, Lund et al., 2018). More recently, GLP-1 and Glucagon receptor co-agonists have been successfully used in preclinical studies for metabolic diseases (Seghieri, Christensen et al., 2018), but additional research is necessary to demonstrate their efficacy in humans.

As of now, most potential therapies to take advantage of interorgan communication in the treatment of metabolic syndrome remain based in lifestyle alterations: increased physical activity, and decreased energy intake.

Concluding remarks

There is still much work to be done to understand the complex inter-organ networks that are needed to coordinate energy homeostasis. Recent studies show that more than 15% of the protein coding genome encodes for roughly 3000 secreted proteins, but only a handful of them has been properly annotated (Lindskog, 2015, Uhlen, Oksvold et al., 2010), suggesting that a very high number of "molecular messengers" remain to be discovered.

More recently, population-based methods taking advantage of the natural variations in between transcript levels between strains of a mouse reference population have been used to identify new inter-organ communication networks involved in metabolism (Seldin et al., 2018). This bioinformatics-based approached allowed the identification of a LCN5, an adipokine that promotes muscle mitochondrial function, and of Notum, an hepatokine that promotes WAT browning and BAT thermogenesis (Seldin et al., 2018). Comparing RNA sequencing approaches of jejununm and stomach when comparing sham and gastric sleeve bypass allowed the identification of LEAP2, an endogenous antagonist of the ghrelin receptor, that may contribute to the efficiency of gastric bypass (Ge et al., 2018). A

similar approach, based on a transcriptomic data-mining strategy, was used to identify CXCL14, a novel batokine that promotes thermogenesis by facilitating the recruitment of anti-inflammatory macrophages to BAT (Cereijo, Gavalda-Navarro et al., 2018).

Moreover, the analysis of large datasets generated with metabolomics and lipidomics studies have shown that different kinds of metabolites, like lipids, amino-acids, ketone bodies and bile-acids can directly modulate cellular metabolic responses not only by acting as substrates for metabolic reactions, but also by directly activating different signaling pathways via specific membrane receptors (Yang, Vijayakumar et al., 2018). An elegant example of the importance of "inter-organ" metabolites in the maintenance of energy homeostasis was published less than two year ago by Simcox and colleagues. They showed that upon cold exposure, WAT produces free fatty acids that, in turn, promote hepatic acyl carnitine production. These acylcarnitine's are in fine used by BAT for adaptive thermogenesis (Simcox, Geoghegan et al., 2017).

Finally, vesicles enabling the transfer of molecules from one tissue to the other may regulate systemic metabolism. Exosomes are such vesicles. More precisely, adipose tissue exosomes carrying circulating miRNAs have been recently been shown to have far-reaching effects in other peripheral tissues, and can therefore be considered the most recent family inside the adipokines (Thomou, Mori et al., 2017). For instance, BAT-produced mir-99b loaded exosomes contribute to the repression of the expression of hepatic FGF21(Thomou et al., 2017).

This suggest that the stimuli modifying the expression/secretion, the function, the molecular action and the targets for potentially thousands of molecules, in a broad sense, affecting whole body energy metabolism remain to be described/identified.

Acknowledgements

References

Al Massadi O, Lopez M, Tschop M, Dieguez C, Nogueiras R (2017) Current Understanding of the Hypothalamic Ghrelin Pathways Inducing Appetite and Adiposity. *Trends Neurosci* 40: 167-180

Aldiss P, Betts J, Sale C, Pope M, Budge H, Symonds ME (2018) Exercise-induced 'browning' of adipose tissues. *Metabolism* 81: 63-70

Ameka M, Markan KR, Morgan DA, BonDurant LD, Idiga SO, Naber MC, Zhu Z, Zingman LV, Grobe JL, Rahmouni K, Potthoff MJ (2019) Liver Derived FGF21 Maintains Core Body Temperature During Acute Cold Exposure. *Sci Rep* 9: 630

Andersen A, Lund A, Knop FK, Vilsboll T (2018) Glucagon-like peptide 1 in health and disease. *Nat Rev Endocrinol* 14: 390-403

Argiles JM, Orpi M, Busquets S, Lopez-Soriano FJ (2012) Myostatin: more than just a regulator of muscle mass. *Drug Discov Today* 17: 702-9

Awazawa M, Ueki K, Inabe K, Yamauchi T, Kubota N, Kaneko K, Kobayashi M, Iwane A, Sasako T, Okazaki Y, Ohsugi M, Takamoto I, Yamashita S, Asahara H, Akira S, Kasuga M, Kadowaki T (2011) Adiponectin enhances insulin sensitivity by increasing hepatic IRS-2 expression via a macrophage-derived IL-6-dependent pathway. *Cell Metab* 13: 401-412

Badman MK, Pissios P, Kennedy AR, Koukos G, Flier JS, Maratos-Flier E (2007) Hepatic fibroblast growth factor 21 is regulated by PPARalpha and is a key mediator of hepatic lipid metabolism in ketotic states. *Cell Metab* 5: 426-37

Bartness TJ, Vaughan CH, Song CK (2010) Sympathetic and sensory innervation of brown adipose tissue. *Int J Obes (Lond)* 34 Suppl 1: S36-42

Batterham RL, Cowley MA, Small CJ, Herzog H, Cohen MA, Dakin CL, Wren AM, Brynes AE, Low MJ, Ghatei MA, Cone RD, Bloom SR (2002) Gut hormone PYY(3-36) physiologically inhibits food intake. *Nature* 418: 650-4

Bayliss WM, Starling EH (1902) The mechanism of pancreatic secretion. *J Physiol* 28: 325-53

Beiroa D, Imbernon M, Gallego R, Senra A, Herranz D, Villarroya F, Serrano M, Ferno J, Salvador J, Escalada J, Dieguez C, Lopez M, Fruhbeck G, Nogueiras R (2014) GLP-1 agonism stimulates brown adipose tissue thermogenesis and browning through hypothalamic AMPK. *Diabetes* 63: 3346-58

Bernard C (1853) Nouvelle fonction du foie considéré comme organe producteur de matière sucrée chez l'homme et les animaux. *Paris:Baillère JB*

Bianco AC, McAninch EA (2013) The role of thyroid hormone and brown adipose tissue in energy homoeostasis. *Lancet Diabetes Endocrinol* 1: 250-8

Blouet C, Schwartz GJ (2012) Duodenal lipid sensing activates vagal afferents to regulate non-shivering brown fat thermogenesis in rats. *PLoS One* 7: e51898

BonDurant LD, Ameka M, Naber MC, Markan KR, Idiga SO, Acevedo MR, Walsh SA, Ornitz DM, Potthoff MJ (2017) FGF21 Regulates Metabolism Through Adipose-Dependent and -Independent Mechanisms. *Cell Metab* 25: 935-944 e4

BonDurant LD, Potthoff MJ (2018) Fibroblast Growth Factor 21: A Versatile Regulator of Metabolic Homeostasis. *Annu Rev Nutr* 38: 173-196

Bostrom P, Wu J, Jedrychowski MP, Korde A, Ye L, Lo JC, Rasbach KA, Bostrom EA, Choi JH, Long JZ, Kajimura S, Zingaretti MC, Vind BF, Tu H, Cinti S, Hojlund K, Gygi SP, Spiegelman BM (2012) A PGC1-alpha-dependent myokine that drives brown-fat-like development of white fat and thermogenesis. *Nature* 481: 463-8

Brent GA (2012) Mechanisms of thyroid hormone action. *J Clin Invest* 122: 3035-43

Briggs DI, Enriori PJ, Lemus MB, Cowley MA, Andrews ZB (2010) Diet-induced obesity causes ghrelin resistance in arcuate NPY/AgRP neurons. *Endocrinology* 151: 4745-55

Bruning JC, Gautam D, Burks DJ, Gillette J, Schubert M, Orban PC, Klein R, Krone W, Muller-Wieland D, Kahn CR (2000) Role of brain insulin receptor in control of body weight and reproduction. *Science* 289: 2122-5

Cannon B, Nedergaard J (2004) Brown adipose tissue: function and physiological significance. *Physiol Rev* 84: 277-359

Cereijo R, Gavalda-Navarro A, Cairo M, Quesada-Lopez T, Villarroya J, Moron-Ros S, Sanchez-Infantes D, Peyrou M, Iglesias R, Mampel T, Turatsinze JV, Eizirik DL, Giralt M, Villarroya F (2018) CXCL14, a Brown Adipokine that Mediates Brown-Fat-to-Macrophage Communication in Thermogenic Adaptation. *Cell Metab* 28: 750-763 e6

Cheng CY, Chu JY, Chow BK (2011) Central and peripheral administration of secretin inhibits food intake in mice through the activation of the melanocortin system. *Neuropsychopharmacology* 36: 459-71

Christoffolete MA, Linardi CC, de Jesus L, Ebina KN, Carvalho SD, Ribeiro MO, Rabelo R, Curcio C, Martins L, Kimura ET, Bianco AC (2004) Mice with targeted disruption of the Dio2 gene have cold-induced overexpression of the uncoupling protein 1 gene but fail to increase brown adipose tissue lipogenesis and adaptive thermogenesis. *Diabetes* 53: 577-84

Chu JY, Cheng CY, Sekar R, Chow BK (2013) Vagal afferent mediates the anorectic effect of peripheral secretin. *PLoS One* 8: e64859

Chuang JC, Sakata I, Kohno D, Perello M, Osborne-Lawrence S, Repa JJ, Zigman JM (2011) Ghrelin directly stimulates glucagon secretion from pancreatic alpha-cells. *Mol Endocrinol* 25: 1600-11

Cori CF, Cori GT (1946) Carbohydrate metabolism. *Annu Rev Biochem* 15: 193-218

Cummings DE, Purnell JQ, Frayo RS, Schmidova K, Wisse BE, Weigle DS (2001) A preprandial rise in plasma ghrelin levels suggests a role in meal initiation in humans. *Diabetes* 50: 1714-9

Cypess AM, Kahn CR (2010) Brown fat as a therapy for obesity and diabetes. *Curr Opin Endocrinol Diabetes Obes* 17: 143-9

D'Souza A M, Neumann UH, Glavas MM, Kieffer TJ (2017) The glucoregulatory actions of leptin. *Mol Metab* 6: 1052-1065

Dinarello CA (2007) Historical insights into cytokines. *Eur J Immunol* 37 Suppl 1: S34-45

Dodd GT, Andrews ZB, Simonds SE, Michael NJ, DeVeer M, Bruning JC, Spanswick D, Cowley MA, Tiganis T (2017) A Hypothalamic Phosphatase Switch Coordinates Energy Expenditure with Feeding. *Cell Metab* 26: 375-393 e7

Dodd GT, Decherf S, Loh K, Simonds SE, Wiede F, Balland E, Merry TL, Munzberg H, Zhang ZY, Kahn BB, Neel BG, Bence KK, Andrews ZB, Cowley MA, Tiganis T (2015) Leptin and insulin act on POMC neurons to promote the browning of white fat. *Cell* 160: 88-104

Fasshauer M, Bluher M (2015) Adipokines in health and disease. *Trends Pharmacol Sci* 36: 461-70

Febbraio MA (2017) Exercise metabolism in 2016: Health benefits of exercise - more than meets the eye! *Nat Rev Endocrinol* 13: 72-74

Fedorenko A, Lishko PV, Kirichok Y (2012) Mechanism of fatty-acid-dependent UCP1 uncoupling in brown fat mitochondria. *Cell* 151: 400-13

Fisher FM, Chui PC, Antonellis PJ, Bina HA, Kharitonenkov A, Flier JS, Maratos-Flier E (2010) Obesity is a fibroblast growth factor 21 (FGF21)-resistant state. *Diabetes* 59: 2781-9

Fisher FM, Kleiner S, Douris N, Fox EC, Mepani RJ, Verdeguer F, Wu J, Kharitonenkov A, Flier JS, Maratos-Flier E, Spiegelman BM (2012) FGF21 regulates PGC-1alpha and browning of white adipose tissues in adaptive thermogenesis. *Genes Dev* 26: 271-81

Fiuza-Luces C, Santos-Lozano A, Joyner M, Carrera-Bastos P, Picazo O, Zugaza JL, Izquierdo M, Ruilope LM, Lucia A (2018) Exercise benefits in cardiovascular disease: beyond attenuation of traditional risk factors. *Nat Rev Cardiol* 15: 731-743

Frederich RC, Hamann A, Anderson S, Lollmann B, Lowell BB, Flier JS (1995) Leptin levels reflect body lipid content in mice: evidence for diet-induced resistance to leptin action. *Nat Med* 1: 1311-4

Gaich G, Chien JY, Fu H, Glass LC, Deeg MA, Holland WL, Kharitonenkov A, Bumol T, Schilske HK, Moller DE (2013) The effects of LY2405319, an FGF21 analog, in obese human subjects with type 2 diabetes. *Cell Metab* 18: 333-40

Garretson JT, Szymanski LA, Schwartz GJ, Xue B, Ryu V, Bartness TJ (2016) Lipolysis sensation by white fat afferent nerves triggers brown fat thermogenesis. *Mol Metab* 5: 626-634

Ge X, Yang H, Bednarek MA, Galon-Tilleman H, Chen P, Chen M, Lichtman JS, Wang Y, Dalmas O, Yin Y, Tian H, Jermutus L, Grimsby J, Rondinone CM, Konkar A, Kaplan DD (2018) LEAP2 Is an Endogenous Antagonist of the Ghrelin Receptor. *Cell Metab* 27: 461-469 e6

Geerling JJ, Boon MR, Kooijman S, Parlevliet ET, Havekes LM, Romijn JA, Meurs IM, Rensen PC (2014) Sympathetic nervous system control of triglyceride metabolism: novel concepts derived from recent studies. *J Lipid Res* 55: 180-9

Gesta S, Tseng YH, Kahn CR (2007) Developmental origin of fat: tracking obesity to its source. *Cell* 131: 242-56

Giudice J, Taylor JM (2017) Muscle as a paracrine and endocrine organ. *Curr Opin Pharmacol* 34: 49-55

Glick Z (1982) Inverse relationship between brown fat thermogenesis and meal size: the thermostatic control of food intake revisited. *Physiol Behav* 29: 1137-40

Gnocchi D, Bruscalupi G (2017) Circadian Rhythms and Hormonal Homeostasis: Pathophysiological Implications. *Biology (Basel)* 6

Goldstein MS (1961) Humoral nature of the hypoglycemic factor of muscular work. *Diabetes* 10: 232-4

Graham TE, Yang Q, Bluher M, Hammarstedt A, Ciaraldi TP, Henry RR, Wason CJ, Oberbach A, Jansson PA, Smith U, Kahn BB (2006) Retinol-binding protein 4 and insulin resistance in lean, obese, and diabetic subjects. *N Engl J Med* 354: 2552-63

Gray SM, Meijer RI, Barrett EJ (2014) Insulin regulates brain function, but how does it get there? *Diabetes* 63: 3992-7

Heymsfield SB, Greenberg AS, Fujioka K, Dixon RM, Kushner R, Hunt T, Lubina JA, Patane J, Self B, Hunt P, McCamish M (1999) Recombinant leptin for weight loss in obese and lean adults: a randomized, controlled, dose-escalation trial. *JAMA* 282: 1568-75

Hoffmann C, Weigert C (2017) Skeletal Muscle as an Endocrine Organ: The Role of Myokines in Exercise Adaptations. *Cold Spring Harb Perspect Med* 7

Holland WL, Adams AC, Brozinick JT, Bui HH, Miyauchi Y, Kusminski CM, Bauer SM, Wade M, Singhal E, Cheng CC, Volk K, Kuo MS, Gordillo R, Kharitonenkov A, Scherer PE (2013) An FGF21-adiponectin-ceramide axis controls energy expenditure and insulin action in mice. *Cell Metab* 17: 790-7

Holland WL, Miller RA, Wang ZV, Sun K, Barth BM, Bui HH, Davis KE, Bikman BT, Halberg N, Rutkowski JM, Wade MR, Tenorio VM, Kuo MS, Brozinick JT, Zhang BB, Birnbaum MJ, Summers SA, Scherer PE (2011) Receptor-mediated activation of ceramidase activity initiates the pleiotropic actions of adiponectin. *Nat Med* 17: 55-63

Hondares E, Iglesias R, Giralt A, Gonzalez FJ, Giralt M, Mampel T, Villarroya F (2011) Thermogenic activation induces FGF21 expression and release in brown adipose tissue. *J Biol Chem* 286: 12983-90

Hukshorn CJ, Saris WH, Westerterp-Plantenga MS, Farid AR, Smith FJ, Campfield LA (2000) Weekly subcutaneous pegylated recombinant native human leptin (PEG-OB) administration in obese men. *J Clin Endocrinol Metab* 85: 4003-9

I OS, Zhang W, Wasserman DH, Liew CW, Liu J, Paik J, DePinho RA, Stolz DB, Kahn CR, Schwartz MW, Unterman TG (2015) FoxO1 integrates direct and indirect effects of insulin on hepatic glucose production and glucose utilization. *Nat Commun* 6: 7079

Inagaki T, Dutchak P, Zhao G, Ding X, Gautron L, Parameswara V, Li Y, Goetz R, Mohammadi M, Esser V, Elmquist JK, Gerard RD, Burgess SC, Hammer RE, Mangelsdorf DJ, Kliewer SA (2007) Endocrine regulation of the fasting response by PPARalpha-mediated induction of fibroblast growth factor 21. *Cell Metab* 5: 415-25

Ingalls AM, Dickie MM, Snell GD (1950) Obese, a new mutation in the house mouse. *J Hered* 41: 317-8

Jackson MB, Ahima RS (2006) Neuroendocrine and metabolic effects of adipocyte-derived hormones. *Clin Sci (Lond)* 110: 143-52

Kahn BB, Flier JS (2000) Obesity and insulin resistance. *J Clin Invest* 106: 473-81

Keipert S, Kutschke M, Ost M, Schwarzmayr T, van Schothorst EM, Lamp D, Brachthauser L, Hamp I, Mazibuko SE, Hartwig S, Lehr S, Graf E, Plettenburg O, Neff F, Tschop MH, Jastroch M (2017) Long-Term Cold Adaptation Does Not Require FGF21 or UCP1. *Cell Metab* 26: 437-446 e5

Kelsey R (2018) BAT is involved in control of satiation. *Nat Rev Endocrinol* 15: 1

Kersten S (2001) Mechanisms of nutritional and hormonal regulation of lipogenesis. *EMBO Rep* 2: 282-6

Kharitonenkov A, Adams AC (2014) Inventing new medicines: The FGF21 story. *Mol Metab* 3: 221-9

Kharitonenkov A, Shiyanova TL, Koester A, Ford AM, Micanovic R, Galbreath EJ, Sandusky GE, Hammond LJ, Moyers JS, Owens RA, Gromada J, Brozinick JT, Hawkins ED, Wroblewski VJ, Li DS, Mehrbod F, Jaskunas SR, Shanafelt AB (2005) FGF-21 as a novel metabolic regulator. *J Clin Invest* 115: 1627-35

Kojima M, Hosoda H, Date Y, Nakazato M, Matsuo H, Kangawa K (1999) Ghrelin is a growth-hormone-releasing acylated peptide from stomach. *Nature* 402: 656-60

Kraakman MJ, Kammoun HL, Allen TL, Deswaerte V, Henstridge DC, Estevez E, Matthews VB, Neill B, White DA, Murphy AJ, Peijs L, Yang C, Risis S, Bruce CR, Du XJ, Bobik A, Lee-Young RS, Kingwell BA, Vasanthakumar A, Shi W et al. (2015) Blocking IL-6 trans-signaling prevents high-fat diet-induced adipose tissue macrophage recruitment but does not improve insulin resistance. *Cell Metab* 21: 403-16

Kubota N, Yano W, Kubota T, Yamauchi T, Itoh S, Kumagai H, Kozono H, Takamoto I, Okamoto S, Shiuchi T, Suzuki R, Satoh H, Tsuchida A, Moroi M, Sugi K, Noda T, Ebinuma H, Ueta Y, Kondo T, Araki E et al. (2007) Adiponectin stimulates AMP-activated protein kinase in the hypothalamus and increases food intake. *Cell Metab* 6: 55-68

Lamy CM, Sanno H, Labouebe G, Picard A, Magnan C, Chatton JY, Thorens B (2014) Hypoglycemia-activated GLUT2 neurons of the nucleus tractus solitarius stimulate vagal activity and glucagon secretion. *Cell Metab* 19: 527-38

Leal LG, Lopes MA, Batista ML, Jr. (2018) Physical Exercise-Induced Myokines and Muscle-Adipose Tissue Crosstalk: A Review of Current Knowledge and the Implications for Health and Metabolic Diseases. *Front Physiol* 9: 1307

LeBrasseur NK, Schelhorn TM, Bernardo BL, Cosgrove PG, Loria PM, Brown TA (2009) Myostatin inhibition enhances the effects of exercise on performance and metabolic outcomes in aged mice. *J Gerontol A Biol Sci Med Sci* 64: 940-8

Lee P, Linderman JD, Smith S, Brychta RJ, Wang J, Idelson C, Perron RM, Werner CD, Phan GQ, Kammula US, Kebebew E, Pacak K, Chen KY, Celi FS (2014) Irisin and FGF21 are cold-induced endocrine activators of brown fat function in humans. *Cell Metab* 19: 302-9

Lee SH, Zabolotny JM, Huang H, Lee H, Kim YB (2016) Insulin in the nervous system and the mind: Functions in metabolism, memory, and mood. *Mol Metab* 5: 589-601

Lee SJ, Sanchez-Watts G, Krieger JP, Pignalosa A, Norell PN, Cortella A, Pettersen KG, Vrdoljak D, Hayes MR, Kanoski SE, Langhans W, Watts AG (2018) Loss of dorsomedial hypothalamic GLP-1 signaling reduces BAT thermogenesis and increases adiposity. *Mol Metab* 11: 33-46

Li Y, Schnabl K, Gabler SM, Willershauser M, Reber J, Karlas A, Laurila S, Lahesmaa M, M UD, Bast-Habersbrunner A, Virtanen KA, Fromme T, Bolze F, O'Farrell LS, Alsina-Fernandez J, Coskun T, Ntziachristos V, Nuutila P, Klingenspor M (2018) Secretin-Activated Brown Fat Mediates Prandial Thermogenesis to Induce Satiation. *Cell* 175: 1561-1574 e12

Lindskog C (2015) The potential clinical impact of the tissue-based map of the human proteome. *Expert Rev Proteomics* 12: 213-5

Long JZ, Roche AM, Berdan CA, Louie SM, Roberts AJ, Svensson KJ, Dou FY, Bateman LA, Mina AI, Deng Z, Jedrychowski MP, Lin H, Kamenecka TM, Asara JM, Griffin PR, Banks AS, Nomura DK, Spiegelman BM (2018) Ablation of PM20D1 reveals N-acyl amino acid control of metabolism and nociception. *Proc Natl Acad Sci U S A* 115: E6937-E6945

Long JZ, Svensson KJ, Bateman LA, Lin H, Kamenecka T, Lokurkar IA, Lou J, Rao RR, Chang MR, Jedrychowski MP, Paulo JA, Gygi SP, Griffin PR, Nomura DK, Spiegelman BM (2016) The Secreted Enzyme PM20D1 Regulates Lipidated Amino Acid Uncouplers of Mitochondria. *Cell* 166: 424-435

Lourenco MV, Frozza RL, de Freitas GB, Zhang H, Kincheski GC, Ribeiro FC, Goncalves RA, Clarke JR, Beckman D, Staniszewski A, Berman H, Guerra LA, Forny-Germano L, Meier S, Wilcock DM, de Souza JM, Alves-Leon S, Prado VF, Prado MAM, Abisambra JF et al. (2019) Exercise-linked FNDC5/irisin rescues synaptic plasticity and memory defects in Alzheimer's models. *Nat Med* 25: 165-175

M UD, Saari T, Raiko J, Kudomi N, Maurer SF, Lahesmaa M, Fromme T, Amri EZ, Klingenspor M, Solin O, Nuutila P, Virtanen KA (2018) Postprandial Oxidative Metabolism of Human Brown Fat Indicates Thermogenesis. *Cell Metab* 28: 207-216 e3

Madsbad S (2014) The role of glucagon-like peptide-1 impairment in obesity and potential therapeutic implications. *Diabetes Obes Metab* 16: 9-21

Martins L, Seoane-Collazo P, Contreras C, Gonzalez-Garcia I, Martinez-Sanchez N, Gonzalez F, Zalvide J, Gallego R, Dieguez C, Nogueiras R, Tena-Sempere M, Lopez M (2016) A Functional Link between AMPK and Orexin Mediates the Effect of BMP8B on Energy Balance. *Cell Rep* 16: 2231-2242

McPherron AC, Lawler AM, Lee SJ (1997) Regulation of skeletal muscle mass in mice by a new TGF-beta superfamily member. *Nature* 387: 83-90

Meex RCR, Watt MJ (2017) Hepatokines: linking nonalcoholic fatty liver disease and insulin resistance. *Nat Rev Endocrinol* 13: 509-520

Minokoshi Y, Kim YB, Peroni OD, Fryer LG, Muller C, Carling D, Kahn BB (2002) Leptin stimulates fatty-acid oxidation by activating AMP-activated protein kinase. *Nature* 415: 339-43

Monda M, Viggiano AN, Viggiano A, Viggiano E, Lanza A, De Luca V (2005) Hyperthermic reactions induced by orexin A: role of the ventromedial hypothalamus. *Eur J Neurosci* 22: 1169-75

Moon HY, Becke A, Berron D, Becker B, Sah N, Benoni G, Janke E, Lubejko ST, Greig NH, Mattison JA, Duzel E, van Praag H (2016) Running-Induced Systemic Cathepsin B Secretion Is Associated with Memory Function. *Cell Metab* 24: 332-40

Munzberg H, Flier JS, Bjorbaek C (2004) Region-specific leptin resistance within the hypothalamus of diet-induced obese mice. *Endocrinology* 145: 4880-9

Obici S, Zhang BB, Karkanias G, Rossetti L (2002) Hypothalamic insulin signaling is required for inhibition of glucose production. *Nat Med* 8: 1376-82

Obregon MJ (2014) Adipose tissues and thyroid hormones. *Front Physiol* 5: 479

Okada-Iwabu M, Yamauchi T, Iwabu M, Honma T, Hamagami K, Matsuda K, Yamaguchi M, Tanabe H, Kimura-Someya T, Shirouzu M, Ogata H, Tokuyama K, Ueki K, Nagano T, Tanaka A, Yokoyama S, Kadowaki T (2013) A small-molecule AdipoR agonist for type 2 diabetes and short life in obesity. *Nature* 503: 493-9

Pan WW, Myers MG, Jr. (2018) Leptin and the maintenance of elevated body weight. *Nat Rev Neurosci* 19: 95-105

Pedersen BK, Febbraio MA (2012) Muscles, exercise and obesity: skeletal muscle as a secretory organ. *Nat Rev Endocrinol* 8: 457-65

Perakakis N, Triantafyllou GA, Fernandez-Real JM, Huh JY, Park KH, Seufert J, Mantzoros CS (2017) Physiology and role of irisin in glucose homeostasis. *Nat Rev Endocrinol* 13: 324-337

Petersen AM, Pedersen BK (2005) The anti-inflammatory effect of exercise. *J Appl Physiol (1985)* 98: 1154-62

Potthoff MJ, Inagaki T, Satapati S, Ding X, He T, Goetz R, Mohammadi M, Finck BN, Mangelsdorf DJ, Kliewer SA, Burgess SC (2009) FGF21 induces PGC-1alpha and regulates carbohydrate and fatty acid metabolism during the adaptive starvation response. *Proc Natl Acad Sci U S A* 106: 10853-8

Qi Y, Takahashi N, Hileman SM, Patel HR, Berg AH, Pajvani UB, Scherer PE, Ahima RS (2004) Adiponectin acts in the brain to decrease body weight. *Nat Med* 10: 524-9

Roca-Rivada A, Castelao C, Senin LL, Landrove MO, Baltar J, Belen Crujeiras A, Seoane LM, Casanueva FF, Pardo M (2013) FNDC5/irisin is not only a myokine but also an adipokine. *PLoS One* 8: e60563

Romere C, Duerrschmid C, Bournat J, Constable P, Jain M, Xia F, Saha PK, Del Solar M, Zhu B, York B, Sarkar P, Rendon DA, Gaber MW, LeMaire SA, Coselli JS,

Milewicz DM, Sutton VR, Butte NF, Moore DD, Chopra AR (2016) Asprosin, a Fasting-Induced Glucogenic Protein Hormone. *Cell* 165: 566-79

Ronveaux CC, Tome D, Raybould HE (2015) Glucagon-like peptide 1 interacts with ghrelin and leptin to regulate glucose metabolism and food intake through vagal afferent neuron signaling. *J Nutr* 145: 672-80

Saito M (2013) Brown adipose tissue as a regulator of energy expenditure and body fat in humans. *Diabetes Metab J* 37: 22-9

Seghieri M, Christensen AS, Andersen A, Solini A, Knop FK, Vilsboll T (2018) Future Perspectives on GLP-1 Receptor Agonists and GLP-1/glucagon Receptor Co-agonists in the Treatment of NAFLD. *Front Endocrinol (Lausanne)* 9: 649

Seldin MM, Koplev S, Rajbhandari P, Vergnes L, Rosenberg GM, Meng Y, Pan C, Phuong TMN, Gharakhanian R, Che N, Makinen S, Shih DM, Civelek M, Parks BW, Kim ED, Norheim F, Chella Krishnan K, Hasin-Brumshtein Y, Mehrabian M, Laakso M et al. (2018) A Strategy for Discovery of Endocrine Interactions with Application to Whole-Body Metabolism. *Cell Metab* 27: 1138-1155 e6

Sellayah D, Bharaj P, Sikder D (2011) Orexin is required for brown adipose tissue development, differentiation, and function. *Cell Metab* 14: 478-90

Shan T, Liang X, Bi P, Kuang S (2013) Myostatin knockout drives browning of white adipose tissue through activating the AMPK-PGC1alpha-Fndc5 pathway in muscle. *FASEB J* 27: 1981-9

Shi YC, Lau J, Lin Z, Zhang H, Zhai L, Sperk G, Heilbronn R, Mietzsch M, Weger S, Huang XF, Enriquez RF, Baldock PA, Zhang L, Sainsbury A, Herzog H, Lin S (2013) Arcuate NPY controls sympathetic output and BAT function via a relay of tyrosine hydroxylase neurons in the PVN. *Cell Metab* 17: 236-48

Simcox J, Geoghegan G, Maschek JA, Bensard CL, Pasquali M, Miao R, Lee S, Jiang L, Huck I, Kershaw EE, Donato AJ, Apte U, Longo N, Rutter J, Schreiber R, Zechner R, Cox J, Villanueva CJ (2017) Global Analysis of Plasma Lipids Identifies Liver-Derived Acylcarnitines as a Fuel Source for Brown Fat Thermogenesis. *Cell Metab* 26: 509-522 e6

Steinberg GR, Kemp BE (2007) Adiponectin: starving for attention. *Cell Metab* 6: 3-4

Stern JH, Rutkowski JM, Scherer PE (2016) Adiponectin, Leptin, and Fatty Acids in the Maintenance of Metabolic Homeostasis through Adipose Tissue Crosstalk. *Cell Metab* 23: 770-84

Suzuki WA (2016) How Body Affects Brain. *Cell Metab* 24: 192-3

Tata JR (2005) One hundred years of hormones. *EMBO Rep* 6: 490-6

Theander-Carrillo C, Wiedmer P, Cettour-Rose P, Nogueiras R, Perez-Tilve D, Pfluger P, Castaneda TR, Muzzin P, Schurmann A, Szanto I, Tschop MH, Rohner-Jeanrenaud F (2006) Ghrelin action in the brain controls adipocyte metabolism. *J Clin Invest* 116: 1983-93

Thomou T, Mori MA, Dreyfuss JM, Konishi M, Sakaguchi M, Wolfrum C, Rao TN, Winnay JN, Garcia-Martin R, Grinspoon SK, Gorden P, Kahn CR (2017) Adipose-derived circulating miRNAs regulate gene expression in other tissues. *Nature* 542: 450-455

Titchenell PM, Chu Q, Monks BR, Birnbaum MJ (2015) Hepatic insulin signalling is dispensable for suppression of glucose output by insulin in vivo. *Nat Commun* 6: 7078

Tokarz VL, MacDonald PE, Klip A (2018) The cell biology of systemic insulin function. *J Cell Biol* 217: 2273-2289

Tschop M, Smiley DL, Heiman ML (2000) Ghrelin induces adiposity in rodents. *Nature* 407: 908-13

Turton MD, O'Shea D, Gunn I, Beak SA, Edwards CM, Meeran K, Choi SJ, Taylor GM, Heath MM, Lambert PD, Wilding JP, Smith DM, Ghatei MA, Herbert J, Bloom SR (1996) A role for glucagon-like peptide-1 in the central regulation of feeding. *Nature* 379: 69-72

Uhlen M, Oksvold P, Fagerberg L, Lundberg E, Jonasson K, Forsberg M, Zwahlen M, Kampf C, Wester K, Hober S, Wernerus H, Bjorling L, Ponten F (2010) Towards a knowledge-based Human Protein Atlas. *Nat Biotechnol* 28: 1248-50

Velazquez-Villegas LA, Perino A, Lemos V, Zietak M, Nomura M, Pols TWH, Schoonjans K (2018) TGR5 signalling promotes mitochondrial fission and beige remodelling of white adipose tissue. *Nat Commun* 9: 245

Veniant MM, Sivits G, Helmering J, Komorowski R, Lee J, Fan W, Moyer C, Lloyd DJ (2015) Pharmacologic Effects of FGF21 Are Independent of the "Browning" of White Adipose Tissue. *Cell Metab* 21: 731-8

Vieira E, Salehi A, Gylfe E (2007) Glucose inhibits glucagon secretion by a direct effect on mouse pancreatic alpha cells. *Diabetologia* 50: 370-9

Villarroya F, Cereijo R, Villarroya J, Giralt M (2017) Brown adipose tissue as a secretory organ. *Nat Rev Endocrinol* 13: 26-35

Virtanen KA (2014) BAT thermogenesis: Linking shivering to exercise. *Cell Metab* 19: 352-4

Watanabe M, Houten SM, Mataki C, Christoffolete MA, Kim BW, Sato H, Messaddeq N, Harney JW, Ezaki O, Kodama T, Schoonjans K, Bianco AC, Auwerx J (2006) Bile acids induce energy expenditure by promoting intracellular thyroid hormone activation. *Nature* 439: 484-9

Wei W, Dutchak PA, Wang X, Ding X, Wang X, Bookout AL, Goetz R, Mohammadi M, Gerard RD, Dechow PC, Mangelsdorf DJ, Kliewer SA, Wan Y (2012) Fibroblast growth factor 21 promotes bone loss by potentiating the effects of peroxisome proliferator-activated receptor gamma. *Proc Natl Acad Sci U S A* 109: 3143-8

Whittle AJ, Carobbio S, Martins L, Slawik M, Hondares E, Vazquez MJ, Morgan D, Csikasz RI, Gallego R, Rodriguez-Cuenca S, Dale M, Virtue S, Villarroya F, Cannon B, Rahmouni K, Lopez M, Vidal-Puig A (2012) BMP8B increases brown adipose tissue thermogenesis through both central and peripheral actions. *Cell* 149: 871-85

Worthmann A, John C, Ruhlemann MC, Baguhl M, Heinsen FA, Schaltenberg N, Heine M, Schlein C, Evangelakos I, Mineo C, Fischer M, Dandri M, Kremoser C, Scheja L, Franke A, Shaul PW, Heeren J (2017) Cold-induced conversion of cholesterol to bile acids in mice shapes the gut microbiome and promotes adaptive thermogenesis. *Nat Med* 23: 839-849

Wu J, Cohen P, Spiegelman BM (2013) Adaptive thermogenesis in adipocytes: is beige the new brown? *Genes Dev* 27: 234-50

Xu J, Lloyd DJ, Hale C, Stanislaus S, Chen M, Sivits G, Vonderfecht S, Hecht R, Li YS, Lindberg RA, Chen JL, Jung DY, Zhang Z, Ko HJ, Kim JK, Veniant MM (2009) Fibroblast growth factor 21 reverses hepatic steatosis, increases energy expenditure, and improves insulin sensitivity in diet-induced obese mice. *Diabetes* 58: 250-9

Yang Q, Graham TE, Mody N, Preitner F, Peroni OD, Zabolotny JM, Kotani K, Quadro L, Kahn BB (2005) Serum retinol binding protein 4 contributes to insulin resistance in obesity and type 2 diabetes. *Nature* 436: 356-62

Yang Q, Vijayakumar A, Kahn BB (2018) Metabolites as regulators of insulin sensitivity and metabolism. *Nat Rev Mol Cell Biol* 19: 654-672

Zaretskaia MV, Zaretsky DV, Shekhar A, DiMicco JA (2002) Chemical stimulation of the dorsomedial hypothalamus evokes non-shivering thermogenesis in anesthetized rats. *Brain Res* 928: 113-25

Zeng W, Pirzgalska RM, Pereira MM, Kubasova N, Barateiro A, Seixas E, Lu YH, Kozlova A, Voss H, Martins GG, Friedman JM, Domingos AI (2015) Sympathetic neuro-adipose connections mediate leptin-driven lipolysis. *Cell* 163: 84-94

Zhang C, Huang Z, Gu J, Yan X, Lu X, Zhou S, Wang S, Shao M, Zhang F, Cheng P, Feng W, Tan Y, Li X (2015) Fibroblast growth factor 21 protects the heart from apoptosis in a diabetic mouse model via extracellular signal-regulated kinase 1/2-dependent signalling pathway. *Diabetologia* 58: 1937-48

Zhang C, McFarlane C, Lokireddy S, Bonala S, Ge X, Masuda S, Gluckman PD, Sharma M, Kambadur R (2011) Myostatin-deficient mice exhibit reduced insulin resistance through activating the AMP-activated protein kinase signalling pathway. *Diabetologia* 54: 1491-501

Zhang W, Bi S (2015) Hypothalamic Regulation of Brown Adipose Tissue Thermogenesis and Energy Homeostasis. *Front Endocrinol (Lausanne)* 6: 136

Zhang Y, Li R, Meng Y, Li S, Donelan W, Zhao Y, Qi L, Zhang M, Wang X, Cui T, Yang LJ, Tang D (2014) Irisin stimulates browning of white adipocytes through mitogen-activated protein kinase p38 MAP kinase and ERK MAP kinase signaling. *Diabetes* 63: 514-25

Zhang Y, Proenca R, Maffei M, Barone M, Leopold L, Friedman JM (1994) Positional cloning of the mouse obese gene and its human homologue. *Nature* 372: 425-32

Zhao B, Wall RJ, Yang J (2005) Transgenic expression of myostatin propeptide prevents diet-induced obesity and insulin resistance. *Biochem Biophys Res Commun* 337: 248-55

Zhu Y, Gao Y, Tao C, Shao M, Zhao S, Huang W, Yao T, Johnson JA, Liu T, Cypess AM, Gupta O, Holland WL, Gupta RK, Spray DC, Tanowitz HB, Cao L, Lynes MD, Tseng YH, Elmquist JK, Williams KW et al. (2016) Connexin 43 Mediates White Adipose Tissue Beiging by Facilitating the Propagation of Sympathetic Neuronal Signals. *Cell Metab* 24: 420-433
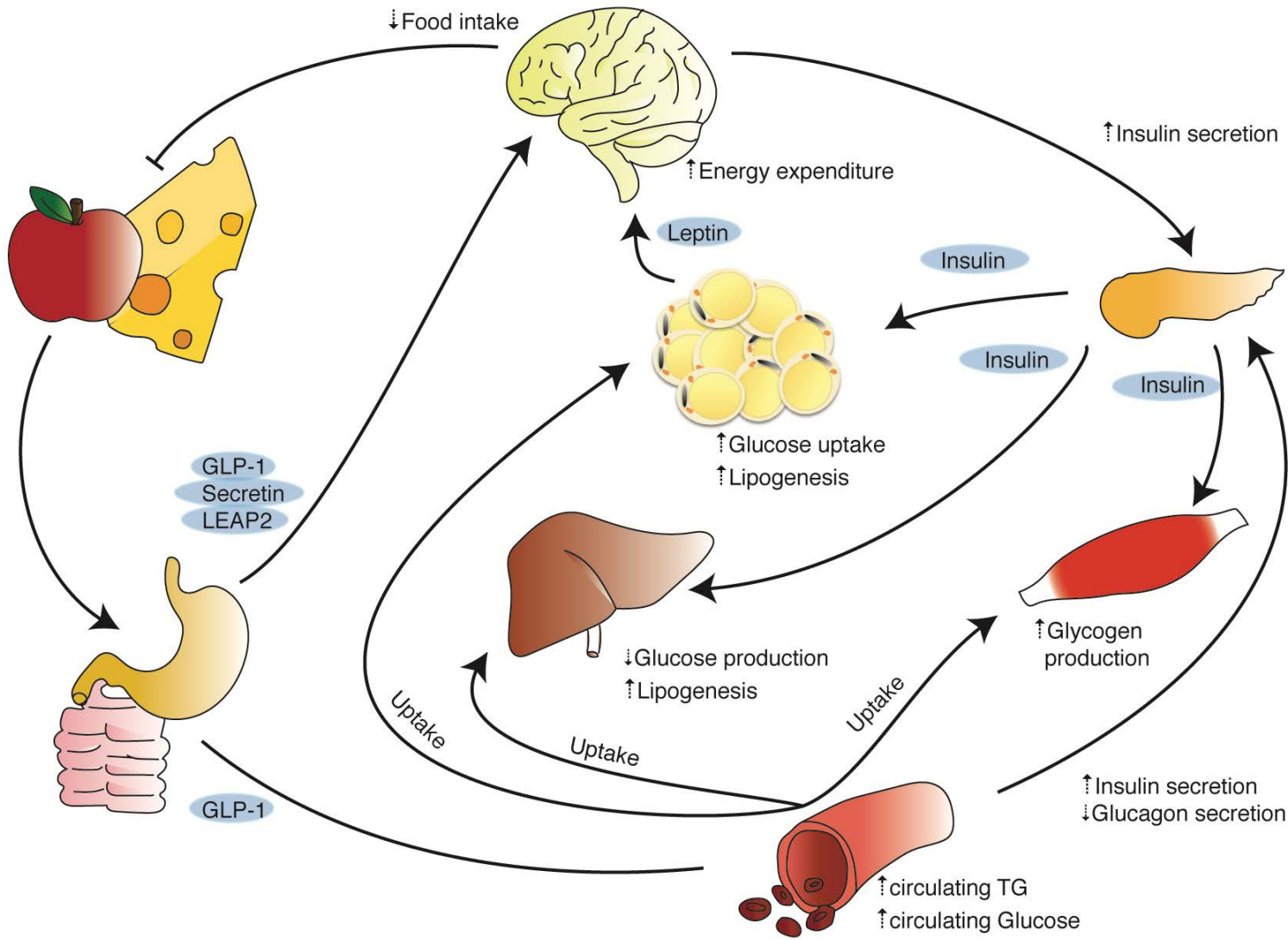
Figure 1. Inter-organ communication under feeding conditions. Food ingestion stimulates the secretion of several molecules such as GLP-1, Secretin and LEAP2. These gut hormones signal to the brain to reduce food intake. GLP-1 will also stimulate insulin (and reduce glucagon) secretion by the pancreas. In turn, insulin will glycogen production in muscle, decrease glucose production in liver and increase glucose uptake and lipogenesis from glucose and triglycerides (TG) in circulation in WAT. Leptin, produced by white adipocytes, will act in the CNS to repress food intake.

Figure 2. Inter-organ communication under fasting conditions. Ghrelin is a gut hormone secreted under fasting conditions. It targets the brain to increase food intake. Pancreatic glucagon secretion is also increased by ghrelin, and directly by low blood glucose levels. Glucagon will target liver to decrease glycolysis and increase hepatic gluconeogenesis and glycogenolysis, as well as WAT to increase lipolysis.

Figure 3. Inter-organ communication under cold exposure. Cold stimuli, sensed by neurons in the skin, activate the thermoregulatory hypothalamic regions of the brain that will secrete Orexin and Bmp8b to stimulate BAT thermogenesis. Moreover, the SNS is responsible for the local production of NE in BAT. The hypothalamic–pituitary–thyroid axis is also activated in response to cold, and promotes the release of thyroid hormones (T3 and T4) in order to contribute to the activation of BAT thermogenesis.
Cold exposure can also trigger muscle shivering and thus the production of the myokine Irisin. Irisin can in turn stimulate BAT thermogenesis. If cold exposure is sustained over time, WAT undergoes browning and can be contribute to thermogenesis. Irisin is one of the molecules that can trigger in this process. In addition, cold-dependent hepatic FGF21 and BA secretion contribute to the browning of WAT. Finally, BAT and WAT FGF21, as well as BAT BMP8b secretion, can also occur after cold activation and promote thermogenesis in a paracrine manner.

Glossary	
ACC	Acetyl-CoA carboxylase
AdipoR1/2	Adiponectin receptor 1/2
ADRB3	Beta3-Adrenergic receptor
AgRP	Agouti-related protein
AKT (PKB)	Protein kinase B
AMPK	AMP-activated protein kinase
ARC	Arcuate nucleus
BA	Bile acids
BAT	Brown adipose tissue
BMP8b	Bone morphogenetic protein 8b
cAMP	Cyclic adenosine monophosphate
CKK	Cholecystokinin
CSF	Cerebrospinal fluid
CTSB	Cathepsin B
CXCL14	Chemokine (C-X-C motif) ligand 14
DIO	Diet-induced obesity
DIO2	Type 2 iodothyronine deiodinase
DMH	Dorsomedial hypothalamus
FBN1	Profibrillin
FDN5	Fibronectin type III domain-containing protein 5
FGF21	Fibroblast growth factor 21
GH	Growth hormone
GHSR	Growth hormone secretagogue receptor
GIP	Glucose-dependent insulinotropic peptide
GLP-1	Glucagon-like peptide 1
GLP-1R	Glucagon-like peptide 1 receptor
GLP-1RA	Glucagon-like peptide-1 receptor agonist
GLUT2	Glucose transporter 2
GLUT4	Glucose transporter 4
HF-HS	High fat – high sucrose
HFD	High fat diet
IL1b	Interleukin 1 beta
ILR1	Interleukin receptor 1
IL1RA	Interleukin 1 receptor antagonist
IL6	Interleukin 6
IL8	Interleukin 8
IL10	Interleukin 10
IL15	Interleukin 15
IRS-2	Insulin receptor substrate 2
JAK2	Janus kinase 2
LCN5	Lipocalin 5
LEAP2	Liver-expressed antimicrobial peptide 2
LepRb	Leptin receptor
LHA	Lateral hypothalamic area
MAPK	Mitogen-activated protein kinase
MCP1	Monocyte chemotactic protein 1
miRNA	Micro RNA

mTOR	Mammalian target of rapamycin
NE	Norepinephrine
NPY	Neuropeptide Y
PGC1a	Peroxisome proliferator-activated receptor gamma coactivator 1-alpha
PI3K	Phosphoinositide 3-kinase
PKA	Protein kinase A
PM20D1	Peptidase M20 domain-containing 1
POA	Preoptic area
POMC	Propiomelanocortin
PVN	Paraventricular nucleus
RBP4	Retinol binding protein 4
RPA	Raphe pallidus
SctR	Secretin receptor
SNS	Sympathetic nervous system
STAT3	Signal transducer and activator of transcription 3
T2D	Type-2 diabetes
T3	Triiodothyronine
T4	Thyroxine
TCPTP	T cell-protein tyrosine phosphatase
TG	Triglycerides
TNFa	Tumor necrosis factor alpha
TSH	Thyroid-stimulating hormone
UCP1	Uncoupling protein 1
VAN	Vagal afferent neuron
VMH	Ventromedial hypothalamus
WAT	White adipose tissue

↓Food intake

↑Insulin secretion

↑Energy expenditure

Leptin

Insulin

GLP-1
Secretin
LEAP2

Insulin

Insulin

↑Glucose uptake
↑Lipogenesis

↑Glycogen
production

GLP-1

Uptake

Uptake

Uptake

↓Glucose production
↑Lipogenesis

↑Insulin secretion
↓Glucagon secretion

↑circulating TG
↑circulating Glucose

↑Food intake

↓Energy expenditure

↑Glucagon secretion

Adiponectin

Glucagon

↑Lipid synthesis
↓FA oxidation

Glucagon

↑Lipolysis

Ghrelin

Adiponectin

↓Lipogenesis
↑FA oxidation

Ghrelin

↓Glycolysis
↑Gluconeogenesis
↑Glycogenolysis

Ghrelin

↓Insulin secretion
↑Glucagon secretion

↓circulating TG
↓circulating Glucose

Cold exposure

Thyroid gland

TSH

CNS

T3, T4

Orexin
BMP8b

NE

FGF21

BAT

BMP8b

Muscle

Liver

Irisin

Irisin

FGF21
BA

FGF21

Browning of WAT

Global kinome analysis in obese subjects reveals PIM-1 as a novel target for the treatment of insulin resistance.

Nasrallah A, Liu PS, Fernandez EA, Li X, Ejarque M, Caputo T, **Castillo-Armengol J**, Martinez-Carreres L, Calvo E, Cheng WC, Bekkar A, Xenarios I, Gilardi F, Pellitero S, Fernandez-Veledo S, Tinahones FJ, Vendrell-Ortega J, Ho PC, Lopez-Mejia IC and Fajas L.

Nature Metabolism (Submitted)

I have also participated to another study from the lab that reveals the differential expression of kinases from human subjects and its relation with insulin resistance. In fact, throughout this study, we have identified PIM-1, a kinase whose regulation could be potentially used to treat insulin resistance. In this project, I worked on the dissection of organs from mice and the isolation of the stromal vascular fraction of white adipose tissue.

Global kinome analysis in obese subjects reveals PIM-1 as a novel target for the treatment of insulin resistance.

Anita Nasrallah[1], Pu-Ste Liu[2,3,4], Eric-Aria Fernandez[1], Xiaoyun Li[2,3], Miriam Ejarque[5,6], Tiziana Caputo[1], Judit Castillo-Armengol[1], Laia Martinez-Carreres[1], Enrique Calvo[5,6], Wan-Chen Cheng[2,3], Amel Bekkar[7], Ioannis Xenarios[7,8,9], Federica Gilardi[1,10], Silvia Pellitero[6,11] Sonia Fernandez-Veledo[5,6], Francisco José Tinahones[12,13], Joan Vendrell-Ortega[5,6,14], Ping Chih Ho[2,3], Isabel C. Lopez-Mejia[1*], and Lluis Fajas[1*]

[1] Center for Integrative Genomics, University of Lausanne, 1015 Lausanne, Switzerland

[2] Department of Fundamental Oncology, University of Lausanne, 1066 Epalinges, Switzerland

[3] Ludwig Cancer Center, Lausanne Branch, Epalinges, Switzerland

[4] Institute of Cellular and System Medicine, National Health Research Institutes, Miaoli County, Taiwan

[5] Institut d´Investigació Sanitària Pere Virgili; Hospital Universitari de Tarragona Joan XXIII-Tarragona Spain.

[6] CIBER de Diabetes y Enfermedades Metabólicas Asociadas (CIBERDEM)-Instituto de Salud Carlos III, Madrid, Spain.

[7] Vital-IT group, SIB Swiss Institute of Bioinformatics, 1015 Lausanne, Switzerland

[8] Swiss-Prot group, SIB Swiss Institute of Bioinformatics, 1211 Geneva, Switzerland

[9] Swiss Insitute of Bioinformatics CITY: Lausanne Switzerland

[10] Faculty Unit of Toxicology, University Center of Legal Medicine, Lausanne University Hospital (CHUV), 1000 Lausanne, Switzerland

[11] Department of Endocrinology and Nutrition. Germans Trias i Pujol Research Institute, Barcelona, Spain

[12] Unidad de Gestión Clínica Endocrinología y Nutrición. Instituto de Investigación Biomédica de Málaga (IBIMA), Complejo Hospitalario de Málaga (Virgen de la Victoria) Málaga (Spain)

[13] CIBER Fisiopatología de la Obesidad y Nutrición (CB06/03), Málaga, Spain.

[14] Universitat Rovira i Virgili, Tarragona, Spain.

[*] Corresponding authors: Isabel C. Lopez-Mejia and Lluis Fajas, University of Lausanne, Center for Integrative Genomics, Quartier UNIL-Sorge, Bâtiment Génopode, CH-1015 Lausanne, Switzerland

E-mail: lluis.fajas@unil.ch, isabel.lopezmejia@unil.ch

Summary

Obesity, the accumulation of excess body fat, is an epidemic leading to numerous human metabolic diseases, such as type 2 diabetes (T2D). T2D is mainly characterized by hyperglycemia, accompanied by local (adipose tissue) and systemic insulin resistance. In the adipose tissue, insulin resistance involves alterations in the cross-talk of various signaling cascades, implicating numerous kinases and phosphatases. To identify molecular changes that occur during the development of insulin resistance, we have used here a new activity-based method to study the global kinase activity in human adipose tissue. Our study is based on the observation that some obese subjects do not develop insulin resistance. This population represents our control group, which avoids confounding results due to obesity by itself rather than to insulin resistance. We found that a specific set of kinase activities are representative of insulin resistance in the obese population. In particular, we found that the Serine/Threonine kinase (STK) PIM-1 has increased activity in the visceral adipose tissue (VAT) of morbid obese diabetic (MOD) insulin resistant (IR) patients. We further show that PIM-1 inhibition decreases the inflammatory capacity of bone marrow-derived macrophages *in vitro*, and leads to a decrease in the inflammatory profile in visceral adipose tissue (VAT), as well as to an increase in insulin sensitivity in diabetic mice.

Key words: PamGene, PIM-1, obesity, T2D, VAT, inflammation

Introduction

The World Health Organization (WHO) has recently announced that worldwide obesity has almost tripled since 1975 (16 February 2018). Obesity is linked to numerous health problems, including insulin resistance, type 2 diabetes, hypertension, dyslipidemia, atherosclerosis, and cancer, among others (Arroyo-Johnson & Mincey, 2016; Y. C. Wang, McPherson, Marsh, Gortmaker, & Brown, 2011; Weitzman & Gordon, 1990). Together, the rising prevalence of obesity and the frequent co-morbidities in affected patients is an important challenge for health care systems. Nevertheless, recent data suggest that the total amount of body fat does not entirely explain the predisposition to cardio-metabolic risk (Goossens, 2017; Wajchenberg, Giannella-Neto, da Silva, & Santos, 2002). Indeed, metabolic complications can be observed in a significant number of non-obese individuals. In sharp contrast, 10 to 35% of obese patients do not appear to develop such complications and are thus considered metabolically healthy (Wildman et al., 2008).

In adipose tissue, insulin resistance is tightly correlated with inflammation as well as with the accumulation of pro-inflammatory macrophages (Lackey & Olefsky, 2016; McLaughlin, Ackerman, Shen, & Engleman, 2017). Adipose tissue consists of mature adipocytes and stromal vascular cells (SVCs). SVCs include premature adipocytes, endothelial cells and immune cells. These immune cells include myeloid cells like macrophages and granulocytes, effector and memory T cells, regulatory T cells and others (Huh, Park, Ham, & Kim, 2014). Macrophages, classified into anti-inflammatory (M2-like) and pro-inflammatory (M1-like) macrophages (Rosen & Spiegelman, 2014), are especially important for adipose tissue homeostasis. Indeed, it is well known that, upon obesity, pro-inflammatory macrophages are recruited (Hotamisligil, Shargill, & Spiegelman, 1993; Nguyen et al., 2007; Weisberg et al., 2003; Xu et al., 2003). Thus, an inflammatory reaction is a pre-requisite for insulin

resistance, locally in the adipose tissue and systemically in the whole organism (Kanda et al., 2006; Patsouris et al., 2008).

Insulin exerts its actions through a cascade of phosphorylation/dephosphorylation reactions of intra-cellular proteins. Insulin signaling in adipocytes has been extensively studied *in vitro* and in animal models, with a particular focus on the effects of insulin receptor, Insulin receptor substrates 1 and 2 (IRS1 and IRS2), and PI3K-protein kinase B (AKT) (Copps & White, 2012). Other known protein kinases that have been involved in the onset of insulin resistance include, but are not limited to, AMP-activated protein kinase (AMPK), IκB kinase (IKK), protein kinase C (PKC), or mitogen-activated protein kinases (MAPKs) (Ye, 2013; Zhang, Zhou, & Li, 2009). However, an extensive study of protein phosphorylation or kinase function alterations in IR has not been performed in human visceral white adipose tissue (VAT).

Describing the changes in the kinome is key to understanding the contributions of signaling cascades in normal or dysfunctional conditions, and therefore for the identification of signaling alterations leading to systemic diseases. The rapid development of techniques, such as genome-wide association study (GWAS), RNA sequencing, or chromatin immunoprecipitation (ChIP) sequencing has paved the way for several scientific breakthroughs (Andersen et al., 2019; Gupta & Vadde, 2019; Ke et al., 2017; Sun et al., 2018). We have chosen now to use a novel technology developed by PamGene to perform a whole kinase activity profiling of human visceral adipose tissue from morbid obese non-diabetic subjects (MOND), compared to morbid-obese diabetic (MOD) patients. Identifying new and specific protein kinases involved in adipose tissue chronic inflammation and insulin resistance may help in developing targeted drug therapies and treatment strategies to minimize insulin resistance in patients.

While analyzing the differences in the kinome of VAT, we found that the activity of the serine/threonine kinase PIM-1 was increased in the VAT of obese insulin resistant patients, compared to metabolically healthy obese subjects. PIM-1 is a member of the PIM family, that is composed of three kinases: PIM-1, PIM-2 and PIM-3. The PIM family plays roles in numerous cellular functions, such as proliferation, cell cycle progression, differentiation, apoptosis, and tumorigenesis (J. Li, Loveland, & Xing, 2011; Narlik-Grassow, Blanco-Aparicio, & Carnero, 2014; Warfel & Kraft, 2015). PIM kinases are important for growth factor signaling (Mikkers et al., 2004) by regulating B- and T- cell responses to cytokines and hematopoietic growth factors (An, Kraft, & Kang, 2013), and are thus known for their role supporting tumor cell growth and survival (Brault et al., 2010). PIM-1 has been specially studied in hematological malignancies and is known to be a major target for cytokine induced STAT signaling (Brault et al., 2010).

We show in this study that PIM-1 activity in the macrophage fraction of adipose tissue mediates their pro-inflammatory effects, thus promoting insulin resistance and type II diabetes. Moreover, we demonstrate that the pharmacological inhibition of PIM-1 alters macrophage polarization *in vitro* and ameliorates insulin resistance in a mouse model of diabetes.

Results

Kinome profiling reveals distinct kinase activities in human visceral adipose tissue from morbid obese diabetic, compared to non-diabetic subjects

The main goal of our study was to identify novel kinases inducing insulin resistance in obese subjects. The insulin signaling cascade is dependent on the rapid activation of a series of tyrosine and serine/threonine protein kinases. We used a technology developed by PamGene to determine differential global kinase activity in human VAT from morbid obese non-diabetic (MOND) and morbid obese diabetic (MOD) patients (Table 1) (Supplemental Figure 1). We used arrays that consist of 140 immobilized serine/threonine containing peptides (STK PamChips). These chips were incubated with the different adipose tissue lysates. Differentially phosphorylated peptides, whose phosphorylation varied significantly between the MOND and MOD samples, were indicative of differential specific kinase activities. More than 60 peptides were highly phosphorylated specifically in the VAT of MOD patients, as compared to MOND patients (Figure 1A and Table S4). Putative upstream kinase analysis was done using the "STK upstream kinase analysis" pipeline from the Bionavigator software. This method takes into account the multiple parallel changes in peptide phosphorylation and both experimental kinase-substrate relationships (Uniprot, HPRD, PhosphositePlus, Phospho.ELM, and Reactome databases), and in silico predictions for upstream kinases (phosphoNET database). The kinases that were identified with "more confidence" using this method were AKT1/PKBα, AKT2/PKBβ, AMPKα1, ANPα, CHK2, mTOR/FRAP, PIM1, PIM2, PIM3, PKAα, PKC (α, δ, ε, η, θ), PKD1, PKG1, PKG2, PRKX and p70S6Kβ (Figure 1B-C). Even though PRKY is shown as a kinase hit in the kinexus-based analysis (Figure 1B), however it is considered as a pseudogene, which is why it is not depicted in the String Plot (Figure 1C). Of note, during the course of this study it was shown that the knockout of PKG1 in TNFα-induced mature adipocytes reverted the insulin resistant phenotype, by rescuing glucose uptake impairment

(Ando et al., 2015), and the adipose tissue specific knockout of PKCε improves diet induced glucose intolerance in mice (Brandon et al., 2019). Importantly, PKA, PKCβ, AKT and AMPK have already been described as involved in the onset of insulin resistance (Huang, Liu, Guo, & Su, 2018; Mehta, 2014). These findings validated our experimental approach, and suggested that the increased activity of the above-mentioned kinases can be either a cause or a consequence of the insulin resistance characterizing MOD subjects.

Pim-1 expression in VAT positively correlates with IR markers and is increased in different mouse models of insulin resistance.

Next, we focused on the PIM family of kinases, because they were not previously described to be involved in insulin resistance or diabetes. PIM kinase activity is constitutively active (Warfel & Kraft, 2015). Thus, unlike other kinases, PIM kinase activity is regulated primarily at the transcriptional level, then by translation efficiency, and finally by proteasomal degradation (Amaravadi & Thompson, 2005). Functional redundancy, at the _in vitro_ and _in vivo_ levels, between the PIM kinases have been shown (Mikkers et al., 2004; Narlik-Grassow et al., 2012).

Thus, we used their transcriptional level as a readout for activity and measured the expression of the different novel kinases in the VAT of more than 80 human patients (Table 2). mRNA levels were correlated to the different IR markers, i.e. body mass index (BMI), insulinemia, and glycemia (Supplemental Figure 2A-I). Of all the identified kinases, _PIM-1_ was the only one to show a positive correlation with all 3 variables (Figure 2 A-C). _PIM-2_ was only correlated to BMI (Figure 2D-F), while _PIM-3_ did not correlate to any of the 3 parameters (Figure 2G-I).

To validate if the increased expression of _PIM-1_ upon insulin resistance is conserved in mice, we quantified mRNA levels in two different mouse models of insulin resistance: mice

under high-fat diet (HFD), and db/db mice. Based on RNA sequencing data, *Pim-1* gene expression was significantly increased in the VAT of mice fed a HFD for 8 weeks, as compared to mice under normal chow diet (CD), which has the exact same composition as the HFD but with lower fat content, otherwise known as low fat diet (LFD) (Figure 2J). This was further increased after 20 weeks of HFD (Figure 2J). It is important to note here that 60% of the calories of the HFD is coming from fat. *Pim-2* expression did not change between the groups (Figure 2K), while *Pim-3* expression significantly decreased in the VAT of mice under HFD (Figure 2L). RTqPCR data showed that *Pim-1* mRNA is also significantly higher in VAT of db/db mice (Figure 2M). However, *Pim-2* expression was also increased in VAT of db/db mice (Figure 2N), while *Pim-3* expression was significantly decreased in the VAT of db/db mice (Figure 2O). Overall, these results prove that *PIM-1* gene expression is increased in adipose tissue from diabetic human subjects and from mouse models of diabetes, suggesting that PIM-1 participates in the development of insulin resistance.

The effects of Pim-1 in insulin resistance are not mediated by adipocytes.

Next, we wanted to analyze the participation of PIM-1 in the onset of insulin-resistance in cellular models of white adipose tissue. Indeed, *Pim-1* is increasingly expressed during adipocyte differentiation in the 3T3L1 model (Figure 3A). Mature 3T3L1 adipocytes treated with TNFα for 72h were used as a model for insulin resistance (Stephens, Lee, & Pilch, 1997). We stimulated these cells with 100nM insulin for 20 minutes and saw a significant decrease in the phosphorylation of AKT at Threonine 308, which is a readout of IS (Figure 3B-C). We treated these insulin-resistant adipocytes with the Pim-1 inhibitor SGI-1776. The inhibition of Pim-1 activity was validated by showing a dose-dependent decrease in the phosphorylation of Bad at Serine 112, which is a target of Pim-1, upon SGI-1776 treatment starting from 0.25μM (Figure 3D-F). The phosphorylation levels of AKT were, however, not increased with any of

the tested doses of Pim-1 inhibitor, showing no rescue of the insulin resistant phenotype of TNFα treated 3T3L1 mature adipocytes (Figure 3D-F). These results suggested that Pim-1 does not directly act on adipocytes to induce insulin resistance in the adipose tissue of obese subjects.

Pim-1 expression and activity are increased in pro-inflammatory macrophages.

Our initial kinome analysis was performed in whole VAT. In addition to adipocytes VAT contains fibroblasts, endothelial cells, and inflammatory cells. Out of those non-adipocyte cells, pro-inflammatory macrophages play a major role in the development of insulin resistance in this tissue. Therefore, we used bone marrow-derived macrophages (BMDMs) treated with lipopolysaccharide (LPS) for 6h, as an _in vitro_ model of pro-inflammatory macrophages. Protein extracts from naive and 6h-LPS-stimulated cells were then submitted to PamChip serine/threonine kinase analyses (Supplemental Figure 4). Pim-1 was among the kinases with increased activity in response to LPS treatment (Figure 4A). Consistently, RNA sequencing data from naïve and LPS-treated macrophages showed an increase in _Pim-1_ mRNA levels in the pro-inflammatory macrophages (Figure 4B). Moreover, the expression of _Pim-1_ was also increased in FACS sorted CD11c$^+$ adipose tissue-derived pro-inflammatory macrophages from mice under HFD, when compared to CD11c$^+$ macrophages from mice under chow diet (Figure 4C), suggesting that our observations in BMDMs can be extended to adipose tissue macrophages.

SGI-1776 decreases pro-inflammatory markers in LPS-stimulated macrophages.

BMDMs were stimulated with LPS for 6h or 24h to induce a pro-inflammatory phenotype. As expected, pro-inflammatory markers (_IL-1ß_, _IL-6_, _TNFα_, _MCP-1_ and _iNOS_) were significantly increased in LPS treated macrophages as compared to naïve macrophages

(Figure 5A). *Pim-1* expression was also increased upon LPS-stimulation in BMDMs, both at the mRNA and protein levels (Figure 5B-D). The phosphorylation of the known Pim-1 targets pS112 Bad and pT146 p21 was also increased upon LPS stimulation (Figure 5E), suggesting an increase in Pim-1 activity in pro-inflammatory macrophages.

The treatment of macrophages with the Pim-1 inhibitor SGI-1776 prior to LPS stimulation decreased the mRNA expression of several pro-inflammatory cytokines, such as *IL-1ß*, *TNFα*, *MCP-1* and *iNOS* (Figure 5F), as well as the expression of *Pim-1* (Figure 5G). These results proved that Pim-1 has a direct role on pro-inflammatory macrophages, and this may participate in the onset of insulin resistance in VAT.

Pim-1 inhibition improves insulin sensitivity in diabetic mice

We next wanted to test the clinical relevance of our findings by treating the db/db diabetic mouse model with the SGI-1776 Pim-1 inhibitor. After 3 weeks of treatment, we did not observe changes in the food intake (Figure 6A) or body weight (Figure 6B). In contrast, the treatment resulted in alterations in body composition; an increase of lean mass and a decrease of fat mass (Figure 6C-D). This correlated with a decreased weight of WAT depots in SGI-1776-treated mice, whereas no differences were observed in the weight of other tissues, such as liver, heart or muscle (Figure 6E). This suggests a specific effect of SGI-1776 on adipose tissue depots. Most important was the finding that the fasting glycemia of the db/db mice treated with the Pim-1 inhibitor was reduced after 3 weeks of treatment, when compared to the vehicle-treated group (Figure 6F). Moreover, SGI-1776 treatment resulted in enhanced insulin sensitivity and glucose disposal, as measured by insulin and glucose tolerance tests (Figure 6G-J).

Gene expression of several cytokines was next assessed. Pro-inflammatory markers, such as *MCP-1*, *TNFα* and *iNOS* decreased in the VAT of SGI-1776-treated mice (Figure 6K).

A higher expression of pro-inflammatory cytokines is often correlated with the aggregation of pro-inflammatory macrophages around dead adipocytes, and is a characteristic feature of inflammation in this tissue. These so-called crown-like structures were indeed apparent in the adipose tissue of vehicle-treated mice (Figure 6L-M), but were much decreased in the VAT of db/db mice treated with SGI-1776 (Figure 6L-M). These results proved that the inhibition of Pim-1 improves adipose tissue inflammation and the overall diabetic phenotype in the db/db mouse model.

Discussion

The use of genomic, proteomic, and transcriptomic techniques in the study of human pathologies has been rapidly expanding. Indeed, the recent identification of new key players in human type 2 diabetes mellitus (T2DM) is based on high throuput techniques. These approaches study potentially pathogenic mutations or SNPs, as well as the expression of protein coding genes and actual protein abundance, whereas functional proteomic methodologies bring more insight on protein activity and how cell signaling works. Actually, in the past five years, proteomic studies have confirmed the importance of inflammatory pathways and cellular stress in the alterations found in adipose tissue of obese subjects (Garrison, Lastwika, Zhang, Li, & Lampe, 2017). A first prediction of upregulated kinases in adipose tissue in conditions of obesity and insulin resistance in mice was performed using phosphoproteomics. However, this study shows very limited overlap with our dataset (Shaik et al., 2016). The kinase activity-based assay from PamGene allows us to detect kinase function directly in order to perform kinome profiling on patients' biopsies.

The aim of our study was to discover new kinases whose activities are deregulated during the development of insulin resistance in obese subjects, independently of adiposity. To implement our strategy, we took advantage of a population of obese subjects that are protected from the development insulin resistance and other obesity-derived pathologies (Wildman et al., 2008). Comparing the global kinase activities in the adipose tissue of these subjects with the kinase activities of the obese diabetic patients allowed us to discover new kinases, specifically active in the adipose tissue of the pathological group. This strategy allows us to overcome any confounding factors that could be related to obesity *per se*, and not to insulin resistance. Moreover, our results shed light on the mechanism behind the ability of a certain population of obese subjects to maintain metabolic health and evade metabolic complications.

We used three criteria to select specific kinase activities for further *in vivo* studies. First, the kinase activity should be significantly modified in validation studies. Second, specific kinase inhibitors should be available for further preclinical testing. And third, a role for the identified kinase in diabetes should not have been previously described. By performing an upstream putative kinase analysis of the differentially phosphorylated peptides in MOD and MOND VAT samples, we identified PIM-1 as a potentially upregulated kinase in diabetic patients. We consequently validated our finding and proposed a mechanism by which Pim-1 modulates insulin sensitivity by integrating cellular models, diabetic mouse models and clinical data from our human cohort.

Emerging evidence proves that PIM-1 is a promising drug target against many types of cancer. It is correlated with tumor aggressiveness and is a marker of poor prognosis in several tumor types, such as prostate cancer and leukemia (Dhanasekaran et al., 2001; Liu, Wang, Wang, & Li, 2010; Shah et al., 2008). Interestingly, in ovarian cancer cells, PIM-1 phosphorylates c-Myc, which in turn induces the expression of several metabolic enzymes: PGK1, LDHA, GLUT1, etc. (Wu et al., 2018), providing a first observation linking PIM-1 activity to the regulation of metabolism, at least in the context of cancer. Moreover, PIM-1 has been shown to play a role in diabetic cardiomyopathy and diabetic nephropathy, which are severe complications associated with diabetes (Agrawal & Kant, 2014; Kannel, Hjortland, & Castelli, 1974). However, PIM-1 has never been directly associated with adipose tissue insulin resistance in the context of T2D. An important role of PIM-1 that strongly places this kinase as a novel target for insulin resistance is its role in the inflammatory response. Indeed, PIM-1 has been linked to placental inflammation (Liong, Barker, & Lappas, 2017), to the stabilization of the p65 subunit of NFκB (Nihira et al., 2009), and to the immunosuppressive activity of human regulatory T cells (Z. Li et al., 2014). It is well established that pro-inflammatory cytokines, such as IL-6 and TNF-α, affect insulin signaling, which in turn is essential to

maintain glucose homeostasis and regulate its metabolism in adipose tissue. We show here that PIM-1 kinase does not mediate cytokine-induced insulin resistance in adipocytes (Figure 3A-D), but rather plays a key role in another cell type mediating insulin resistance in adipose tissue: pro-inflammatory macrophages.

PIM kinases are arising as significant mediators in cytokine signaling pathways. *Pim-1* is highly expressed in the bone marrow, spleen, thymus, fetal liver, and non-hematopoietic tissues such as hippocampus, prostate, and epithelia (Eichmann, Yuan, Breant, Alitalo, & Koskinen, 2000). *Pim-1* transcription is activated in response to numerous cytokines through JAK-STAT signaling (Brault et al., 2010). PIM-1 is also involved in myeloid cell differentiation, indeed when the levels of active PIM-1 are manipulated, the rate of differentiation of U937 cells is altered (Z. Wang et al., 2001). Importantly, PIM-1 has been shown to promote NFκB transactivation by preventing its degradation in HeLa cells (Nihira et al., 2009), and by promoting RANKL-induced NFκB transcriptional activity in osteoclasts (Kim, Kim, Youn, Jin, & Kim, 2010). We propose here an additional role for PIM-1 in macrophage polarization in response to pro-inflammatory stimuli.

In conclusion, this study has identified a subset of novel kinases potentially involved in adipose tissue insulin resistance through an activity-based screen and elucidated yet another important role of PIM-1 kinase, linking its canonical role in cancer and inflammation to metabolism, specifically insulin resistance in diabetic patients. This will now pave the way for more studies, investigating the mechanisms by which PIM-1 participates in adipose tissue inflammation in obese subjects, and thus in the onset of T2D. This will also help develop new targeted drug therapies in the field of diabetes, a worldwide epidemic, with no clear therapeutic strategies yet.

Tables

Table 1: Cohort 1 (discovery cohort)

Morbid obese non-diabetic (MOND) and morbid obese type 2 diabetic (MOD) patients used for PamGene data analysis

Patients	n	Females	Males	Age (years)	BMI (kg/m^2)	Insulinemia (mIU/mL)	Glycaemia (mg/dL)	HOMA-IR
MOND	23	16	7	47 ± 2	46.3 ± 1.0	17.8 ± 2.3	94.6 ± 2.6	4.4 ± 0.6
MOD	21	11	10	52 ± 2	48.5 ± 1.7	25.4 ± 4.8	133.5 ± 9.8	10.7 ± 2.7

Table 2: Cohort 2 (confirmatory cohort)

Lean (L), obese (O) and morbid obese (MO) patients that are diabetic and non-diabetic used for the correlations between mRNA expression and IR markers (BMI, Glycemia, and Insulinemia)

Patients	n	Females	Males	Age (years)	BMI (kg/m^2)	Insulinemia (mIU/mL)	Glycaemia (mg/dL)	HOMA-IR
L	20	13	7	55 ± 3	23.7 ± 0.4	7.5 ± 1.2	100.8 ± 4.2	1.9 ± 0.3
O	23	12	11	59 ± 3	32.8 ± 0.4	11.1 ± 1.4	110.8 ± 5.1	3.0 ± 0.4
MO	43	33	10	49 ± 1	46.6 ± 0.9	19.9 ± 2.3	114.4 ± 5.0	6.2 ± 1.0

Table S 1: Primers used for qPCR analysis of housekeeping genes (human and mouse)

Gene	Forward	Reverse
RS9	CACACTCTCCCCAACGTTCT	ACCACCTGCTTGCGGACCCTGATA
Actin	TCCATCATGAAGTGTGACGT	TACTCCTGCTTGCTGATCCAC

Table S 2: Primers used for qPCR analysis of kinases upregulated in VAT of MOD patients

Gene	Forward	Reverse
Pim-1 (human)	CCTGGGGATCCTGCTGTATG	CAGGGCCAAGCACCATCTAA
Pim-1 (mouse)	GCGGCGAAATCAAACTCA	TCATAGAGCAGGATCCCAAG

Pim-2 (human)	AGCTCATCGACTTCGGTTCG	TATCGTAGAGAAGCACGCCC
Pim-2 (mouse)	AGCTTTCGAGGCCGAATA	GGTTCCGGGAGATTACTTTG
Pim-3 (human)	GTTCTGGTGCCCTGCTTCAT	TGCATGGTACTGGTGTCGAG
Pim-3 (mouse)	AGCTGAAGCTCATCGACT	GTAGAGCAGTACACCCAGA
PRKG1 (human)	ATCAGGCAAGGTGCAAGAGG	CCTGCAAGGCTTTCTCTCCA
PRKG2 (human)	TCCTGCACAATGGGAAGAGG	ATGGGGTAGCCTCTAGCAGT
CHK2 (human)	GCAGGTTTAGCGCCACTCTG	TCCGACTCCCGAGACATCAC

Table S 3: Primers used for qPCR analysis of pro-inflammatory markers (mouse)

Gene	Forward	Reverse
IL-1β	GCAACTGTTCCTGAACTCAACT	ATCTTTTGGGGTCCGTCAACT
IL-6	TAGTCCTTCCTACCCCAATTTCC	TTGGTCCTTAGCCACTCCTTC
iNOS	CCAAGCCCTCACCTACTTCC	CTCTGAGGGCTGACACAAGG
MCP-1	CCACTCACCTGCTGCTACTCA	TGGTGATCCTCTTGTAGCTCTCC
TNFα	ACGGCATGGATCTCAAAGAC	AGATAGCAAATCGGCTGACG

Table S 4: Peptides highly phosphorylated in hVAT of MOD as compared to MOND patients

Rank	ID	UniprotAccession	Sequence	Ser	Thr	p-value
1	NCF1_296_308	P14598	RGAPPRRSSIRNA	[303, 304]	[]	1.42E-03
2	NCF1_321_333	P14598	QDAYRRNSVRFLQ	[328]	[]	2.09E-03
3	SCN7A_898_910	Q01118	KNGCRRGSSLGQI	[905, 906]	[]	3.31E-03
4	PTN12_32_44	Q05209	FMRLRRLSTKYRT	[39]	[40, 44]	3.84E-03
5	VTNC_390_402	P04004	NQNSRRPSRATWL	[393, 397]	[400]	4.14E-03
6	ADRB2_338_350	P07550	ELLCLRRSSLKAY	[345, 346]	[]	5.74E-03
7	GBRB2_427_439	P47870	SRLRRRASQLKIT	[427, 434]	[439]	5.74E-03
8	CAC1C_1974_1986	Q13936	ASLGRRASFHLEC	[1975, 1981]	[]	6.50E-03
9	BAD_69_81	Q92934	IRSRHSSYPAGTE	[71, 74, 75]	[80]	6.59E-03
10	EPB42_241_253	P16452	LLNKRRGSVPILR	[248]	[]	6.59E-03
11	GPSM2_394_406	P81274	PKLGRRHSMENME	[401]	[]	6.70E-03
12	MYPC3_268_280	Q14896	LSAFRRTSLAGGG	[269, 275]	[274]	6.71E-03
13	NFKB1_330_342	P19838	FVQLRRKSDLETS	[337, 342]	[341]	6.76E-03
14	VASP_150_162	P50552	EHIERRVSNAGGP	[157]	[]	7.15E-03
15	DESP_2842_2854	P15924	RSGSRRGSFDATG	[2843, 2845, 2849]	[2853]	7.76E-03
16	VASP_271_283	P50552	LARRRKATQVGEK	[]	[278]	8.65E-03
17	CGHB_109_121	P01233	QCALCRRSTTDCG	[116]	[117, 118]	8.97E-03
18	KPB1_1011_1023	P46020	QVEFRRLSISAES	[1018, 1020, 1023]	[]	9.05E-03
19	CFTR_730_742	P13569	EPLERRLSLVPDS	[737, 742]	[]	9.24E-03
20	LIPS_944_956	Q05469	GFHPRRSSQGATQ	[950, 951]	[955]	9.53E-03
21	KAP2_92_104	P13861	SRFNRRVSVCAET	[92, 99]	[104]	9.63E-03
22	KCNA6_504_516	P17658	ANRERRPSYLPTP	[511]	[515]	1.00E-02

23	CREB1_126_138	P16220	EILSRRPSYRKIL	[129, 133]	[]	1.01E-02
24	ANDR_785_797	P10275	VRMRHLSQEFGWL	[791]	[]	1.11E-02
25	RYR1_4317_4329	P21817	VRRLRRLTAREAA	[]	[4324]	1.15E-02
26	KAP3_107_119	P31323	NRFTRRASVCAEA	[114]	[110]	1.20E-02
27	E1A_ADE05_212_224	P03255	AILRRPTSPVSRE	[219, 222]	[218]	1.20E-02
28	F263_454_466	Q16875	NPLMRRNSVTPLA	[461]	[463]	1.27E-02
29	ANXA1_209_221	P04083	AGERRKGTDVNVF	[]	[216]	1.29E-02
30	RAP1B_172_184	P61224	PGKARKKSSCQLL	[179, 180]	[]	1.29E-02
31	KCNA1_438_450	Q09470	DSDLSRRSSSTMS	[439, 442, 445, 446, 447, 450]	[448]	1.31E-02
32	CENPA_1_14	P49450	MGPRRRSRKPEAPR	[7]	[]	1.32E-02
33	REL_260_272	Q04864	KMQLRRPSDQEVS	[267, 272]	[]	1.35E-02
34	TY3H_65_77	P07101	FIGRRQSLIEDAR	[71]	[]	1.35E-02
35	STMN2_90_102	Q93045	AAGERRKSQEAQV	[97]	[]	1.42E-02
36	NMDZ1_890_902	Q05586	SFKRRRSSKDTST	[890, 896, 897, 901]	[900, 902]	1.47E-02
37	PPR1A_28_40	Q13522	QIRRRPTPATLV	[]	[35, 38]	1.51E-02
38	PLM_76_88	O00168	EEGTFRSSIRRLS	[82, 83, 88]	[79]	1.57E-02
39	NOS3_1171_1183	P29474	SRIRTQSFSLQER	[1171, 1177, 1179]	[1175]	1.57E-02
40	GPR6_349_361	P46095	QSKVPFRSRSPSE	[350, 356, 358, 360]	[]	1.60E-02
41	CSF1R_701_713	P07333	NIHLEKKYVRRDS	[713]	[]	1.74E-02
42	RS6_228_240	P62753	IAKRRLSSLRAS	[235, 236, 240]	[]	1.85E-02
43	PTK6_436_448	Q13882	ALRERLSSFTSYE	[442, 443, 446]	[445]	1.98E-02
44	FRAP_2443_2455	P42345	RTRTDSYSAGQSV	[2448, 2450, 2454]	[2444, 2446]	2.02E-02
45	PDE5A_95_107	O76074	GTPTRKISASEFD	[102, 104]	[96, 98]	2.09E-02

46	TOP2A_1463_1475	P11388	RRKRKPSTSDDSD	[1469, 1471, 1474]	[1470]	2.10E-02
47	H32_3_18	Q71DI3	RTKQTARKSTGGKAPR	[11]	[4, 7, 12]	2.12E-02
48	KCNA2_442_454	P16389	PDLKKSRSASTIS	[447, 449, 451, 454]	[452]	2.13E-02
49	K6PL_766_778	P17858	LEHVTRRTLSMDK	[775]	[770, 773]	2.15E-02
50	COF1_17_29	P23528	DMKVRKSSTPEEV	[23, 24]	[25]	2.36E-02
51	ADDB_706_718	P35612	KKKFRTPSFLKKS	[713, 718]	[711]	2.38E-02
52	ESR1_160_172	P03372	GGRERLASTNDKG	[167]	[168]	2.42E-02
53	STK6_283_295	O14965	SSRRTTLCGTLDY	[283, 284]	[287, 288, 292]	2.45E-02
54	H2B1B_ 27_40	P33778	GKKRKRSRKESYSI	[33, 37, 39]	[]	2.47E-02
55	KIF2C_105_118_S106G	Q99661	EGLRSRSTRMSTVS	[109, 111, 115, 118]	[112, 116]	2.57E-02
56	RAF1_253_265	P04049	QRQRSTSTPNVHM	[257, 259]	[258, 260]	2.62E-02
57	PLEK_106_118	P08567	GQKFARKSTRRSI	[113, 117]	[114]	2.63E-02
58	KPCB_19_31_A25S	P05771	RFARKGSLRQKNV	[25]	[]	2.88E-02
59	BAD_93_105	Q92934	FRGRSRSAPPNLW	[97, 99]	[]	3.08E-02
60	BAD_112_124	Q92934	RELRRMSDEFVDS	[118, 124]	[]	3.30E-02
61	RBL2_655_667	Q08999	GLGRSITSPTTLY	[659, 662]	[661, 664, 665]	3.37E-02
62	KCNA3_461_473	P22001	EELRKARSNSTLS	[468, 470, 473]	[471]	3.40E-02
63	GYS2_1_13	P54840	MLRGRSLSVTSLG	[6, 8, 11]	[10]	3.81E-02
64	RB_242_254	P06400	AVIPINGSPRTPR	[249]	[252]	4.66E-02
65	ACM1_444_456	P11229	KIPKRPGSVHRTP	[451]	[455]	4.93E-02

Figure Legends

Figure 1: Pim-1 kinase activity is upregulated in human visceral adipose tissue (hVAT) of morbid obese diabetic (MOD) patients as seen in upstream score plot using kinexus-based analysis.

The heatmap shows that more than 60 peptides were highly phosphorylated in visceral adipose tissue samples from morbid obese diabetic (IR) as compared to samples from morbid obese non-diabetic (IS) patients (A). Upstream kinase analysis was done using the Bionavigator software of the PamGene, which bases its assumption on kinexus. Peptide set size corresponding to each kinase is denoted by the size of the dot. As for the specificity of these peptides to the kinase, it ranges from black (0) to red (2). The darker the red color, the higher the specificity of the peptide set to the kinase. Negative values indicate higher kinase activity in the MOD group. As seen in this score plot, PKG1, PKG2, PKA, Pim-1, Pim-2, Pim-3, PRKX, PKC, p70S6Kβ, CHK2, PKD1, Akt1/PKB, etc. have higher kinase activity in the hVAT samples from MOD patients, as compared to the hVAT samples from morbid obese non-diabetic (MOND) patients (B). An interaction network was constructed using the STRING tool and the selected kinases as input. The width of the interactions depends on the confidence score to each association in STRING, i.e. the thickness of the lines indicates the strength of the data support. Each color group of the kinases is attributed to a kinase cluster, giving a total of 5 different groups of interacting kinases (C). More detailed information is found in the Materials and Methods section. n = 21-24.

Figure 2: Pim-1 gene expression positively correlates to IR markers in hVAT and is upregulated in mVAT of 2 IR mouse models.

RTqPCR was performed on visceral adipose tissue samples taken from more than 80 lean, obese, and morbid obese healthy and diabetic patients. Pim-1 relative gene expression

positively correlates with BMI (A), insulinemia (B), and glycemia (C). Pim-2 positively correlates with BMI (D), but not with insulinemia (E) or glycemia (F). Pim-3 does not correlate with any of the three markers (G-I). Pim expression was also checked in visceral adipose tissue from 2 mouse models of insulin resistance (J-O). RNA sequencing data of VAT from male mice under CHOW or HFD (8 or 20 weeks) show that Pim-1 expression was significantly increased in VAT of mice under HFD, with higher values in the 20 weeks' duration (J), Pim-2 does not differ (K), and Pim-3 significantly decreases in mice under HFD (L). Pim-1 and Pim-2 gene expression significantly increase in VAT of male db/db mice (M-N), while Pim-3 significantly decreases (O). RS9 and 18S were used as housekeeping genes. Significance of the correlation data was determined using the Pearson correlation coefficients, with * $p < 0.05$, ** $p < 0.01$. Results of panels D-E represent the average ± SEM. n= 5-7 mice. Significance was determined using the Bonferroni-Dunn method, with * $p < 0.05$, ** $p < 0.01$, *** $p < 0.001$, **** $p < 0.0001$.

Figure 3: Pim-1 inhibition does not promote insulin sensitivity in TNFα-treated mature adipocytes.

Pim-1 mRNA is highly expressed in mature adipocytes as compared to pre-mature adipocytes (A). Western blot analysis of mature adipocytes with or without 48h of 10ng/mL TNFα, stimulated with 100nM insulin for 15' (B). pT308 Akt, readout for insulin resistance, was significantly decreased in TNFα-treated mature adipocytes (C). Western blot analysis of IS and IR mature adipocytes treated with SGI-1776 (0.1, 0.25, 0.5, and 1μM) and stimulated with 100nM insulin for 15' (D). pS112 Bad, Pim-1 phospho-target, was significantly decreased at 0.25, 0.5, and 1μM of the inhibitor (E). pT308 Akt was not rescued with the inhibitor treatment (F). RS9 and 18S were used as housekeeping genes in RTqPCR experiments. 10μg of extracted protein was blotted, and α-Tubulin was used as the loading control. Western blot quantification

is done using ImageJ. Results represent the average ± SEM, with n=3. Significance was determined using the Bonferroni-Dunn method, with * $p < 0.05$, ** $p < 0.01$, *** $p < 0.001$, **** $p < 0.0001$.

Figure 4: Pim-1 kinase activity and gene expression are upregulated in pro-inflammatory macrophages.

Protein was extracted from naive and 6h-LPS-stimulated pro-inflammatory BMDMs, and then incubated on PamChip Serine/Threonine kinase microarrays to detect peptide phosphorylation. Upstream kinase analysis was done using the Bionavigator software of the PamGene, which bases its assumption on kinexus. Peptide set size corresponding to each kinase is denoted by the size of the dot. As for the specificity of these peptides to the kinase, it ranges from black (0) to red (2). The darker the red color, the higher the specificity of the peptide set to the kinase. Positive values indicate higher kinase activity in LPS-stimulated macrophages. As seen in the score plot, PKA, AMPK, several CDKs, and Pim-1 have higher kinase activity in the pro-inflammatory LPS-stimulated macrophages (A). Heat map of the RNA sequencing data from naive and LPS-treated macrophages show that PRKX, Pim-1, and Pim-2 genes are significantly high in the pro-inflammatory as compared to naïve BMDMs (B). RTqPCR data show that Pim-1 mRNA expression is significantly higher in M1-sorted macrophages from VAT of HFD mice (C). PamGene results are the average of 3 independent experiments, each with 4 replicates. B2M was used as the housekeeping gene in RTqPCR experiments, and results represent the average ± SEM, n = 6. Significance was determined using the Bonferroni-Dunn method, with * $p < 0.05$, ** $p < 0.01$, *** $p < 0.001$, **** $p < 0.0001$.

Figure 5: Pim-1 expression is high in LPS-stimulated macrophages, and its inhibition decreases the expression of pro-inflammatory markers.

RTqPCR was performed on naïve and LPS-stimulated (6h, 24h) macrophages (A-B). Expression of pro-inflammatory markers IL-1β, IL-6, TNFα, and MCP-1 significantly increase in LPS-treated macrophages for 6h (A). Pim-1 expression is significantly high in LPS-treated pro-inflammatory macrophages (B). Western blot analysis of naïve and LPS-stimulated macrophages (6h, 24h) against Pim-1, pS112 Bad, and pT145p21 (C). Pim-1 protein expression decreases in LPS-treated macrophages for 6h, while it increases back to normal levels in LPS-treated macrophages for 24h (D). pS112 Bad and pT145p21, Pim-1 phospho targets, significantly increase in LPS-treated macrophages (E). Pro-inflammatory macrophages that are LPS-stimulated for 6h were treated with DMSO or 0.25μM SGI-1776 for 24h. Pro-inflammatory markers IL-1β, TNFα, MCP-1, and iNOS gene expression significantly decrease upon inhibitor treatment (F). Pim-1 gene expression tends to decrease upon inhibitor treatment (G). RS9 and actin were used as housekeeping genes in RTqPCR experiments. 10μg of extracted protein was blotted, and α-Tubulin was used as the loading control. Western blot quantification is done using ImageJ. Results represent the average ± SEM, with n = 3. Significance was determined using the Bonferroni-Dunn method, with * p < 0.05, ** p < 0.01, *** p < 0.001.

Figure 6: db/db mice treated with SGI-1776 for 3 weeks have lower fat mass, increased glucose and insulin sensitivity, and decreased VAT inflammation.

Gavaged mice with DMSO or the Pim-1 inhibitor do not differ in food intake (A) or total body weight (B). However, their % lean mass increases (C), and their % fat mass decreases (D) as compared to the control group. The relative masses of VAT and SAT of treated mice significantly decrease in the treated group, while the relative masses of the liver, heart, and gastrocnemius do not change between the groups (E). The % change in fasting glycemia before and after treatment tends to decrease in the treated group (F). Mice underwent an insulin

tolerance test at day 9 post-treatment, in which the treated db/db mice became more insulin sensitive after 1h of insulin injection (G), and had a significant decrease in the Area Under Curve (H). Glucose tolerance test was done on both groups at day 18 post-treatment. Treated mice became more glucose tolerant after 30' of glucose injection (I), and had a significant decrease in the area under curve in SGI-1776-gavaged mice (J). RTqPCR was done on VAT of all mice, and gene expression of several pro-inflammatory macrophage markers was measured. iNOS, TNFα, and MCP-1 decrease in the SGI-1776-gavaged group, while IL-1β and IL-6 tend to increase (K). Cross-sections of the mVAT of control and treated mice were stained for H/E and F4/80, a macrophage marker (L). An example of a crown-like structure is depicted in the magnified image. For each mVAT sample, 20 images were taken and all crown-like structures were counted, and shown to be significantly decreased in mVAT of treated mice (M). Results represent the average ± SEM, n = 8-9 mice. Significance was determined using the Bonferroni-Dunn method, with * $p < 0.05$, ** $p < 0.01$, *** $p < 0.001$, **** $p < 0.0001$.

Supplemental Figure 1: Kinome profiling of human visceral adipose tissue (hVAT) samples from morbid obese diabetic (MOD) and morbid obese non-diabetic MOND) patients.

The protein lysate was extracted from morbid obese visceral adipose tissue from IS and IR patients, and were passed into the PamStation, where the samples were incubated on PamChip Serine/Threonine kinase microarrays to detect kinase activity readout, by peptide phosphorylation and FITC labelling. The Log Data is then displayed as a heat map showing that more than 60 peptides were highly phosphorylated in visceral adipose tissue samples from morbid obese diabetic (IR) as compared to samples from morbid obese non-diabetic (IS) patients. The darker the red color, the higher the phosphorylation. The darker the blue color, the lower the phosphorylation. n = 21-24.

Supplemental Figure 2: Gene expression correlations to IR markers in hVAT and kinase activity validation of Pim family in mVAT.

RTqPCR was performed on visceral adipose tissue samples taken from more than 80 lean, obese, and morbid obese healthy and diabetic patients (A-I). PRKG1 relative gene expression negatively correlates with BMI (A) not insulinemia (B) or glycemia (C). PRKG2 (D-F) and CHK2 (G-I) do not correlate with any of the IR markers. RS9 and 18S were used as housekeeping genes. Significance was determined using the Pearson correlation coefficients, with * $p < 0.05$, ** $p < 0.01$.

Supplemental Figure 3: Kinome profiling of naïve and pro-inflammatory macrophages.

Protein was extracted from naïve and 6h-LPS-stimulated pro-inflammatory macrophages. Samples were then incubated on PamChip Serine/Threonine kinase microarrays to detect peptide phosphorylation. As seen in this heat map, the upper 45 peptides were highly phosphorylated in the pro-inflammatory LPS-stimulated macrophages. The darker the red color, the higher the phosphorylation, and the darker the blue color, the lower the phosphorylation (A). RTqPCR data show that Pim-2 and Pim-3 mRNA expression does not change in M1-sorted macrophages from VAT of HFD mice as compared to mice under CHOW diet (B). PamGene results are the average of 3 independent experiments, each with 4 replicates. B2M was used as the housekeeping gene in RTqPCR experiments, and results represent the average ± SEM, with n = 5.

Materials and Methods

Human Samples

Cohort 1: Patients scheduled for a bariatric surgery procedure were recruited from the obesity outpatient clinic of Hospital Universitari Germans Trias, Badalona (Spain) and from the Hospital Universitario Virgen de la Victoria, Malaga (Spain). The study was conducted according to the principles of the Declaration of Helsinki. All patients signed an informed consent form approved by the corresponding institutional ethics committee. Inclusion criteria were as follows: age between 18 and 60 years, BMI >35 kg/m2. Exclusion criteria were type 1 diabetes or positivity for GAD autoantibodies, secondary forms of diabetes, acute metabolic complications, liver disease, renal dysfunction or patients under anticoagulant treatment, pregnancy and corticoid use by oral or intravenous route for more than 14 consecutive days in the last 3 months. Patients were classified as having type 2 diabetes (MOD) according to ADA criteria (American Diabetes, 2010) or as morbid obese non-diabetic subjects (MOND). A physical examination with determination of anthropometrical parameters and a complete biochemical analysis was performed before bariatric surgery (Table 1). A sample of visceral fat was obtained during the surgical bariatric procedure.

Cohort 2: lean (20), obese (23) and morbid obese (43) patients were included in the study from a biobank adipose tissue collection (registry number C.0001665 from the national registry of biobank collections at the Instituto de Salud Carlos III (ISCIII) (Spain) managed by the Institut d'Investigacio Sanitaria Pere Virgili (IISPV). Visceral adipose tissue samples with clinical and analytical variables were obtained from this collection and registry. All samples had the corresponding informed consent approved by the IISPV ethics committee. The main clinical and analytical characteristics are shown in table 2.

Glucose, cholesterol and triglycerides were determined using standard enzymatic methods. Plasma insulin was analyzed by immunoassay (Coat-A-Count Insulin; Diagnostic Products Corp., Los Angeles, CA). Glycated haemoglobin (HbA1c) was measured by high-pressure liquid chromatography using a fully automated analyzer system (Hitachi L-9100). The homeostatic model assessment insulin resistance index (HOMA-IR) was calculated by the formula: (plasma glucose (mmol/l) x serum insulin (mU/L)) / 22.5.

Isolation of mature adipocytes and stromal vascular fraction

SVF was obtained from human adipose tissue biopsies as described (Ceperuelo-Mallafre et al., 2016; Serena et al., 2016; Serena et al., 2017). Briefly, sub-cutaneous white adipose tissue (scWAT) and visceral white adipose tissue (vWAT) was washed extensively with PBS to remove debris and treated with 0.1% collagenase in PBS and 1% BSA for 1 hr at 37°C with gentle agitation. Digested samples were centrifuged at 300 × g at 4°C for 5 min to separate adipocytes from the SVF. Adipocytes were directly used for RNA isolation and the cell pellet containing the SVF was resuspended in red-blood-cell lysis buffer (10 mM KHCO3, 150 mM NH4Cl, 0.1 mM EDTA) for 2 min, then washed with PBS and passed through a 40-μm filter (Fisher Scientific). To isolate ultrapure ATMs, the SVF was incubated with F4/80 MicroBeads (130-110-443, MiltenyiBiotec S.L. Madrid, Spain) for 30 min and positive selection was performed with an autoMACS separator (MiltenyiBiotec).

Flow cytometry

The SVF from scWAT and vWAT was isolated as described above. To isolate myeloid lineage cells, SVF was incubated with CD11b MicroBeads (130-049-601, MiltenyiBiotec) for 30 min, and positive selection was performed with an autoMACS separator. Magnetically isolated CD11b+ cells were washed and incubated with the desired combination of fluorochrome-conjugated monoclonal antibodies, including FITC-anti-F4/80 (clone BM8), APC-anti-CD11c

(clone N418), PE-anti-CD206 (clone MR6F3) and PE-Cy7-anti-Ly-6G (clone RB6-8C5) (all from eBiosciences, San Diego, CA) for 20 min. Data were acquired on a FACS Aria III (BD Biosciences) and analysis was performed using FACSDivaTM software (BD Biosciences).

Kinome Profiling (PamGene):

For kinome analysis, serine/threonine (STK) kinase microarrays were purchased from PamGene International BV. Each array contained 140 phosphorylatable peptides, as well as 4 control peptides. Sample incubation, detection, and analysis were performed according to the manufacturer's instructions in a PamStation 12. Briefly, extracts from human adipose tissue were made using M-PER mammalian extraction buffer (Thermo Scientific) containing 1:50 Halt phosphatase inhibitor cocktail (Thermo Scientific) and 1:50 Halt protease inhibitor cocktail EDTA-free (Thermo Scientific) for 20 min on a spinning wheel at 4°C. The lysates were then centrifuged at 13,000 r.p.m. for 20 min to remove all debris. The supernatant was aliquoted, snap-frozen in liquid nitrogen, and stored at -80°C until further processing. Prior to incubation with the kinase reaction mix, the arrays were blocked with 2% BSA for 30 cycles and washed three times with PK assay buffer. Kinase reactions were performed over 1 h with 5 µg total extract and 400 µM ATP at 30°C. Phosphorylated peptides were detected with a secondary anti rabbit-FITC antibody that recognizes a pool of anti-phospho serine/threonine antibodies. The instrument contains a 12-bit CCD camera suitable for imaging of FITC-labelled arrays. The images obtained from the phosphorylated arrays were quantified using the bionavigator software (PamGene International BV). Generated heat maps and kinexus plots are further explained in the results and figures sections.

STRING Analysis

Based on the kinexus plot generated by the bionavigator software (PamGene International BV), we chose the top 20 kinases. The hit kinases were then used as input in the STRING software. A kinase interaction network was constructed with a minimum required interaction score or medium confidence of 0.4 and several criteria for linkage, i.e. co-expression, experimental evidence, existing databases, text mining, as well as co-occurrence and neighborhood. Further explanation is found in the figure legend.

Mouse Strains and Diet Information

BKS(D)-Lepr db/+JOrlRj and BKS(D)-Lepr db/db JOrlRj male mice were obtained from Janvier Labs. Mice had free access to standard rodent chow diet and water, unless stated otherwise. They were housed 5 mice per cage in a 12h-day 12h-night cycle, unless stated differently. Animals were gavaged daily with 75mg/kg of vehicle or SGI-1776 (HY-13287) purchased from MedChemTronics, the European branch of MedChemExpress, for 21 consecutive days. Mice were acclimated and submitted to the PhenoMaster (metabolic phenocage) throughout the treatment, by which food intake was measured. Body weight was controlled daily. Following the protocol, mice were killed by cervical dislocation and tissues were isolated for analysis.

Male C57Bl6 mice were fed with HFD with 60% calories from fat (Research Diet D12492) or matched control diet (D12450J) starting from 5 weeks of age.

All animal care and treatment procedures were performed in accordance with Swiss guidelines and were approved by the Canton of Vaud, Service de la Consommation et des Affaires Vétérinaires (SCAV) (authorization VD 3371.b).

Glucose and Insulin Tolerance Tests

For the Glucose Tolerance Test, mice were starved for 16h and then injected intraperitoneally with glucose (2g/kg). Tail vein blood glucose was checked at the indicated time points. For the

Insulin Tolerance Test, mice were fasted for 6h, after which they were injected intraperitoneally with 1.125 U/kg insulin, and tail vein blood glucose was then measured at the indicated time.

Metabolic Phenocage of the PhenoMaster

This special automated cage construct separates, collects, and quantifies urine and feces of mice or rats, and thus provides important information about the animal's energy balance. Dedicated urine and feces collection funnels direct urine and feces into standard lab tubes. Weighing sensors below the collection containers quantify urine and feces by amount and time. Before measurement, mice were adapted for five days, after which the mice stayed throughout the whole period of treatment. Individual mice were housed in a single test chamber (size, 8" x 5" x 4"). Animals had free access to food and water during the entire experiment period.

Body Composition Analysis Using the EchoMRI

Lean body mass, fat mass, free water, and total water were measured on live animals by quantitative magnetic resonance (QMR) using an EchoMRI instrument. Mice were not restrained nor anesthetized.

Immunohistochemistry

Adipose Tissue samples were fixed overnight at 4°C with 4% paraformaldehyde, and then washed 3 times with cold PBS and embedded in parafinn. 4μm sections cut at 50μm intervals were mounted on charged glass slides, deparaffinized in xylene, and stained for expression of F4/80 as described by (Cecchini et al., 1994) with anti-F4/80 monoclonal antibody (ab6640) from Abcam, and hematoxylin and eosin as described in (Ni et al., 2018). Histological observation was done using light microscopy (Olympus Upright Motorized Microscope, Olympus Corporation, Tokyo, Japan). Image acquisition and processing was performed using the AxioVision software. 2 tissue sections were selected from each mouse, and 20 random non-

overlapping fields at 10x magnification were taken. In a blinded manner, crown-like structures of the F4/80 staining were manually counted.

3T3L1 Differentiation

3T3-L1 were cultured in Dulbecco's modified Eagle's medium (DMEM) with 10% foetal bovine serum (FBS, PAA Laboratories) in 5% CO_2. Two days after reaching confluence, they were differentiated with DMEM, 10% FBS, 0.5 mM 3-isobutyl-1methylxanthine (IBMX), 1.7 µM insulin, 1 µM dexamethasone, and 1 µM rosiglitazone for 2 days. From day 3 onward, cells were incubated with DMEM, 10% FBS, 10 µg/ml insulin. Media was changed every 2 days until day 8 of differentiation. 3T3-L1 mature adipocytes were maintained in medium containing 10% FBS only.

3T3L1 Insulin Resistance Models and Treatment

After differentiation, mature 3T3L1 adipocytes were washed with PBS and incubated with or without 20 ng/ml TNFα in DMEM containing 0.2% bovine serum albumin (BSA). Insulin resistant mature adipocytes were treated overnight with DMSO, 0.1µM, 0.25µM, 0.5µM or 1µM SGI-1776. Then, cells were starved and stimulated with or without insulin, at 100 nM. Cells were washed with cold PBS and lysed as described later.

BMDM Treatment

Bone marrow-derived macrophages (BMDMs) were seeded in 10cm petri-dishes. After cells attached, they were treated with control or 100ng/mL LPS for 6h or 24h. As for treatment with the inhibitor, BMDMs were seeded in 6-well plates. After they attached, BMDMs were treated with DMSO or 0.25µM SGI-1776 for 24h, and then 100ng/mL LPS was added for 6h.

Protein Extraction and Western Blotting:

For Western blot (WB) analysis, protein extraction from different mouse tissues, cell lysates, and human adipose tissue samples was obtained with M-PER mammalian extraction buffer

(Thermo Scientific, USA) containing 1:100 Halt phosphatase inhibitor cocktail (Thermo Scientific, USA) and 1:100 Halt protease inhibitor cocktail, EDTA-free (Thermo Scientific, USA). Membranes were incubated over night at 4°C with the corresponding primary antibodies. The following day, membranes were washed and incubated with the corresponding secondary antibodies, washed and revealed with ECL in the fusion Fx. WB bands were quantified using ImageJ or Fiji software.

The following antibodies were used for Western blot analysis: anti-phospho AKT-T308 (4056), anti AKT (9272), anti-phospho IKKα/β-S176/180 (2697) and anti IKKβ (8943) from cell signaling, anti-phospho Bad-S112 (ab129192) and anti-phospho p21-T145 (ab135553) from Abcam, anti-PIM1 (AP7932d) from Abgent, and anti-Tubulin (T6199) from Sigma.

RNA Extraction and RTqPCR:

Samples were lysed using TRI-reagent (T9424, Sigma Aldrich), according to the manufacturer's instructions. An additional centrifugation step immediately after lysis was included in order to remove the lipid layer when adipose tissue samples or mature 3T3L1 adipocytes were extracted. For adipose tissue samples, a second chloroform wash step, followed by an overnight precipitation using ammonium acetate and absolute ethanol, was performed to remove phenol contaminations. Quality check and quantification of the RNA was done using the Nanodrop. cDNA was prepared using 1μg of total RNA (unless stated otherwise), using Superscript II (Invitrogen). cDNAs were diluted 20 times and used for qPCR. qPCR experiments were done using the FastStart Universal SYBR Green Master (Rox) from Roche and a 7900HT Fast Real-Time PCR System (Applied Biosystems), with a mix of 10μM forward and reverse primers of the targeted genes. Relative mRNA expression levels were calculated from the comparative threshold cycle (Ct) values of the gene of interest relative to RS9 and actin mRNA (unless stated otherwise). Specific primer sequences are listed in Table S1, S2 and S3.

Data Analysis:

All statistics are described in the figure legends. All *P*-values below 0.05 were considered significant. The results were expressed as means ± standard error of the means (s.e.m). Statistical significance values were represented by asterisks corresponding to *p<0.05, **p<0.01, ***p<0.001, and ****p<0.0001.

Acknowledgements

Author Contributions

A.N., I.C.L-M and L.F. designed the study. A.N. and I.C.L-M performed kinome experiments. A.N., I.C.L-M., A.B. and I.X. analyzed the kinome experiments. A.N. performed *in vitro* and

in vivo experiments and their analysis, with the help of I.C.L-M. P-S.L., X.L, W-C.C. and P-C.H performed BMDM cultures and provided BMDM RNA Sequencing data for the top 20 kinase candidates. M.E. and S.F-V. performed the ATM sorting. E-A.F., J.C-A, L.M-C. and E.C. provided technical assistance. T.C. and F.G. provided mouse VAT RNA Sequencing data for the top 20 kinase candidates. F-J.T. and J.V-O. and S.P. provided the human samples, performed anthropometric studies and classified metabolic status of cohorts. A.N., I.C.L-M and L.F. wrote the manuscript.

Declaration of Interests

The authors declare no competing interests.

References

Agrawal, N. K., & Kant, S. (2014). Targeting inflammation in diabetes: Newer therapeutic options. *World J Diabetes, 5*(5), 697-710. Retrieved from https://www.ncbi.nlm.nih.gov/pubmed/25317247. doi:10.4239/wjd.v5.i5.697

Amaravadi, R., & Thompson, C. B. (2005). The survival kinases Akt and Pim as potential pharmacological targets. *J Clin Invest, 115*(10), 2618-2624. Retrieved from https://www.ncbi.nlm.nih.gov/pubmed/16200194. doi:10.1172/JCI26273

American Diabetes, A. (2010). Diagnosis and classification of diabetes mellitus. *Diabetes Care, 33 Suppl 1*, S62-69. Retrieved from https://www.ncbi.nlm.nih.gov/pubmed/20042775. doi:10.2337/dc10-S062

An, N., Kraft, A. S., & Kang, Y. (2013). Abnormal hematopoietic phenotypes in Pim kinase triple knockout mice. *J Hematol Oncol, 6*, 12. Retrieved from https://www.ncbi.nlm.nih.gov/pubmed/23360755. doi:10.1186/1756-8722-6-12

Andersen, E., Ingerslev, L. R., Fabre, O., Donkin, I., Altintas, A., Versteyhe, S., . . . Barres, R. (2019). Preadipocytes from obese humans with type 2 diabetes are epigenetically reprogrammed at genes controlling adipose tissue function. *Int J Obes (Lond), 43*(2), 306-318. Retrieved from https://www.ncbi.nlm.nih.gov/pubmed/29511320. doi:10.1038/s41366-018-0031-3

Ando, Y., Shinozawa, Y., Iijima, Y., Yu, B. C., Sone, M., Ooi, Y., . . . Takahashi, S. (2015). Tumor necrosis factor (TNF)-alpha-induced repression of GKAP42 protein levels through cGMP-dependent kinase (cGK)-Ialpha causes insulin resistance in 3T3-L1 adipocytes. *J Biol Chem, 290*(9), 5881-5892. Retrieved from https://www.ncbi.nlm.nih.gov/pubmed/25586176. doi:10.1074/jbc.M114.624759

Arroyo-Johnson, C., & Mincey, K. D. (2016). Obesity Epidemiology Worldwide. *Gastroenterol Clin North Am, 45*(4), 571-579. Retrieved from https://www.ncbi.nlm.nih.gov/pubmed/27837773. doi:10.1016/j.gtc.2016.07.012

Brandon, A. E., Liao, B. M., Diakanastasis, B., Parker, B. L., Raddatz, K., McManus, S. A., . . . Schmitz-Peiffer, C. (2019). Protein Kinase C Epsilon Deletion in Adipose Tissue, but Not in Liver, Improves Glucose Tolerance. *Cell Metab, 29*(1), 183-191 e187. Retrieved from https://www.ncbi.nlm.nih.gov/pubmed/30318338. doi:10.1016/j.cmet.2018.09.013

Brault, L., Gasser, C., Bracher, F., Huber, K., Knapp, S., & Schwaller, J. (2010). PIM serine/threonine kinases in the pathogenesis and therapy of hematologic malignancies and solid cancers. *Haematologica, 95*(6), 1004-1015. Retrieved from https://www.ncbi.nlm.nih.gov/pubmed/20145274. doi:10.3324/haematol.2009.017079

Cecchini, M. G., Dominguez, M. G., Mocci, S., Wetterwald, A., Felix, R., Fleisch, H., . . . Stanley, E. R. (1994). Role of colony stimulating factor-1 in the establishment and regulation of tissue macrophages during postnatal development of the mouse. *Development, 120*(6), 1357-1372. Retrieved from https://www.ncbi.nlm.nih.gov/pubmed/8050349.

Ceperuelo-Mallafre, V., Ejarque, M., Serena, C., Duran, X., Montori-Grau, M., Rodriguez, M. A., . . . Fernandez-Veledo, S. (2016). Adipose tissue glycogen accumulation is associated with obesity-linked inflammation in humans. *Mol Metab, 5*(1), 5-18. Retrieved from https://www.ncbi.nlm.nih.gov/pubmed/26844203. doi:10.1016/j.molmet.2015.10.001

Copps, K. D., & White, M. F. (2012). Regulation of insulin sensitivity by serine/threonine phosphorylation of insulin receptor substrate proteins IRS1 and IRS2. *Diabetologia,*

55(10), 2565-2582. Retrieved from http://www.ncbi.nlm.nih.gov/pubmed/22869320. doi:10.1007/s00125-012-2644-8

Dhanasekaran, S. M., Barrette, T. R., Ghosh, D., Shah, R., Varambally, S., Kurachi, K., . . . Chinnaiyan, A. M. (2001). Delineation of prognostic biomarkers in prostate cancer. *Nature, 412*(6849), 822-826. Retrieved from https://www.ncbi.nlm.nih.gov/pubmed/11518967. doi:10.1038/35090585

Eichmann, A., Yuan, L., Breant, C., Alitalo, K., & Koskinen, P. J. (2000). Developmental expression of pim kinases suggests functions also outside of the hematopoietic system. *Oncogene, 19*(9), 1215-1224. Retrieved from https://www.ncbi.nlm.nih.gov/pubmed/10713710. doi:10.1038/sj.onc.1203355

Garrison, C. B., Lastwika, K. J., Zhang, Y., Li, C. I., & Lampe, P. D. (2017). Proteomic Analysis, Immune Dysregulation, and Pathway Interconnections with Obesity. *J Proteome Res, 16*(1), 274-287. Retrieved from https://www.ncbi.nlm.nih.gov/pubmed/27769113. doi:10.1021/acs.jproteome.6b00611

Goossens, G. H. (2017). The Metabolic Phenotype in Obesity: Fat Mass, Body Fat Distribution, and Adipose Tissue Function. *Obes Facts, 10*(3), 207-215. Retrieved from https://www.ncbi.nlm.nih.gov/pubmed/28564650. doi:10.1159/000471488

Gupta, M. K., & Vadde, R. (2019). Identification and characterization of differentially expressed genes in Type 2 Diabetes using in silico approach. *Comput Biol Chem, 79*, 24-35. Retrieved from https://www.ncbi.nlm.nih.gov/pubmed/30708140. doi:10.1016/j.compbiolchem.2019.01.010

Hotamisligil, G. S., Shargill, N. S., & Spiegelman, B. M. (1993). Adipose expression of tumor necrosis factor-alpha: direct role in obesity-linked insulin resistance. *Science, 259*(5091), 87-91. Retrieved from https://www.ncbi.nlm.nih.gov/pubmed/7678183.

Huang, X., Liu, G., Guo, J., & Su, Z. (2018). The PI3K/AKT pathway in obesity and type 2 diabetes. *Int J Biol Sci, 14*(11), 1483-1496. Retrieved from https://www.ncbi.nlm.nih.gov/pubmed/30263000. doi:10.7150/ijbs.27173

Huh, J. Y., Park, Y. J., Ham, M., & Kim, J. B. (2014). Crosstalk between adipocytes and immune cells in adipose tissue inflammation and metabolic dysregulation in obesity. *Mol Cells, 37*(5), 365-371. Retrieved from https://www.ncbi.nlm.nih.gov/pubmed/24781408. doi:10.14348/molcells.2014.0074

Kanda, H., Tateya, S., Tamori, Y., Kotani, K., Hiasa, K., Kitazawa, R., . . . Kasuga, M. (2006). MCP-1 contributes to macrophage infiltration into adipose tissue, insulin resistance, and hepatic steatosis in obesity. *J Clin Invest, 116*(6), 1494-1505. Retrieved from https://www.ncbi.nlm.nih.gov/pubmed/16691291. doi:10.1172/JCI26498

Kannel, W. B., Hjortland, M., & Castelli, W. P. (1974). Role of diabetes in congestive heart failure: the Framingham study. *Am J Cardiol, 34*(1), 29-34. Retrieved from https://www.ncbi.nlm.nih.gov/pubmed/4835750.

Ke, M., Wu, H., Zhu, Z., Zhang, C., Zhang, Y., & Deng, Y. (2017). Differential proteomic analysis of white adipose tissues from T2D KKAy mice by LC-ESI-QTOF. *Proteomics, 17*(5). Retrieved from https://www.ncbi.nlm.nih.gov/pubmed/27995753. doi:10.1002/pmic.201600219

Kim, K., Kim, J. H., Youn, B. U., Jin, H. M., & Kim, N. (2010). Pim-1 regulates RANKL-induced osteoclastogenesis via NF-kappaB activation and NFATc1 induction. *J Immunol, 185*(12), 7460-7466. Retrieved from https://www.ncbi.nlm.nih.gov/pubmed/21068407. doi:10.4049/jimmunol.1000885

Lackey, D. E., & Olefsky, J. M. (2016). Regulation of metabolism by the innate immune system. *Nat Rev Endocrinol, 12*(1), 15-28. Retrieved from https://www.ncbi.nlm.nih.gov/pubmed/26553134. doi:10.1038/nrendo.2015.189

Li, J., Loveland, B. E., & Xing, P. X. (2011). Anti-Pim-1 mAb inhibits activation and proliferation of T lymphocytes and prolongs mouse skin allograft survival. *Cell Immunol, 272*(1), 87-93. Retrieved from https://www.ncbi.nlm.nih.gov/pubmed/21974958. doi:10.1016/j.cellimm.2011.09.002

Li, Z., Lin, F., Zhuo, C., Deng, G., Chen, Z., Yin, S., . . . Li, B. (2014). PIM1 kinase phosphorylates the human transcription factor FOXP3 at serine 422 to negatively regulate its activity under inflammation. *J Biol Chem, 289*(39), 26872-26881. Retrieved from https://www.ncbi.nlm.nih.gov/pubmed/25096571. doi:10.1074/jbc.M114.586651

Liong, S., Barker, G., & Lappas, M. (2017). Placental Pim-1 expression is increased in obesity and regulates cytokine- and toll-like receptor-mediated inflammation. *Placenta, 53*, 101-112. Retrieved from https://www.ncbi.nlm.nih.gov/pubmed/28487013. doi:10.1016/j.placenta.2017.04.010

Liu, H. T., Wang, N., Wang, X., & Li, S. L. (2010). Overexpression of Pim-1 is associated with poor prognosis in patients with esophageal squamous cell carcinoma. *J Surg Oncol, 102*(6), 683-688. Retrieved from https://www.ncbi.nlm.nih.gov/pubmed/20544717. doi:10.1002/jso.21627

McLaughlin, T., Ackerman, S. E., Shen, L., & Engleman, E. (2017). Role of innate and adaptive immunity in obesity-associated metabolic disease. *J Clin Invest, 127*(1), 5-13. Retrieved from https://www.ncbi.nlm.nih.gov/pubmed/28045397. doi:10.1172/JCI88876

Mehta, K. D. (2014). Emerging role of protein kinase C in energy homeostasis: A brief overview. *World J Diabetes, 5*(3), 385-392. Retrieved from https://www.ncbi.nlm.nih.gov/pubmed/24936260. doi:10.4239/wjd.v5.i3.385

Mikkers, H., Nawijn, M., Allen, J., Brouwers, C., Verhoeven, E., Jonkers, J., & Berns, A. (2004). Mice deficient for all PIM kinases display reduced body size and impaired responses to hematopoietic growth factors. *Mol Cell Biol, 24*(13), 6104-6115. Retrieved from https://www.ncbi.nlm.nih.gov/pubmed/15199164. doi:10.1128/MCB.24.13.6104-6115.2004

Narlik-Grassow, M., Blanco-Aparicio, C., & Carnero, A. (2014). The PIM family of serine/threonine kinases in cancer. *Med Res Rev, 34*(1), 136-159. Retrieved from https://www.ncbi.nlm.nih.gov/pubmed/23576269. doi:10.1002/med.21284

Narlik-Grassow, M., Blanco-Aparicio, C., Cecilia, Y., Peregrina, S., Garcia-Serelde, B., Munoz-Galvan, S., . . . Carnero, A. (2012). The essential role of PIM kinases in sarcoma growth and bone invasion. *Carcinogenesis, 33*(8), 1479-1486. Retrieved from https://www.ncbi.nlm.nih.gov/pubmed/22623646. doi:10.1093/carcin/bgs176

Nguyen, M. T., Favelyukis, S., Nguyen, A. K., Reichart, D., Scott, P. A., Jenn, A., . . . Olefsky, J. M. (2007). A subpopulation of macrophages infiltrates hypertrophic adipose tissue and is activated by free fatty acids via Toll-like receptors 2 and 4 and JNK-dependent pathways. *J Biol Chem, 282*(48), 35279-35292. Retrieved from https://www.ncbi.nlm.nih.gov/pubmed/17916553. doi:10.1074/jbc.M706762200

Ni, X., Zhang, L., Peng, M., Shen, T. W., Yu, X. S., Shan, L. Y., . . . Ma, K. T. (2018). Hydrogen Sulfide Attenuates Hypertensive Inflammation via Regulating Connexin Expression in Spontaneously Hypertensive Rats. *Med Sci Monit, 24*, 1205-1218. Retrieved from https://www.ncbi.nlm.nih.gov/pubmed/29485979.

Nihira, K., Ando, Y., Yamaguchi, T., Kagami, Y., Miki, Y., & Yoshida, K. (2009). Pim-1 controls NF-κB signalling by stabilizing RelA/p65. *Cell Death And Differentiation, 17*, 689. Retrieved from https://doi.org/10.1038/cdd.2009.174. doi:10.1038/cdd.2009.174 https://www.nature.com/articles/cdd2009174#supplementary-information

Patsouris, D., Li, P. P., Thapar, D., Chapman, J., Olefsky, J. M., & Neels, J. G. (2008). Ablation of CD11c-positive cells normalizes insulin sensitivity in obese insulin resistant animals. *Cell Metab, 8*(4), 301-309. Retrieved from https://www.ncbi.nlm.nih.gov/pubmed/18840360. doi:10.1016/j.cmet.2008.08.015

Rosen, E. D., & Spiegelman, B. M. (2014). What we talk about when we talk about fat. *Cell, 156*(1-2), 20-44. Retrieved from https://www.ncbi.nlm.nih.gov/pubmed/24439368. doi:10.1016/j.cell.2013.12.012

Serena, C., Keiran, N., Ceperuelo-Mallafre, V., Ejarque, M., Fradera, R., Roche, K., . . . Fernandez-Veledo, S. (2016). Obesity and Type 2 Diabetes Alters the Immune Properties of Human Adipose Derived Stem Cells. *Stem Cells, 34*(10), 2559-2573. Retrieved from https://www.ncbi.nlm.nih.gov/pubmed/27352919. doi:10.1002/stem.2429

Serena, C., Keiran, N., Madeira, A., Maymo-Masip, E., Ejarque, M., Terron-Puig, M., . . . Vendrell, J. (2017). Crohn's Disease Disturbs the Immune Properties of Human Adipose-Derived Stem Cells Related to Inflammasome Activation. *Stem Cell Reports, 9*(4), 1109-1123. Retrieved from https://www.ncbi.nlm.nih.gov/pubmed/28966116. doi:10.1016/j.stemcr.2017.07.014

Shah, N., Pang, B., Yeoh, K. G., Thorn, S., Chen, C. S., Lilly, M. B., & Salto-Tellez, M. (2008). Potential roles for the PIM1 kinase in human cancer - a molecular and therapeutic appraisal. *Eur J Cancer, 44*(15), 2144-2151. Retrieved from https://www.ncbi.nlm.nih.gov/pubmed/18715779. doi:10.1016/j.ejca.2008.06.044

Shaik, A. A., Qiu, B., Wee, S., Choi, H., Gunaratne, J., & Tergaonkar, V. (2016). Phosphoprotein network analysis of white adipose tissues unveils deregulated pathways in response to high-fat diet. *Sci Rep, 6*, 25844. Retrieved from https://www.ncbi.nlm.nih.gov/pubmed/27180971. doi:10.1038/srep25844

Stephens, J. M., Lee, J., & Pilch, P. F. (1997). Tumor necrosis factor-alpha-induced insulin resistance in 3T3-L1 adipocytes is accompanied by a loss of insulin receptor substrate-1 and GLUT4 expression without a loss of insulin receptor-mediated signal transduction. *J Biol Chem, 272*(2), 971-976. Retrieved from https://www.ncbi.nlm.nih.gov/pubmed/8995390.

Sun, W., Yao, S., Tang, J., Liu, S., Chen, J., Deng, D., & Zeng, C. (2018). Integrative analysis of super enhancer SNPs for type 2 diabetes. *PLoS One, 13*(1), e0192105. Retrieved from https://www.ncbi.nlm.nih.gov/pubmed/29385209. doi:10.1371/journal.pone.0192105

Wajchenberg, B. L., Giannella-Neto, D., da Silva, M. E., & Santos, R. F. (2002). Depot-specific hormonal characteristics of subcutaneous and visceral adipose tissue and their relation to the metabolic syndrome. *Horm Metab Res, 34*(11-12), 616-621. Retrieved from http://www.ncbi.nlm.nih.gov/pubmed/12660870. doi:10.1055/s-2002-38256

Wang, Y. C., McPherson, K., Marsh, T., Gortmaker, S. L., & Brown, M. (2011). Health and economic burden of the projected obesity trends in the USA and the UK. *Lancet, 378*(9793), 815-825. Retrieved from https://www.ncbi.nlm.nih.gov/pubmed/21872750. doi:10.1016/S0140-6736(11)60814-3

Wang, Z., Bhattacharya, N., Meyer, M. K., Seimiya, H., Tsuruo, T., Tonani, J. A., & Magnuson, N. S. (2001). Pim-1 negatively regulates the activity of PTP-U2S phosphatase and influences terminal differentiation and apoptosis of monoblastoid leukemia cells. *Arch Biochem Biophys, 390*(1), 9-18. Retrieved from https://www.ncbi.nlm.nih.gov/pubmed/11368509. doi:10.1006/abbi.2001.2370

Warfel, N. A., & Kraft, A. S. (2015). PIM kinase (and Akt) biology and signaling in tumors. *Pharmacol Ther, 151*, 41-49. Retrieved from https://www.ncbi.nlm.nih.gov/pubmed/25749412. doi:10.1016/j.pharmthera.2015.03.001

Weisberg, S. P., McCann, D., Desai, M., Rosenbaum, M., Leibel, R. L., & Ferrante, A. W., Jr. (2003). Obesity is associated with macrophage accumulation in adipose tissue. *J Clin Invest, 112*(12), 1796-1808. Retrieved from https://www.ncbi.nlm.nih.gov/pubmed/14679176. doi:10.1172/JCI19246

Weitzman, S. A., & Gordon, L. I. (1990). Inflammation and cancer: role of phagocyte-generated oxidants in carcinogenesis. *Blood, 76*(4), 655-663. Retrieved from https://www.ncbi.nlm.nih.gov/pubmed/2200535.

Wildman, R. P., Muntner, P., Reynolds, K., McGinn, A. P., Rajpathak, S., Wylie-Rosett, J., & Sowers, M. R. (2008). The obese without cardiometabolic risk factor clustering and the normal weight with cardiometabolic risk factor clustering: prevalence and correlates of 2 phenotypes among the US population (NHANES 1999-2004). *Arch Intern Med, 168*(15), 1617-1624. Retrieved from http://www.ncbi.nlm.nih.gov/pubmed/18695075. doi:10.1001/archinte.168.15.1617

World Health Organization (16 February 2018). Obesity and overweight. Retrieved from: https://www.who.int/en/news-room/fact-sheets/detail/obesity-and-overweight.

Wu, Y., Deng, Y., Zhu, J., Duan, Y., Weng, W., & Wu, X. (2018). Pim1 promotes cell proliferation and regulates glycolysis via interaction with MYC in ovarian cancer. *Onco Targets Ther, 11*, 6647-6656. Retrieved from https://www.ncbi.nlm.nih.gov/pubmed/30349298. doi:10.2147/OTT.S180520

Xu, H., Barnes, G. T., Yang, Q., Tan, G., Yang, D., Chou, C. J., . . . Chen, H. (2003). Chronic inflammation in fat plays a crucial role in the development of obesity-related insulin resistance. *J Clin Invest, 112*(12), 1821-1830. Retrieved from https://www.ncbi.nlm.nih.gov/pubmed/14679177. doi:10.1172/JCI19451

Ye, J. (2013). Mechanisms of insulin resistance in obesity. *Front Med, 7*(1), 14-24. Retrieved from https://www.ncbi.nlm.nih.gov/pubmed/23471659. doi:10.1007/s11684-013-0262-6

Zhang, B. B., Zhou, G., & Li, C. (2009). AMPK: an emerging drug target for diabetes and the metabolic syndrome. *Cell Metab, 9*(5), 407-416. Retrieved from https://www.ncbi.nlm.nih.gov/pubmed/19416711. doi:10.1016/j.cmet.2009.03.012

Figure 1

Figure 2

Figure 3

Figure 4
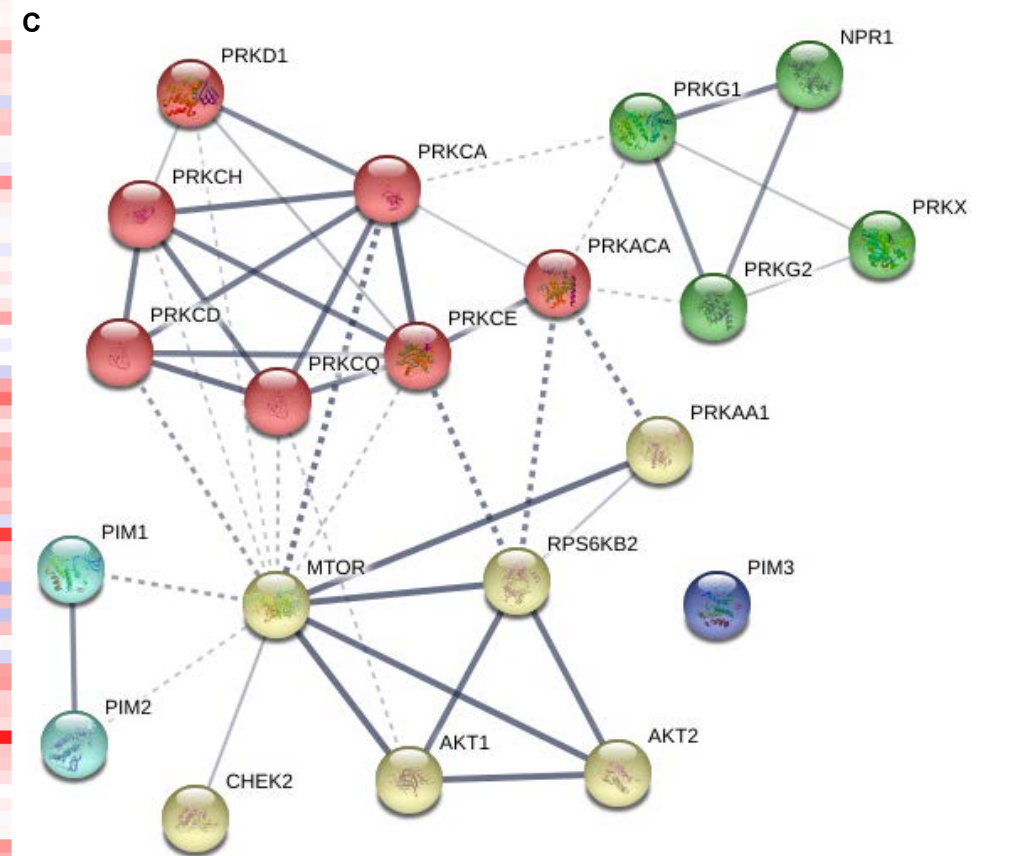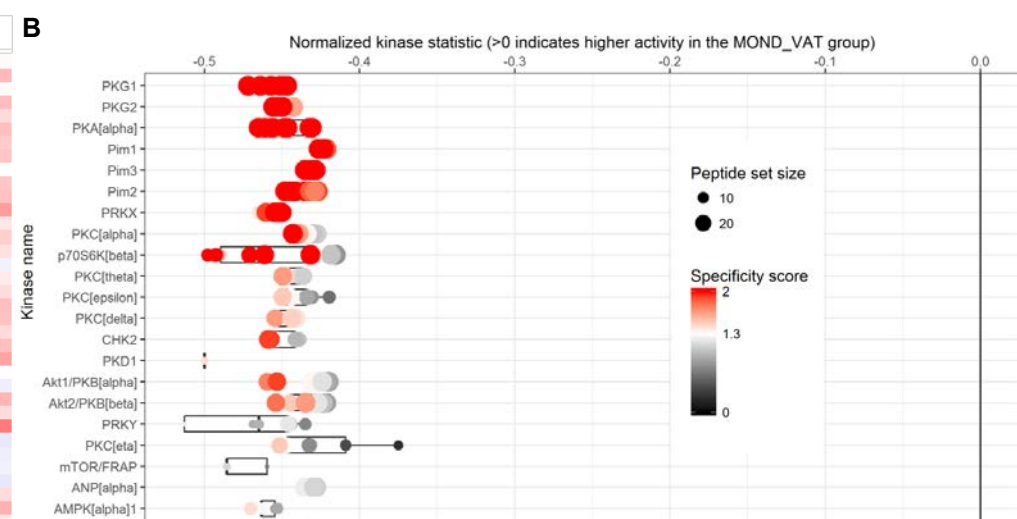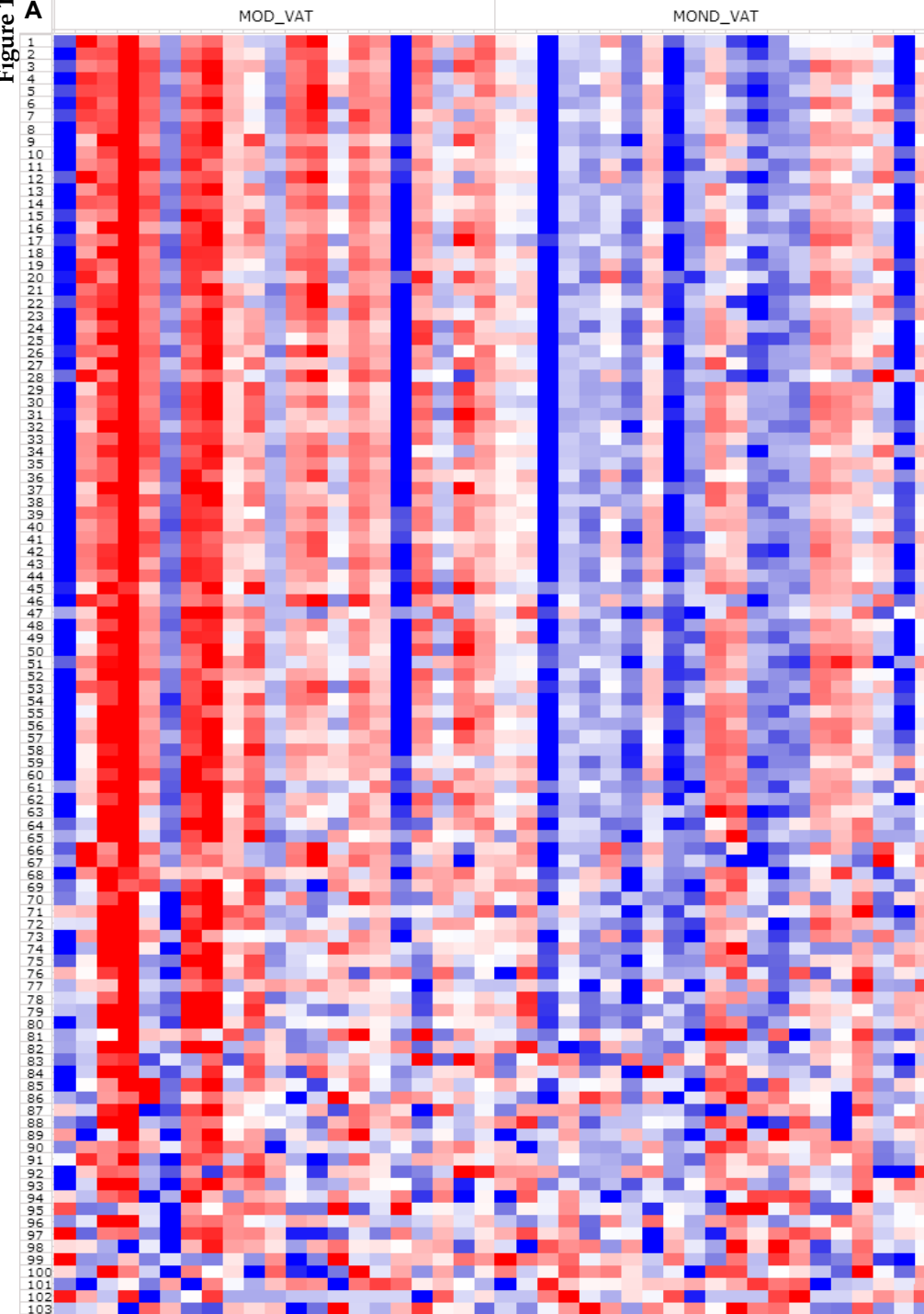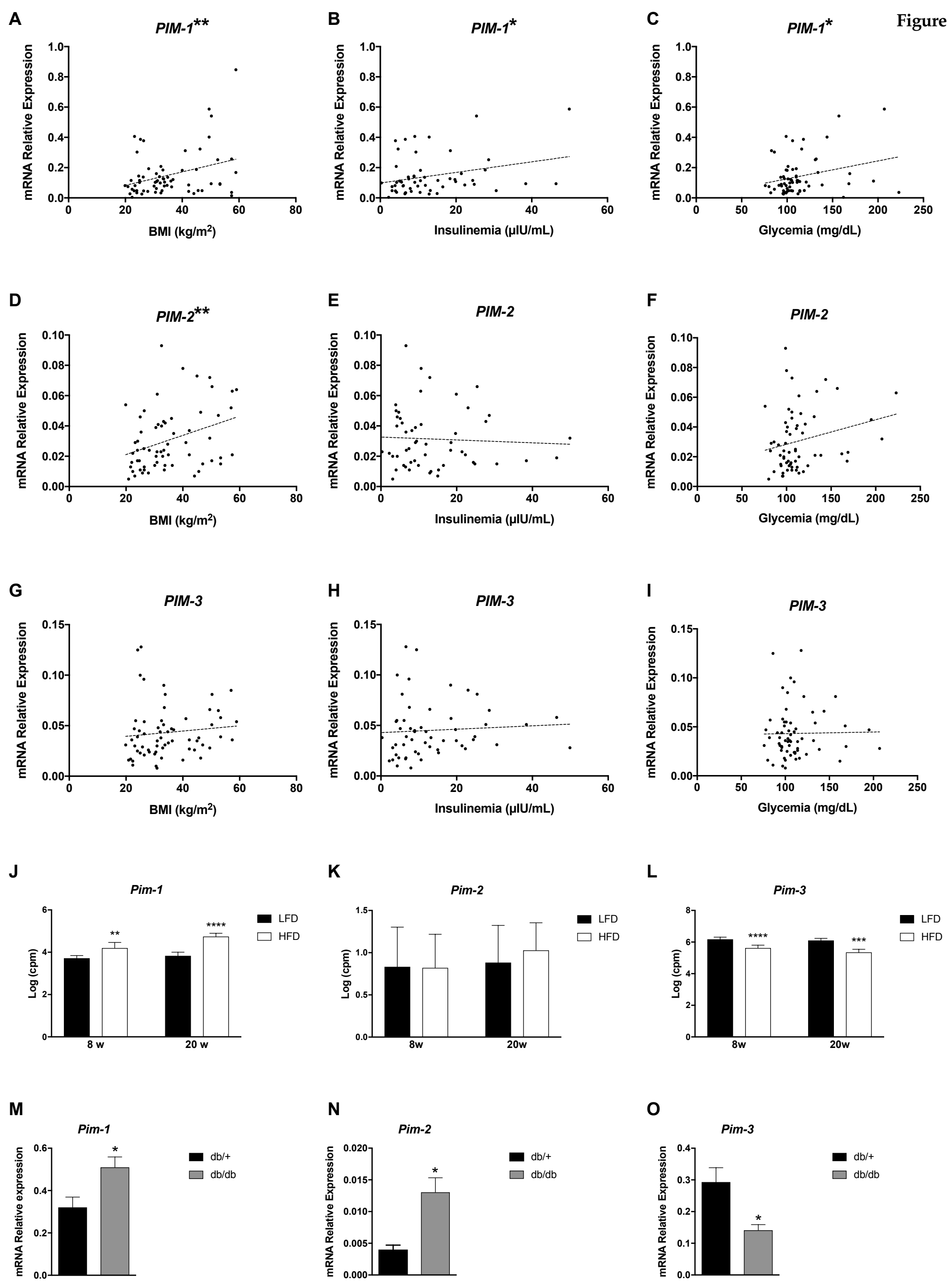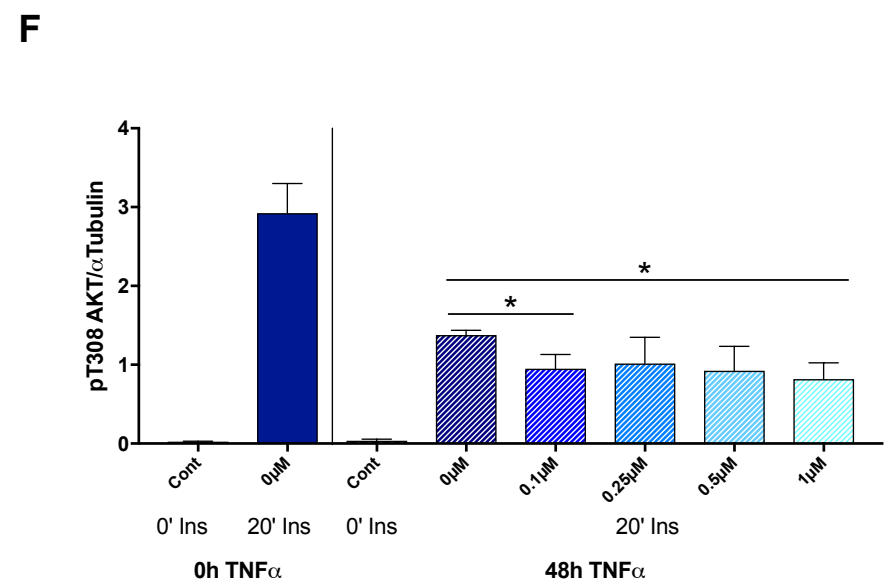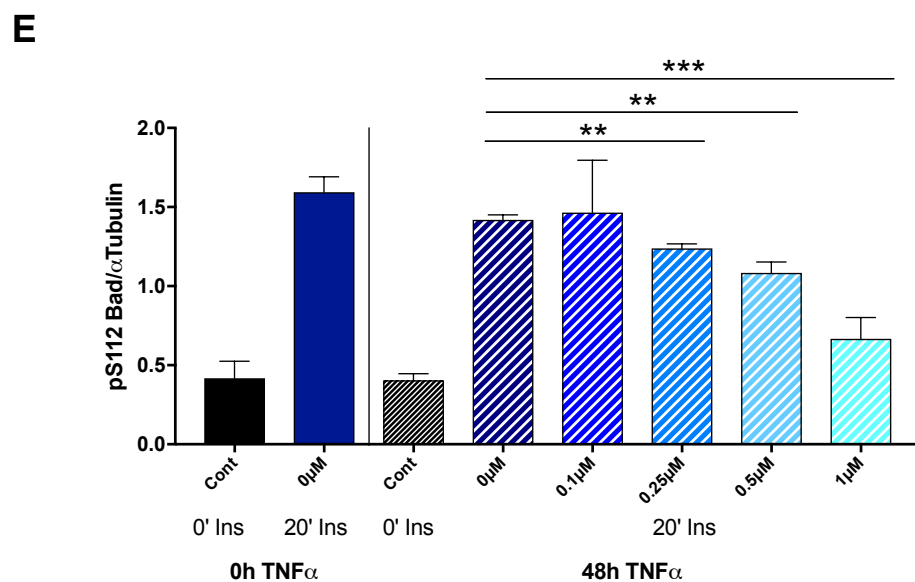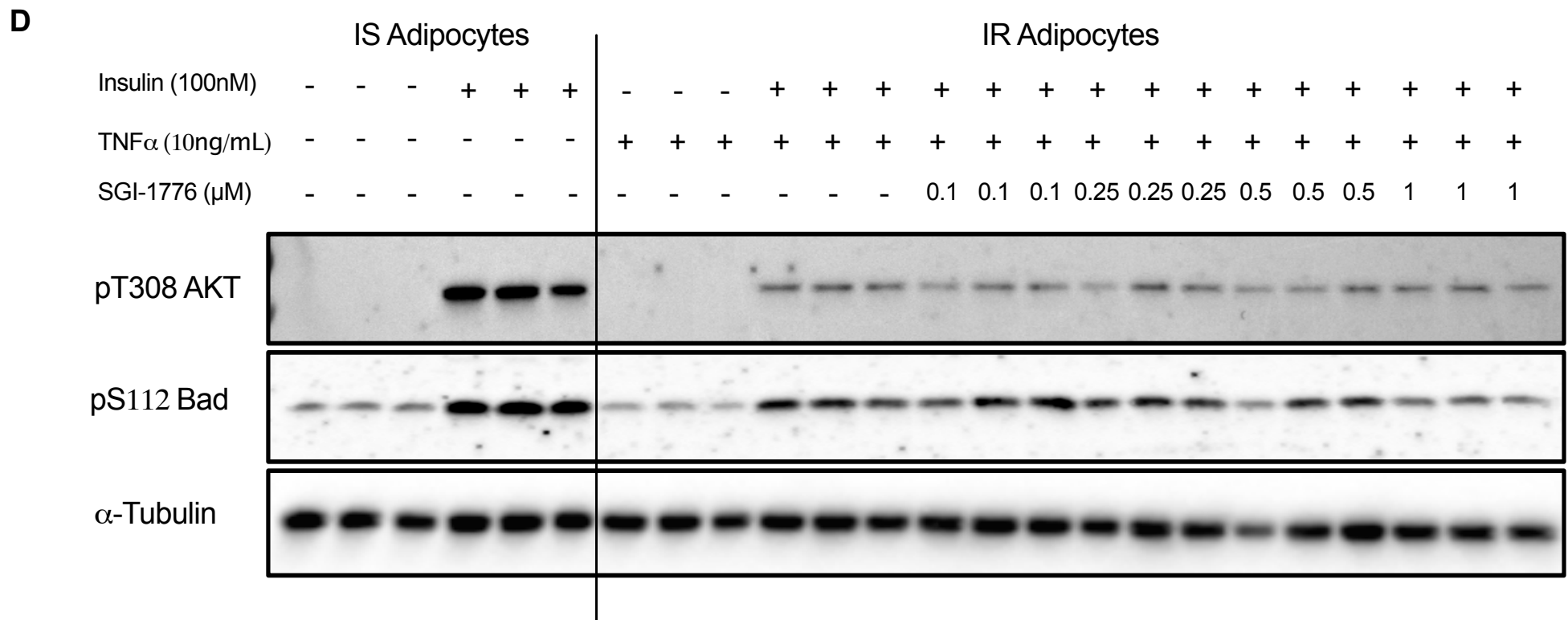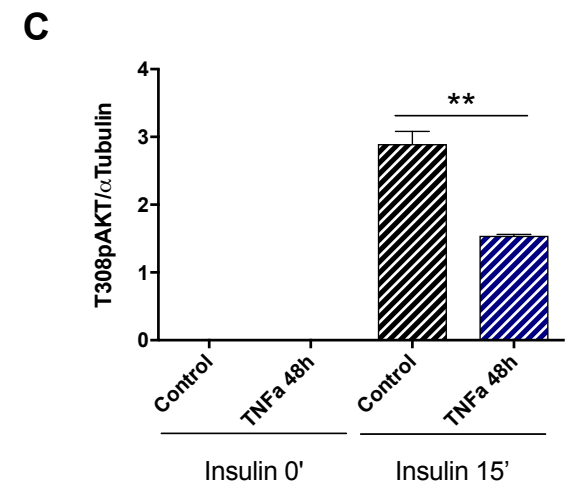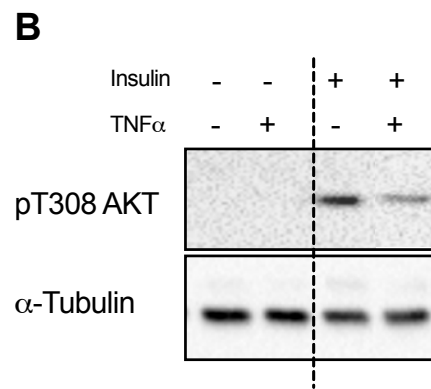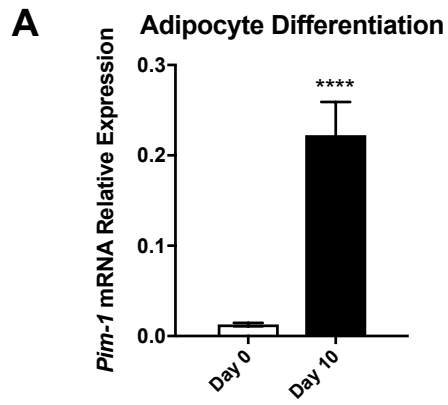
A Normalized kinase statistic (>0 indicates higher activity in the Macrophages_LPS6h group)

Figure 5

Figure 6
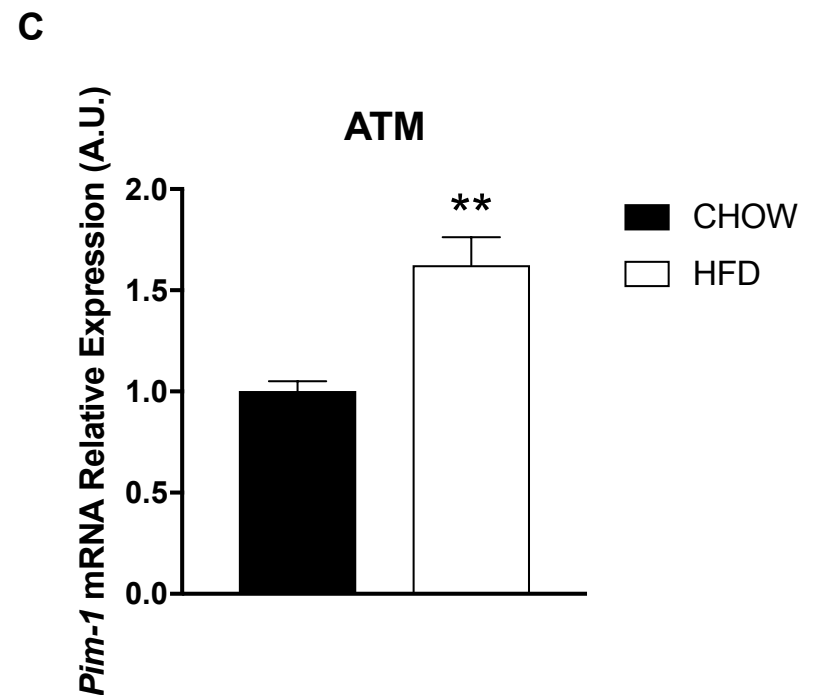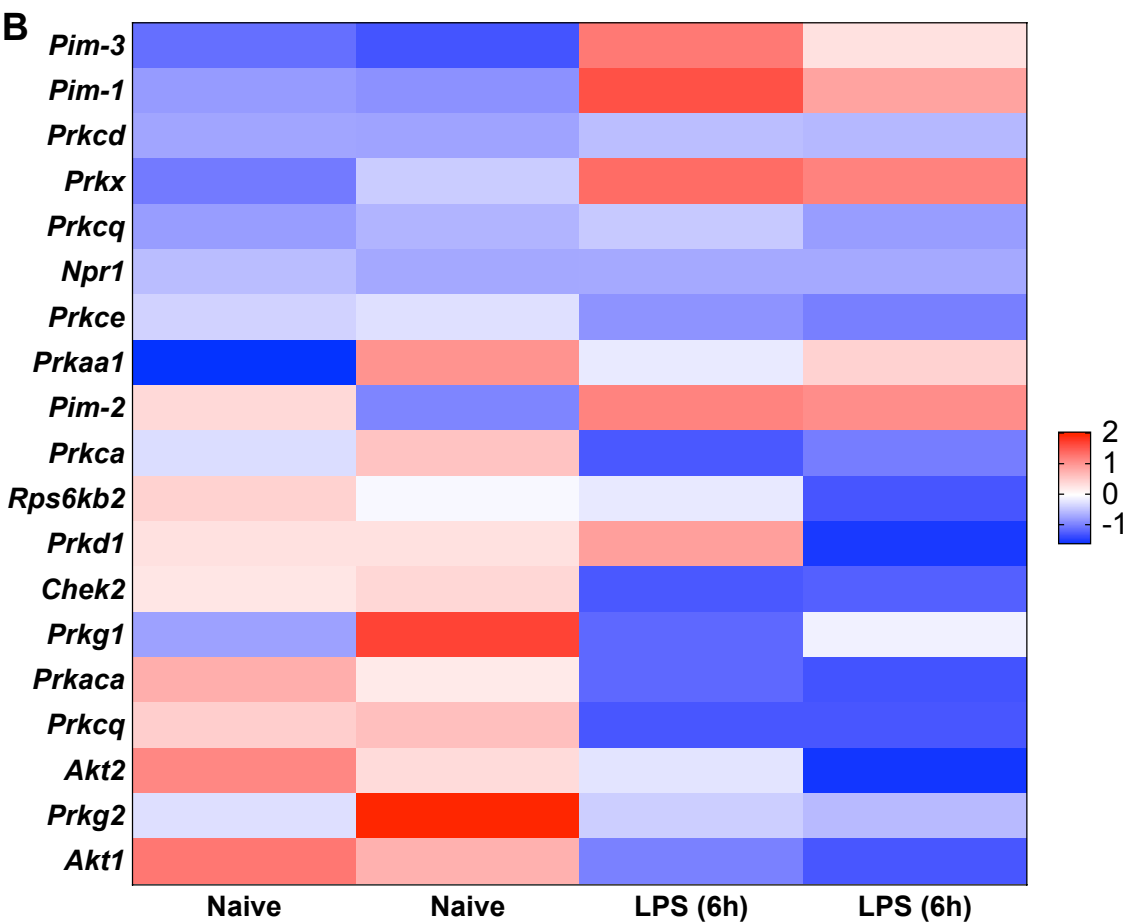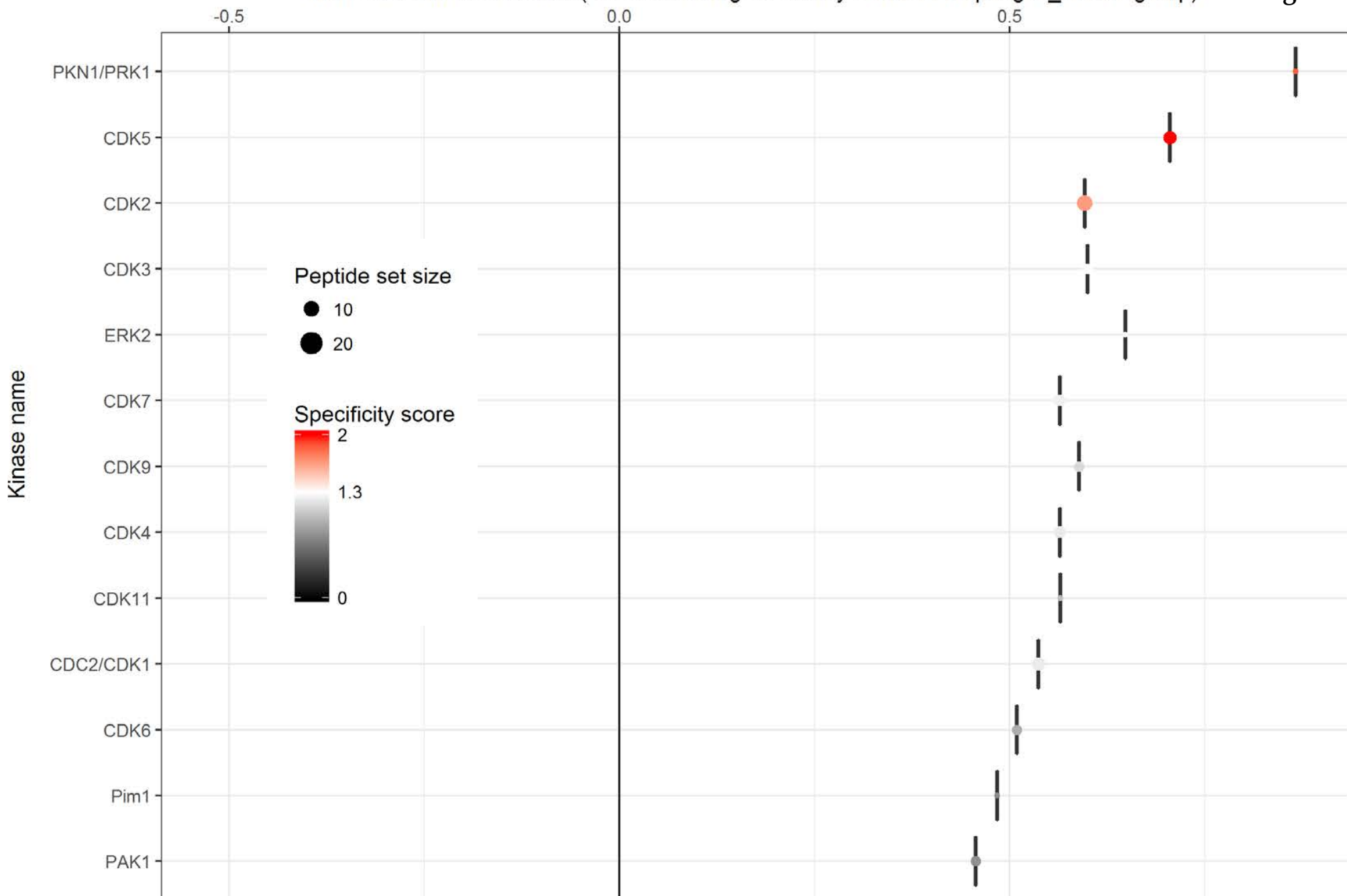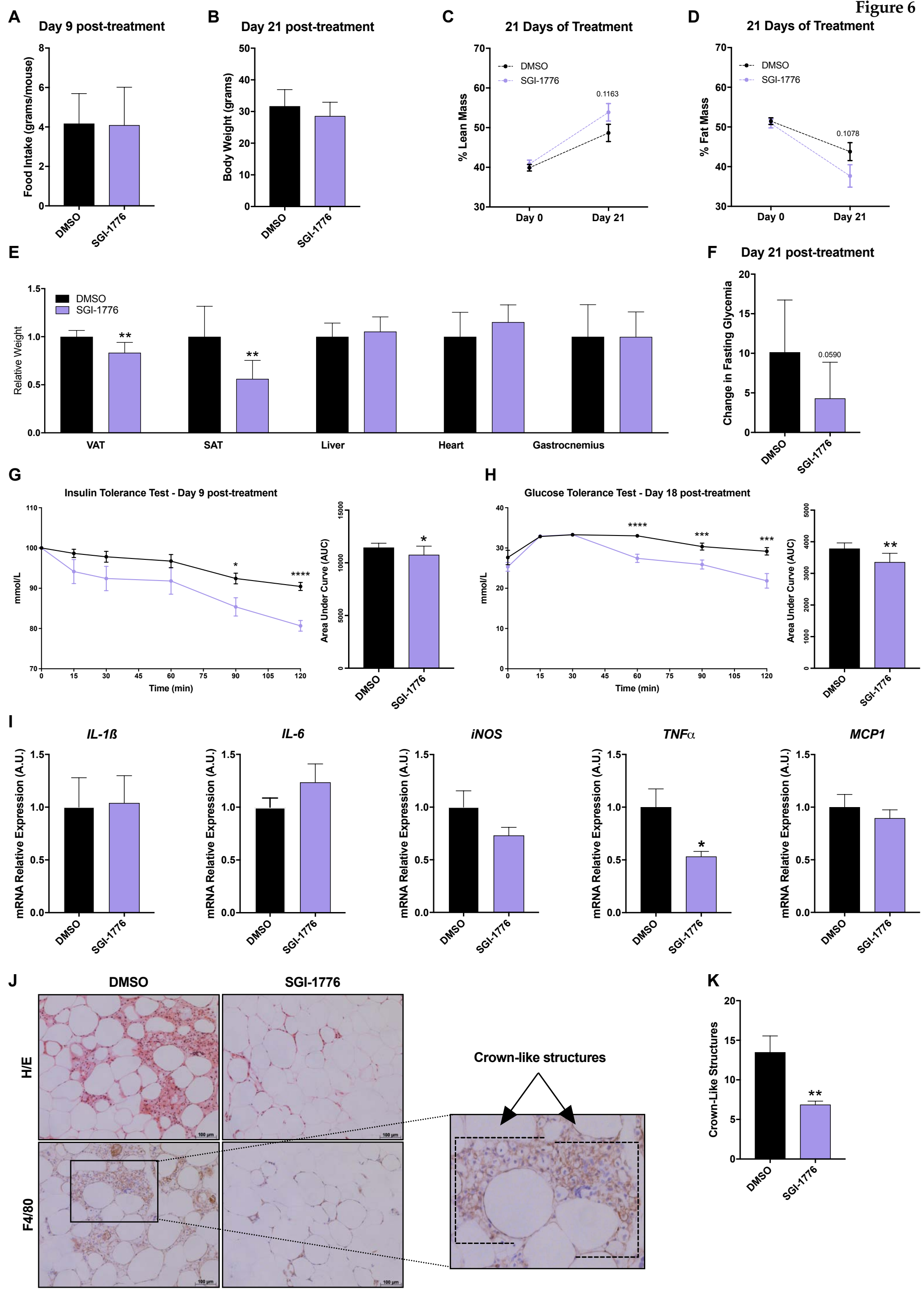
Morbid Obese Visceral Adipose Tissue
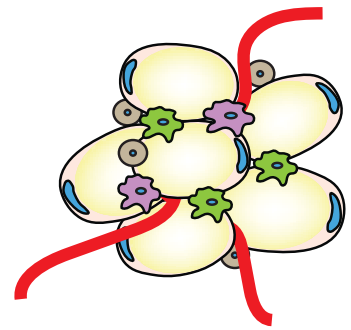
- Adipocyte
- M1 Macrophage
- M2 Macrophage
- Other Cell Types
- Blood Vessel

Lysate

IS

IR

Kinase Activity

ATP

ADP

- Serine/Threonine
- Kinase
- Phosphate
- 1° Antibody
- 2° Antibody
- FITC

Kinase Activity Readout

Peptide Heatmap

MOD_VAT   MOND_VAT

A

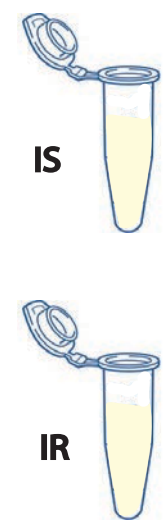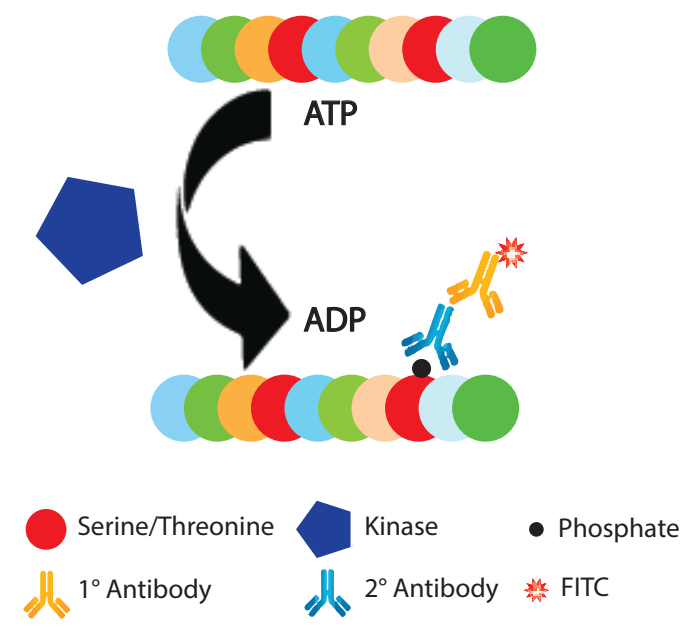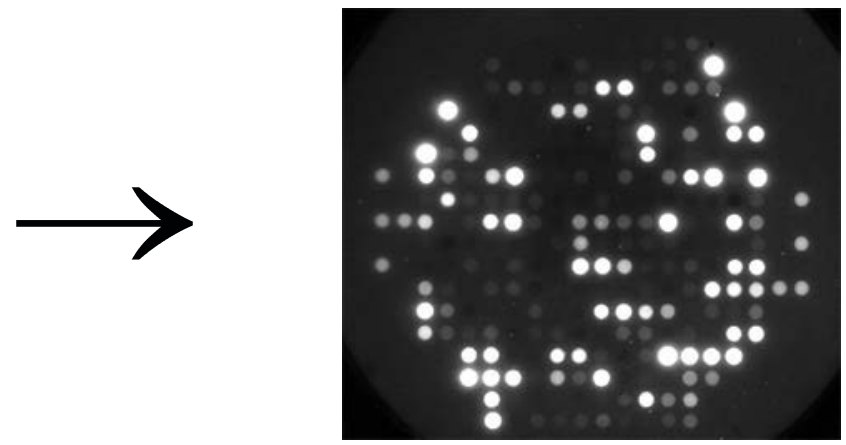| 2GC_	ID
110	MARCS_152_164
109	ADDB_696_708
108	GSUB_61_73
107	C1R_201_213
106	MP2K1_287_299
105	IF4E_203_215
104	ACM1_444_456
103	CD27_212_224
102	NEK3_158_170
101	NR4A1_344_356
100	BAD_93_105
99	LMNB1_16_28
98	ACM4_456_468
97	FOXO3_25_37
96	MARCS_160_172
95	ACM5_494_506
94	ACM5_498_510
93	NEK2_172_184
92	RB_803_815
91	RB_350_362
90	ACM1_421_433
89	CDC2_154_169
88	ANDR_785_797
87	FIBA_569_581
86	P53_308_323
85	ERF_519_531
84	CA2D1_494_506
83	KS6A1_374_386
82	H32_3_18
81	PP2AB_297_309
80	MBP_222_234
79	KAPCG_192_206
78	BCKD_45_57
77	KCNB1_489_501
76	DCX_49_61
75	MPIP1_172_184
74	ESR1_160_172
73	RB_242_254
72	BAD_69_81
71	PDE5A_95_107
70	TAU_524_536
69	CENPA_1_14
68	MPIP3_208_220
67	GYS2_1_13
66	CDK7_163_175
65	KPCB_626_639
64	PRKDC_2618_2630
63	H2B1B_27_40
62	RB_774_786
61	ANXA1_209_221
60	COF1_17_29
59	KCC2G_278_289
58	PPR1A_28_40
57	ADDB_706_718
56	KPCB_19_31_A25S
55	RAP1B_172_184
54	RYR1_4317_4329
53	BAD_112_124
52	K6PL_766_778
51	GPR6_349_361
50	RAF1_253_265
49	DESP_2842_2854
48	KIF2C_105_118_S106G
47	KCNA1_438_450
46	KCNA3_461_473
45	PLM_76_88
44	STMN2_90_102
43	REL_260_272
42	KPB1_1011_1023
41	GPSM2_394_406
40	CGHB_109_121
39	NFKB1_330_342
38	LIPS_944_956
37	CFTR_730_742
36	ERBB2_679_691
35	ART_025_CXGLRRWSLGGLRRWSL
34	SCN7A_898_910
33	VASP_150_162
32	RBL2_655_667
31	CSF1R_701_713
30	PLEK_106_118
29	PTK6_436_448
28	NMDZ1_890_902
27	TY3H_65_77
26	CAC1C_1974_1986
25	KAP2_92_104
24	EPB42_241_253
23	KCNA2_442_454
22	ADRB2_338_350
21	VASP_271_283
20	STK6_283_295
19	TOP2A_1463_1475
18	FRAP_2443_2455
17	VTNC_390_402
16	E1A_ADE05_212_224
15	KAP3_107_119
14	CDN1A_139_151
13	NCF1_321_333
12	MYPC3_268_280
11	RS6_228_240
10	KCNA6_504_516
9	GRIK2_708_720
8	NCF1_296_308
7	F263_454_466
6	CREB1_126_138
5	GBRB2_427_439
4	PTN12_32_44
3	CFTR_761_773
2	LMNA_192_204
1	NOS3_1171_1183

Comment 1 | Macrophages_control | Macrophages_LPS6h

2GC_Ctrl_LPS::Input_Row Scale

B

ATM

Pim-2 mRNA Relative Expression (A.U.)

CHOW
HFD

ATM

Pim-3 mRNA Relative Expression (A.U.)

CHOW
HFD